

Characterisation and Biological Impact of Wear Particles from
Composite Ceramic Hip Replacements

Imran Mohammed Asif

Submitted in accordance with the requirements for the degree of
Doctor of Philosophy

The University of Leeds
School of Mechanical Engineering

January 2018

The candidate confirms that the work submitted is his own and that appropriate credit has been given where reference has been made to the work of others.

This copy has been supplied on the understanding that it is copyright material and that no quotation from the thesis may be published without proper acknowledgement.

The right of Imran Mohammed Asif to be identified as Author of this work has been asserted by him in accordance with the Copyright, Designs and Patents Act 1988.

© 2018 The University of Leeds and Imran Mohammed Asif

Acknowledgements

I begin in the name of Allah, the most beneficent and most merciful.

First and foremost, I would like to thank and express my sincere appreciation to Professor Joanne Tipper. As my primary supervisor, she guided me throughout the journey of my PhD with invaluable motivation and ideas, as well as patience during the ups and downs of my PhD and personal life. From my first meeting with Joanne, she has been my professional mentor and I am truly grateful to her for everything I have achieved over the past four years. I would also like to thank my co-supervisors, Dr Sophie Williams, Dr Mazen Al-Hajjar, Dr James Anderson and Professor John Fisher. My project would have been so much more difficult without their expert knowledge they provided to me and I feel very lucky to have had such a strong supervision team behind me. Special regards and thanks to Dr Sophie Williams for her straightforwardness and support during my supervision meetings and whilst writing my thesis. Her advice and critique really helped me overcome many challenges I faced throughout my PhD.

I would like to thank everyone in the both the engineering and biology labs. Thanks to Dr Daniel Thomas, Sha Zhang and Irvin Homan for their help and technical support. I would also like to thank my peers during my time at Leeds. In particular, Andres Barco, Saurabh Lal, Laura Edwards and Ama Frimpong for their infinite sources of advice, motivation and laughs, you all made my journey so much more enjoyable. I have amazing memories with you all, and I wish you continued success both professionally and personally.

I would like to give my deepest thanks and appreciation to my wife for her support, wisdom, advice and most of all for her understanding during the hard times of my PhD. Your support has been unlimited, and my time at Leeds would have not been the same without you. The happiness you bring, and the love you constantly show, allows me to conquer anything.

I want to express an enormous gratitude and eternal appreciation to my parents for their unlimited support throughout my PhD and my life. You have always encouraged me to achieve high goals and given me the drive to succeed in everything I do. I would especially like to thank my mum who would always give me multiple containers of food to take back to Leeds every time I visited home. I must also thank my sisters who also helped and supported me during my time at Leeds. Finally, my parents have given me the best upbringing and tools to succeed in life. Your love, encouragement and support has allowed me to follow my dreams and complete this PhD. This thesis is dedicated to you both, mum and dad!

Abstract

The high prevalence of osteolysis and aseptic loosening associated with the wear particles of conventional metal-on-UHMWPE (MoP) total hip replacements (THRs), and concerns over the release of metal wear particles and metal ions around the body from metal-on-metal (MoM) THRs, led to the development of alternative ceramic-on-ceramic (CoC) THRs. CoC bearings are of great interest due to their superior wear properties, compared to MoP and MoM bearings. Historically, ceramic THRs had a reputation for fracture, and recent issues have centred around surgical positioning and squeaking. The development of improved manufacturing methods allowed major improvements of ceramics which led to the introduction of composite ceramics for example, zirconia-toughened, platelet reinforced alumina or ZTA, otherwise commercially known as BIOLOX[®] Delta. The wear performance of composite CoC THRs such as those using BIOLOX[®] Delta has been extensively investigated, however no studies have reported the combined characteristics and biocompatibility of the wear debris generated from these bearings.

Understanding wear particle characteristics and their biological activity is an essential step in the pre-clinical testing of joint replacements. However, currently for composite ZTA CoC bearings there is a lack of relevant studies, due to difficulties in generating high volumes of clinically-relevant ceramic wear debris *in vitro*, in addition current particle isolation methods are not sensitive enough to reliably isolate wear particles from hip simulator lubricants, due to the inherent low wear rates of the composite ZTA ceramics. Hence, the particles have not been systematically characterised and therefore little is known about their size, morphology and biological responses. Therefore, the aim of this study was to investigate the characteristics and biological activity of wear particles generated from composite BIOLOX[®] Delta ZTA CoC THRs.

This study developed a two-step particle isolation method and subsequently applied it to hip simulator lubricants for the isolation of composite ceramic wear particles generated from BIOLOX[®] Delta CoC bearings tested under edge loading conditions. The high sensitivity of this new particle isolation method coupled with its effective removal of protein, allowed the successful recovery and characterisation of very low volumes of both micro and nano-scale wear particles, generated from composite ZTA CoC hip replacements for the first time. The recovered wear particles demonstrated a bimodal size range, which has been previously reported for wear particles generated from alumina ceramic hip replacements.

A comprehensive evaluation of the biological impact of commercially-obtained composite BIOLOX[®] Delta ZTA ceramic model particles and clinically-relevant composite BIOLOX[®] Delta ZTA ceramic wear particles was investigated in terms of cytotoxicity, inflammation, genotoxicity and oxidative stress. The clinically-relevant composite ZTA ceramic wear particles were generated in water lubricant using a hip simulator under severe edge loading

conditions. The biological impact of the ceramic particles was assessed using L929 fibroblast cells and peripheral blood mononuclear cells (PBMNCs) isolated from healthy human donors. Both the model and clinically-relevant BIOLOX[®] Delta ceramic wear particles demonstrated significant reduction in the viability of L929 fibroblast cells at very high doses (500 μm^3 of particles per cell), however no cytotoxic effects were observed at the lower clinically-relevant doses (0.5-0.05 μm^3 per cell). The BIOLOX[®] Delta ZTA ceramic model particles failed to stimulate an inflammatory response in terms of TNF- α release and did not cause any significant DNA damage or production of reactive oxygen species (oxidative stress) in PBMNCs from all donors. However, high doses (50 μm^3 per cell) of clinically-relevant BIOLOX[®] Delta ZTA ceramic wear particles caused significantly elevated levels of TNF- α release from PBMNCs. But, there were no significant effects in terms of DNA damage and oxidative stress in PBMNCs from all donors. This study demonstrated that there was a threshold volume of clinically-relevant ceramic wear particles required to stimulate significant TNF- α release from PBMNCs. However, these doses were not clinically-relevant and highly unlikely to occur in vivo due to the extremely low wear rates of CoC bearings. This comprehensive study indicated that composite ZTA Delta ceramic hip replacements had a low biological impact, which may enhance long-term clinical performance. The results from this study are only relevant for BIOLOX[®] Delta ZTA ceramics and not other manufacturers ceramics.

Table of Contents

ACKNOWLEDGEMENTS	I
ABSTRACT	II
TABLE OF CONTENTS	IV
LIST OF TABLES	X
LIST OF FIGURES	XII
LIST OF ABBREVIATIONS	XIX
1 LITERATURE REVIEW	1
1.1 INTRODUCTION	1
1.2 CERAMICS AS A BEARING MATERIAL FOR THA	2
1.2.1 History of ceramic-on-ceramic total hip replacements	2
1.2.2 Development of manufacturing methods for ceramic hip components	5
1.2.3 Introduction of zirconia femoral heads	5
1.2.3.1 Phase changes in zirconia heads	6
1.2.4 Introduction of composite ceramics	6
1.2.4.1 Strengthening mechanism in BIOLOX [®] Delta ceramic hips	7
1.2.4.2 Clinical Performance of BIOLOX [®] Delta ceramic hips	9
1.3 WEAR	10
1.3.1 Types of wear	10
1.3.2 Friction and Lubrication	11
1.3.3 Wear simulation testing	11
1.3.4 Simulator testing of CoC bearings	12
1.3.4.1 Microseparation in a hip simulator	13
1.3.5 CoC hip simulation under microseparation conditions	14
1.3.5.1 Wear testing of alumina ceramics	14
1.3.5.2 Wear testing of composite ceramics	15
1.4 ISOLATION AND CHARACTERISATION OF WEAR PARTICLES FROM THRS	16
1.4.1 Wear particle analysis in vivo	17
1.4.1.1 Isolation of wear particles by tissue digestion	17
1.4.2 Isolation and characterisation of ceramic wear particles	18
1.4.2.1 Isolation of ceramic wear particles from retrieved tissues	18
1.4.2.2 Isolation of nanometre-sized ceramic wear particles	19
1.4.2.3 Isolation of ceramic wear particles from hip simulator lubricants	19
1.4.3 Comparison of wear particle isolation techniques	21
1.4.3.1 Base, acid or enzymatic digestion	21

1.4.4	Isolation of nano-metre sized wear particles from hip simulator lubricants	22
1.5	FAILURES OF TOTAL HIP REPLACEMENTS	24
1.5.1	Introduction	24
1.5.2	Mechanical factors	25
1.5.2.1	Implant design and material properties	25
1.5.3	Biological Factors	26
1.5.3.1	Osteolysis	26
1.5.3.2	Cytokines and mediators released by macrophages and their roles in osteolysis	26
1.5.4	Biological effects of wear particles generated from different bearing materials	33
1.5.4.1	Wear particles generated from metal-on-UHMWPE hips	33
1.5.4.2	Wear particles generated from metal-on-metal hips	37
1.5.4.3	Wear particles generated from ceramic-on-ceramic hips	41
1.6	SUMMARY	45
1.7	PROJECT AIMS AND OBJECTIVES	47
1.7.1	Aims	47
1.7.2	Objectives	47
2	OPTIMISATION AND VALIDATION OF A NOVEL PARTICLE ISOLATION METHOD FOR ULTRA-LOW VOLUMES OF CERAMIC WEAR DEBRIS	48
2.1	INTRODUCTION	48
2.2	AIMS AND OBJECTIVES	50
2.3	MATERIALS AND METHODS	51
2.3.1	Introduction	51
2.3.2	Materials	51
2.3.2.1	Ceramic particles	51
2.3.2.2	Chemicals and reagents used in this study	51
2.3.2.3	Equipment	52
2.3.2.4	Consumables, plasticware and glassware	53
2.3.3	Validation of sensitivity for the novel particle isolation method	53
2.3.3.1	Introduction	53
2.3.3.2	Characterisation of the particles	54
2.3.3.3	Preparation of particle spiked serum lubricants	55
2.3.3.4	Particle isolation methodology	57
2.3.3.5	Gravimetric measurements of the recovered particles	59
2.3.3.6	Characterisation of the recovered ZTA particles	59
2.3.3.7	Statistical analysis	59

2.3.4	Application of validated novel particle isolation method to hip simulator serum	59
2.3.5	Optimisation of the novel particle isolation method	60
2.3.5.1	Incorporation of papain enzymatic digestion	60
2.3.5.2	Incorporation of lysozyme enzyme	61
2.3.6	Particle isolation from serum lubricants produced from one million cycles of hip simulation	61
2.3.6.1	Isolation of metal particle contaminants using a magnet	62
2.3.7	Particle isolation using two-step digestion and density gradient ultra-centrifugation	62
2.4	RESULTS	65
2.4.1	Validation of sensitivity for the novel particle isolation method	65
2.4.1.1	Particle recovery rates for the isolation method using serum spiked with ZTA ceramic model particles	65
2.4.2	Characterisation of ZTA ceramic model particles before and after isolation	66
2.4.3	Application of validated particle isolation method to hip simulator lubricants	71
2.4.4	Optimisation of digestion regime for novel particle isolation method	72
2.4.4.1	Incorporation of papain enzyme digestion step	72
2.4.4.2	Incorporation of lysozyme enzyme	73
2.4.5	Application of optimised method to hip simulator lubricants collected from one million cycles (0-1Mc)	74
2.4.5.1	Separation of stainless-steel wear particle contaminants from ceramic wear debris	76
2.4.5.2	Recovery of large micrometre ceramic wear particles from hip simulator lubricants	77
2.4.6	Recovery of clinically-relevant BIOLOX [®] Delta ceramic wear debris from hip simulator lubricants using two-step particle isolation protocol	79
2.4.6.1	Characterisation of the clinically-relevant BIOLOX [®] Delta ceramic wear particles recovered from hip simulator lubricants	80
2.5	DISCUSSION	82
2.5.1	Current particle isolation methods	82
2.5.2	Validation of novel particle isolation method	84
2.5.3	Optimisation of particle isolation method	85
2.5.4	Successful recovery of composite ceramic wear particles	88
2.6	LIMITATIONS OF STUDY	89
2.7	SUMMARY OF FINDINGS	89
3	WEAR SIMULATION OF CLINICALLY-RELEVANT CERAMIC WEAR PARTICLES	90

3.1	INTRODUCTION	90
3.2	AIMS AND OBJECTIVES	93
3.3	MATERIALS AND METHODS	94
3.3.1	Introduction	94
3.3.2	Materials	95
3.3.2.1	Chemicals and reagents used in this study	95
3.3.2.2	Equipment	95
3.3.2.3	Ceramic hip components	96
3.3.2.4	Cobalt-chromium pins and plates	96
3.3.2.5	Wear simulators	97
3.3.3	Methods	97
3.3.3.1	Generation of ceramic wear particles using hip simulation	97
3.3.3.2	Pre-test and Post-test analysis of the ceramic hip components	103
3.3.3.3	Generation of cobalt chromium wear particles using a six-station pin-on-plate wear simulator	106
3.3.3.4	Recovery of the wear particles generated	109
3.3.3.5	Characterisation of the recovered ceramic wear particles	110
3.3.3.6	Preparation of particles for cell culture studies	111
3.3.4	Statistical Analysis	112
3.3.4.1	Wear rates and Penetration depths	112
3.3.4.2	Characteristics of wear particles	112
3.4	RESULTS	113
3.4.1	Wear testing of ceramic-on-ceramic hip bearings	113
3.4.1.1	Gravimetric analysis	113
3.4.1.2	Dynamic separation	119
3.4.1.3	Surface analysis ceramic hip components	120
3.4.2	Characterisation of the recovered wear particles	126
3.4.2.1	Characterisation of ceramic wear particles	126
3.4.2.2	Percentage ratio between ceramic and stainless-steel wear particles using EDX elemental mapping	133
3.4.2.3	Characteristics of CoCr wear particles	135
3.5	DISCUSSION	137
3.5.1	Wear rates of CoC bearings	137
3.5.2	Dynamic separation	138
3.5.3	Surface analysis of wear scar	139
3.5.4	Characterisation of recovered wear particles	140
3.5.5	Limitations of study	142
3.6	SUMMARY OF FINDINGS	143

4	BIOLOGICAL IMPACT OF CERAMIC HIP REPLACEMENTS	144
4.1	INTRODUCTION	144
4.2	AIMS AND OBJECTIVES	149
4.3	MATERIALS AND METHODS	150
4.3.1	Materials	150
4.3.1.1	Particles	150
4.3.1.2	Cell lines and primary cells	150
4.3.1.3	Chemicals and reagents used in this chapter	151
4.3.1.4	Equipment	153
4.3.1.5	Consumables, plasticware and glassware	154
4.3.2	Methods	155
4.3.2.1	Measurement of pH	155
4.3.2.2	Microscopy	155
4.3.2.3	Sterilisation	156
4.3.2.4	Stock solutions	156
4.3.2.5	Cell culture	156
4.3.2.6	Determination of cell number using Trypan blue exclusion assay	158
4.3.2.7	Biological impact of ceramic particles	159
4.3.2.8	Culturing cells with particles to determine the biological impact	167
4.3.3	Statistical analysis	170
4.4	RESULTS	171
4.4.1	Characteristics of the model ceramic particles	171
4.4.1.1	BIOLOX® Forte model ceramic particles	171
4.4.1.2	BIOLOX® Delta model ceramic particles	173
4.4.2	Biological impact of ceramic model particles	178
4.4.2.1	The cytotoxic effects of ceramic model particles on L929 fibroblast cells	178
4.4.2.2	The cytotoxic and inflammatory effects of BIOLOX® Delta ceramic model particles in PBMNCs	182
4.4.2.3	The genotoxic effects of BIOLOX® Delta ceramic model particles in PBMNCs	189
4.4.2.4	Oxidative stress in PBMNCs in response to model ceramic particles	197
4.4.3	Biological impact of clinically-relevant ceramic particles	203
4.4.3.1	The cytotoxic effects of clinically-relevant BIOLOX® Delta ceramic wear particles in L929 fibroblast cells	203
4.4.3.2	The cytotoxic and inflammatory effects of clinically-relevant ceramic wear particles on PBMNCs	206
4.4.3.3	The genotoxic effects of clinically-relevant ceramic wear particles in PBMNCs	213

4.4.3.4	Oxidative stress in PBMNCs in response to clinically-relevant ceramic wear particles	220
4.5	DISCUSSION	226
4.5.1	Characteristics of ceramic model particles compared to clinically-relevant ceramic wear particles	226
4.5.2	Cytotoxic effects of ceramic wear particles	228
4.5.3	Inflammatory response to ceramic wear particles	239
4.5.4	Genotoxic effects of ceramic wear particles	244
4.5.5	Oxidative stress in response to ceramic wear particles	246
4.5.6	Limitations of study	248
4.6	SUMMARY OF FINDINGS	249
5	FINAL DISCUSSION	250
5.1	INTRODUCTION	250
5.2	DEVELOPMENT OF PARTICLE ISOLATION METHODOLOGY FOR ULTRA-LOW WEARING COMPOSITE ZTA CERAMIC BEARINGS	252
5.3	GENERATION OF CLINICALLY-RELEVANT COMPOSITE ZTA CERAMIC WEAR PARTICLES IN VITRO	254
5.4	BIOLOGICAL IMPACT OF MODEL AND CLINICALLY-RELEVANT COMPOSITE ZTA CERAMIC WEAR PARTICLES	256
5.5	FUTURE WORK	260
5.6	CONCLUSIONS	262
	REFERENCES	264

List of Tables

Table 1.1: Summary of the mechanical properties of different ceramics used for THA.	4
Table 1.2 - Summary of primary and secondary effects of osteolytic mediators.	30
Table 2.1 - Supplier of the ceramic powder used in this chapter.	51
Table 2.2 – List of chemicals and reagents used in this study.	51
Table 2.3 - List of equipment used in this chapter.	52
Table 2.4 – List of consumables, plasticware and glassware used in this study	53
Table 2.5 – Weights of the ZTA powder required for different volumes of ZTA particles.	55
Table 2.6 – Weights of the ZTA powder for each particle volume.	65
Table 2.7 - Mean size (feret diameter) and morphology (aspect ratio and circularity) values for ZTA ceramic model particle before and after isolation.	70
Table 2.8 - Mean size (feret diameter) and morphology (aspect ratio and circularity) values for clinically-relevant BIOLOX [®] Delta ZTA ceramic wear particle recovered from three different samples of hip simulator serum lubricants.	81
Table 3.1 - List of chemicals and reagents used in this study	95
Table 3.2 – List of equipment used in this study	95
Table 3.3 – Components used for generation of wear particle from ceramic bearings on the hip simulator	96
Table 3.4 – Changes in simulator set-up to reduce contamination of water lubricant	101
Table 3.5: Conditions used for each test for both materials. Two simulator inclination angles of 45 ⁰ and 55 ⁰ were used in the tests, which are equivalent to 55 ⁰ and 65 ⁰ clinical inclination angles, respectively.	103
Table 3.6 - The mean surface roughness characterisation parameters before and after wear simulation testing for BIOLOX [®] Forte and BIOLOX [®] delta heads and cups.	120
Table 3.7 – Morphology (ferret diameter, aspect ratio and circularity) values for BIOLOX [®] Forte ceramic wear particles generated in water.	130
Table 3.8 – Mean size (feret diameter) and morphology (aspect ratio and circularity) values for BIOLOX [®] Delta ceramic wear particles generated in water and serum.	133
Table 4.1 – Composition and source of particles used for biological impact experiments	150
Table 4.2 – Cells used throughout the study.	150
Table 4.3 – List of chemicals and reagents used in this study	151
Table 4.4– List of equipment used in this study	153
Table 4.5– List of consumables, plasticware and glassware used in this study	154
Table 4.6 – The reagents prepared for use with the ELISA kit	160
Table 4.7 – The reagents provided with the ELISA kit and the preparation required prior to use.	160
Table 4.8 – The reagents prepared for use with the comet assay	163

Table 4.9 – The reagents prepared for use with the cellular ROS detection assay	166
Table 4.10 – Seeding density, type of culture vessel and repeats used for each assay.	169
Table 4.11 – Positive controls used for each assay.	169
Table 4.12 - Mean size (feret diameter) and morphology (aspect ratio and circularity) values for BIOLOX [®] Forte ceramic wear particles generated in water and BIOLOX [®] Forte ceramic model particles.	173
Table 4.13 - Mean size (feret diameter) and morphology (aspect ratio and circularity) values for BIOLOX [®] Delta ceramic wear particles generated in water and BIOLOX [®] Delta ceramic model particles.	177
Table 4.14 – Summary of previous studies that have investigated the biological response to ceramic particles.	232

List of Figures

Figure 1.1 – Microstructure of alumina before and after hot isostatic pressing.	5
Figure 1.2 - The microstructure of BIOLOX® Delta.	8
Figure 1.3: The application of microseparation during hip simulation.	14
Figure 1.4: The potential mechanisms that can occur when macrophages are stimulated by wear particles.	27
Figure 1.5. Relationship between RANK, RANKL and OPG.	29
Figure 1.6: Diagrams showing the inversion technique that is used for co-culturing polyethylene particles with cells.	37
Figure 2.1 – Flow diagram showing the work in this chapter in relation to other chapters	49
Figure 2.2 – The particle isolation technique described in three main steps; (1) concentration, (2) enzymatic digestion and (3) separation.	56
Figure 2.3- The spiked and recovered masses for the different volumes of ZTA ceramic model particles isolated using the novel particle isolation method.	66
Figure 2.4- The percentage particle recovery rates of the different volumes of ZTA ceramic model particles isolated using the novel particle isolation method.	66
Figure 2.5 - CFE-SEM images of (A) larger micron size alumina particles and (B) smaller nano-scale zirconia/alumina particles before the particle isolation protocol. CFE-SEM images of (C) larger micron size alumina particles and (D) smaller nano-scale zirconia/alumina particles after the particle isolation protocol.	68
Figure 2.6 - EDX analysis of ZTA ceramic model particles (A) before particle isolation and corresponding EDX spectrum (B). EDX analysis of ZTA ceramic model particles (C) after particle isolation and (D) corresponding EDX spectrum.	69
Figure 2.7 - Comparison of frequency size distribution of the ZTA particles before and after the particle isolation protocol.	70
Figure 2.8 – (A) CFE-SEM image of particles isolated from CoC hip simulator lubricant tested under standard gait conditions and (B) corresponding EDX spectrum.	71
Figure 2.9 – (A) CFE-SEM image of particles isolated from CoC hip simulator lubricant tested under severe microseparation conditions and (B) corresponding EDX spectrum.	72
Figure 2.10 - Formation of a band of CoCr wear debris at the interface between the bottom two layers of the SPT density gradient after ultra-centrifugation.	73
Figure 2.11 - CFE-SEM images of CoCr nano-particles isolated from the band of CoCr wear debris separated using density gradient ultra-centrifugation.	73
Figure 2.12 - CFE-SEM images of BIOLOX® Delta ceramic wear particles (A) standard digestion method and (B) standard digestion method with lysozyme digestion.	74

Figure 2.13 Centrifuge tubes containing digested serum lubricant on top of the SPT density gradient layers.	75
Figure 2.14 Particles recovered from hip simulator lubricant that was collected from one million cycles of testing (0-1Mc).	75
Figure 2.15 CFE-SEM analysis of the recovered particles from hip simulator lubricant that was collected from one million cycles of testing (0-1Mc).	76
Figure 2.16 Magnetic particle isolation technique showing the separation of the magnetic metal particles from the ceramic wear debris.	77
Figure 2.17 CFE-SEM and EDX analysis of the recovered ceramic wear debris.	78
Figure 2.18 - CFE-SEM of the recovered large Alumina micrometre ceramic particles. (B) CFE-SEM of the recovered small Zirconia nano-scale ceramic particles.	79
Figure 2.19 - EDX analysis of the BIOLOX [®] Delta ceramic wear debris recovered from hip simulator lubricant.	80
Figure 2.20 - Frequency size distribution of clinically-relevant BIOLOX [®] Delta ceramic wear particle recovered from three different samples of hip simulator serum lubricants.	81
Figure 3.1 – Flow diagram showing the work in this chapter in relation to other chapters	92
Figure 3.2 – Overview of the experimental methods for generating clinically-relevant wear particles for subsequent testing of biological impact.	94
Figure 3.3 – The dimensions of the pins (A) and plates (B) used in the six-station pin-on-plate wear tests.	97
Figure 3.4 - Leeds Mark II Physiological Anatomical Six Station Hip Joint Simulator.	98
Figure 3.5 – Tools used for compacting the (A) femoral heads and (B) acetabular cups on their corresponding stems and shells, respectively.	99
Figure 3.6 – Removal of acetabular cup from the cup holder after impaction.	99
Figure 3.7 – Simulator set-up of stem and cup holder. (A) Stem holders were attached to the simulator at their corresponding station and thereafter the silicon gaiters were attached. (B) Cup holders were placed into their corresponding stations. (C) Cup holders were covered with the silicon gaiters.	100
Figure 3.8 – Water lubricant collected from Test 2 after 779634 cycles.	101
Figure 3.9 – Conventional bath set-up of the ceramic components in the Leeds II hip simulator.	102
Figure 3.10 - Loading and motion profiles for one gait cycle on the Leeds II hip simulator.	103
Figure 3.11 - Data points taken using a CMM on the surfaces of the (A) femoral heads and (B) acetabular cups to ascertain the geometrical changes after wear simulation testing.	105

Figure 3.12 - Schematic of the three traces performed on the femoral head and acetabular cup components in relation to the alignment mark in order to obtain the surface roughness before and after the wear simulation test.	106
Figure 3.13 – Components of the six-station pin-on-plate wear rig simulator.	107
Figure 3.14 – Assembly of the six-station pin-on-plate wear rig simulator.	108
Figure 3.15 – Assembled station on the six-station wear rig simulator with (1) cantilever arm and (2) weight.	109
Figure 3.16 - Wear volumes generated by ceramic-on-ceramic bearings after 1 million cycles of testing under 4mm translational mismatch and 55° (clinical equivalence) cup inclination angle conditions (Test 1).	114
Figure 3.17 - Mean wear rate of ceramic-on-ceramic bearings after 1 million cycles of testing under 4mm translational mismatch and 55° (clinical equivalence) cup inclination angle conditions (Test 1).	114
Figure 3.18 - Wear volumes generated by ceramic-on-ceramic bearings after 1 million cycles of testing under 4mm translational mismatch and 65° (clinical equivalence) cup inclination angle conditions (Test 2).	115
Figure 3.19 - Mean wear rate of BIOLOX® Forte ceramic-on-ceramic bearings after 1 million cycles of testing under 4mm translational mismatch and 65° (clinical equivalence) cup inclination angle conditions (Test 2).	115
Figure 3.20 - Wear volumes generated by ceramic-on-ceramic bearings after 1 million cycles of testing under 3mm translational mismatch and 65° (clinical equivalence) cup inclination angle conditions (Test 3).	116
Figure 3.21 - Mean wear rate of BIOLOX® Forte ceramic-on-ceramic bearings after 1 million cycles of testing under 3mm translational mismatch and 65° (clinical equivalence) cup inclination angle conditions (Test 3).	117
Figure 3.22 - Wear volume generated from ceramic-on-ceramic bearings after 1 million cycles of testing under 3mm translational mismatch and 65° (clinical equivalence) cup inclination angle conditions (Test 4).	118
Figure 3.23 - Mean wear rate of BIOLOX® Forte ceramic-on-ceramic bearings after 1 million cycles of testing under 3mm translational mismatch and 65° (clinical equivalence) cup inclination angle conditions (Test 4).	118
Figure 3.24 – Wear rate of BIOLOX® Forte components plotted against the medial-lateral displacement or dynamic (micro) separation measured using a LVDT (Tests 1-4).	119
Figure 3.25 - Wear rate of BIOLOX® Delta components plotted against the medial-lateral displacement or dynamic (micro) measured using a LVDT (Tests 1-4).	119
Figure 3.26 - SEM images of a BIOLOX® Forte ceramic femoral head post wear simulation (Test 1, station 1).	122

Figure 3.27 - SEM images of a BIOLOX® Delta ceramic femoral head post wear simulation (Test 1, station 2).	123
Figure 3.28 – Three-dimensional reconstruction of the wear stripe area over three BIOLOX® Forte and BIOLOX® Delta femoral heads tested (test 1) under severe edge loading conditions (4mm translational mismatch and 45° (clinical equivalence) cup inclination angle).	125
Figure 3.29 – Mean penetration depths for BIOLOX® Forte and BIOLOX® Delta tested under severe edge loading conditions (4mm translational mismatch and 45° (clinical equivalence) cup inclination angle).	126
Figure 3.30 - CFE-SEM and EDX analysis of the recovered BIOLOX® Delta ceramic wear particles and stainless-steel particle contaminants generated in the Leeds II hip simulator.	127
Figure 3.31 - CFE-SEM images of wear particles generated from BIOLOX® Forte using the Leeds II hip simulator.	128
Figure 3.32 - CFE-SEM and EDX analysis of the recovered BIOLOX® Forte ceramic wear particles and stainless-steel particle contaminants generated using the Leeds II hip simulator.	129
Figure 3.33 - CFE-SEM and EDX analysis of the recovered BIOLOX® Forte ceramic wear particles (A) SEM image of the nano-scale alumina particles analysed using EDX and (B) corresponding EDX spectrum.	129
Figure 3.34 - Frequency size distribution of clinically-relevant BIOLOX® Forte ceramic particles that were generated in water lubricant using the Leeds II hip simulator under edge loading conditions due to dynamic separation between the head and cup centres.	130
Figure 3.35 - CFE-SEM images of wear particles generated from BIOLOX® Delta using the Leeds II hip simulator.	131
Figure 3.36 - CFE-SEM and EDX analysis of the recovered BIOLOX® Delta ceramic wear particles and stainless-steel particle contaminants generated using the Leeds II hip simulator.	132
Figure 3.37 - CFE-SEM and EDX analysis of the recovered BIOLOX® Delta ceramic wear particles.	132
Figure 3.38 - Frequency size distribution of clinically-relevant BIOLOX® Delta ceramic particles that were generated in water lubricant using the Leeds II hip simulator that were generated under edge loading conditions due to dynamic separation between the head and cup centres.	133
Figure 3.39 – Percentage (weight %) of ceramic and stainless-steel wear particles present in the (A) BIOLOX® Forte and (B) BIOLOX® Delta final particle suspensions.	

Aluminium (Al) was indicative of ceramic and iron (Fe) was indicative of stainless-steel.	134
Figure 3.40 - CFE-SEM images of agglomerated CoCr nano-particles generated using the six-station pin-on-plate wear simulator.	135
Figure 3.41 - Frequency size distribution of clinically-relevant CoCr nano-particles generated using the six-station pin-on-plate wear simulator. The right Y-axis shows the cumulative size frequency of the particles (red line).	136
Figure 4.1 – Flow diagram showing the work in this chapter in relation to other chapters.	149
Figure 4.2 - Example plate layout for performing one ELISA.	162
Figure 4.3 – L929 cells cultured with ceramic model particles.	167
Figure 4.4 – Flow diagram showing the different assays completed on PBMNCs isolated from blood collected from a single donor.	168
Figure 4.5 - CFE-SEM images of BIOLOX® Forte ceramic model particles, which consisted of (A) large micron sized alumina particles and (B) small nano-scale alumina particles.	172
Figure 4.6 - CFE-SEM and EDX analysis of the BIOLOX® Forte ceramic model particles. (A) SEM image of the large alumina particles analysed using EDX and (B) corresponding EDX spectrum.	172
Figure 4.7 - Frequency size distribution of alumina BIOLOX® Forte ceramic model particles.	173
Figure 4.8 - CFE-SEM images of BIOLOX® Delta ceramic model particles.	175
Figure 4.9 - EDX element map of BIOLOX® Delta ceramic model particles at 20K magnification showing the distribution of elements within the composite ceramic.	176
Figure 4.10 - CFE-SEM and EDX analysis of the micron and sub-micron BIOLOX® Delta ceramic model particles.	176
Figure 4.11 - CFE-SEM and EDX analysis of smaller nano-scale BIOLOX Delta ceramic model particles.	177
Figure 4.12 - Frequency size distribution of composite BIOLOX® Delta ceramic model particles.	177
Figure 4.13 –Effects of BIOLOX® Forte ceramic model particles in L929 murine fibroblast cells using the ATP-Lite assay.	180
Figure 4.14 - Effects of BIOLOX® Delta ceramic model particles in L929 murine fibroblast cells using the ATP-Lite assay.	181
Figure 4.15 – (A) Cell viability and (B) TNF- α release from PBMNCs isolated from Donor 2 in response to BIOLOX® Delta model ceramic particles.	183
Figure 4.16 - (A) Cell viability and (B) TNF- α release from PBMNCs isolated from Donor 5 in response to BIOLOX® Delta model ceramic particles.	184

Figure 4.17 - (A) Cell viability and (B) TNF- α release from PBMNCs isolated from Donor 7 in response to BIOLOX® Delta model ceramic particles.	185
Figure 4.18 - (A) Cell viability and (B) TNF- α release from PBMNCs isolated from Donor 25 in response to BIOLOX® Delta model ceramic particles.	186
Figure 4.19 - (A) Cell viability and (B) TNF- α release from PBMNCs isolated from Donor 26 in response to BIOLOX® Delta model ceramic particles.	187
Figure 4.20 – Inter-donor and intra-donor variability in PBMNC responses for (A) cell only control and PBMNCs cultured with 50 μm^3 per cell of CoCr nano-particles and (B) PBMNCs treated with LPS.	189
Figure 4.21 – Tail moment length is measured from the centre of the head to the centre of the tail.	190
Figure 4.22 – The genotoxic effects of BIOLOX® Delta ceramic model particles in PBMNCs isolated from Donor 2.	192
Figure 4.23 - The genotoxic effects of BIOLOX® Delta model ceramic particles in PBMNCs isolated from Donor 5.	193
Figure 4.24 - The genotoxic effects of BIOLOX® Delta model ceramic particles in PBMNCs isolated from Donor 7.	194
Figure 4.25 - The genotoxic effects of BIOLOX® Delta model ceramic particles in PBMNCs isolated from Donor 25.	195
Figure 4.26 - The genotoxic effects of BIOLOX® Delta model ceramic particles in PBMNCs isolated from Donor 26.	196
Figure 4.27 – Visualisation of the presence of ROS in PBMNCs (donor 2) cultured with BIOLOX® Delta ceramic model particles.	199
Figure 4.28 – Oxidative stress in PBMNCs isolated from Donor 2 in response to BIOLOX® Delta ceramic model particles.	200
Figure 4.29 – Oxidative stress in PBMNCs isolated from Donor 5 in response to BIOLOX® Delta model ceramic particles.	200
Figure 4.30 – Oxidative stress in PBMNCs isolated from Donor 7 in response to BIOLOX® Delta model ceramic particles.	201
Figure 4.31 - Oxidative stress in PBMNCs isolated from Donor 25 in response to BIOLOX® Delta model ceramic particles.	201
Figure 4.32 - Oxidative stress in PBMNCs isolated from Donor 26 in response to BIOLOX® Delta model ceramic particles.	202
Figure 4.33 - Effects of clinically-relevant BIOLOX Delta wear particles on L929 fibroblast cells using the ATP-Lite assay.	205
Figure 4.34 – (A) Cell viability and (B) TNF- α release from PBMNCs isolated from Donor 2 in response to clinically-relevant BIOLOX® Delta ceramic wear particles.	208

Figure 4.35 – (A) Cell viability and (B) TNF- α release from PBMNCs isolated from Donor 5 in response to clinically-relevant BIOLOX® Delta ceramic wear particles.	209
Figure 4.36 – (A) Cell viability and (B) TNF- α release from PBMNCs isolated from Donor 7 in response to clinically-relevant BIOLOX® Delta ceramic wear particles.	210
Figure 4.37 – (A) Cell viability and (B) TNF- α release from PBMNCs isolated from Donor 25 in response to clinically-relevant BIOLOX® Delta ceramic wear particles.	211
Figure 4.38 – (A) Cell viability and (B) TNF- α release from PBMNCs isolated from Donor 26 in response to clinically-relevant BIOLOX® Delta ceramic wear particles.	212
Figure 4.39 – The genotoxic effects of clinically-relevant BIOLOX® Delta ceramic particles wear in PBMNCs isolated from Donor 2.	215
Figure 4.40 – The genotoxic effects of clinically-relevant BIOLOX® Delta ceramic particles wear in PBMNCs isolated from Donor 5.	216
Figure 4.41 – The genotoxic effects of clinically-relevant BIOLOX® Delta ceramic particles wear in PBMNCs isolated from Donor 7.	217
Figure 4.42 – The genotoxic effects of clinically-relevant BIOLOX® Delta ceramic particles wear in PBMNCs isolated from Donor 25.	218
Figure 4.43 – The genotoxic effects of clinically-relevant BIOLOX® Delta ceramic particles wear in PBMNCs isolated from Donor 26.	219
Figure 4.44 – Visualisation of the presence of ROS in PBMNCs isolated from Donor 2.	222
Figure 4.45 - Oxidative stress in PBMNCs isolated from Donor 2 in response to BIOLOX® Delta model ceramic particles.	223
Figure 4.46 - Oxidative stress in PBMNCs isolated from Donor 5 in response to BIOLOX® Delta model ceramic particles.	223
Figure 4.47 - Oxidative stress in PBMNCs isolated from Donor 7 in response to BIOLOX® Delta model ceramic particles.	224
Figure 4.48 - Oxidative stress in PBMNCs isolated from Donor 25 in response to BIOLOX® Delta model ceramic particles.	224
Figure 4.49 - Oxidative stress in PBMNCs isolated from Donor 26 in response to BIOLOX® Delta model ceramic particles.	225

List of Abbreviations

Al ₂ O ₃	Alumina
ANOVA	Analysis of variance
APCs	Antigen presenting cells
ATP	Adenosine triphosphate
ATZ	Alumina-toughened zirconia
BSA	Bovine serum albumin
BSE	Back-scattered electrons
CFE-SEM	Cold field emission gun scanning electron microscopy
CMM	Coordinate measurement machine
CO ₂	Carbon dioxide
CoC	Ceramic-on-ceramic
CoCr	Cobalt chromium
CoM	Ceramic-on-metal
CPS	Counts per second
Delta	BIOLOX [®] Delta
d _{max}	Feret diameter
DMEM	Dulbecco's modified eagle's medium
DMSO	Dimethyl sulphoxide
DNA	Deoxyribonucleic acid
DPBS	Dulbecco's phosphate buffered saline
EDTA	Ethlenediaminetetraacetic acid
EDX	Energy-dispersive x-ray spectroscopy
FBS	Foetal bovine serum
FCS	Foetal calf serum
FEG-SEM	Field emission gun scanning electron microscopy
Forte	BIOLOX [®] Forte
GM-CSF	Granulocyte-macrophage colony stimulating factor
HCL	Hydrochloric acid
HIP	Hot-isostatic pressing
IL-1	Interleikin-1
IL-6	Interleikin-6
IL-8	Interleikin-8
LCM	Laser capture microdissection
LPS	Lipopolysaccharide
LVDT	Linear variable differential transformer

MCP-1	Monocyte chemoattractant protein-1
M-CSF	Macrophage colony stimulating factor
MC-SWD	Metal and ceramic silicon wafer display
MIP-1 α	Macrophages inflammatory protein-1 α
MoM	Metal-on-metal
MoP	Metal-on-polymer
NaOH	Sodium hydroxide
NF- κ B	Nuclear kappa B
OA	Osteoarthritis
OPG	Osteoprotegrin
PBMNCs	Peripheral blood mononuclear cells
PBS	phosphate buffered saline
PDGF- α	Platelet-derived growth factor - alpha
PGE ₂	Prostaglandin E-2
PMMA	Polymethylmethacrylate
RANK	Receptor activator of nuclear factor kappa-B
RANKL	Receptor activator of nuclear factor kappa-B ligand
ROS	Reactive oxygen species
RPMI	Roswell Park Memorial Institute
SCF	Stem cell factor
SDS	Sodium dodecyl sulphate
SEM	Scanning electron microscopy
SPT	Sodium polytungstate
TEM	Transmission electron microscopy
THA	Total hip arthroplasty
THR	Total hip replacement
TNF- α	Tumour necrosis factor-alpha
TRAP	Tartrate-resistant acid phosphatase positive
U937	Histiocyte cell line
UHMWPE	Ultra-high molecular weight polyethylene
VNR+	Vitronectin positive
WD	Working distance
Y-TZP	Yttria Stabilized Zirconia
ZrO ₂	Zirconia
ZTA	Zirconia-toughened alumina

CHAPTER 1

1 Literature review

1.1 Introduction

Osteoarthritis (OA) is a degenerative joint disease that affects many joints within the body. Synovial joints are more commonly affected such as the hip and knee joints, hence it is the leading cause of lower extremity disability amongst older adults. The disease causes breakdown of the articular cartilage and can result from a combination of factors including ageing, obesity, muscle weakness, inflammation of the joints and wear and abrasion (Tortora and Derrickson, 2009). For patients with severe OA the last resort treatment would be surgery. The main surgical treatment that is performed and has a high success rate is total hip arthroplasty (THA). This procedure involves surgical replacement of the natural hip joint with an artificial prosthesis. THA is a reconstructive surgical technique, which has allowed better management of OA of the hip joint, that has otherwise responded inadequately to conventional medical treatments (Siopack and Jergesen, 1995).

Metal-on-polyethylene (MoP) bearings have been the most commonly used bearing combination for total hip replacements (THRs) since they were first developed by Sir John Charnley in the early 1960's. The vast majority of total hip replacements implanted today still follow the principles of Charnley's low frictional torque arthroplasty, which consisted of a hard metal femoral head that articulated against an ultra-high molecular weight polyethylene (UHMWPE) acetabular cup with cement fixation (Knight et al., 2011). The national joint registry for the UK reported that out of the approximately 87,733 THRs in 2016, around 51,236 (58.4%) were MoP bearings (National Joint Registry, 2017). This is because MoP bearings are considered to be the gold standard in UK THA and currently provide a safe, predictable and cost-effective bearing for the majority of patients over the age of 55. Hard-on-soft bearings have been shown to be successful in the short term, however, historically high rates of failure due to high wear rates resulted in periprosthetic osteolysis and aseptic loosening in the longer term. Thus, the need for improved bearing surfaces in THA led to the development and study of alternative hard-on-hard bearings such as metal-on-metal and ceramic-on-ceramic.

These alternative hard-on-hard bearings have been of great interest recently due to their superior wear properties. Early generation MoM hip bearings had poor results, and concerns over the release of metal wear particles (metallosis) and metal ions that may be associated with increased risk of carcinogenicity and/or hypersensitivity resulted in rapid declined use of MoM THRs. However, the catastrophic failure of early generation MoM bearings is now believed to have been due to poor design, poor manufacturing tolerances/techniques and improper implantation techniques, hence there has been renewed interest into these alternative bearings throughout the 1990's which resulted in the development of second and third generation MoM bearings (Amstutz and Grigoris, 1996; Knight et al., 2011). Nevertheless, soft tissue reactions to metal wear debris and metal ions has been extensively reported and resulted in implant failure (Haddad et al., 2011). The concerns surrounding MoM THRs led to an increase in the use of ceramic component bearings, from 23.7% of all uncemented THRs in 2003 to 57.7% in 2017 in England and Wales (National Joint Registry, 2017). This is due to ceramics being used in combination with UHMWPE cups. Furthermore, ceramic-on-ceramic (CoC) bearings have demonstrated the best overall tribological and biological performance compared to other bearing materials (MoP and MoM), and so are increasingly being used in younger and more active patients.

1.2 Ceramics as a bearing material for THA

1.2.1 History of ceramic-on-ceramic total hip replacements

Ceramic-on-Ceramic (CoC) total hip replacements (THRs) were first introduced by the French Surgeon Pierre Boutin in 1970 (Boutin, 2000). CoC hip replacements have now been in use for more than 40 years, mainly in Europe, Korea and Australia with a much lower usage in the USA (Knight et al., 2011). Alumina bearings were initially developed to overcome the problems of friction and wear of other bearing materials, since alumina has excellent wear resistance properties and high hardness (Table 1.1). Since its introduction, alumina has also been widely used in combination with UHMWPE acetabular cups (Callaghan and Liu, 2009; Garino, 2011). The first alumina hip implant was performed without cement for the polymer acetabular component and cemented for the ceramic head component (Garino, 2011). Fixation proved to be inadequate and resulted in aseptic loosening in addition to high rates of fracture (Griss and Heimke, 1981; Jeffers and Walter, 2012). A new fixation method was developed by Mittelmeier, from Germany in 1985, who used a threaded ceramic cup that was screwed into the acetabulum. This new method (Autophor design) also employed a press-fit femoral component that eliminated the use of cement fixation, which showed some early success (Garino, 2011). Premarket approval of the Autophor design by the Food and Drug Administration (FDA) resulted in more than 3500 total hip arthroplasty (THA) procedures

being performed in the USA over a three-year period (1982-1985) using the Mittelmeier CoC prosthesis. However, very high incidences of stem loosening (>30% within 3 years) resulted in the Mittelmeier Autophor design being discontinued by the manufacturer (Smith and Nephew, Memphis, Tennessee) (Tateiwa et al., 2008). Clinical studies of the CoC Mittelmeier Autophor design conducted by Yoon et al. (1998) and Nevelos et al. (1999) reported that osteolysis occurred as a result of ceramic debris in periprosthetic tissues. It was also reported that majority of the implants investigated had minimal linear wear penetration (<100µm), but some implants showed very high volumetric wear (3mm³), which was comparable with severe UHMWPE wear. There was no obvious explanation for this high wear, but it was suggested that implant loosening was design related. However, an important finding was that periprosthetic osteolysis due to ceramic wear debris was considerably less when compared with metal-on-polymer (MoP) bearings (Yoon et al., 1998; Nevelos et al., 1999).

Table 1.1: Summary of the mechanical properties of different ceramics used for THA.

Mechanical Property	Units	Forte - Alumina (99.95 Al₂O₃)	Delta - Zirconia, Platelet Toughened Alumina (ZTA) (Al₂O₃ + ZrO₂ + Y₂O₃ + Cr₂O₃ + SrO)
Density	g/cm ³	3.97	4.37
Average Grain Size	μm	≤ 1.8	---
Bending Strength	MPa	>650	1380
Compression Strength	MPa	5000	4700
Young's Modulus	GPa	407	358
Fracture Toughness (K_{IC})	MPa m ^{1/2}	3.5	5.9
Micro-hardness (HV)	GPa	>8.9	>7.7

Note: The average grain size values for ZTA are not stated due to their mixed structure (Kuntz and Krueger, 2018).

1.2.2 Development of manufacturing methods for ceramic hip components

The early ceramic bearings used for THA had a coarse-grained microstructure with limited purity and low density, which led to poor mechanical properties and high rates of fracture of up to 13.4% (Willmann, 2000). Alumina implant technology has improved over the past 40 years with the development of improved manufacturing methods, which included the use of laser markings. Laser markings replaced engraving methods in the 1980s, as engraving have been a source of stress concentration within the alumina ceramic that could cause fracture. In 1995, hot isostatic pressing (HIP) was introduced, which produced a highly pure, more dense ceramic with a smaller grain size and full density (Figure 1.1) (Tateiwa et al., 2008). The manufacturing process of HIPing involves simultaneous application of elevated high temperature and isostatic pressure. The pressure is achieved by pumping inert gas such as argon or nitrogen, into a pressure vessel and pressurising up to 200 MPa. The elevated temperature is achieved by a furnace in the vessel which produces temperatures of up to 2000°C. Before the HIPing process a green body of the ceramic component is formed which is sintered to remove interconnected pores (Loh and Sia, 1992). In 1995, the introduction of HIPing led to the development of HIPed alumina that is commercially known as BIOLOX® Forte (CeramTec, Germany), which was reported to have a lower mean wear rate of $0.09 \pm 0.04\text{mm}^3$ per million cycles compared to non-HIPed alumina ($0.15 \pm 0.06\text{mm}^3$ per million cycles) (Nevelos, Ingham, et al., 2001) .

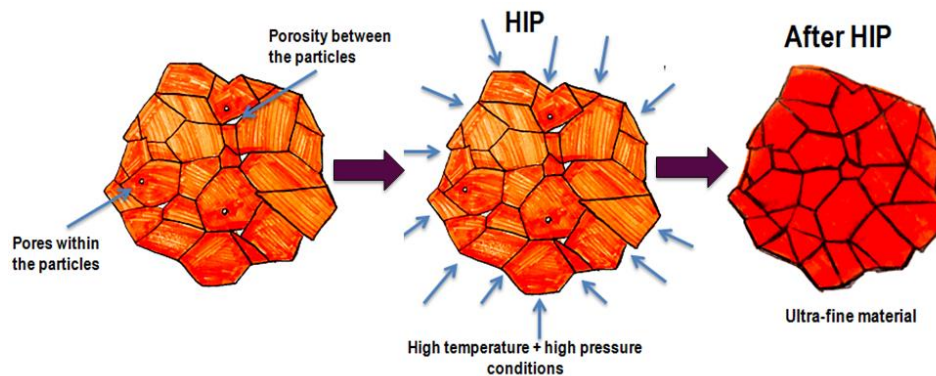


Figure 1.1 – Microstructure of alumina before and after hot isostatic pressing.

1.2.3 Introduction of zirconia femoral heads

Due to the high rates of fracture associated with alumina, in 1985, zirconia heads were introduced in Europe and then in 1989 the FDA approved zirconia ceramic femoral head-on-UHMWPE cup combinations (Zr-on-PE) for use in North America. The use of zirconia for the femoral head component began to dominate the markets in the USA and Europe, particularly for younger patients, due to its significantly greater fracture toughness and superior mechanical properties compared to alumina (Table 1.1). However, there were

concerns over the hydrothermal degradation of zirconia with its simultaneous ability to undergo phase changes that resulted in increased surface roughness (surface degradation and compression strength) and thus increased wear (Clarke et al., 2005; Tateiwa et al., 2008; Garino, 2011). In 2001, Prozyr St. Gobain Desmarquest the largest manufacture of zirconia heads, recalled a selected batch of heads as there were reports of high rates of head fractures *in vivo* (Masonis et al., 2004).

1.2.3.1 Phase changes in zirconia heads

The most common form of zirconia used for femoral heads is tetragonal zirconia stabilised by yttria (Y-TZP), which is a metastable ceramic. The ability of zirconia to transform from the tetragonal to the monoclinic phase gives a transformation-toughening mechanism effect with a small increase in volume of about 5%. The Y-TZP strengthening effect, while very useful in increasing the mechanical strength, can also be a problem as it can cause phase transformations after THA, which presents many problems such as an increase in surface roughness of the zirconia ceramic femoral head (Clarke et al., 2005).

Phase transformations in Y-TZP can be induced at room temperatures in the presence of water and pressure compared to sintering temperatures. Thus, it is speculated that the heat and pressure generated during articulation could be a contributor in the phase transformations described in Y-TZP heads (Haraguchi et al., 2001). Lu and McKellop (1997) reported that the temperature at the surface of the polyethylene cup increased to 99°C when articulated against a Y-TZP head in a hip simulator (Lu and McKellop, 1997). A study by Hernigou et al. (2003) reported a six-fold increase in wear for zirconia heads with phase transformation compared to alumina heads after 8 years follow-up (Hernigou and Bahrami, 2003). The x-ray diffraction results from this study revealed monoclinic transformation increased from <4% to 19-30% in conjunction with increased roughness of the zirconia femoral heads from 5 nm to 50 nm. Clinical studies of Zr-on-PE have demonstrated mixed results in terms of performance, however, the majority of studies have reported higher wear rates, osteolysis and revision rates compared to conventional MoP and alumina-on-UHMWPE (Clarke et al., 2005). Consequently, the popularity of pure zirconia as a bearing material has decreased, however there is still interest in this biomaterial due to its superior mechanical properties and high resistance to crack propagation.

1.2.4 Introduction of composite ceramics

The introduction of alumina matrix composite (AMC) ceramics began in the 1970s with the investigation of transformation toughening as a technique to improve the strength of alumina materials (Garvie et al., 1975). Zirconia-toughened alumina (ZTA) is the most commonly used composite ceramic for artificial hip joint replacements worldwide. This is due to the superior combined material properties of alumina and zirconia, which combines the high

hardness and wear properties of alumina with the high strength and toughness of zirconia (Burger and Richter, 2000a). BIOLOX[®] Delta by CeramTec (Plochingen, Germany) is a well-known ZTA material that contains 80% (volume) alumina, 17% (volume) zirconia and 3% (volume) strontium aluminate platelets (Kuntz and Krueger, 2018).

1.2.4.1 **Strengthening mechanism in BIOLOX[®] Delta ceramic hips**

The toughening effect of zirconia in ZTA materials gives this material its high strength. Stress-induced phase transformations in zirconia, from the metastable tetragonal phase to the monoclinic phase at room temperature causes a volume increase (3-5%). This volume increase by phase transformation prevents crack propagation and leads to microcracking, both of which increase the fracture toughness and overall strength of the material by dissipating the stress effect on the main crack. Hence, phase transformation from tetragonal to monoclinic of the zirconia particles gives a toughening mechanism to the ceramic (Chevalier et al., 2009; Maccauro et al., 2011; Kurtz et al., 2014).

The introduction of zirconia (17%) in the alumina matrix results in a significant increase in strength and fracture toughness in comparison to pure alumina. The fracture toughness of ZTA is approximately 6 MPa m^{1/2}, which is almost double that of pure alumina (3.5 MPa m^{1/2}). Furthermore, ZTA is reported to have an average strength of 1380MPa, an increase of more than 50% when compared to pure alumina (>650 MPa). However, there is a small reduction in hardness of the composite ZTA (>7.7 GPa) ceramic material in comparison to pure alumina (>8.9 GPa). Nevertheless, controlling the grain size and density of the ZTA composite ceramic material through manufacturing processes ensures the maximum hardness of the material is achieved. Furthermore, the addition of other elements such chromium and strontium in the form of platelets have been to increase the hardness of this material. However, recent studies have shown that the addition of chromium does not affect or increase the hardness of ZTA ceramic (Kuntz and Krueger, 2018). The addition of chromium rather slows down the hydrothermal degradation in the zirconia and enhances the protective effect against phase transformation in zirconia (Pezzotti et al., 2010). The addition of strontium oxide (SrO) to ZTA by in situ solid state reaction during sintering produces elongated grains or platelets within the structure of a ZTA ceramic (Figure 1.2). These deflect the crack and increase the distance the crack needs to travel, thus increasing the energy required for the propagation of the crack (Burger and Richter, 2000a; Jeffers and Walter, 2012). The resulting mechanical properties of BIOLOX[®] Delta and other ceramics used for THA are reported in Table 1.1.

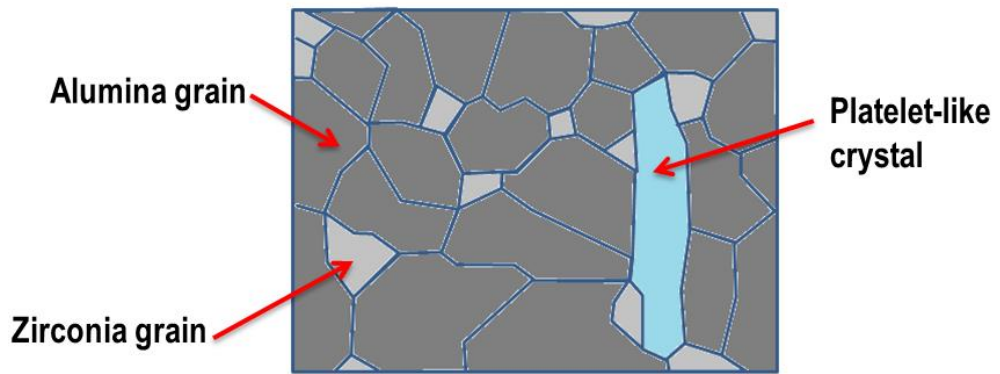


Figure 1.2 - The microstructure of BIOLOX® Delta. ZTA consists of an alpha matrix, which is toughened by phase transformation of dispersed tetragonal zirconia particles. Further reinforcement is achieved by the presence of strontium aluminate platelets that are crystallised in a magnetoplumbite structure.

1.2.4.2 Clinical Performance of BIOLOX® Delta ceramic hips

1.2.4.2.1 Fracture rates

Many of the fractures reported are related to the early non-HIPed pure alumina ceramics that were implanted more than 20 years ago. A study by Willmann et al. (2000) reported the fracture rates for BIOLOX® Forte ceramic heads. The fracture rate for HIPed BIOLOX® Forte heads was 0.004%, which was significantly lower than the early non-HIPed BIOLOX® I: 0.026% and BIOLOX® II: 0.014%. This difference in fracture rates was due to the introduction of improved materials and manufacturing methods, namely HIPing which significantly improved the mechanical properties of pure alumina. These statistics demonstrated a significant decrease in the incidence of fractures over the three generations of alumina i.e. more than a six-fold decrease from the 1970s to the 1990s (fracture rates ranging between 0.026-13.4%) (Willmann, 2000). BIOLOX® Delta CoC bearings have demonstrated a further reduction in fracture rates representing 1 in 50,000, as reported by the manufacturer (CeramTec) (Jeffers and Walter, 2012). A recent article reported no fractures after a 6-year follow-up for BIOLOX® Delta bearings, where more than 100, 000 components (heads and inserts) have been implanted (Masson, 2009). This extremely low incidence of fracture as mentioned earlier is due to the superior mechanical properties of BIOLOX® Delta described in Table 1.1.

1.2.4.2.2 Phase Transformations *in vivo*

As stated earlier, zirconia has a monoclinic structure at room temperature, but changes to a tetragonal structure at temperatures greater than 1100°C with a small change in volume. This tetragonal phase can be maintained at room temperature by stabilisation with yttria. It has been reported that zirconia can undergo phase transformations in a physiological environment resulting in reduced mechanical properties and increased surface roughness that can lead to catastrophic failures (Clarke et al., 2005). This concern was also apparent for BIOLOX® Delta when it was first introduced, as it may be possible for the zirconia phase in ZTA to become unstable in the physiological environment at body temperature as was observed for zirconia-yttria femoral heads in the 1980s and 1990s (Hernigou and Bahrami, 2003). An *in vitro* study by Pezzotti et al. (2009) reported an increase in monoclinic microstructure after BIOLOX® Delta was exposed to a moist environment (139°C) for 300 hours. This caused a 30% decrease in fracture toughness, but this was still higher than the fracture toughness of pure alumina. However, a more clinically-relevant exposure time of 10 hours that was equivalent to 39 years *in vivo*, demonstrated no significant change of monoclinic volume fraction and no change in fracture toughness was detected (Pezzotti et al., 2009). However, an interesting study by Medel et al. (2009) reported changes in the zirconia microstructure *in vivo* of BIOLOX® Delta, but no changes in surface roughness. It was stated that due to the high content of alumina and low content (17%) of zirconia, the alumina maintains the stability of zirconia, thus inhibiting phase transformation (Medel et al., 2009).

1.2.4.2.3 Squeaking

Squeaking is another unusual phenomenon that has attracted much attention in the orthopaedic community as it presents an unwanted complication that can affect the performance of the bearing. Squeaking from CoC THRs has been attributed to adverse conditions that increased wear or impingement (Wu et al., 2016). Squeaking arising from CoC THR may cause patient distress and in some cases, lead the patient to seek revision surgery. A recent meta-analysis study by Owen et al. (2014), reviewed published literature for the incidence of squeaking for CoC bearings and the incidence of revision surgery for squeaking. The incidence of squeaking was reported as 4.2% and the incidence of revision surgery for squeaking was 0.2% (Owen et al., 2014). Another recent prospective observational study by Restrepo et al. (2010) followed-up patients for a minimum of 2.5 years after CoC THR. Ninety-five of the 1468 patients or 6% of the patients with CoC THR developed squeaking. The squeaking was present during walking for 38% of these patients and the intensity and frequency remained similar over time for 70% of the patients (Restrepo et al., 2010).

1.3 Wear

1.3.1 Types of wear

Wear is defined as the loss of material in the form of wear particles, which results from the relative motion between two opposing surfaces (Schmalzried and Callaghan, 2000). This phenomenon also occurs in the bearing components of total hip replacements and can limit the performance and functional life of a joint replacement. In addition, the relative features (size and shape) of the wear particles generated from the bearing surface, can cause many clinical problems, such as osteolysis and aseptic loosening, which can ultimately lead to implant failure. There are many types of wear that can occur in the complex mechanical-biological environment of the total hip replacement, which can include a combination of adhesion, abrasion, third body, fatigue and corrosion (Wright and Goodman, 2001). Adhesive wear is the displacement of material as wear particles from one surface to another due to shearing of junctions between contacting asperities under a sufficient load. Abrasive wear occurs between two materials with different relative hardness i.e. asperities on the harder material cut and plow through the surface of the softer material, resulting in removal of materials as wear debris. Third body wear is a form of abrasive wear that occurs through the embedment of particles (metal, ceramic or bone particles) in a soft surface. Surface fatigue occurs when the local stresses exceed the fatigue limit or strength of a material. The forces from these cyclic conditions can result in subsurface delamination and cracking of the material, thus causing release of wear particles and eventually leading to failure of the material. Corrosive wear is an indirect wear mechanism and occurs due to the chemical interaction of the material with the surrounding environment. The forces and motions resulting from articulation can damage the protective passive layer of the articulating surface and enhance

the corrosion of the surface and liberation of corrosive products that can result in removal of material and production of wear debris (Schmalzried and Callaghan, 2000; Wright and Goodman, 2001).

1.3.2 Friction and Lubrication

Friction and lubrication have a major influence on the wear of hip bearings. Friction can be described as the force that opposes the motion between two articulating surfaces. Lubrication is the addition of a fluid to reduce the friction and wear between the two articulating surfaces. There are three types of lubrication regimes that can exist between two articulation surfaces i.e. boundary, mixed and fluid film lubrication. Boundary lubrication is when the thickness of the fluid is less than or equal to the average surface roughness of the articulating surface, which causes the articulating surfaces to be in contact at all times. Fluid film lubrication is when there is no contact between the articulating surfaces resulting in complete separation between the two materials. Mixed lubrication is a combination of fluid film and boundary lubrication. The lubrication mechanism of the bearing material is dependent upon several properties, which include the lubricant properties, surface roughness, clearance between the bearings, loading and sliding distance (Jin et al., 2006; Kamali, 2009).

The understanding of the tribological performance of bearing materials is important for the development of low-wearing and longer lasting bearing materials for total hip replacements. Wear is an inevitable phenomenon of any hip replacement and is a major clinical problem that can cause periprosthetic osteolysis and aseptic loosening. These adverse tissue reactions, particularly to metal wear debris resulted in thousands of revision surgeries every year. According to the National Joint Registry, 17% (4,103) of the primary revisions (24,065) were due to adverse soft tissue reaction to particulate wear debris (National Joint Registry, 2017). This phenomenon therefore necessitates pre-clinical wear testing and validation of a prosthesis in order to gain valuable information about the tribological characteristics of a hip implant prosthesis (Affatato et al., 2008).

1.3.3 Wear simulation testing

Hip wear simulators are complex and sophisticated and can be described as “machines, which under appropriate test conditions, cause prostheses to wear in a manner equivalent to that which it would experience in typical clinical use in a patient” (Affatato et al., 2008). Specific tests can be run on these hip wear simulators using advanced protocols that reproduce severe conditions, which thereby allow the optimal performance of a material to be established. These tests are necessary and are a prerequisite for a new design or material combination as they provide pre-clinical validation of hip implants prior to implantation in the human body. In addition to predicting the performance of a material, these simulators can be used to develop an understanding of wear mechanisms and the influence of environmental, design, and material

parameters on wear behaviour. However, the reliability of the results will depend on the validity of reproducing *in vitro* the conditions of a prosthetic implant *in vivo* (Affatato et al., 2008).

The data received from hip simulators has been validated through the testing of MoP bearings due to the large numbers of retrieved prosthesis available for direct comparison of wear rates, wear debris morphology and wear mechanisms (Hatton, 2001). This validation of whether wear generated from hip simulators is clinically relevant or not has to be applied for all different bearing materials and combinations.

1.3.4 Simulator testing of CoC bearings

The wear performance of CoC bearings have been extensively investigated *in vitro* under standard and adverse loading conditions. Previous studies of alumina CoC bearings under standard simulation conditions where implants were positioned in their optimum position, reported extremely low wear rates, in the order of 0.01-0.1 mm³/million cycles (Taylor et al., 1998; Oonishi et al., 1999). These wear rates were, however, considerably lower than those produced by retrieved alumina CoC bearings, which have been reported as typically being between 1-5 mm³ per year (Nevelos et al., 1999). Therefore, it was apparent from previous studies that wear rates for failed alumina-alumina bearings *in vivo* were considerably greater than the wear rates produced in physiological hip simulators. In addition, the hip simulators were not reproducing the wear stripe and wear patterns observed in retrieval studies of alumina-alumina total hip prostheses. This led to studies more focussed on reproducing clinically relevant wear rates *in vitro* (Nevelos et al., 1999).

Standard simulation tests use ideal conditions, whereby the head and cup are precisely placed in the correct position throughout the test cycle. However, the loading conditions experienced clinically are more complex and variable (Nevelos et al., 2000a). Nevelos et al. (2001) used water as a lubricant, as opposed to serum, to produce harsher testing conditions in an attempt to increase the wear rates of alumina CoC bearings and replicate those observed *in vivo*. However, water lubricants had no effect on the wear rates (Nevelos, Ingham, et al., 2001). Retrieval studies of alumina ceramic components showed increased wear with steeper cup angles, which indicated that an increased angle of inclination of the acetabular cup may be a possible cause of accelerated wear of CoC hip bearings *in vivo*. This phenomenon may be associated with the depletion of lubricant film when the contact reaches the edge of the cup, on the other hand it is more likely to be associated with increased contact stresses adjacent to the rim of the cup (Nevelos et al., 1999). This led Nevelos et al. (2001) to investigate the influence of acetabular cup angle on the wear of CoC bearings in a hip joint simulator. These authors found that increasing the inclination angle conditions from 45 to 60 degrees in hip simulator studies failed to replicate the higher wear rates observed *in vivo* (Nevelos, Ingham, et al., 2001).

Stripe wear, associated with early generation alumina-alumina ceramic bearings, was also prevalent and has also been observed in modern HIPed alumina-alumina bearings (Nevelos et al.,

1999; Nevelos et al., 2000a). Fluoroscopy studies by Lombardi et al. (2000) reported the occurrence of separation of the ball and socket in patients with MoP THRs during the swing phase of the gait cycle. It was previously thought that this “microseparation” of the components was more prominent in MoP bearings, however recent studies have reported it could occur in any hip prosthesis (Dennis et al., 2001; Glaser et al., 2008). For that reason, Nevelos et al. (2000) introduced microseparation of the CoC hip prosthesis components into *in vitro* hip simulations, as it was believed that this could be a factor in stripe wear production as observed on retrieved CoC hip implants. These authors for the first time reproduced clinically relevant wear patterns in the form of a stripe, wear rates and mechanisms as those observed *in vivo*.

1.3.4.1 Microseparation in a hip simulator

Microseparation occurs during swing phase when the load is minimal and could occur clinically due to different factors such as head offset deficiency, laxity of the joint, medialised cup, impingement or subluxation. These factors cause the femoral head to be translated inferiorly and laterally relative to the acetabular cup during swing phase. During heel strike in the stance phase, there is a rapid increase in load which results in edge loading and causes the femoral head to contact the rim of the acetabular cup before relocating back in the centre of the cup (Figure 1.3) (Williams et al., 2003). The high load applied during rim contact results in the production of stripe wear and increased wear rates of CoC bearings during *in vitro* wear testing (Nevelos et al., 2000; Al-Hajjar et al., 2010; Al-Hajjar, Fisher, Tipper, et al., 2013; Al-Hajjar, Jennings, Begand, et al., 2013a). This was the only laboratory condition that successfully reproduced *in vitro*, stripe wear and bimodal micron and nano-metre sized ceramic wear particles that resembled those observed in retrieval studies (Hatton et al., 2002; Tipper et al., 2002a). Microseparation during hip simulation was achieved by applying a 0.4-0.5 mm lateral displacement of the cup relative to the head during swing phase of the gait cycle, which ultimately allowed edge loading to occur at heel strike (Nevelos et al., 2000a). The microseparation required to cause edge contact must be greater than the radial clearance. It is important to mention that physical separation of the head and cup is not essential in microseparation, rather translational malpositioning of the centre of the head relative to the cup is sufficient (Al-Hajjar, Jennings, Begand, et al., 2013). Mak et al. (2002) reported that a smaller microseparation distance is required to cause edge contact for MoM or CoC bearings compared with MoP bearings, since a small clearance is usually required in these hard-on-hard bearings. For that reason, microseparation can occur at displacements as low as 0.5 mm, thus causing edge loading and increased wear (Mak et al., 2002; Al-Hajjar, Jennings, Begand, et al., 2013).

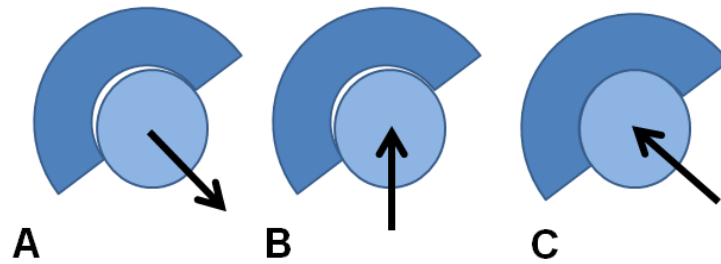


Figure 1.3: The application of microseparation during hip simulation. (A) Swing phase: microseparation. (B) Heel-strike: rim contact. (C) Stance phase: relocation (Williams et al., 2003). Arrows indicate direction of femoral head movement/ motion relative to the acetabular cup.

1.3.5 CoC hip simulation under microseparation conditions

1.3.5.1 Wear testing of alumina ceramics

Considerable research and incorporation of microseparation in hip simulation studies to assess the performance of CoC hip joint replacements has been conducted. A study by Affatato et al. (2011) investigated the effects of different angles of inclination with microseparation during the swing phase of the gait cycle (Affatato et al., 2011). Their findings were in agreement with the findings of Nevelos et al. (2001), who found no significant differences between the two different angles of inclination in terms of wear for BIOLOX[®] Forte alumina ceramic bearings. Similarly, the introduction of microseparation was found to considerably increase the wear of alumina CoC bearings in conjunction with the production of a stripe wear pattern, which was observed to be identical to the stripe wear pattern seen clinically. Stewart et al. (2001) investigated the long term tribological wear performance of HIPed alumina on alumina bearings under mild (400N swing phase load) and severe (50N swing phase load) microseparation conditions. These authors reported wear rates of 0.2 and 1.84 mm³ per million cycles under mild and severe conditions, respectively, which was considerably greater than the wear rate measured under standard conditions (0.09 mm³ /million cycles) (Stewart et al., 2001). The wear rates and wear stripe patterns generated under microseparation conditions were comparable to clinically relevant levels of wear and wear patterns found in early retrieval studies. Furthermore, the wear debris morphology was also similar to debris from retrieved tissues with both small nanometre sized and larger micrometre sized particles (Tipper et al., 2002a).

Femoral heads consisting of zirconium oxide have also been in use to overcome the problems of alumina head fracture. Zirconia heads are considered to be less likely to fracture and have been reported as having lower wear rates against UHMWPE cups than stainless steel and cobalt chromium femoral heads (Derbyshire et al., 1994). Stewart et al. (2003) investigated the wear of zirconia femoral heads against alumina acetabular inserts under microseparation conditions. These authors reported high wear rates and femoral head fracture associated with severe microseparation conditions representative of greater joint laxity. It was concluded that this

combination of zirconia femoral head against alumina acetabular cup is not recommended for clinical use (Stewart et al., 2003b).

1.3.5.2 **Wear testing of composite ceramics**

The introduction of composite ceramics was believed to have overcome the problems of fracture. As previously mentioned, the ZTA composite ceramics have double the strength and fracture toughness compared to alumina. The ZTA or BIOLOX® Delta CoC bearing has had considerable amount of literature published on its wear performance since it was first introduced to the marketplace in the year 2000 (Clarke et al., 2007). A study by Stewart et al. (2003) investigated the long term tribological wear performance of ZTA composite ceramics (BIOLOX® Delta) under severe microseparation conditions. The authors reported the ZTA composite ceramic components had significantly lower wear rates (0.16 mm^3 /million cycles) compared to the previously tested HIPed alumina components, which had an average wear rate of 1.84 mm^3 per million cycles (Stewart et al., 2003a). In addition, the wear mechanisms and wear debris of the ZTA ceramic components were similar to those observed in previous alumina retrieval studies with the presence of stripe wear and wear particles with a bimodal size range i.e. smaller particles that were 10-20 nm and larger particles that were up to $3 \mu\text{m}$ in size (Tipper et al., 2002a). Another study by Al-Hajjar et al. (2010) investigated the effects of cup inclination angle during microseparation on wear of BIOLOX® Delta hip components. Their findings were consistent with previous studies in that the cup inclination angle had no significant effect on the wear rate (Nevelos, Prudhommeaux, et al., 2001; Affatato et al., 2011). The introduction of microseparation increased the wear rate of BIOLOX® Delta components to 0.13 mm^3 per million cycles compared to 0.05 mm^3 per million cycles under standard conditions. However, this was still very low compared to the third generation HIPed alumina ceramic hips (BIOLOX® Forte), which had wear rate of 1.84 mm^3 per million cycles under the same microseparation conditions (Stewart et al., 2001). A more recent study by Al-Hajjar et al. 2013 investigated the wear of different combinations of ceramic matrix composites, ZTA and alumina-toughened zirconia (ATZ) compared with alumina-on-alumina under microseparation conditions. Both ZTA-on-ZTA and ATZ-on-ATZ bearings showed extremely low wear rates of 0.14 mm^3 per million cycles and 0.06 mm^3 per million cycles, respectively, compared with a wear rate of 0.74 mm^3 per million cycles for alumina-on-alumina. Stripe wear was prevalent for all bearing combinations, however, the stripe wear formed on the ZTA and ATZ femoral heads was narrower and shallower than that formed on the alumina heads (Al-Hajjar, Jennings, Begand, et al., 2013).

The superior mechanical properties of BIOLOX® Delta has allowed greater design flexibility to produce larger sized femoral heads, which have shown a significant reduction in dislocation rate by reduced impingement and improved stability (Zagra and Ceroni, 2007). A study by Al-Hajjar et al. (2013) investigated the effect of increasing head size (from 28 mm to 36 mm) on the wear of BIOLOX® Delta CoC bearings under microseparation ($0.4 -0.5 \text{ mm}$ medial displacement) and

steep cup inclination angle (65°) conditions. Similar to previous studies, the steep cup inclination angle conditions did not affect the wear rates, whereas introduction of microseparation increased wear rates and stripe wear pattern on the femoral heads. The wear rate for the larger (36 mm) bearings was 0.22 mm³ per million cycles which was significantly higher than the smaller (28 mm) bearings, which had a wear rate of 0.13 mm³ per million cycles. This increase of wear rate for the larger size CoC bearings was attributed to the larger contact area for larger bearings and also deprived lubrication due to edge loading conditions (Al-Hajjar, Fisher, Tipper, et al., 2013a). Tribological studies of hip implant bearings has demonstrated that edge loading due to separation can result in increased wear in hard-on-hard bearings and increased deformation in polyethylene bearings (Nevelos et al., 2000; Stewart et al., 2001; Stewart et al., 2003; Williams et al., 2003; Al-Hajjar et al., 2010; Al-Hajjar, Fisher, Tipper, et al., 2013; Al-Hajjar, Jennings, Begand, et al., 2013; Al-Hajjar, Fisher, Williams, et al., 2013). However, all these previous studies used a fixed level of separation (0.4-0.5mm) between the head and the cup during swing phase as an input to simulate edge loading, thus the wear was measured for a predetermined level of severity of edge loading. A recent study by O'Dwyer Lancaster-Jones et al. (2017) investigated surgical positioning of CoC hip implants (BIOLOX® Delta) as an input in order to simulate dynamic (micro) separation and create edge loading conditions. The experimental setup created a surgical mismatch (1-4mm) between the centres of rotation of the femoral head and acetabular cup in the medial-lateral axis and the rotational positioning (inclination angle: 45-65 degrees). The resultant dynamic separation between the head and acetabular components created from these conditions was measured and the wear rates were reported for the different levels of medial-lateral translational mismatch. The authors reported that an increase in the mismatch between the centres of rotation of the femoral head and acetabular cup resulted in increased levels of dynamic separation, thus causing an increase in the severity of edge loading condition, which led to increased wear rate in CoC bearings. Furthermore, the mismatch coupled with increased cup inclination angles resulted in increased dynamic separation and caused severed edge loading condition, which increased the wear rates further. The combination of high levels of mismatch (4mm) and steep cup inclination angle (65 degrees) resulted in mean wear rates of up to 1.01 ± 0.17mm³ per million cycles. These severe edge loading conditions demonstrated >1mm of dynamic separation between the femoral head and acetabular cup. This study demonstrated the occurrence and severity of edge loading that can occur as a result of mal-positioned implants, and the impact these conditions can have on the performance of CoC bearings.

1.4 Isolation and characterisation of wear particles from THRs

The isolation and characterisation of wear particles from hip replacements, be it from *in vivo* or *in vitro* samples is important, as the data obtained can be used to predict the severity of the biological response *in vivo*, which is largely dependent on the relative features (size and shape) of the wear particles (Green et al., 1998). Hence, a search of the literature was performed to

identify the current published particle isolation methods to understand their limitations and how these could be improved for the isolation of ceramic wear particles.

1.4.1 Wear particle analysis *in vivo*

The generation of wear particles from articulating surfaces of total joint replacements is inevitable and wear particles have been implicated as the cause of osteolysis and aseptic loosening. In the early 1990s the evidence to support this statement was initially observed through the examination of retrieved implants and tissues, whereby particulate metal and/or UHMWPE were observed within tissue sections. The relative features of the particles in terms of size, shape, composition and quantity were unclear due to the inherent difficulties of particle characterisation. Histologic examination of the wear particles had many limitations, which included tissue processing and sectioning that affected the final size and appearance of the particles. The resolution of light microscopy was limited to large particles only, generally $>0.5 \mu\text{m}$ sized particles. In addition, the particles had to be recognised within tissues, so observer bias or experience may have influenced the accuracy of the assessment of particles in tissues (Campbell et al., 1994; Campbell et al., 1995).

1.4.1.1 Isolation of wear particles by tissue digestion

An alternative approach to tissue sectioning and histologic examination was to isolate the particles from the tissues and subsequently characterise them using scanning electron microscopy (SEM). In the early 1990s, several studies reported on the use of tissue digestion for isolation of metal or bone cement particles (Lee et al., 1992). The high density of metal and bone cement particles allowed these particles to pellet during centrifugation. However, the isolation of polyethylene particles required new techniques for recovery, due to their intrinsic low density which is less than that of water ($0.93\text{-}0.94 \text{ g/cm}^3$). Campbell et al. (1994) devised a suitable method for the isolation of both metallic and polyethylene wear particles from periprosthetic tissues (Campbell et al., 1994). This method was reported as successful when filtered reagents and ultracentrifugation were used to separate the particles from the cellular debris. This was because, it was demonstrated that cellular debris and reagent particles could cause contamination of the wear particles when examined by SEM. The use of filtered reagents and the inclusion of ultracentrifugation overcame these problems. Another study by Campbell et al. (1995) assessed the reproducibility of this method for the isolation of UHMWPE wear particles from a number of periprosthetic tissues (Campbell et al., 1995). The wear particles isolated had consistent morphology, being either rounded or elongated in shape. In addition, the method was described as relatively simple, involving fewer steps and less time compared to previous methods (Shanbhag et al., 1994).

1.4.2 Isolation and characterisation of ceramic wear particles

1.4.2.1 Isolation of ceramic wear particles from retrieved tissues

The particles generated from CoC bearings have also been investigated through histological examination of retrieval tissues. A study by Kummer et al. (1990) investigated pseudosynovial tissues obtained from revisions due to aseptic loosening of Autophor CoC prostheses (Kummer et al., 1990). The revisions were performed 8 to 54 months following implantation and the results revealed numerous particles with a size of 5µm in tissues. Another study by Henssge et al. (1994) reported on ceramic wear particles in retrieved pseudocapsules and soft tissue membranes retrieved from cemented alumina-on-alumina prostheses that were revised for loosening after 6-12 years (Henssge et al., 1994). For comparison purposes, autopsy specimens were also retrieved from patients that had CoC bearings for more than 5 years. The authors observed ceramic wear particles in all the tissue specimens, which appeared as polygonal yellow-brown particles of up to 5 µm in diameter and smaller granular wear particles inside macrophages. However, fewer particles were observed in the tissue from the autopsy compared to the tissue obtained from revision surgery. Yoon et al. (1998) examined tissue samples of interface membranes obtained from ten Mittelmeier THRs failed and revised for aseptic loosening. Transmission electron microscopy (TEM) revealed the presence of abundant ceramic wear particles with a mean size of 0.71 µm (range, 0.13 to 7.2 µm) (Yoon et al., 1998).

All these previous studies, examined wear particles within retrieved tissues using histological methods. Lerouge et al. (1996) used two methods to analyse the wear debris in tissues retrieved from CoC THA revised for aseptic loosening; 1), semi-quantitative histological analysis and 2), tissue digestion to isolate the particles and evaluate them using SEM, EDX and image analysis (Lerouge et al., 1996). The non-isolation technique revealed ceramic particles in the submicron size, ranging from the limits of the microscope resolution (0.3 µm) up to a few microns in size. The isolation technique revealed alumina wear particles with a mean size of 0.44 ± 0.25 µm. In addition to alumina wear particles, zirconia and titanium particles were also observed. This study highlighted the importance of isolating wear particles for accurate evaluation in terms of composition and size distribution. Bohler et al. (2000) used nitric acid for tissue digestion to isolate alumina ceramic wear particles from periprosthetic tissues (Bohler et al., 2000). The particles were collected using filters and subsequently counted and measured using coulter analysis, but this technique had a detection limit of 0.5µm. Hence, particles smaller than 0.5µm and larger than 10µm were collected on filters, gold coated and analysed using SEM. The use of SEM in parallel with electronic counting methods highlighted the limitations of the available methods at that time. Furthermore, the use of nitric acid has been reported as having minimal deleterious effects, however, there remain concerns over the use of such strong acids, which may have affected the morphology and size of the wear particles. Also, the use of micro-pore filters

may have resulted in loss of particles that were smaller than the pore size of the filter (Margevicius et al., 1994).

1.4.2.2 Isolation of nanometre-sized ceramic wear particles

Due to the limitations discussed above, Hatton et al. (2002) used a novel technique, laser capture microdissection (LCM) to isolate ceramic wear debris from tissues retrieved at revision (Hatton et al., 2002). This method was developed as a research tool at the National Institutes of Health (NIH) and originally used to obtain pure populations of targeted cells from specific regions of tissue sections for extraction of molecules and analysis (Bonner et al., 1997). This study was the first to apply LCM for the isolation and analysis of wear debris in retrieved tissues. LCM would effectively preserve the particles in the state in which they were found *in vivo* allowing accurate analysis of their size and morphology. The tissues were obtained from around 10 non-cemented Mittlemeier alumina CoC THR's from patients undergoing revision surgery. Wear particles were extracted from tissue sections using LCM and subsequently characterised using SEM and TEM. TEM of the laser captured tissue revealed the presence of very small alumina wear debris, in the size range of 5-90 nm, with a mean size of 24 ± 19 nm, whereas SEM, which has a lower resolution, revealed particles in the size range of 0.05-3.2 μm . This study for the first time demonstrated that wear particles from alumina CoC bearing have a bimodal size range. Prior to this study, alumina ceramic wear particles have been reported as being in the submicron size range, however this study reported for the first time descriptions of nanometre sized ceramic wear particles in retrieval tissues (Hatton et al., 2002).

1.4.2.3 Isolation of ceramic wear particles from hip simulator lubricants

The reproduction of clinically relevant wear rates and wear patterns *in vitro* in hip simulators for CoC THR's was not possible until Nevelos et al. (2000), introduced microseparation of CoC hip prostheses into the *in vitro* wear simulation (Nevelos et al., 2000a). This led Tipper et al. (2002) to investigate the characteristics of wear particles generated *in vitro* under standard and microseparation conditions from HIPed and non-HIPed alumina CoC hip prostheses and compared these particles to those previously studied *in vivo* (Hatton et al., 2002; Tipper et al., 2002a). Under standard simulation conditions both HIPed and non-HIPed alumina CoC prostheses produced very low wear rates of 0.08 and 0.11 mm^3 per million cycles, respectively. Contact profilometry revealed no change in surface roughness for either HIPed or non-HIPed alumina and the wear particles generated under standard simulation conditions were only observed in the nanometre size range. These particles were thought to be generated as a result of surface relief polishing of the alumina ceramic and had mean sizes of 9.19 ± 0.52 nm and 9.22 ± 0.52 nm, respectively for the HIPed and non-HIPed alumina.

The introduction of microseparation considerably increased the wear rates to 1.24 mm^3 per million cycles for HIPed alumina and 1.74 mm^3 per million cycles for the non-HIPed alumina. Both prosthesis types revealed the presence of a wear stripe, which was comparable with those

often observed clinically. SEM analysis of the wear stripes revealed intergranular fracture of the femoral heads for both types of alumina. In addition, surface roughness increased after microseparation for both HIPed and non-HIPed alumina from an average of R_a of $0.007\ \mu\text{m}$ to R_a $0.03\ \mu\text{m}$ for the HIPed heads and $0.06\ \mu\text{m}$ for the non-HIPed alumina heads. These values of surface roughness are comparable with retrieved components indicating that similar wear mechanisms may have occurred *in vitro* during microseparation in the hip simulators. The wear particles generated in the serum lubricant were isolated using two different methods for SEM and TEM analysis. The particles analysed using TEM were isolated by centrifuging the serum lubricant containing the wear particles and fixing the pellet of wear particles in 2.5% (v/v) glutaraldehyde in phosphate buffered saline (PBS). The wear particles were stained and fixed with 1% (w/v) osmium tetroxide before being dehydrated using ethanol. The samples were polymerised in araldite resin and 100nm sections were cut with a diamond knife for TEM analysis. The particles analysed using SEM were isolated by centrifuging the serum lubricant containing the wear particles and then washing the pellet of particles and proteins with PBS to remove proteins. Thereafter, the wear debris were heat treated at 180°C for four hours to denature any residual proteins and remove any bacterial contamination from the wear particles. Thereafter the wear particles were filtered onto 15nm pore filters and analysed using SEM. The wear particles generated consisted of small (1-35 nm) and larger (0.02-0.94 μm) sizes of particles. TEM analyses revealed the small wear particles as dense aggregates with a round/oval shape and were thought to be as a result of relief polishing. The larger particles also had a round/oval shape with some polygonal particles and were thought to have originated from within the wear stripe by transgranular fracture of the alumina ceramic material. This bimodal size range of wear particles produced was also observed in the analysis of tissues from retrieved components (Hatton et al., 2002). Therefore, it is evident from these studies that the introduction of microseparation during wear simulation produced clinically relevant wear rates, wear stripe patterns and bimodal distribution of wear particles as clearly seen *in vivo*. The particle isolation methods used by Tipper et al. (2002) were successful in characterising alumina ceramic wear particles recovered from serum lubricants, but these methods may lack the sensitivity to isolate wear particles generated from composite CoC bearings due to their extremely low wear rates, even under microseparation conditions. There is a high risk of particle loss during the fixing of the particles in resin and heat treatment of the particles to remove proteins and endotoxins may not effectively remove all the proteins, which can cause contamination issues and difficulties during imaging of the particles. Nevertheless, these studies were a major breakthrough in terms of isolation and characterisation of ceramic wear particles, as this study demonstrated for the first time successful isolation of low volumes of wear particles generated from alumina CoC bearings and also revealed for the first time the characteristics of ceramic wear particles in the nanometre size range (Hatton et al., 2002; Tipper et al., 2002a).

1.4.3 Comparison of wear particle isolation techniques

Due to ethical issues associated with retrieved implants and limited number of tissues samples from retrieved implants, the isolation and characterisation of wear particles from hip simulator lubricants has been the focus of many studies to obtain the characteristics of wear particles *in vitro*. However, as mentioned previously, even with the introduction of severe edge loading conditions the superior wear properties of ZTA composite CoC bearings still produces extremely low wear volumes, which present major challenges for the isolation and characterisation of wear particles generated from composite ceramics such as BIOLOX® Delta. A comparison between the different types of digestion techniques was conducted in order to find the most suitable digestion technique for ceramic wear particles in hip simulator serum lubricants.

1.4.3.1 Base, acid or enzymatic digestion

Quantification of wear debris was traditionally and still is practiced using the weight loss method. This method has been successful in determining the amount of wear but it is limited in the sense that it does not provide valuable information about the wear debris characteristics in terms of size distribution and morphology. The conventional isolation methods as described previously used the base digestion technique whereby a strong base such as sodium hydroxide (NaOH) was used to digest tissue before centrifugation and filtration to isolate the wear particles (Campbell et al., 1994; Campbell et al., 1995). Niedzwiecki et al. (2001) compared three polymer wear particle isolation methods that used different reagents for the digestion of serum i.e. acid, base or enzymes. It was concluded that all three methods were viable at preserving the particle morphology and yielded similar particle size distributions for the same simulator serum. It was further stated, that the acid and enzyme methods did not require ultracentrifugation or gradient filtration. The enzyme method was considered as the optimum choice since it generated the least amount of hazardous waste (Niedzwiecki et al., 2001).

The accurate measurements of particle size, shape and composition is important in determining the wear performance and tissue response to particulate material from THRs. This can only be done by optimising particle isolation methods and minimising wear particle changes due to the effects of the reagents. Catelas et al. (2001) investigated the effects of different digestion techniques on the isolation and characterisation of wear particles from simulator lubricants generated from MoM bearings *in vitro*. The effects were analysed in terms of particle size, shape, composition and the release of metal ions. Metal wear particles present a much more challenging problem compared to polymer wear debris because of their smaller size, their tendency to agglomerate and their potential for chemical damage and degradation by digestion reagents. TEM revealed that particles generated in water experienced changes in size with both enzymatic and alkaline digestion treatments. These changes were more pronounced for the alkaline protocols and increased with alkali concentration and time in solution (Catelas, Bobyn, J.B. Medley, et al., 2001). This was previously mentioned by Campbell et al. (1994) who postulated that strong

alkaline solutions may affect particle morphology. In contrast, the changes in particles generated in hip simulator in 95% (v/v) serum lubricant, were considerably less extensive for both the alkaline and enzyme digestion protocols. It was suggested that serum proteins or lipids initially covered the particles and protected them against the oxidising action of the solutions. Hence, both digestion techniques could be used for particle isolation from simulator serum without extensive size and shape changes to the particles. However, it was noticed that alkaline digestion caused the particles to agglomerate more easily (Catelas, Bobyn, J.B. Medley, et al., 2001). This problem of agglomeration after alkaline treatment was also previously reported by Campbell et al. (1994). In addition, particles treated with alkaline solutions appeared to have more uniform and high contrast appearance in TEM, whereas particles isolated by enzymatic treatments were more diverse with varying contrast intensities. This suggested that the alkaline treatments modified the wear particle composition. Furthermore, the release of Co and Cr ions after alkaline treatment also provided further evidence of composition change, whereas enzymatic treatment resulted in negligible release of Co and Cr ions into solution. It was concluded that from all the protocols tested, the enzymatic digestion technique was the least damaging to the wear particles and most likely an optimum choice for isolation and characterisation of metal wear particles, especially for those generated in serum (Catelas, Bobyn, J.B. Medley, et al., 2001). This may also apply to ceramic wear particles, as the characteristics for ceramic particles in terms of size and shape are similar to metal wear particles.

1.4.4 Isolation of nano-metre sized wear particles from hip simulator lubricants

Brown et al. (2007) developed a novel method for the isolation of wear particles generated from MoM hip bearings. This method employed an enzymatic digestion technique to avoid the use of acids or bases, thus preventing damage of the wear particles during isolation. The method was successful in isolating wear particles from both MoM and alumina ceramic-on-metal (CoM) tested under both standard and microseparation simulation conditions. The wear particles were characterised using high resolution field emission gun scanning electron microscopy (FEGSEM) which revealed significant differences in particle morphology and size distribution for the MoM and ceramic-on-metal (CoM) bearing combinations and different simulation conditions. In addition, FEG-SEM was used as an alternative to TEM because it provided high resolution imaging and avoided inaccurate sampling due to the use of only a small amount of sample, which was the case for TEM. Also, the small amount of sample can result in the loss of larger particles and unevenly distributed particles. SEM also has its problems, such as resolving small particles requires the use of high accelerating voltages to improve the resolution of SEM, which can cause particle damage and errors in particle area measurement (Yanez and Barbosa, 2003). Nevertheless, the method developed by Brown et al. (2007) presented attractive advantages over other methods in that it was successful in isolating wear particles from low volumes of wear (0.3 mm³ per million cycles) generated from MoM bearings.

Due to the limitations of previous particle isolation methods, including particle loss, agglomeration and chemical damage, Billi et al. (2012) developed a new award-winning method that claimed to overcome all of the shortcomings of previous methods (Billi, Benya, Kavanaugh, Adams, McKellop, et al., 2012). The method involved a two-step process; 1) particle isolation, and 2) particle purification. This method was designed for wear debris from any material having a density greater than 2.0 g/mL i.e. metal or ceramic. The method employed enzymatic digestion and was referred to as "Metal and ceramic silicon wafer display" (MC-SWD), since it uses a featureless wafer to collect and display the particles without the use of filtration. This was previously attempted by Catelas et al. (2004) who used a similar approach where after centrifugation, the wear particles were embedded in a resin to minimise particle loss and promote dispersion of the wear particles. The results displayed evenly distributed wear particles when analysed using TEM (Catelas et al., 2004). The MC-SWD method was evaluated to determine its efficiency and accuracy by recovering gold nano-beads and metal and ceramic particles from hip simulator wear lubricants. The method demonstrated a $92 \pm 5\%$ recovery rate of the gold beads. Particle concentration before digestion and decreased handling ensured maximum particle recovery and reduced particle loss. This was further supported by particle loss evaluation where the concentration of Co before centrifugation was 37.5 ± 1.5 ppm and after centrifugation it was 37.3 ± 1.6 ppm, which demonstrated that virtually no particles remained in the supernatant. The adoption of the wafer instead of filtration ensured the particles were displayed well separated with few agglomerates. In addition, the distribution of the wear particles was uniform i.e. similar at different locations on the wafer. This allowed for precise and individual chemical characterisation of particles as small as 12nm, thus ensuring accurate and reliable morphological characterisation of the wear particles.

Despite the evidence and reported success of the MC-SWD particle isolation method, this method has not been reproduced or tested in any other laboratory. There are no other studies that have implemented this method, hence a sense of uncertainty exists regarding this protocol as they are no external reviews of whether this method produces the results that it claims. Also, the complexity of this method will make it very difficult to replicate since many steps are specialised and require sophisticated equipment. In addition, the cost of the reagents that this method uses is extremely high, for example mussel glue (Cell-Tak) used to coat the silicon wafer display costs around two hundred dollars (Fisher Scientific, USA) for one milligram of adhesive. Another issue with this method is that the particles are irreversibly stuck to the silicon wafer and cannot be recovered for subsequent biological testing. All these factors make the MC-SWD particle isolation method less attractive to implement, even though it is reportedly a successful method. More recently a novel particle isolation method was developed by Lal et al. (2016), who also employed enzymatic digestion and density gradients to separate the proteins from the wear particles. However, this method used a different medium i.e. sodium polytungstate to form the density gradient. The metal/ceramic wear particles were recovered from the proteins by placing

the digested serum containing the wear particles on a sodium polytungstate density gradient and centrifuging the samples at an average RCF of 202,048g. After centrifugation, the wear particles would collect at the bottom of the tube, whilst the broken-down protein and other impurities were suspended higher up the tube due to their lower density compared to the metal/ceramic wear particles. This method was developed for the isolation of ultra-low volumes of ceramic or ceramic-like coating particles and metal wear particles from serum lubricants. The authors demonstrated a particle recovery rate of >80% and they also reported that the enzymatic digestion did not alter the size or morphology of ceramic and metal particles during the isolation process. The particle recovery rate value for this particle isolation technique could be considered more reliable compared to the particle recovery rate value for the particle isolation method developed by Billi et al. (2012). This is because Lal et al. (2016), used actual ceramic particles (silicon nitride) to assess the particle recovery rate, whereas Billi et al. (2012) used gold beads. Nevertheless, Lal et al. 2016 did not test their method on hip simulator serum lubricants, instead only results for particles recovered from serum spiked with silicon nitride particles was reported, hence the efficacy of this method to recover particles from hip simulator lubricants is unknown. An extensive search in the literature found no studies that reported the recovery and characterisation of wear particles generated from ZTA composite ceramic hip replacements. This may be due to the limitations of the current particle isolation methods not being reliable enough to isolate the challenging ultra-low wear volumes exhibited by CoC bearings. This gap in the literature presents a difficult challenge for the development of a method that will successfully recover wear particles generated from ZTA composite ceramic hip replacements.

1.5 Failures of Total Hip Replacements

1.5.1 Introduction

There is a large body of evidence in the literature that indicates the life expectancy of an artificial hip is limited and that small numbers of devices survive beyond 25 years (Learmonth et al., 2007). However, the survivorship of the age of the patient is a major contributor to implant survival rate; the survivorship for older patients (>55 years) is more than 90% at 15 years, whereas the survival rate falls to 70% at 10 years for patients under 55 years of age (Hartofilakidis et al., 2005). It has been predicted that the number of THAs will increase by 174% by 2030, because younger and more active patients are increasingly having joint replacements (Kurtz et al., 2007). A search in the literature was conducted to evaluate the biological responses to wear particles generated from different bearing materials used for THA. The longevity of an implant has been reported to be directly affected by and related to the biological response to wear particles generated from THRs (Suner et al., 2012). Therefore, the need to understand the biological impact of wear particles and the mechanisms which may result in implant failure have become more important. Nevertheless, the landscape is changing due to the introduction of alternative bearing materials such as MoM

and CoC bearings. Hip implants are no longer failing due to osteolysis and/or wear particle production as wear rates of current THRs have decreased dramatically. Instead, other factors such as mechanical failure and failure of fixation also contribute towards the failure of modern hip implant bearings. In addition, aseptic loosening is reported to be one of the most commonly cited causes of THR failures that were revised during the period between 2003-2016 (National Joint Registry, 2016). Aseptic loosening is a process of bone loss without infection and may even occur without any symptoms. Osteolysis causing the bone loss may be linear (equally distributed around the implant) or focal (specific areas of bone loss relative to the implant) (Sundfeldt et al., 2006). The cause of aseptic loosening has been reported as being mainly due to two factors, namely mechanical and biological factors.

1.5.2 Mechanical factors

1.5.2.1 Implant design and material properties

Implant design, material properties and surgical technique are mechanical factors that contribute to the cause of aseptic loosening. For example, a study by White et al. (2012) reported that the Accolade cementless femoral stem design was associated with high incidence of migration, as a result of poor fixation due to lack of osteointegration, which caused poor initial stability (White et al., 2012). Material properties are also an important factor as stress shielding can result, which is a mechanical phenomenon caused by stiff and inflexible materials in the femoral component of THRs. Stress shielding can cause bone resorption as the intramedullary stem absorbs all the stresses that the femur would have carried in its natural state, therefore the bone is subjected to reduced stresses, hence shielded from stress. The redistribution of load causes bone resorption as an effect of bone adaptation to stress shielding that can eventually result in aseptic loosening. Many implant designs have been changed to reduce stress shielding such as introducing a flexible stem, implant geometry and shape (hollow stem) (Huiskes et al., 1992; Joshi et al., 2000).

1.5.2.1.1 Surgical positioning

Surgical malpositioning of THRs as a result of poor alignment or poor fixation of the implant can lead to micromotion and fluid pressure, as well as instability of the implant inevitably resulting in aseptic loosening and failure of the implant (Aspenberg and Herbertsson, 1996). The correct positioning of the acetabular cup with respect to inclination and anteversion is very important as it can affect the rate of wear, range of motion, dislocation and aseptic loosening. Surgical experience was reported not to statistically influence the accuracy of acetabular cup positioning, rather it was the alignment of devices and insertion guides themselves that determined the accuracy of cup positioning (Reize et al., 2008). Jolles et al. (2004) reported that the use of computer assisted cup placement was significantly more accurate than conventional methods of cup positioning. This technique could provide better or even optimum positioning of hip implants, thus resulting in a decrease of revision rates (Jolles et al., 2004).

1.5.3 Biological Factors

1.5.3.1 Osteolysis

Excessive wear particles have been linked with the aetiology of periprosthetic osteolysis and aseptic loosening. Osteolysis is the active resorption of bone by osteoclasts and is commonly associated with aseptic loosening of artificial joint replacements. The initial stages of osteolysis involves wear particles that are generated at the articulating surfaces, entering the periprosthetic tissue (Brown et al., 2006). Here, macrophages and multinucleated giant cells engulf the wear particles that are in the critical size range (0.2-0.8 μm) for phagocytosis (Ingham and Fisher, 2000; Brown et al., 2006). Histological studies of periprosthetic tissues have shown that small particles (<10 μm) were engulfed by macrophages whereas larger particles (>10 μm) were engulfed by multinucleated giant cells (Pazzaglia et al., 1987; Ingham and Fisher, 2005). Macrophages and giant cells are part of the mononuclear phagocyte system and are produced by the differentiation of monocytes in tissues. These cells play a key role in the immune response, whereby they detect, phagocytose and degrade foreign matter. The primary role of macrophages is to engulf and digest micro-organisms and initiate the processes of inflammation by releasing a range of pro-inflammatory cytokines and other mediators of inflammation (Ingham and Fisher, 2000). The release of these mediators results in the recruitment, migration and stimulation of other cell types involved in the immune response and host defence. However, in response to wear particles macrophages are unable to degrade the wear particles due to their inert nature (Brown et al., 2006). Consequently, the macrophages release cytokines and mediators to recruit other cells to the site of the foreign wear particles. As a result, the formation of a granulomatous periprosthetic tissue, which is rich in macrophages, forms around the implant to isolate the foreign matter from the surrounding tissues (Ingham and Fisher, 2005).

1.5.3.2 Cytokines and mediators released by macrophages and their roles in osteolysis

Previous studies of periprosthetic tissues have shown the presence of many inflammatory mediators and cytokines associated with the biological response to wear particles. These include tumour necrosis factor- α (TNF- α), receptor activator of nuclear factor kappa-B (RANK)/RANK ligand (RANKL), interleukin-1 (IL-1), interleukin-1 β (IL-1 β), interleukin-6 (IL-6), interleukin-8 (IL-8), granulocyte-macrophage colony stimulating factor (GM-CSF), macrophage colony stimulating factor (M-CSF), stem cell factor (SCF) and prostaglandin E₂ (PGE₂) (Kim et al., 1993; Sabokbar and Rushton, 1995; Goodman et al., 1998; Neale and Athanasou, 1999; Ingham and Fisher, 2000; Abu-Amer et al., 2007; Goodman et al., 2013).

These inflammatory mediators and cytokines affect the behaviour of many cell types, particularly the interaction of osteoblasts, osteoclasts and fibroblasts which ultimately leads to bone loss and aseptic loosening (Figure 1.4). The roles that these mediators play in the process of wear particle induced-osteolysis are summarised in Table 1.2.

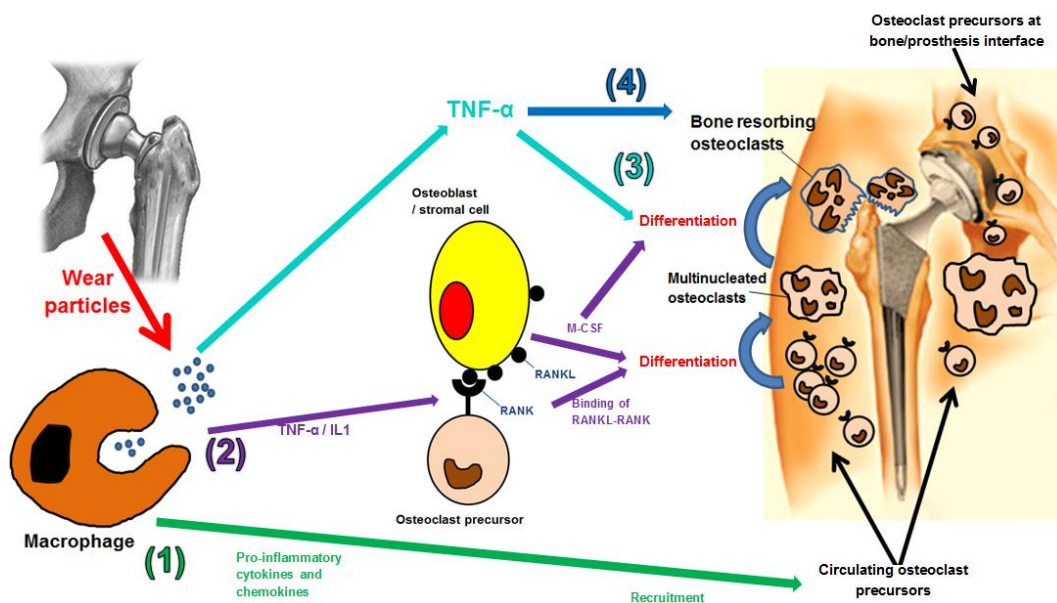


Figure 1.4: The potential mechanisms that can occur when macrophages are stimulated by wear particles. There are several potential pathways after macrophage activation by wear particles that can result in bone resorption and ultimately osteolysis in THRs. (1) The release of pro-inflammatory cytokines and chemokines may increase the recruitment of haematopoietic osteoclast precursors from local blood vessels. (2) The release of TNF- α / IL-1 by macrophages may lead to enhanced expression of RANKL and M-CSF by osteoblasts/ stromal cells. Binding of RANK to RANKL and release of M-CSF stimulates osteoclast differentiation and activates mature osteoclasts to resorb bone. (3) TNF- α may directly enhance the differentiation of osteoclast precursors independent of RANK/RANKL mechanisms. (4) TNF- α may directly activate mature osteoclasts to resorb bone (Ingham and Fisher, 2005).

TNF- α is a key osteolytic cytokine released by macrophages stimulated by wear particles. TNF- α enhances the expression of RANKL by acting on mesenchymal and osteoblastic cells. RANKL is a surface-bound molecule which is part of the TNF superfamily and is expressed by osteoblasts/bone marrow stromal cells (Ingham and Fisher, 2005). The receptor for RANKL, RANK is expressed on the surface of osteoclast pre-cursors and mature osteoclasts. The binding of RANKL to RANK has been shown to stimulate osteoclast differentiation and activate mature osteoclasts to resorb bone (Wei and Siegal, 2008). A study by Mandelin et al. (2003) of periprosthetic tissue investigated RANKL/RANK and their association with osteolysis. It was found that RANKL and RANK were both upregulated compared to control synovial tissue (Mandelin et al., 2003). TNF- α has also been reported to directly stimulate the recruitment of osteoclasts (Azuma et al., 2000; Kobayashi et al., 2000; Fuller et al., 2002; Tsuboi et al., 2003). The importance of TNF- α has been highlighted by *in vitro* studies of TNF-knockout mice. Clohisy et al. (2002) investigated the effects of PMMA particles on osteoclast precursors derived from murine bone marrow. The cells showed an increase in NF κ B nuclear translocation which was dependent upon TNF- α signalling, whereas cells from TNF-knockout mice demonstrated a null response to the PMMA particles (Clohisy et al., 2002; Ingham and Fisher, 2005). Similarly, another study on RANK deficient mice exhibited no osteolytic response to wear particles. These results indicated that these two mediators; TNF- α and RANK/RANKL work synergistically to

directly inducing macrophages towards the osteoclastic phenotype for bone resorption (Wei and Siegal, 2008).

Several *in vitro* studies have revealed that some of the macrophages within the periprosthetic tissue retrieved from revision surgeries may have the potential to differentiate into osteoclasts capable of bone resorption. Sabokbar et al. (2003) reported that these cells differentiated into tartrate-resistant acid phosphatase positive (TRAP+) and vitronectin positive (VNR+) multinucleated cells capable of extensive lacunar resorption in the presence of M-CSF and TNF- α (Sabokbar et al., 2003). TRAP and VNF are osteoclast markers used to characterise cells *in vitro*. The addition of antibodies to act against the TNFp55 receptor protein resulted in fewer TRAP+ cells and so it was concluded that macrophages isolated directly from the periprosthetic tissues can differentiate in the presence of TNF- α into multi-nucleated giant cells that can express the phenotype of osteoclasts (Sabokbar et al., 1997; Sabokbar et al., 2003). This study added weight to previous findings that TNF- α can directly induce macrophages to differentiate into osteoclasts independent of RANK mechanisms. These findings were also in agreement with *in vitro* studies by Darowish et al. (2009) who demonstrated that TNF- α can induce its effects on osteoclast precursor differentiation independent of RANKL, but only in the presence of M-CSF (Darowish et al., 2009).

IL-1 and IL-6 are also important cytokines released by macrophages during the inflammatory response to wear particles. Similar to TNF- α , IL-1 is a osteoclastogenic cytokine that promotes the expression of RANKL in bone marrow stromal cells and osteoblasts. IL-1 increases the expression of its receptor IL-1R1 and thus mediates TNF- α induction of RANKL expression. Jimi et al. (1999) reported that precursors of osteoclasts and osteoclast like cells expressed IL-1R1 receptors to which IL-1 binds, and then promotes longer survival, induces fusion, and activates osteoclast function (Jimi et al., 1999). The role of IL-1 seems to be one that promotes the destruction of cartilage and bone (Dayer, 2002). IL-6 is expressed in high levels by macrophages and fibroblasts as a result of stimulation by wear particles *in vitro* (Darowish et al., 2009). The role of IL-6 is not clearly defined, as some studies suggest it functions as a pro-osteoclastogenic and pro-inflammatory cytokine, whilst others have suggested it is an inhibitor having both anti-inflammatory and anti-osteoclastogenic effects. Most studies of IL-6 have reported its role as primarily being anti-inflammatory and anti-osteoclastogenic (Table 1.2). IL-1 and IL-6 are also involved in the synthesis of collagenase and prostaglandin E₂ (PGE₂), which are associated with the bone remodelling (Goodman et al., 1998).

Osteoprotegerin (OPG) is also an inhibitory cytokine that is produced by osteoblasts/bone marrow stromal cells (Ingham and Fisher, 2005). OPG is an anti-osteoclastogenic decoy receptor which binds to RANKL and inhibits nuclear kappa B (NF- κ B), thus preventing the differentiation of osteoclast precursors. Molecules capable of bone resorption exert their effects by directly promoting RANKL expression and inhibiting the synthesis of OPG (Wei et al., 2005). The interactions between RANK, RANKL and OPG are illustrated in Figure 1.5.

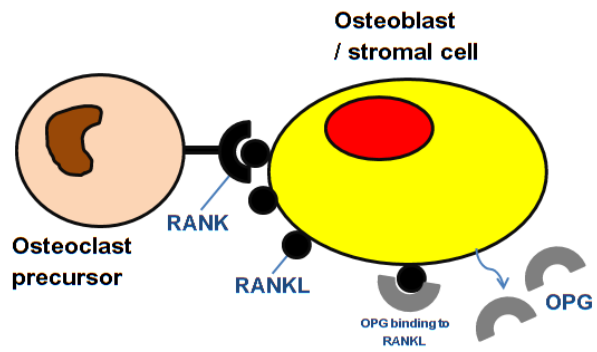


Figure 1.5. Relationship between RANK, RANKL and OPG. OPG acts as a decoy protein, binding to RANKL on osteoblasts/stromal cells and preventing interaction with RANK on osteoclast precursors, thus inhibiting the process of osteoclastogenesis (Ingham and Fisher, 2005).

Table 1.2 - Summary of primary and secondary effects of osteolytic mediators.

Name	Type	Source	Primary effects	Secondary effects	Reference
Tumour necrosis factor- α (TNF- α)	Cytokine	Monocytes and macrophages	<p>Enhances the expression of RANKL on mesenchymal and osteoblastic cells.</p> <p>Directly stimulates the recruitment of osteoclasts independent of RANK/RANKL mechanism in the presence of M-CSF.</p> <p>Promotes the survival of terminally differentiated osteoclasts to maintain their intensification of osteolysis.</p> <p>Directly induces macrophages to differentiate into osteoclasts independent of RANK/RANKL mechanisms.</p> <p>Interacts with synoviocytes and chondrocytes in the superficial layers of cartilage.</p> <p>Elevated levels of TNF-α have been reported in retrieved tissues from revision hips with osteolysis.</p>	<p>Binding of RANKL to RANK stimulates osteoclast differentiation and activates mature osteoclasts to resorb bone.</p> <p>Causes the release of enzymes, metalloproteinases that breakdown cartilage and proteoglycans, which cause cartilage destruction.</p> <p>Narrowing of the joint space.</p>	<p>(Sabokbar et al., 1997; Goodman et al., 1998; Azuma et al., 2000; Kobayashi et al., 2000; Fuller et al., 2002; Clohisy et al., 2002; Arend, 2002; Sabokbar et al., 2003; Mandelin et al., 2003; Ingham and Fisher, 2005; Darowish et al., 2009)</p>
Macrophage colony stimulating factor (M-CSF)	Cytokine	Osteoblasts/stromal cells	<p>Plays a role in organising the cytoskeleton of mature osteoclasts</p> <p>Induces the fusion of osteoclast precursor cells.</p> <p>Reduces caspase activity within osteoclast precursor cells.</p>	<p>Maintains and prolongs the survival and longevity of osteoclast precursors.</p> <p>Increases bone resorption.</p>	<p>(Jimi et al., 1999; Kitaura et al., 2005)</p>

Interleuken-1 (IL-1)	Cytokine	Monocytes and macrophages	<p>Promotes the expression of RANKL in bone marrow stromal cells and osteoblasts.</p> <p>Binds to its receptor IL-1R1 expressed on precursors of osteoclasts and osteoclast like cells, which promotes longer survival, induces fusion and activates osteoclast function.</p> <p>Directly stimulates the differentiation of mononuclear osteoclast precursors in the presence of sub-osteoclastogenic concentrations of RANKL.</p> <p>Directly induces the differentiation of macrophages into osteoclasts in the presence of RANKL.</p> <p>Interacts with synoviocytes and chondrocytes in the superficial layers of cartilage.</p> <p>Stimulate fibroblasts and synovial cells to synthesise enzymes.</p>	<p>Increases bone resorption</p> <p>Causes the release of enzymes, metalloproteinases that breakdown cartilage and proteoglycans, which cause cartilage destruction.</p> <p>Narrowing of the joint space.</p>	(Jimi et al., 1999; Arend, 2002; Wei et al., 2005)
Interleuken-6 (IL-6)	Cytokine	Monocytes/macrophages and fibroblasts	<p>Functions as an anti-inflammatory and anti-osteoclastogenic cytokine.</p> <p>Reduces the expression of TNF-α.</p> <p>Inhibits the differentiation of osteoblast progenitor cells.</p> <p>Stimulate fibroblasts and synovial cells to synthesise enzymes.</p>	Decreases bone resorption.	(Kopf et al., 1994; Balto et al., 2001; Darowish et al., 2009)
Interleukin-8 (IL-8)	Cytokine	Monocytes/macrophages and fibroblasts	<p>Stimulates the recruitment of both osteoclasts and mononuclear osteoclast-like cells.</p> <p>Stimulates the release of degradative enzymes (collagenase) and other pro-inflammatory cytokines.</p> <p>Elevated levels have been found in retrieved tissues from failed THAs.</p>	Enhances the stimulation of osteoclastogenesis and bone resorption in osteoclasts.	(Peichl et al., 1991; Sabokbar and Rushton, 1995)

Osteoprotegerin (OPG)	Cytokine receptor/ glycoprotein	Osteoblasts/bone marrow stromal cells	OPG plays a role as an anti-osteoclastogenic decoy receptor which binds to RANKL and inhibits nuclear kappa B (NF-κB), thus preventing the differentiation of osteoclast precursors (monocytes/macrophages).	Decreases bone resorption.	(Ingham and Fisher, 2005; Wei et al., 2005)
Collagenase and gelatinase	Enzymes	Fibroblasts and synovial cells	These enzymes play a role in the digestion and degradation of collagen and gelatin found within connective tissue and extracellular matrix. Collagenase may be directly associated with bone resorption by degrading the osteoid layer of bone, thus exposing the surface for osteoclast resorption.	Increases bone resorption by exposing the surface for osteoclastic activity.	(Kim et al., 1993; Sabokbar and Rushton, 1995)
Prostaglandin E ₂ (PGE ₂)	Eicosanoid signalling molecule	Fibroblasts and monocytes/macrophages	Inflammatory mediator associated with the resorption of bone Increased production by macrophages in response to wear particles.	Implant loosening.	(Goodman et al., 1989; Sabokbar and Rushton, 1995)
Monocyte chemoattractant protein-1 (MCP-1)	Chemokines	Monocytes and macrophages	Regulates the recruitment and migration of lymphocytes and monocytes/macrophages to the site of injury. Released in response to phagocytosis or adherence to wear particles. High expression observed in tissues from THAs failed from loosening. Stimulates the release of IL-1 and IL-6 from monocytes/macrophages.	Stimulates the production of osteolytic cytokines and thus results in bone resorption.	(Goodman et al., 1989; Nakashima et al., 1999; Goodman and Ma, 2010)
Macrophages inflammatory protein-1α (MIP-1α)	Chemokines	Monocytes and macrophages	Potent chemoattractants for monocytes/macrophages and lymphocytes. Stimulates the production of pro-inflammatory cytokines; IL-1, IL-6 and TNF-α.	Plays a role in the recruitment and differentiation of osteoclasts.	(Goodman et al., 1989; Goodman and Ma, 2010)

1.5.4 Biological effects of wear particles generated from different bearing materials

Evidence to support the mechanisms involved in the biological response to wear particles is ever increasing. The innovation of new techniques has allowed the analysis of retrieved periprosthetic tissues, in addition to *in vitro* and *in vivo* studies of the direct biological effects of wear debris. *In vitro* studies provide vital knowledge of cellular responses to wear particles, however these controlled environments are limited in the sense that they do not take into account other biological systems and mechanical stimuli from other cells and tissues that would otherwise be found in a clinical environment. Nevertheless, if replicated as close to a clinical situation as possible, vital information can be extrapolated from *in vitro* experiments. It is important to mention that caution should be taken when reviewing literature published on *in vitro* studies of the biological response to wear particles, since sterile, non-endotoxin contaminated, wear particles have not been used by many investigators, which may produce misleading results (Ingham and Fisher, 2000). Brooks et al. (2002) reported that even a minor contamination with endotoxin could result in the release of cytokines and hence, produce erroneous results (Brooks et al., 2002). In addition, clinically-relevant wear particles in terms of size and shape, have not been used by many researchers, instead they have used commercially available particles that differ greatly in terms of characteristics i.e. size, morphology, surface area and texture, from clinically generated particles resulting in discrepancies within the data. The prevalence of use of commercially available particles may be due to the difficulty in generating clinically-relevant wear particles *in vitro* that are free from endotoxins.

1.5.4.1 Wear particles generated from metal-on-UHMWPE hips

Following a total hip replacement particulate debris can be generated either due to wear or corrosion. Wear generated due to the normal functioning of the bearing is inevitable and can have devastating consequences in terms of the biological response. Osteolysis induced by polyethylene wear debris is most prevalent in long term implants (Brown et al., 2006). There is ample evidence published on the biological effects of UHMWPE wear debris through both retrieval analyses of periprosthetic tissue and *in vivo/in vitro* studies.

1.5.4.1.1 Biological response to UHMWPE wear particles *in vivo*

The formation of a pseudosynovial membrane around the articulation occurs after implantation. It has been reported by Bullough et al. (1988) that the formation of this membrane can take up to 2 years after implantation (Bullough et al., 1988). The interfacial membranes have the same features as synovial membranes i.e. thin in structure with few cells and vessels. Retrieval studies of MoP hip implants recovered after revision surgery for aseptic loosening have clearly shown the formation of a thicker and highly vascularised fibrous tissue

membrane which is highly populated with macrophages and multinucleated giant cells (Ingham and Fisher, 2000; Ingham and Fisher, 2005).

Polyethylene wear particles extracted from periprosthetic tissues have been reported as having a wide size distribution ranging from 10nm up to 3mm (Hailey et al., 1996; Richards et al., 2008). However, the majority of the particles were found to be in the sub-micrometre (0.1-0.99 μ m) range (Rajpura, Kendoff et al. 2014). It has been reported that when there is a concentration of more than 1×10^{10} wear particles with a size of less than 5 μ m, per gram of tissue, the occurrence of osteolysis is greater (Kobayashi et al., 1997). This was in agreement with the findings of Tipper et al. (2000) who isolated particles in the size range 0.1 -0.5 μ m from periprosthetic tissue from patients with osteolysis. Histology studies of retrieved tissues have revealed UHMWPE wear particles associated with macrophages and multinuclear giant cells. Small wear particles (<5 μ m) were located within macrophages, whereas larger wear particles (>10 μ m) were located within multinucleated giant cells (Tipper et al., 1999; Ingham and Fisher, 2000). Goodman et al. (1990) investigated the effects of implantation of different sizes of polyethylene particles in the tibia of rabbits. It was found that smaller particles were engulfed by macrophages and larger particles were engulfed by giant cells within the fibrous tissue. The largest of particles with an average size of 67.29 μ m were more readily fibrous encapsulated due to their less large size, which was not compatible with phagocytosis by macrophages (Goodman et al., 1990). A large variation in the morphology of UHMWPE particles is also apparent from many studies, small particles range from granular and round shaped to larger particles in the form of platelets, shards and fibrils (Ingham and Fisher, 2000; Suner et al., 2012).

1.5.4.1.2 Biological response to UHMWPE wear particles *in vitro*

A considerable amount of literature has been published on *in vitro* studies of UHMWPE wear debris. Shanbhag et al. (1995) investigated the difference in human monocyte response to commercially obtained and retrieved UHMWPE particles and demonstrated that cytokines IL-1 α , IL-1 β and IL-6 cytokines were produced at significantly higher levels for commercially obtained particles compared to retrieved UHMWPE particles. This study showed that the human monocytes responded differently in terms of cytokine release to the different grades of polyethylene (Shanbhag et al., 1995). Despite the lack of clinical relevance when using commercial particles, important knowledge can still be extrapolated. For example, a study by Green et al. (1998) tested the inflammatory response to low molecular weight polyethylene (ceridust, GUR416) within different size ranges using primary murine macrophages and human peripheral blood mononuclear phagocytes. The critical size range for biological activity in terms of cytokine release was reported to be between 0.2 and 0.8 μ m.

In addition to using clinically relevant wear particles, previous studies have used model cell lines such as murine cells that respond differently to human cells (Glant and Jacobs, 1994; Algan et al., 1996; Horowitz and Gonzales, 1997). Glant and Jacobs. (1994) distinguished that even macrophages from different cell populations may have various responses to the same micro-environmental signal. Matthews et al. (2000) reported that different cell types i.e. human, nonhuman, transformed and primary, vary in their ability to distinguish the distinct morphological characteristics of wear particles. This statement was made due to the fact that the size of the most reactive particles for primary human macrophages was different when compared to murine macrophages (Matthews, Besong, et al., 2000). Another study by Matthews et al. (2000) using human primary peripheral blood mononuclear cells revealed a great deal of variation in the level of cytokines produced in response to the UHMWPE particles between individuals. One donor consistently produced a response that was between 2 and 15-fold lower compared to the other five donors. This study demonstrated that the heterogeneity of humans can result in a variation in the reactivity of different individuals to particle stimulation for the first time. The observed variation in the reactivity of different human individuals to particle stimulation may have highlighted another major contributory factor in determining implant failure (Matthews, Green, et al., 2000). There has been much interest in the role that cytokine gene polymorphisms play in various diseases such as rheumatoid arthritis. Evidence is now emerging that the severity of a disease such as rheumatoid arthritis is determined by the genetic capacity of an individual to express genetic factors that activate or deactivate immunological processes. These factors will most definitely have implications for clinical implantation and may also be a major element in determining the life of an implant *in vivo* (Wilkinson et al., 2003; Kotake and Kamatani, 2005; Pawlik et al., 2005; Paradowska and Lacki, 2006; Correia et al., 2007; Xu et al., 2014).

Furthermore, the low-density of polyethylene wear particles presents difficulties where it is inherently difficult to manipulate in *in vitro* studies as it is less dense than culture medium and invariably floats on the medium surface preventing interaction with cultured monolayers of macrophages. Many studies have conducted experiments where no physical interaction existed between the cells and the polymer particles as they were not in the same plane. However, solutions to overcome this problem have been employed by many researchers, for example, cells have been cultured on the underside of culture well inserts and inverted over floating particles to allow interaction between the particles and cells (Horowitz and Gonzales, 1997). This method termed as the 'inversion technique' (Figure 1.6) has since been adapted by many studies (Matthews, Besong, et al., 2000; Matthews, Green, et al., 2000b). Other studies have utilised agarose gel (Green et al., 1998; Green et al., 2000) or collagen coated coverslips (Voronov et al., 1998) as an alternative for the immobilisation of particles to expose to cells.

The employment of these methods allowed a more accurate evaluation of the response to polyethylene wear debris *in vitro*. The size and dose of clinically relevant UHMWPE wear particles has been reported by Green et al. (2000) as being critically important in determining the biological response of macrophages *in vitro*. It was found that particles of size 0.24 μm of volumetric concentration $10\mu\text{m}^3$ debris per cell was required for stimulation of release of pro-inflammatory cytokines TNF- α , IL-1 β and IL-6 and the mediator of inflammation PGE₂, whereas a volumetric concentration of $100\mu\text{m}^3$ debris per cell of size 0.45 and 1.7 μm were required to stimulate macrophages to release these cytokines and mediators. The largest particles (88 μm) were found not to activate the cells at any volumetric concentrations. Other studies using murine and human macrophages also confirmed that the most biologically active size range was sub-micrometre particles (0.1-1.0 μm) (Green et al., 1998; Matthews, Green, et al., 2000a; Green et al., 2000).

The introduction of crosslinking of UHMWPE has been employed to improve the wear characteristics resulting in a highly cross-linked polyethylene (HXPE). Even though the crosslinking resulted in a reduction of volumetric wear of between 73 - 87%, HXPE generated a higher proportion of wear debris in the size range of 0.1 - 0.5 μm (88%) compared with conventional UHMWPE (68%) (Rajpura et al., 2014). Ingram et al. (2004) reported that just 0.1 μm^3 of HXPE wear particles per cell was needed to significantly increase the levels of TNF- α release whereas $10\mu\text{m}^3$ of conventional UHMWPE wear particles per cell was needed to stimulate macrophages to produce elevated levels of cytokines *in vitro*, indicating the increased biological activity of HXPE wear particles (Ingram et al., 2004). This study was in agreement with Illgen et al. (2009), who reported HXPE was significantly more inflammatory than conventional UHMWPE *in vitro* and *in vivo* with regards to elevated levels of TNF- α and vascular endothelial growth factor (Illgen II et al., 2008; Illgen II et al., 2009). This increased inflammatory response was attributed to the generation of more wear particles in the nanometre range as a result of crosslinking. Richards et al. (2008) isolated wear particles in the nanometre size range from tissues retrieved from hip replacements which confirmed the presence of nanometre sized wear particles retained in periprosthetic tissue. It has been previously suggested that wear particles in the nanometre range have the potential to disseminate throughout the body via the lymphatic system and end up in lymph nodes and distal organs (Urban et al., 2000; Richards et al., 2008).

A study by Liu et al. 2015 showed that nanometre particles have the potential to provoke inflammatory cytokine release from macrophage activation. UHMWPE particles in the 40nm size range were reported to show a higher inflammatory response in terms of cytokine release than micrometre-sized UHMWPE wear particles. The mechanism by which the nanometre wear particles were taken up by and activated the macrophages was believed to be by non-active processes such as pinocytosis. The authors investigated the cellular uptake of

UHMWPE wear particles and found that pinocytosis via the clathrin- and caveolae-mediated endocytosis pathways were responsible for the uptake of both nanometre-sized and micrometre-sized UHMWPE wear particles. Furthermore, it was reported that these cellular uptake mechanisms are affected by particle size and morphology, as it was observed that only one of the pinocytosis pathways, clathrin-mediated endocytosis was involved in the cellular uptake of 40nm UHMWPE manufactured by FluoSpheres. These 40nm particles had a more regular morphology and narrow size distribution which may have contributed to the different cellular uptake mechanism (Liu et al., 2015).

While the particle size and volumetric concentration of wear particles are critical factors in determining the biological reaction, the shape/morphology and composition of wear particles are just as important as indicated in a study by Fang et al. (2006). These authors investigated the ability of macrophages to engulf wear particles of different shapes (phagocytic capacity) and found that elongated particles had a smaller phagocytic capacity than spherical particles of the same volume (Fang et al., 2006). Other studies by Yang et al. (2002) and Ren et al. (2003) demonstrated that elongated UHMWPE particles were more inflammatory than globular/round UHMWPE particles. This was characterised by a more severe local inflammatory response in terms of over-expression of IL-1 β and TNF- α and macrophage infiltration. Hence, these studies showed that the shape of wear debris from failed THRs influences the severity of the biological response where elongated fibrils could provoke a more adverse inflammatory reaction (Yang et al., 2002; Ren et al., 2003).

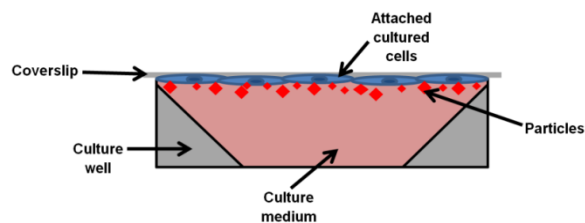


Figure 1.6: Diagrams showing the inversion technique that is used for co-culturing polyethylene particles with cells.

1.5.4.2 Wear particles generated from metal-on-metal hips

MoP has been the most common choice bearing combination for THRs since the early 1960's (Knight et al., 2011). However, problems with osteolysis induced by polyethylene wear particles led to increased interest in and development of low wearing alternative bearing materials such as metal-on-metal and ceramic-on-ceramic THRs. MoM bearings demonstrated lower wear rates compared to MoP bearings, however the release of nano-scale wear particles and metal ions was of great concern in terms of biological response.

1.5.4.2.1 Biological response to metal wear particles *in vivo*

The release of large numbers of nano-scale wear particles and metal ions is of great biological concern to clinicians in the long term. Doorn et al. (1998) used an enzymatic tissue digestion method to isolate metal wear particles from periprosthetic tissues followed by characterisation using TEM. The tissues were obtained from 13 patients undergoing revision of cobalt-chromium-molybdenum (CoCrMo) THR implants. The study revealed metal wear particles in the size range of 51-116nm, with a mean size of 81nm, which was substantially smaller than the UHMWPE particles. The shapes of the particles were mostly round or oval-like with some shard/needle-like particles, and remarkably there was very little difference in the shape and size of the particles between different patients. Using volumetric wear data from previous studies, Doorn et al. (1998) estimated that between 6.7×10^{12} to 2.5×10^{14} metal particles were produced per year in three of the patients. This was stated as being 13 to 500 times more than the 5×10^{11} UHMWPE wear particles generated from MoP hips (Doorn et al., 1998a). An *in vitro* study by Firkins et al. (2001), of metal wear particles generated from MoM hip prostheses in a physiological hip simulator was in agreement with the annual estimation of wear particle generation reported by Doorn et al. (1998). Firkins et al. (2001) reported that an average number of between 10^{13} and 10^{14} wear particles would be generated per year based on estimates of wear in the hip simulator (Firkins et al., 2001a). The size and shape of the particles were also consistent with the findings of Doorn et al. (1998) i.e. the particles generated in the hip simulator were round/oval and of uniform shape with sizes in the range of 25-36nm. These studies therefore provide evidence that wear particles generated from MoM hips are consistently in the nanometre size range and uniform in size and shape.

There are concerns over the possible distribution of these small particles in the body, and their biological effects on cells and tissues. Metal particles have been shown to disseminate throughout the body and have been found in the lymph nodes, liver, spleen and bone marrow (Case et al., 1994; Urban et al., 2000). The release of metal wear particles and metal ions from MoM hips can thus have potential local and systemic effects in the body. Potential local effects may include the deposition of metal particles which can lead to metallosis which has been reported by many retrieval studies of revision THR (Chang et al., 2005). Metallosis is defined as the infiltration of metallic wear debris into periprosthetic hard and soft tissues, and its occurrence has been reported as frequently causing osteolysis (Korovessis et al., 2006). In addition to metallosis, the the production of cytokine and osteolytic mediators by macrophages in response to metallic wear debris can lead to periprosthetic osteolysis and aseptic loosening (Campbell et al., 2004). Campbell et al. (2002) reported that MoM hips had similar cytokine profiles to MoP hips, in terms of IL1 β , IL-6 and PDGF- α release, demonstrating that CoCr particles can induce cytokine production that can result in osteolysis, despite the small size of the metal wear particles. However, only low levels of TNF- α were

observed, which may explain the lower incidence of osteolysis associated with MoM implants compared with MoP implants (Campbell et al., 2002). Overall, in comparison to MoP hip implants, significant amounts of literature state that MoM implants demonstrate a lower incidence of osteolysis (Long, 2005). Despite the low incidence of osteolysis, MoM implants have been reported to be associated with pseudotumours, described as soft tissue masses that can lead to devastating short term implant failures. The cause of these reactions is highly controversial, however some studies have associated pseudotumours with excessive wear and/or metal hypersensitivity (Haddad et al., 2011; Catelas, 2011). Mahendra et al. (2009) reported the presence of macrophages and lymphocytes in the periprosthetic tissues (pseudocapsule and pseudomembrane) of revised MoM implants, which was indicative of an inflammatory reaction to the metal wear debris. Tissue necrosis and pseudotumours were observed in the periprosthetic tissues of all 28 cases studied, the pathogenesis of which was mainly associated with both a cytotoxic and delayed hypersensitivity response to the metal wear debris (Mahendra et al., 2009). Campbell et al. (2010) reported that pseudotumours can also occur around implants with low wear, suggesting hypersensitivity as the underlying cause which was the case for some patients (Campbell et al., 2010).

The release of metal ions and metal particles from MoM bearings can act as antigens and stimulate allergic reactions causing hypersensitivity. Hypersensitivity is defined as an overreaction of the specific immune system to an allergen and can be mediated by either antibodies (type I, II, III) or cells (type IV/delayed type hypersensitivity) (Brown et al., 2006). Metals and metal ions elicit type IV hypersensitivity which is mediated by class II restricted CD4 positive T-lymphocytes, reactive against metal-ion specific major histocompatibility complexes (MHC) which are presented on antigen presenting cells (APCs) (Jacobs et al., 2008). A study by Howie et al. (1993) reported the presence of lymphocytes associated with metal wear particles in tissues around failed MoM hip implants, suggesting a substantially different immune response than the histocytic response observed with UHMWPE wear debris (Howie, 1993). The lymphocytic response to metal wear debris is well documented, and has been linked to metal hypersensitivity reactions in patients with MoM bearings as suggested by increased Co and Cr ions levels in patient serum (Kwon et al., 2010).

1.5.4.2.2 Biological response to metal wear particles *in vitro*

Previous studies have established that wear particles generated from MoM implants are in the nanometre size range (Doorn et al., 1998a; Firkins et al., 2001b; Brown et al., 2007). It is important to take into consideration the relevance of *in vitro* studies on metal wear particles, as only those studies that use metal wear particles in the nanometre size range are relevant. Brown et al. (2006) used clinically relevant endotoxin-free CoCr wear particles to investigate the response of human peripheral blood mononuclear cells in terms of TNF- α production *in*

vitro. TNF- α production was observed when the cells were stimulated with doses of $50\mu\text{m}^3$ per cell of CoCr wear particles. As well as cytokine release, high concentrations of CoCr particles were found to be cytotoxic to the cells. Brown et al. (2006) suggested that the metal wear particles may have become aggregated, forming larger particles. These larger particles may have then been phagocytosed by macrophages, resulting in activation of the macrophages and release of cytokines (TNF- α).

The cytotoxic effects of clinically relevant CoCr nanoparticles and ions on macrophages were investigated by Kwon et al. (2009). The authors reported that only cobalt ions at high concentrations were cytotoxic to macrophages suggesting the possible consequences that could occur from high levels of metal wear particles *in vivo*. Cobalt ions have been extensively studied *in vitro* where they have been shown to reduce cell viability at low concentrations (Ingham and Fisher, 2000; Kwon et al., 2009). A more recent study by VanOs et al. (2014) investigated the effects of chromium oxide particles on macrophages *in vitro*. They found an increase in necrosis and decrease in cell viability with high concentrations of chromium oxide. These authors also reported no significant increase in TNF- α cytokine release in response to the chromium oxide particles, when compared to the cell only control. Overall this study concluded that chromium oxide presents low cytotoxic effects on macrophages and these particles may not be the main contributor to the inflammatory reaction around MoM implants (VanOs et al., 2014). Another study by Behl et al. (2013) investigated the biological effects of clinically relevant CoCr nanoparticles and ions on dural fibroblasts and dural epithelial cells. It was reported that specific concentrations of CoCr particles (6.05 , 60.5 , $121\mu\text{m}^3$ per cell) and ions ($121\mu\text{m}^3$ per cell) significantly reduced the viability of epithelial cells, whereas no effect on the cell viability of fibroblasts was observed. In terms of cytokine release, both cell types released IL-8 in response to particle concentrations of $60.5\mu\text{m}^3$ per cell (epithelial cells) and $121\mu\text{m}^3$ per cell (epithelial and fibroblast cells). In addition to cell viability and cytokine release, oxidative stress was also assessed and observed at a concentration of $50\mu\text{m}^3/\text{cell}$ for both cell types at 24 hours. This study indicated that different cell types showed different responses to CoCr nanoparticles and ions (Behl et al., 2013).

Genotoxicity is also another phenomenon that is cause for concern regarding CoCr wear particles (Brown et al., 2006; Suner et al., 2012). Numerous studies have investigated chromosome aberrations in patients with MoM implants. Ladon et al. (2004) observed an increase in chromosomal aberrations and aneuploidy in the peripheral blood of patients after 2 years of MoM implantation (Ladon et al., 2004). The cause for these changes is not known, but it was suggested that it may have been due to exposure to metal wear particles (Doherty et al., 2001). A more recent *in vitro* study by Tsaousi et al. (2010) demonstrated high numbers of chromosomal aberrations and variation of lesions in primary human fibroblasts induced by CoCr wear particles. It was suggested that the *in vitro* genotoxicity of CoCr particles is a

chemically induced effect rather than a particle effect whereby after phagocytosis the build-up of Cr ions at the surface of particles may induce genotoxic effects (Tsaousi et al., 2010).

1.5.4.3 Wear particles generated from ceramic-on-ceramic hips

CoC hip implants have now been in clinical use for more than 40 years, however they are not as commonly used as MoM or MoP hip implants, hence there are a limited number of studies available on the biological response to ceramic wear debris. Even so, studies that have been conducted, have shown that out of the three main types of bearing combinations (MoP, MoM and CoC), CoC bearings have the best tribological performance, produced the lowest wear, and generated wear particles with the lowest biological reactivity (Fisher et al., 2006).

1.5.4.3.1 Biological response to ceramic wear particles *in vivo*

Early retrieval studies of alumina CoC hip replacements reported no difference in terms of the tissue reaction around the implant compared with tissues from failed MoP implants. Both groups of tissues had an intense macrophage reaction. However, it was concluded that the tissue reaction in the CoC implant was due to the abundant zirconia particles from the cement, which represented 76% of the debris present, rather than the alumina particles which represented only 12% of the wear debris present (Lerouge et al., 1997). A more recent study by Esposito et al. (2013) analysed pseudocapsules retrieved from revision surgeries of alumina-on-alumina hip replacements and found that none of the patients developed evidence of osteolysis. None of the patients showed severe local tissue reactions characteristic of MoM implants or severe foreign body reaction characteristic of MoP implants. They instead found a rather moderate infiltration of mononuclear macrophages and occasional lymphocytes which are typical features of a response to foreign material. However it should be noted that the initial reasons for revision were not osteolysis (Esposito et al., 2013). In contrast, Nam et al. (2007) reported a case report of a 63-year-old female patient, that had revision surgery due to osteolytic lesions identified during follow-up radiographs. Histological analysis of these osteolytic lesions showed the presence of abundant ceramic wear particles ($\leq 5 \mu\text{m}$) and macrophage and lymphocyte infiltrates. This study demonstrated that if alumina wear particles were in the critical size ($< 5 \mu\text{m}$), shape and volume ($100 \mu\text{m}^3$ per cell), they can induce biological responses similar to those induced by UHMWPE wear particles. However, it should be noted that this was an isolated case where extensive volumes of wear particles were generated due to grain pull-out (Nam et al., 2007). Osteolysis in association with CoC bearings has rarely been reported, and is generally limited to isolated cases of excessive wear (Shishido et al., 2006; Nam et al., 2007).

Hatton et al. (2002) analysed tissues retrieved from around CoC bearings compared with tissues retrieved from around MoP bearings at revision surgery. All the CoC tissues showed the presence of wear particles either as agglomerates or in distinct channels in the tissues. The

CoC tissues showed mixed pathology and were relatively rich in macrophages as well as over half of the tissues showing necrosis/necrobiosis. On the other hand, the MoP tissues showed a granulomatous cellular reaction infiltrated with a dense population of macrophages and giant cells and less than 30% of tissues demonstrated necrosis/necrobiosis. Interestingly, the CoC tissues also showed the presence of neutrophils and lymphocytes. The mixed pathology observed in the CoC tissues was suggested as being attributed to the bimodal size ranges of the wear particles. The larger particles may have been phagocytosed by macrophages resulting in cytokine release and further recruitment of macrophages. The smaller particles may have contributed to the necrosis/necrobiosis via the release of ions that may be toxic to cells. However, other reasons suggested as being the possible causes of necrosis/necrobiosis included fretting wear of the stem, or even physical damage to the surrounding tissues as a result of micro-motion (Hatton et al., 2002).

1.5.4.3.2 CoC wear particles *in vitro*

There have been few studies of the biological effects of ceramic wear debris in comparison to other bearing materials. However, of the studies that are available, very few researchers use clinically relevant wear particles, and so their studies are not representative of what may occur *in vivo*. Endotoxin-free particles are not as much of an issue with wear particles generated from hard-on-hard bearings such as MoM and CoC as it is with UHMWPE wear particles due to the fact that ceramic and metal wear particles can be heat treated to remove the endotoxins. The low melting point (130-136°C) of UHMWPE wear particles prevents the use of heat to destroy endotoxins; instead many studies used gamma irradiation (Premnath et al., 1996; Besong et al., 1998). More recently however, many studies have resorted to generating clinically relevant wear particles in a sterile environment such as Class I laminar flow cabinet using an aseptic technique throughout. All the components of the wear test rigs are sterilised by either exposure to UV light or dry heat sterilisation. This innovative technique ensures minimal contamination by endotoxin giving more accurate results in terms of biological response to wear debris (Ingram et al., 2004; Liu et al., 2015).

The use of commercially-obtained ceramic wear particles is a very common practice in previous studies. For example, a study by Catelas et al. 1998 used commercially obtained alumina and zirconia particles in the phagocytosable range; 0.6-4.5µm and 0.6 µm, respectively. These authors found that the cell viability decreased with increased alumina particle size and concentration in that a higher concentration of smaller particles (1.3µm) compared to larger particles (2.4µm) was required to induce cytotoxic effects. This pattern was also observed for the release of TNF-α from macrophages. Another similar study by Catelas et al. (1999) investigated the ability of alumina ceramic particles to induce apoptotic cell death. This study showed that ceramic particles induced DNA fragmentation into

oligonucleosomes, which is a characteristic of apoptosis. However, it was hypothesised that the programmed cell death in response to the ceramic particles may explain the lower levels of TNF- α released from the macrophages in response to alumina particles. This observation may explain the low incidence of osteolysis observed in CoC bearings (Petit et al., 2002).

Different biological effects between alumina and zirconia particles have also been reported. Nkamgueu et al. (2000) observed a higher cytotoxicity associated with alumina particles (10%) compared to zirconia particles (8%). The zirconia and alumina particles affected the intracellular electrolyte concentration, where sodium concentration increased and potassium content decreased, thus resulting in increased cell mortality. Changes in cellular ionic concentration reduced phagocytic activity and oxidative metabolism, thus resulting in reduced production of hydrogen peroxide. These effects were attributed to the wear particles inhibiting or altering the oxidative metabolism mechanism within cells (Nkamgueu et al., 2000a). All these results from the previous mentioned studies give vital information about the response of cells to wear particles *in vitro*, however it should be taken into account that certain aspects of these types of studies are not accurately representative of the *in vivo* scenario.

The differences between biological activity of ceramic wear particles compared to UHMWPE wear particles has been reported in many studies. Savarino et al. (2009) compared the biological activity of alumina ceramic wear particles with polyethylene wear particles that were both clinically relevant as they were extracted from tissue sections obtained from revision THA. These authors reported a higher release of PGE₂ for the polyethylene (150-160 ng.ml⁻¹) compared to ceramic (40-65 ng/mL) wear particles. PGE₂ is an inflammatory mediator which functions in the recruitment and differentiation of macrophages and pre-osteoclast cells (Savarino et al., 2009). Granchi et al. (2004) also highlighted the differences between alumina ceramic and polyethylene wear particle in terms of the wear particles effects on osteoblast-osteoclast interaction. These authors reported that the alumina particles were less inductive of osteoclastogenesis compared to polyethylene wear particles. The polyethylene wear particles increased the release of RANKL, whilst simultaneously decreasing the release of OPG, which as mentioned earlier is an inhibitor of osteoclastogenesis. This study demonstrated that alumina ceramic wear particles were less active in promoting osteoclast formation (Granchi et al., 2004). Other studies have compared the biological activity of alumina ceramic wear particles with CoCr wear particles that are generated from MoM hip bearings. Tsaousi et al. (2010) reported that alumina ceramic wear particles were weakly genotoxic to human cells *in vitro* when compared with metal CoCr wear particles, because the CoCr wear particles caused a greater number of and variation of chromosomal aberrations and lesions (Tsaousi et al., 2010).

The lack of relevant studies is hypothesised to be due to the difficulties in generating high volumes of clinically relevant ceramic wear particles *in vitro*. The recent introduction of

microseparation during hip simulation of CoC bearings has allowed the generation of clinically relevant wear rates, wear patterns and wear particles *in vitro* (Tipper et al., 2002a). Very few studies have used this technique to generate and investigate the biological effects of ceramic wear particles *in vitro*. A study by Hatton et al. (2003) investigated the effects of clinically relevant alumina ceramic wear particles on human peripheral blood mononuclear cells (PBMNCs) *in vitro*. The alumina ceramic wear particles were generated using a hip simulator under microseparation conditions. The clinically-relevant alumina ceramic wear particles showed a bimodal size distribution with nanometre sized (5-20 nm) particles and larger particles (0.2 - >10 μm). The results were compared with commercially-obtained alumina powder which had a uniform morphology and average particle size of 0.5 μm . The effects of the particles were measured in terms of TNF- α production by PBMNCs. Higher volumes (500 μm^3 per cell) of the clinically-relevant wear particles were required to stimulate the PBMNCs than the alumina powder (100 μm^3 per cell). The authors suggested that this may be due to the clinically relevant wear particles having fewer particles in the critical size range (0.1-1 μm) for macrophage activation compared to the alumina powder which had considerably larger particles. This study therefore demonstrated that clinically relevant ceramic wear particles can stimulate the release of osteolytic cytokines by macrophages. However, extremely large volumes are required to initiate this response, which is very unlikely to occur *in vivo*, even under microseparation, due to the superior low wear rates (<1.74 mm^3 per million cycles) of alumina CoC bearings (Tipper et al., 2002a). A similar study by Germain et al. (2003) compared the effects of clinically-relevant alumina ceramic and CoCr wear particles on the viability of U937 histiocytes and L929 fibroblasts *in vitro*. The clinically-relevant alumina ceramic wear particles were generated in a hip simulator under microseparation conditions and the CoCr wear particles were generated using a pin-on-plate tribometer. The cytotoxicity of the clinically-relevant alumina wear particles was compared with commercially-obtained CoCr and alumina powder. It was found that the clinically-relevant alumina ceramic wear particles were mildly cytotoxic in only histiocytic cells at a concentration of 50 μm^3 per cell, all other concentrations induced no effect. On the other hand, clinically relevant CoCr wear particles were cytotoxic to both histiocytes and fibroblasts, at all concentrations (50 and 5 μm^3 per cell, respectively). Interestingly the commercial CoCr and alumina particles did not affect the viability of either histiocytes and fibroblasts. The authors concluded that the composition, size and volume of the wear particles were critical factors in determining the biological effects of wear debris on cells *in vitro* (Germain et al., 2003a).

1.6 Summary

Overall, the literature review has highlighted the concerns and problems that exist for different bearing materials. All bearing combinations have advantages and disadvantages. Some have completely fallen out of favour, particularly MoM bearings. It is evident that there is a lack of studies that accurately represent the *in vivo* situation. This may be due to the difficulties of methods and technologies available at the time of the studies. However, as methods and research technologies develop, the experimental designs should reflect the *in vivo* and clinical situation more accurately.

Clinically-relevant sterile endotoxin-free UHMWPE wear particles in the critical size range and volumetric concentration, when cultured *in vitro*, activate macrophages to release a range of osteolytic cytokines i.e. IL-1 and IL-6, TNF- α and M-CSF. *In vitro* studies of both human and murine macrophages have shown that wear particles in the size range 0.1-1.0 μm are the most biologically active (Green et al., 1998). In addition, these studies have allowed us to extrapolate that from all the many cytokines that are released, TNF- α is a key cytokine released by wear particle activated macrophages (Matthews, Green, et al., 2000a). MoM bearings were considered to be an alternative bearing to MoP bearings, however, implants that are malfunctioning can produce high wear rates that can have devastating consequences and in some cases, osteolysis. In addition, the release of nanometre sized metal wear particles and metal ions are of concern, as they can cause adverse biological reactions as discussed earlier (Haddad et al., 2011). Thus, the need for alternative bearing materials, such as ceramic-on-ceramic hip implants has become more important.

CoC bearings have demonstrated the best tribological performance compared to other bearing materials (Fisher et al., 2006). Wear simulation testing of CoC bearings under edge loading conditions has allowed reproduction of wear rates and wear mechanisms similar to those observed *in vivo* (Nevelos et al., 2000a). The wear performance of composite ceramic hip replacements has been extensively investigated using standard and severe edge loading conditions (Al-Hajjar, Jennings, Begand, et al., 2013). However, no studies have reported the characteristics or biological activity of the wear particles generated from composite ZTA CoC bearings. Alumina ceramic wear particles have shown to produce a minimal biological response, with low cytotoxicity and inflammatory potential at the volumes representative of alumina CoC bearings (I Catelas, Petit, Zukor, et al., 1999; Germain et al., 2003a). The number of studies carried out for MoP and MoM bearings in terms of assessing biocompatibility far exceed those for CoC bearings. However, these studies are largely limited to the cytotoxic and inflammatory effects (cytokine release) of wear particles. Other assays that measure DNA damage or oxidative stress in response to wear particles are also important, especially for ceramic wear particles as they are generally considered to be biocompatible. Moreover, these subtle changes such as DNA damage and oxidative stress have been linked

to osteolysis, hence it is important to investigate these biological effects, in addition to cytotoxicity testing and cytokine release. Cytotoxicity and inflammatory cytokine release has predominantly been linked to high volumes of wear particles. However, CoC bearings have lower wear rates compared to other bearing materials and the long-term effects of these low volumes of ceramic wear particles in terms of genotoxicity and oxidative stress is currently unknown.

1.7 Project aims and objectives

1.7.1 Aims

The aim of this project was to understand the characteristics and conduct a comprehensive evaluation of the biological impact of clinically-relevant ceramic wear particles generated from composite ZTA BIOLOX® Delta ceramic-on-ceramic total hip replacements. This project will generate benchmark data on composite ZTA Delta ceramic bearings, which could be used for the evaluation of new biomaterials against this data. In addition, this project will provide a more clinically-relevant understanding of the biological impact of the wear particles generated from composite ZTA Delta ceramic hip replacements. Thus, clinicians and surgeons will have more confidence in this bearing and will be better able to provide a long-term prognosis to patients.

1.7.2 Objectives

The objectives of the study were as follows:

- To develop and optimise a novel particle isolation method for the recovery and characterisation of very low volumes of composite ZTA ceramic wear particles generated under edge loading conditions in hip simulator serum lubricants
- To generate clinically-relevant ceramic wear particles from alumina (BIOLOX® Forte) and composite ZTA (BIOLOX® Delta) CoC hip replacements under severe edge loading conditions for subsequent testing of biological impact
- To investigate the biological impact of composite ZTA Delta ceramic model particles and composite ZTA Delta ceramic wear particles generated from ceramic-on-ceramic total hip replacements, in terms of cytotoxicity, inflammatory cytokine release, genotoxicity and oxidative stress.

CHAPTER 2

2 Optimisation and validation of a novel particle isolation method for ultra-low volumes of ceramic wear debris

2.1 Introduction

Excessive wear particles have been linked with the aetiology of periprosthetic osteolysis and aseptic loosening. The initial stages of osteolysis involve wear particles which are generated at the articulating surfaces, entering the periprosthetic tissue where they are phagocytosed by macrophages. The macrophages then initiate the processes of inflammation by releasing pro-inflammatory cytokines and other mediators of inflammation that stimulate osteoclastic bone resorption, leading to osteolysis and inevitable loosening of the hip implant (Ingham and Fisher, 2000; Ingham and Fisher, 2005; Brown et al., 2006; Purdue et al., 2006; Sukur et al., 2016; Kandahari et al., 2016). The relative features of prosthetic wear particles in terms of their size and shape determines the severity of the biological response. It is well established that polyethylene wear particles within the critical size range (0.2–0.8 μ m) cause macrophage activation (Green et al., 1998). In addition to particle size, the volume of particles has also been reported as being critically important in determining the biological response (Isabelle Catelas et al., 1999; Ingham and Fisher, 2000; Matthews, Besong, et al., 2000). The characteristics data of wear particles in conjunction with the wear rates of different types of bearing couples has previously been used to predict the functional biological activity of wear debris generated from THRs (Fisher et al., 2001; Tipper et al., 2003). Hence, understanding wear particle characteristics and their biological activity is an essential step in the pre-clinical testing of joint replacements (Ingham and Fisher, 2000). Currently, the best technique to obtain the characteristics of prosthetic wear particles is to isolate the particles from tissues or simulator lubricants, and analyse the characteristics of the recovered particles using SEM (Galvin et al., 2007; Brown et al., 2006). Whilst this has been successful for polyethylene and metal wear debris from MoP and MoM, respectively, the isolation of ceramic wear particles from CoC bearings has been very challenging. Hence, there is currently a lack of clinically-relevant studies on the characteristics and biological activity of ceramic wear particles.

The wear performance of the composite CoC total hip replacements such as those using BIOLOX[®] Delta (CeramTec, Germany), has been extensively investigated (Stewart et al., 2003a; Al-Hajjar, Jennings, Begand, et al., 2013b; Al-Hajjar, Fisher, Tipper, et al., 2013a; O'Dwyer Lancaster-Jones et al., 2017), however no studies have reported the characteristics

of the wear debris generated from these bearings. The lack of clinically-relevant studies may be due to difficulties in generating high volumes of clinically-relevant ceramic wear debris *in vitro*. In addition, current particle isolation methods are not sensitive enough to reliably isolate the extremely low wear volumes (0.1-1mm³ per million cycles) of composite wear particles that are generated in hip simulator lubricants. Current particle isolation methods have many limitations including multiple steps, insufficient speeds for nano-particle sedimentation and ineffective protein digestion, which all increase particle loss during the process of isolation (Doorn et al., 1998b; Catelas, Bobyn, J.B. Medley, et al., 2001; Brown et al., 2007). Such particle loss cannot be tolerated for ceramic wear debris due to the inherent low wear rates of CoC bearings. A particle isolation method developed by Lal et al. (2016) recently reported recovery rates of >80% for ceramic-like particles at very low wear rates in the order of 0.01 mm³ - 0.1 mm³ per million cycles from serum. These wear rates are comparable with the wear rates of composite ceramic bearings, hence this method was optimised and validated for the isolation of ZTA ceramic particles generated from composite CoC couples tested in a hip simulator under microseparation conditions. The work in the current chapter in relation to the other chapters is presented in Figure 2.1.

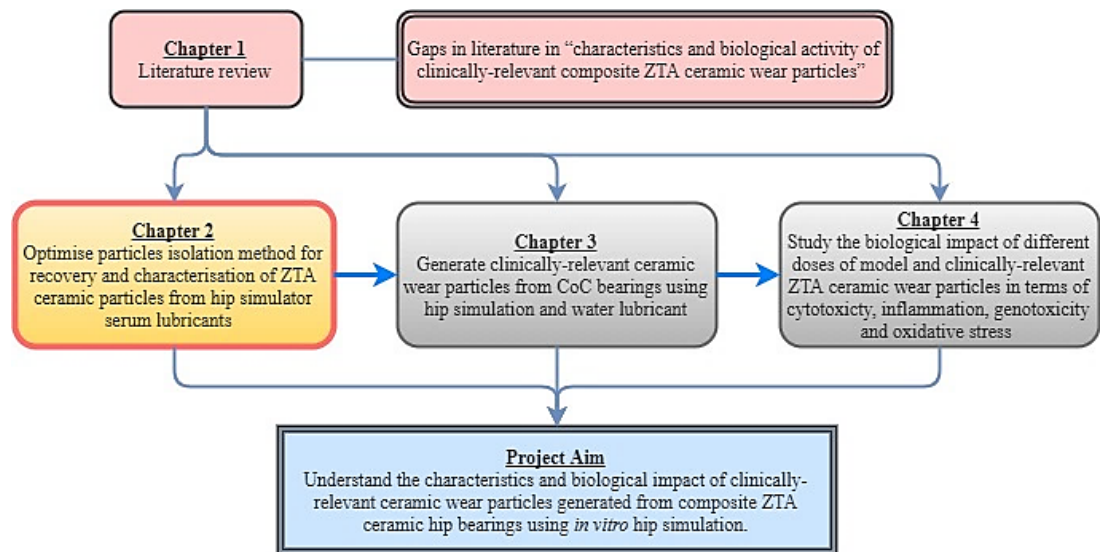


Figure 2.1 – Flow diagram showing the work in this chapter in relation to other chapters, with the current chapter highlighted in yellow.

2.2 Aims and objectives

Aims:

The aim of the study presented in this chapter was to optimise and validate a novel particle isolation method for ultra-low wearing ceramic materials. This was subsequently applied to hip simulator lubricants for the isolation and characterisation of very low volumes of composite ZTA ceramic wear particles generated under edge loading conditions.

Objectives:

- To validate the sensitivity and repeatability of the novel particle isolation method in terms of particle recovery rates using spiking of serum with composite ZTA ceramic model particles.
- To optimise the method for the isolation of composite ZTA ceramic wear debris from hip simulator lubricant serum.
- To characterise the recovered ceramic wear particles in terms of their size, morphology and composition.

2.3 Materials and Methods

2.3.1 Introduction

The method developed by Lal et al. (2016) was initially validated in terms of sensitivity and repeatability to obtain the recovery rates using serum pre-loaded with a known volume of ZTA ceramic model particles (0.05-5mm³). Thereafter, the validated method was applied to hip simulator serum lubricant, which contained ZTA ceramic wear particles generated from BIOLOX[®] Delta CoC bearings under microseparation conditions. The validated method demonstrated insufficient digestion of the hip simulator serum lubricant as considerable protein contamination was observed when the recovered particles were analysed using SEM. Hence, the method was further optimised and as a result a two-step digestion protocol followed by density gradient purification was devised.

2.3.2 Materials

2.3.2.1 Ceramic particles

Commercially-obtained zirconia-toughened alumina (ZTA) powder was used to validate the method as it had a similar composition to that of BIOLOX[®] Delta i.e. ~80% (w/w) alumina and ~20% (w/w) zirconia (Table 2.1).

Table 2.1 - Supplier of the ceramic powder used in this chapter.

Material name	Composition (wt.%)	Supplier/Source
Zirconia toughened alumina (ZTA) ceramic powder (agglomerated particle size: 20-150 µm)	Al ₂ O ₃ ~80% (w/w) and ZrO ₂ ~20% (w/w)	Inframat Advanced Materials, Connecticut, USA

2.3.2.2 Chemicals and reagents used in this study

The chemicals and reagents used in this study are listed in Table 2.2.

Table 2.2 – List of chemicals and reagents used in this study.

Chemical/Reagent	Supplier	Storage/Preparation
Calcium chloride	Fisher Scientific, Loughborough, UK	4°C
Foetal Bovine Serum (FBS)	Lonza Biologics, Cambridge, UK	-20°C
HEPES buffer	Melford Laboratories LTD, Ipswich, UK	Room temperature
Lysozyme	Sigma-Aldrich, Irvine, UK	-20°C

Methanol	Atom Scientific LTD, Manchester, UK	Room temperature
Non-pyrogenic water	Baxter, UK	Room temperature
Proteinase K (20 mg per ml)	VWR International LTD, Poole, UK	-20°C
Sodium dodecyl sulphate (SDS) 2 % (w/v) and 10% (w/v)	Sigma-Aldrich, Irvine, UK	Room temperature
Sodium polytungstate solution - 85 % (w/v)	Sigma-Aldrich, Irvine, UK	Room temperature
SurfaSil™ Silconizing Fluid	Thermo Scientific, Rockford, USA	Room temperature
Tris (trizma base) (50 mM)	Sigma-Aldrich, Irvine, UK	Room temperature

2.3.2.3 Equipment

The equipment used in this chapter are listed in Table 2.3.

Table 2.3 - List of equipment used in this chapter.

Materials and Equipment	Supplier
Aluminium stubs, adhesive carbon tabs and conductive carbon cement	Agar scientific, Elektron Technology UK Ltd, Essex, UK
Balance X205	Mettler Toledo Ltd., Beaumont Leys, Leicester, UK
Beckman polypropylene centrifuge tubes (331374) SW40 and SW32	Beckman Coulter Ltd., High Wycombe, UK
Filtration kit	Millipore
Hitachi SU8230 Cold FE SEM	Hitachi High-Technologies Europe Gmbh, Maidenhead, Berkshire, UK
Incubator	Sanyo Electronic Co. Ltd, China
Infrared (IR) lamp	Goldmark, China
Lint-free wipes	RS Components Ltd, Corby, UK
Optima L-90K ultra-centrifuge, SW-40 titanium (Ti) rotor and Ti swinging buckets, SW32 Ti rotor and Ti swinging buckets.	Beckman Coulter Ltd., High Wycombe, UK

Polycarbonate filter membranes (0.015µm pore size)	Whatman, UK
PSU-10i orbital shaker	Grant instruments, Cambridgeshire, UK
Quorum Q15OT carbon coater	Quorum Technologies Ltd., East Sussex, UK
Ultra-sonic water bath	VWR International Ltd. Leicestershire, UK
X-Max EDX system	Oxford Instruments Aztec Energy, Oxford, UK

2.3.2.4 Consumables, plasticware and glassware

The consumables, plasticware and glassware used in this chapter are listed in Table 2.4.

Table 2.4 – List of consumables, plasticware and glassware used in this study

Item	Size	Supplier
Bijous	5ml	Scientific Laboratory Supplies, Nottingham, UK
Falcon tubes	50ml	Starstedt Ltd, Leicester, UK
Glass duran bottles	100ml, 500ml	Duran Group, Wertheim am Main, Germany
Glass bijous	5ml	Faculty of Biological Sciences, University of Leeds, UK
Serological pipettes	25ml, 10ml, 5ml	Starstedt Ltd, Leicester, UK
Sterile pipette tips	1000µl, 200µl, 20µl, 2µl	Starlab UK, Milton Keynes, UK
Sterile plastic pots	250ml, 150ml, 60ml	Thermo Scientific, Massachusetts, USA
Universals	20ml	Scientific Laboratory Supplies, Nottingham, UK

2.3.3 Validation of sensitivity for the novel particle isolation method

2.3.3.1 Introduction

Commercially-obtained ZTA ceramic model particles were used to assess and validate the sensitivity of the ceramic wear particle isolation method in terms of recovery rates. Foetal bovine serum (25% (v/v)) was spiked with a range of volume concentrations of ZTA particles

(5mm³, 1mm³, 0.5mm³, 0.1mm³ and 0.05mm³), which were subsequently digested with proteinase K. The digested serum was centrifuged on a sodium polytungstate gradient at 270,000g. The ZTA ceramic model particles were filtered onto pre-weighed 0.015µm filter membranes which were subsequently dried and weighed to obtain the recovery weight of the ZTA ceramic model particles. The ZTA particles were characterised in terms of size and morphology using SEM, EDX analysis and image analysis software. The ZTA ceramic model particles were compared before and after isolation to assess if the digestion caused any changes in size distribution and particle morphology.

2.3.3.2 Characterisation of the particles

2.3.3.2.1 Calculating particle volumes

The ZTA particles at a volume of 0.1 mm³ (n=3) were suspended in 10 ml sterile water and sonicated for 10 mins to disperse the particles. The following formula was used to calculate the weight of ZTA powder required for a specific particle volume: -

Equation 1

$$density = \frac{mass}{volume}$$

For example, the calculations to work out how many milligrams (mg) of ZTA powder was required for a volume of 5mm³ is presented below: -

1. Rearrange formula to make mass the subject

$$mass = density \times volume$$

2. Input the required volume and density of ZTA (5.0g/cm³ or 0.005g/mm³)

$$mass = 0.005 \times 5$$

3. Mass= 0.025g or 25mg of ZTA powder required for 5mm³

2.3.3.2.2 Filtration and characterisation using SEM

The ZTA particle solution was filtered in a class II cabinet through a 0.015µm pore size polycarbonate filter membrane using the Millipore filtration kit, before being dried under an infrared lamp for at least 1 hour. The filter membrane was mounted on to an aluminium stub before coating with carbon to a thickness of 5 nm using the Quorum Q150T carbon coater. The filter membrane was then imaged using the Hitachi SU8230 Cold field emission gun scanning electron microscope (CFE-SEM) at 1 kV (beam deceleration mode), mixed signal; secondary electrons (SE) and back-scattered electrons (BSE) and at a working distance (WD) of 1-3 mm. The use of the Hitachi SU8230 CFE-SEM allowed a resolution of approximately 1.0nm/15kV (SE resolution). Five random fields of view were imaged for each magnification;

5K, 60K, 90K and 150K. Chemical characterisation of the ZTA model ceramic particles was carried out by energy dispersive x-ray (EDX) analysis (X-Max EDX system, Oxford, UK) to confirm the chemical composition of the particles. The CFE-SEM micrographs of the ZTA particles were subsequently analysed using computer software, ImageJ version 1.49, to measure the Feret's diameter (d_{max}), aspect ratio and circularity of the particles. The Feret's diameter is the longest distance between any 2 points along the particle boundary. A minimum of 150 were characterised in accordance with the standard practice for characterisation of particles; ASTM F1877-05:2010 and international standard for Wear of implant materials – Polymer and metal wear particles – Isolation and characterisation; BS ISO 17853:2011.

2.3.3.3 Preparation of particle spiked serum lubricants

A range of volumes of ZTA ceramic model particles (5mm^3 , 1mm^3 , 0.5mm^3 , 0.1mm^3 and 0.05mm^3), were directly spiked into 38ml of fresh 25% (v/v) foetal bovine serum (FBS). Each sample was prepared in triplicate ($n=3$) using 38.5ml thin wall polypropylene tubes. The weights of the ZTA powder required for different volumes of ZTA particles are shown in Table 2.5.

Table 2.5 – Weights of the ZTA powder required for different volumes of ZTA particles.

Volume	5mm^3	1mm^3	0.5mm^3	0.1mm^3	0.05mm^3
Weight of ZTA powder (mg)	25	5	2.5	0.5	0.25

The lower volumes of ZTA particles (0.1mm^3 and 0.05mm^3) are representative of the clinically relevant wear rates of BIOLOX[®] Delta CoC hip replacements ($0.1\text{-}1\text{ mm}^3/\text{million}$ cycles). The serum lubricants spiked with different volumes ($0.05\text{-}5\text{mm}^3$) of commercially-obtained ZTA ceramic particles were used to assess and validate the sensitivity and repeatability of the novel ceramic wear particle isolation method in terms of recovery rates. The control sample contained 25% (v/v) FBS with no ZTA particles added. Each sample was sonicated for 10 minutes and incubated at 37°C for 24 hours before being treated according to an optimised proteolytic digestion protocol which is illustrated in Figure 2.2 (Lal et al., 2016).

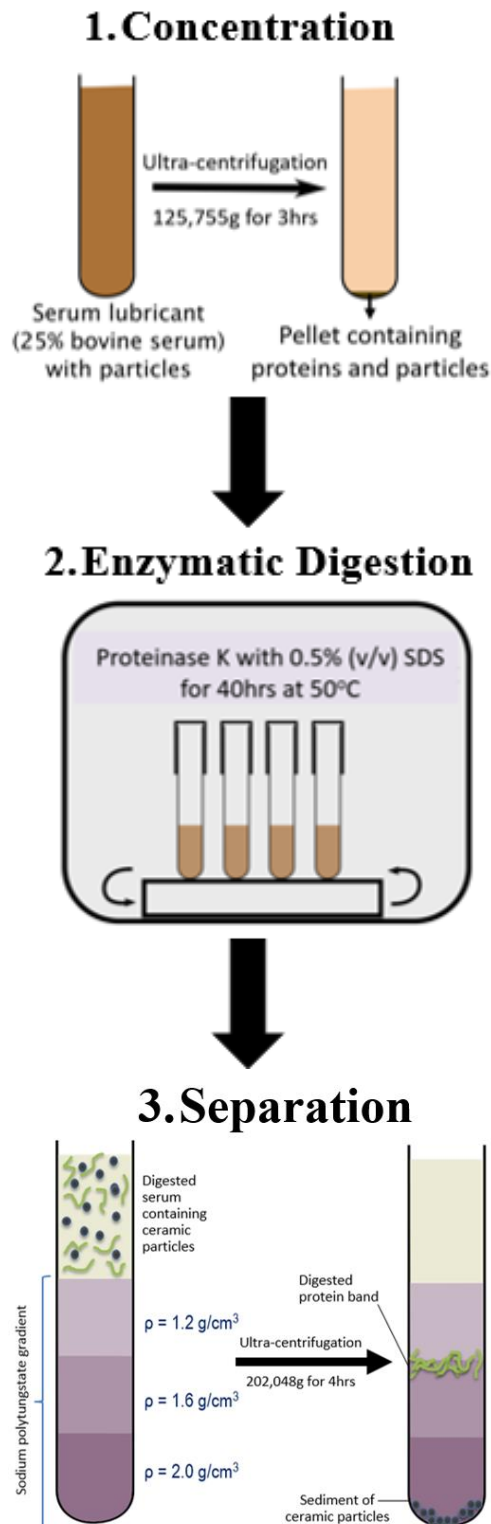


Figure 2.2 – The particle isolation technique described in three main steps; (1) concentration, (2) enzymatic digestion and (3) separation. The concentration step involves reducing the sample volume by concentrating the particulate matter in the serum lubricant. Thereafter the concentrated pellet of particles and proteins is digested using proteolytic enzymes before separating the particles from the digested proteins using density-gradient ultra-centrifugation in the isolation step (Lal et al., 2016).

2.3.3.4 Particle isolation methodology

All solutions used within this study were filtered using 20 nm Whatman[®] Anodisc membrane filters (GE Whatman, UK) to minimise contamination by external impurities.

2.3.3.4.1 Pre-treatment of the centrifuge tubes

All centrifuge tubes were pre-treated with siliconising fluid surfactant using lint free wipes and tweezers. Specifically, lint-free wipes were immersed in the surfactant before wiping the inside of the tubes. This was done twice before wiping away the excess with a dry lint-free wipe. The coating was set by rinsing the tubes with methanol (maximum volume capacity of the tube) before finalising the pre-treatment by rinsing the tubes with non-pyrogenic water. The purpose of the coating was to prevent adhesion of the ceramic particles to the sides and bottom of the tube, hence minimising particles loss.

2.3.3.4.2 Concentration of particles using centrifugation

Since CoC bearings exhibit extremely low wear, a centrifugation step (Beckman Optima L-90K ultra-centrifuge and SW-32 rotor) at 125,755g for 3 hours at 25°C, preceded the enzymatic digestion to concentrate the ZTA ceramic model particles and proteins present in the 25% (v/v) FBS. The supernatant was carefully removed by aspiration leaving behind a volume of 3ml to re-suspend the pellet, which was located at the bottom of the tube. Centrifugation speeds and times were calculated based on the Stokes law equations; particle sedimentation:

Equation 2

$$V_t = \frac{gd^2(\rho_p - \rho_m)}{18\mu}$$

In Equation 2, 'g' is acceleration of gravity, 'd' is particle diameter, 'pp' is density of particle, 'pm' is density of medium and 'μ' is viscosity of medium was used to calculate the terminal velocity (Vt), which in turn was used to calculate the time it took the particles to travel the length of the centrifuge tube. For instance, during the concentration step, the serum lubricant was centrifuged at 125,755g using a Beckman Coulter SW32Ti rotor. Based on the centrifugal sedimentation calculations, the time required to cover the distance of 89mm (maximum displacement of particles in SW-32 tubes) for 20nm sized particles would be 2 hours and 31 minutes. However, centrifugation was carried out for 3 hours, which was theoretically sufficient to completely sediment all particles >18nm.

2.3.3.4.3 Enzymatic digestion

The concentrated pellet of particles and proteins from the 25% (v/v) FBS spiked with ZTA particles was subsequently re-suspended in 500 μ l of HEPES buffer (working concentration 0.1M) and digested with 250 μ l of 20mg.ml⁻¹ proteinase-K (working concentration 1mg.ml⁻¹) at 50°C for 18 hours in the presence of 0.5% (w/v) sodium dodecyl sulphate (SDS) and 3mM calcium chloride. During incubation, the tubes were shaken at 320 rpm using the PSU-10i orbital shaker. After digestion, the particle solution was sonicated for 10 minutes before the enzymatic digestion was repeated by the addition of proteinase K (working concentration (1mg.ml⁻¹) and the samples were incubated for a further 22 hours at 50°C, whilst being shaken at 320 rpm.

2.3.3.4.4 Separation of proteins from particles

Sodium polytungstate (SPT) gradients were prepared by sequentially layering 60% (v/v) SPT ($\rho=2.0$ g/cm³), 40% (v/v) SPT ($\rho=1.6$ g/cm³) and 20% (v/v) SPT ($\rho=1.2$ g/cm³) in thin wall Polypropylene 14ml tubes. After 40 hours of enzymatic digestion, the digest was sonicated for 10 minutes before it was dispensed slowly on top of the sodium polytungstate density gradient. The tubes were then filled to the top of the tube with sterile water. The samples were centrifuged (Beckman Optima L-90K ultra-centrifuge and SW40 rotor) at 202,048g for 4 hours at 25°C. After centrifugation, the particles were collected at the bottom of the tube in the form of a pellet, whilst the proteins fragments and other impurities with lower density remained higher up the tube. The supernatant was slowly aspirated and discarded, and the pellet of particles was re-suspended in 1ml of sterile water and sonicated for 10 minutes before being transferred to clean pre-coated (section 2.3.3.4.1) centrifuge tubes (14ml, Thinwall Polypropylene, Beckman, UK). The transfer step was repeated three times to ensure all the particles were transferred to the clean tube.

2.3.3.4.5 Washing of the recovered particles

The recovered particles were then washed three times in sterile water using Beckman Optima L-90K ultra-centrifuge and SW40 rotor at 154,693g for 1 hour at 37°C. Between each wash, the supernatant was collected and the particles were re-suspended in sterile water before sonication for 10 minutes.

2.3.3.5 Gravimetric measurements of the recovered particles

After washing, the recovered particles were re-suspended in 1ml of sterile water and sonicated for 10 minutes before being transferred to pre-weighed sterile glass vials. This transfer step was repeated three times to ensure all the particles were transferred to the glass vial. The weight of each glass vial was measured three times using the X205 balance (sensitive to 10^{-5} grams) ensuring each reading was within $10\mu\text{g}$ of each other to produce a mean weight of each glass vial. The balance was zeroed if necessary, between each repeat. Thereafter the glass vial was heat treated for 4 hours at 190°C to remove the water from the particles. The glass vial was then weighed gravimetrically to obtain the recovery rate of the ZTA particles using the same technique as described above.

2.3.3.6 Characterisation of the recovered ZTA particles

The isolated ZTA ceramic model particles were re-suspended in sterile water, filtered onto $0.015\mu\text{m}$ filter membranes and analysed using CFE-SEM as described in section 2.3.3.2.2.

2.3.3.7 Statistical analysis

Statistical differences in the particles size distributions, aspect ratio values and circularity values before and after the isolation process were tested using an Independent Samples T-Test (SPSS Statistics Version 24, IBM Corp. USA). The tests were carried out on the original un-binned data for increased accuracy.

2.3.4 Application of validated novel particle isolation method to hip simulator serum

The validated method was subsequently applied to a range of hip simulator serum lubricant samples (25% (v/v) foetal calf serum (FCS), supplemented with 0.03% (v/v) sodium azide to inhibit bacterial growth) provided by Dr Mazen Al-Hajjar (School of Mechanical Engineering, University of Leeds), which was collected from a previous wear test on the Leeds MkII hip simulator, which were stored at -20°C . The method was initially applied to two serum samples, which were collected at the 3 million cycles (Mc) time point (2-3Mc) and contained a reported volume of 0.01mm^3 and 0.85mm^3 , of ceramic wear debris generated from 36mm BIOLOX[®] Delta ceramic-on-ceramic bearings under standard gait or severe microseparation conditions, respectively. The severe microseparation condition was similar to that as previously described by Nevelos et al. (2000) and Stewart et al. (2001).

The serum was thawed in a water bath at 37°C and sonicated for 10 minutes before three aliquots of 38ml from each sample were subjected to the particle isolation method described in section 2.3.3.4. The recovered particles were analysed using CFE-SEM, as described in section 2.3.3.2.2.

2.3.5 Optimisation of the novel particle isolation method

Further optimisation of the digestion regime was required to isolate the particles from the serum proteins. The incorporation of papain and other enzymes that breakdown the cell wall of bacteria e.g. lysozyme was investigated to improve the efficiency of protein removal from the wear particles.

2.3.5.1 Incorporation of papain enzymatic digestion

The efficacy of the digestion was assessed using serum from 36mm cobalt-chromium metal-on-metal hip replacements tested under high inclination angle (65°) and microseparation conditions. The serum (stored at -18°C) was provided by Dr Mazen Al-Hajjar (School of Mechanical Engineering, University of Leeds), which was collected from 2.33 Mc time point and contained a reported volume of 4.05mm³ metal wear debris. The rationale for using serum with MoM wear debris was because unlike the ceramic wear particles, the black colour of the metal wear debris permitted easier visualisation of the wear debris during the isolation process.

The serum was thawed in a water bath at 37°C and sonicated for 10 minutes before three aliquots of 38ml were taken and concentrated using the method described in section 2.3.3.4.2. Thereafter, the supernatant was discarded and the pellet was digested with papain at a working concentration of 0.21mg.ml⁻¹ in 9mM TCEP in MOPS (pH 6.5) at 55°C for 3 hours. This was repeated in total for three times, whereby the third addition of papain was followed by overnight incubation at 55°C (Brown et al., 2007). The digested particle solutions were centrifuged at 125,755g using a Beckman Coulter SW32Ti rotor. Thereafter, the supernatant was discarded and the remainder of the particle isolation was performed in the same manner as described in section 2.3.3.4.3-2.3.3.4.5. Briefly, the pellet was digested with 20mg.ml⁻¹ proteinase-K (working concentration 1mg.ml⁻¹) at 50°C for 40 hours in the presence of 0.5% (w/v) sodium dodecyl sulphate (SDS) and 3mM calcium chloride. After 40 hours of enzymatic digestion, the digest was sonicated for 10 minutes before it was dispensed slowly on top of the sodium polytungstate density gradient. The samples were centrifuged (Beckman Optima L-90K ultra-centrifuge and SW40 rotor) at 202,048g for 4 hours at 25°C. After centrifugation, the particles were collected at the bottom of the tube in the form of a pellet, whilst the protein fragments and other impurities with lower density remained higher up the tube. The supernatant was slowly aspirated and discarded, and the recovered particles were then washed three times in sterile water using Beckman Optima L-90K ultra-centrifuge and SW40 rotor at 154,693g for 1 hour at 37°C. Between each wash, the supernatant was collected and the particles were re-suspended in sterile water before sonication for 10 minutes. Following this, samples were then filtered onto 0.015µm filter membranes and analysed using CFE-SEM as detailed in section 2.3.3.2.2.

2.3.5.2 Incorporation of lysozyme enzyme

The efficacy of the digestion was assessed using serum from 36mm CoC BIOLOX® Delta bearings tested under severe edge loading conditions that caused dynamic separation due to high cup inclination angle (65°) and 4mm translational mismatch in the centres of rotation of the femoral head and acetabular cup. The lubricant serum (stored at -18°C) was provided by Dr Mazen Al-Hajjar (School of Mechanical Engineering, University of Leeds), which was collected from one million cycles of testing on the hip simulator (0-1 Mc), and contained a reported volume of 0.98mm³ ceramic wear debris.

The serum was thawed in a water bath at 37°C and sonicated for 10 minutes before two aliquots of 38 ml were taken and concentrated using the method described in section 2.3.3.4.2. One aliquot was processed through the standard method described in section 2.3.3.4. However, after the enzymatic digestion with proteinase-K, aliquot two was concentrated at 125,755g for 3 hours at 25°C, the supernatant was discarded and the pellet was digested with freshly prepared lysozyme (20mg.ml⁻¹ in 10mM Tris-HCl, pH 8.0) in the presence of STET (Saline/Tris/EDTA/Triton) buffer (10 mM Tris-HCl, pH 8.0, with 0.1 M NaCl, 1 mM EDTA, and 5% (v/v) Triton X-100) at a working concentration of 10mg.ml⁻¹. Lysozyme hydrolyses linkages between N-acetylmuramic acid and N-acetyl-D-glucosamine residues in peptidoglycan and between N-acetyl-D-glucosamine residues in chitodextrin. Gram-positive bacteria are more susceptible to this hydrolysis due to the high proportion of peptidoglycan in their cell walls. (Osserman, 2012). After incubation, the tube containing the lysis mixture was placed in boiling water for exactly 40 seconds. Thereafter both samples were subjected to density gradient ultra-centrifugation and washing as described in section 2.3.3.4. Following this, the samples were washed with sterile water, filtered onto a 0.015µm filter membrane and then analysed using CFE-SEM as detailed in section 2.3.3.2.2.

2.3.6 Particle isolation from serum lubricants produced from one million cycles of hip simulation

Gaiters made of silicon were used to hold the 25% (v/v) FCS lubricant during wear simulation and have a volume capacity of approximately 500ml. The serum lubricant is changed every 330,000 cycles, as a result approximately 1.5L of serum lubricant is produced for every million cycles of simulation. Due to the extremely low volume of ceramic wear debris generated from BIOLOX® Delta CoC bearings (0.1-1mm³/million cycles), the entire batch of serum from one million cycles was processed using the optimised digestion protocol (2.3.5.2). This approach was taken to manipulate the volume of the wear particles by pooling together the concentrated pellets obtained from serum concentration steps in order to increase the volume of wear debris. The sample of lubricant serum (stored at -18°C) was provided by Dr Mazen Al-Hajjar (School of Mechanical Engineering, University of Leeds), which was

collected from one million cycles of testing on the hip simulator (0-1 Mc), and contained a volume of 1.29mm³ of BIOLOX[®] Delta ceramic wear debris. The ceramic wear debris were generated from 36mm CoC BIOLOX[®] delta bearings tested under severe edge loading conditions due to by dynamic separation due to high cup inclination angle (65°) and 4mm translational mismatch in the centres of rotation of the femoral head and acetabular cup.

The serum lubricant from one million cycles of hip simulator testing was thawed in a water bath at 37°C and sonicated for 10 minutes before aliquots of 38ml were taken and concentrated by centrifugation using the method described in section 2.3.3.4.2. This was repeated until all (approximately 1.5L) of the serum lubricant had been concentrated. Thereafter the concentrated pellets were processed through the standard method described in section 2.3.3.4. However, after the enzymatic digestion with proteinase-K, the samples were pooled together in six tubes and concentrated at 125,755g for 3 hours at 25°C. The supernatant was discarded and the pellets were digested with freshly prepared lysozyme (20mg.ml⁻¹) by the method described in section 2.3.5.2. Thereafter, all the samples were subjected to density gradient ultra-centrifugation as described in section 2.3.3.4. Following this, the thick band of protein along with the rest of the supernatant was removed, before the particles collected at the base of the tube were resuspended in water, sonicated for 10 minutes and transferred to clean tubes for washing with sterile water as described in section 2.3.3.4.5. During the transfer step, the six tubes were pooled into two tubes. During the washing steps a pellet was observed, which was filtered onto a 0.015µm filter membrane and then analysed using CFE-SEM as detailed in section 2.3.3.2.

2.3.6.1 Isolation of metal particle contaminants using a magnet

Due to the presence of stainless-steel wear particle contaminants in the lubricant serum containing ceramic wear debris, an attempt was made to remove or minimise the stainless-steel wear particles using a magnet. The particle suspension from section 2.3.6 was added to a clear polypropylene tube, which was placed on top of a powerful magnet (Miltenyi Biotec Ltd). The particle suspension was immediately removed using a p1000 Gilson pipette, leaving behind the magnetic metal particles. This step was repeated three times whereby a clean clear polypropylene tube was used each time. The particle suspension was then filtered onto a 0.015µm filter membrane and analysed using CFE-SEM as detailed in section 2.3.3.2.

2.3.7 Particle isolation using two-step digestion and density gradient ultra-centrifugation

Particle isolation from the entire volume of lubricant serum produced from one million cycles on the hip simulator serum became necessary due to the extremely low volumes of ceramic wear debris present in serum lubricant. However, this presented a large protein burden on the nano-scale particles, whereby it was hypothesised that the protein adsorption layer, otherwise

known as the protein corona that forms on the surface of colloidal nano-scale particles was changing their intrinsic density, thus inhibiting particle sedimentation during density gradient ultra-centrifugation. For this reason, a two-step digestion protocol followed by density gradient purification was devised, which theoretically allowed the sedimentation of the nano-scale particles with attached proteins during the initial modified density gradient ultra-centrifugation step. The density of the SPT layers in the initial density gradient ultra-centrifugation step were changed in that the density ($\rho=1.1\text{g/cm}^3$) of the bottom layer was less than the average density ($\rho=1.22\text{g/cm}^3$) of proteins (Quillin and Matthews, 2000). This would theoretically allow the nano-scale particles to pellet with the attached proteins after the initial density gradient ultra-centrifugation step. The recovered particles would then be subjected to further enzymatic digestion and purification.

The hip simulator serum lubricant (stored at -18°C) was provided by Oscar O'Dwyer Lancaster Jones (School of Mechanical Engineering, University of Leeds), which was collected from one million cycle's (0-1Mc) of testing on the hip simulator and contained a volume of 1.58mm^3 of ceramic wear debris. The wear debris were generated from 36mm CoC BIOLOX[®] Delta bearings tested under severe edge loading conditions due to by dynamic separation due to high cup inclination angle (65°) and 4mm translational mismatch in the centres of rotation of the femoral head and acetabular cup.

The serum lubricant from one million cycles of hip simulator testing was thawed in a water bath at 37°C and sonicated for 10 minutes before aliquots of 38 ml were taken and concentrated by centrifugation using the method described in section 2.3.3.4.2. This was repeated until all the approximately 1.5L of serum was concentrated. Thereafter, the concentrated pellets were processed through the standard method described in section 2.3.3.4. However, after the 18 hours enzymatic digestion step with proteinase-K, the samples were pooled together in six tubes and concentrated at 125,755g for 3 hours at 25°C . The supernatant was discarded and the pellets were digested with freshly prepared lysozyme by the same method described in section 2.3.5.2. Thereafter, the samples were pooled together in two tubes and concentrated at 125,755g for 3 hours at 25°C . The supernatant was discarded and the pellets were digested with proteinase K for 22 hours as described in section 2.3.3.4.3. Subsequently, the particles were separated from the proteins via density gradient ultra-centrifugation as described in section 2.3.3.4.4. However, the density of the gradient layers was modified in this step whereby sodium polytungstate (SPT) gradients were prepared by sequentially layering 45% (v/v) SPT ($\rho=1.5\text{g/cm}^3$), 39% (v/v) SPT ($\rho=1.3\text{g/cm}^3$) and 33% (v/v) SPT ($\rho=1.1\text{g/cm}^3$) in thin walled polypropylene 14ml tubes. Following this, the band of protein was first carefully aspirated, before discarding the rest of the supernatant. The particles collected at the base of the tube were then re-suspended in water, sonicated for 10 minutes and transferred to clean tubes for washing as described in section 2.3.3.4.5. The

isolated particles were only washed once before commencing a further enzymatic digestion for 40 hours using proteinase K at a working concentration of 2 mg/ml following the method described in section 2.3.3.4.3. An additional dose of proteinase (working concentration of 2 mg.ml⁻¹) was added after 18 hours. Thereafter, both the samples were subjected to the original density gradient ultra-centrifugation as described in section 2.3.3.4.4. Following this, the band of separated protein was carefully aspirated, before discarding the rest of the supernatant. The particles collected at the base of the tube were re-suspended in water, sonicated for 10 minutes and transferred to clean tubes for washing as described in section 2.3.3.4.5. During the washing steps, a pellet was observed for both samples, which was filtered onto a 0.015µm filter membrane and then analysed in terms of size, composition and morphology using CFE-SEM as detailed in section 2.3.3.2. EDX analysis was used to identify the elemental composition of every particle imaged to ensure that the particles being measured were indeed ceramic i.e. particles that showed aluminium (Al) and zirconia (Zr) and/or strontium (Sr) peaks were imaged and subsequently measured using Image J software. This technique minimised the incorrect measurement of contaminating particles, which may otherwise have the same geometry/morphology as ceramic particles and therefore be indistinguishable.

In order to obtain three replicates, the two-step particle isolation protocol was repeated on two more samples of serum lubricants (stored at -18°C) that contained 1.93mm³ and 1.65mm³ of ceramic wear debris generated from 36mm CoC BIOLOX[®] Delta bearings tested under severe edge loading conditions due to by dynamic separation due to high cup inclination angle (65°) and 4mm translational mismatch in the centres of rotation of the femoral head and acetabular cup. The serum lubricant was collected from one million cycle's testing on the hip simulator by Oscar O'Dwyer Lancaster Jones (School of Mechanical Engineering, University of Leeds).

2.4 Results

2.4.1 Validation of sensitivity for the novel particle isolation method

2.4.1.1 Particle recovery rates for the isolation method using serum spiked with ZTA ceramic model particles

The particle isolation method was validated for sensitivity and repeatability by determining the recovery rates of different volumes (0.05-5mm³) of ZTA ceramic model particles which had been spiked into 25% (v/v) FBS. The measured weights of the ZTA particles for different volumes used in this study are shown in Table 2.6. The variability in the weights was due to difficulties in accurately measuring such small weights. The serum spiked with ZTA powder was then processed through the novel particle isolation method and the mass of the recovered ZTA model particles was measured gravimetrically in order to determine the particle recovery rates. The spiked and recovered masses for the different volumes of ZTA particles is shown in Figure 2.3. For the control sample, a recovered mass of 0.02 mg was measured. The percentage particle recovery rates for the novel method are presented in Figure 2.4. The control sample generated an average recovery rate of 0% from the non-spiked 25% (v/v) FBS. The high volumes (0.5-5mm³) of ZTA particles had a percentage particle recovery rate ranging between 93-96%. The lowest volumes of ZTA particles (0.1 and 0.05 mm³), which are representative of the wear rates of CoC bearings, both demonstrated an average percentage recovery rate of approximately 89%.

Table 2.6 – Weights of the ZTA powder for each particle volume.

	Volume of ZTA particles					
Repeat	5mm ³	1mm ³	0.5mm ³	0.1mm ³	0.05mm ³	Control
i	25.18mg	5.24mg	2.50mg	0.54mg	0.28mg	0mg
ii	25.25mg	5.08mg	2.52mg	0.52mg	0.28mg	0mg
iii	25.09mg	4.94mg	2.52mg	0.55mg	0.25mg	0mg
Average	25.17mg	5.09mg	2.51mg	0.54mg	0.27mg	0mg
±95% CL	0.20	0.37	0.03	0.04	0.04	0.00

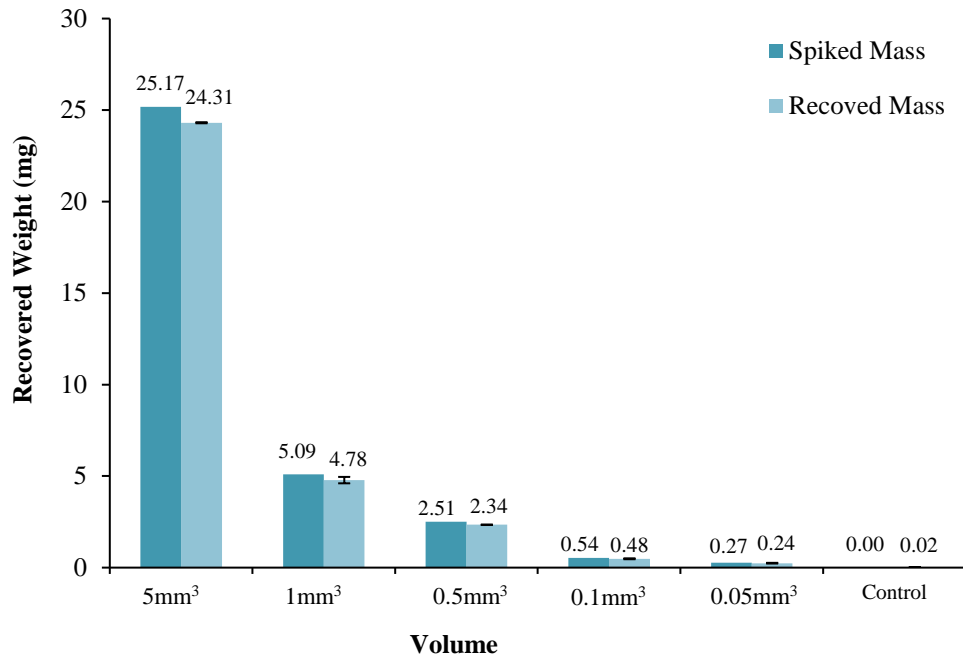


Figure 2.3- The spiked and recovered masses for the different volumes of ZTA ceramic model particles isolated using the novel particle isolation method. Each sample was performed in triplicate (n=3). The values are expressed as mean and the error bars represent \pm standard deviations.

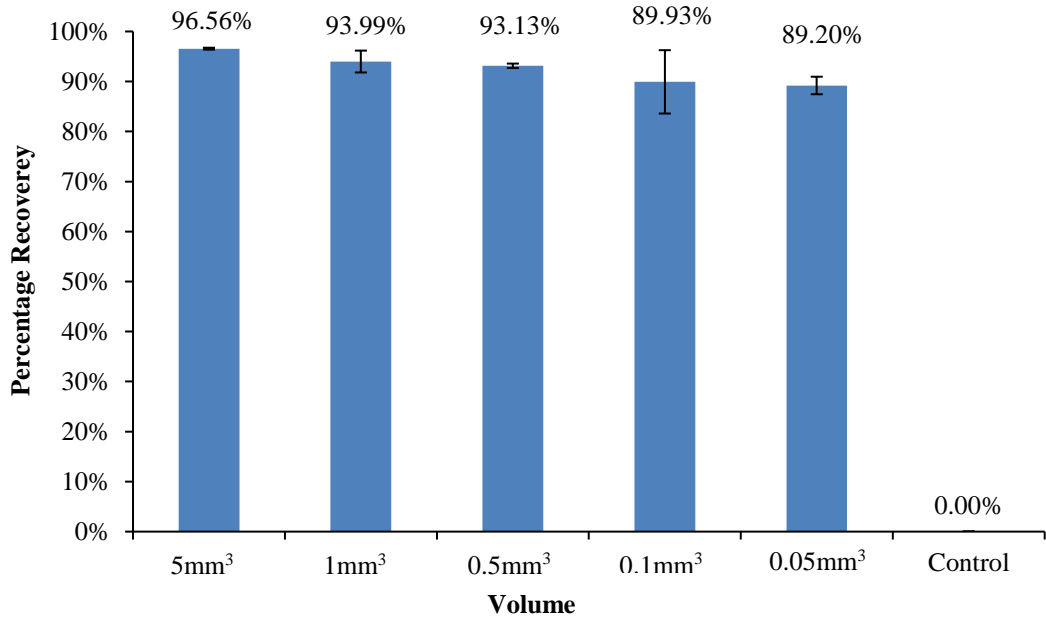


Figure 2.4- The percentage particle recovery rates of the different volumes of ZTA ceramic model particles isolated using the novel particle isolation method. Each sample was performed in triplicate (n=3). The values are expressed as mean and the error bars represent \pm standard deviations.

2.4.2 Characterisation of ZTA ceramic model particles before and after isolation

The characteristics in terms of size and morphology, and the composition of the ZTA particles before and after isolation from spiked 25% (v/v) FBS were determined and analysed after filtration on 0.015 μ m filter membrane using CFE-SEM and EDX analysis as described in section 2.3.3.2.2. Image analysis software (ImageJ version 1.49) was used to measure the Feret diameter (d_{max}), aspect ratio and circularity of the particles (minimum of 150 particles).

CFE-SEM analysis of the ZTA ceramic model particles revealed larger micrometre particles that had a polygonal shard-like morphology. The smaller nano-scale particles were round in morphology and existed as large agglomerates (Figure 2.5). EDX analysis of the larger irregular/shard-like micron and sub-micron sized particles shown in Figure 2.6 were comprised of alumina or zirconia as indicated by EDX analysis that showed elemental peaks of Al (aluminium), O (oxygen) and Zr (zirconia). The nano-scale particles mainly consisted of zirconia as indicated by EDX analysis that showed elemental peaks of Zr (zirconia), Al (aluminium) and O (oxygen). Furthermore, a peak of Na (sodium) and W (tungsten) was observed due to the sodium polytungstate density gradient medium during the isolation process. The carbon (C) peak that can be seen in all EDX spectra was due to the carbon coating and polycarbonate membrane.

The mean feret diameter, mean aspect ratio and mean circularity values (value of 1.0 indicates a perfect circle) are shown in Table 2.7. An independent-samples t-test was conducted to compare the size distribution (feret diameter) and morphology (aspect ratio and circularity) of ZTA ceramic model particles before and after isolation. The morphology of the particles was unaffected by the isolation process, as there were no significant differences in the aspect ratio and circularity values before and after the isolation process (Table 2.7). Moreover, there was no significant difference in size distribution of the ZTA ceramic model particles before and after isolation from 25% (v/v) FBS. The frequency as a function of size of the ZTA ceramic model particles before and after isolation is presented in Figure 2.7, which revealed a bimodal size distribution. Before isolation, the larger micron and submicron size particles ranged between 100-9915nm with a mean size of $2655.09 \pm 267.27\text{nm}$, whereas the small nano-scale particles ranged between 10-80nm with a mean size of $38.43 \pm 1.49\text{nm}$. After isolation, the larger micron and submicron size particles ranged between 100-8834nm with a mean size of $2993.88 \pm 254.21\text{nm}$, whereas the small nano-scale particles ranged between 10-80nm with a mean size of $44.30 \pm 1.61\text{nm}$. The ZTA particles before isolation had a mode size distribution of 2000-3000nm for the larger particles and a mode size of 30-40nm for the small nano-scale particles, whereas the ZTA particles after isolation had a mode size distribution of 1000-2000nm for the larger particles and a mode size of 30-40nm for the small nano-scale particles.

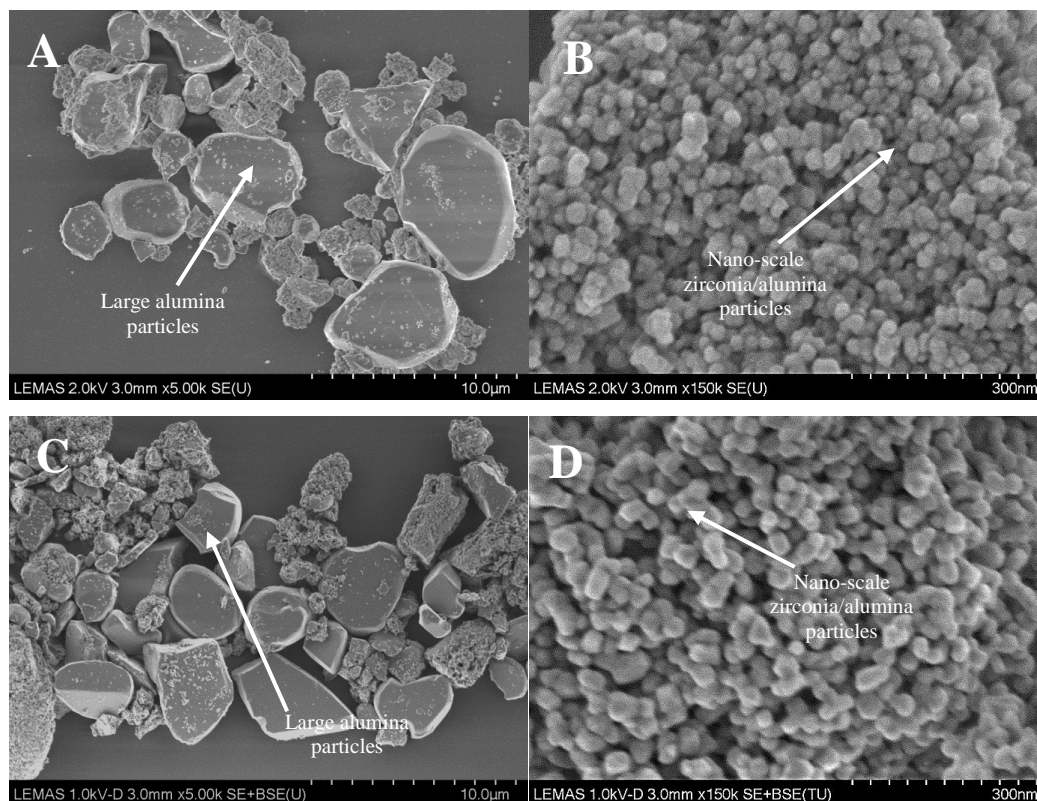


Figure 2.5 - CFE-SEM images of (A) larger micron size alumina particles and (B) smaller nano-scale zirconia/alumina particles before the particle isolation protocol. CFE-SEM images of (C) larger micron size alumina particles and (D) smaller nano-scale zirconia/alumina particles after the particle isolation protocol. The proteolytic digestion did not affect the size or morphology of the particles. The particles were imaged at 5K, 60K, 90K and 150K magnification at a 1-2kV voltage and at a working distance of 3mm.

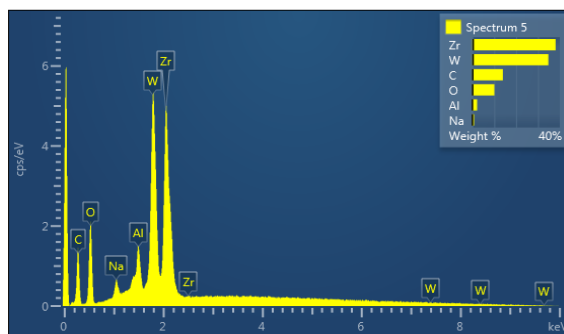
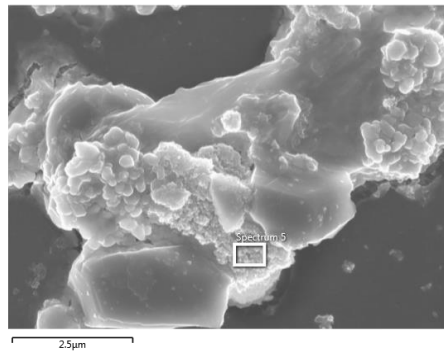
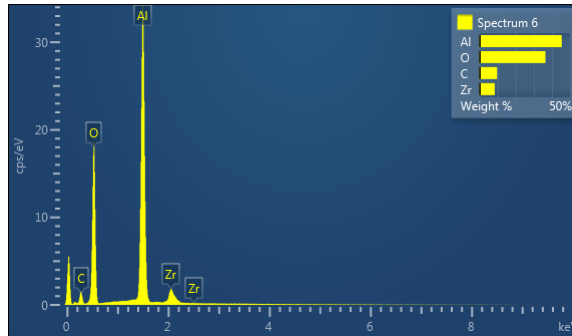
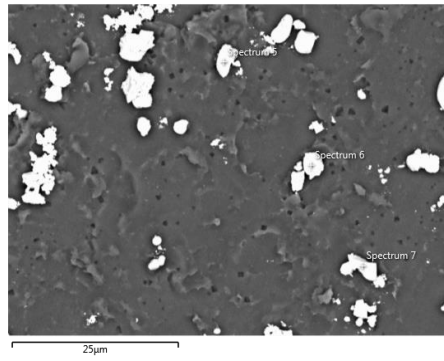


Figure 2.6 - EDX analysis of ZTA ceramic model particles (A) before particle isolation and corresponding EDX spectrum (B). EDX analysis of ZTA ceramic model particles (C) after particle isolation and (D) corresponding EDX spectrum. Pin-point or area selection analysis of the particles was performed at a working distance of 15mm, 10 kV and suitable magnification to maintain focus.

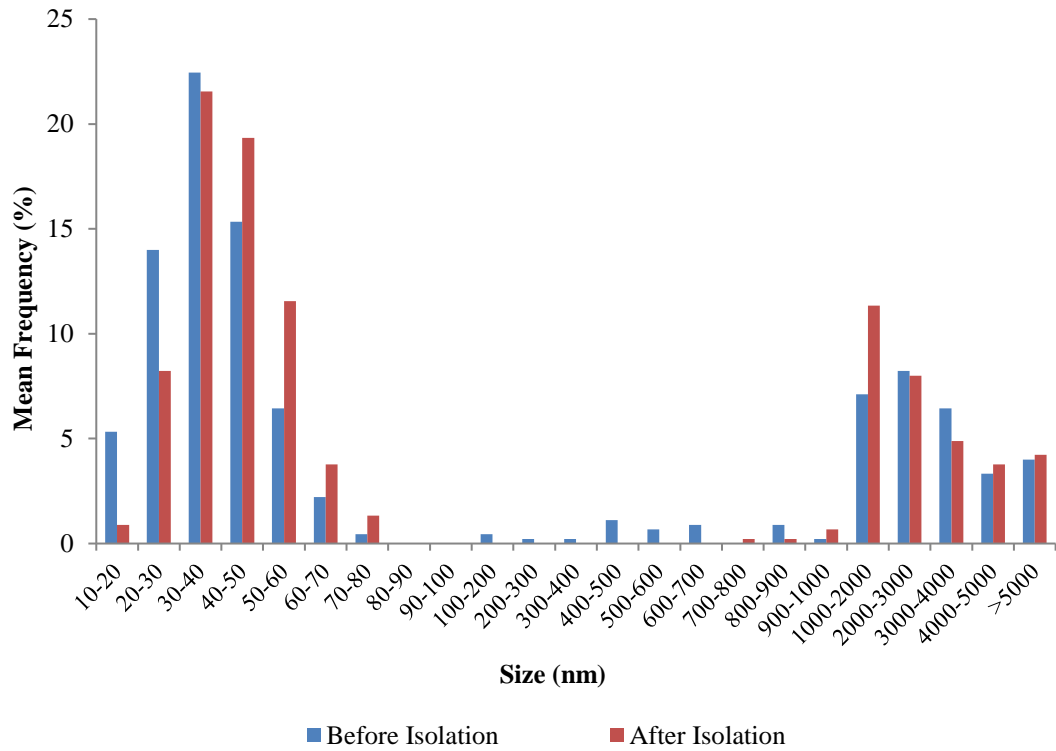


Figure 2.7 - Comparison of frequency size distribution of the ZTA particles before and after the particle isolation protocol. A minimum of 150 particles were measured.

Table 2.7 - Mean size (feret diameter) and morphology (aspect ratio and circularity) values for ZTA ceramic model particle before and after isolation.

	BEFORE ISOLATION; Larger particles (100 - >5000nm)	BEFORE ISOLATION; Smaller particles (0 - 100nm)	AFTER ISOLATION; Larger particles (100 - >5000nm)	AFTER ISOLATION; Smaller particles (0 - 100nm)
Feret diameter (nm)	2655.09 ± 267.27	38.43 ± 1.49	2993.88 ± 254.21	44.30 ± 1.61
Aspect ratio	1.48 ± 0.04	1.34 ± 0.24	1.44 ± 0.36	1.28 ± 0.13
Circularity	0.80 ± 0.01	0.93 ± 0.01	0.83 ± 0.09	0.92 ± 0.01

Note: All values expressed as mean ±95% Confidence Interval.

2.4.3 Application of validated particle isolation method to hip simulator lubricants

The validated method was subsequently applied to hip simulator lubricant serum containing a reported wear volume of either 0.01mm³ or 0.85mm³ of ceramic wear debris generated from 36mm BIOLOX[®] Delta ceramic-on-ceramic bearings under standard gait or severe microseparation conditions, respectively. The two serum samples were collected from 2-3 million cycles time point, from which three aliquots of 38ml was taken from each sample and subjected to the particle isolation method described in section 2.3.3.4. CFE-SEM and EDX analysis revealed that the recovered wear debris generated under standard gait conditions were nano-scale in size, and appeared as large (>5µm) agglomerates (Figure 2.8). EDX analysis showed elemental peaks of a range of elements including aluminium (Al), strontium (Sr), zirconia (Zr), oxygen (O), sodium (Na), sulphur (S), titanium (Ti), iron (Fe) and tungsten (W). The recovered wear debris generated under severe microseparation conditions was not adequately separated from the proteins (Figure 2.9), which made it very difficult to identify the ceramic wear debris. The proteins appeared as globular-like structures that had irregular morphology and covered a large proportion of the filter membrane. However, EDX analysis confirmed the particles within the proteins were indeed ceramic wear debris with elemental peaks of aluminium (Al), oxygen (O), zirconia (Zr), and strontium (Sr). Additionally, it was extremely difficult to identify the ceramic particles due to the inherently low volumes of ceramic wear debris present in the serum.

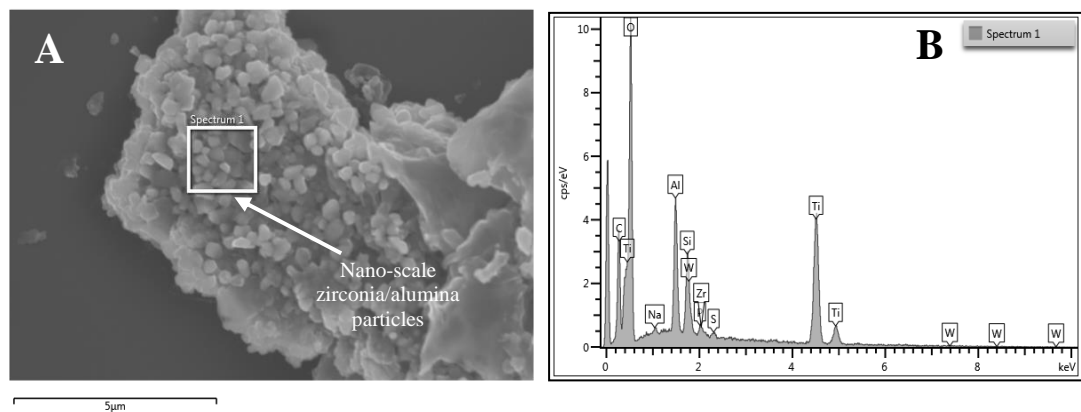


Figure 2.8 – (A) CFE-SEM image of particles isolated from CoC hip simulator lubricant tested under standard gait conditions and (B) corresponding EDX spectrum. The area selection tool was used to analyse the composition of the particles at a working distance of 15 mm and 10 kV and suitable magnification to maintain focus.

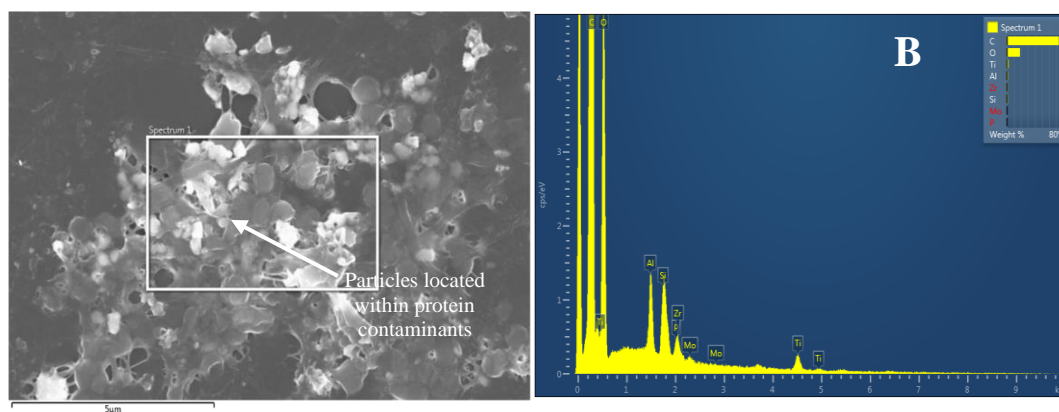


Figure 2.9 – (A) CFE-SEM image of particles isolated from CoC hip simulator lubricant tested under severe microseparation conditions and (B) corresponding EDX spectrum. The area selection tool was used to analyse the composition of the particles at a working distance of 15 mm and 10 kV and suitable magnification to maintain focus.

2.4.4 Optimisation of digestion regime for novel particle isolation method

The application of the particle isolation method developed by Lal et al. 2016 was not successful at recovering purified ceramic wear debris from hip simulator serum, which could be used for subsequent characterisation. This led to the optimisation of the method where numerous alterations were made to the digestion regime, whereby papain and lysozyme was incorporated into the digestion, the results of which are documented below.

2.4.4.1 Incorporation of papain enzyme digestion step

Papain was incorporated into the digestion regime to address the issue of inefficient proteolysis, which was observed in previous experiments (section 2.3.4) where the initial digestion method was applied. Lubricant containing cobalt-chrome wear debris generated from metal-on-metal total hip replacements in a hip simulator was used to assess the efficiency of the enzymatic digestion. Three aliquots of 38ml were taken and concentrated using the method described in section 2.3.3.4.2. The pellet of CoCr wear particles and concentrated proteins was initially digested with papain followed by proteinase K. Thereafter the remainder of the particle isolation was performed in the same manner as described in section 2.3.3.4.3-2.3.3.4.5. Post-density gradient ultra-centrifugation revealed that the metal wear debris did not form a pellet at the bottom of the tube, instead the debris formed a band at the interface between the bottom two layers of the SPT density gradient (Figure 2.10). CFE-SEM analysis of the wear debris recovered from the band of CoCr wear particles located between the 2x and 4x SPT layers, revealed that the particles were nano-scale in size and round in morphology (Figure 2.11A). However, the CoCr nano-particles were highly agglomerated and contaminated with proteins (Figure 2.11B).

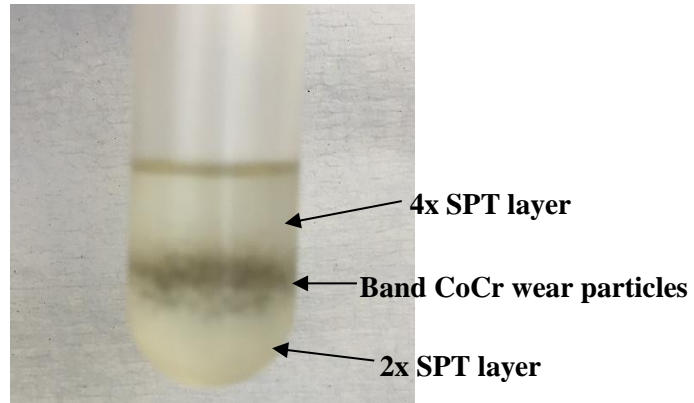


Figure 2.10 - Formation of a band of CoCr wear debris at the interface between the bottom two layers of the SPT density gradient after ultra-centrifugation. The digested serum containing CoCr wear debris generated from MoM bearings was centrifuged on a SPT gradient at 40,000 rpm (average RCF 202,048g) for 4 hours at 25°C.

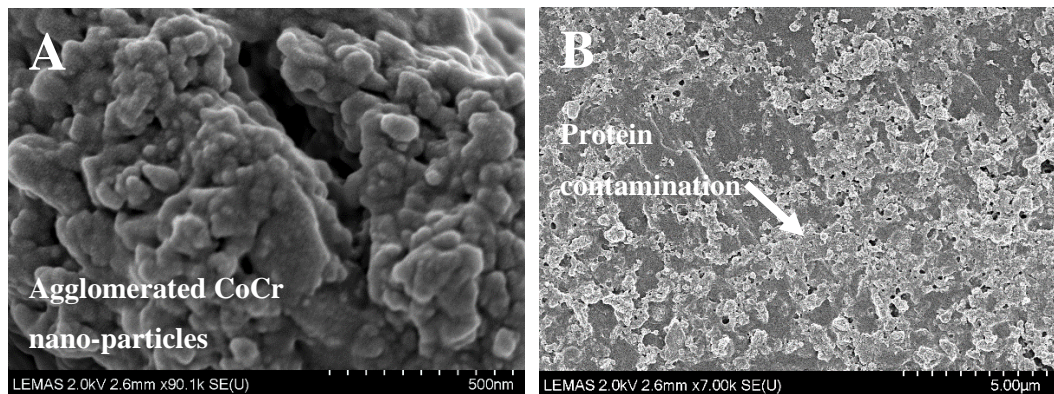


Figure 2.11 - CFE-SEM images of CoCr nano-particles isolated from the band of CoCr wear debris separated using density gradient ultra-centrifugation. (A) The CoCr wear particles were nano-scale in size and round in morphology. (B) The recovered CoCr nano-particles were heavily contaminated with proteins. The particles were imaged at 7-90K magnification at 2kV voltage and at a working distance of 2-3mm.

2.4.4.2 Incorporation of lysozyme enzyme

Lysozyme enzyme was incorporated into the digestion regime to target the breakdown of bacterial proteins, which may have contaminated the serum lubricant during wear simulation testing. Lubricant containing ceramic wear debris generated from 36mm CoC BIOLOX[®] Delta bearings tested under severe edge loading conditions due to dynamic separation due to high cup inclination angle (65°) and 4mm translational mismatch in the centres of rotation of the femoral head and acetabular cup was used to assess the efficiency of the lysozyme digestion. Six aliquots of 38ml were taken and concentrated using the method described in section 2.3.3.4.2. Three aliquots were processed through the standard method described in section 2.3.3.4. However, after the enzymatic digestion with proteinase-K, the other three aliquots were digested with freshly prepared lysozyme (section 2.3.5.2). Thereafter both sets of samples were subjected to density gradient ultra-centrifugation and washing as described in section 2.3.3.4. SEM analysis of the recovered wear particles subjected to this digestion revealed that the filter membrane had lower levels of contaminating proteins (Figure 2.12A)

compared to the standard method, which had large areas of the filter membrane covered with proteins (Figure 2.12B).

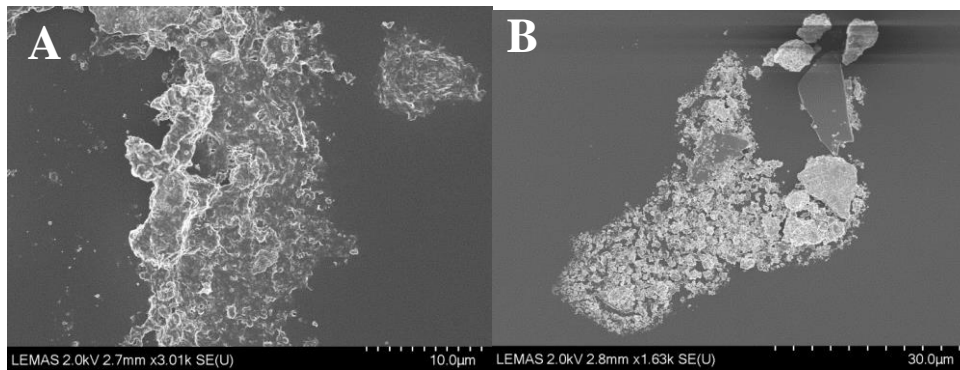


Figure 2.12 - CFE-SEM images of BIOLOX[®] Delta ceramic wear particles (A) standard digestion method and (B) standard digestion method with lysozyme digestion. Lower levels of protein contamination were observed on the filter membrane that incorporated lysozyme digestion. The particles were imaged at 2kV voltage, working distance of 2-3mm and 1-3k magnification.

2.4.5 Application of optimised method to hip simulator lubricants collected from one million cycles (0-1Mc)

Due to the extremely low volume of ceramic wear debris present in the lubricant serum, the entire batch of serum lubricant collected from one million cycles (0-1Mc) was processed using the particle isolation method. Three different serum lubricant samples were used that were provided by Dr Mazen Al-Hajjar, which were collected from one million cycles (0-1Mc) time point and contained a volume of 1.29mm³ BIOLOX[®] Delta ceramic wear debris. The ceramic wear debris were generated from 36mm CoC BIOLOX[®] Delta bearings tested under severe edge loading conditions created by dynamic separation due to high cup inclination angle (65°) and 4mm translational mismatch in the centres of rotation of the femoral head and acetabular cup.

All the serum lubricant from one million cycles (0-1Mc) of hip simulator testing was concentrated in aliquots of 38ml by centrifugation using the method described in section 2.3.3.4.2. Thereafter the concentrated pellets were processed through the standard method described in section 2.3.3.4, with the additional lysozyme step that preceded density gradient ultra-centrifugation. After density gradient ultra-centrifugation, it was clear that the digested protein was successfully separated, as a thick band of protein was formed above the third layer of the SPT (Figure 2.13). During the washing step, it became visibly apparent that a large volume of wear particles was recovered from the hip simulator lubricant (Figure 2.14). CFE-SEM analysis of the recovered wear debris revealed large irregular-shaped particles that were up to 50µm in size. High magnification revealed these larger particles were comprised of smaller nano-particles. EDX analysis revealed these larger particles may be stainless-steel as they had a high percentage composition of iron, as confirmed by the Fe (iron) elemental peaks in the EDX spectrum (Figure 2.15).

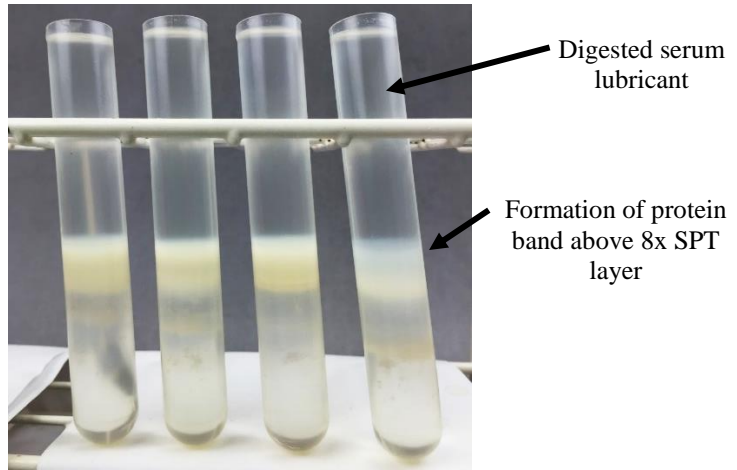


Figure 2.13 - Centrifuge tubes containing digested serum lubricant on top of the SPT density gradient layers. The arrow is pointing at the separated band of digested protein after density gradient ultra-centrifugation. The digested proteins containing ceramic wear particles was centrifuged at 202,048g.

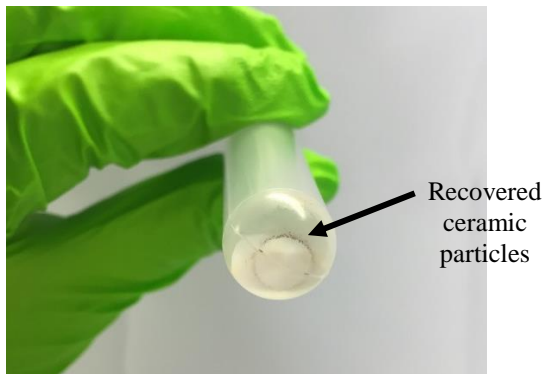


Figure 2.14 - Particles recovered from hip simulator lubricant that was collected from one million cycles of testing (0-1Mc). The serum lubricant contained a volume of 1.29mm³ BIOLOX[®] delta ceramic wear debris generated from 36mm BIOLOX[®] Delta CoC bearings tested under severe edge loading conditions due to dynamic separation due to high cup inclination angle (65°) and 4mm translational mismatch in the centres of rotation of the femoral head and acetabular cup.

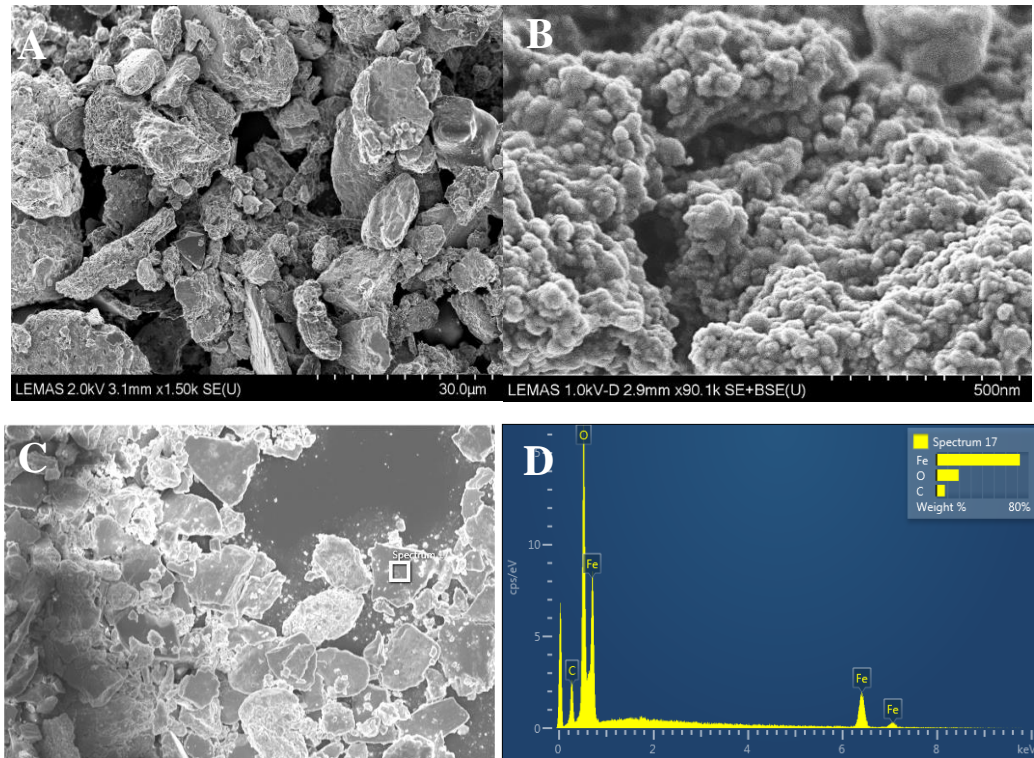


Figure 2.15 CFE-SEM analysis of the recovered particles from hip simulator lubricant that was collected from one million cycles of testing (0-1Mc). (A) Large irregular shaped particles, (B) Small nano-scale particles that constituted the large particles, (C) Image of particles analysed using EDX and (D) corresponding EDX spectrum). The particles were imaged at 1kV (deceleration mode) voltage, working distance of 2-3mm and 1.5-90k magnification. Area selection EDX analysis of the particles was performed at a working distance of 15mm, 10kV and a suitable magnification to maintain focus.

2.4.5.1 Separation of stainless-steel wear particle contaminants from ceramic wear debris

A magnet was used to attempt to separate the stainless-steel particles from the ceramic particles. CFE-SEM analysis of the particles recovered from serum lubricant described in section 2.4.5, revealed an abundance of stainless-steel wear particles. These particles were re-suspended in sterile water and dispensed in a plastic tube that was placed on top of a magnet. After the particle solution was aspirated from the plastic transparent tube placed on the magnet, it could be clearly seen the magnetic metal particles were left behind (Figure 2.16).

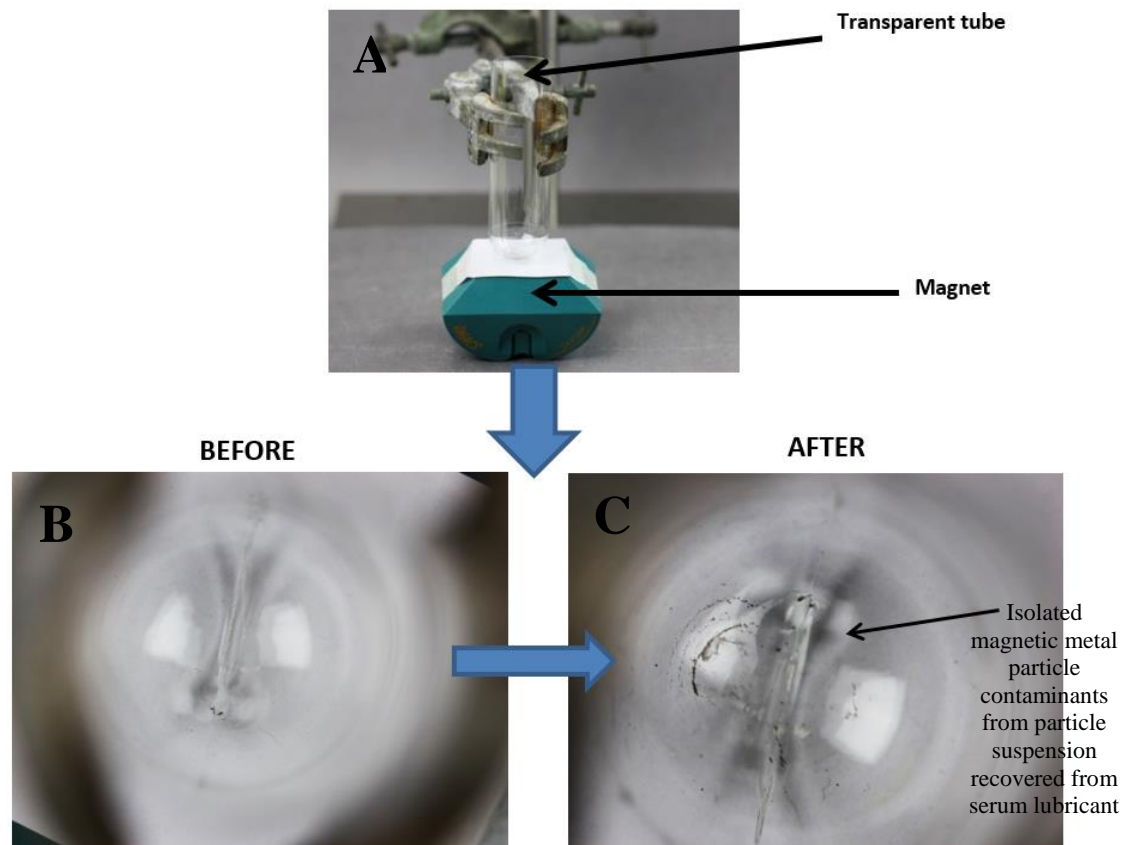


Figure 2.16 Magnetic particle isolation technique showing the separation of the magnetic metal particles from the ceramic wear debris. (A) Plastic transparent tube placed on the magnet. (B) Inside of plastic transparent tube BEFORE dispensing the particle suspension. (C) Inside of plastic transparent tube AFTER aspirating the particle suspension.

2.4.5.2 Recovery of large micrometre ceramic wear particles from hip simulator lubricants

After the magnetic particle separation technique, the particle suspension was filtered and analysed using CFE-SEM. CFE-SEM analysis revealed a significant reduction in the presence of stainless-steel particles, thus allowing the identification of BIOLOX[®] Delta ceramic wear debris in the form of large micrometre ceramic wear particles, that were up to 10 microns in size (Figure 2.17). Furthermore, nano-scale ceramic particles were also identified, however these were enveloped in protein. EDX analysis of the larger micrometre ceramic wear particles showed elemental peaks of aluminium (Al), carbon (C), oxygen (O), copper (Cu) and tungsten (W) and EDX analysis of the nanoscale ceramic particles showed elemental peaks of aluminium (Al), zirconia (Zr), iron (Fe), oxygen (O), carbon (C), and tungsten (W), thus confirming these particles were indeed from BIOLOX[®] Delta ceramic. The elemental peaks of W were contamination from the sodium polytungstate density gradient.

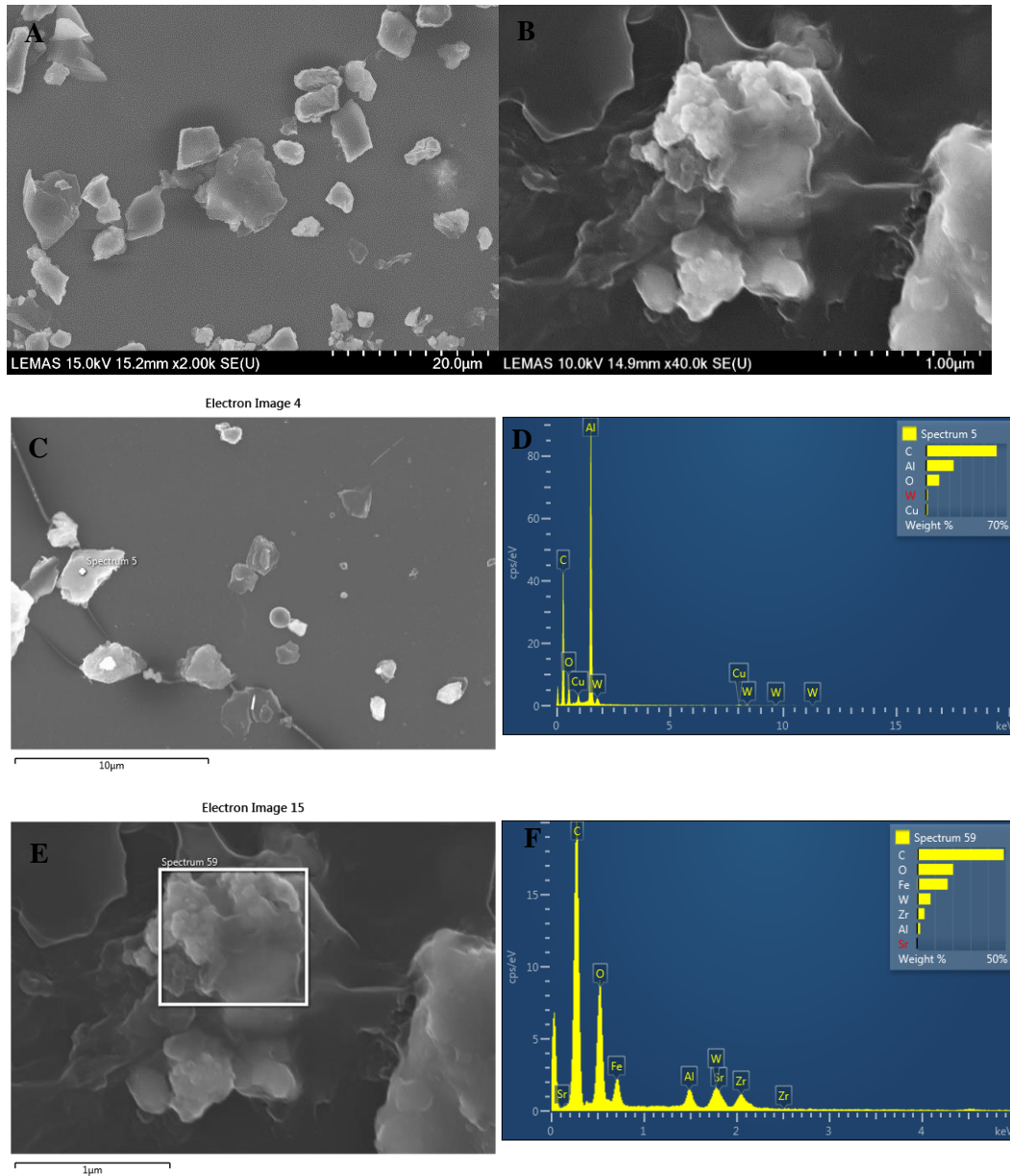


Figure 2.17 CFE-SEM and EDX analysis of the recovered ceramic wear debris. The lubricant serum contained a volume of 1.29mm³ BIOLOX® Delta ceramic wear debris generated from 36mm BIOLOX® Delta CoC bearings tested under severe edge loading conditions due to dynamic separation due to high cup inclination angle (65°) and 4mm translational mismatch in the centres of rotation of the femoral head and acetabular cup. (A) CFE-SEM of the recovered of large micrometre ceramic particles. (B) CFE-SEM of the recovered small nano-scale ceramic particles. (C) EDX image of the large micrometre particles and (D) corresponding EDX spectrum. EDX image of the small nano-scale particles and (E) corresponding EDX spectrum. Area selection and pin point EDX analysis of the particles was performed at a working distance of 15mm, 10kV and a suitable magnification to maintain focus.

2.4.6 Recovery of clinically-relevant BIOLOX[®] Delta ceramic wear debris from hip simulator lubricants using two-step particle isolation protocol

A two-step particle isolation protocol (section 2.3.7) was devised to enable the sedimentation of the nano-scale ceramic wear particles. The serum lubricant contained a volume of 1.58mm³ of ceramic wear debris. The wear debris were generated from 36mm CoC BIOLOX[®] Delta bearings tested under severe edge loading conditions due to dynamic separation due to high cup inclination angle (65°) and 4mm translational mismatch in the centres of rotation of the femoral head and acetabular cup. The density of the STP layers in the initial density gradient ultra-centrifugation step were changed in that the density ($\rho=1.1\text{g/cm}^3$) of the bottom layer was less than the average density ($\rho=1.22\text{g/cm}^3$) of proteins, which would theoretically allow the nano-scale particles to pellet with the attached proteins after the initial optimised digestion regime (section 2.3.5.2) and density gradient ultra-centrifugation step (section 2.3.7). The recovered particles were then subjected to further enzymatic digestion and purification using the original published method (Lal et al., 2016) as described in section 2.3.3.4.

CFE-SEM analysis of the recovered ZTA ceramic wear particles using the two-step particle isolation protocol method revealed both large micrometre and small nano-scale particles (Figure 2.18). EDX analysis confirmed the large micrometre particles were indeed Alumina with elemental peaks of aluminium (Al) and oxygen (O) (Figure 2.19A, B). The small nano-scale particles were comprised of Alumina, Zirconia and Strontium as confirmed by the elemental peaks of aluminium (Al), oxygen (O), zirconia (Zr) and strontium (Sr) from EDX analysis (Figure 2.19C, D). The elemental peaks of tungsten (W) represents contamination from the sodium polytungstate density gradient.

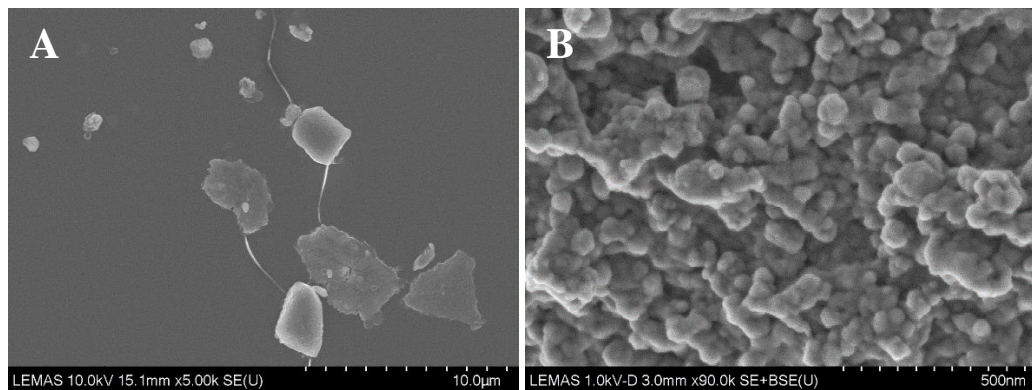


Figure 2.18 - CFE-SEM of the recovered large alumina micrometre ceramic particles. (B) CFE-SEM of the recovered small Zirconia nano-scale ceramic particles. The larger particles were imaged at 10kV voltage, working distance of 15mm and 5K magnification to capture groups of the particles. The smaller nano-scale particles were imaged at 1kV (deceleration mode) voltage, working distance of 2-3mm and 90k magnification.

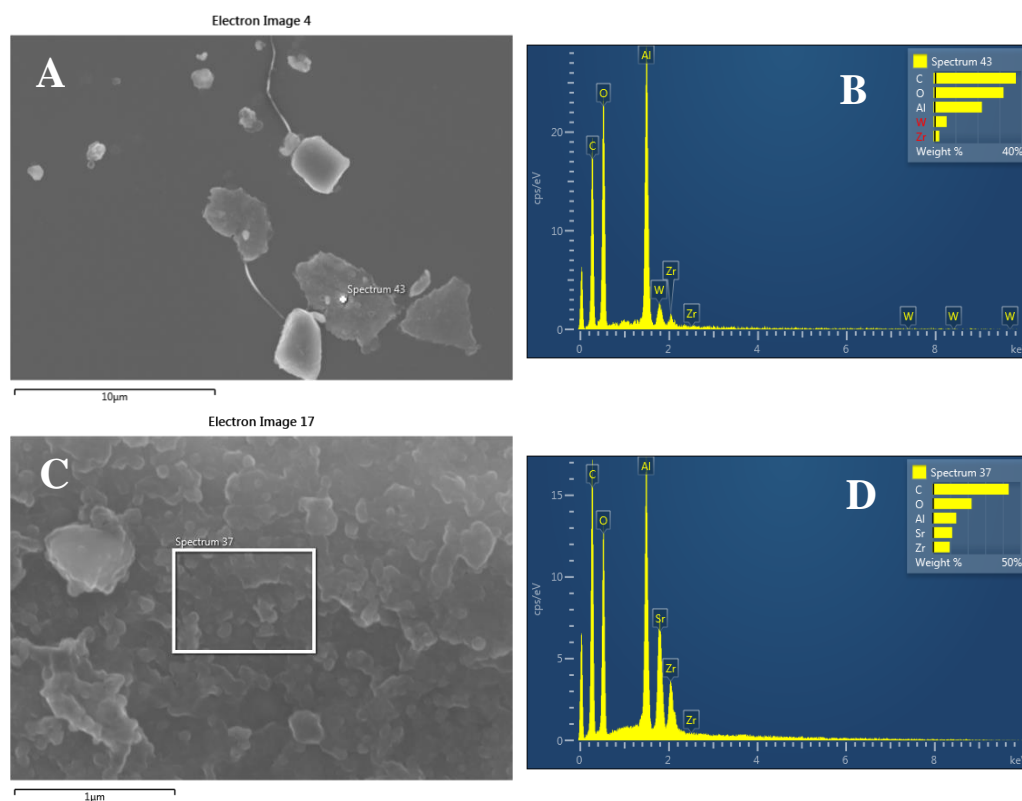


Figure 2.19 - EDX analysis of the BIOLOX[®] Delta ceramic wear debris recovered from hip simulator lubricant. (A) EDX image of the large alumina micrometre particles and (B) corresponding EDX spectrum. (C) EDX image of the small zirconia nano-scale particles and (D) corresponding EDX spectrum. Area selection and pin point EDX analysis of the particles was performed at a working distance of 15mm, 10kV and a suitable magnification to maintain focus.

2.4.6.1 Characterisation of the clinically-relevant BIOLOX[®] Delta ceramic wear particles recovered from hip simulator lubricants

The recovered clinically-relevant BIOLOX[®] Delta ZTA ceramic wear particles showed a bimodal size distribution of larger micron sized particles and nano-scale particles. The frequency as a function of size of the recovered particles are presented in Figure 2.20. The larger micron/submicron sized particles ranged between 100–32,980nm with a mean size of 2308.11 ± 243.58 nm, whereas the small nano-scale particles ranged between 10-100nm with a mean size of 43.73 ± 0.97 nm. The larger alumina particles had a mode of distribution in the 1-2µm size range and were irregular/shard-like in morphology, whereas the smaller zirconia particles were round in morphology with a mode size of 30-40nm. The mean ferret diameter, mean aspect ratio and mean circularity values (value of 1.0 indicates a perfect circle) are shown in Table 2.8. The larger particles (100 - >5000nm) had a higher mean aspect ratio (1.47 ± 0.02), which indicated that they were more elongated and irregular in shape compared to the smaller (0-100nm) nano-scale particles (1.29 ± 0.01), as they were more round and consistent in shape. The smaller (0-100nm) nano-scale particles had a higher mean circularity value (0.91 ± 0.02) compared to the larger particles (0.80 ± 0.01), which indicated the smaller nano-scale particles were more circular in shape than the larger particles.

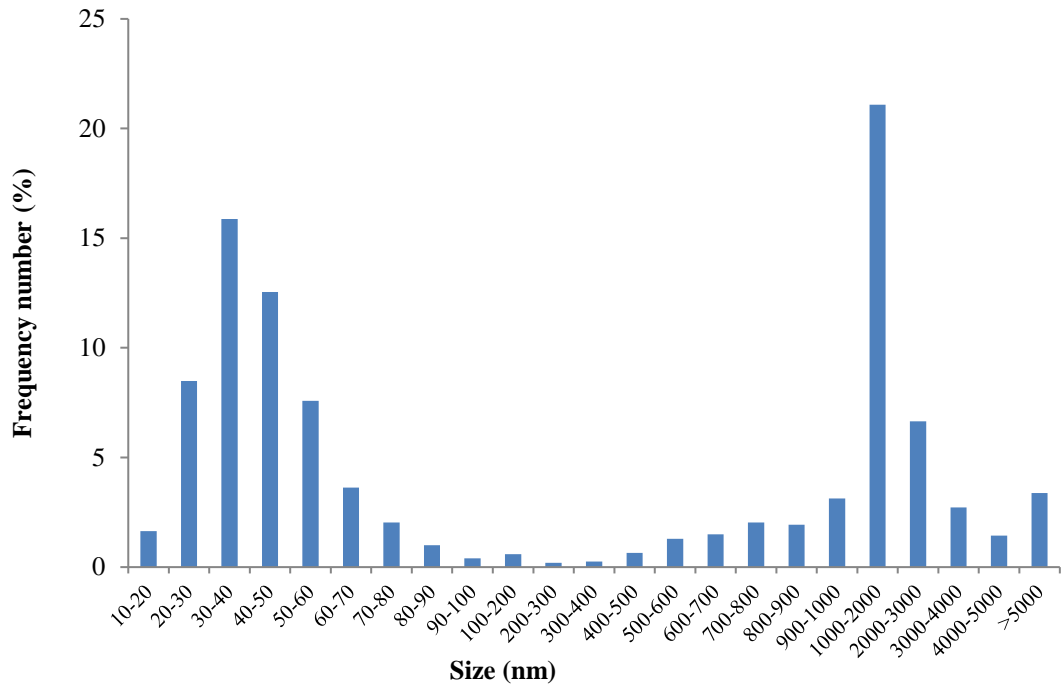


Figure 2.20 - Frequency size distribution of clinically-relevant BIOLOX® Delta ceramic wear particle recovered from three different samples of hip simulator serum lubricants. The ceramic wear particles were generated under edge loading conditions due to dynamic separation between the head and cup centres. A minimum of 150 particles were analysed from each sample (n=3).

Table 2.8 - Mean size (feret diameter) and morphology (aspect ratio and circularity) values for clinically-relevant BIOLOX® Delta ZTA ceramic wear particle recovered from three different samples of hip simulator serum lubricants.

	Larger micron/submicron sized particles (100 - >5000nm)	Nano-scale particles (0 - 100nm)
Feret diameter (nm)	2308.11 ± 243.58	43.73 ± 0.97
Aspect ratio	1.47 ± 0.02	1.29 ± 0.01
Circularity	0.80 ± 0.01	0.91 ± 0.02

Note: All values expressed as mean ±95% Confidence Interval.

2.5 Discussion

This study had the following two aims: -

1. To optimise and validate a novel particle isolation method for ultra-low wearing ceramic materials.
2. To isolate and characterise composite ZTA ceramic wear particles generated under edge loading conditions.

In order to meet these aims, commercially-obtained ZTA ceramic model particles were initially spiked into 25% (v/v) FBS at a range of volumes to assess the sensitivity of the novel particle isolation method in terms of recovery rates. Thereafter the method was applied to hip simulator lubricant serum that contained composite ZTA ceramic wear debris generated under edge loading conditions. However, the method demonstrated ineffective removal of contaminating proteins from the ceramic wear particles, thus the particle isolation method was further optimised. The optimisation process ultimately resulted in a two-step particle isolation method, which allowed for the first time the successful recovery and characterisation of very low volumes of both micrometre and nano-scale wear particles, generated from composite CoC hip replacements (BIOLOX[®] Delta). The discussion is divided into the following sections: -

1. Current particle isolation methods
2. Validation of a novel particle isolation method
3. Optimisation of particle isolation method
4. Successful recovery of composite ceramic wear particles

2.5.1 Current particle isolation methods

Characterisation of wear particles from CoC bearings has historically been extremely challenging due to the low volume and nano-scale nature of the wear particles. The composite CoC bearings have extremely low wear rates, which are approximately twenty-to eighty-fold lower than the current generation of highly cross-linked UHMWPE-on-metal total hip replacements (Galvin et al., 2007; Al-Hajjar, Fisher, Tipper, et al., 2013a). Whilst these low wear rates of composite ceramic hip replacements are highly beneficial, it has made it extremely challenging to isolate the wear particles generated *in vitro* using hip simulators, and so at present no studies have reported their characteristics or biological activity. Current established particle isolation methods (Doorn et al., 1998b; Catelas, Bobyn, J.B. Medley, et al., 2001a; Catelas, Bobyn, J.J. Medley, et al., 2001b; Brown et al., 2007; Billi et al., 2012) lack the sensitivity to reliably isolate very low wear volumes such as those produced by the latest generation composite or BIOLOX[®] Delta CoC bearings. However, a novel particle isolation method was developed by Lal et al. (2016) to tackle the challenge of isolating ultra-low volumes of particles from large volumes of serum lubricants, which is often used in hip

simulators. This novel method was originally developed for the isolation of silicon-nitride ceramic-like particles from coatings for total hip replacements. Hence, this study was undertaken to optimise and validate this recently published novel particle isolation method (Lal et al., 2016) for the recovery and characterisation of wear particles generated from BIOLOX® Delta CoC hip replacements using hip simulation. The validated method was applied to hip simulator serum lubricant that contained ceramic wear debris generated from BIOLOX® Delta CoC bearings.

This novel particle isolation method developed by Lal et al. (2016) has many attractive features over other methods, as it was developed for the isolation of ultra-low wearing materials, such as composite ZTA CoC bearings. The method used enzymatic digestion and sodium polytungstate density gradient ultra-centrifugation technology to isolate wear particles from low wearing ceramic bearing materials. Enzymatic digestion is advantageous over other digestion methods i.e. acid or base digestion in that it preserves the characteristic features of wear particles and minimises chemical damage (Catelas, Bobyn, J.B. Medley, et al., 2001a; Catelas, Bobyn, J.J. Medley, et al., 2001b). The protein digestion process in this method also utilised a denaturing agent; sodium dodecyl sulphate (SDS) to breakdown the secondary and non-disulfide-linked tertiary structures of the serum proteins, thus increasing the efficiency of the digestion. The uniqueness of this method however, is in employment of a novel gradient technique, which uses sodium polytungstate. A recently developed particle isolation method (Billi, Benya, Kavanaugh, Adams, Ebrahimzadeh, et al., 2012) used caesium trifluoroacetate for density gradients, however this is highly toxic and not readily available. Common conventional gradient materials consist of sucrose or caesium chloride (Chauhan, 2008), these have a limited density range and hence are not suitable for particle separation from proteins. On the contrary, sodium polytungstate has a wide density range of 1.1 to 3.0 g/cm³ in water. The average density of proteins is 1.22g/cm³, which is approximately four-fold lower than alumina ceramic particles and six-fold lower than CoCr metal particles (Quillin and Matthews, 2000). This large difference in density allows easy separation of the particles from the proteins using density gradients, however in contrast this is difficult for UHMWPE particles as it has a lower intrinsic density (0.928-0.941g/cm³) compared to the average density of proteins (1.22g/cm³). Furthermore, sodium polytungstate is non-toxic and has a low viscosity, hence it is easy to work with (Savage, 1988). It also comes with an additional benefit, whereby it has been reported to act as a protein denaturant and so can assist in the breakdown of the proteins present in the serum lubricant (Seidl et al., 2012). However, a limitation of this novel method is that the medium used for the density gradient i.e. sodium polytungstate, contaminated the recovered particles and thus necessitated a subsequent wash step to remove this medium before analysing the particles. The EDX spectrum clearly showed peaks of sodium and tungsten, which are the major constituents of sodium polytungstate.

Nevertheless, the soluble nature of sodium polytungstate allowed easy separation from the isolated particles by repeated washing steps.

2.5.2 Validation of novel particle isolation method

The particle isolation method was validated for sensitivity and repeatability by determining the recovery rates of different volumes (0.05-5mm³) of ZTA ceramic particles which had been spiked into 25% (v/v) FBS. The serum spiked with ZTA powder was then processed through the novel particle isolation method and the mass of the recovered ZTA particles was measured gravimetrically in order to determine the particle recovery rates. The method demonstrated a high average recovery rate of 89% for the low volumes of ZTA particles (0.1-0.05mm³), which was comparable with the recovery rate of 84.7% reported by Lal et al. (2016) who developed the method for isolation of silicon-nitride particles. The control sample recovered a mass of 0.02mg, which may have been due to the unavoidable introduction of contamination during the particle isolation process. The high recovery rate observed in this study may result from fewer steps, decreased handling, fewer vessel changes and sufficient ultracentrifugation speeds, all of which contribute towards minimising particle loss. Whereas previous methods (Doorn et al., 1998b; Catelas, Bobyn, J.B. Medley, et al., 2001a; Catelas, Bobyn, J.J. Medley, et al., 2001b; Brown et al., 2007; Billi et al., 2012) have multiple and complex steps, many vessel changes and lower centrifugation speeds, which collectively reduce particle recovery. Moreover, the sensitivity of this novel method was comparable with the 92% ±5% reported by Billi et al. (2012) for their metal-ceramic silicon wafer display (MC-SWD) protocol. However, the advantages of this method over the Billi et al. (2012) method are its simplicity, cost effective reagents and non-specialist equipment, and most importantly, the ability to use the recovered particles for subsequent assays, for example biocompatibility testing of clinically-relevant wear particles. This is not possible with the Billi et al. (2012) protocol as the particles become embedded within the silicon wafer during the purification process, thus only allowing visualisation of the particles using SEM/TEM. The MC-SWD method does not allow physical recovery of the wear particles, hence subsequent biocompatibility testing of the particles is not possible.

The relative features of wear particles in terms of their size, morphology, quantity and composition determine the severity of the biological response (Green et al., 1998). Hence it is essential to understand the characteristics of wear particles and their biological activity for the pre-clinical testing of joint replacements (Ingham and Fisher, 2000). Particles of less than 1µm are considered to be more biologically active than larger sized particles (Green et al., 1998; Ingham and Fisher, 2000; Ingham and Fisher, 2005). Similarly elongated particles may induce a stronger biological response than round particles (Billi et al., 2009). Therefore, it is important that particle isolation methods preserve the size and morphological characteristics of wear particles. There was no significant difference observed for the size distribution of the

ZTA particles before and after the isolation protocol. Similarly, there was no significant difference in the aspect ratio and circularity of the ZTA particles before and after the isolation method. Thus, the method employed here demonstrated effective proteolytic digestion and particle recovery without effecting the particle size and morphology of the ZTA particles spiked into 25% (v/v) FBS. Catelas et al. (2001) reported that enzymatic digestion techniques were least damaging to metal wear particles and hence were an optimum choice for isolation and characterisation of wear particles. Furthermore, effective removal of protein minimised agglomeration of the particles, as a result the method in the present study allowed for precise chemical characterisation of the ZTA ceramic model particles using EDX analysis. However, as mentioned previously, contamination by sodium polytungstate was observed as indicated by the Na (Sodium) and W (Tungsten) elemental peaks observed during EDX analysis. However, incorporation of centrifugal washes and subsequent CFE-SEM analysis found that this did not affect characterisation of the recovered particles.

2.5.3 Optimisation of particle isolation method

The validated method was subsequently applied to hip simulator serum lubricant from BIOLOX® Delta CoC bearings tested under severe edge loading conditions due to dynamic separation due to high cup inclination angle (65°) and 4mm translational mismatch in the centres of rotation of the femoral head and acetabular cup (Al-Hajjar et al., 2015; O'Dwyer Lancaster-Jones et al., 2017). These kinematic conditions have been reported to produce wear patterns (stripe wear) and wear mechanisms in CoC bearings, similar to those found *in vivo* (Nevelos et al., 2000a). The initial application of the validated novel method was unsuccessful in isolating the ceramic wear debris generated from 36mm BIOLOX® Delta ceramic-on-ceramic bearings under standard gait or severe microseparation conditions. The serum proteins were not fully removed, thus making it difficult to identify and observe the ceramic wear debris, which were enveloped in the protein. The use of EDX confirmed that the ceramic wear debris were indeed present, as elemental peaks of Al, O, Zr, and Sr were observed in the EDX spectrum. However, the protein corona that forms on the surface of colloidal nanoparticles was not successfully removed causing a charging effect that resulted in abnormal contrast and made the particles appear flat and deformed. Furthermore, in addition to the protein contamination, very few particles were recovered making it extremely difficult to conduct a comprehensive characteristic analysis. Thus, a more robust digestion protocol was required for the complete removal of serum proteins from the particles.

Other enzymes to breakdown the serum proteins were introduced, such as papain, as previous methods have used this enzyme and demonstrated successful recovery of wear particles from tissues or simulator lubricants (Schmiedberg et al., 1994; Doorn et al., 1998a; Tipper et al., 1999; Catelas, Bobyn, J.B. Medley, et al., 2001; Catelas, Bobyn, J.J. Medley, et al., 2001; Brown et al., 2007). Hence, this enzyme was incorporated into the digestion protocol,

whereby it is reported to hydrolyse esters, amides and breakdown peptide bonds of basic amino acids e.g. leucine and glycine (Barrett et al., 2013). In order to visibly assess the efficacy of this enzyme, serum containing CoCr wear debris generated from metal-on-metal bearings tested under microseparation conditions was used as the black colour of the CoCr wear particles could be easily observed. The results from this digestion demonstrated that the metal wear debris formed a band at the interface between the bottom two layers of the SPT density gradient and did not pellet at the bottom of the tube as expected. This was indicative of insufficient digestion of the proteins, which remained attached to the metal wear debris, thus altering the density and preventing sedimentation. The physico-chemical properties (surface charge, size, shape and composition) of the nano-particles determines the structure and composition of the protein corona (Rahman et al., 2013). Metal nano-particles typically have a high surface charge, hence a hard protein corona forms as protein adsorption increases with increasing surface charge (Abbas et al., 2008; Rahman et al., 2013). The protein corona on the metal wear debris may have changed the intrinsic density of the CoCr nano-particles, thus inhibiting sedimentation. Furthermore, CFE-SEM of the particles recovered from the metal band revealed the CoCr nano-particles were highly agglomerated and contaminated with proteins. This showed that papain was ineffective at breaking down the proteins in serum lubricants and an alternative solution was required.

The elevated temperatures generated during wear simulation coupled with the serum proteins provides ideal conditions for microorganisms to thrive (Liao and Hanes, 2006). For that reason, it became necessary to introduce lysozyme into the digestion protocol. Lysozyme is an enzyme that breaks down the cell wall of both Gram-positive and Gram-negative bacteria resulting in the formation of protoplasts and spheroplasts. Lysozyme is found naturally in the human body and is abundant in secretions including tears, saliva, human milk and mucus. The enzyme occurs in the innate immune system, which forms the first line of defence against infections (Osserman, 2012). SEM analysis of the recovered wear particles subjected to digestion with lysozyme revealed that the filter membrane had a lower level of protein contamination compared to the standard digestion method, in which large areas of the filter membrane were observed to be covered with proteins. However, despite the reduced protein contamination observed on the filter membranes after lysozyme digestion, the identification of ceramic wear particles was unsuccessful.

Previous attempts at ceramic particle isolation in this study processed aliquots taken from serum lubricants that contained approximately 0.02-0.05mm³ of ceramic wear debris, as the particles were diluted due to the high volume of serum. The aliquot technique was clearly not a viable approach, since the ratio of volume of particles to volume of serum was extremely high (0.1:1500 - 2:1500). Furthermore, the serum lubricant was heavily contaminated with bacteria and other contaminants from the hip simulators, thus making it even more difficult

to isolate the ultra-low volume of ceramic wear debris. Therefore, it became necessary to process the entire batch of serum produced from one million cycles of hip simulation, which equated to approximately 1.5 litres of serum lubricant and contained between 1.58-1.93mm³ of ZTA ceramic wear particles.

During the batch processing of the lubricant serum, the volumes of the wear particles were manipulated by pooling together the concentrated pellets obtained from the serum concentration steps in order to increase the volume of wear debris present in a small volume of solution. This enabled the visualisation of a particle pellet after the washing step, which was not previously observed when isolating particles from smaller aliquots of serum lubricant. This was indicative of successful recovery of ceramic particles from the hip simulator serum lubricant, which was confirmed by CFE-SEM analysis that showed an abundance of particles on the filter membrane. However, EDX analysis confirmed that the majority of the recovered particles were stainless-steel as indicated by the Fe elemental peaks. The source of these stainless wear particle contaminants is unknown, however it was postulated that they may have been released from fretting wear of the taper or fixtures of the Leeds II hip simulator. Nonetheless, the overwhelming large volume of these stainless-steel particle contaminants masked the presence of the ceramic wear debris that were recovered from the serum lubricant. Therefore, a separation technique using a magnet was devised to separate the stainless-steel particle contaminants from the ceramic wear particles.

A clear polystyrene tube placed on top of a MidiMACS™ magnet was used to capture the stainless-steel particles from the particle suspension. The taper and fixtures of the hip simulator are made from type 316 stainless-steel which is a non-magnetic austenitic chromium-nickel stainless-steel containing molybdenum. Nevertheless, this technique significantly reduced the number of stainless-steel particles present in the particle suspension. The ferromagnetic properties exhibited by some of these stainless-steel particles may have been due to their small size (nm-µm) or a change in their microstructure from austenitic to martensitic. It has been reported that deformation induced phase transformation of stainless-steel can occur under cyclic loading, which may have taken place during wear simulation (Solomon and Solomon, 2010). Furthermore, the adhesive sliding during fretting wear of the taper or fixtures may also induce martensitic phase transformation, rendering the particles magnetic (Maruyama et al., 2013). The reduction in stainless-steel particle contaminants allowed the identification of larger micrometre-sized ceramic wear particles that were up to 10 microns in size. Additionally, agglomerated nano-scale zirconia particles (30-50nm) were also identified, however these were enveloped in proteins, which demonstrated insufficient digestion. It was therefore postulated that despite the sedimentation of the larger micrometre particles, the protein corona on the surface of the nano-scale particles may be inhibiting their sedimentation during density gradient ultra-centrifugation. For this reason, a two-step

digestion and density gradient protocol was devised, whereby the density of the initial SPT layers were modified to allow the sedimentation of nanoscale particles and proteins during the first step. This was followed by a second proteolytic digestion and a second density gradient ultra-centrifugation step utilising densities of SPT as described by Lal et al. (2016). This resulted in successful isolation of both large micrometre and small nano-scale BIOLOX® Delta ceramic wear particles.

2.5.4 Successful recovery of composite ceramic wear particles

The high sensitivity of this optimised novel two-step particle isolation method coupled with its effective removal of protein, allowed for the first time the successful recovery and characterisation of very low volumes (0.1-1.93mm³) of both micrometre and nano-scale wear particles, generated from composite ZTA CoC hip replacements (BIOLOX® Delta), from protein containing lubricants. CFE-SEM analysis revealed that the particles had a bimodal size range, with larger polygonal shaped particles of alumina that ranged between 100->5000nm with a mean size of 2308nm, and small round (granular) zirconia particles that were agglomerated and ranged between 10-100nm with a mean size of 43.7nm. Since no previous studies have reported the characteristics of wear particles generated from composite ceramic hip replacements, a comparison with the early generation pure alumina ceramic was made. The bimodal size range of the recovered ceramic wear particles is in agreement with previous studies (Hatton et al., 2002; Tipper et al., 2002b; Stewart et al., 2003a), since analysis of retrieved tissues from CoC THR revision surgeries has identified ceramic wear particles as having a bimodal distribution of particle sizes ranging from 5 – 90 nm (mean size: 24 ± 19nm), and larger particles similar to UHMWPE debris ranging in size from 46 – 3,200 (mean size: 438 ± 325nm) (Hatton, 2001). The large size distribution for clinically-relevant ZTA ceramic wear particles is thought to be caused by the introduction of microseparation conditions during articulation, causing a bimodal size distribution. The nanometre-sized particles are believed to be produced by relief polishing of the ceramic bearing, whereas the larger particles are produced by trans-granular fracture of the ceramic bearing that results in the formation of a wear stripe during edge loading (Nevelos et al., 2000a; Tipper et al., 2002b). The larger micrometre/ submicron sized wear particles generated from this wear mechanism i.e. transgranular/intergranular fracture as a result of rim contact during edge loading, may be critical in determining the severity of the biological response as it is well established that this size range can induce an inflammatory response (Green et al., 1998). This novel two-step particle isolation is a major breakthrough since it has allowed for the first time comprehensive particle characteristic analysis of clinically-relevant ZTA ceramic wear particles generated *in vitro*.

2.6 Limitations of study

The work in the current chapter demonstrated successful recovery of wear particles generated from composite ZTA BIOLOX[®] Delta CoC THR's for the first time. However, the recovered particles from the hip simulator lubricants also contained stainless-steel wear particle contaminations, the likely source of which may have been from the fixtures and components of the hip simulator. This is a limitation of the current study as it cannot be certain that all the particles characterised were indeed ceramic. However, a technique was devised using EDX analysis to ensure the elemental composition of every particle that was being imaged. This technique minimised the incorrect measurement of contaminating particles, and increased the reliability of the findings of the present study. This work continues to increase the understanding of the characteristics of wear debris generated from ceramic hip replacements.

2.7 Summary of findings

- Validation of the novel method developed by Lal et al. (2016), demonstrated a recovery rate of 89% for wear volumes (0.05-0.5mm³) that were representative of the wear rates of CoC bearings
- Further optimisation of the novel method resulted in the development of a two-step particle isolation method that allowed successful recovery of extremely low volumes of wear particles generated from composite ZTA BIOLOX[®] Delta CoC hips
- CFE-SEM analysis revealed that the composite ZTA ceramic wear particles had a bimodal size range, with larger polygonal shaped particles of alumina that had a mean size of $2308 \pm 243.58\text{nm}$, and small round granular zirconia particles that had a mean size of $43.7 \pm 0.97\text{nm}$

CHAPTER 3

3 Wear Simulation of clinically-relevant ceramic wear particles

3.1 Introduction

The wear performance of composite ZTA CoC total hip replacements such as those using BIOLOX® Delta has been extensively investigated using hip simulators, however no studies have reported the characteristics and biological impact of the wear debris generated from these bearings. The lack of studies may be due to difficulties in generating high volumes of clinically-relevant ceramic wear debris *in vitro*, in addition to the fact that current particle isolation methods are not sensitive enough to reliably isolate the wear particles from hip simulator lubricants, due to the inherent low wear rates of composite ZTA ceramics (Doorn et al., 1998a; Catelas, Bobyn, J.J. Medley, et al., 2001; Brown et al., 2007; Billi, Benya, Kavanaugh, Adams, McKellop, et al., 2012). Whilst these extremely low wear rates of CoC bearings are highly beneficial, the high ratio between the volume of serum lubricant and volume of ceramic wear debris has made it extremely challenging to reliably isolate ceramic wear debris generated *in vitro* using hip simulators to be used for biological testing. Hence, the majority of previous studies have used commercially available ceramic powders to assess biological activity (Nagase et al., 1995; Isabelle Catelas et al., 1999; Nkamgueu et al., 2000b; Granchi et al., 2004; Tsaousi et al., 2010). However, these particles may not be clinically-relevant in terms of their characteristics, which is extremely important as the relative features of wear particles in terms of their size, morphology, quantity and composition determines the severity of the biological response (Green et al., 1998). But with the recent development and optimisation of a novel particle isolation method (Lal et al., 2016), the challenge of being unable to recover ceramic wear debris has now been addressed to some extent.

The present study successfully recovered composite ZTA ceramic wear particles from hip simulator serum lubricants that were generated under edge loading conditions (Chapter 2). The recovered particles demonstrated a bimodal size range, which consisted of large micron/submicron size alumina particles and smaller nano-scale zirconia granular particles. This was in agreement with previous studies (Hatton et al., 2002; Tipper et al., 2002b; Stewart et al., 2003a), where analysis of retrieved tissues from first generation alumina CoC THR revision surgeries also identified ceramic wear particles with a bimodal size distribution. However, these particles could not be used for biological testing due to the potential problem of adherent endotoxins and a protein corona that may be present on any particles recovered

from simulator testing, which may lead to cell activation that may not have been due to the ceramic wear particles, thus causing misleading results. In addition, the extremely low volumes of ceramic wear particles generated from CoC bearings mean that particles lost during the isolation process is potentially very costly. Hence, Hatton et al. (2003) used the hip simulators as a tool to generate clinically-relevant ceramic wear particles in water lubricant for subsequent biological testing. The particles were generated under microseparation conditions to replicate stripe wear, which is known to produce wear particles with bimodal size distribution. Thereafter the ceramic wear particles were subsequently heat treated (180°C for 4 hours) to evaporate the water, leaving behind sterile wear particles for biological testing. This technique was also employed in the present study, however the use of water as the lubricant necessitated subsequent characterisation of the wear particles generated to ensure that they were clinically relevant i.e. comparable with those wear particles generated in serum lubricant. The characteristics data of the composite ZTA ceramic wear particles obtained from simulator testing in serum lubricants (Chapter 2) was used to verify that the characteristics (size and morphology) of the composite ZTA ceramic wear particles generated in water in the present chapter were the same as those generated in serum. Following this, the particles were used for testing biological impact using a range of biological assays (Chapter 4). The work in this chapter in relation to other chapters is presented in Figure 3.1.

Previous wear simulation studies (Stewart et al., 2003c; Al-Hajjar et al., 2010; Affatato et al., 2011; Al-Hajjar, Fisher, Tipper, et al., 2013a; Al-Hajjar et al., 2015; O'Dwyer Lancaster-Jones et al., 2017) of the composite ZTA BIOLOX[®] Delta ceramic bearings have reported extremely low wear rates of between 0.1-1mm³ per million cycles, which is twenty to eighty fold lower than the highly cross-linked UHMWPE-on-metal bearings (Galvin et al., 2007). Furthermore, retrieval studies of CoC bearings have shown extremely low volumes of wear compared to other bearing couples (Refior et al., 1997; Nevelos et al., 1999; Nevelos, Ingham, et al., 2001c). However, recent issues centred around component positioning have revealed that CoC bearings can exhibit component separation, which can result in edge loading (Nevelos et al., 2000b; Dennis et al., 2001; Fisher, 2011), and increased wear of hard-on-hard bearings, thus eventually leading to implant failure. Microseparation is introduced into wear simulation tests to replicate stripe wear that was often seen on retrieved ceramic hip implants (Nevelos et al., 2000a). This was achieved by applying a 0.4-0.5mm medial-lateral displacement of the cup relative to the head using a spring during the swing phase of the gait cycle, which ultimately caused edge loading during heel strike (Nevelos et al., 2000a; Stewart et al., 2001; Stewart et al., 2003a; Stewart et al., 2003b). Nevertheless, fluoroscopic studies of patients with total hip replacements has shown that the level of dynamic (micro) separation and severity of edge loading can vary considerably i.e. 1.9-5.2mm (Lombardi et al., 2000; Dennis et al., 2001). Hence, the effect of variations in translational positioning with different

levels of mismatch between the centres of the cup and head on the magnitude of dynamic separation and severity of edge loading have been investigated by Lancaster-Jones., et al. (2016). In the present study, dynamic separation due to translational mismatch of up to 4mm in the centres of rotation of the femoral head and acetabular cup were employed to create severe edge loading conditions to ensure maximum wear rates in order to produce enough volume of wear particles for determination of biological impact of composite ZTA ceramic wear particles.

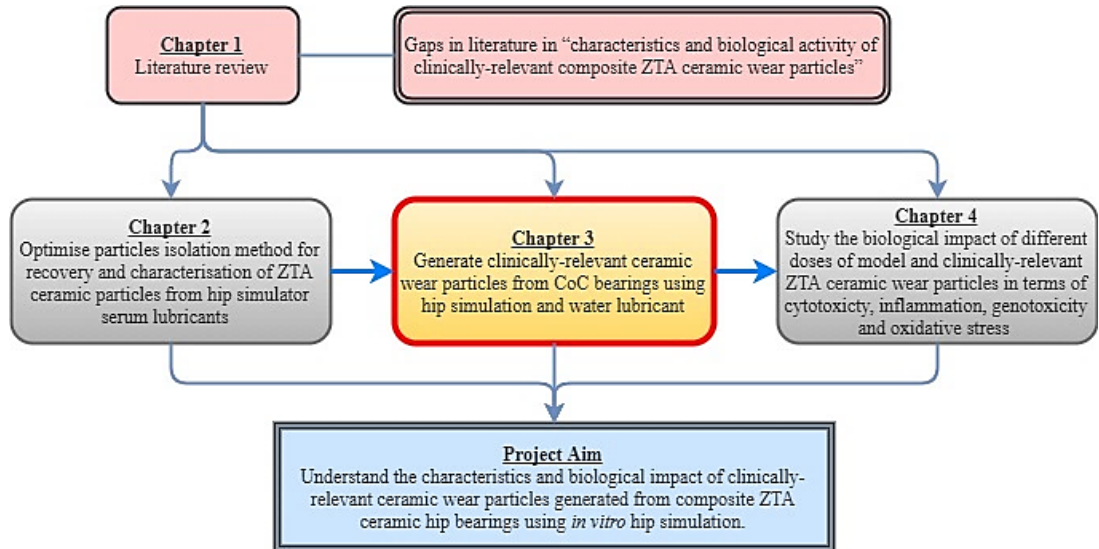


Figure 3.1 – Flow diagram showing the work in this chapter in relation to other chapters, with the current chapter highlighted in yellow.

3.2 Aims and objectives

Aims:

The aim of this chapter was to generate clinically-relevant ceramic wear particles from alumina (BIOLOX[®] Forte) and composite ZTA (BIOLOX[®] Delta) CoC hip replacements for subsequent testing of biological impact.

Objectives:

- To generate ceramic wear debris (in water lubricant) from BIOLOX[®] Forte and BIOLOX[®] Delta ceramic bearings under severe edge loading conditions caused by dynamic separation due to translational mismatch in the centres of rotation of the femoral head and acetabular cup
- To quantify the wear rates and surface characteristics of the ceramic bearings after testing
- To recover and characterise the wear particles in terms of their size and morphology
- To compare the characteristics to ZTA wear particles generated in hip simulator tests using serum as a lubricant
- To generate CoCr wear particles using the pin-on-plate wear rig to use as positive particle control

3.3 Materials and methods

3.3.1 Introduction

Clinically-relevant ceramic wear particles were generated from ceramic-on-ceramic bearings under severe edge loading conditions using the hip simulator and clinically-relevant CoCr wear particles were generated from CoCr pins and plates using the pin-on-plate wear rig. Water was used as the lubricant to generate both the ceramic and metal wear particles. The characteristics of the wear particles generated were analysed using cold-field emission gun scanning electron microscopy. The water lubricant containing the wear particles was processed to recover the wear particles, which were stored at -20°C until required for subsequent biological testing. A flow diagram of the method can be seen in Figure 3.2.

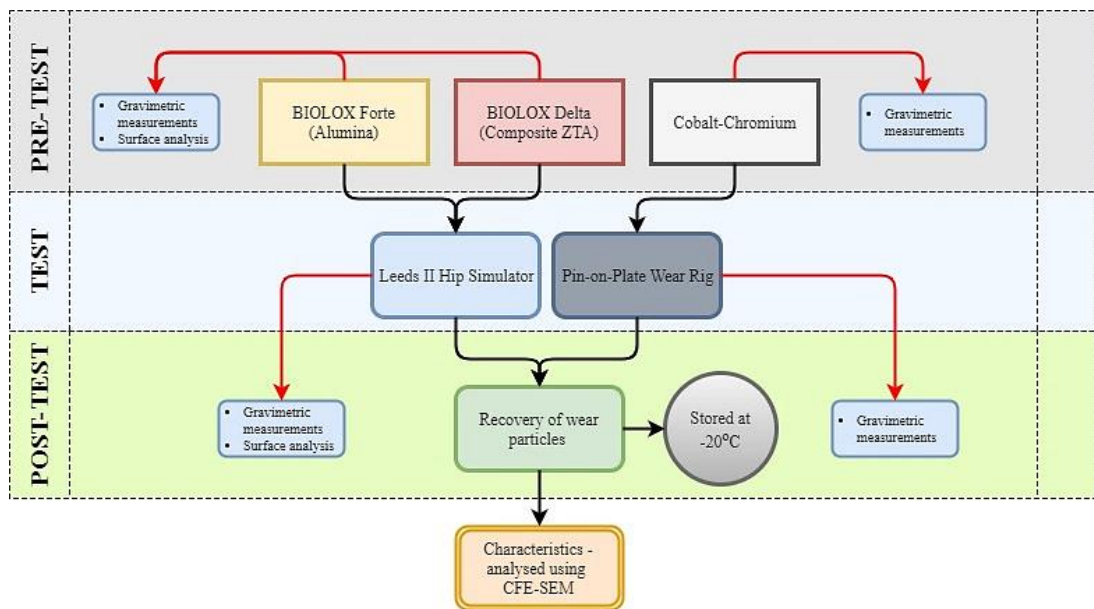


Figure 3.2 –Overview of the experimental methods for generating clinically-relevant wear particles for subsequent testing of biological impact.

3.3.2 Materials

3.3.2.1 Chemicals and reagents used in this study

The chemicals and reagents used in this study are listed in Table 3.1.

Table 3.1 - List of chemicals and reagents used in this study

Chemical/Reagent	Supplier	Storage/Preparation
Ethanol, absolute	VWR International LTD, Poole, UK	Room temperature in flammables cupboard
Grease (Kluber Petamo 133N)	Mitchell Fox, Leeds, UK	Room temperature
Isopropanol	VWR International LTD, Poole, UK	Room temperature in flammables cupboard
Sterile ultra-pure water	Baxter Healthcare, UK	Room temperature
Trigene	Scientific Laboratory Supplies Ltd, Nottingham, UK	Room temperature

3.3.2.2 Equipment

The equipment used in this study are listed in Table 3.2.

Table 3.2 – List of equipment used in this study

Item	Model/Size	Supplier
Balance (accuracy of 10 μ g)	XP205	Mettler-Toledo Ltd, Leicester, UK
Contacting surface profilometer	Talysurf 120L	Taylor-Hobson, UK
Coordinate measuring machine	Legex 322	Mitutoyo, Japan
Freeze dryer	ModulyoD-230	Thermo Savant, UK
Scanning electron microscope	Carl Zeiss EVO MA15 high definition scanning electron microscopy	Zeiss, UK
Sputter coater and thickness monitor	B7341 and B7348 respectively	Agar Scientific Limited, Stanstead, UK
Ultra-sonicator	XB3	Grant Instruments Ltd, Shepreth, UK

3.3.2.3 Ceramic hip components

Two different types of ceramics (32mm in diameter) were used for the hip wear simulation tests i.e. alumina ceramic, which is known commercially as BIOLOX[®] Forte (CeramTec, Germany) and composite ceramic, zirconia-toughened platelet reinforced alumina (ZTA), otherwise commercially known as BIOLOX[®] Delta (CeramTec, Germany). The composition of the different ceramics is shown in Table 1.1, section 1.2.

Heads of both ceramics (BIOLOX[®] Forte and BIOLOX[®] Delta) were mounted onto stainless-steel C-STEM AMT cemented femoral stems (DePuy Synthes). Cups were mounted in titanium alloy acetabular shells (Duraloc[®] for BIOLOX[®] Forte and Pinnacle[®] for BIOLOX[®] Delta, DePuy Synthes, Leeds, UK). The details of the components used in the hip simulator are shown in Table 3.3. All the heads, cups, shells and stem components were supplied by DePuy Synthes Joint Reconstruction, Leeds, UK.

Table 3.3 – Components used for generation of wear particle from ceramic bearings on the hip simulator

	Stem	Head	Cup	Shell
BIOLOX[®] Delta	Stainless-steel C-STEM AMT	Delta head (32mm ID)	Delta insert (32mm ID, 48mm OD)	Pinnacle 100 acetabular cup (48mm OD)
BIOLOX[®] Forte	Stainless-steel C-STEM AMT	Forte head (32mm ID)	Forte insert (32mm ID, 52mm OD)	Duraloc option cup (52mm OD)

ID - inner diameter; OD - outer diameter

3.3.2.4 Cobalt-chromium pins and plates

Six pins and plates were manufactured in house (School of Mechanical Engineering, University of Leeds) from a high carbon >0.2% (w/w) wrought cobalt-28 chromium-6 molybdenum alloy (ASTM F1537). The pins were polished to a surface roughness (R_a) of 0.02-0.04 μm and the plates were polished to a surface roughness of (R_a) of 0.01-0.02 μm to create a smooth contact surface. The dimensions of the pins and plates are shown in Figure 3.3. The pins and plates were engraved with a number on the non-contact face of the component for identification and continuity of positioning in the test rig. The pins and plates were sonicated in 70% (v/v) isopropanol for 10 minutes to ensure the components were clean before using in wear simulation.

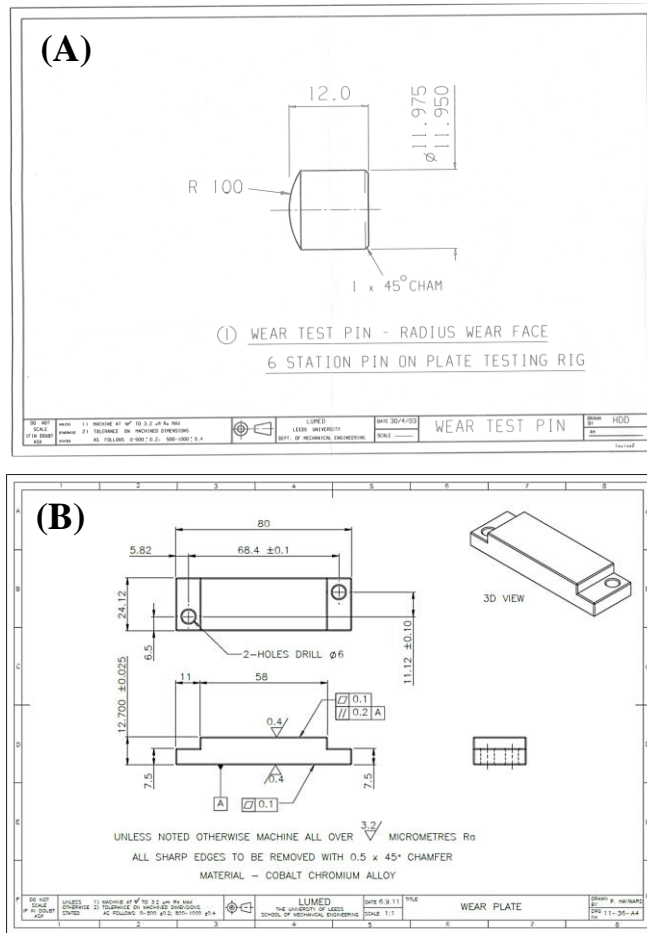


Figure 3.3 – The dimensions of the pins (A) and plates (B) used in the six-station pin-on-plate wear tests. The measurement ‘R’ refers to the 100° radius of the contact face.

3.3.2.5 Wear simulators

3.3.2.5.1 Pin-on-plate wear rig

A six-station pin-on-plate reciprocating wear test rig was used to generate metal wear particles from CoCr pins and plates (built in house, School of Mechanical Engineering, University of Leeds, UK).

3.3.2.5.2 Hip joint wear simulator

The Leeds II B hip joint simulator was used to generate ceramic wear particles from ceramic-on-ceramic hip bearings.

3.3.3 Methods

3.3.3.1 Generation of ceramic wear particles using hip simulation

Clinically-relevant ceramic wear particles were generated in water under adverse edge loading conditions using the Leeds II hip joint simulator. BIOLOX[®] Forte and BIOLOX[®]

Delta ceramic-on-ceramic hip components were used as described in section 3.3.2.3. In total, four million cycles over four different tests were completed, which generated sufficient volumes of wear debris for subsequent biological testing (chapter 4).

3.3.3.1.1 Leeds Mark II Physiological Anatomical Hip Joint Wear Simulator

Hip joint wear simulators are used to predict the wear performance of artificial hip replacements *in vitro*. The Leeds Mark II Physiological Anatomical hip joint simulator B (Figure 3.4) was used to generate ceramic wear debris from BIOLOX® Forte and BIOLOX® Delta ceramic bearing components. The simulator consisted of six stations that simulate dynamic vertical loading, flexion/extension and internal/external rotation (Barbour et al., 1999).



Figure 3.4 - Leeds Mark II Physiological Anatomical Six Station Hip Joint Simulator.

3.3.3.1.2 Component pre-test preparation

The ceramic femoral heads and acetabular cups for both BIOLOX® Delta and BIOLOX® Forte were inserted on top of their corresponding stainless-steel stems (C-STEM™ AMT, DePuy Synthes, UK) and into their corresponding titanium shells (BIOLOX® Forte; Duraloc® OPTION CUP and BIOLOX® Delta; PINNACLE™, DePuy Synthes, UK), respectively, to allow for metal transfer prior to pre-test gravimetric measurements. The ceramic femoral heads were inserted onto the stainless-steel stems (pre-cemented in stem holders by a technician) and using a compaction tool and soft-face club hammer the head was impacted three times. The heads were removed using a wedge and the compaction was repeated twice (Figure 3.5A). The acetabular cups were inserted into the titanium shells (pre-cemented into the cup holders by a technician) and using a round plastic piece (similar diameter to ceramic cup) and soft-face club hammer the cup was impacted three times (Figure 3.5B). The cup was removed by inserting the fixed angle plastic mould into the cup holder and turning the Allen key clockwise until the cup was removed from the shell (Figure 3.6). During removal of the cup, the screw pushes against a small round plastic piece, which in turn pushes against the ceramic cup for removal. The small round plastic piece was placed in the cup holder prior to

inserting the acetabular cup to ensure no damage is inflicted on the ceramic cup during removal.

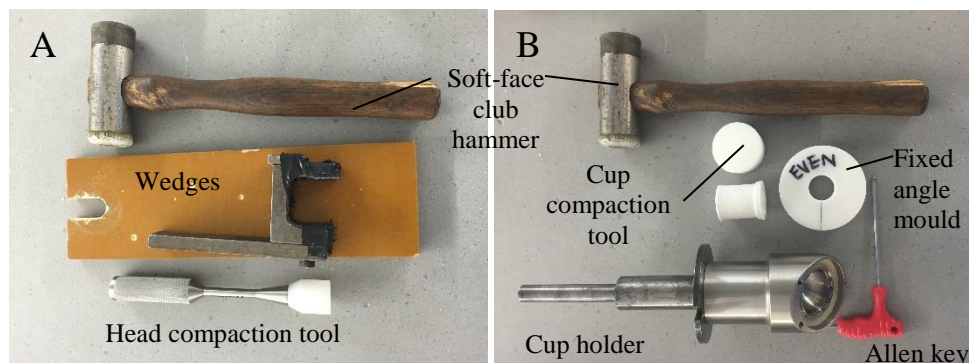


Figure 3.5 – Tools used for compacting the (A) femoral heads and (B) acetabular cups on their corresponding stems and shells, respectively.

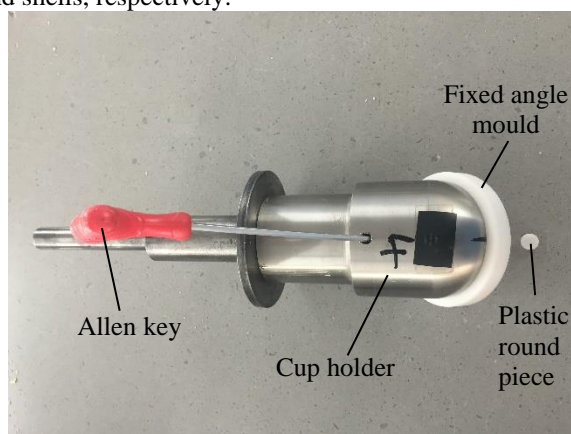


Figure 3.6 – Removal of acetabular cup from the cup holder after impaction.

3.3.3.1.3 Simulator set up

The components were set up on the machine to ensure the centres of rotation of the femoral head and acetabular cup coincided with the centre of rotation of the simulator. All the components and fixtures were etched/marked with identification numbers and alignment marks to ensure they could be re-assembled in the same position after measurement. The BIOLOX[®] Forte components were fixed into the odd numbered stations (one, three and five) whereas the BIOLOX[®] Delta components were fixed into the even numbered stations (two, four and six). This gave $n=3$ for each of the two different types of ceramic bearing materials. The femoral heads were mounted on the taper of stainless-steel stems ensuring the alignment mark on the head was aligned with a manufacturing mark on the stem. The head was then taper locked by impacting the heads with a soft-face club hammer. The stem was previously mounted by a technician in stainless steel holders using poly-methyl methacrylate (PMMA) resin and a bespoke alignment jig to ensure the stem was cemented centrally and vertically in the holder. The same stainless-steel stems were used for all tests, however new ceramic bearing components were used for test 1-3. The the stem holder was attached to the simulator

at its corresponding station and silicon was used to seal any gaps to prevent leaking of the lubricant. The silicon gaiters were attached to each station and secured in place using jubilee stainless-steel high torque hose clips (Figure 3.7A). Using a soft-face club hammer and fixed angle plastic mould (35° or 45°), each acetabular cup was tapped and taper locked into a titanium shell (BIOLOX® Forte; Duraloc® OPTION CUP and BIOLOX® Delta; PINNACLE™) which were previously cemented into a stainless-steel cup holder using PMMA cement. Shells cemented at 45° (clinically 55°) inclination angle were used for test one, whereas new shells cemented at 55° (clinically 65°) inclination angle were used for the remaining tests (Table 3.5). The alignment marks on both the cup and shell were matched to ensure continuity of the positioning throughout the test. Thereafter, grease was applied to the cup holder and inserted into its corresponding test station (Figure 3.7B). The silicon gaiters were then placed over the cup holder and secured in place using jubilee stainless-steel high torque hose clips (Figure 3.7C). The simulator could not be kept sterile during the test, but in order to reduce contamination from microorganisms, all of the components coming into contact with the water lubricant were cleaned by spraying with 1% (v/v) Trigene followed by 70% (v/v) ethanol. The components were dried using paper towels.

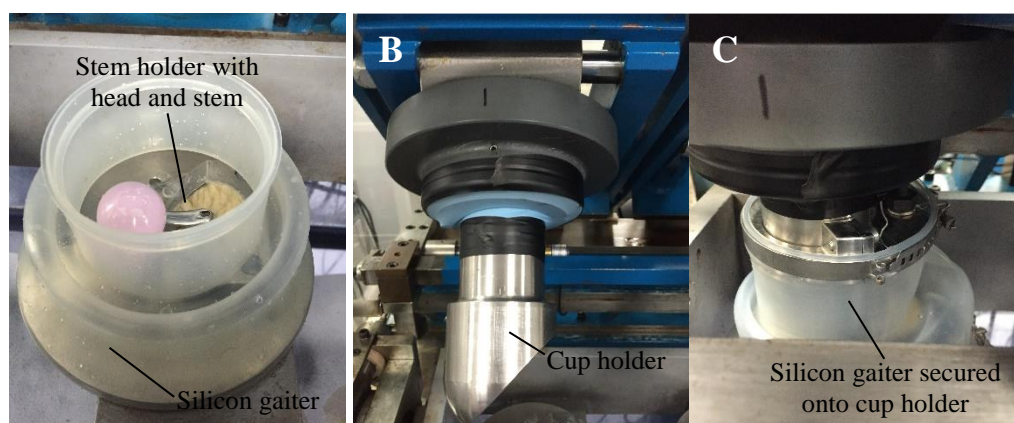


Figure 3.7 – Simulator set-up of stem and cup holder. (A) Stem holders were attached to the simulator at their corresponding station and thereafter the silicon gaiters were attached. (B) Cup holders were placed into their corresponding stations. (C) Cup holders were covered with the silicon gaiters.

3.3.3.1.4 Lubricant used in test stations

Sterile ultra-pure water was used as the lubricant for all the wear simulation tests. The water lubricant was held in silicon gaiters for the initial tests 1 and 2, but these were replaced with open plastic baths for tests 3 and 4 due to silicon contamination issues. Approximately, 450ml of water lubricant was added to each station, which was checked regularly during the test and topped up if the water level dropped. The water lubricant was changed every 330,000 cycles and stored in plastic pots at -20°C.

3.3.3.1.4.1 Contamination of water lubricant

During the lubricant changes the water was noticeably contaminated as indicated by a change in colour and opacity (Figure 3.8). This was of great concern for subsequent biological testing, which required a pure yield of ceramic wear debris. Hence, many changes were made for subsequent tests (Tests 2-4) in an attempt to reduce the contamination levels (Table 3.4). Despite all these changes, the contamination of the water lubricant was still prominent. It was therefore decided to proceed with wear simulation with the contamination issues and resort to post-test processing of the water in order to purify the yield of ceramic wear debris.

Table 3.4 – Changes in simulator set-up to reduce contamination of water lubricant

Test number	Number of cycles (million)	Change in set-up
2	0.77	Silicone barrier applied at the taper-head interface
3	1	-Marine silicone applied to all metal surfaces (Figure 3.9)
4	1	-Conventional-bath set-up was implemented - Cup holders were covered with duct-tape to reduce the number of metal surfaces in contact with the water lubricant

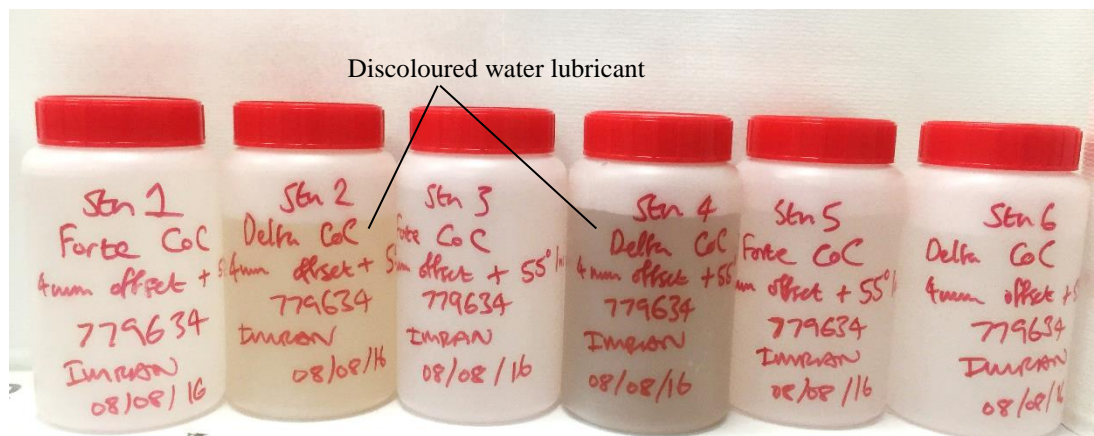


Figure 3.8 – Water lubricant collected from Test 2 after 779634 cycles. The water was visibly discoloured, mainly in stations 2 and 4 due to contaminants present in the water from the simulator.

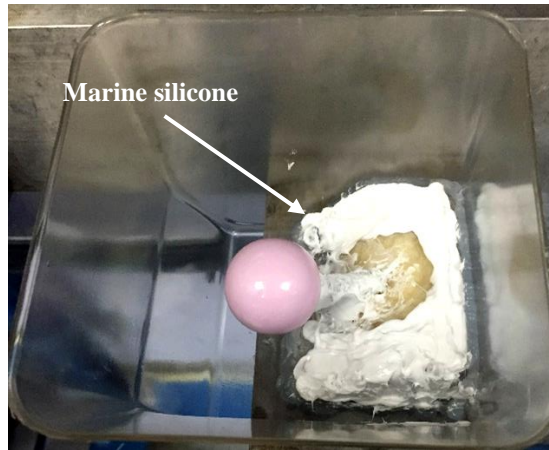


Figure 3.9 – Conventional bath set-up of the ceramic components in the Leeds II hip simulator. Marine silicone was applied to all the metal surfaces (stem and stem holder) that were contact with the lubricant.

3.3.3.1.5 Simulator kinetics and kinematics

The Leeds II hip simulator is capable of generating multi-directional motion between the femoral head and acetabular cup, which includes flexion/extension (applied to the head) and internal/external rotation (applied to the cup). It can generate between 50-3000N of load, which was applied vertically through the centre of the acetabular component. The load was applied and controlled via a single feedback loop system and the input was controlled by SimSol software, the profile of which is shown in Figure 3.10.

Each test was run for one million cycles at a frequency of 1 Hz. A gait cycle was simulated for each cycle that comprised flexion/extension of $-15^{\circ}/+30^{\circ}$ on the femoral head and internal/external rotation ($\pm 10^{\circ}$) on the cup using a Paul-type twin-peak dynamic vertical load of 50N swing phase load and 3kN peak load that was applied through the centre of the acetabular cup. A mismatch or medial-lateral displacement between the centres of rotations of the head and the cup, representing translational surgical mal-positioning, was applied to all the stations using a spring to the lateral side of the cup holder (see Table 3.5). Two acetabular cup inclination angles (45° and 55°) were used throughout this study (Table 3.5). An inclination of 45° that is clinically equivalent to 55° was used for test 1. An inclination angle of 55° that is clinically equivalent to 65° was used for tests 2-4, in order to simulate severe edge loading conditions and attempt to increase the wear rates. The cup inclination angle was increased after Test 1 to increase the wear rates and volume of ceramic wear debris generated. However, the increased cup inclination angle coupled with the high medial-lateral mismatch resulted in fracturing of the BIOLOX[®] Delta cups in stations 4 and 6. Hence, the medial-lateral mismatch was decreased from 4mm to 3mm. The medial-lateral displacement or dynamic (micro) separation was measured and monitored routinely using a calibrated linear variable differential transformer (LVDT) position sensor, which was connected to an oscilloscope (Tektronix, USA) that displayed a graph of the displacement being produced.

Table 3.5 - Conditions used for each test for both materials. Two simulator inclination angles of 45° and 55° were used in the tests, which are equivalent to 55° and 65° clinical inclination angles, respectively.

Test number	Simulator inclination angle (clinical equivalent inclination angle)	Medial-lateral mismatch
1	45 (55) degrees	4mm
2	55 (65) degrees	4mm
3	55 (65) degrees	3mm
4	55 (65) degrees	3mm

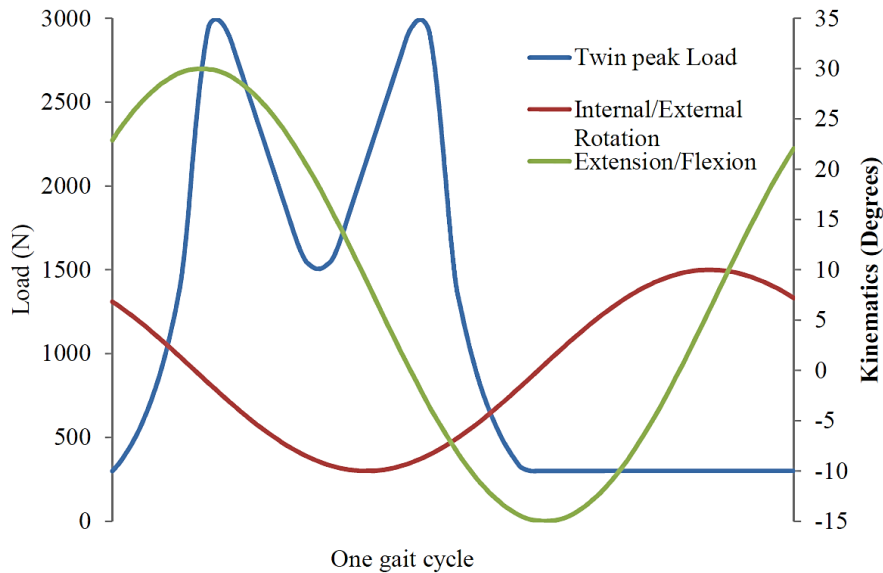


Figure 3.10 - Loading and motion profiles for one gait cycle on the Leeds II hip simulator. Loading and motion profiles for one gait cycle on the Leeds II hip simulator illustrating the relationship between the twin peak axial load and simultaneous motion in the flexion-extension, anterior-posterior and internal-external directions.

3.3.3.2 Pre-test and Post-test analysis of the ceramic hip components

The weight, geometry and surface topography of the ceramic heads and cups was analysed before and after the test to determine the effects of the testing conditions on the components in terms of wear rates, wear stripe pattern, surface roughness and changes in geometry.

3.3.3.2.1 Cleaning of the ceramic hip components

The test components (femoral heads and acetabular cups) were carefully removed from the stems and shells and cleaned using household detergent to remove visible contaminants followed by sonication in 1% (v/v) Trigene solution for 10 minutes. Thereafter the components were rinsed with deionised water and then sonicated for 10 minutes in 70% (v/v)

isopropanol. The components were air dried for 1hr and then transferred to the measurements lab for post-test analysis.

3.3.3.2.2 Measuring clearance between the head and cup ceramic hip components

The diameter and form of the components were measured using the coordinate measuring machine. The option “measure a sphere” was used to obtain twenty-five measurement points (a ring of 10 points at approximately 20 degrees and a ring of 14 points at approximately 110 degrees), which commenced after the initial manual point was measured at the pole. The clearance was calculated by subtracting the external diameter of the head from the internal diameter of the cup.

3.3.3.2.3 Gravimetric measurements of ceramic hip components

The components were weighed before and after the wear simulation testing to determine the volume of wear that was generated. Prior to testing, the ceramic heads and cups were compacted into their corresponding metal backings to allow for metal transfer (section 3.3.3.1.2). Gravimetric measurements were obtained using the XP205 microbalance, where each component was weighed five times and an average weight was determined. A control head and cup component for both BIOLOX® Delta and BIOLOX® Forte (stored in the measurements lab climate controlled room) was used as a reference weight to ensure the difference in weight of the components between different tests was due to wear and no other factors. Cumulative volumetric wear was calculated using the Equation 3 and 3.98g/cm³ density for BIOLOX® Forte and 4.36g/cm³ density for BIOLOX® Delta.

Equation 3

$$Volume = \frac{Weight}{Density}.$$

3.3.3.2.4 Geometric analysis of ceramic hip components

Three-dimensional geometrical characteristics of the surface of the femoral heads and acetabular cups were obtained by using a coordinate measuring machine and RedLux software. The femoral heads and acetabular cups were measured by taking 72 traces over each surface with five degrees spacing about the vertical axis (Figure 3.11). Each trace started at the crest of the component and had a 0.2mm pitch resulting in a total number of 9,936 points on the femoral heads and 8,928 points on the acetabular cups. In order to get the best resolution, for these particular measurements, a 3mm stylus was used with a vertical probe. RedLux software was used to visualise the size, shape and penetration depth of the wear areas.

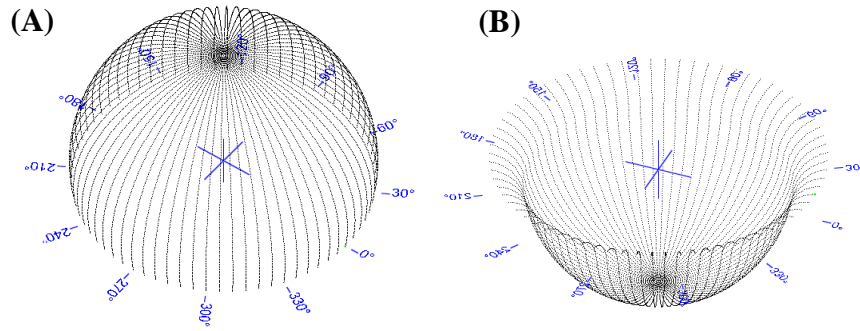


Figure 3.11 - Data points taken using a CMM on the surfaces of the (A) femoral heads and (B) acetabular cups to ascertain the geometrical changes after wear simulation testing.

3.3.3.2.5 Surface topography analysis of the ceramic hip components

3.3.3.2.5.1 Surface roughness of the ceramic hip components

Surface roughness of the articulating surfaces for the heads and cups was measured using the Form Talysurf 120L contacting surface profilometer, which maps out irregularities on a surface. The arithmetic mean deviation, also known as the average roughness or centre line average (R_a), is the average from the centre line of the sampling length. R_a values are high when the surface is rough, represented by a large number of peaks across the sampling area. The skewness (R_{sk}) measured the symmetry of the profile about the mean line and therefore allowed differentiation between asymmetrical profiles that may have the same R_a . The maximum peak height (R_p) and the minimum valley height (R_v) were also investigated together with R_a and R_{sk} to provide a more accurate description of the bearing surface. Roughness parameters R_a , R_{sk} , R_p and R_v were assessed before and after wear simulation test 1 in accordance with ISO 4288:1998. Three 15mm traces (P1, P2 and P3) were taken in relation to the alignment mark (Figure 3.12). P1 and P2 were perpendicular to each other and taken along the flexion-extension path. The P3 trace was taken on an area of the bearing not in contact during the test. The femoral head was positioned on its side, by rotating the component 90° so trace P3 could be obtained. The acetabular cup was tilted approximately 45° so trace P3 could be obtained. Due to the hemispherical nature of ceramic hip components, the traces were taken using least square arcs with a Gaussian filter to suppress the waviness and form of the components, allowing only roughness to be assessed. A Gaussian cut-off of 0.08mm with a bandwidth of 100:1 was used as recommended in ISO 4288:1998 for ceramic components with initial R_a below $0.02\mu\text{m}$.

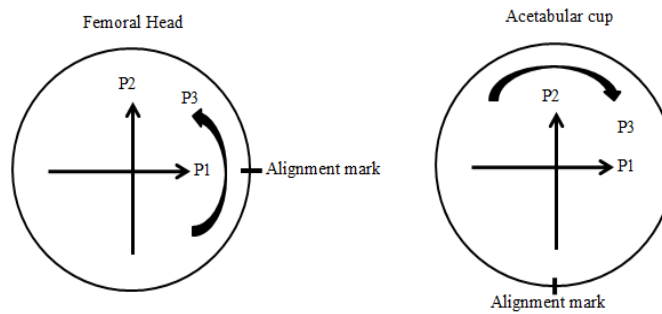


Figure 3.12 - Schematic of the three traces performed on the femoral head and acetabular cup components in relation to the alignment mark in order to obtain the surface roughness before and after the wear simulation test.

3.3.3.2.5.2 Scanning electron microscopy of the wear scar on the ceramic femoral heads

A Carl Zeiss EVO MA15 high definition scanning electron microscopy was used to obtain high magnification images of the wear areas of the bearing surfaces after simulator testing. The images were used to analyse the features of the wear pattern and in turn identify the wear mechanism. Prior to imaging, the ceramic wear surface was coated with 20nm layer of Iridium to allow conduction of the electron beam. The whole femoral head component was placed on the stage of the SEM for imaging.

3.3.3.3 Generation of cobalt chromium wear particles using a six-station pin-on-plate wear simulator

Clinically-relevant CoCr wear particles were generated in water using the six-station pin-on-plate wear simulator. Smooth, high carbon CoCr alloy pins and plates were used as described in section 3.3.2.4.

3.3.3.3.1 Cleaning of rig components

The CoCr pins and plates were cleaned by ultra-sonication in 70% (v/v) isopropanol for 10 minutes at room temperature. The components of the six-station rig were cleaned using household detergent solution and then immersed in 1% (v/v) Trigene for 20 minutes. Thereafter all the components were rinsed in deionised water before drying using disposable paper towels Figure 3.13. The cleaning of the components was to minimise contamination of from previous tests.

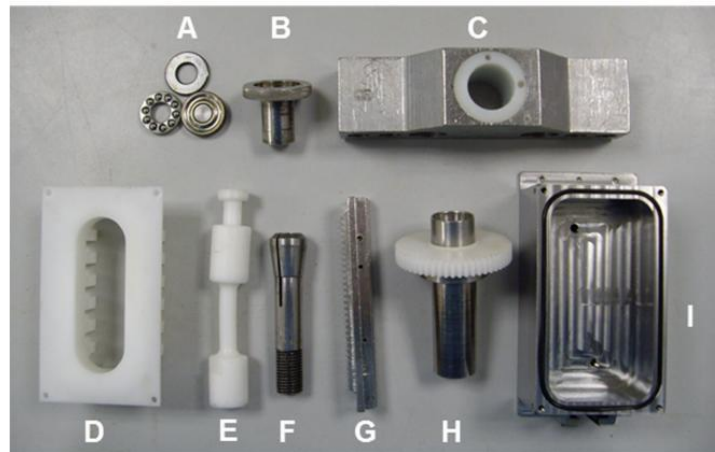


Figure 3.13 – Components of the six-station pin-on-plate wear rig simulator. (A) Ball bearing assembly components, (B) threaded nut, (C) bridge section, (D) polymer baffle, (E) connecting rod, (F) collet, (G) toothed rack, (H) pin holder with polymer gear, (I) stainless-steel bath with seal inside the side groove.

3.3.3.3.2 Assembly of the six-station pin-on-plate wear rig

The plates were fixed into the stainless-steel baths noting the orientation and numbers of both the plates and bath to ensure this remained constant throughout the test. A rubber seal was placed into the groove of the bath before a plastic baffle was inserted into the bath and secured in place using screws. The toothed racks were then screwed onto the side of each bath before each numbered bath was fixed on the rig at the corresponding station number (Figure 3.14A). The pins were assigned to individual stations and remained constant throughout the test. The pins were placed in a pin collet, using metal spacers to ensure that at least 5mm of the pin was protruding from the pin holder (Figure 3.14B). The pin collet containing the pin was then placed into the pin holder outer sleeve, which was then inserted into the corresponding bridge section and secured in place using a threaded nut that was screwed onto the end of the pin holder (Figure 3.14C). Thereafter the complete bridge section and pin holder was slotted into the support brackets of the corresponding station and secured in place by tightening the clamps (Figure 3.14D). The pins were checked to ensure contact with the plates, and that the threaded nut was not in contact with the bridge. This was to ensure that the loading was applied axially throughout the test. Thereafter, the connecting rods were screwed into place, connecting the scotch yolk mechanism to the trays (Figure 3.14E).

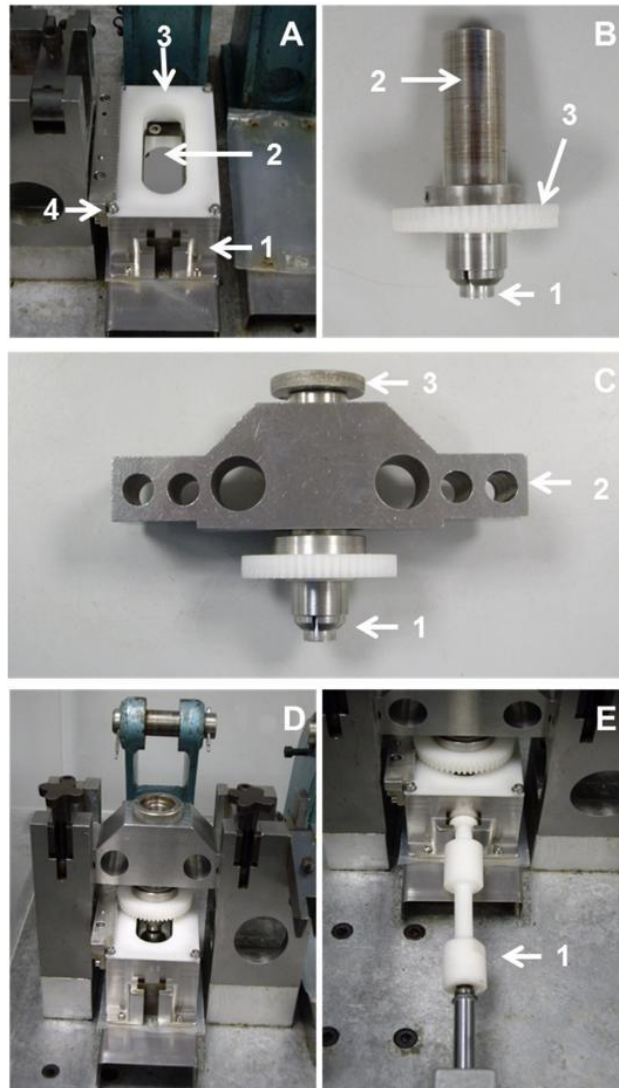


Figure 3.14 – Assembly of the six-station pin-on-plate wear rig simulator. A - The pre-assembled stainless-steel bath (1) containing the CoCr plate (2), corresponding baffle (3) and toothed rack (4) was secured into position on the rig. B – The pin (1) was placed in the collet and pin holder (2) with plastic gear wheel attached. C – The pin holder (1) was slotted into the corresponding bridge section (2) and secured into position using a threaded nut (3). D – The bridge section and pin holder were secured into position over the bath. E – The plastic connecting rods (1) were screwed into place, connecting the scotch yolk mechanism to the trays.

3.3.3.3.3 Generation of cobalt-chromium wear particles using the six-station pin-on-plate wear rig simulator

Using a syringe, approximately 50ml of ultra-pure water was added to each bath, ensuring the level of water was sufficient enough so the pin surface was under water. Thereafter, the appropriately numbered cantilever arm was secured onto each station using the pivot pins and levelled using a spirit level. The thrust bearing assembly was inserted in the top of the threaded nut to provide a sitting point for the load screw in the cantilever.

The cycle counter was set to zero before the rig was started. The frequency was increased slowly to the required setting i.e. 1 Hz or 60 cycles per minute (cpm), with a stroke length of 28mm and a rotation of $\pm 30^\circ$ (calibration of the stroke length and reciprocating speed was

performed by a lab technician). Thereafter the weights were placed onto each cantilever arm at the correct position to give an application load of 80 N (Figure 3.15). The test was run for continuously for 2 weeks whereby the lubricant was topped up to ensure the fluid level was 1-2mm above the plate wear surface. Upon completion of the wear test, the water lubricant containing the wear particles for each station was transferred into appropriately labelled sterile plastic pots and stored at -20°C. The number of cycles was recorded and the rig was dismantled.

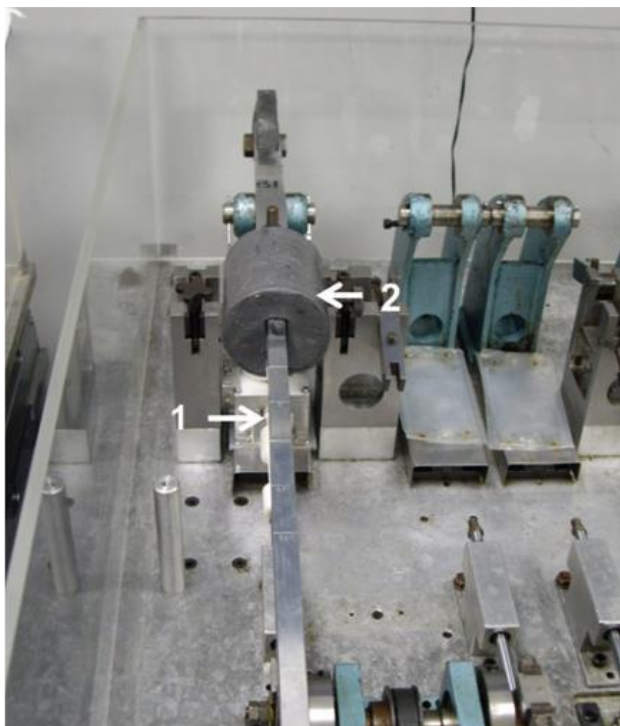


Figure 3.15 – Assembled station on the six-station wear rig simulator with (1) cantilever arm and (2) weight.

3.3.3.4 Recovery of the wear particles generated

The water lubricants containing the ceramic or metal wear particles were processed to recover the wear particles, which were stored until required for subsequent testing to determine biological impact.

3.3.3.4.1 Ceramic wear particles

The water lubricants containing the ceramic (BIOLOX[®] Forte or BIOLOX[®] Delta) wear particles generated using the hip simulator were initially reduced in volume using a freeze dryer. The water lubricant was dried for 1-2 weeks until all or most of the ice sublimed away, leaving behind particulate matter. Thereafter, the remaining particle matter was re-suspended in a 10ml of sterile water and sonicated for 10 minutes before pooling the particle suspensions for BIOLOX[®] Forte from stations 1, 3 and 5 and for BIOLOX[®] Delta from stations 2, 4 and

6. Thereafter, the particle suspensions were transferred to SW32 polypropylene centrifuge tubes and centrifuged at 125,755g for 1 hour at 25°C. The supernatant was removed and the particle pellets were re-suspended in 3ml of ultra-pure deionised water. Each particle suspension was then placed on a sodium polytungstate density gradient and centrifuged (Beckman Optima L-90K ultra-centrifuge and SW40 rotor) at 202,048g for 4 hours and 25°C (section 2.3.3.4.4). After centrifugation, the particles were collected at the bottom of the tube in the form of a pellet, whilst the contaminating particulate matter and other impurities, which was darker in colour and had a lower density remained higher up the tube. The supernatant was slowly aspirated and discarded, and the pellet of particles was re-suspended in 1ml of sterile water and sonicated for 10 minutes before being transferred to a clean centrifuge tube (14ml, Thinwall Polypropylene). This was repeated three times to ensure all the particles were transferred to the clean tube. The recovered particles were then washed five times in sterile water using Beckman Optima L-90K ultra-centrifuge and SW40 rotor at 154,693g for 1 hour at 37°C. Between each wash, the supernatant was discarded and the particles were re-suspended in sterile water before sonication for 10 minutes. After the final wash, the particle pellet was re-suspended in 3ml of ultra-pure deionised water and stored at -20°C until required.

3.3.3.4.2 Cobalt-chromium wear particles

The water lubricant containing the CoCr nano-particles that were generated using the six-station pin-on-plate wear simulator was thawed at 37°C for 1 hour before being sonicated for 30 minutes to disperse the particles. Thereafter, the particle suspension was transferred to SW32 polypropylene centrifuge tubes and centrifuged at 125,755g for 1 hour at 25°C. The supernatant was removed and the particle pellet was re-suspended in 3ml of ultra-pure deionised water and stored at -20°C until required.

3.3.3.5 Characterisation of the recovered ceramic wear particles

The characteristics of the ceramic wear particles generated in water required subsequent validation against the ceramic wear particles generated in the conventional serum lubricant (25% FBS (v/v)). An aliquot from the particle suspension containing the wear particles recovered from the water lubricant used in wear simulation was subjected to sonication and filtered through a 0.015 filter membrane. Images and the composition of the wear particles generated *in vitro* were captured and analysed using CFE-SEM and EDX analysis as described in section 2.3.3.2.2. The CFE-SEM micrographs of the wear particles were subsequently analysed using computer software, ImageJ version 1.49, to measure the Feret diameter (d_{max}), aspect ratio and circularity of the particles. A minimum of 150 particles were characterised in accordance with the standard practice for characterisation of particles; ASTM

F1877-05:2010, and International Standard for wear of implant materials; BS ISO 17853:2011.

3.3.3.5.1 Calculating percentage ratio between ceramic and stainless-steel wear particles using EDX elemental mapping

The ceramic wear particles generated using the hip simulator were contaminated with stainless-steel wear particles, which could not be separated from the ceramic wear particles. This resulted in a mix population of ceramic and stainless-steel wear particles that would be presented to the cells. Hence, EDX elemental mapping was used to calculate the percentage ratio between the ceramic wear particles (BIOLOX[®] Forte and BIOLOX[®] Delta) and stainless-steel particle contaminants.

An aliquot (100 μ l) from the recovered wear particle suspension (1mg/ml) was subjected to sonication and filtered through a 0.015 filter membrane. Thereafter, images and the composition of the wear particles generated *in vitro* were captured and analysed using CFE-SEM and EDX analysis. The CFE-SEM was set to a working distance of 15mm and 10Kv voltage. Using the EDX elemental mapping tool, five random fields of view at 100x magnification were analysed for the major elements (wt%) iron (Fe) for the stainless-steel wear particles and aluminium (Al) for the ceramic wear particles. An average of the weight % for each element was calculated and presented in a histogram.

3.3.3.6 Preparation of particles for cell culture studies

A glass vial was cleaned by sonication in sterile water and 70% (v/v) ethanol before heat treatment at 180°C for 4 hours. The glass vial was then weighed using the XP205 microbalance, which is sensitive to 10⁻⁵ grams. A reference glass vial was also weighed as changes in atmospheric conditions can cause differences that need to be accounted for before and after adding particles to the glass vial. The glass vials were weighed five times (within 100 μ g) to provide an average weight. The particle suspension (section 3.3.3.4) was thawed and transferred to the glass vial; all of the particle suspension for the ceramic particles and a small amount (2-3ml) for the CoCr particles was transferred into the pre-weighed glass vial. The glass vials containing the particle suspensions were then heat treated in the oven at 190°C for 4 hours to sterilise the particles and remove the water and endotoxins. Thereafter, the glass vials with the particles were weighed again using the same technique described previously. The mass of the particles was calculated by subtracting the average weight of the vial without the particles from the average weight of the glass vial with the particles. This mass was then adjusted according to the average weight of the reference glass vial before and after adding the particles to the other glass vials. The particles were suspended in an appropriate volume

of sterile water to produce a stock particle suspension with a concentration of $1\text{ mg}\cdot\text{ml}^{-1}$ which were stored at -20°C until required.

3.3.4 Statistical Analysis

3.3.4.1 Wear rates and Penetration depths

Statistical analysis was performed on measurements data using one-way analysis of variance (ANOVA) and 95% confidence limits (95% CL) were calculated.

3.3.4.2 Characteristics of wear particles

Statistical differences in the particles size distributions, aspect ratio values and circularity values between different types of particles were tested using an Independent Samples T-Test (SPSS Statistics Version 24, IBM Corp. USA). The tests were carried out on the original un-binned data produced from Image J.

3.4 Results

The aim of this study was to generate clinically-relevant ceramic wear particles to be used for subsequent determination of biological impact of ceramic wear particles. In order to do this the Leeds II hip simulator was used to generate clinically relevant ceramic wear particles from CoC bearings and the pin-on-plate wear rig was used to generate clinically-relevant CoCr wear particles from CoCr pins and plates. The wear rates were determined using gravimetric analysis, which are presented in this section.

3.4.1 Wear testing of ceramic-on-ceramic hip bearings

3.4.1.1 Gravimetric analysis

The Leeds II hip simulator was used to generate clinically-relevant ceramic wear debris from the BIOLOX® Forte (n=3) and BIOLOX® Delta (n=3) ceramic-on-ceramic hip replacements. Four tests were completed in total, where each test was run for one million cycles under severe edge loading conditions caused by dynamic separation due to translational mismatch between the centres of rotation of the femoral head and acetabular cup (test conditions used are shown in Table 3.5). A Paul-type twin-peak dynamic vertical load of 50N swing phase load and 3kN peak load was applied through the centre of the acetabular cup. Two acetabular cup inclination angles (45° and 55°) were used throughout this study (Table 3.5).

3.4.1.1.1 Wear simulation – Test 1

During Test 1, the components were tested under 4mm translational mismatch with a 55° (clinical equivalence) cup inclination angle for one million cycles. The three stations for BIOLOX® Forte and stations 4 and 6 for BIOLOX® Delta generated similar amounts of wear, however the components in station 2 for BIOLOX® Delta generated considerably lower wear compared to the other stations (Figure 3.16). Overall, the test generated higher cumulative wear from BIOLOX® Delta (1.27mm³) than BIOLOX® Forte (0.94mm³). BIOLOX® Delta experienced a higher mean wear rate of $0.42 \pm 0.66\text{mm}^3/\text{million cycles}$ compared to BIOLOX® Forte ($0.31 \pm 0.12\text{mm}^3/\text{million cycles}$) (Figure 3.17) using water as the lubricant, however there was no significant difference in wear rate between the two different materials ($p>0.05$, ANOVA).

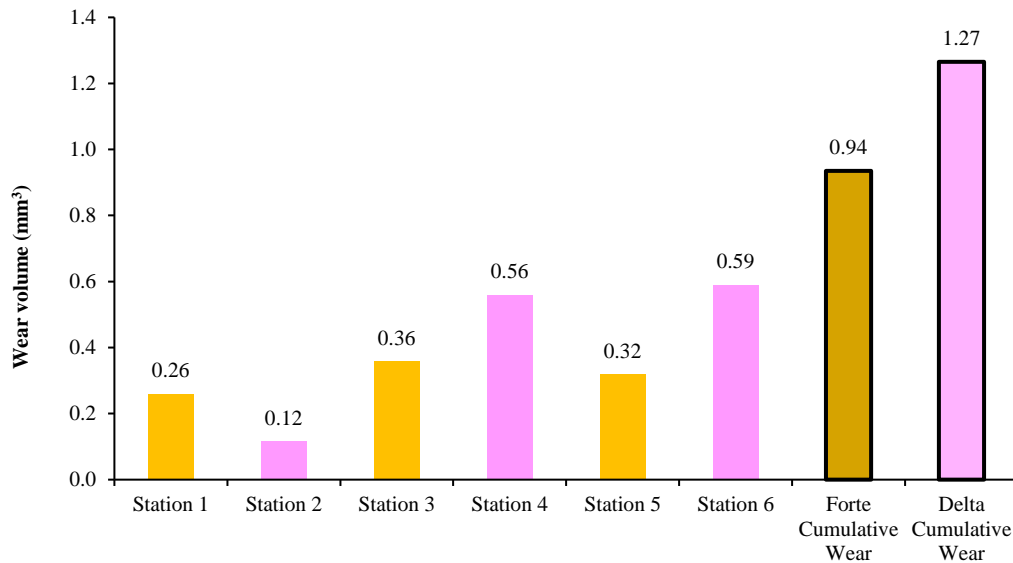


Figure 3.16 - Wear volumes generated by ceramic-on-ceramic bearings after 1 million cycles of testing under 4mm translational mismatch and 55° (clinical equivalence) cup inclination angle conditions (Test 1). Stations 1, 3 and 5 housed BIOLOX® Forte components and stations 2, 4 and 6 housed BIOLOX® Delta components. Total wear volume across stations for both materials is also shown.

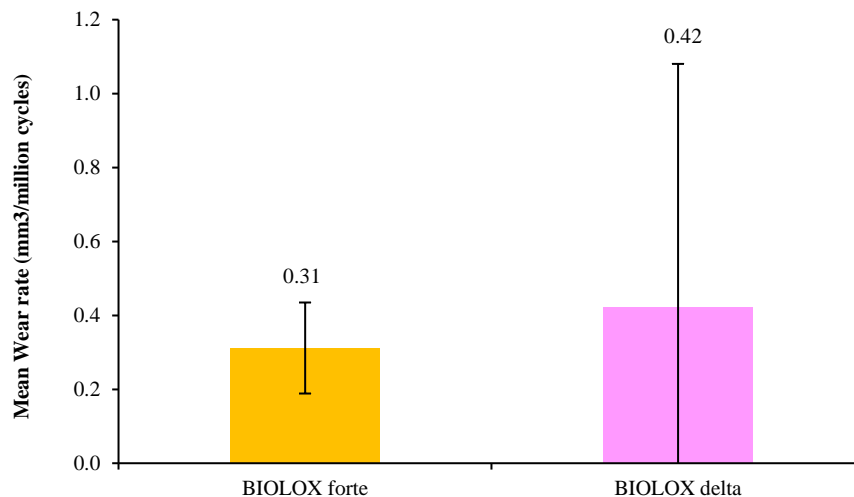


Figure 3.17 - Mean wear rate of ceramic-on-ceramic bearings after 1 million cycles of testing under 4mm translational mismatch and 55° (clinical equivalence) cup inclination angle conditions (Test 1). Error bars represent 95% confidence limits (n=3).

3.4.1.1.2 Wear simulation – Test 2

During Test 2, the components were tested under 4mm translational mismatch with 65° (clinical equivalence) cup inclination angle. The increase in inclination angle was implemented as higher volumes of wear particles was required from the ceramic bearings. The simulator was stopped at 780,000 cycles due to fracturing of the BIOLOX® Delta cup components on stations 4 and 6. However, the BIOLOX® Delta components on station 2 generated extensive amounts of wear compared to the BIOLOX® Forte components (Figure 3.18), where the volume of wear from BIOLOX® Delta (4.66mm³) was higher than the cumulative wear volume (4.07mm³) for BIOLOX® Forte. The components from Stations 4

and 6 were not analysed due to fracture of the acetabular cup components. Hence only the mean wear rate for BIOLOX® Forte was calculated, which was $1.36 \pm 0.12 \text{mm}^3/0.78 \text{million}$ cycles (Figure 3.19).

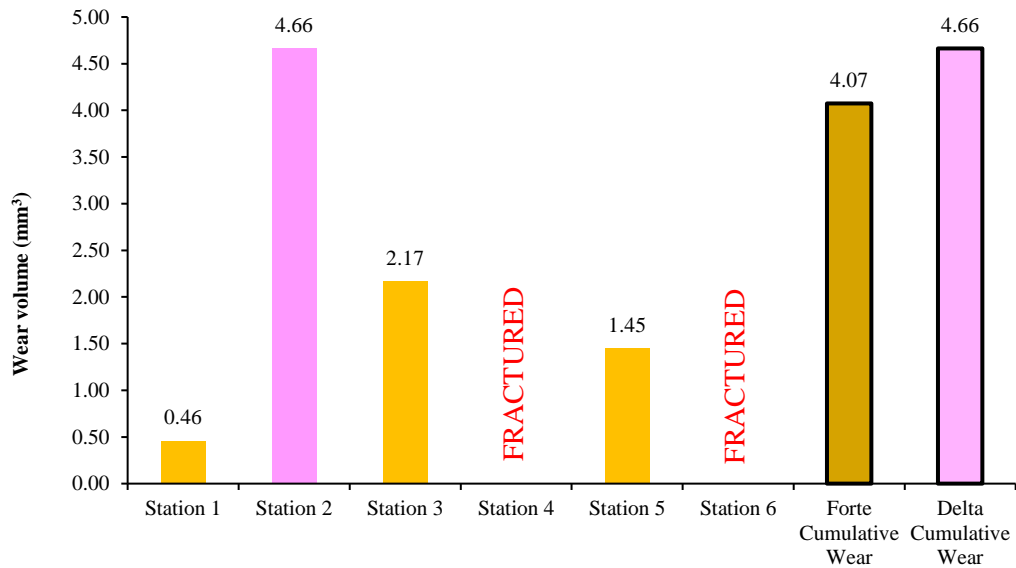


Figure 3.18 - Wear volumes generated by ceramic-on-ceramic bearings after 1 million cycles of testing under 4mm translational mismatch and 65° (clinical equivalence) cup inclination angle conditions (Test 2). Stations 1, 3 and 5 housed BIOLOX® Forte components and stations 2, 4 and 6 housed BIOLOX® Delta components. Total wear volume across stations for both materials is also shown. The components from Stations 4 and 6 were not analysed due to fracture of the acetabular cup components.

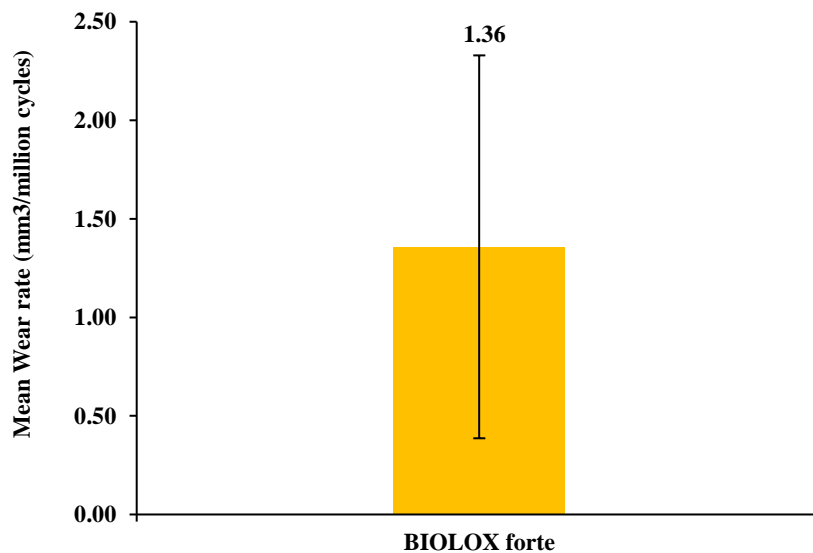


Figure 3.19 - Mean wear rate of BIOLOX® Forte ceramic-on-ceramic bearings after 1 million cycles of testing under 4mm translational mismatch and 65° (clinical equivalence) cup inclination angle conditions (Test 2). The mean wear rate of BIOLOX® Delta was not presented due to the fracture of the acetabular cup components that resulted in n=1. Error bars represent 95% confidence limits (n=3).

3.4.1.1.3 Wear simulation – Test 3

The cup inclination angle was increased in test 2 to increase the wear rates and volume of ceramic wear debris generated. However, the increased cup inclination angle coupled with the high medial-lateral mismatch resulted in fracturing of the BIOLOX[®] Delta cups in stations 4 and 6. Therefore, the medial-lateral mismatch was decreased from 4mm to 3mm. Hence during test 3, the components were tested under 3mm translational mismatch with 65° (clinical equivalence) cup inclination angle for one million cycles. All three stations for BIOLOX[®] Forte and stations 2 and 4 for BIOLOX[®] Delta generated similar amounts of wear, whereas the wear volume generated in station 6 for BIOLOX[®] Delta was considerably higher (0.92mm³), in the order of 10-fold higher compared to station 2 (0.09mm³) and station 4 (0.07mm³) (Figure 3.20). The higher wear rate for station 6 was due to stainless steel third body wear, which was generated from the cup holder impacting against the stem holder because of a failed screw that holds the cup holder in place. For this reason, station 6 was not included in the cumulative wear and the mean wear rate was not calculated for BIOLOX[®] Delta components. Overall, the test generated higher cumulative wear from BIOLOX[®] Forte (0.34mm³) than BIOLOX[®] Delta (0.16mm³) components. The BIOLOX[®] Forte components experienced a mean wear rate of $0.11 \pm 0.05\text{mm}^3/\text{million cycle}$ (Figure 3.21).

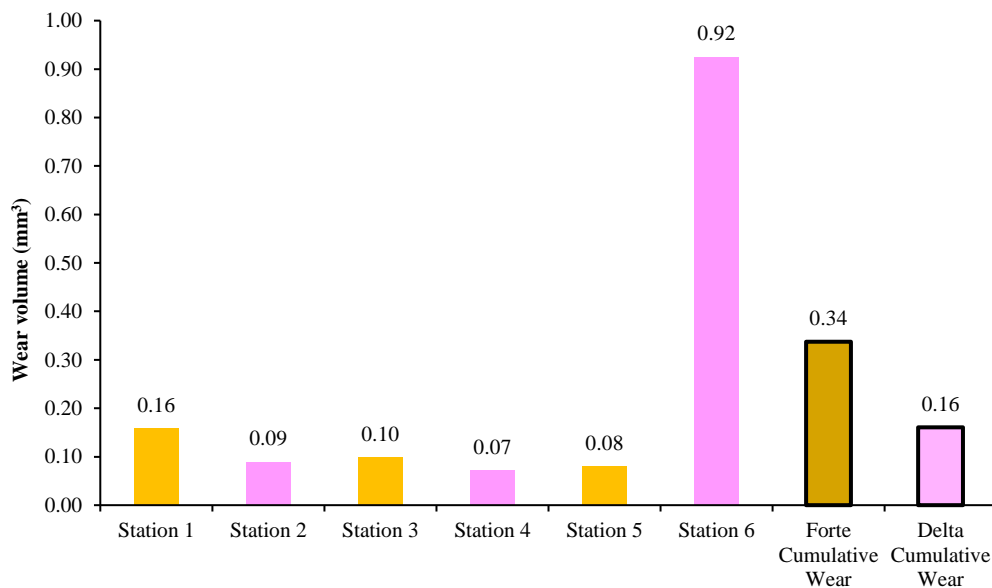


Figure 3.20 - Wear volumes generated by ceramic-on-ceramic bearings after 1 million cycles of testing under 3mm translational mismatch and 65° (clinical equivalence) cup inclination angle conditions (Test 3). Stations 1, 3 and 5 housed BIOLOX[®] Forte components and stations 2, 4 and 6 housed BIOLOX[®] Delta components. Total wear volume across stations for both materials is also shown. The BIOLOX[®] Delta components from station 6 were not included in the cumulative wear due to complications during the test.

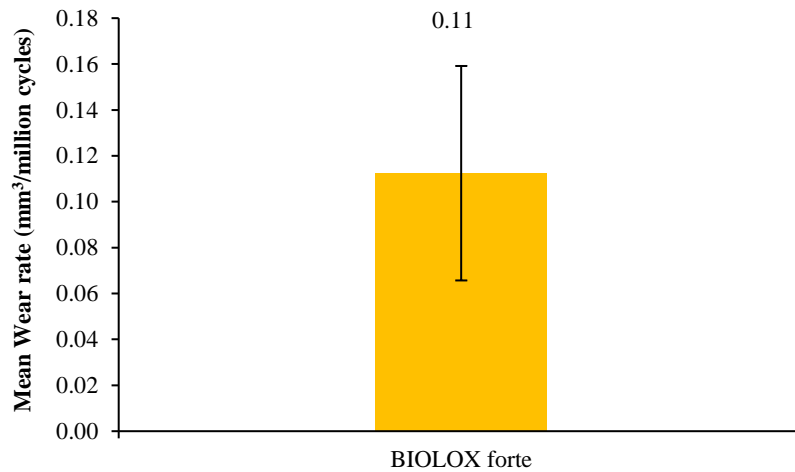


Figure 3.21 - Mean wear rate of BIOLOX Forte ceramic-on-ceramic bearings after 1 million cycles of testing under 3mm translational mismatch and 65° (clinical equivalence) cup inclination angle conditions (Test 3). The mean wear rate of BIOLOX® Delta components was not presented due to complications during the test, which resulted in n=2. Error bars represent 95% confidence limits (n=3).

3.4.1.1.4 Wear simulation – Test 4

During Test 4, the components were tested under 3mm translational mismatch with 65° (clinical equivalence) cup inclination angle for one million cycles. The same conditions as test 3 were employed as these conditions generated a sufficient volume of ceramic wear debris required for biological testing. The three stations which housed BIOLOX Forte and BIOLOX Delta components varied in the amount of wear generated (Figure 3.22). Station 6 for BIOLOX® Delta experienced high levels of contamination by stainless steel wear particles, which may have been due to the complications from test 3 that may have resulted in a faulty testing station. For this reason, station 6 was not included in the cumulative wear and the mean wear rate was not calculated for BIOLOX® Delta components. Overall, the test generated higher cumulative wear volumes from BIOLOX® Forte (0.95mm³) compared to BIOLOX® Delta (0.29mm³). The BIOLOX® Forte components experienced a mean wear rate of $0.32 \pm 0.19\text{mm}^3/\text{million cycle}$ (Figure 3.23).

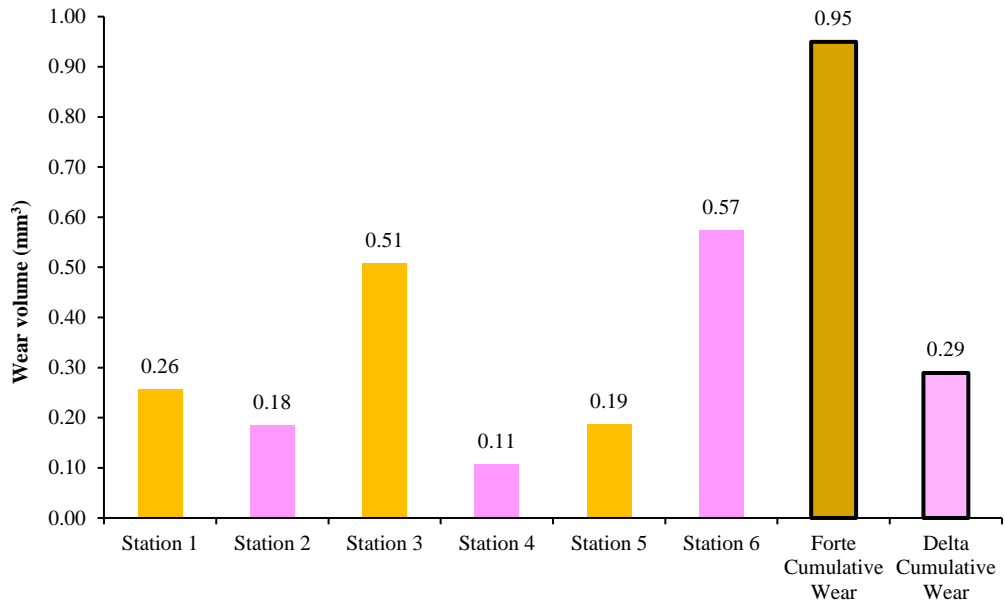


Figure 3.22 - Wear volume generated from ceramic-on-ceramic bearings after 1 million cycles of testing under 3mm translational mismatch and 65° (clinical equivalence) cup inclination angle conditions (Test 4). Stations 1, 3 and 5 housed BIOLOX® Forte components and stations 2, 4 and 6 housed BIOLOX® Delta components. Total wear volume across stations for both materials is also shown. The BIOLOX® Delta components from station 6 were not included in the cumulative wear due to complications during the test.

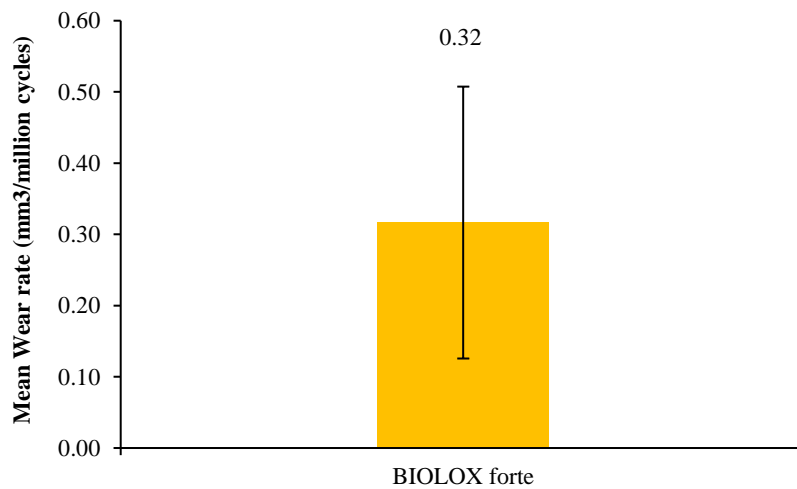


Figure 3.23 - Mean wear rate of BIOLOX Forte ceramic-on-ceramic bearings after 1 million cycles of testing under 3mm translational mismatch and 65° (clinical equivalence) cup inclination angle conditions (Test 4). The mean wear rate of BIOLOX® Delta components was not presented due to complications during the test, which resulted in n=2. Error bars represent 95% confidence limits (n=3).

3.4.1.2 Dynamic separation

The dynamic (micro) separation achieved from each station was measured using a LVDT and plotted against the wear rate for both BIOLOX® Forte (Figure 3.24) and BIOLOX® Delta (Figure 3.25). A weak positive correlation was observed for both BIOLOX® Forte ($R^2=0.56$) and BIOLOX® Delta ($R^2=0.59$), where an increase in the level of dynamic (micro) separation resulted in increased wear.

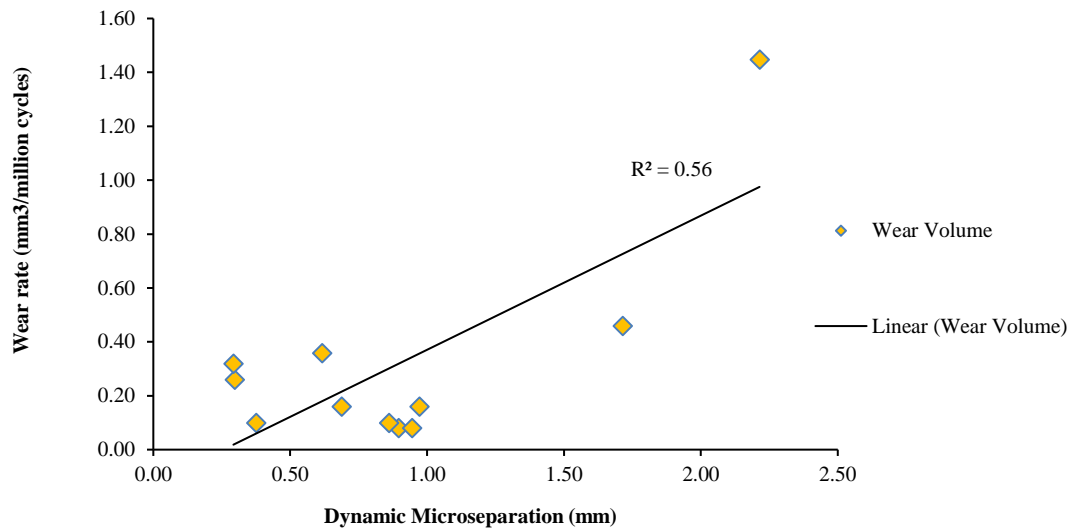


Figure 3.24 – Wear rate of BIOLOX® Forte components plotted against the medial-lateral displacement or dynamic (micro) separation measured using a LVDT (Tests 1-4).

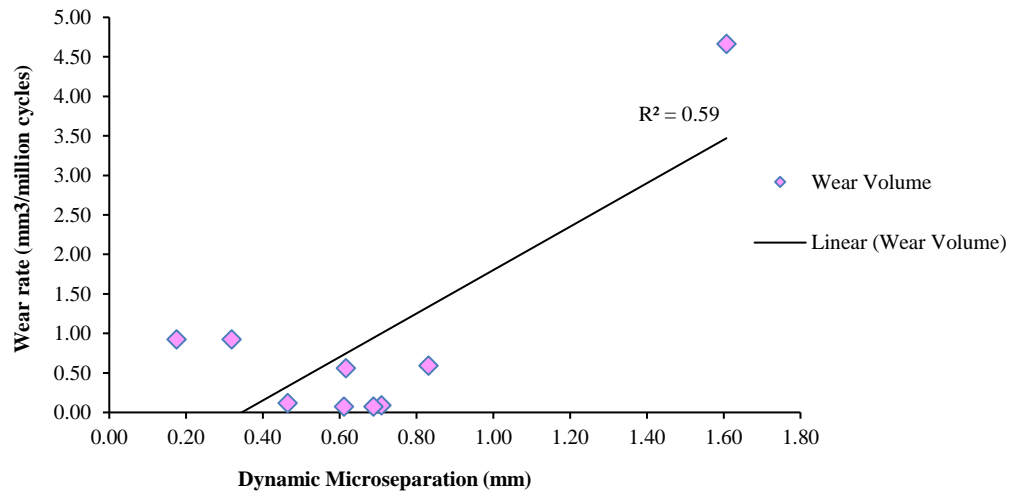


Figure 3.25 - Wear rate of BIOLOX® Delta components plotted against the medial-lateral displacement or dynamic (micro) measured using a LVDT (Tests 1-4).

3.4.1.3 Surface analysis ceramic hip components

3.4.1.3.1 Roughness of ceramic hip components

The introduction of translational medial-lateral mismatch between the head and the cup resulted in the formation of stripe wear on the femoral head and a corresponding wear scar on the acetabular cup. The surface roughness of the articulating surfaces was measured using the Form Talysurf 120L contacting surface profilometer, which maps irregularities on the surface. The severe edge loading conditions caused an increase in the surface roughness (R_a) for all the heads and cups for both BIOLOX[®] Forte and BIOLOX[®] Delta (Table 3.6). However, there was no significant difference in all the surface roughness parameters (R_a , R_{sk} , R_p and R_v), before or after the wear simulation test.

Table 3.6 - The mean surface roughness characterisation parameters before and after wear simulation testing for BIOLOX[®] Forte and BIOLOX[®] delta heads and cups.

	Pre-test		Post-test	
	Forte Heads	Forte Cups	Forte Heads	Forte Cups
Ra (µm)	0.004 ± 0.001	0.006 ± 0.001	0.006 ± 0.002	0.015 ± 0.008
Rp (µm)	0.011 ± 0.003	0.016 ± 0.001	0.018 ± 0.004	0.039 ± 0.008
Rv (µm)	0.016 ± 0.005	0.022 ± 0.002	0.023 ± 0.007	0.062 ± 0.028
Rsk	-1.475 ± 1.037	-0.780 ± 0.076	-2.226 ± 1.911	-1.370 ± 0.828
	Pre-test		Post-test	
	Delta Heads	Delta Cups	Delta Heads	Delta Cups
Ra (µm)	0.005 ± 0.000	0.007 ± 0.001	0.006 ± 0.001	0.010 ± 0.001
Rp (µm)	0.013 ± 0.001	0.018 ± 0.004	0.014 ± 0.003	0.029 ± 0.003
Rv (µm)	0.016 ± 0.002	0.025 ± 0.006	0.018 ± 0.004	0.037 ± 0.002
Rsk	-0.389 ± 0.203	-0.720 ± 0.072	-0.703 ± 0.125	-0.972 ± 0.557

Note: All values expressed as ±95% confidence interval.

3.4.1.3.2 Scanning electron microscopy of wear scar

A high definition scanning electron microscope was used to obtain high magnification images of the wear area of the femoral head bearing surfaces from test 1 (wear stripes of test 1 components are representative of all the tests). High magnification (x200) images of the femoral head articulation surfaces showed a smooth uniform surface in the unworn areas and a roughened surface in the adjacent worn areas for both BIOLOX[®] Forte and BIOLOX[®] Delta (Figure 3.26 & Figure 3.27). The lower magnification (x200) images also showed the overall wear track and the distribution of grain pull-outs, which resulted in the formation of pits within the surface. Pits ranging between 0-20 μ m in length were observed for BIOLOX[®] Forte (Figure 3.26), whereas BIOLOX[®] Delta (Figure 3.27) had larger pits ranging between 0-60 μ m in length at x1000 magnification. The x200 magnification images for BIOLOX[®] Delta showed the boundary between the unworn and worn surface areas that was characterised by a line of exposed grains and individual grain pull-outs in the unworn area, which may eventually wear away a resemble the unworn surface.

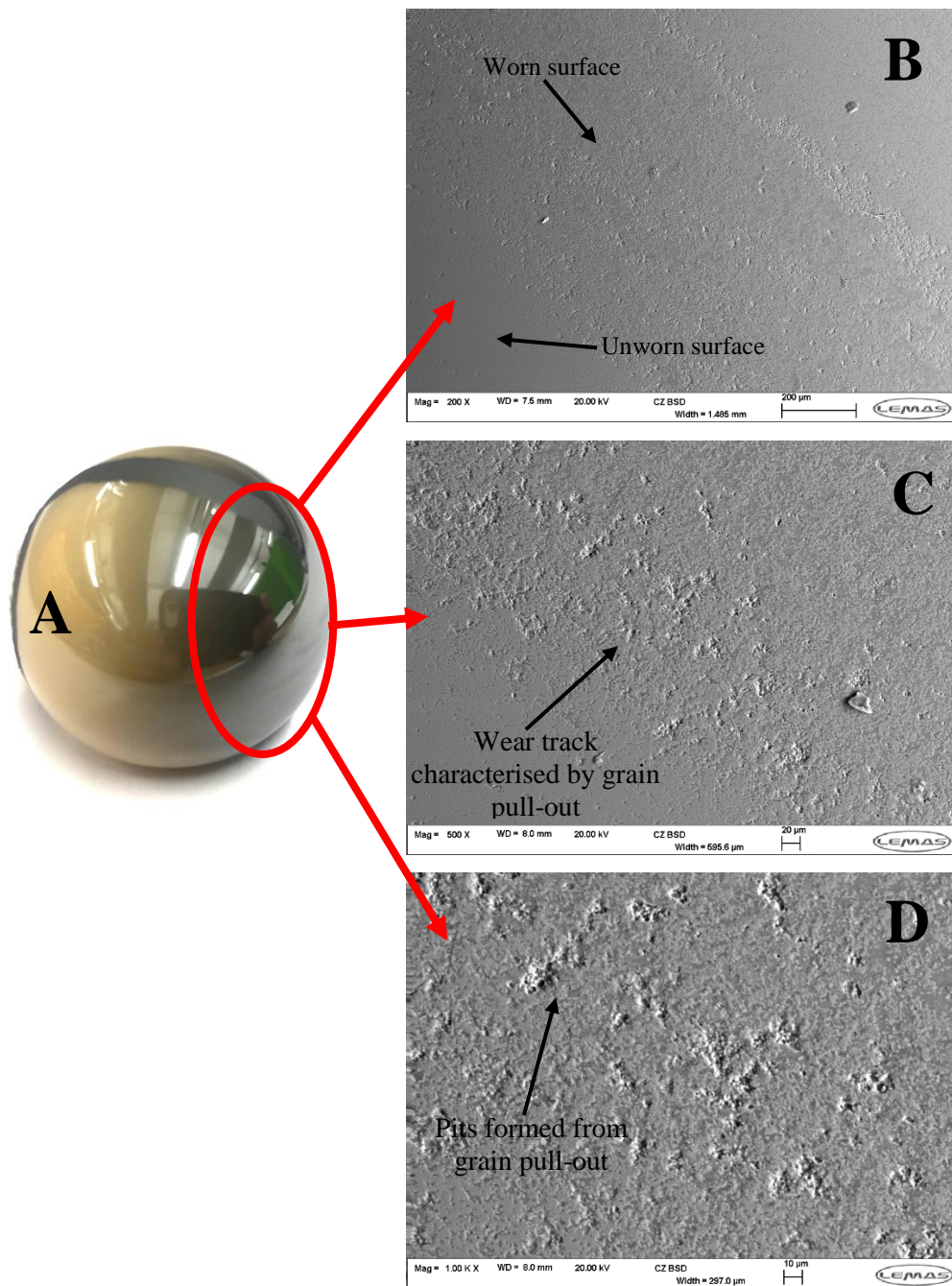


Figure 3.26 - SEM images of a BIOLOX[®] Forte ceramic femoral head post wear simulation (Test 1, station 1). The components were tested under 4mm translational mismatch with a 55° (clinical equivalence) cup inclination angle for one million cycles. (A) BIOLOX[®] Forte ceramic femoral head coated with iridium over the wear scar; (B) x200 magnification of wear scar and unworn surface; (C) x500 magnification of wear scar; (D) x1000 magnification of wear scar.

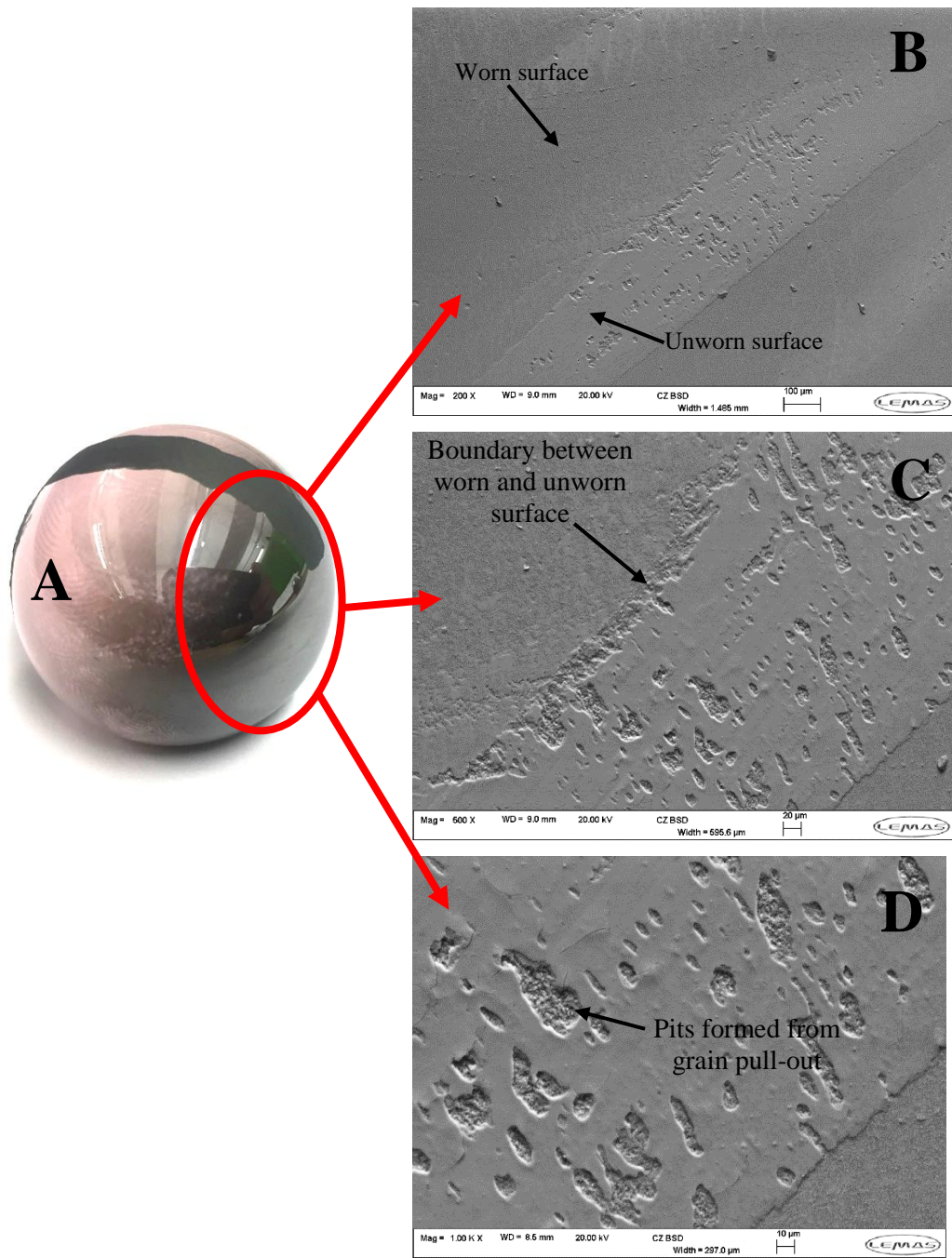


Figure 3.27 - SEM images of a BIOLOX[®] Delta ceramic femoral head post wear simulation (Test 1, station 2). The components were tested under 4mm translational mismatch with a 55° (clinical equivalence) cup inclination angle for one million cycles. (A) BIOLOX[®] Delta ceramic femoral head coated with iridium over the wear scar; (B) x200 magnification of wear scar and unworn surface; (C) x500 magnification of wear scar; (D) x1000 magnification of wear scar.

3.4.1.3.3 Stripe analysis

Three-dimensional representation of the surface of the heads and cups from test 1 (representative of all tests as all components were tested under same conditions) were generated using a CMM to analyse the characteristics of the wear scar after wear simulation for one million cycles. Furthermore, a CMM was used to ascertain the penetration depth of the wear scar. The wear stripes for BIOLOX[®] Forte and BIOLOX[®] Delta produced under the severe edge loading conditions due to dynamic (micro) separation are shown in Figure 3.28. The wear stripes on the BIOLOX[®] Forte heads appeared to be wider compared to the wear stripes on the BIOLOX[®] Delta heads. The wear stripe on the BIOLOX[®] Forte heads had a mean penetration depth of 9.25 μ m, whereas the wear stripe on the BIOLOX[®] Delta heads had a mean penetration depth of 15.91 μ m (Figure 3.29). However, there was no significant difference in the mean penetration depth between the two different materials. Furthermore, there was a larger variation in penetration depths for BIOLOX[®] Delta compared to BIOLOX[®] Forte, as illustrated by the large error bar (95% confidence limit) in Figure 3.29.

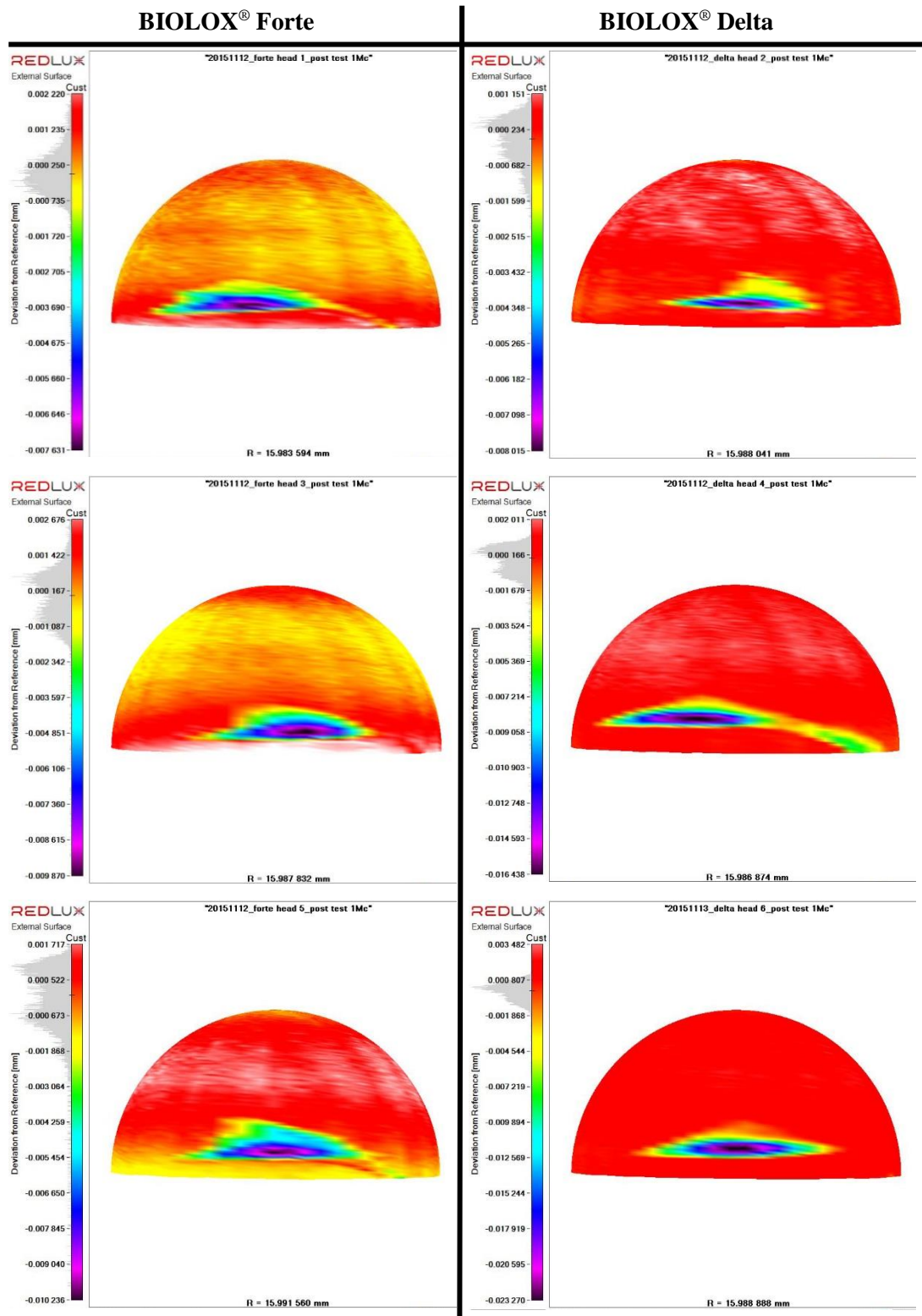


Figure 3.28 – Three-dimensional reconstruction of the wear stripe area over three BIOLOX[®] Forte and BIOLOX[®] Delta femoral heads tested (test 1) under severe edge loading conditions (4mm translational mismatch and 45° (clinical equivalence) cup inclination angle).

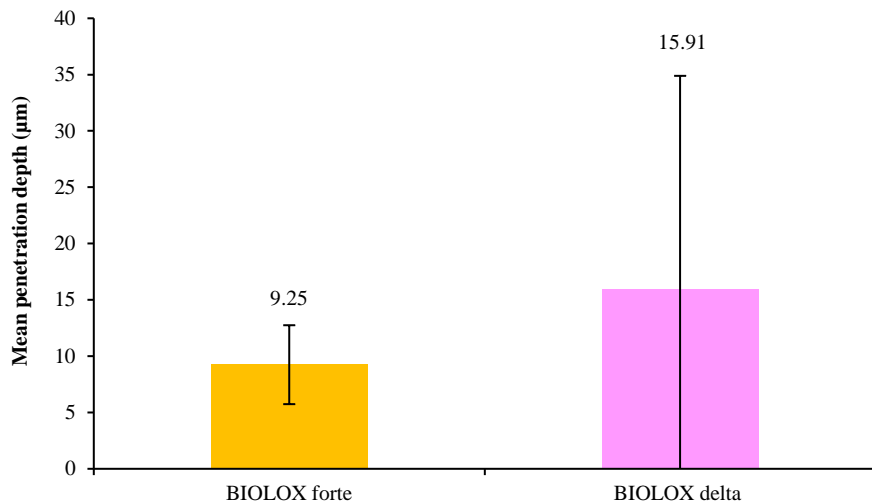


Figure 3.29 – Mean penetration depths for BIOLOX® Forte and BIOLOX® Delta tested under severe edge loading conditions (4mm translational mismatch and 45° (clinical equivalence) cup inclination angle). Error bars represent 95% confidence limits.

3.4.2 Characterisation of the recovered wear particles

The characteristics in terms of size and morphology, and the composition of the recovered wear particles generated in water were determined and analysed after filtration on 0.015µm filter membrane using CFE-SEM and EDX analysis as described in section 2.3.3.2.2. Image analysis software (ImageJ version 1.49) was used to measure the Feret diameter (d_{max}), aspect ratio and circularity of the particles (minimum of 150 particles).

3.4.2.1 Characterisation of ceramic wear particles

CFE-SEM analysis of the ceramic wear particles generated using the Leeds II hip simulator revealed an abundance of stainless steel particle contaminants from all the tests as indicated by detection of the iron (Fe) elemental peaks in EDX analysis (Figure 3.30). This was also observed for the particles isolated from serum lubricant as described in section 2.4.5, and was of great concern for accurately obtaining the characteristics of ceramic wear particles and also for subsequent biological testing. Hence, the same imaging technique was also applied here whereby EDX analysis was used to identify the elemental composition of every particle imaged to ensure that the particles being measured were indeed ceramic i.e. particles that showed aluminium (Al) peak for the BIOLOX® Forte samples were measured and particles that showed aluminium (Al) and zirconia (Zr) and/or strontium (Sr) peaks for the BIOLOX® Delta samples were measured. For example, Figure 3.30 shows an SEM image of the particles analysed using EDX and corresponding EDX spectrums (Figure 3.30B, C). The Al (aluminium) and O (oxygen) peaks in Figure 3.30B are indicative of alumina, similarly the Fe (iron) peaks in Figure 3.30C are indicative of stainless steel. This technique minimised the incorrect measurement of contaminating particles, which may otherwise have the same

geometry/morphology as ceramic particles and therefore be indistinguishable. The carbon (C) peak was due to the carbon coating and the other peaks of silica (Si) and chromium (Cr) may have been due to contaminants that were present in the water lubricant from wear simulation testing.

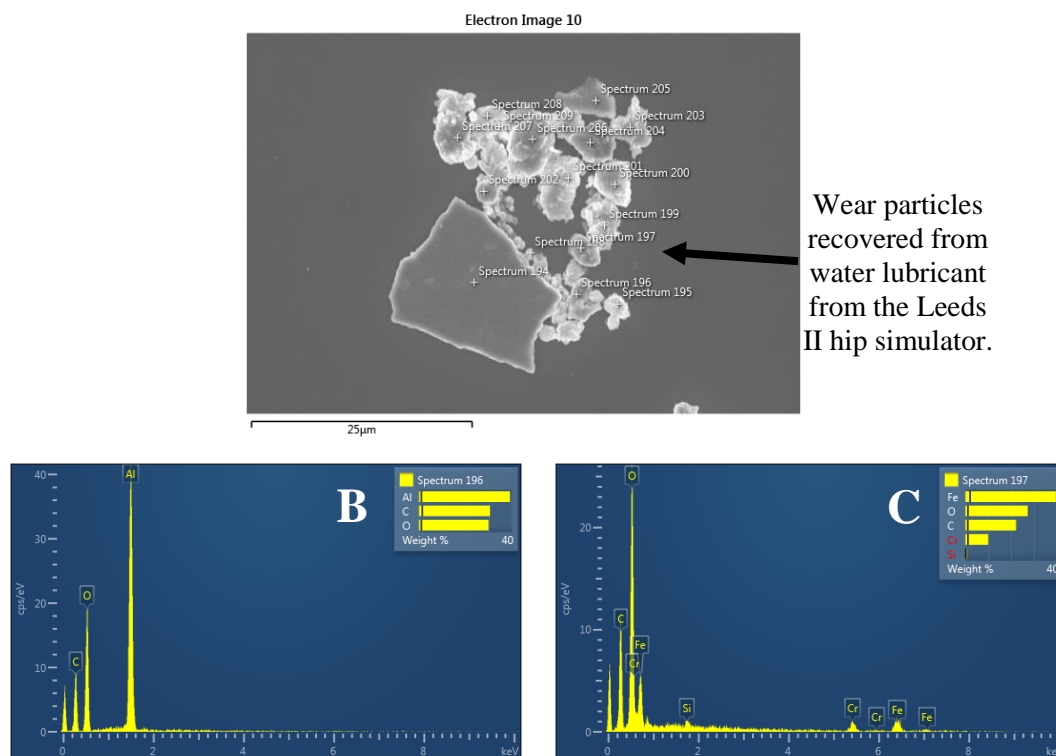


Figure 3.30 - CFE-SEM and EDX analysis of the recovered BIOLOX[®] Delta ceramic wear particles and stainless-steel particle contaminants generated in the Leeds II hip simulator. (A) SEM image of the particles analysed using EDX and (B & C) corresponding EDX spectra. (B) EDX spectrum of alumina particles as indicated by Al (aluminium) and O (oxygen) peaks and (C) EDX spectrum of stainless-steel particles as indicated by the Fe (iron) peaks. Pin point EDX analysis of the particles was performed at a working distance of 15mm, 10kV and a suitable magnification to maintain focus.

3.4.2.1.1 Characteristics of BIOLOX[®] Forte ceramic wear particles

CFE-SEM analysis of the recovered ceramic wear particles from BIOLOX[®] Forte revealed large micrometre particles (Figure 3.31A) that were irregular/shard-like in shape and small nano-scale particles (Figure 3.31B) that were round in morphology. EDX analysis confirmed these larger wear particles were indeed comprised of alumina as indicated by the elemental peaks of aluminium (Al) and oxygen (O) (Figure 3.32B). The presence of stainless steel particle contaminants was also detected, which were indicated by the elemental peaks of iron (Fe) in the EDX spectrum (Figure 3.32C). EDX analysis confirmed that the smaller nano-scale particles were also alumina as indicated by the elemental peaks of aluminium (Al) and oxygen (O) (Figure 3.33). The carbon (C) peak was due to the carbon coating and the tungsten (W) peak was due to the sodium polytungstate density gradient medium that was used to separate the wear particles from the low-density contaminants.

The frequency as a function of size of the recovered particles is presented in Figure 3.34, which revealed a bimodal size distribution. The larger micron and sub-micron size particles ranged between 100-4000nm with a mean size of $736 \pm 99.45\text{nm}$ ($\pm 95\%$ CL), whereas the small nano-scale particles ranged between 10-90nm with a mean size of $50 \pm 7.11\text{nm}$ ($\pm 95\%$ CL). The BIOLOX[®] Forte wear particles had a mode size distribution of 300-400nm for the larger particles and a mode size of 40-50nm for the smaller nano-scale particles. The mean feret diameter, mean aspect ratio and mean circularity values (value of 1.0 indicates a perfect circle) are shown in Table 3.7. The larger particles (100 - >5000nm) had a higher mean aspect ratio (1.52 ± 0.06), thus they were more elongated and irregular in shape compared to the smaller (0-100nm) nano-scale particles (1.34 ± 0.04), which were more round and consistent in shape. The smaller (0-100nm) nano-scale particles had a higher mean circularity value (0.91 ± 0.01) compared to the larger particles (0.76 ± 0.02), which indicated that the smaller nano-scale particles were more circular in shape than the larger particles.

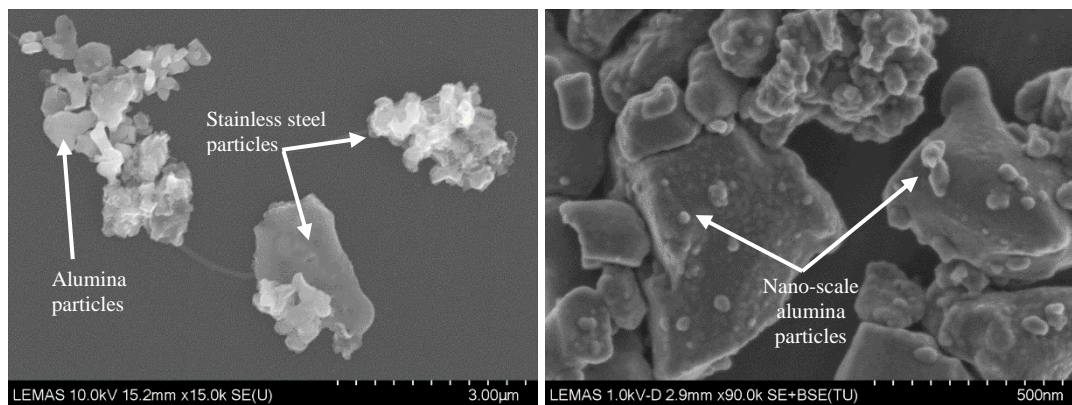


Figure 3.31 - CFE-SEM images of wear particles generated from BIOLOX[®] Forte using the Leeds II hip simulator. (A) SEM image of large micron size alumina particles and (B) smaller nano-scale alumina. The larger particles were imaged at 10kV (secondary electrons; SE) voltage, working distance of 15mm and 15K magnification to capture groups of large particles. The smaller nano-scale particles were imaged at 1kV (deceleration mode) voltage, working distance of 2-3mm and at 60k, 90k and 150k magnification.

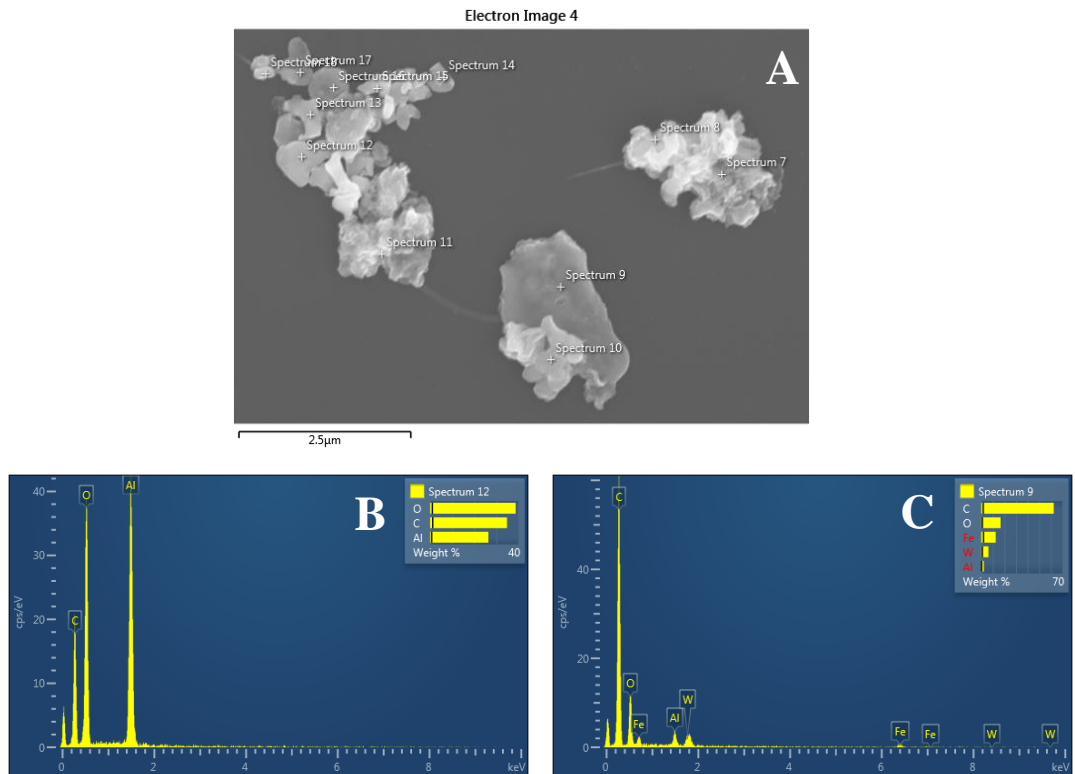


Figure 3.32 - CFE-SEM and EDX analysis of the recovered BIOLOX[®] Forte ceramic wear particles and stainless-steel particle contaminants generated using the Leeds II hip simulator. (A) SEM image of the larger alumina particles analysed using EDX and (B & C) corresponding EDX spectra. Pin point EDX analysis of the particles was performed at a working distance of 15mm, 10kV and a suitable magnification to maintain focus. EDX spectrum B showed elemental peaks of Al (aluminium) and O (oxygen), which is indicative of alumina ceramic particles. EDX spectrum C showed elemental peaks of Fe (iron), which is indicative of stainless steel. The W (tungsten) peak was from the particle isolation procedure.

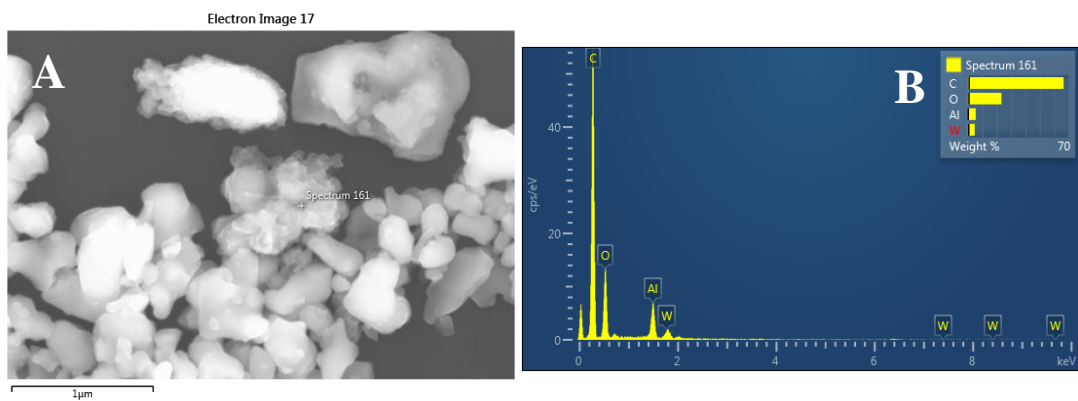


Figure 3.33 - CFE-SEM and EDX analysis of the recovered BIOLOX[®] Forte ceramic wear particles (A) SEM image of the nano-scale alumina particles analysed using EDX and (B) corresponding EDX spectrum. Pin point EDX analysis of the particles was performed at a working distance of 15mm, 10kV and a suitable magnification to maintain focus. The W (tungsten) peak was from the particle isolation procedure.

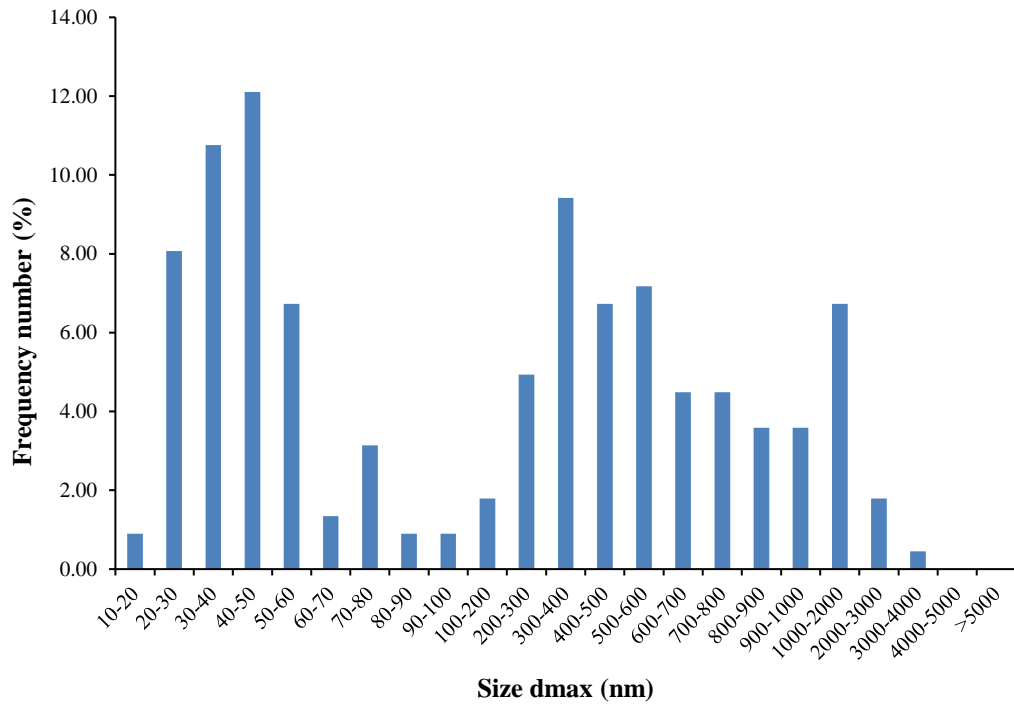


Figure 3.34 - Frequency size distribution of BIOLOX® Forte ceramic wear particles that were generated in water lubricant using the Leeds II hip simulator under edge loading conditions due to dynamic separation between the head and cup centres. A minimum of 150 particles were measured.

Table 3.7 – Morphology (ferret diameter, aspect ratio and circularity) values for BIOLOX® Forte ceramic wear particles generated in water.

	BIOLOX® Forte wear debris generated in water; Larger particles (100 - >5000nm)	BIOLOX® Forte wear debris generated in water; Smaller particles (0 - 100nm)
Feret diameter (nm)	736.48 ± 99.45	50.16 ± 7.11
Aspect ratio	1.52 ± 0.06	1.34 ± 0.04
Circularity	0.76 ± 0.02	0.91 ± 0.01

Note: All values expressed as mean ±95% Confidence Interval.

3.4.2.1.2 Characteristics of BIOLOX® Delta ceramic wear particles

CFE-SEM analysis of the recovered ceramic wear particles from BIOLOX® Delta revealed large micrometre particles (Figure 3.35A) that were irregular/shard-like in shape and smaller nano-scale particles (Figure 3.35B) that were round in morphology. EDX analysis confirmed the larger micron-size particles were alumina with elemental peaks of aluminium (Al) and oxygen (O) (Figure 3.36B), whereas the smaller nano-scale particles consisted of alumina and Zirconia as indicated by the elemental peaks of aluminium (Al) and zirconia (Zr) (Figure 3.37B). The presence of stainless steel particle contaminants was also detected, which was indicated by the elemental peaks of iron (Fe) in the EDX spectrums (Figure 3.36C). The carbon (C) peak was due to the carbon coating and the chromium (Cr) peak may have been from stainless-steel wear particles as it is present in trace amounts.

The frequency as a function of size for the recovered BIOLOX[®] Delta particles generated in water is presented in

Figure 3.38, which revealed a bimodal size distribution. The larger micron and sub-micron size particles ranged between 200-20,000nm, with a mean size of $3900 \pm 447.52\text{nm}$ ($\pm 95\%$ CL), whereas the smaller nano-scale particles ranged between 20-90nm with a mean size of $48 \pm 1.41\text{nm}$ ($\pm 95\%$ CL). The BIOLOX[®] Delta particles had a mode size distribution of 2000-4000nm for the larger particles and a mode size of 40-50nm for the smaller nano-scale particles. The mean ferret diameter, mean aspect ratio and mean circularity values (value of 1.0 indicates a perfect circle) are shown in Table 3.8. The larger particles (100 - >5000nm) had a higher mean aspect ratio (1.58 ± 0.08), which indicated that they were more elongated and irregular in shape compared to the smaller (0-100nm) nano-scale particles (1.27 ± 0.02), as they were more round and consistent in shape. The smaller (0-100nm) nano-scale particles had a higher mean circularity value ($0.91 \pm 0.01\text{nm}$) compared to the larger particles ($0.68 \pm 0.02\text{nm}$), which indicated the smaller nano-scale particles were more circular in shape than the larger particles. The same pattern was observed for the BIOLOX[®] Delta ceramic wear particles generated in serum lubricant. An independent-samples t-test was conducted to compare the size distribution (feret diameter) and morphology (aspect ratio and circularity) of the BIOLOX[®] Delta ceramic wear particles generated in water with those generated in serum (section 3.3.4.2). Particle morphology of the BIOLOX[®] Delta ceramic wear particles was unaffected by the lubricant i.e. no statistically significant differences in the aspect ratio ($p=0.571$) and circularity ($p=0.088$) values were observed between the BIOLOX[®] Delta ceramic wear particles generated in serum and water. Moreover, the particle size distribution (feret diameter) for the BIOLOX[®] Delta wear particles generated in water and serum were also statistically similar ($p=0.057$).

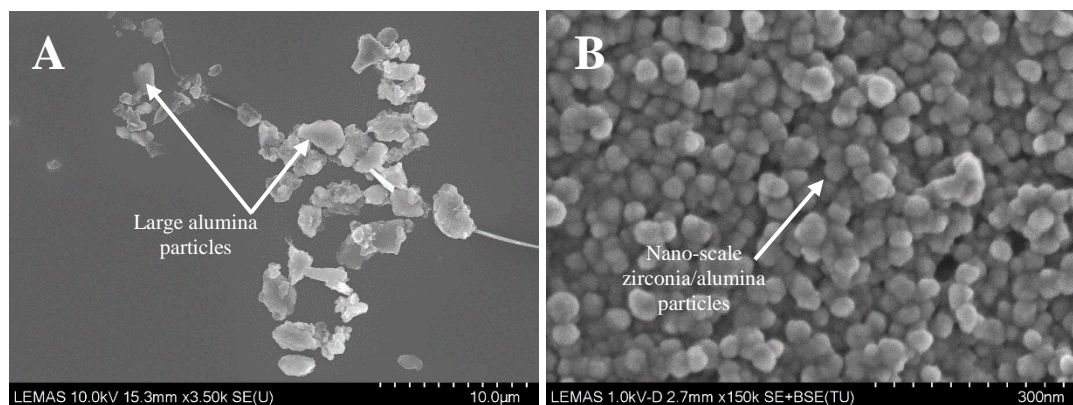


Figure 3.35 - CFE-SEM images of wear particles generated from BIOLOX[®] Delta using the Leeds II hip simulator. SEM images of (A) large micron size alumina particles and (B) smaller nano-scale alumina and zirconia particles. The larger particles were imaged at 10kV voltage, working distance of 15mm and 3.5K magnification to capture groups of the particles. The smaller nano-scale particles were imaged at 1kV (deceleration mode) voltage, working distance of 2-3mm and 60k, 90k and 150k magnification.

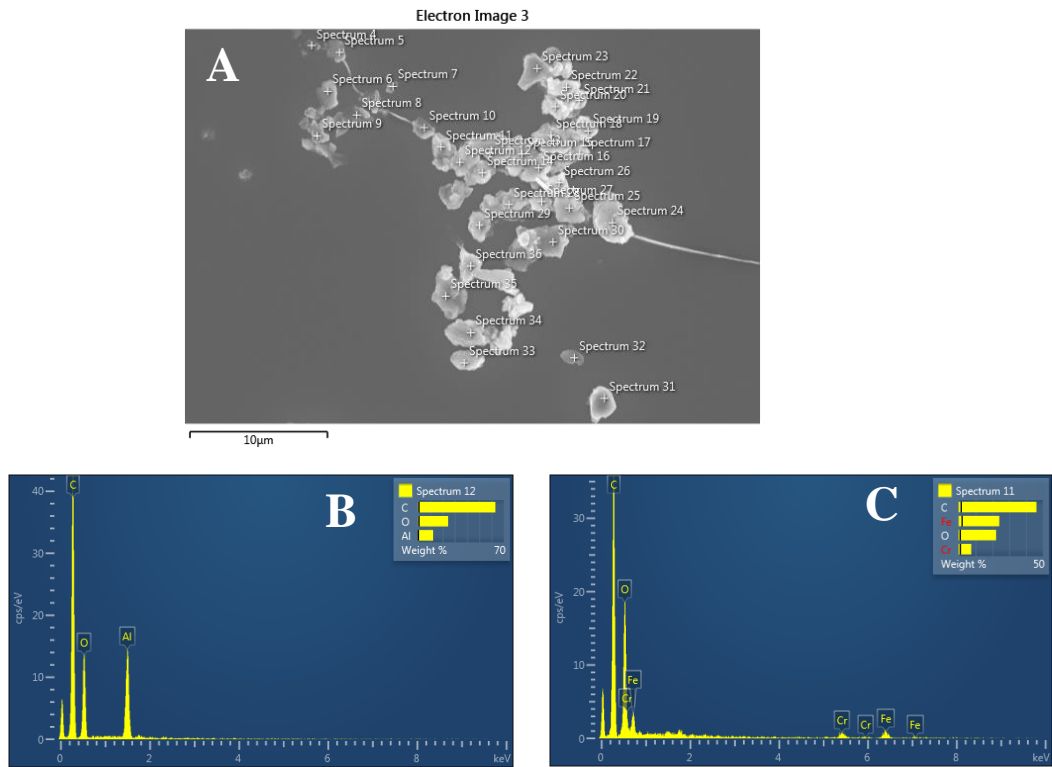


Figure 3.36 - CFE-SEM and EDX analysis of the recovered BIOLOX[®] Delta ceramic wear particles and stainless-steel particle contaminants generated using the Leeds II hip simulator. (A) SEM image of the large alumina particles analysed using EDX and (B & C) corresponding EDX spectra. EDX spectrum B showed elemental peaks of Fe (iron), which is indicative of stainless steel. EDX spectrum C showed elemental peaks of Al (aluminium) and O (oxygen), which is indicative of alumina ceramic particles. Pin point EDX analysis of the particles was performed at a working distance of 15mm, 10kV and a suitable magnification to maintain focus.

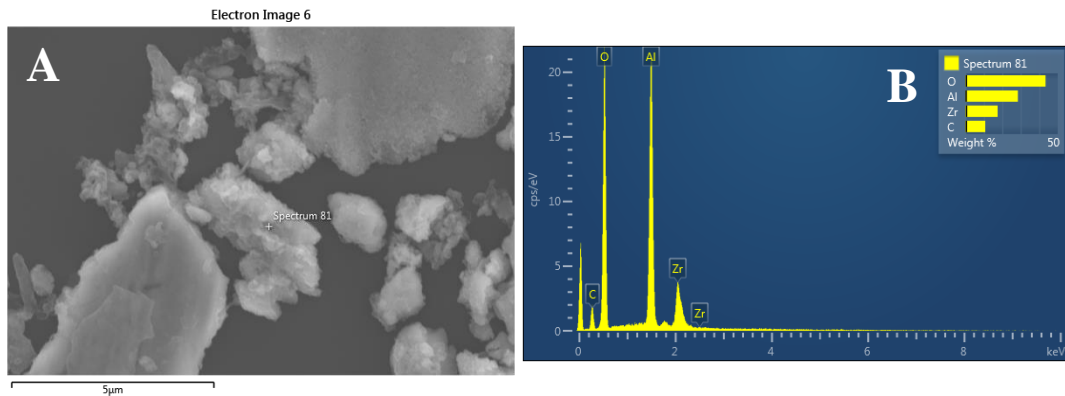


Figure 3.37 - CFE-SEM and EDX analysis of the recovered BIOLOX[®] Delta ceramic wear particles. (A) SEM image of the nano-scale alumina and zirconia particles analysed using EDX and (B) corresponding EDX spectrum. Pin point EDX analysis of the particles was performed at a working distance of 15mm, 10kV and a suitable magnification to maintain focus.

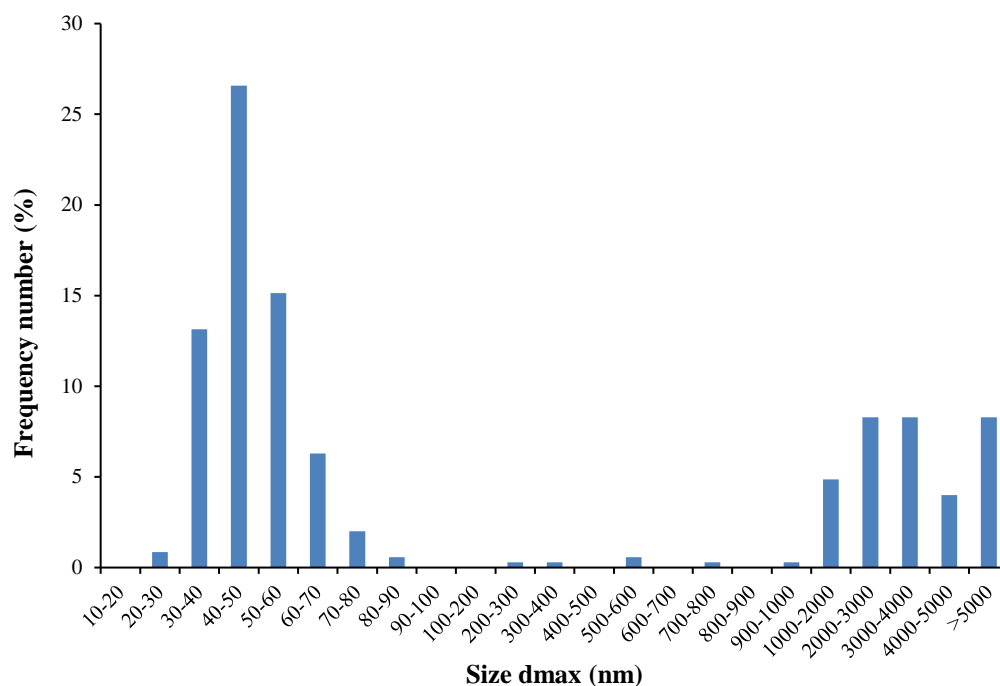


Figure 3.38 - Frequency size distribution of BIOLOX® Delta ceramic wear particles that were generated in water lubricant using the Leeds II hip simulator that were generated under edge loading conditions due to dynamic separation between the head and cup centres. A minimum of 150 particles were measured.

Table 3.8 – Mean size (feret diameter) and morphology (aspect ratio and circularity) values for BIOLOX® Delta ceramic wear particles generated in water and serum.

	BIOLOX® Delta wear debris generated in water; Larger particles (100 - >5000nm)	BIOLOX® Delta wear debris generated in water; Smaller particles (0 - 100nm)	BIOLOX® Delta wear debris generated in serum; Larger particles (100 - >5000nm)	BIOLOX® Delta wear debris generated in serum; Smaller particles (0 - 100nm)
Feret diameter (nm)	3877.53 ± 447.52	48.19 ± 1.41	2308.11 ± 243.58	43.73 ± 0.97
Aspect ratio	1.58 ± 0.08	1.265 ± 0.02	1.47 ± 0.02	1.29 ± 0.01
Circularity	0.68 ± 0.02	0.913 ± 0.01	0.80 ± 0.01	0.91 ± 0.02

Note: All values expressed as mean ±95% Confidence Interval.

3.4.2.2 Percentage ratio between ceramic and stainless-steel wear particles using EDX elemental mapping

The mixed population of ceramic and stainless-steel wear particles recovered from the water lubricant of both BIOLOX® Forte and BIOLOX® Delta simulations were analysed using EDX elemental mapping to calculate the percentage ratio between the ceramic wear particles and stainless-steel particle contaminants. The recovered wear particles were filtered onto a 0.015 filter membrane and analysed using CFE-SEM and EDX analysis. Five random areas of the filter membrane were analysed for elements (wt %) iron (Fe) for the stainless-steel wear particles and alumina (Al) for the ceramic wear particles. An average of the weight % for each

element was calculated, which are presented in Figure 3.39A and Figure 3.39B for both BIOLOX® Forte and BIOLOX® Delta, respectively.

Both types of ceramic had an approximately 50%:50% ratio between ceramic wear particles and stainless-steel wear particles. EDX mapping of particle suspension generated in the BIOLOX® Forte test stations demonstrated $44.13 \pm 31.48\%$ of aluminium (Al), which was indicative of alumina ceramic. EDX mapping of particle suspension generated in the BIOLOX® Delta test stations demonstrated $47.06 \pm 42.75\%$ of aluminium (Al), which was indicative of alumina ceramic.

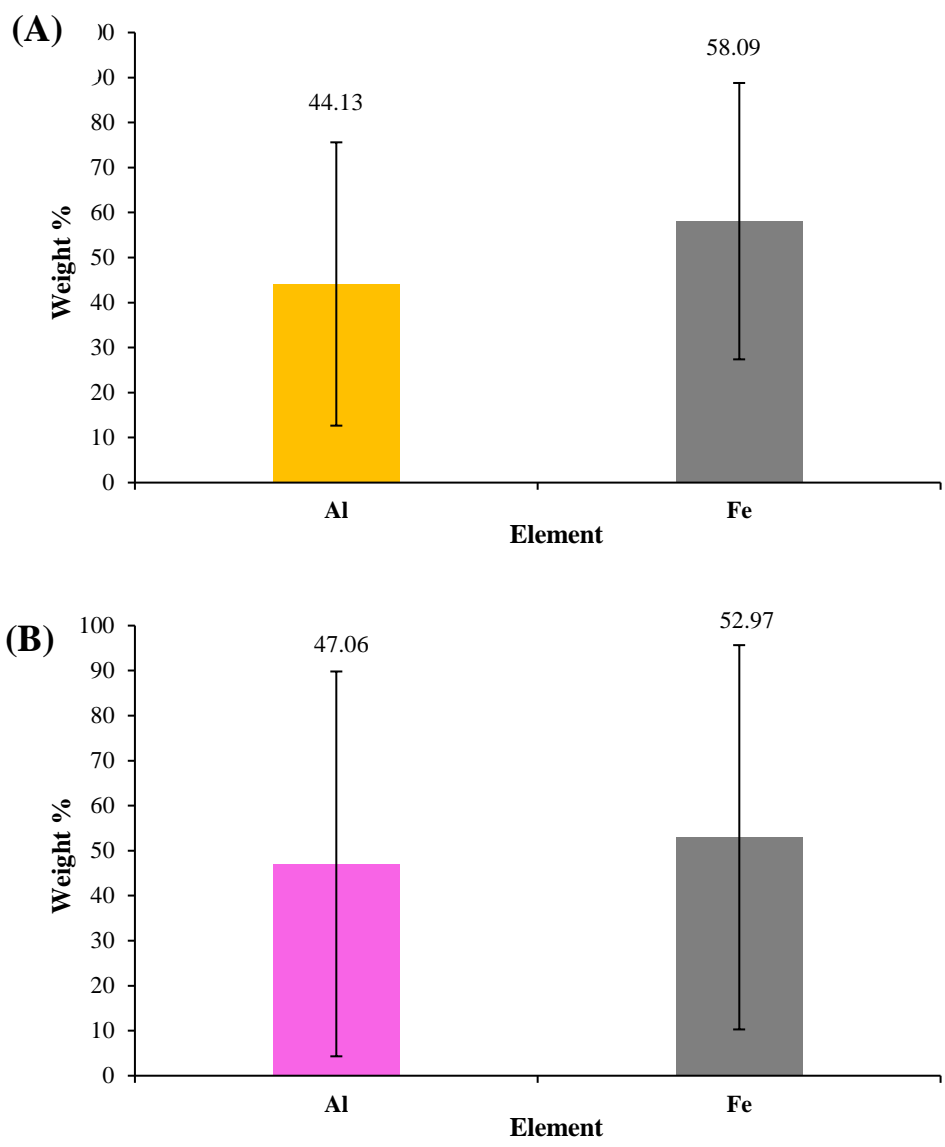


Figure 3.39 – Percentage (weight %) of ceramic and stainless-steel wear particles present in the (A) BIOLOX® Forte and (B) BIOLOX® Delta final particle suspensions. Aluminium (Al) was indicative of ceramic and iron (Fe) was indicative of stainless-steel. Error bars represent 95% confidence limits.

3.4.2.3 Characteristics of CoCr wear particles

The clinically-relevant CoCr nano-particles appeared as large agglomerates that were up to 10µm in size at low magnification (x5k) (Figure 3.40A). At higher magnifications of x90k and x150k, small nano-scale particles were revealed that were round to oval in morphology (Figure 3.40B, C). The frequency as a function of particle size of the recovered CoCr nano-particles is presented in Figure 3.41. Characterisation of the CoCr nano-particles indicated that the particles ranged between 30-200nm, with a mean size of $66.01 \pm 2.65\text{nm}$ ($\pm 95\%$ CL) and mode size of 50-70nm.

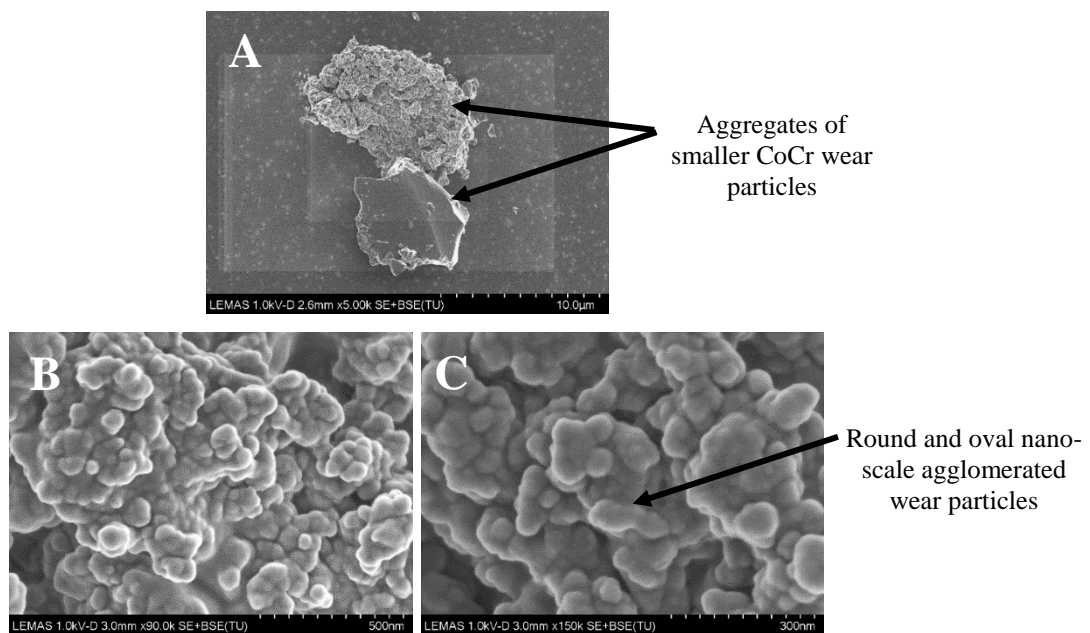


Figure 3.40 - CFE-SEM images of agglomerated CoCr nano-particles generated using the six-station pin-on-plate wear simulator. The particles were imaged at (A) 5K, (B) 90K and (C) 150K magnification with a 1kV (deceleration mode) voltage and working distance of 2-3mm.

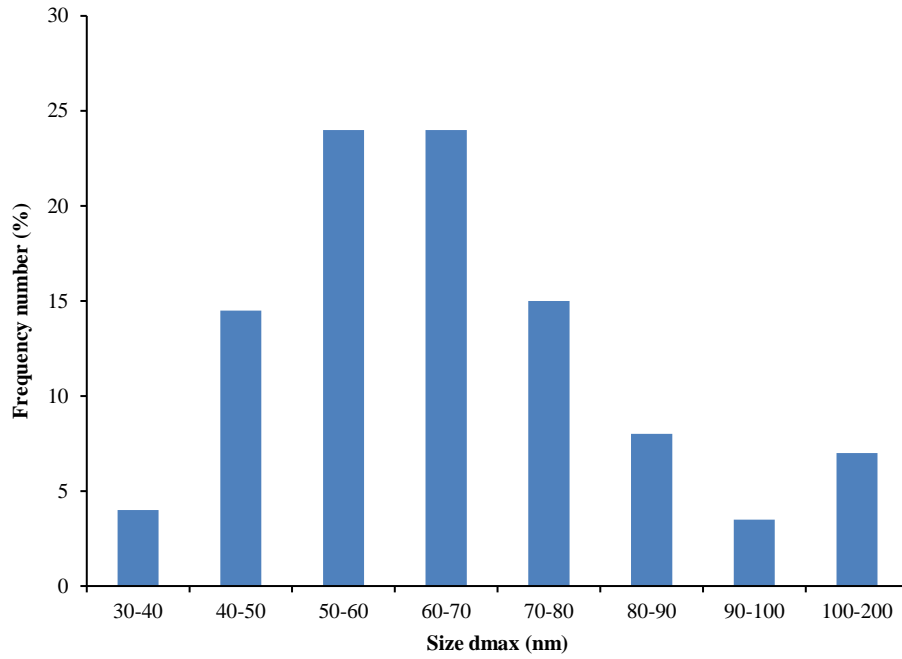


Figure 3.41 - Frequency size distribution of clinically-relevant CoCr nano-particles generated using the six-station pin-on-plate wear simulator. The right Y-axis shows the cumulative size frequency of the particles (red line). A minimum of 150 particles were measured.

3.5 Discussion

This study had the following two aims: -

1. To generate clinically-relevant ceramic (alumina and composite ZTA) and CoCr wear particles.
2. To compare the characteristics of the ceramic wear particles generated in water to those generated in serum.

In order to meet these aims, BIOLOX® Forte and BIOLOX® Delta CoC bearings were used to generate ceramic wear particles in water lubricants using the Leeds II hip simulator. Severe edge loading conditions were employed to maximise the wear rates and volume of ceramic wear particles produced. The characteristics of the ceramic wear particles generated in water were compared with ceramic wear particles generated in serum lubricants under similar kinematic conditions in the same Leeds II hip simulator. The findings of this study are divided into the following sections: -

1. Wear rates of CoC bearings
2. Dynamic separation
3. Surface analysis of CoC bearings
4. Characteristics of recovered wear particles
5. Limitations of the study

3.5.1 Wear rates of CoC bearings

The wear tests conducted in this study produced mean wear rates for BIOLOX® Delta ($0.42 \pm 0.66 \text{mm}^3$ per million cycles; test 1 only) that were comparable with previous studies ($0.32 \pm 0.04 \text{mm}^3/\text{million cycles}$), which employed similar test conditions i.e. severe edge loading conditions caused by dynamic separation due to translational mismatch in the centres of rotation of the femoral head and acetabular cup (Lancaster-Jones et al., 2016). However, it is important to note that in the present study, water was used as the lubricant, whereas previous studies used 25% (v/v) new-born calf serum. The mean wear rates for BIOLOX® Forte ranged between 0.11 ± 0.5 and $1.36 \pm 0.97 \text{mm}^3$ per million cycles and were also similar to the wear rates reported by Stewart et al. (2001) for BIOLOX® Forte CoC bearings that produced overall mean wear rates of 0.2 and $1.84 \text{mm}^3/\text{million cycles}$ under mild and severe microseparation conditions, respectively. The variation in microseparation conditions from mild to severe was controlled by altering the swing phase load from 400N for mild to 50N for severe separations. There were no significant differences in the mean wear rates (test 1 only) between the two different material types in the present study (the mean wear rates for the two different materials was not compared in the other tests as the mean wear rates for BIOLOX® Delta was not calculated due to complications during the tests that resulted in less than n=3 repeats). The cumulative wear volumes produced from all four tests were 6.30mm^3 and 6.20mm^3 for

BIOLOX[®] Forte and BIOLOX[®] Delta, respectively. However, due to the complications experienced in station 6 (BIOLOX[®] Delta) from tests 3 & 4, the volumes of wear for this station were excluded from the total cumulative wear volume, resulting in a final volume of 4.70mm³. These wear volumes were believed to be sufficient for subsequent biological impact testing as it was calculated that approximately 1mm³ of ceramic wear particles was required to complete all four biological assays for PBMNCs from five donors and cytotoxicity testing using L929 cells. Hence, no further wear simulation was required.

The severity of the edge loading conditions (4mm translational mismatch with 65° (clinical equivalence) cup inclination angle) applied during test 2 resulted in fracturing of the BIOLOX[®] Delta acetabular liners on stations 4 and 6. The fracturing of the BIOLOX[®] Delta components during *in vitro* wear simulation testing was unprecedented and in contrast with previous studies (Al-Hajjar et al., 2010; Al-Hajjar, Fisher, Tipper, et al., 2013a; Al-Hajjar, Jennings, Begand, et al., 2013b; O'Dwyer Lancaster-Jones et al., 2017), hence it was believed that the fracturing may have been due to the adverse test conditions employed in the test combined with the use of water as the lubricant, which may have increased friction between the head and cup during articulation. However, it has been reported that the coefficient of friction in water lubricant is relatively similar to that when 25% (v/v) new-born calf serum was used to test BIOLOX[®] Delta discs against a high purity alumina ball using a reciprocating ball-on-flat tribometer (Ma and Rainforth, 2012). Furthermore, the thickness of the 32mm diameter BIOLOX[®] Delta acetabular cups used in these tests, was smaller at the rim than the 36mm components used in previous studies (Al-Hajjar et al., 2010; Al-Hajjar, Fisher, Tipper, et al., 2013a; Al-Hajjar, Jennings, Begand, et al., 2013b; Lancaster-Jones et al., 2016), which may have been a contributing factor towards failure of the implants. Nevertheless, this is highly speculative and further tests would need to be conducted to evaluate the mechanism of this failure. Due to the fracturing phenomenon, the medial-lateral mismatch between the head and the cup was reduced to 3mm in all subsequent tests, in order to decrease the magnitude of dynamic separation and risk of fracturing, whilst ensuring the highest possible volume of ceramic wear debris was being generated.

3.5.2 Dynamic separation

The medial-lateral displacement or dynamic (micro) separation was measured for each station using a LVDT and the results demonstrated a positive correlation between the dynamic (micro) separation and wear rate. This was supported by Lancaster-Jones et al. (2016) who reported the magnitude of dynamic separation increased as the level of translational mismatch between the head and cup increased from 1 to 4mm. These authors reported that dynamic separation was at its highest when the 4mm level of mismatch was coupled with high cup inclination angles (55-65°). The magnitudes of dynamic separation observed in the present

study were in a similar range to those measured clinically in other studies (Lombardi et al., 2000; Tsai et al., 2014). Lombardi et al., (2000) reported an average hip separation of 1.2mm for stance phase, which increased to 2.4mm during swing phase and recommended that these phenomena should be included in hip simulator studies to replicate clinically-relevant wear patterns observed *in vivo* and to assess the detrimental effects that these conditions may pose to the components. However, it is important to mention that the separation measured in the present study was the medial-lateral separation between the head and the cup, whereas Lombardi et al. (2000) reported the total separation between the head and cup centres.

3.5.3 Surface analysis of wear scar

Surface analysis of the heads and cups using surface profilometry did not reveal any significant differences in terms of surface roughness, before and after the wear simulation tests. The traces post-test may have included unworn areas due to the narrow stripe of wear and the curvature of the trace, which may have resulted in the underestimation of surface roughness values. Nevertheless, SEM analysis of the surface of the ceramic head components revealed both BIOLOX[®] Forte and BIOLOX[®] Delta had pit formations over the worn area, likely to be as a result of grain pull-out due to edge loading. This was in agreement with previous studies (Nevelos et al., 2000; Shishido et al., 2006; Affatato et al., 2011; Ma and Rainforth, 2010; Affatato et al., 2012), where wear stripe formation was attributed to inter-granular fracture and gross deformation of the alumina. Ma and Rainforth (2010) reported that BIOLOX[®] Delta subjected to water lubricated reciprocating wear experienced two lubrication regimes during testing, which included full fluid-film lubrication and mixed lubrication, the latter being more likely for this study as contact is required to produce the magnitude of wear observed in the present study. Fluid-film lubrication occurs in normal hip articulation where the articulating surfaces are completely separated by a continuous lubricant film, which results in differential wear between the grains in the form of pits and grooves. Differential wear is mainly associated with tribochemical wear and occurs under standard conditions. The wear from mechanical damage is associated with edge loading conditions, which results in wear scar formation. The formation of pits is from inter-granular pull-out of single alumina grains, which causes subsequent fracturing around the pit and thus results in the initiation of stripe wear formation (Ma and Rainforth, 2010; Ma and Rainforth, 2012). The SEM images of the wear stripe for the BIOLOX[®] Delta femoral head from test 1 showed the formation of larger pits, compared to BIOLOX[®] Forte. However, high magnification of the wear stripe on the BIOLOX[®] Forte head showed a different superficial grain microstructure compared to BIOLOX[®] Forte, where there was a wider distribution of pits in the worn surface area indicating higher incidence of inter-granular fracture of the alumina. The edge loading conditions caused an inter-granular fracturing wear mechanism in both

materials that resulted in more surface damage on the BIOLOX[®] Forte femoral head, which may be due to the lower material toughness compared to BIOLOX[®] Delta. However, a possible reason for the larger pits observed in the BIOLOX[®] Delta heads may be due to the loss of both alumina and zirconia grains. The size of the pits were much greater than the size of alumina grains, suggesting loss of both grain types resulting in the formation of enlarged pits (Ma and Rainforth, 2010). Furthermore, the coordinate measurement machine was used to produce a three-dimensional construct and provide characteristic information about the wear stripes generated on the femoral heads and acetabular cups after wear simulation testing. The wear stripe on the BIOLOX[®] Forte heads had a lower mean penetration depth of 9.25 μ m, compared to the BIOLOX[®] Delta heads, which had a mean penetration depth of 15.91 μ m for the wear stripe. However, there was no significant difference in the mean penetration depth between the two different materials. The wear stripes on the BIOLOX[®] Forte heads appeared to be wider compared to the wear stripes on the BIOLOX[®] Delta heads, indicating a larger wear area due to inter-granular fracturing. The small wear area on the BIOLOX[®] Delta heads may have been due to its improved wear properties, making it more resistant to harsher conditions, which younger and more active patients may exert on hip prostheses.

3.5.4 Characterisation of recovered wear particles

The ceramic wear particles generated in water lubricant using the Leeds II hip simulator were recovered using the density gradient separation technique described in chapter 2 (section 2.3.3.2.2), and analysed using CFE-SEM and EDX, which revealed an abundance of stainless steel particle contaminants present in both BIOLOX[®] Forte and BIOLOX[®] Delta recovered particle samples. The presence of large volumes of stainless steel particle contaminants masked the very low volume of ceramic wear particles generated, making it extremely challenging to identify and image the ceramic particles. Hence, the ceramic particles were identified using the technique described in section 2.3.6.1, whereby every particle was analysed using EDX analysis to confirm its elemental composition in order to ensure that it was indeed comprised of ceramic. Characterisation of the wear particles generated from BIOLOX[®] Forte revealed a bimodal size range, with large shard-like shaped particles that ranged between 100-4000nm (mean size: 736.48 \pm 99.45nm), and smaller round granular particles that ranged between 10-90nm (mean size: 50.16 \pm 7.11nm), which were observed as agglomerations or as single particles. These particles had a similar size distribution to those isolated from retrieved tissues by Hatton et al. (2001) using laser micro-dissection. These authors used SEM to identify the large micron sized particles and TEM to identify nano-scale particles. They reported the presence of large polygonal-shaped micron size alumina particles that ranged between 46-3200nm (mean size; 438 \pm 325nm) and smaller nano-scale alumina particles that ranged between 5-90nm (mean size; 24 \pm 19nm).

Characterisation of the wear particles generated from BIOLOX[®] Delta components also revealed a bimodal size range, with large shard-like alumina particles that ranged between 200-20,000nm (mean size: 3877.53 ± 447.52 nm), and smaller round granular alumina/zirconia particles that ranged between 20-90nm (mean size: 48.19 ± 1.41 nm) that were agglomerated. Since no previous studies have isolated BIOLOX[®] Delta ceramic wear particles from retrieved tissues, the size distribution and morphology of these particles was compared to the BIOLOX[®] Delta ceramic wear particles isolated from hip simulator serum lubricants in chapter 3. The isolated particles were generated from BIOLOX[®] Delta CoC bearings under severe edge loading conditions using 25% (v/v) serum as the lubricant as these conditions are believed to reproduce clinically-relevant wear rates, wear patterns (stripe wear) and wear mechanisms as those observed *in vivo* (Nevelos et al., 2000a). There were no significant differences in size distribution and morphology between the BIOLOX[®] Delta wear particles generated in serum or water. The BIOLOX[®] Delta ceramic wear particles generated in serum ranged between 100-32,980nm (mean size: 2308.11 ± 243.58) for the larger alumina particles and 10-90nm (mean size: 43.73 ± 0.97 nm) for the nano-scale zirconia/alumina particles. Despite the use of water as the lubricant, the comparison with ceramic particles isolated from tissue for BIOLOX[®] Forte and from hip simulator serum lubricant for BIOLOX[®] Delta allowed validation of the characteristics of these particles as being representative of those generated *in vivo*, thus successfully addressing the aim of this chapter. Having said that, the contamination issues with stainless steel wear particles was not ideal and a limitation that needs to be considered for *in vitro* particle generation using hip simulators.

CoCr nano-scale wear particles were generated using a six-station pin-on-plate wear simulator as these conditions have been used previously in the literature for simple pin-on-plate wear studies and represent the loading and kinematic conditions of a standard gait cycle in the hip (Jin et al., 2000). Hip simulators have also been used previously to generate clinically-relevant CoCr nano-particles using 25% (v/v) lubricant serum (Brown et al., 2007). However, as mentioned previously the limitations of particle isolation methods and the problem of residual serum proteins and endotoxins in causing cell activation necessitated an alternative solution. Many previous studies have used a simplified pin-on-plate wear simulator to generate clinically-relevant CoCr wear particles for subsequent biological testing (Germain et al., 2003a; Behl et al., 2013; Papageorgiou et al., 2014). Characterisation of the CoCr nano-particles revealed round to oval particles that ranged between 30-200nm (mean size; 66.01 ± 2.65 nm), with a mode size of 50-70nm. This was similar to the reported literature where Doorn et al. (1998) used an enzymatic tissue digestion method to isolate CoCr wear particles from periprosthetic tissues obtained from 13 patients with MoM hips followed by characterisation using TEM. This study revealed metal wear particles in the size range of 51-

116 nm, with a mean size of 81 nm. Furthermore, an *in vitro* study by Firkins et al. (2001) reported the particles generated in the hip simulator were round/oval and of uniform shape with sizes in the range of 25-36 nm. These studies therefore provide evidence that wear particles generated from MoM hips are consistently in the nanometre size range and uniform in size and shape. The small size of the wear particles gives rise to large numbers of particles which causes great concern over the possible distribution of these small particles in the body, and their biological effects on cells and tissues. Metal particles have been shown to disseminate throughout the body and have been found in the lymph nodes, liver, spleen and bone marrow (Case et al., 1994). Furthermore, CoCr particles have been shown to cause reduced cell viability, TNF- release, DNA damage and oxidative stress (Fleury et al., 2006; Tsaousi et al., 2010; Papageorgiou et al., 2014; Posada et al., 2015). Hence, the *in vitro* generated CoCr wear particles were used as a positive particle control in the present study for biological impact testing experiments.

3.5.5 Limitations of study

The use of water as the lubricant to generate wear particles *in vitro* eradicates the risk of residual proteins and adherent endotoxins that can cause positive mis-leading results, which may have not been a response due to the wear particles. However, the present study has shown that contamination by stainless steel wear particles in the hip simulator complicated the initial purpose of generating ceramic wear debris *in vitro*. The resultant ceramic particle suspensions consisted of both ceramic wear debris and stainless-steel wear particles. The biological impact of the stainless-steel wear particles will therefore need to be investigated before commencing the *in vitro* biological testing of the ceramic wear debris. Furthermore, stainless wear particle controls will need to be included in all biological tests to elucidate the response to the stainless-steel wear particles and the ceramic wear particles as the particles presented to the cells will be a mixed population of both ceramic and metal particles. This highlighted the limitation of hip simulators when used to generate wear particles *in vitro*. A more efficient technique needs to be developed in order to produce a pure yield of clinically-relevant ceramic wear debris *in vitro*.

3.6 Summary of findings

- Severe edge loading conditions caused by dynamic separation due to translational mismatch between the centres of rotation of the femoral head and acetabular cup resulted in stripe wear on the CoC bearings.
- Water lubricant did not alter the characteristics (size and morphology) of the ceramic wear particles generated, thus producing ceramic wear particles that were representative of those generated *in vivo*.
- *In vitro* wear testing of the CoC bearings using the hip simulator produced unwanted stainless-steel wear particles, which contaminated the water lubricant and resulted in a mixed population of ceramic and stainless-steel wear particles that will be used for subsequent biocompatibility testing.

CHAPTER 4

4 Biological impact of ceramic hip replacements

4.1 Introduction

The biological activity and mechanisms by which cells interact with ceramic wear particles released from CoC THRs is not currently fully understood. Wear simulation studies have provided a better understanding of the wear mechanisms of UHMWPE and metal bearings, and have also provided a plentiful supply of clinically relevant wear particles that could be used for *in vitro* cell studies. Hence, a considerable amount of literature has been published on the biological activity of wear particles generated from MoP and MoM THRs, such as the cytotoxic effects and the release of inflammatory cytokines from cells in response to wear particles. However, it is important to remember the conditions of these assays do not always consistently represent clinically relevant conditions. Biological assays using the conventional two-dimensional monolayer cells cultured on flat substrates do not consider the natural three-dimensional environment of cells *in vivo*, such as other surrounding cells, extra-cellular matrix, blood supply and normal supply of nutrients. Hence, it is extremely important to consider these factors when extrapolating *in vitro* results to predict the phenomena *in vivo* and avoid providing misleading and nonpredictive data for *in vivo* responses (Edmondson et al., 2014).

The ideal THR bearing would consist of an articulating surface that has virtually no wear or even if debris were produced, a host immune response should not be evoked (Rajpura et al., 2014). Biocompatibility is described as “the ability of a material to perform with an appropriate host response in a specific application” (Williams, 1999). High density, pure alumina is used in load-bearing applications such as hip prostheses because of its excellent corrosion resistance, biocompatibility, high wear resistance and high strength (Ratner et al., 2012). Early studies of the evaluation of the biocompatibility of alumina considered this material to be bioinert and so alumina was used as a reference material for biocompatibility tests. A bioinert material is defined as a material that induces no tissue response post-surgical implantation. While this may be true for alumina in bulk form, the same cannot be said when alumina is in particulate form. Indeed, this applies to majority of biomaterials, whereby they may elicit an immune response when presented to tissues in particulate form. After implantation of alumina in bulk form, a connective tissue capsule is formed at the ceramic-tissue interface. The features of this encapsulating membrane are indicative of a minimal response i.e. many fibroblasts and few inflammatory cells, nevertheless this shows that alumina ceramic implants can elicit and maintain a foreign body reaction (Christel, 1992).

Having said that, no material is bioinert, instead the characteristics of that induced response in terms of cells present at the material-tissue interface can either be categorised as biocompatible or cytotoxic (Christel, 1993).

Wear is an inevitable phenomenon of artificial joint replacements and so the pre-clinical testing of any new materials for joint replacements must include an analysis of the wear particle characteristics and their biological impact. However, this has been challenging for ceramic hip replacements, particularly for ZTA composite ceramic hips (BIOLOX[®] Delta), due to their extremely low wear rates that has made it difficult to generate and recover enough clinically-relevant ceramic wear particles for biocompatibility testing. For these reasons, no studies have reported the characteristics or biological impact of the wear debris generated from ZTA composite ceramic bearings. Wear particles produced by alumina ceramic-on-ceramic bearings have been reported to cause minimal immunological responses, with low cytotoxicity and inflammatory potential (Germain et al., 2003a; Hatton et al., 2003a). However, comprehensive immunological and biological studies are yet to be completed for the composite BIOLOX[®] Delta CoC hip replacements due to difficulties in isolating the very low volume of clinically relevant wear debris generated by such materials *in vitro*. Due to the extremely low wear rates of CoC bearings, the majority of the previous studies (Nagase et al., 1995; Catelas et al., 1998; I Catelas, Petit, Zukor, et al., 1999; Nkamgueu et al., 2000a; Petit et al., 2002; Warashina et al., 2003; Granchi et al., 2004; Tsaousi et al., 2010; Faye et al., 2017) have used commercially-obtained ceramic powders to test the *in vitro* biological activity of ceramic particles. The main finding from these studies indicated that the reactivity of the commercially-obtained ceramic particles was dose dependent in that cell death increased with the concentration of alumina particles. Whilst these studies provided vital information about the biological response to ceramic wear particles *in vitro*, it is important to consider that the characteristics i.e. size and shape of these commercially-obtained ceramic particles may not accurately represent ceramic wear debris generated *in vivo*. This is extremely important as the relative features of wear particles in terms of their size, morphology, quantity and composition determines the severity of the biological response. The manufacturing process involves compressing and sintering the ceramic powder to form the final components. Thus, the size of the particles in the powder may be different to the particles released from the microstructure of the ceramic component.

The introduction of microseparation by Nevelos et al. (2000) into *in vitro* wear testing of CoC bearings resulted in stripe wear production, which was often observed on retrieved CoC hip implants. These authors for the first time reproduced clinically-relevant wear patterns, wear rates and wear mechanisms as those observed *in vivo* (Nevelos et al., 1999; Nevelos, Prudhommeaux, et al., 2001; Hatton et al., 2002; Tipper et al., 2002a). The wear particles from composite ceramic hip replacements generated under microseparation conditions are

bimodal in size as demonstrated by the work in chapter 3. The literature review revealed only two previous studies (Hatton et al., 2003b; Germain et al., 2003a) used clinically-relevant ceramic wear particles to test the biocompatibility of alumina ceramic hip replacements. Hatton et al., (2003) reported that a larger volume ($500\mu\text{m}^3$) of clinically-relevant alumina ceramic wear particles than alumina powder ($100\mu\text{m}^3$) was required to stimulate the release of the inflammatory TNF- α (cytokine) from PBMNCs. Similar findings by Germain et al. (2003) reported high particle volumes of clinically-relevant alumina ceramic wear particles were required to induce cytotoxic effects in U937 human histocytes. These studies demonstrated the potential cytotoxic and inflammatory effects of wear particles from alumina ceramic hip replacements. However, given the low wear rates of CoC bearings, it is unlikely that these high volumes ($100\text{-}500\mu\text{m}^3$ per cell) will be produced *in vivo*, even under mal-positioning conditions.

A range of biocompatibility tests can be used to evaluate the biological impact of particulate wear debris. The FDA recommends that biocompatibility testing should include the identification of any toxicities or adverse effects in response to the material of the medical device as per ISO 10993-5 “Biological evaluation of medical devices – Part 5: Tests for *in vitro* cytotoxicity”. The FDA also published a document; Use of International Standard ISO 10993-1, "Biological evaluation of medical devices - Part 1: Evaluation and testing within a risk management process" (Food and Drug Administration, 2016), which recommends the consideration of “biological hazards arising from any mechanical failure... For example, if coating particles or wear debris are released from a device, those particles could lead to a biological response...” (Food and Drug Administration, 2016). However, no specific tests for the evaluation of the biological effects of wear particles resulting from mechanical failure was specified. Nevertheless, biocompatibility testing of materials as a result of device mechanical failure typically involves cytotoxicity evaluation using L929 murine fibroblast cells and a suitable biological assay. For example, the cytotoxic effects of a material can be assessed by measuring the amount of ATP, which is used as a marker for cell viability because it is present in all metabolically active cells. ATP decreases very rapidly within cells when they undergo necrosis or apoptosis which can occur in response to cytotoxic materials (Crouch et al., 1993). Due to previous experience with UHMWPE wear particles it is known that wear particles induce an inflammatory response, whereby macrophages release pro-inflammatory cytokines and other mediators of inflammation which stimulate osteoclastic bone resorption leading to osteolysis (Ingham and Fisher, 2000). Therefore, it seems pertinent for studies to investigate the release of inflammatory cytokines after exposure of cells to other particle types/materials. A sandwich ELISA or enzyme-linked immunosorbent assay is a sensitive technique used in the previous studies (Table 4.14) to identify the concentration of an antigen such as TNF- α that is present in the supernatants collected from the cells. The antigen of interest is quantified

between two layers of antibodies i.e. the capture and detection antibody, which bind to the non-overlapping epitopes on the antigen. An enzyme binds to this complex, which catalyses a substrate added during the process resulting in a colour change, the intensity of which is used to determine the concentration of the cytokine in the sample (Grebentchikov et al., 2005).

Majority of the previous studies (Nagase et al., 1995; Catelas et al., 1998; I Catelas, Petit, Zukor, et al., 1999; Nkamgueu et al., 2000a; Petit et al., 2002; Warashina et al., 2003; Germain et al., 2003a; Hatton et al., 2003a; Granchi et al., 2004; Tsaousi et al., 2010; Faye et al., 2017) demonstrated that ceramic particles, be it clinically-relevant or commercially-obtained have demonstrated a benign cellular response, with low cytotoxicity and inflammatory potential at the volumes or doses representative of the wear rates of CoC bearings. Therefore, due to the low wear rates of CoC THR, the cytotoxic and inflammatory effects of ceramic wear particles was not of real concern. However, the subtle changes that may occur intracellularly because of phagocytosis of wear particles also need to be investigated. Hence, the evaluation of DNA damage is another common test listed in previous studies, which have reported genotoxicity in response to metal wear particles from metal-on-metal hips. Ladon et al. (2004) observed an increase in chromosomal aberrations and aneuploidy in the peripheral blood of patients after 2 years of MoM implantation. Genotoxicity was also reported for commercially-obtained alumina nano-particles, though this was only mildly genotoxic when compared with commercially-obtained CoCr alloy particles (Tsaousi et al., 2010). Single-cell gel electrophoresis or comet assay is a simple uncomplicated test that can be used to test for DNA damage. It works on the principle of measuring DNA strand breaks in eukaryotic cells (Collins, 2004).

Oxidative stress occurs when there is an imbalance between the formation of oxidants and the rate of metabolism and the ability of antioxidant systems to remove reactive oxygen species (ROS), such as free radicals. Elevated oxidative stress has been suggested to be a critical factor in many inflammatory and degenerative disorders resulting in tissue damage and fibrosis in different parts of the body (Kinov et al., 2010). Inflammation is a definitive characteristic of aseptic loosening of THRs, therefore it is very likely that free radicals play a major role in this condition (Kinov et al., 2006). Free radicals can cause damage to cells in several ways such as DNA and protein damage, as well as disruption to cell proliferation, DNA and protein synthesis and metabolic activity. Thus, many studies (Nagase et al., 1995; Wang et al., 2002; Prabhakar et al., 2012; Steinbeck et al., 2014) have investigated the role of oxidative stress in aseptic loosening of THAs. It has been reported that wear particles generated from MoM bearings induce oxidative stress in cells (osteoblasts, fibroblasts and macrophages) where metal ions induce the production of ROS (Fleury et al., 2006; Wei et al., 2009). Little is currently known about the potential of ceramic wear particles to induce the

production of ROS, and hence oxidative stress. Therefore, this remains a gap in knowledge and so remains to be investigated.

4.2 Aims and objectives

Aims:

The aim of the research in this chapter was to investigate the biological impact of wear particles generated from ceramic-on-ceramic total hip replacements. The first part of this study was concerned with determining if the biological activity of BIOLOX® Delta ceramic model particles were comparable to the published literature on commercially-obtained alumina and zirconia particles. Hence, a comprehensive evaluation of the biological impact of ZTA model ceramic particles in terms of cytotoxicity, inflammation, genotoxicity and oxidative stress was initially conducted. Thereafter, the biological impact of clinically-relevant ceramic wear particles generated *in vitro* from ceramic bearings using the hip simulator was investigated (Figure 4.1).

Objectives:

- To assess the cytotoxic effects of BIOLOX® Forte ceramic model particles, BIOLOX® Delta ceramic model particles and clinically-relevant BIOLOX® Delta ceramic wear particles on the viability of L929 murine fibroblast cells over a period of 6 days.
- To assess the biological impact of BIOLOX® Delta ceramic model particles and clinically-relevant BIOLOX® Delta ceramic wear particles on peripheral blood mononuclear cells in terms of cytotoxicity (viability), inflammation (release of TNF- α), genotoxicity (DNA damage) and oxidative stress (production of reactive oxygen species) and compare with BIOLOX® Forte ceramic model particles and clinically-relevant BIOLOX® Forte ceramic wear particles, respectively.

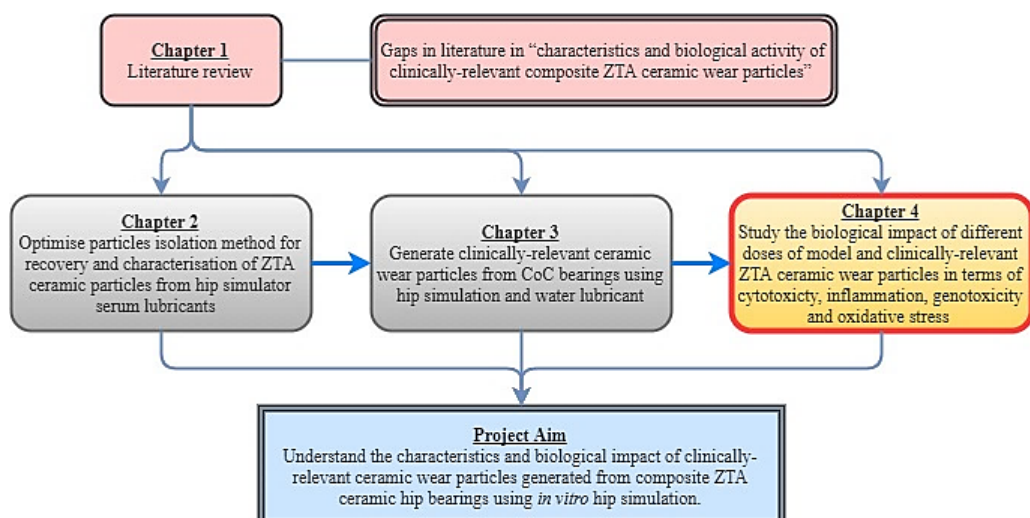


Figure 4.1 – Flow diagram showing the work in this chapter in relation to other chapters, with the current chapter highlighted in yellow.

4.3 Materials and methods

4.3.1 Materials

4.3.1.1 Particles

The sources or suppliers of the particles are listed in Table 4.1. The commercial BIOLOX[®] Forte and BIOLOX[®] Delta powders were manufactured by Ceramtec GmbH (Germany) using their pre-approved powder preparation formula, which consists of binding and sintering agents in the raw materials (not disclosed by Ceramtec). The resulting powder is subjected to a number of milling cycles to avoid agglomeration and homogenise the material. The slurry produced is subsequently processed (drying, filtering, moisturising, quality control) to produce a final powder ready for pressing (Palmero et al., 2014).

Table 4.1 – Composition and source of particles used for biological impact experiments

Material name	Composition (wt.%)	Supplier/Source
BIOLOX [®] Forte powder	Al ₂ O ₃ (99.95%)	Ceramtec GmbH, Germany
BIOLOX [®] Delta powder	Al ₂ O ₃ (76.1%), ZrO ₂ (22.5%), Y ₂ O ₃ (1%), Cr ₂ O ₃ (>1%), SrO (>1%)	Ceramtec GmbH, Germany
BIOLOX [®] Forte wear particles	Al ₂ O ₃ (99.95%)	Generated in house using the Leeds II hip simulator
BIOLOX [®] Delta wear particles	Al ₂ O ₃ (76.1%), ZrO ₂ (22.5%), Y ₂ O ₃ (1%), Cr ₂ O ₃ (>1%), SrO (>1%)	Generated in house using the Leeds II hip simulator
CoCr wear particles	Co (balance), Cr (30%), Mo (6%), C (0.2%), other elements (0.8%)	Generated in house using the pin-on-plate wear rig

4.3.1.2 Cell lines and primary cells

The cells used in this chapter and suppliers are listed in Table 4.2.

Table 4.2 – Cells used throughout the study.

Cells	Type	Species	Supplier
L929 cells	Fibroblasts	Murine	European collection of cell cultures
Primary peripheral blood mononuclear cells (PBMNCs)	Monocytes/ Macrophages	Human	Blood collected from healthy volunteers

4.3.1.3 Chemicals and reagents used in this chapter

The chemicals and reagents used in this study are listed in Table 4.3

Table 4.3 – List of chemicals and reagents used in this study

Chemical/Reagent	Supplier	Storage/Preparation
ATPlite™ ATP detection assay	PerkinElmer, Massachusetts, USA	4°C
Bovine Serum Albumin (BSA)	Sigma-Aldrich, Dorset, UK	4°C
Camptothecin	Sigma-Aldrich, Dorset, UK	Room temperature
Carbon paste	Agar Scientific, Stanstead, Essex, UK	Room temperature
DCFDA / H2DCFDA - Cellular Reactive Oxygen Species Detection Assay Kit (ab113851)	Abcam, Cambridge, UK	4°C
Dimethyl sulphoxide (DMSO)	Sigma-Aldrich, Dorset, UK	Room temperature
Dulbecco's modified Eagle's medium (DMEM)	Lonza Biological, Cambridge, UK	4°C
Dulbecco's Phosphate Buffered Saline (DPBS)	Sigma-Aldrich, Dorset, UK	Room temperature
ELISA Kit (Human TNF α)	Diaclone, France	4°C
Ethanol, absolute	VWR International LTD, Poole, UK	Room temperature in flammables cupboard
Ethlenediaminetetraacetic acid (EDTA)	Sigma-Aldrich, Dorset, UK	Room temperature
Foetal bovine serum (FBS)	Bio-Whittaker, Lonza, Verviers, Belgium	-20°C
Hydrochloric acid (HCL) 12M	Sigma-Aldrich, Dorset, UK	Room temperature
Hydrogen peroxide	Sigma-Aldrich, Dorset, UK	4°C
L-glutamine (200mM)	Sigma-Aldrich, Dorset, UK	-20°C
Lipopolysaccharide (LPS)	Sigma-Aldrich, Dorset, UK	-20°C
Lymphoprep	Axis-Shield PoC AS, Oslo, Norway	Room temperature

Lysis solution	Trevigen, Gaithersburg, Maryland, USA	Room temperature
N-(2- hydroxyethyl) piperazine- N'-(2- ethanulfonic acid) (HEPES)	Bio-Whittaker, Lonza, Verviers, Belgium	Room temperature
Penicillin (5000U)/Streptomycin (5mg.ml ⁻¹)	Bio-Whittaker, Lonza, Verviers, Belgium	-20°C
Phosphate Buffered Saline (PBS) tablets	Oxoid Thermo Scientific, Northumberland, UK	Room temperature
Potassium hydroxide	Sigma-Aldrich, Dorset, UK	Room temperature
Roslyn Park Memorial Institute (RPMI) 1640 medium	Bio-Whittaker, Lonza, Verviers, Belgium	4°C
Sodium hydroxide (NaOH)	Fisher Scientific, Loughborough, UK	Room temperature
Sterile water	Baxter Healthcare, UK	Room temperature
Sulphuric acid solution	VWR International LTD, Poole, UK	Room temperature
SYBR Gold	Fisher Scientific, Loughborough, UK	-20°C
Trigene	Scientific Laboratory Supplies Ltd, Nottingham, UK	Room temperature
Tris-HCL	Sigma-Aldrich, Dorset, UK	Room temperature
Triton X-100	BDH laboratory supplies, Poole, UK	Room temperature
Trizma-hydrochloride	Sigma-Aldrich, Dorset, UK	Room temperature
Trypan blue (0.4%)	Sigma-Aldrich, Dorset, UK	Room temperature
Trypsin-EDTA	Sigma-Aldrich, Dorset, UK	-20°C
Tween 20	Sigma-Aldrich, Dorset, UK	Room temperature
Ultra-pure low melting point agarose	Invitrogen Life Technologies Ltd, Paisley, UK	Room temperature

4.3.1.4 Equipment

The equipment used in this chapter are listed in Table 4.4.

Table 4.4– List of equipment used in this study

Item	Model/Size	Supplier
Absorbance plate reader	Multiskan Spectrum	Thermo LabSystems, Franklin, USA
Automatic pipette	Multipette® stream	Eppendorf UK Ltd, Stevenage, UK
Automatic pipette (Pipetboy®)	Ergo One®	Starlab, Milton Keynes, UK
Balance (accuracy of 0.1mg)	ABJ 220-4NM	KERN-SOHN GmbH, Balingen, Germany
Balance (accuracy of 1µg)	XP26	Mettler-Toledo Ltd, Leicester, UK
Balance (accuracy of 10µg)	XP205	Mettler-Toledo Ltd, Leicester, UK
Benchtop centrifuge	5415R	Eppendorf UK Ltd, Stevenage, UK
Cell culture centrifuge	Harrier 15/80	MSE (UK) Ltd, London, UK
Cell culture incubator	Sanyo MCO-20AIC	SANYA Biomedical Europe BV, UK
Cell culture water bath	NE2-D	Clifton, Weston-Super- Mare, UK
Distilled water reservoir and filter	ELGA, Reservoir 75L	ELGA, High Wymcombe, UK
Electrophoresis bath	SUB-CELL® GT	Bio-Rad, Watford, UK
Electrophoresis power supply	GPS 200/400	Pharmacia LKB, Sweden
Eppendorf Thermomixer comfort	5355 000.038	Eppendorf UK Ltd, Stevenage, UK
Luminescent plate reader	Chameleon	Hidex, Turku, Finland
Magnetic stirrer	Stuart SB161	Scientific Laboratory Supplies Ltd., Nottingham, UK

Microlitre plate shaker	Stuart® SSM5	Cole-Parmer, Staffordshire, UK
Oven	OMT225	IDEX Health & Science GmbH, Wertheim, Germany
pH metre	Jenway 3010	VWR International
Ultra-pure distilled water	QEARD00R1	Merck Millipore, Cork, Ireland
Ultrasonicator	XB3	Grant Instruments Ltd, Cambridge, UK
Vortexer	Topomix FB15024	Fisher Scientific, Loughborough, UK
Water bath	JBN12	Grant Instruments Ltd, Cambridge, UK

4.3.1.5 Consumables, plasticware and glassware

The consumables, plasticware and glassware used in this study are listed in Table 4.5.

Table 4.5– List of consumables, plasticware and glassware used in this study

Item	Size	Supplier
Bijous	5ml	Scientific Laboratory Supplies, Nottingham, UK
Cell culture flasks	T175, T75	Thermo Scientific, Massachusetts, USA
Combi tips	10ml, 5ml	Eppendorf, Stevenage, UK
Comet slides	20 wells	Trevigen, Gaithersburg, Maryland, USA
Eppendorf tubes	2ml, 1.5ml	Starstedt Ltd, Leicester, UK
Falcon tubes	50ml	Starstedt Ltd, Leicester, UK
Glass duran bottles	100ml, 500ml, 1000ml, 2000ml	Duran Group, Wertheim am Main, Germany
Glass universals	20ml	Faculty of Biological Sciences, University of Leeds, UK
Haemocytometer	-	Marienfield, Germany
Maxisorb™ plate	96 well	Scientific Laboratory Supplies, Nottingham, UK

Microplate adhesive sealing film	96 well	PerkinElmer, Berkshire, UK
Optiplat TM	96 well	PerkinElmer, Berkshire, UK
Petri dish	30mm diameter	Bibby Sterilin, Staffordshire, UK
SepMate TM tubes	50ml	Stemcell technologies UK Ltd, Cambridge, UK
Serological pipettes	25ml, 10ml, 5ml	Starstedt Ltd, Leicester, UK
Sterile pipette tips	1000 μ l, 200 μ l, 20 μ l, 2 μ l	Starlab UK, Milton Keynes, UK
Sterile plastic pots	250ml, 150ml, 60ml	Thermo Scientific, Massachusetts, USA
Sterile plastic syringes	10ml, 5ml, 2ml, 1ml	Scientific Laboratory Supplies, Nottingham, UK
Universals	20ml	Scientific Laboratory Supplies, Nottingham, UK
Well plates (Nunc [®]), flat bottomed	96 well, 48well, 96-Well Clear Bottom Black	Scientific Laboratory Supplies, Nottingham, UK

4.3.2 Methods

4.3.2.1 Measurement of pH

The pH of solutions was measured using a Jenway 3510 pH meter. The pH meter was calibrated using purchased calibration solutions of pH 4, pH 7 and pH 10, at room temperature. The pH of solutions was also measured at room temperature.

4.3.2.2 Microscopy

4.3.2.2.1 Bright field

An optical Olympus CK-40-SLP microscope was used to view cells during cell culture experiments, such as cell seeding or culture of cells with particles. The microscope was set up for standard Köhler illumination.

4.3.2.2.2 Confocal

A Zeiss LSM700 inverted confocal microscope was used to image immunostained slides and gels. The laser settings used were laser Diode: 405nm (Hoechst; blue) and 488nm GFP; green).

4.3.2.2.3 Phase contrast

An Olympus IX71 inverted microscope setup for phase contrast microscopy was used to view and capture images of cells co-cultured with particles. Images were captured using Cell[^]B image acquisition software.

4.3.2.3 Sterilisation

All particles were sterilised using heat treatment at 190°C for 4 hours before being used for cell culture experiments.

4.3.2.3.1 Filter sterilisation

Solutions not suitable for heat sterilisation were filtered using 0.2µm pore sized filters using a disposable syringe in a class II safety cabinet.

4.3.2.4 Stock solutions

4.3.2.4.1 Phosphate buffered saline

Phosphate buffered saline (PBS) was prepared by adding one PBS tablets to 100ml of distilled water. The pH was adjusted to 7.2-7.4.

4.3.2.4.2 Supplemented phosphate buffered saline

PBS supplemented with 2% (v/v) foetal bovine serum was used to dilute the whole blood during the PBMNC isolation process.

4.3.2.4.3 DMEM culture medium for L929 cells

Dulbecco's modified Eagle's medium (DMEM) was used with 10% (v/v) FBS, 2mM L-glutamine, 100 U.ml⁻¹ penicillin and 100 µg.ml⁻¹ streptomycin. Supplemented cell culture medium was stored 4°C for a maximum of 4 weeks.

4.3.2.4.4 RPMI culture medium for PBMNCs

Roswell Park Memorial Institute (RPMI) 1640 medium was used with 10% (v/v) FBS, 2mM L-glutamine, 100 U.ml⁻¹ penicillin and 100 µg.ml⁻¹ streptomycin. Supplemented cell culture medium was stored 4°C for a maximum of 4 weeks.

4.3.2.5 Cell culture

4.3.2.5.1 Resurrection of L929 cells

A cryovial of approximately 1x10⁶ cells was removed from liquid nitrogen and allowed to thaw slowly at room temperature. Once the cells were thawed they were immediately

transferred to a sterile universal containing 10ml of pre-warmed (37°C) fresh DMEM culture medium. The cell suspension was centrifuged at 150g for 10 minutes at room temperature. After centrifugation, the supernatant was discarded and the pellet of cells was suspended in 2ml of DMEM culture medium. The cell suspension was added to a sterile culture flask (T-75), which was pre-loaded with 10ml of DMEM culture medium. Thereafter, the T-75 culture flask containing the L929 cells was incubated at 37°C in 5% (v/v) CO₂ in air until the cells were approximately 80% confluent, which was determined using a light microscope. The cell culture medium was changed every 2-3 days until passaging was required.

4.3.2.5.1.1 Cell culture maintenance

Once the cells achieved approximately 80% confluency the cell culture medium was removed from the flask, and the cells were gently washed with sterile DPBS (without calcium and magnesium). The cells were treated with trypsin-EDTA (2ml for T75 or 5ml for T175) for upto 10 minutes in 5% (v/v) CO₂ in air at 37°C to detach the cells from the flask. The bottom of the flask was tapped gently to dislodge the cells from the plastic and the trypsin-EDTA was inhibited by the addition of equivalent volume of culture medium containing 10% (v/v) FBS (1:1) to that of trypsin-EDTA. Thereafter, the cell suspension was transferred to a sterile universal and centrifuged at 150g for 10 minutes. After centrifugation, the supernatant was carefully aspirated and the pellet was suspended in 5ml of DMEM culture medium. A trypan blue exclusion assay (section 4.3.2.6) was performed to ascertain the cell number and the cells were seeded into a fresh culture flask (T75 or T175) at an appropriate seeding density (1×10^4 per cm²). A final volume of DMEM culture medium was added to the culture flask (10ml for T75 or 17ml for T175). Thereafter, the cells were incubated in 5% (v/v) CO₂ in air at 37°C and the cell culture medium was replaced every 3-4 days until confluent. Cells were maintained up to 10 passages before being discarded.

Cells were stored in longer term storage by passaging the cells as described above. The cells were suspended at a density of 1×10^6 cells.ml⁻¹ in DMEM supplemented with 10% (v/v) FBS and 10% (v/v) dimethyl sulphoxide (DMSO). A volume of 1.5ml of the cell suspension was transferred into each sterile cryovial and placed in a freezing pot containing isopropanol. The cryovials were placed in a -80°C freezer for 24hrs before being transferred into liquid nitrogen for long term storage.

4.3.2.5.2 Isolation of primary peripheral blood mononuclear cells

This study used five healthy donors aged between 24-60 years. The blood was collected by a trained phlebotomist (Dr Daniel Thomas, School of Biomedical Sciences, University of Leeds) in accordance with the Faculty of Biological Sciences Ethics Committee approval (BIOSCI 10-018). Informed consent was obtained from the donor before collecting the blood,

which was recorded and tracked using the Achiever tissue tracking system (Leeds Teaching Hospital NHS Trust and University of Leeds). Approximately 30ml of blood was collected using a 21G needle and sodium heparinised vacuum collection tubes. The blood was collected in the morning and processed on the same day to minimise activation of platelets and clotting of the blood.

Isolation of the PBMNCs was performed in a class II safety cabinet designated for human tissue only. The blood sample, PBS with 2% (v/v) FBS and density gradient medium (lymphoprep) were incubated at room temperature for 1 hour prior to isolation. The SepMate™ procedure was used to isolate the PBMNCs from the blood. The SepMate™ tubes used in this procedure were specifically designed for the isolation of mononuclear cells from human whole peripheral blood and cord samples by density gradient centrifugation.

Specifically, the whole blood was diluted with an equal volume (1:1) PBS of supplemented with 2% FBS (v/v) and mixed gently. The density gradient medium i.e. lymphoprep (15ml), was added to the 50ml SepMate™ tube by carefully pipetting it through the central hole of the SepMate™ insert. Thereafter, keeping the SepMate™ tube vertical, the diluted blood sample was added to the tube by slowly pipetting it down the side of the tube. The loaded SepMate™ tube was then centrifuged at 1200g for 10 minutes at room temperature. After centrifugation, the enriched layer of isolated PBMNCs was poured into a separate falcon tube (50ml) ensuring the SepMate™ tube was not inverted for longer than 2 seconds. The isolated PBMNCs were washed in PBS with 2% (v/v) FBS and centrifuged at 300g for 8 minutes at room temperature. This was repeated (2-3 times) until the supernatant was clear. The isolated PBMNCs were then re-suspended in 5ml of supplemented RPMI culture medium and the cells were counted using the trypan blue dye exclusion method, before seeding the cells.

4.3.2.6 Determination of cell number using Trypan blue exclusion assay

The trypan blue exclusion assay was used to determine the number of viable cells in an isolated cell suspension. The trypan blue dye enters the dead cells due to a loss of membrane potential, which results in blue appearance of dead cells, whereas live cells appear colourless. To perform a cell count, 90µl was taken from a cell suspension and transferred to a sterile bijou. A volume of 10µl of trypan blue dye was added to the cell suspension and thoroughly mixed by pipetting up and down. Thereafter, 10µl of the trypan blue: cell suspension mixture was added to a haemocytometer and using an inverted light microscope, the viable cells (colourless cells) were counted, whilst the dead cells (stained blue) were not included in the count. A minimum of 100 cells and a maximum of 300 cells were counted within the 25 squares of the haemocytometer. The number of viable cells per ml was calculated according to Equation 4.

Equation 4

$$\text{number of viable cells. ml}^{-1} = \frac{\text{number of viable cells}}{n} \times 10^4 \times \text{dilution factor}$$

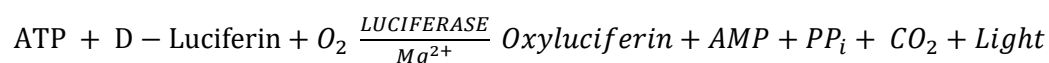
- n= number of grid squares used in cell count
- dilution factor = 10/9

4.3.2.7 Biological impact of ceramic particles

The following assays were used to assess the biological impact of ceramic particles on L929 murine cell fibroblasts and PBMNCs. All assays were conducted using the PBMNCs, whereas only cytotoxicity assessment was conducted with L929 murine cell fibroblasts.

4.3.2.7.1 Cytotoxicity assessment using ATP-Lite assay

The ATP detection kit assay (ATP-lite assay) measures the levels of ATP present within cells by the production of luminescence caused by the reaction of ATP with added luciferase and D-luciferin. Based on this reaction (see below), the concentration of ATP present can be determined by measuring the emission of light from the sample, which is proportional to the ATP concentration.



4.3.2.7.1.1 Performing the ATP Lite assay

Culture medium was removed from each well of the 96-well plate and either discarded (L929 cells) or stored (PBMNCs) in 96-well plates for further analysis. A volume of 50µl of mammalian cell lysis solution was added to each well and the plate was shaken (320rpm) for 5 minutes. Reconstituted lyophilised substrate solution at a volume of 50µl was added to each well and the plate was shaken (320rpm) for 5 minutes. The solution in each well was transferred to the corresponding well of a 96-well Optiplate® and an adhesive clear film seal was placed over the plate to prevent contamination. The plate was adapted to the dark for 10 minutes before measuring the luminescence in each well for 10 seconds using the luminescent plate reader and MiroWin 2000 software.

The output measurements were expressed as counts per second (CPS) and were exported to Microsoft Excel software. The average of the blank measurements was subtracted from all the results, however for the cells cultured with the highest particle volume, the average of the particle control was subtracted instead. This was to ensure that the particles did not interfere with the assay reagents and produce false positive or false negative results.

4.3.2.7.2 Inflammatory response assessment using ELISA

A sandwich enzyme-linked immunosorbent assay (ELISA) was used to determine the concentration of TNF- α , an important cytokine involved in osteolysis. The assay was completed by following these steps: -

4.3.2.7.2.1 Preparation of reagents for the ELISA

The reagents used in the ELISA, but not provided with the kit are listed in Table 4.6. Prior to the assay, two litres of PBS solution were prepared (section 4.3.2.4.1) and autoclaved at 121°C for 20 minutes, at 103 kPa, and stored at room temperature. The reagents were prepared and stored at 2-8°C and used for up to one week. The reagents provided with the ELISA kit are shown in Table 4.7, which were stored at 2-8°C.

Table 4.6 – The reagents prepared for use with the ELISA kit

Reagent	Composition
Coating buffer	PBS (pH 7.2-7.4)
Wash buffer	PBS with 0.05% (v/v) Tween
Reconstitution buffer	PBS with 0.09% (v/v) Sodium azide
Blocking buffer	PBS with 5% (w/v) BSA
Standard dilution buffer and secondary antibody dilution buffer	PBS with 1% (w/v) BSA
HRP dilution buffer	PBS with 1% (w/v) BSA and 0.1% (v/v) Tween

Table 4.7 – The reagents provided with the ELISA kit and the preparation required prior to use

Reagent	Preparation
TNF- α standard; 800pg.ml ⁻¹	Reconstituted with PBMNCs culture medium as directed on the vial
Capture antibody	Sterile and diluted prior to use
Biotinylated anti-TNF- α detection antibody	Reconstituted with 0.55ml of reconstitution buffer prior to use
Streptavidin-HRP	Diluted prior to use
TMB substrate	Ready to use

4.3.2.7.2.2 Preparation of ELISA plate

The Diaclone Human TNF- α ELISA set was used in this study to quantify the concentration of TNF- α released from PBMNCs in response to different doses of ceramic particles. Typically, 100 μ l of capture antibody was added to 10ml of coating buffer, which was enough to coat a full 96-well Maxisorp plate. A volume of 100 μ l of diluted capture antibody was

added to each well using an automated pipette. Thereafter, the plate was incubated overnight at 4°C. The diluted capture antibody was discarded and washed with 350µl of wash buffer per well. The wash buffer was aspirated and tapped firmly against absorbent paper to remove any residual liquid. The wash step was repeated once. A volume of 250µl of blocking buffer was added to each well and the plate was covered with the lid and incubated at room temperature for 2 hours. After incubation, the plate was washed with wash buffer a further three times and either used immediately or wrapped in parafilm and stored at 2-8°C in a seal bag containing desiccant for up to one month.

4.3.2.7.2.3 Performing the ELISA method

The supernatants collected from the PBMNCs (4.3.2.8.2) cultured with ceramic particles was thawed at room temperature for one hour prior to performing the ELISA. The reagents in Table 4.7 were prepared as and when required before each step. The following steps were performed to complete the ELISA: -

The TNF- α standards were prepared by reconstituting the standard vial with RPMI 1640 culture medium to give an 800pg.ml⁻¹ sample. This was dispensed in duplicate at a volume of 200µl in the appropriate wells (A1 and A2) according to the plate layout illustrated in Figure 4.2. Thereafter, 100µl of the PBMNCs culture medium (diluent buffer) was added to the remaining wells B1 and B2 through to G1 and G2. The highest concentration (800pg.ml⁻¹) of the TNF- standard was diluted using these well, whereby 100µl from wells A1 and A2 was transferred to B1 and B2, respectively, by mixing the contents of the well by repeated aspirations using a P200 Gilson pipette. This 1:1 dilution step was continued using 100µl from wells B1 and B2 through to wells G1 and G2 providing a serial diluted standard curve ranging from 800pg.ml⁻¹ to 12.5pg.ml⁻¹. The PBMNCs culture medium was added as the blank standard in wells H1 and H2. The test samples were dispensed in duplicate at a volume of 100µl in each well. The lipopolysaccharide (LPS) positive control sample was diluted 1:2 using RPMI 1640 culture medium before adding to the plate. This was to ensure the levels of TNF- α did not exceed the maximum standard concentration as high levels of TNF- α release was anticipated.

	Standards		Sample wells									
	1	2	3	4	5	6	7	8	9	10	11	12
A	800	800										
B	400	400										
C	200	200										
D	100	100										
E	50	50										
F	25	25										
G	12.5	12.5										
H	B	B										

*Standards were in pg.ml^{-1} . B (Blank).

Figure 4.2 - Example plate layout for performing one ELISA.

The biotinylated anti-TNF- α detection antibody was reconstituted with 550 μl of reconstitution buffer prior to use. For one plate, 100 μl of the reconstituted detection antibody was diluted with 5ml of secondary antibody dilution buffer. Thereafter, 50 μl of diluted detection antibody was added to each well and the plate was incubated for at room temperature for three hours. Following the incubation, the contents in each well was aspirated and washed with wash buffer three times using the same technique described previously (section 4.3.2.7.2.2).

The streptavidin-HRP (5 μl) provided with the kit was diluted with 500 μl of HRP dilution buffer immediately before use. This was further diluted, whereby for one plate 150 μl of the diluted streptavidin-HRP solution was added to 10ml of HRP dilution buffer and 100 μl of this diluted solution was added to each well. The plate was covered and incubated at room temperature for 30 minutes. After incubation, the streptavidin-HRP solution was aspirated and the wells were washed three times with wash buffer using the same technique described previously (section 4.3.2.7.2.2).

A volume of 100 μl of ready-to-use TMB (3,3',5,5'-Tetramethylbenzidine) substrate was added to each well and the plate was covered and wrapped in aluminium foil immediately to incubate in the dark at room temperature for 15 minutes. During the incubation period, the TMB solution turned blue in the presence of TNF- α . Thereafter, a volume of 100 μl of 1M sulphuric acid was added to each well, which terminated the reaction and turned the solution yellow. The absorbance value of each well was read on a multi-scan spectrum micro-plate spectrophotometer using a 450nm as the primary wavelength and 630nm as the reference wavelength.

4.3.2.7.2.4 Analysis of ELISA results

The average optical density was plotted against each standard concentration of TNF- α to generate a linear standard curve. The standard curve was used to determine the TNF- α concentration (pg.ml⁻¹) of each sample using the average optical density, for each sample. The positive LPS control was diluted, and so the values obtained were multiplied by the dilution factor. The data from the cell only negative control and the treatments that stimulated PBMNCs to produce a statistically significant increase in the levels of TNF- α PBMNCs from all donors, were used to generate box plots in order to analyse the variability in inflammatory response between different donors.

4.3.2.7.3 Genotoxicity assessment using the Comet assay

Single cell gel electrophoresis or the comet assay is a sensitive and rapid technique for quantifying DNA damage from *in vivo* and *in vitro* samples of eukaryotic cells. The assay produces images of single cells embedded in agarose gel that resembles a 'comet' with a distinct head and tail. The head contains intact DNA, whilst the tail is composed of single-stranded or double-stranded DNA with breaks. The extent of DNA migrated from the head of the comet is directly proportional to the level of DNA damage.

4.3.2.7.3.1 Preparation of reagents

The reagents prepared for the comet assay are listed in Table 4.8.

Table 4.8 – The reagents prepared for use with the comet assay

Reagent	Composition	Storage
TE buffer	10mM Tris-HCL with 1mM EDTA (pH 7.5)	Stored at room temperature
Alkaline unwinding solution	200mM NaOH with 1mM EDTA	Stored at room temperature
Alkaline electrophoresis solution	300mM NaOH with 1mM EDTA	Stored at 4°C
SYBR Gold	1 μ l of 10,000x diluted in 30ml TE buffer	Stored at 4°C
PBMNC detaching solution	DPBS with 2.5mM EDTA	Stored on ice
LMAgarose	Provided by Trivegen	Melted using microwave and then place in thermomixer set at 37°C

4.3.2.7.3.2 Performing the Comet assay

The assay was completed by following these steps:

The cell culture media was aspirated from all the wells in the 48-well plate and discarded, before washing the cells with 100 μ l of sterile DPBS. Thereafter, 1ml of ice-cold PBMNC detaching solution was added to each well and the 48-well plate was incubated on ice for 30 minutes. After incubation, the contents of the well were aspirated and dispensed several times to dislodge any remaining attached cells. Thereafter, the cell suspension from each well was transferred to pre-labelled sterile 1.5ml Eppendorf tubes, which were centrifuged at 200g for 10 minutes at 4°C. After centrifugation, the supernatant was carefully discarded ensuring the pellet was not disturbed.

As there were many cell samples due to the different particle dose treatments, the LMAgarose was aliquoted (1ml) into 1.5ml Eppendorf tubes and placed in the thermomixer set to 37°C. The cells were resuspended in 100 μ l of molten LMAgarose gel (37°C) and the agarose cell suspension was mixed gently by inversion several times to evenly disperse the cells. Thereafter, 30 μ l of agarose cell suspension was immediately pipetted on the 20 well CometSlide™. The tip of the pipette tip was used to spread the agarose/cells over the sample area to ensure complete coverage of the sample area. This was done for all different samples, except for the positive control, which was incubated at 37°C with 5 μ l of 100 μ M hydrogen peroxide prior to placing the agarose cell suspension on the slide. The slide was incubated at 4°C in the dark for 30 minutes. This was to set the gel and ensure adherence of the sample to the slide. A 0.5mm clear ring appeared at the edge of the CometSlide™ area once the gel was set.

The slides were immersed in pre-cooled (4°C) lysis solution and incubated at 4°C for 1 hour, in the dark. Thereafter, the slides were immersed in freshly prepared alkaline unwinding solution for 20 minutes at room temperature, in the dark.

The slides were then placed in the electrophoresis tank containing electrophoresis solution that was pre-cooled for 1 hour at 4°C. The electrophoresis tank was set at 1 volt/cm e.g. 30V in a 30cm tank. The mAmp was adjusted to 300 by adding or removing electrophoresis buffer before the samples were electrophoresed at 4°C in the dark for 20 minutes. Thereafter the slides were immersed in distilled water for 5 minutes. This was repeated once. The slides were then immersed in 70% (v/v) ethanol for 5 minutes, in the dark. The slide was stored in the dark at room temperature with a desiccant prior to scoring.

The SYBR Gold x10,000 was diluted by adding 1 μ l to 30 μ l of TE buffer. A volume of 50 μ l of the diluted SYBR Gold stain was placed onto each circle of dried agarose and stained for 30 minutes at room temperature, in the dark. The slides were gently tapped onto absorbed paper to remove the SYBR solution and then rinsed briefly in water. The slides were dried at

37°C in an incubator for 2 hours before imaging using a Zeiss upright microscope using the following settings: -

- HXP 120 V power was set to 10
- 10x objective
- GFP channel (excitation at 509nm)
- Exposure time 1500ms
- Intensity set to min/max after image was taken

The automatic tiling tool was used to take images of the entire sample area. This technique ensured all the cells present in the gel were imaged. Images were captured and exported using ZEN 2009 software (Carl Zeiss Microscopy Ltd).

The SYBR gold nucleic acid gel stain allowed visualisation of the nuclear DNA within the cell. Cell nuclei that appeared circular indicated intact nuclei and no (or minimal) detectable DNA damage, whereas nuclei that had tails resembling a comet, indicated DNA damage. All images were oriented where the head was on the right and the tail to the left for the software to correctly detect the comets. Only single cells were measured, cells which were overlapping or too close to each other or surrounded by debris were not measured. A minimum of 100 cells were scored per condition. The data was exported to Microsoft Excel, and the 'Olive tail moment' was presented for each treatment.

4.3.2.7.4 Oxidative stress assessment using cellular reactive oxygen species detection assay

The cellular reactive oxygen species (ROS) detection assay uses the 2',7' -dichlorofluorescein diacetate (DCFDA) fluorogenic dye that measures hydroxyl, peroxy and other ROS activity/presence within the cell. The DCFDA diffuses into the cell via the cell membrane and undergoes deacetylation by cellular esterases to a non-fluorescent compound. In the presence of ROS, the DCFDA is oxidised into 2',7' -dichlorofluorescein (DCF), which is a highly fluorescent compound that can be detected by fluorescence spectroscopy by 495nm excitation and 529nm emission (Eruslanov and Kusmartsev, 2010).

4.3.2.7.4.1 Preparation of reagents

The reagents prepared for the cellular reactive oxygen species (ROS) detection assay are listed in Table 4.9.

Table 4.9 – The reagents prepared for use with the cellular ROS detection assay

Reagent	Reagent preparation	Storage
1x buffer	10x buffer supplied with the kit was diluted with sterile water (1:10)	Stored at 4°C
1x supplemented buffer with 10% (v/v) FBS	1x buffer was supplemented with 10% (v/v) FBS	Stored at 4°C
25µM DCFDA (2',7' – dichlorofluorescein diacetate) solution	20mM DCFDA was diluted with sterile water to give a 25µM final concentration solution of DCFDA	Stored at 4°C
200µM TBHP (tert-Butyl hydroperoxide)	55mM was diluted with sterile water to give a 200µM final concentration solution of TBHP	Stored at 4°C

4.3.2.7.4.2 Performing the cellular reactive oxygen species detection assay

The assay was completed by following these steps: -

The cell culture media was aspirated from all the wells in the 96-well plate and discarded, before washing the cells with 100µl of 1x buffer. Thereafter, the 1x buffer was aspirated and discarded before staining the cells by adding 100µl of 25µM DCFDA in 1x buffer and incubated at 37°C for 45 minutes. A volume of 100µl of 200µM TBHP was added to the column of wells designated as the positive control treatment. The plate was incubated for 2 hours at 37°C.

The fluorescence at excitation 485nm and emission 535nm of each well was measured using the plate reader and MiroWin 2000 software. The output measurements were expressed as fluorescence intensity and was exported to the Microsoft Excel software and the average of the blank readings was subtracted from all the measurements. The contents of each well were dispensed and the plate was immediately imaged with the Zeiss upright microscope using the following settings: -

- HXP 120 V power was set to 10
- 20x objective
- eGFP channel (excitation at 485nm)
- Exposure time 1000ms

The eGFP channel allowed imaging of the green fluorescent ROS (485nm) that was present in the cells. Images were captured and exported using ZEN 2009 software (Carl Zeiss Microscopy Ltd). Images were captured at random locations, and a minimum of four non-overlapping images from each treatment were captured (n=4).

4.3.2.8 Culturing cells with particles to determine the biological impact

4.3.2.8.1 Culture of L929 cells with particles to determine the cytotoxic effects of ceramic model particles and clinically-relevant ceramic wear particles

The L929 murine fibroblast cell line was used as per ISO 10993-5 “Biological evaluation of medical devices – Part 5: Tests for *in vitro* cytotoxicity”, to determine the cytotoxic effects of ceramic model particles and clinically-relevant ceramic wear particles to select the appropriate doses for subsequent experiments using PBMNCs. L929 cells were resurrected and passaged using standard cell culture methods outlined in section 4.3.2.5.1.

The effects of the ceramic model particles and clinically-relevant ceramic wear particles on the viability of L929 cells in co-culture were determined using the ATP-Lite™ assay, which is described in section 4.3.2.7.1. The L929 cells were seeded into 96 well plates at a seeding density of 1×10^4 cells per well and cultured with increasing doses of BIOLOX® Delta ceramic model particles (0.05-500 μm^3 per cell), or BIOLOX® Forte ceramic model particles (0.05-500 μm^3 per cell) or clinically-relevant BIOLOX® Delta ceramic wear particles (0.05-500 μm^3 per cell). Six wells in total were used for each treatment (n=6). The negative control was seeded in the same way but with no particles or treatment. The cytotoxic effects of the ceramic particles were compared with clinically-relevant CoCr nano-particles at a dose of 50 μm^3 per cell, which was used as the positive particle control. Camptothecin, at a final concentration of 2 $\mu\text{g} \cdot \text{ml}^{-1}$ was included as the positive control to induce apoptosis. The plates were incubated for 0, 1, 3 and 6 days at 37°C in 5% (v/v) CO₂ in air. After the appropriate incubation period with the particles, an ATP-Lite™ assay was performed, which is described in section 4.3.2.7.1. The L929 cells cultured with Delta ceramic model particles is shown in Figure 4.3.

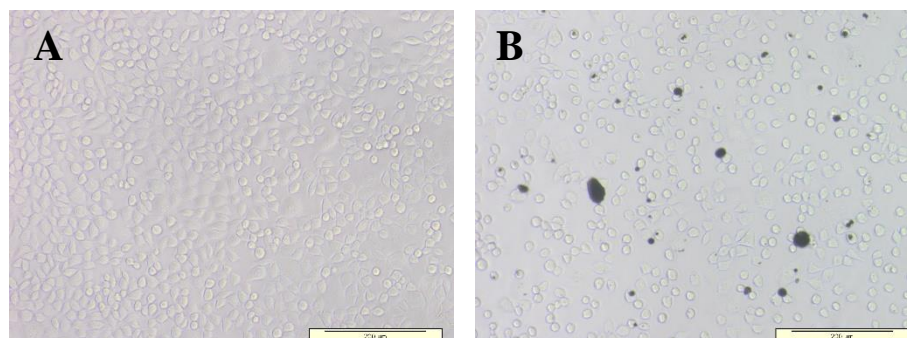


Figure 4.3 – L929 cells cultured with ceramic model particles. (A) L929 cells with no particles and (B) L929 cells cultured with 500 μm^3 per cell of BIOLOX® Delta model ceramic particles.

4.3.2.8.2 Culture of PBMCs with model or clinically-relevant ceramic wear particles to determine the biological impact in terms of cytotoxicity, inflammation, genotoxicity and oxidative stress

4.3.2.8.2.1 Methodology to assess the biological impact of ceramic model particles

PBMCs were isolated from blood taken from five healthy volunteer donors (Donor 2, Donor 5, Donor 7, Donor 25 and Donor 26) as described in section 4.3.2.5.2. The PBMCs isolated from the blood of a single donor were used to conduct all four assays as described in section 4.3.2.7 and illustrated in Figure 4.4.

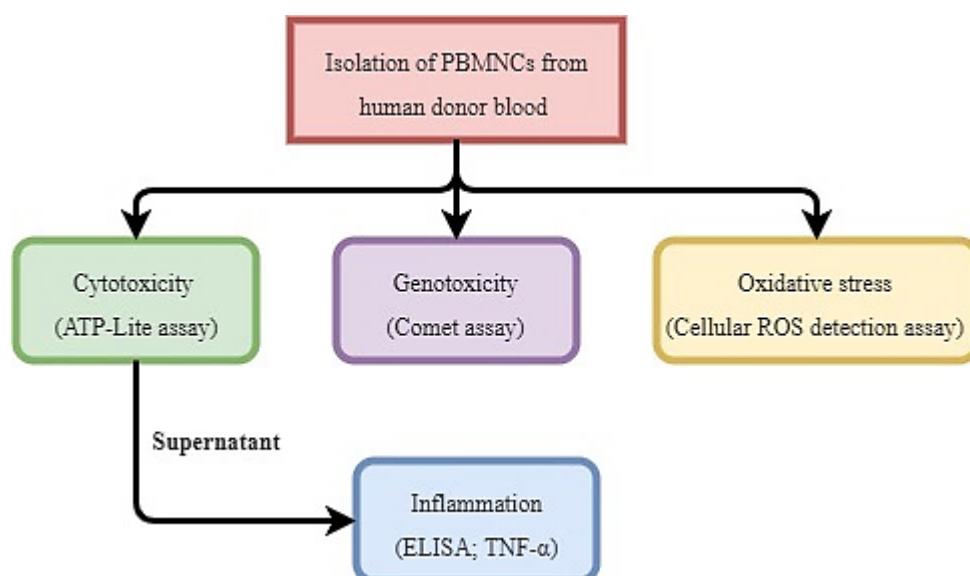


Figure 4.4 – Flow diagram showing the different assays completed on PBMCs isolated from blood collected from a single donor.

The PBMCs from each donor were seeded into the appropriate well plate at the appropriate seeding density and repeats for each assay as described in Table 4.10. The effects of increasing doses ($0.05\text{-}50\mu\text{m}^3$ per cell) of BIOLOX[®] Delta ceramic model particles was initially investigated in terms of cytotoxicity, inflammation, genotoxicity and oxidative stress, and compared with the effects of low ($0.5\mu\text{m}^3$ per cell) and high ($50\mu\text{m}^3$ per cell) doses of BIOLOX[®] Forte ceramic model particles and low ($0.5\mu\text{m}^3$ per cell) and high ($50\mu\text{m}^3$ per cell) doses of clinically-relevant CoCr nano-particles (generated using the PoP wear rig; section 3.3.3.3), which was used as the positive particle control. The positive controls for each assay are listed Table 4.11. The negative control was seeded in the same way but with no particles or treatment for all the assays. The plates were incubated for 24 hours at 37°C in 5% (v/v) CO_2 in air. After the incubation period with the particles, the cytotoxic effects of the particles were assessed using the ATP-Lite assay as described in section 4.3.2.7.1.

Table 4.10 – Seeding density, type of culture vessel and repeats used for each assay.

Biological assessment (assay type)	Seeding density (per well)	Culture vessel	Repeats
Cytotoxicity (ATP-Lite assay)	2×10^4	96-well plate	6 wells per treatment
Inflammation (ELISA; TNF- α)	2×10^4	96-well plate	Supernatants harvested from 4 wells
Genotoxicity (Comet assay)	1×10^5	48-well plate	2 wells per treatment (100 cells scored per treatment)
Oxidative stress (Cellular ROS detection)	2×10^4	96-well plate (Clear Bottom Black)	6 wells per treatment

Table 4.11 – Positive controls used for each assay.

Biological assessment	Assay type	Positive control (concentration)
Cytotoxicity	ATP-Lite assay	Camptothecin ($2 \mu\text{g} \cdot \text{ml}^{-1}$)
Inflammation	ELISA (TNF- α)	LPS ($200 \text{ng} \cdot \text{ml}^{-1}$)
Genotoxicity	Comet assay	Hydrogen peroxide ($100 \mu\text{M}$)
Oxidative stress	Cellular ROS detection	TBHP ($200 \mu\text{M}$)

The inflammatory response to the ceramic model particles was assessed in terms of cytokine (TNF- α) release through harvesting of the supernatant to be used in an ELISA. The supernatant ($200 \mu\text{l}$) was collected and aliquoted in duplicate ($n=4$) i.e. a volume of $100 \mu\text{l}$ into each well of 96-well plate. These plates were wrapped in Parafilm and stored at -80°C until an ELISA was performed as described in section 4.3.2.7.2.

In addition to the ATP-Lite assay, the other assays for genotoxicity and oxidative stress were also performed on the same day. The genotoxic effects of the ceramic model particles were assessed using the comet assay as described in section 4.3.2.7.3. The production of ROS in response to the ceramic model particles was assessed using the cellular reactive oxygen species detection assay as described in section 4.3.2.7.4.

4.3.2.8.2.2 Methodology to assess the biological impact of clinically-relevant ceramic wear particles

PBMNCs isolated from blood taken from the same five healthy volunteer donors was co-cultured with increasing doses (0.05-50 μm^3 per cell) of clinically-relevant BIOLOX[®] Delta ceramic wear particles that were generated using the Leeds II hip simulator as described in section 3.3.3.1. The effects of these wear particles were compared with low (0.5 μm^3 per cell) and high (50 μm^3 per cell) doses of clinically-relevant BIOLOX[®] Forte ceramic wear particles (generated using the Leeds II hip simulator) and low (0.5 μm^3 per cell) and high (50 μm^3 per cell) doses of clinically-relevant CoCr nano-particles, which was used as the positive particle control. The positive controls for each assay are listed in table Table 4.11. Furthermore, due to contamination issues with stainless wear particles as described in section Percentage ratio between ceramic and stainless-steel wear particles using EDX elemental mapping, stainless steel wear particles at dose 50 μm^3 per cell were introduced. These stainless-steel wear particles were a gift from another researcher (Helen Lee) and were generated using the six-station pin-on-plate wear rig and smooth (Ra value of $\leq 0.01\mu\text{m}$) medical grade stainless-steel pins articulated against smooth stainless-steel plates in water lubricant. The negative control cell only was seeded in the same way but with no particles or treatment for all the assays. The plates were incubated for 24 hours at 37°C in 5% (v/v) CO₂ in air. After the incubation period with the particles, the same assays described in section 4.3.2.8.2.1 were used to assess the effects of clinically-relevant ceramic wear particles in terms of cytotoxicity (ATP-Lite assay), inflammation (ELISA), genotoxicity (comet assay) and oxidative stress (cellular ROS detection assay).

4.3.3 Statistical analysis

Values were presented as means $\pm 95\%$ confidence limits and analysed using one-way ANOVA. Differences between the different treatment groups and the negative control were determined by calculating the minimum significant differences (MSD) value ($p < 0.05$) using the Tukey-method.

4.4 Results

The results of the characterises of the ceramic model particles is first presented (4.4.1). Thereafter the biological impact in terms of cytotoxicity, inflammation, genotoxicity and oxidative stress was initially presented for the ceramic model particles (4.4.2) followed by the biological impact of the clinically-relevant ceramic wear particles (4.4.3) in terms of the same four biological assays.

4.4.1 Characteristics of the model ceramic particles

The size, morphology and composition of the ceramic model particles were determined and analysed using CFE-SEM and EDX analysis. The ceramic model particles were filtered on a 0.015 μ m filter membrane and imaged using CFE-SEM at 1 kV (beam deceleration mode), mixed signal; secondary electrons (SE) and back-scattered electrons (BSE) and at a working distance (WD) of 1-3 mm. Five random fields of view were imaged for each magnification; 5K, 60K, 90K and 150K. Chemical characterisation of the ceramic model particles was carried out by EDX analysis to confirm the chemical composition of the particles. The CFE-SEM micrographs of the ceramic model particles were subsequently analysed using computer software, ImageJ version 1.49, to measure the Feret's diameter (d_{max}), aspect ratio and circularity of the particles as described in section 2.3.3.2.2. A minimum of 150 particles were measured.

4.4.1.1 BIOLOX[®] Forte model ceramic particles

CFE-SEM analysis of the alumina BIOLOX[®] Forte ceramic model particles filtered on the 0.015 μ m filter membrane revealed large micron sized particles that were irregular/shard-like in shape (Figure 4.5A). High magnification of these particles showed the presence of small nano-scale particles (Figure 4.5B) that were round in morphology. EDX analysis confirmed that the larger particles were indeed comprised of alumina as indicated by the elemental peaks of aluminium (Al) and oxygen (O) (Figure 4.6B). The carbon (C) peak was due to the carbon coating. The mean ferret diameter, mean aspect ratio and mean circularity values (value of 1.0 indicates a perfect circle) for BIOLOX[®] Forte ceramic model particles are shown in Table 4.12. These values were compared with the values for the morphology of alumina BIOLOX Forte ceramic wear particles that were generated in Chapter 3, section 3.4.2.1.1, which are also listed in Table 4.12. An independent-samples t-test was conducted to compare the size distribution (feret diameter) and morphology (aspect ratio and circularity) of BIOLOX[®] Forte ceramic model particles with clinically-relevant BIOLOX[®] Forte wear particles generated in water (section 3.4.2.1.1). There were no significant differences in the values for aspect ratio ($p=0.835$) and circularity ($p=0.179$) between the clinically-relevant BIOLOX[®] Forte ceramic wear particles generated in water and BIOLOX[®] Forte ceramic model particles. Moreover,

the particle size distributions (feret diameter) for the clinically-relevant BIOLOX[®] Forte wear particles generated in water and BIOLOX[®] Forte ceramic model particles were also statistically similar (p=0.059). The frequency as a function of size of the BIOLOX[®] Forte ceramic model particles is presented in Figure 4.7, which revealed a bimodal size distribution. The larger micron and submicron size particles ranged between 100-3000nm with a mean size of 613nm ± 34.93nm, whereas the small nano-scale particles ranged between 10-80nm with a mean size of 44nm ± 2.6nm. The BIOLOX[®] Forte ceramic model particles had a mode size distribution of 300-400nm for the larger particles and a mode size of 30-40nm for the small nano-scale particles.

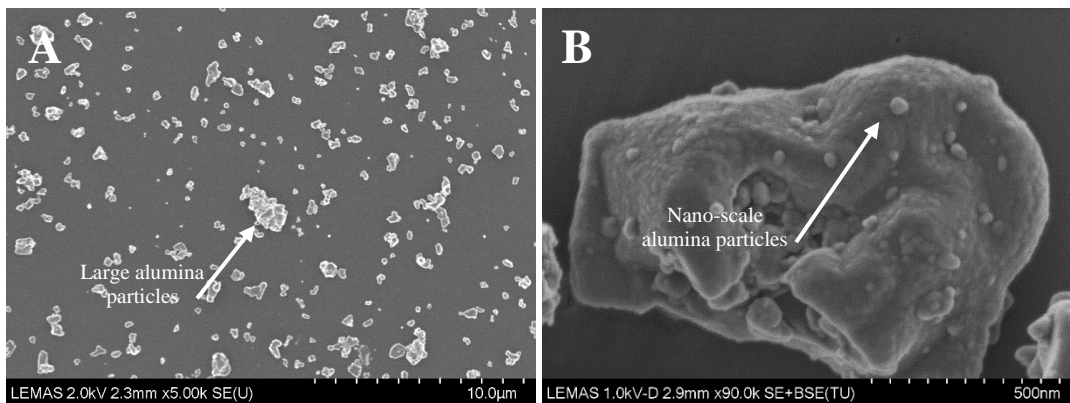


Figure 4.5 - CFE-SEM images of BIOLOX[®] Forte ceramic model particles, which consisted of (A) large micron sized alumina particles and (B) small nano-scale alumina particles. The particles were imaged at 1-2kV voltage and working distance of 2-3mm. The larger particles were imaged at 5K magnification to capture groups of particles. The smaller nano-scale particles were imaged at 60k, 90k and 150k magnification.

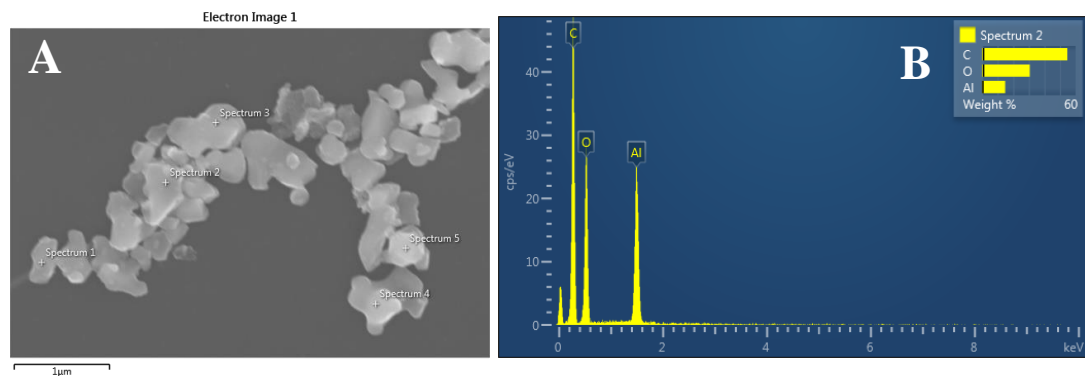


Figure 4.6 - CFE-SEM and EDX analysis of the BIOLOX[®] Forte ceramic model particles. (A) SEM image of the large alumina particles analysed using EDX and (B) corresponding EDX spectrum. Pin point EDX analysis of the particles was performed at a working distance of 15mm, 10kV and a suitable magnification to maintain focus. EDX spectrum B showed elemental peaks of Al (aluminium) and O (oxygen), which is indicative of alumina ceramic particles.

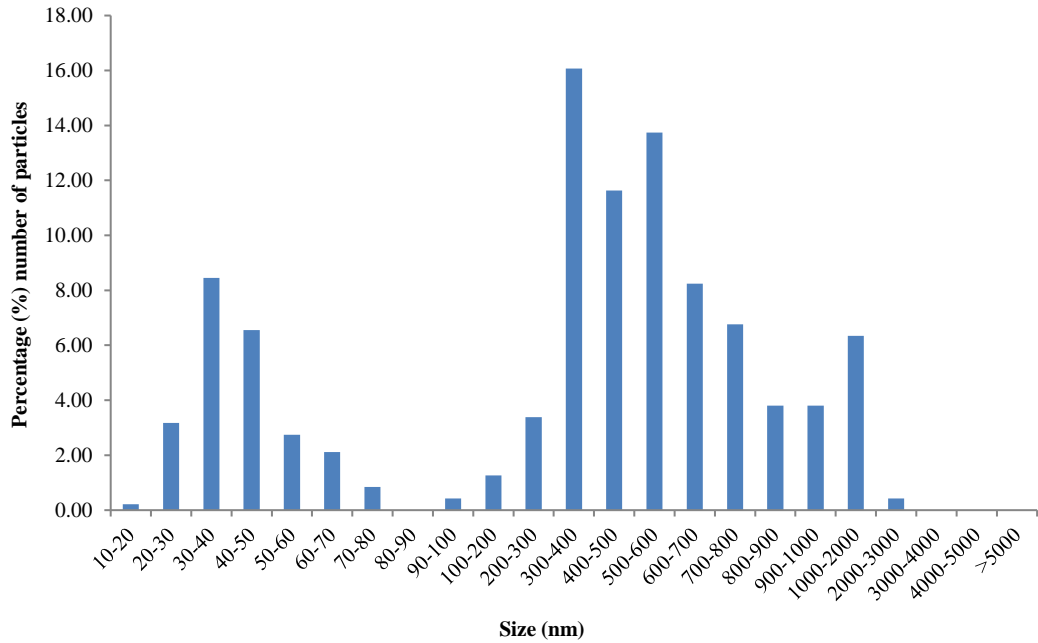


Figure 4.7 - Frequency size distribution of alumina BIOLOX® Forte ceramic model particles. A minimum of 150 particles were measured.

Table 4.12 - Mean size (feret diameter) and morphology (aspect ratio and circularity) values for BIOLOX® Forte ceramic wear particles generated in water and BIOLOX® Forte ceramic model particles.

	BIOLOX® Forte wear debris generated in water; Larger particles (100 - >5000nm)	BIOLOX® Forte wear debris generated in water; Smaller particles (0 - 100nm)	BIOLOX® Forte model; Larger particles (100 - >5000nm)	BIOLOX® Forte model; Smaller particles (0 - 100nm)
Feret diameter (nm)	736.478 ± 99.449	50.162 ± 7.105	613.275 ± 34.924	43.554 ± 2.595
Aspect ratio	1.521 ± 0.060	1.336 ± 0.042	1.458 ± 0.030	1.337 ± 0.035
Circularity	0.762 ± 0.017	0.905 ± 0.008	0.790 ± 0.012	0.905 ± 0.006

Note: All values expressed as mean ±95% Confidence Interval.

4.4.1.2 BIOLOX® Delta model ceramic particles

CFE-SEM analysis of the composite BIOLOX® Delta ceramic model particles revealed large grain-like structures that formed individual powder grains (Figure 4.8A). At high magnification (6-20K), these grain-like structures revealed the micro-structure of the BIOLOX® Delta powder, which consisted of tetragonal zirconia particles and strontium platelets dispersed within an alumina matrix (Figure 4.8B, C). The individual micron/sub-micron sized particles can be seen in Figure 4.8D, which were irregular/shard-like in morphology. The nano-scale particles were round in morphology and existed as large agglomerates (Figure 4.8E, F). EDX mapping of the large grain-like structures clearly showed the presence of strontium platelets (yellow) and zirconia particles (blue) within the alumina

matrix (green) as indicated by the individual element maps (Sr, Zr and Al) (Figure 4.9). The irregular/shard-like micron and sub-micron sized particles shown in Figure 4.8D were comprised of alumina or zirconia as indicated by EDX analysis that showed elemental peaks of Al (aluminium), O (oxygen) and Zr (zirconia) (Figure 4.10). The nano-scale particles also consisted of alumina and zirconia as indicated by EDX analysis that showed elemental peaks of Al (aluminium), Zr (zirconia) and O (oxygen) (Figure 4.11). Furthermore, a peak of Sr (strontium) was also observed due to the platelet present within the microstructure, which can be clearly seen in the corresponding SEM image in Figure 4.11A. The carbon (C) peak that can be seen in all EDX spectra was due to the carbon coating. The mean ferret diameter, mean aspect ratio and mean circularity values (value of 1.0 indicates a perfect circle) are shown in Table 4.13. An independent-samples t-test was conducted to compare the size distribution (feret diameter) and morphology (aspect ratio and circularity) of BIOLOX[®] Delta ceramic model particles with clinically-relevant BIOLOX[®] Delta ceramic wear particles generated in water (section 3.4.2.1.2). There was a significant difference in the values for aspect ratio ($p < 0.05$) and circularity ($p < 0.05$) between the clinically-relevant BIOLOX[®] Delta ceramic wear particles generated in serum and BIOLOX[®] Forte ceramic model particles. Moreover, the particle size distribution (feret diameter) for the clinically-relevant BIOLOX[®] Delta wear particles generated in water and BIOLOX[®] Delta ceramic model particles were also statistically different ($p < 0.05$). The frequency as a function of size of the BIOLOX[®] Delta ceramic model particles is presented in Figure 4.12, which revealed a multimodal size distribution. The micron and sub-micron size alumina particles ranged between 100-2000nm with a mean size of 508nm, whereas the small nano-scale particles ranged between 30-100nm with a mean size of 64nm. Furthermore, the large grain-like structures that are represented in the $>5000\mu\text{m}$ size range (Figure 4.12), ranged between 4-49.8 μm , with a mean size of 14.5 μm . The BIOLOX[®] Delta ceramic model particles had a mode size distribution of 500-600nm for the micron/sub-micron size alumina particles and a mode size of 60-70nm for the small nano-scale particles. Large grain-like structures ($>5\mu\text{m}$) made up more than 14% of the number of particles that were analysed.

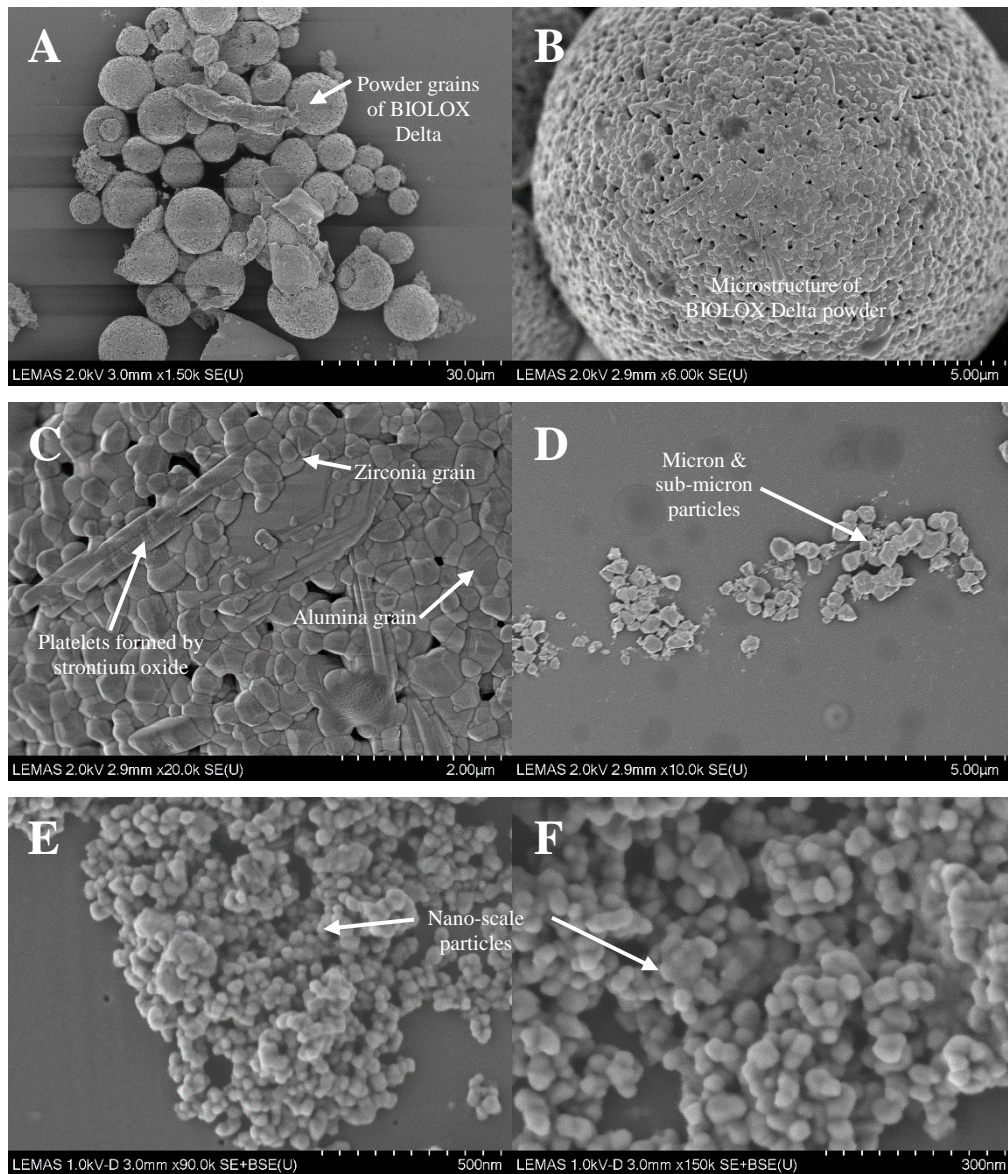


Figure 4.8 - CFE-SEM images of BIOLOX[®] Delta ceramic model particles. (A) Individual powder grains, (B & C) Large grain-like structures that shows the microstructure of the composite ceramic. (D) Large micron and sub-micron size particles and (E & F) small nano-scale particles. The particles were imaged at 1-2kV voltage, working distance of 3mm and magnification ranging between 1.5-150K.

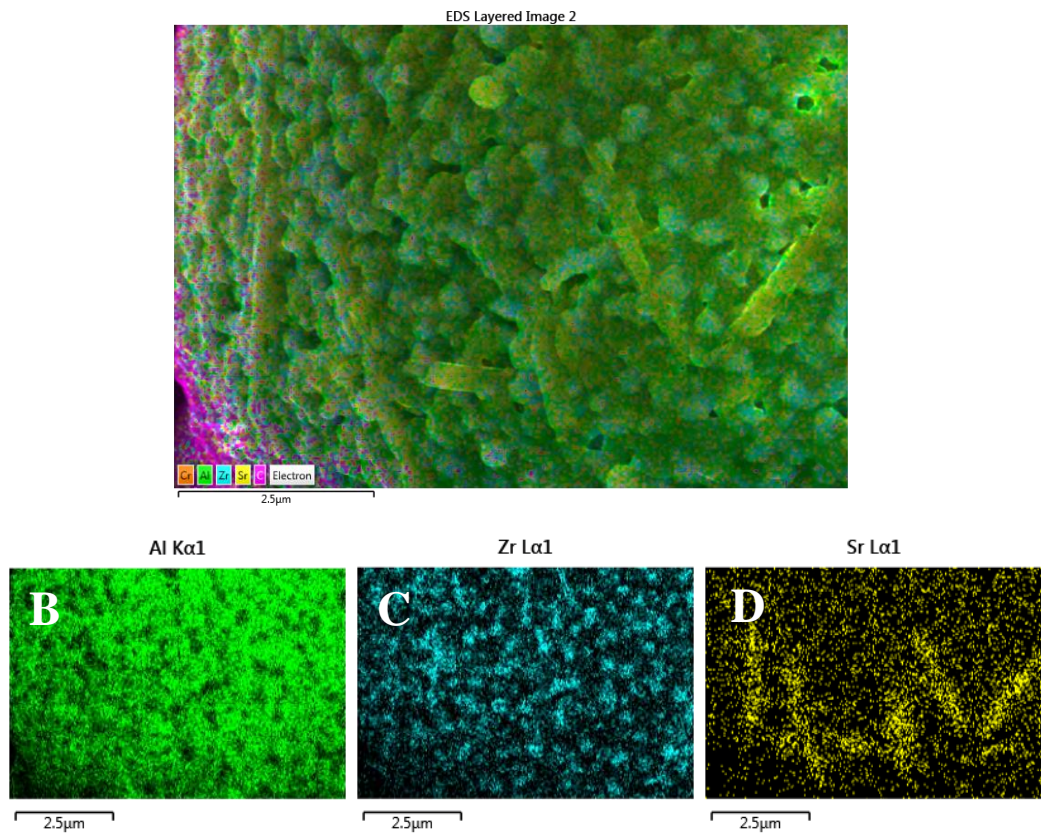


Figure 4.9 - EDX element map of BIOLOX[®] Delta ceramic model particles at 20K magnification showing the distribution of elements within the composite ceramic. EDX mapping was performed using the EDX element mapping tool at a working distance of 15 mm, 10kV. (A) EDX layered image of the elements identified on the area of the filter membrane; (B-D) Individual layers that correlate to the x-ray map colours of the different elements identified i.e. Al (aluminium), Zr (zirconia) and Sr (strontium).

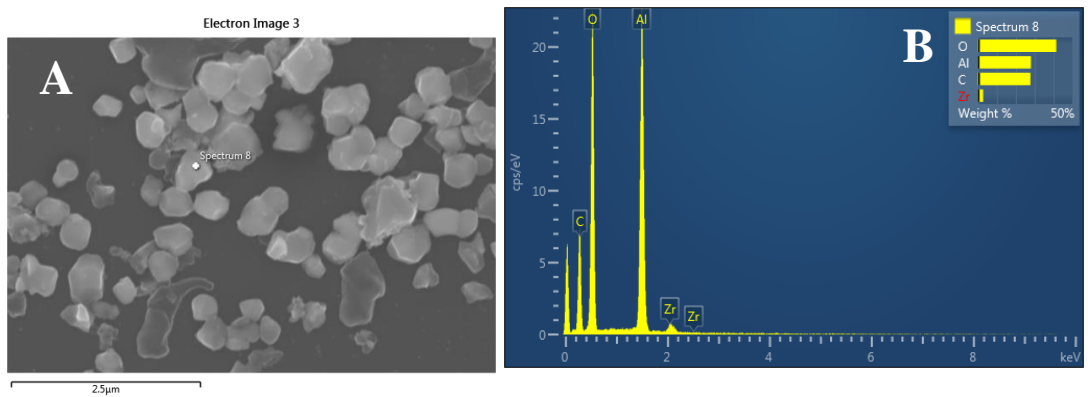


Figure 4.10 - CFE-SEM and EDX analysis of the micron and sub-micron BIOLOX[®] Delta ceramic model particles. (A) SEM image of the larger particles analysed using EDX and (B) corresponding EDX spectrum. Pin point EDX analysis of the particles was performed at a working distance of 15mm, 10kV and a suitable magnification to maintain focus.

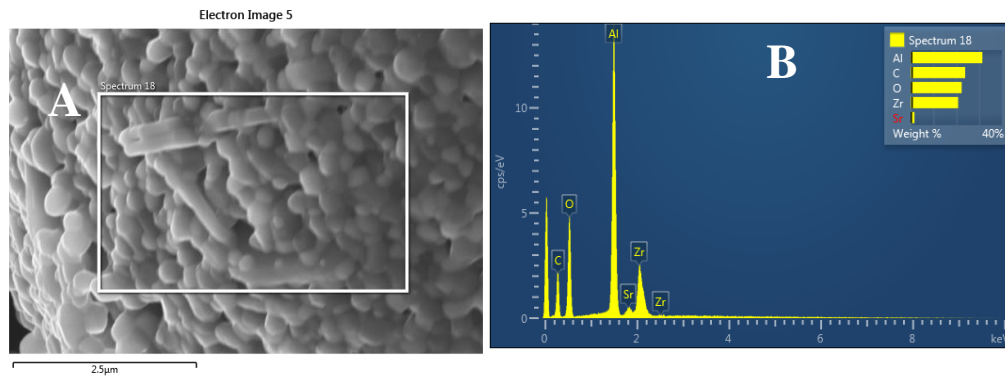


Figure 4.11 - CFE-SEM and EDX analysis of smaller nano-scale BIOLOX[®] Delta ceramic model particles. (A) SEM image of the nano-scale particles analysed using EDX and (B) corresponding EDX spectrum. Pin point EDX analysis of the particles was performed at a working distance of 15mm, 10kV and a suitable magnification to maintain focus.

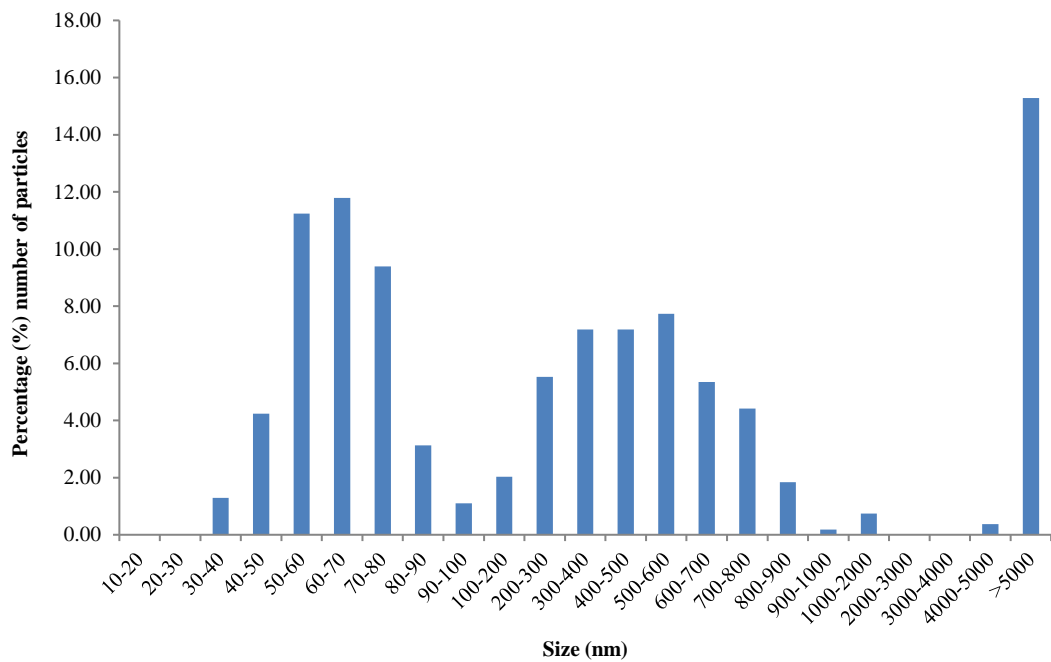


Figure 4.12 - Frequency size distribution of composite BIOLOX[®] Delta ceramic model particles. A minimum of 150 particles were measured.

Table 4.13 - Mean size (feret diameter) and morphology (aspect ratio and circularity) values for BIOLOX[®] Delta ceramic wear particles generated in water and BIOLOX[®] Delta ceramic model particles.

	BIOLOX [®] Delta model particles; Larger particles (100 - >5000nm)	BIOLOX [®] Delta model particles; Smaller particles (0 - 100nm)	BIOLOX [®] Delta wear particles generated in serum; Larger particles (100 - >5000nm)	BIOLOX [®] Delta wear particles generated in serum; Smaller particles (0 - 100nm)
Feret diameter (nm)	507.895 ± 24.742	64.367 ± 1.753	2308.105 ± 243.576	43.729 ± 0.968
Aspect ratio	1.344 ± 0.030	1.257 ± 0.020	1.471 ± 0.021	1.289 ± 0.010
Circularity	0.848 ± 0.009	0.908 ± 0.004	0.801 ± 0.005	0.911 ± 0.002

Note: All values expressed as mean ±95% Confidence Interval.

4.4.2 Biological impact of ceramic model particles

The biological response to commercially obtained ceramic powder (ceramic model particles) that is used to manufacture ceramic hip replacements BIOLOX[®] Delta and BIOLOX[®] Forte, was tested in terms of cytotoxic effects on L929 murine fibroblast cells as an initial assessment of biocompatibility. These results were used to determine the concentration(s) at which the ceramic particles induced cytotoxic effects, which was subsequently used to select the appropriate doses of ceramic particles for the biocompatibility assessment using primary cells. This step was necessary to elucidate the cytotoxic dose(s) of ceramic particles, as this phenomenon is highly unlikely to occur *in vivo* due to the low wear rates of CoC bearings, hence it was important to ensure that the doses were representative of the clinical scenario. A comprehensive evaluation of the biological impact of BIOLOX[®] Delta ceramic model particles in terms of cytotoxicity, inflammation, genotoxicity and oxidative stress was subsequently conducted using human PBMNCs.

4.4.2.1 The cytotoxic effects of ceramic model particles on L929 fibroblast cells

L929 murine fibroblast cells were seeded at a density of 1×10^4 cells per well ($n=6$) in 96-well plates and cultured in DMEM culture media with increasing doses of ceramic model particles (BIOLOX[®] Forte or BIOLOX[®] Delta) at low to high volumes ranging from 0.05 - $500 \mu\text{m}^3$ per cell. The negative control was seeded in the same way but with no particles. The cytotoxic effects of the ceramic particles were compared with clinically-relevant CoCr nano-particles at a dose of $50 \mu\text{m}^3$ per cell, which was used as the positive particle control. Camptothecin, at a final concentration of $2 \mu\text{g} \cdot \text{ml}^{-1}$ was included as the positive control to induce apoptosis. The plates were incubated for 0, 1, 3 and 6 days at 37°C in 5% (v/v) CO_2 in air. The results of the ATP-Lite assay were expressed as average absorbance values (counts per second) and as a percentage relative to the cell only negative control. The data was analysed using a one-way ANOVA and Tukey Post hoc analysis.

The cytotoxic effect of increasing doses of ceramic model particles in L929 murine fibroblast cells is demonstrated in Figure 4.13A (BIOLOX[®] Forte) and Figure 4.14A (BIOLOX[®] Delta). The average absorbance values, which are indicative of cellular metabolic activity and thus viability, for the cell only negative control continued to increase over the course of the 6-day culture period. The average absorbance values from day 0 to day 6 for the cells only negative control increased by approximately 10-fold in the BIOLOX[®] Forte particles experiment and by 6-fold in the BIOLOX[®] Delta particles experiment, which was indicative of cell proliferation. The cell growth was adversely affected in the presence of high particle volumes, whereby the ceramic model particles of BIOLOX[®] Forte (Figure 4.13) and BIOLOX[®] Delta (Figure 4.14) at a dose of $500 \mu\text{m}^3$ per cell caused a significant reduction in cell viability after 6 days (ANOVA; $p < 0.05$). Whereas, the CoCr nano-particles at a dose of $50 \mu\text{m}^3$ per cell had

a significant cytotoxic affect from day 1 (ANOVA; $p < 0.05$), where viability was reduced to 84.3% in the BIOLOX[®] Forte treatment (Figure 4.13B) and to 51.7% in the BIOLOX[®] Delta treatment (Figure 4.14B). There was no significant reduction in cell viability for all the other particle doses tested for both BIOLOX[®] Forte and BIOLOX[®] Delta ceramic model particles. In fact, on occasion the cell viability increased after 1 day with both BIOLOX[®] Forte (all doses) and BIOLOX[®] Delta (0.5 and 500 μm^3 per cell) ceramic model particles, however this difference was not statistically significant. A significant reduction (ANOVA; $p < 0.05$) in cell viability was measured for the positive control (2 $\mu\text{g}\cdot\text{ml}^{-1}$ camptothecin), where after 6 days cell viability reduced by approximately 93% for both the BIOLOX[®] Forte (Figure 4.13) and BIOLOX[®] Delta (Figure 4.14) experiments.

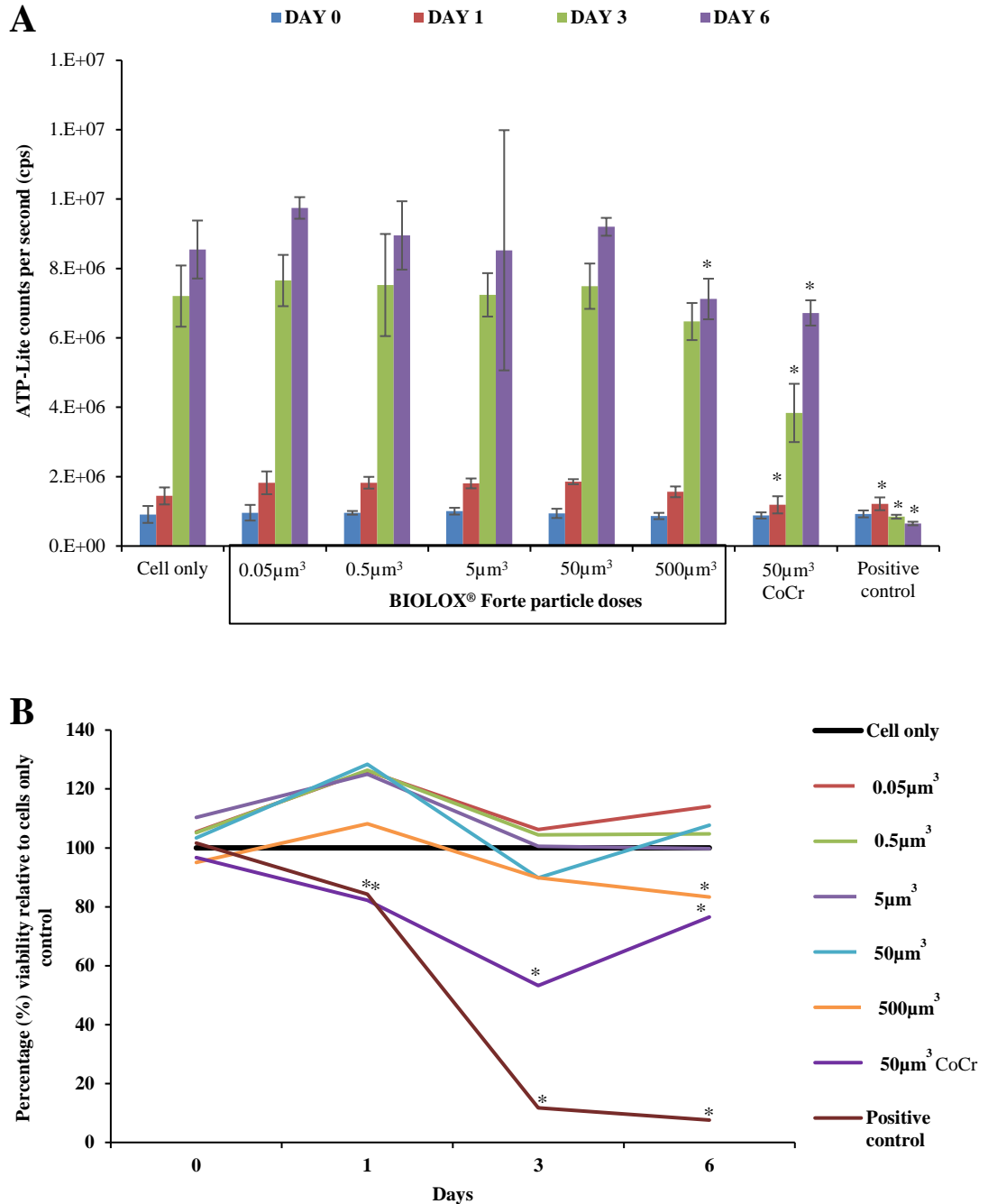


Figure 4.13 –Effects of BIOLOX® Forte ceramic model particles in L929 murine fibroblast cells using the ATP-Lite assay. L929 cells were cultured with bimodal sized micrometre and nanoscale alumina ceramic particles for 6 days. Cell viability was determined using the ATP-Lite assay and presented as (A) mean counts per second and (B) percentage viability relative to the cell only negative control. Positive controls were camptothecin (2 µg.ml⁻¹) and clinically relevant CoCr nano-particles (50µm³ per cell) as a positive particle control. A statistically significant reduction ($p < 0.05$ ANOVA with post hoc Tukey test) in cell viability in comparison to the cell only control, at given time points, is indicated by an asterisk (*). Error bars represent $\pm 95\%$ confidence limits, $n=6$.

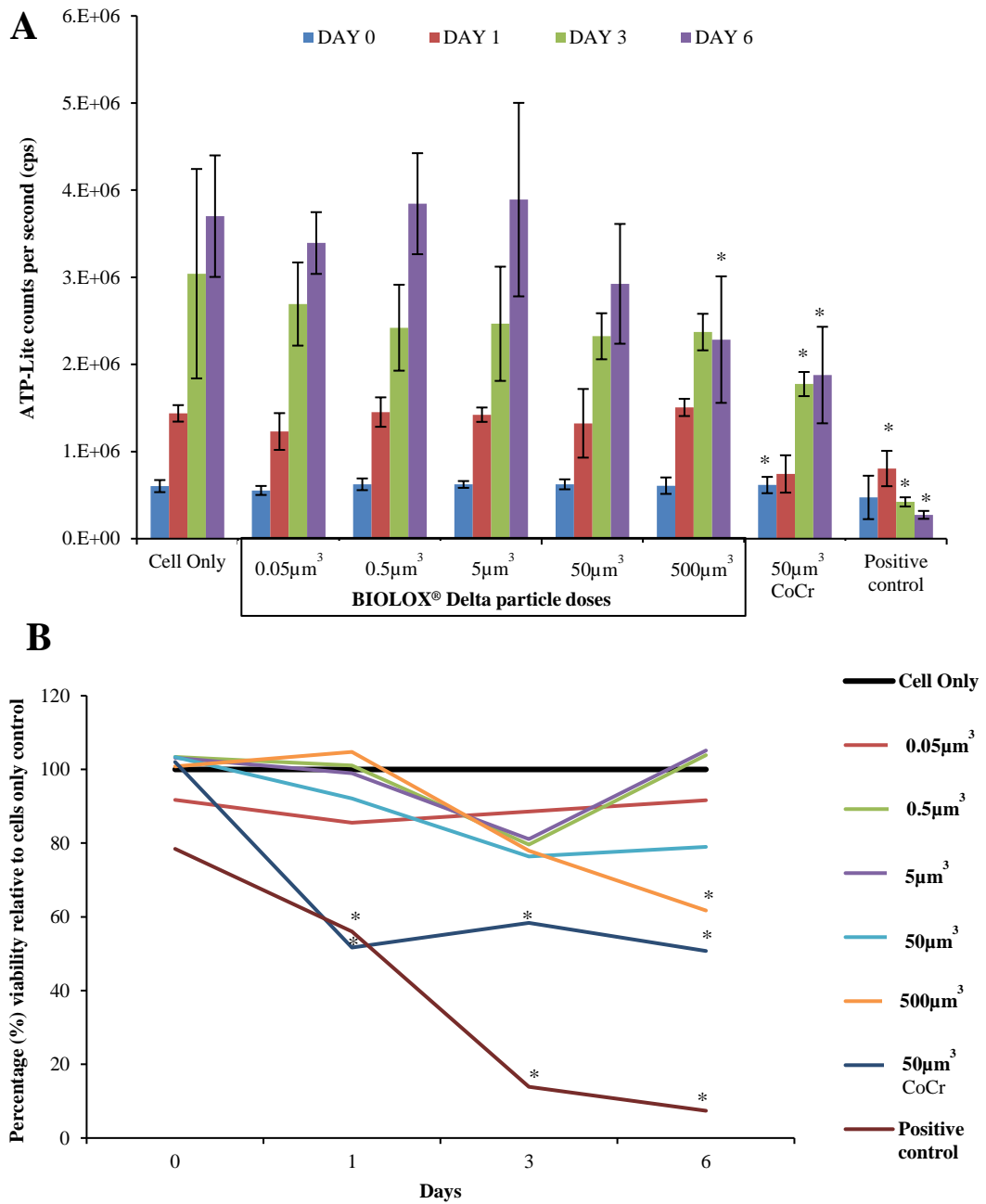


Figure 4.14 - Effects of BIOLOX[®] Delta ceramic model particles in L929 murine fibroblast cells using the ATP-Lite assay. L929 cells were cultured with bimodal sized micrometre and nanoscale composite ceramic particles for 6 days. Cell viability was determined using the ATP-Lite assay and presented as (A) mean counts per second and (B) percentage viability relative to the cell only negative control. Positive controls were camptothecin (2 $\mu\text{g}\cdot\text{ml}^{-1}$) and clinically relevant CoCr nano-particles (50 μm^3 per cell) as positive particle control. A statistically significant reduction ($p < 0.05$ ANOVA with post hoc Tukey test) in cell viability in comparison to the cell only control, at given time points, is indicated by an asterisk (*). Error bars represent $\pm 95\%$ confidence limits, $n=6$.

4.4.2.2 The cytotoxic and inflammatory effects of BIOLOX® Delta ceramic model particles in PBMNCs

The aim of this part of the study was to determine the release of TNF- α from PBMNCs in response to the increasing doses (0.05-50 μm^3 per cell) of commercially obtained BIOLOX® Delta ceramic model particles. This assessment was completed using PBMNCs isolated from five different healthy volunteer donors (donor 2, donor 5, donor 7, donor 25 and donor 26) to evaluate the variability in response to the particles and controls.

4.4.2.2.1 TNF- α release from PBMNCs in response to BIOLOX® Delta ceramic model particles

PBMNCs isolated from five donors (donor 2, donor 5, donor 7, donor 25 and donor 26) were seeded at a density of 2×10^4 cells per well ($n=6$) in 96-well plates and cultured in RPMI culture media with increasing doses (0.05, 0.5, 5 & 50 μm^3 per cell) of BIOLOX® Delta ceramic model particles. The negative control was seeded in the same way but with no particles. LPS (20ng.ml⁻¹) was used as the positive control. The cytotoxic and inflammatory effects of the BIOLOX® Delta ceramic model particles were compared with high (50 μm^3 per cell) and low (0.5 μm^3 per cell) doses of BIOLOX® Forte ceramic model particles and high (50 μm^3 per cell) and low (0.5 μm^3 per cell) doses of clinically-relevant CoCr nano-particles (positive particle control). The plates were incubated for 24 hours at 37°C in 5% (v/v) CO₂ in air. The cell viability of the PBMNCs following incubation with the particles and controls was determined using the ATP-Lite assay, and an ELISA was conducted on the culture supernatants to determine the concentration of TNF- α released from the cells after the 24hr culture period. The results of the ATP-Lite assay and ELISA were expressed as average absorbance values and were analysed using one-way ANOVA and Tukey Post hoc analysis.

The cell viability and TNF- α released from PBMNCs after 24 hours incubation with the particles and controls are shown in Figure 4.15 (Donor 2), Figure 4.16 (Donor 5), Figure 4.17 (Donor 7), Figure 4.18 (Donor 25) and Figure 4.19 (Donor 26). None of the particle doses (0.05, 0.5, 5 & 50 μm^3 per cell) had a significant effect on the viability of PBMNCs from any of the donors compared to the cell only negative control. There was no significant increase in the level of TNF- α released for all the donors in response to the BIOLOX® Delta ceramic model particles compared to the cell only negative control, for all the particle volumes tested. The BIOLOX® Forte ceramic model particles at low (0.5 μm^3 per cell) and high (50 μm^3 per cell) doses also did not elicit a significant increase in TNF- α release for all the donors compared to the cell only negative control. In addition, the low dose (0.5 μm^3 per cell) of clinically-relevant CoCr nano-particles showed no significant increase in TNF- α release in any of the donors compared to the cell only negative control. However, the high dose (50 μm^3 per cell) of clinically-relevant CoCr nano-particles caused a significant increase in the levels

of TNF- α for all the donors tested when compared to the cell only negative control (ANOVA; $p < 0.05$). The positive control of 20ng.ml⁻¹ LPS caused significant levels of TNF- α release from PBMNCs from all donors compared to the cell only negative control (ANOVA; $p < 0.05$).

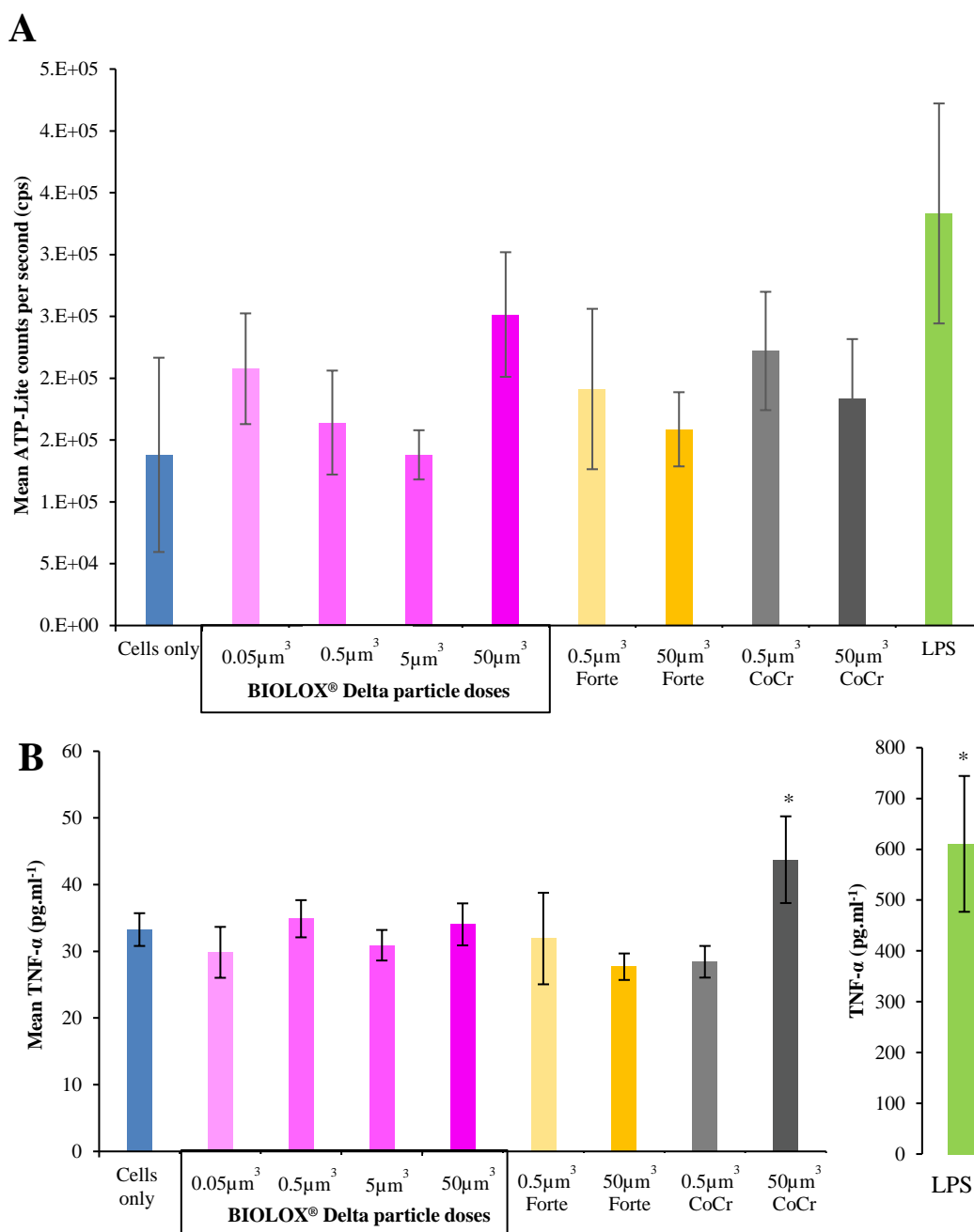


Figure 4.15 – (A) Cell viability and (B) TNF- α release from PBMNCs isolated from Donor 2 in response to BIOLOX® Delta model ceramic particles. PBMNCs were cultured with multimodal sized micrometre and nanoscale composite (BIOLOX® Delta) and alumina (BIOLOX® Forte) ceramic and particles, and clinically-relevant CoCr nano-particles for 24 hours. Cell viability was determined using the ATP-Lite assay and presented as (A) mean counts per second and (B) release of TNF- α was measured using ELISA. The positive control was 200ng.ml⁻¹ lipopolysaccharide (LPS). A statistically significant reduction ($p < 0.05$ ANOVA with post hoc Tukey test) in cell viability in comparison to the cell only control is indicated by an asterisk (*). Error bars represent $\pm 95\%$ confidence limits, $n = 6$.

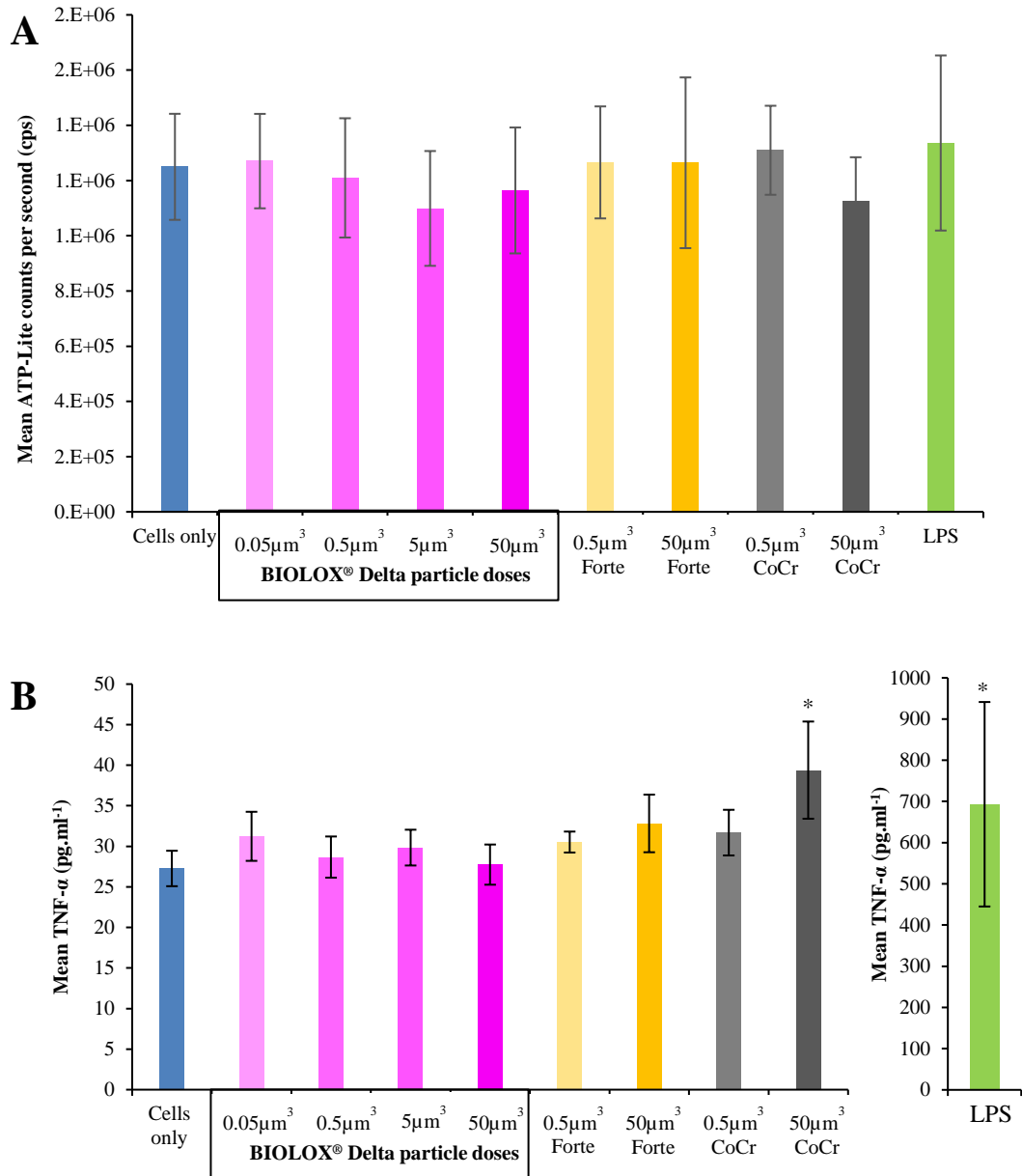


Figure 4.16 - (A) Cell viability and (B) TNF- α release from PBMCs isolated from Donor 5 in response to BIOLOX[®] Delta model ceramic particles. PBMCs were cultured with multimodal sized micrometre and nanoscale composite (BIOLOX[®] Delta) and alumina (BIOLOX[®] Forte) ceramic and particles, and clinically-relevant CoCr nano-particles for 24 hours. Cell viability was determined using the ATP-Lite assay and presented as (A) mean counts per second and (B) release of TNF- α was measured using ELISA. The positive control was 200ng.ml⁻¹ lipopolysaccharide (LPS). A statistically significant reduction ($p < 0.05$ ANOVA with post hoc Tukey test) in cell viability in comparison to the cell only control is indicated by an asterisk (*). Error bars represent $\pm 95\%$ confidence limits, $n=6$.

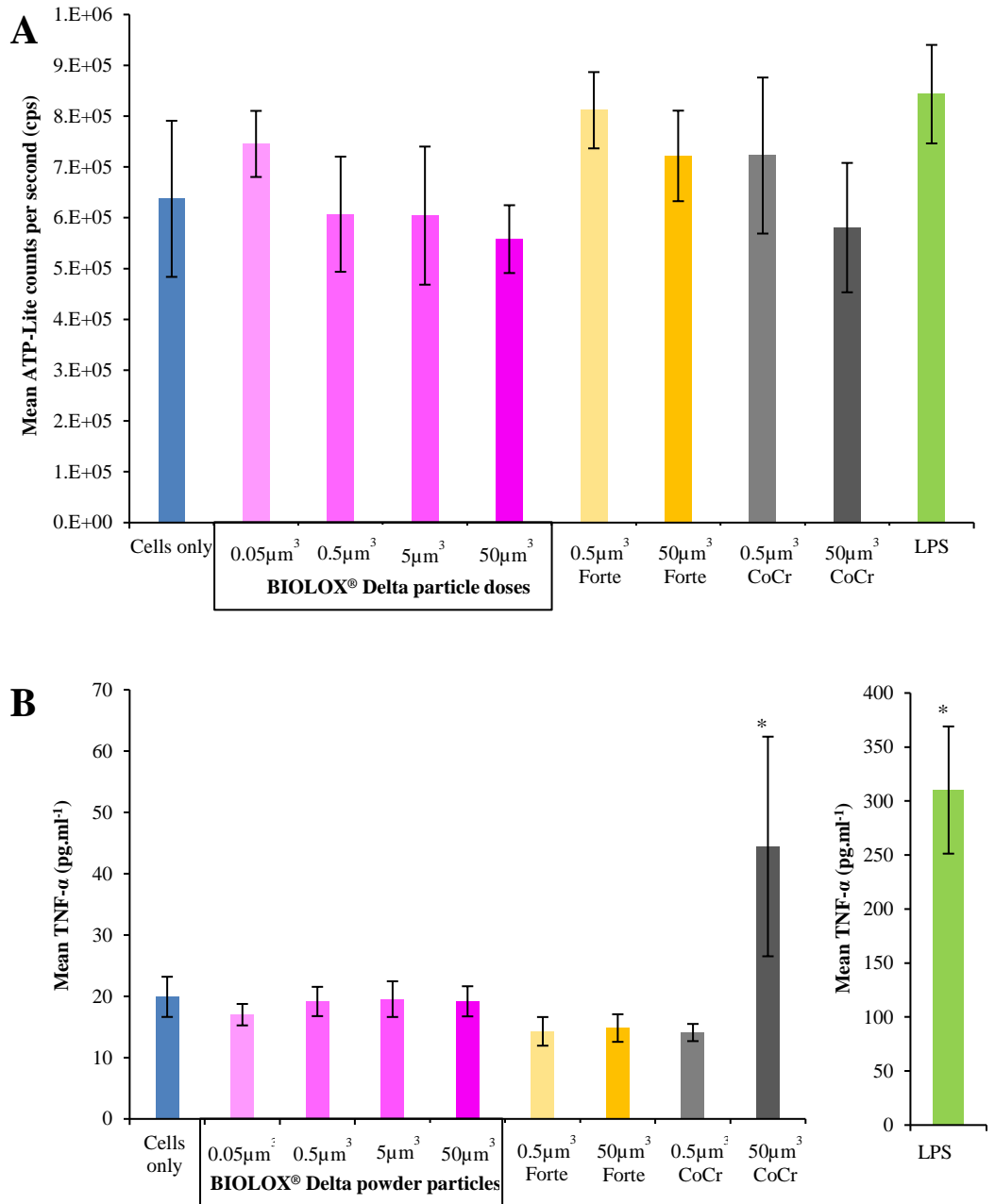


Figure 4.17 - (A) Cell viability and (B) TNF- α release from PBMNCs isolated from Donor 7 in response to BIOLOX[®] Delta model ceramic particles. PBMNCs were cultured with multimodal sized micrometre and nanoscale composite (BIOLOX[®] Delta) and alumina (BIOLOX[®] Forte) ceramic and particles, and clinically-relevant CoCr nano-particles for 24 hours. Cell viability was determined using the ATP-Lite assay and presented as (A) mean counts per second and (B) release of TNF- α was measured using ELISA. The positive control was 200ng.ml⁻¹ lipopolysaccharide (LPS). A statistically significant reduction ($p < 0.05$ ANOVA with post hoc Tukey test) in cell viability in comparison to the cell only control is indicated by an asterisk (*). Error bars represent $\pm 95\%$ confidence limits, $n = 6$.

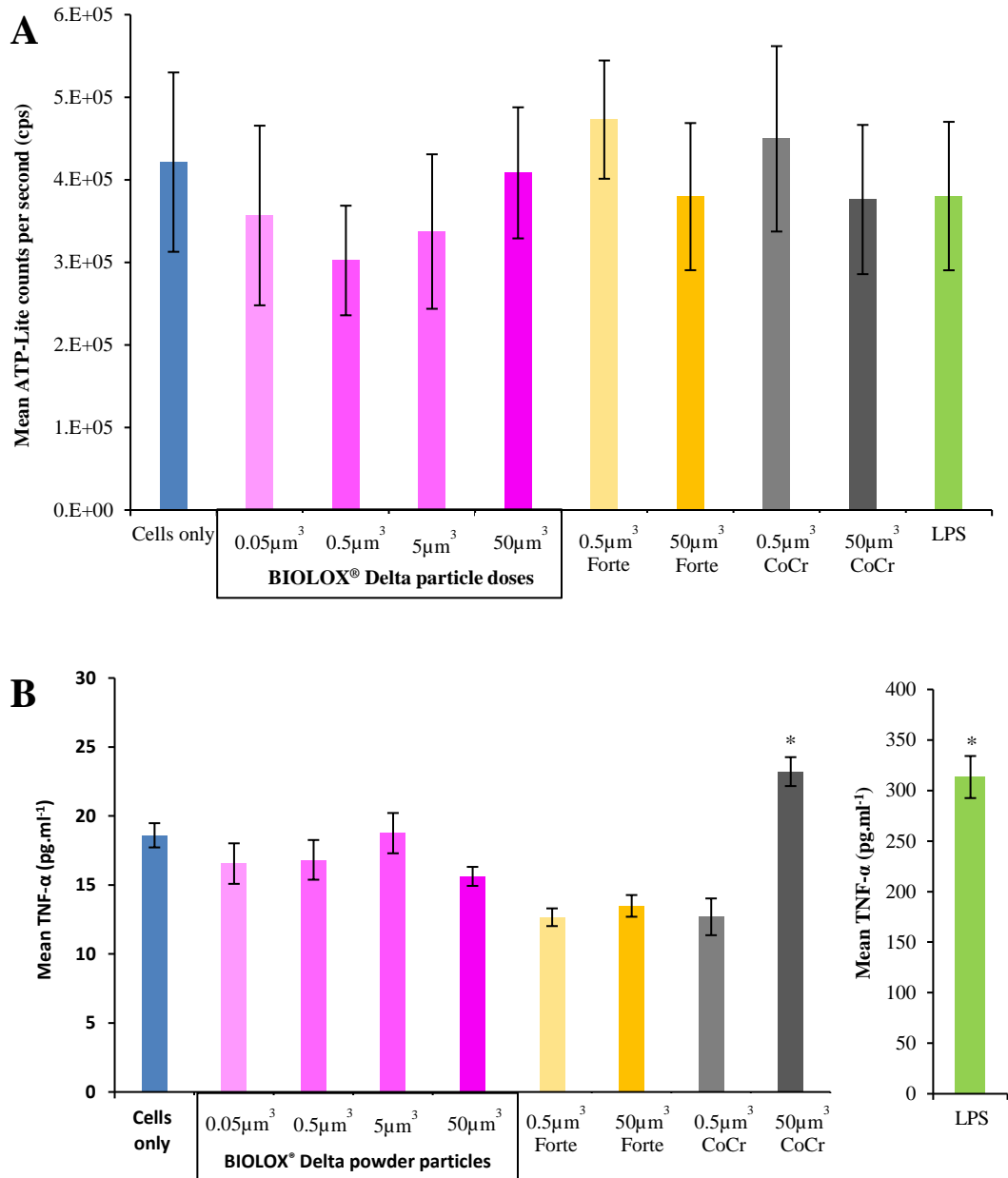


Figure 4.18 - (A) Cell viability and (B) TNF- α release from PBMNCs isolated from Donor 25 in response to BIOLOX[®] Delta model ceramic particles. PBMNCs were cultured with multimodal sized micrometre and nanoscale composite (BIOLOX[®] Delta) and alumina (BIOLOX[®] Forte) ceramic and particles, and clinically-relevant CoCr nano-particles for 24 hours. Cell viability was determined using the ATP-Lite assay and presented as (A) mean counts per second and (B) release of TNF- α was measured using ELISA. The positive control was 200ng.ml⁻¹ lipopolysaccharide (LPS). A statistically significant reduction ($p < 0.05$ ANOVA with post hoc Tukey test) in cell viability in comparison to the cell only control is indicated by an asterisk (*). Error bars represent $\pm 95\%$ confidence limits, $n = 6$.

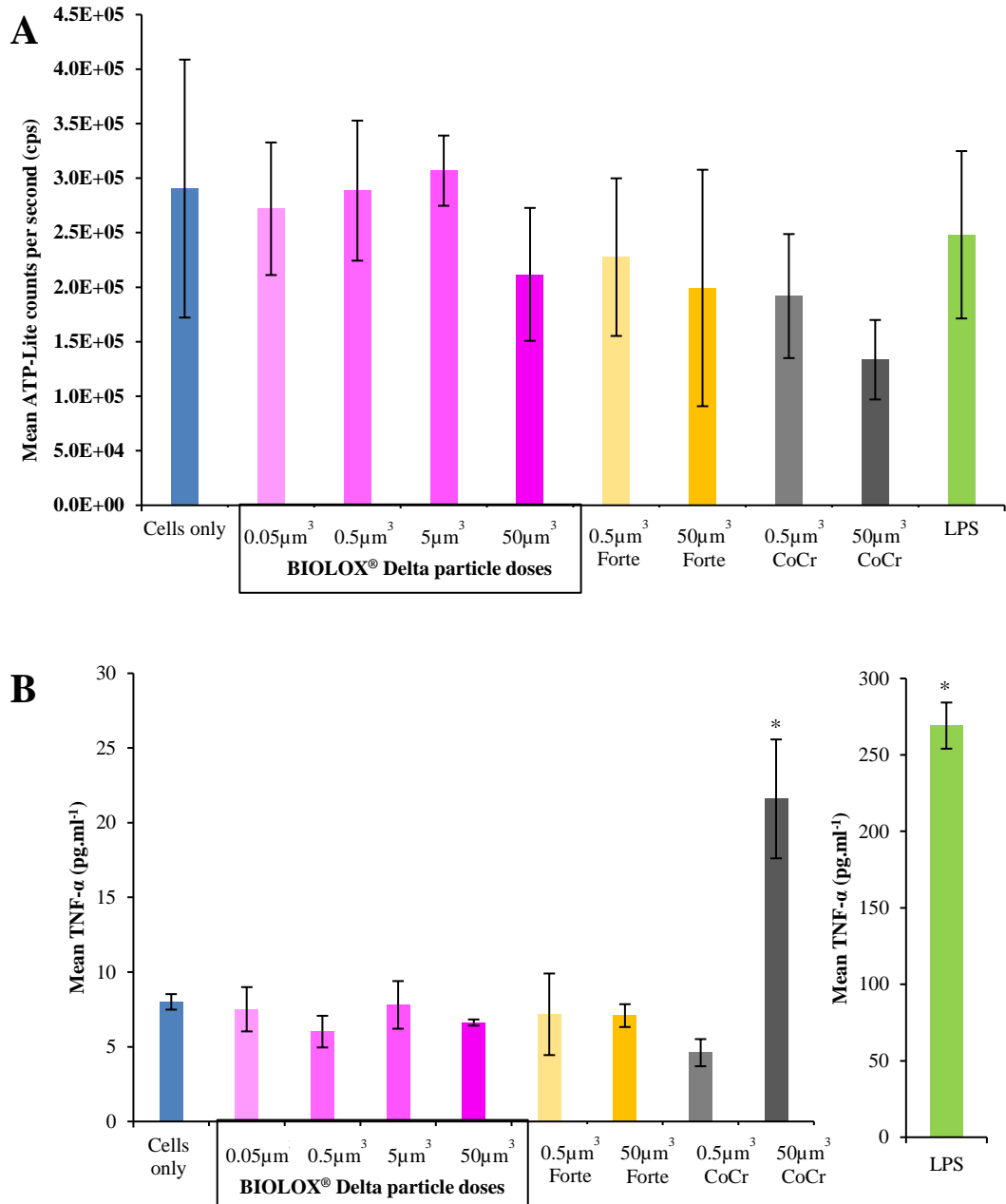


Figure 4.19 - (A) Cell viability and (B) TNF- α release from PBMCs isolated from Donor 26 in response to BIOLOX[®] Delta model ceramic particles. PBMCs were cultured with multimodal sized micrometre and nanoscale composite (BIOLOX[®] Delta) and alumina (BIOLOX[®] Forte) ceramic and particles, and clinically-relevant CoCr nano-particles for 24 hours. Cell viability was determined using the ATP-Lite assay and presented as (A) mean counts per second and (B) release of TNF- α was measured using ELISA. The positive control was 200ng.ml⁻¹ lipopolysaccharide (LPS). A statistically significant reduction ($p < 0.05$ ANOVA with post hoc Tukey test) in cell viability in comparison to the cell only control is indicated by an asterisk (*). Error bars represent $\pm 95\%$ confidence limits, $n = 6$.

4.4.2.2.2 Inter-donor and intra-donor variability in TNF- α production by PBMNCs in response to CoCr nano-particles and LPS

The production of TNF- α in response to BIOLOX[®] Delta ceramic model particles was measured and compared to clinically-relevant CoCr nano-particles and LPS (positive control). Despite the inherent donor variability in inflammatory response, the BIOLOX[®] Delta ceramic model particles consistently failed to stimulate a statistically significant inflammatory response compared to the cell only negative control, in terms of TNF- α production by PBMNCs from all donors for all the particle volumes tested. However, LPS (positive control) and CoCr nano-particles at a dose of 50 μm^3 per cell resulted in significant levels of TNF- α when compared to the cell only negative control (ANOVA; $p < 0.05$). Hence, the TNF- α data for the cell only negative control, CoCr nano-particles and LPS (positive control) from all the donors was presented as box plots to demonstrate the inter-donor and intra-donor variability in terms of TNF- release from PBMNCs isolated from different donors (Figure 4.20).

In terms of inter-donor variability, donor 2, donor 5 and donor 7 produced higher concentrations of TNF- α compared to donor 25 and donor 26, in the cell only negative control and 50 μm^3 CoCr nano-particles. Donor 2 and donor 5 produced a two-fold increase in TNF- α when stimulated with 20ng.ml⁻¹ of LPS compared to the other donors. Furthermore, donor 7 for the cell only negative control showed the highest level of intra-donor variability relative to all the other donors. All the donors stimulated with 50 μm^3 per cell of CoCr nano-particles showed high levels of intra-donor variability whereby donor 25 showed the least variation in TNF- α production compared to the other donors. Donor 2, donor 5 and donor 7 showed the highest level of intra-donor variation in TNF- α production compared to the other donors.

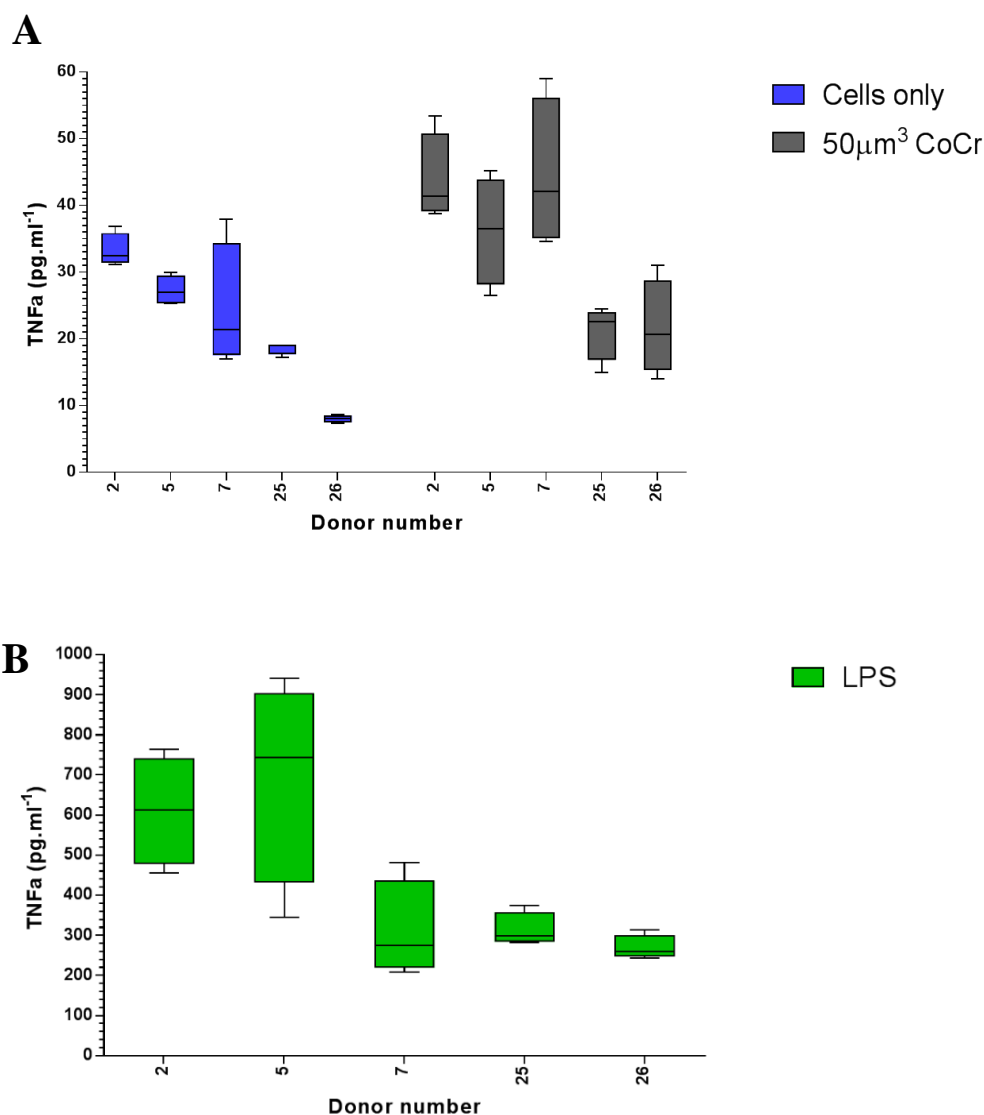


Figure 4.20 – Inter-donor and intra-donor variability in PBMNC responses for (A) cell only control and PBMNCs cultured with 50µm³ per cell of CoCr nano-particles and (B) PBMNCs treated with LPS.

4.4.2.3 The genotoxic effects of BIOLOX[®] Delta ceramic model particles in PBMNCs

The aim of this part of the study was to assess the genotoxicity of increasing doses (0.05-50 µm³ per cell) of commercially obtained BIOLOX[®] Delta ceramic model particles in PBMNCs. This assessment was completed in PBMNCs isolated from five different healthy volunteer donors to evaluate the variability in response to the particles and controls. DNA damage in PBMNCs following a 24hr incubation period with the particles and controls was determined using the comet assay (protocol described in section 4.3.2.7.3). DNA damage was quantified as the comet tail moment (Figure 4.21), which represents the extent of DNA damage in individual cells and is defined as the product of the percentage of total DNA in the tail and the distance between the centres of the mass of head and tail regions (Equation 5).

Equation 5

$$\text{Tail moment} = \text{tail length} \times \text{percentage of DNA in tail}$$

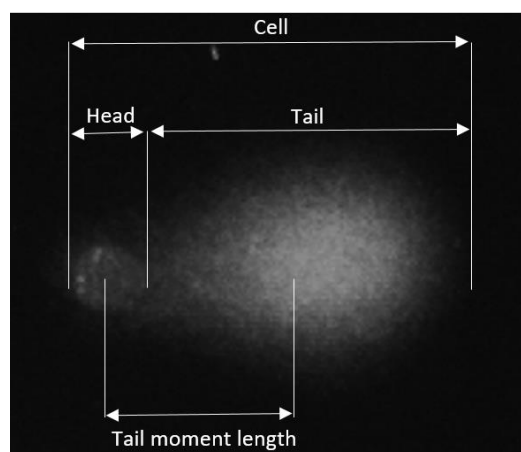
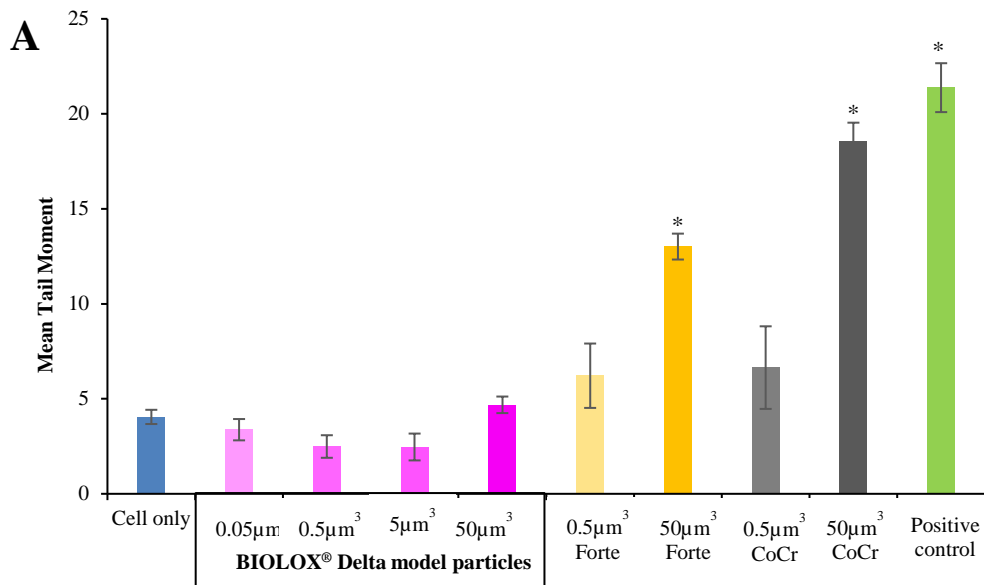


Figure 4.21 – Tail moment length is measured from the centre of the head to the centre of the tail.

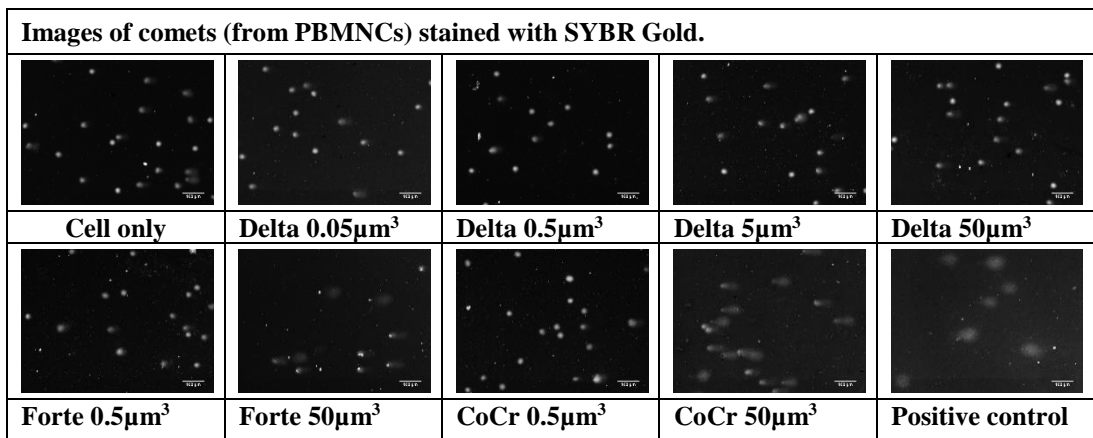
4.4.2.3.1 DNA damage in PBMNCs in response to BIOLOX® Delta ceramic model particles

PBMNCs isolated from five donors (Donor 2, Donor 5, Donor 7, Donor 25 and Donor 26) were seeded at a density of 1×10^5 cells per well ($n=2$) in 48-well plates and cultured in RPMI culture media with increasing doses of (0.05, 0.5, 5 & $50 \mu\text{m}^3$ per cell) of BIOLOX® Delta ceramic model particles. The negative control was seeded in the same way but with no particles. Hydrogen peroxide ($100 \mu\text{M}$) was used as the positive control as it is known to induce single and double strand DNA damage (Driessens et al., 2009). The genotoxic effects of BIOLOX® Delta ceramic model particles were compared with high ($50 \mu\text{m}^3$ per cell) and low ($0.5 \mu\text{m}^3$ per cell) doses of BIOLOX® Forte ceramic model particles and high ($50 \mu\text{m}^3$ per cell) and low ($0.5 \mu\text{m}^3$ per cell) doses of clinically-relevant CoCr nano-particles (positive particle control). The plates were incubated for 24 hours at 37°C in 5% (v/v) CO_2 in air and DNA damage in the PBMNCs following incubation with the particles and controls was determined using the comet assay (protocol described in section 4.3.2.7.3). During the assay protocol, the cells were embedded in agarose gel and underwent single cell electrophoresis. The output of the assay output was images of single cells that were analysed using the Comet IV software. The results were expressed as the comet tail moment and were analysed using one-way ANOVA and Tukey Post hoc analysis. The genotoxic effects of the particles and controls are shown in Figure 4.22 (Donor 2), Figure 4.23 (Donor 5), Figure 4.24 (Donor 7), Figure 4.25 (Donor 25) and Figure 4.26 (Donor 26). High levels of DNA damage are indicated by longer tails in the images and higher values of tail moment relative to the cell only control. Cell nuclei that appear completely circular are indicative of no DNA damage. The BIOLOX® Delta ceramic model particles did not cause DNA damage in PBMNCs from all donors as there was no statistical difference in comet tail moment for all the particle doses when compared to the cell only negative control. This was also evident for the BIOLOX® Forte ceramic model particles at low doses ($0.5 \mu\text{m}^3$ per cell) where there was no significant increase

in tail moment compared to the cell only negative control for all the donors. However, for the BIOLOX[®] Forte ceramic model particles at high doses ($50\mu\text{m}^3$ per cell) there was a significant increase in tail moment compared to the cell only negative control for all donors, except donor 5 (ANOVA; $p<0.05$). PBMNCs from donor 5 demonstrated no significant increase in DNA damage (tail moment) in response to the high dose ($50\mu\text{m}^3$ per cell) of BIOLOX[®] Forte ceramic model particles. Similarly, the high dose ($50\mu\text{m}^3$) of clinically-relevant CoCr nano-particles caused a significant increase in DNA damage as indicated by the high values for tail moment compared to the cell only negative control (ANOVA; $p<0.05$). The low dose ($0.5\mu\text{m}^3$) of clinically-relevant CoCr nano-particles demonstrated no genotoxic effects (no significant increase in tail moment) in PBMNCs from all donors when compared to the cell only negative control. The positive control of hydrogen peroxide caused significant levels of DNA damage in PBMNCs from all donors compared to the cell only negative control (ANOVA; $p<0.05$).

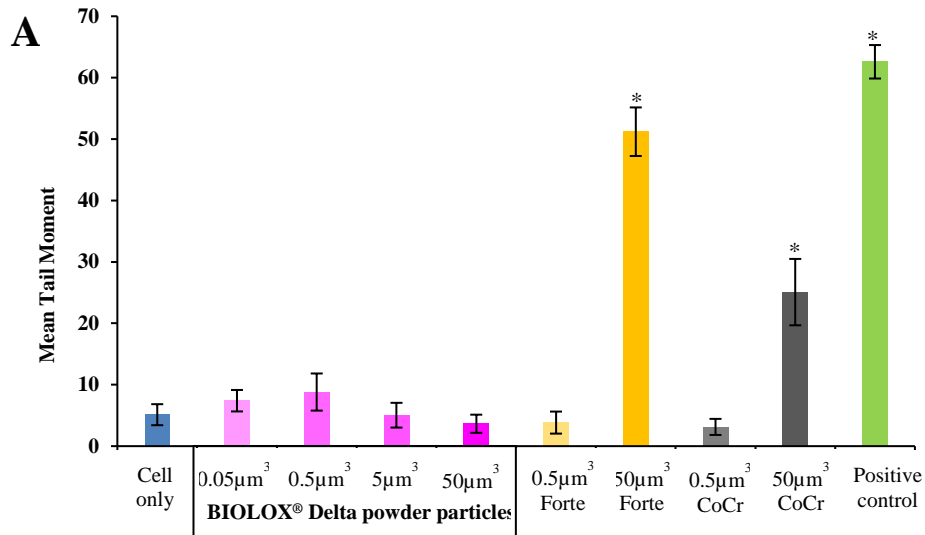


B

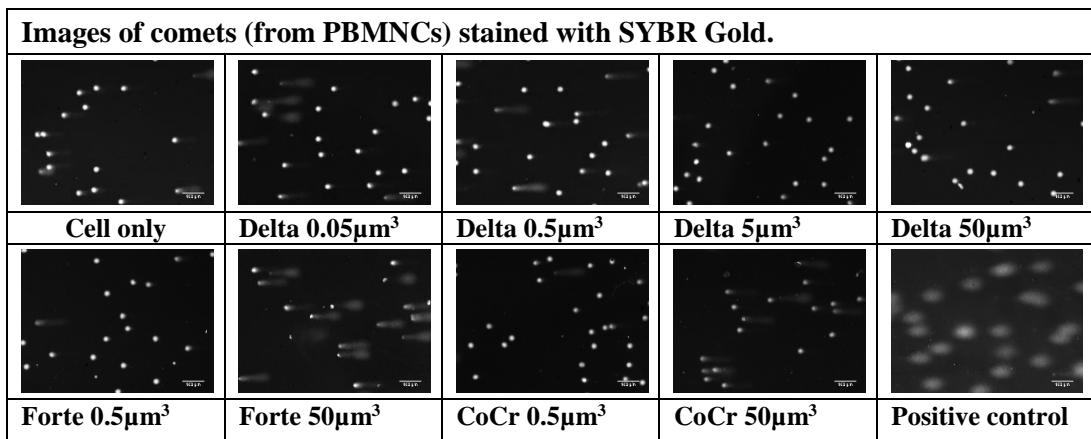


Scale bar 50µm

Figure 4.22 – The genotoxic effects of BIOLOX® Delta ceramic model particles in PBMNCs isolated from Donor 2. PBMNCs were cultured with bimodal size micrometre/sub-micron and nanoscale composite (BIOLOX® Delta) and alumina (BIOLOX® Forte) ceramic model particles, and clinically-relevant CoCr nano-particles for 24 hours. DNA damage was determined using the comet assay and presented as (A) mean tail moment and (B) images of single cells. Cells that appear circular have no DNA damage, whereas nuclei that have tails are indicative of DNA damage. A statistically significant difference ($p < 0.05$ ANOVA with post hoc Tukey test) in tail moment compared to the cells only control is indicated by an asterisk (*). A minimum of 100 cells were scored using the Comet IV software. Error bars represent $\pm 95\%$ confidence limits.

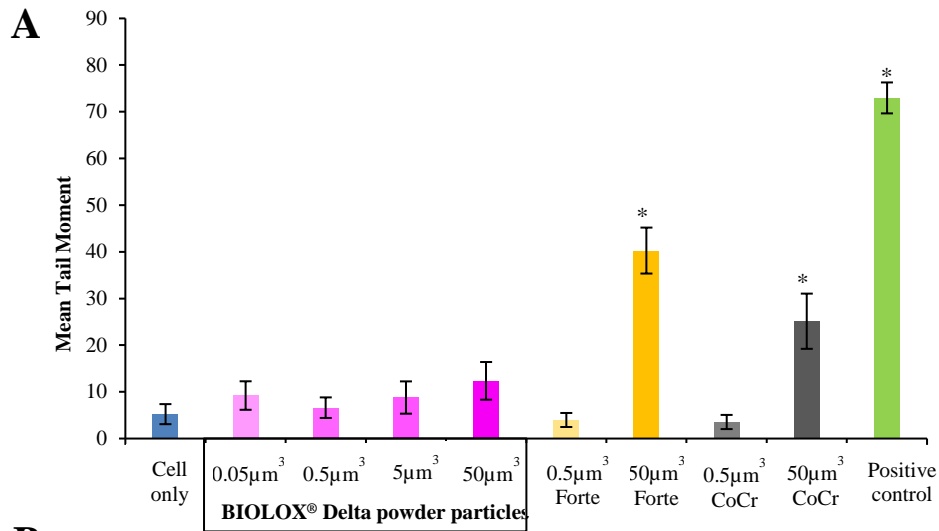


B

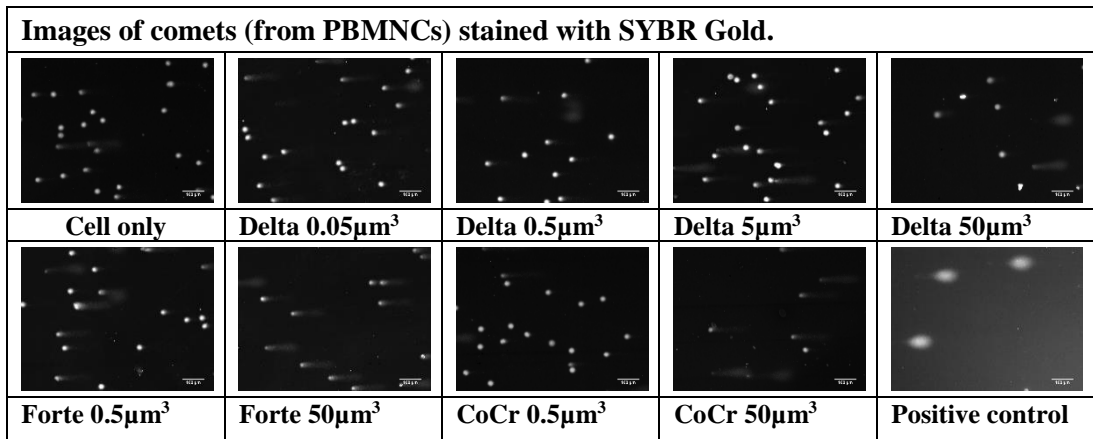


Scale bar 50µm

Figure 4.23 - The genotoxic effects of BIOLOX[®] Delta model ceramic particles in PBMNCs isolated from Donor 5. PBMNCs were cultured with bimodal size micrometre/sub-micron and nanoscale composite (BIOLOX[®] Delta) and alumina (BIOLOX[®] Forte) ceramic model particles, and clinically-relevant CoCr nano-particles for 24 hours. DNA damage was determined using the comet assay and presented as (A) mean tail moment and (B) images of single cells. Cells that appear circular have no DNA damage, whereas nuclei that have tails are indicative of DNA damage. A statistically significant difference ($p < 0.05$ ANOVA with post hoc Tukey test) in tail moment compared to the cells only control is indicated by an asterisk (*). A minimum of 100 cells were scored using the Comet IV software. Error bars represent $\pm 95\%$ confidence limits.

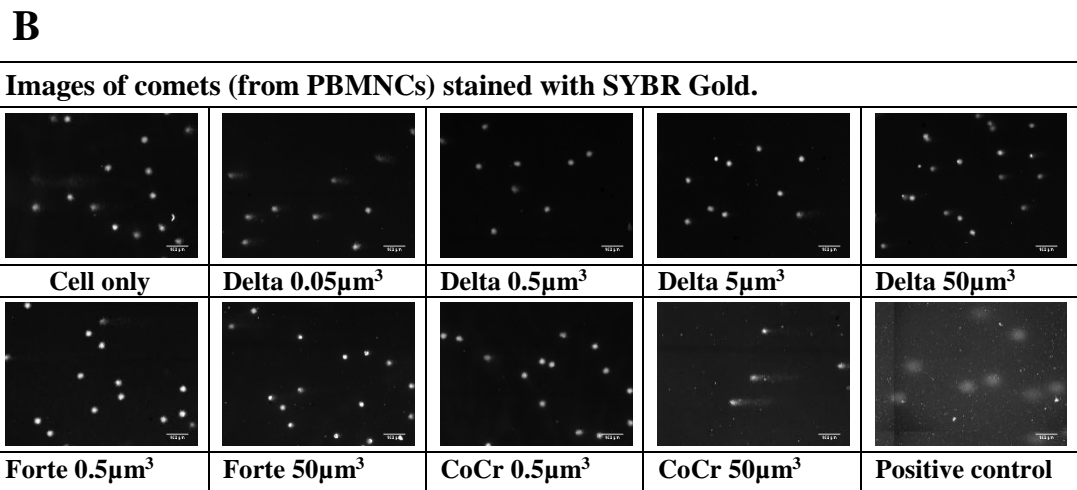
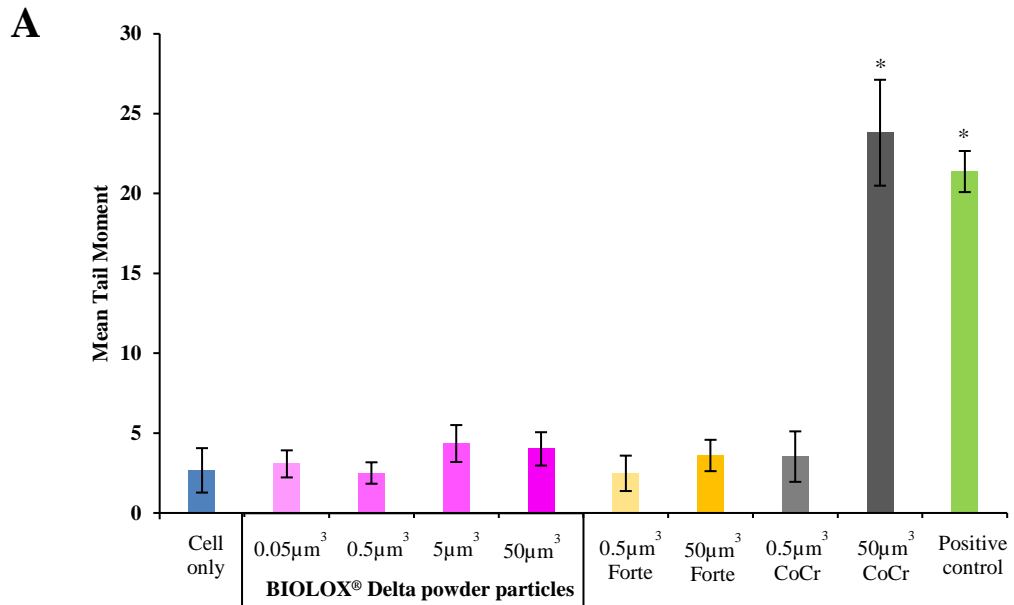


B



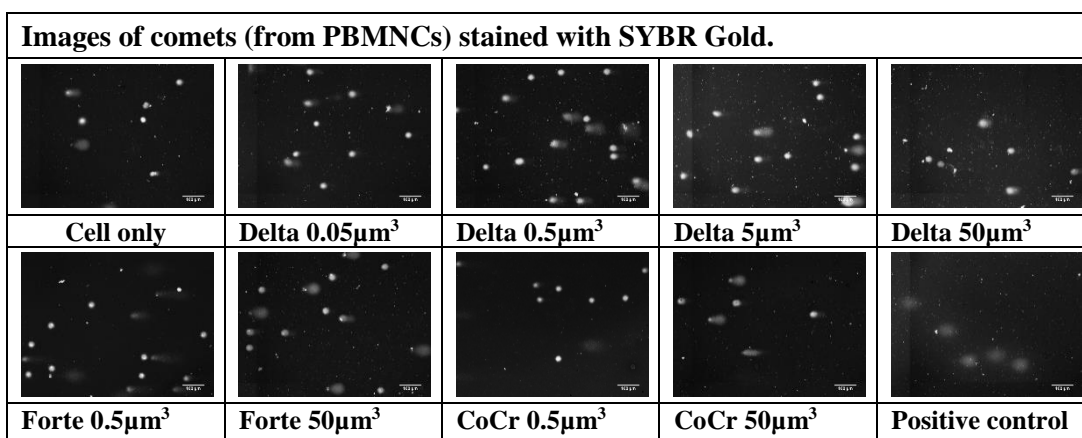
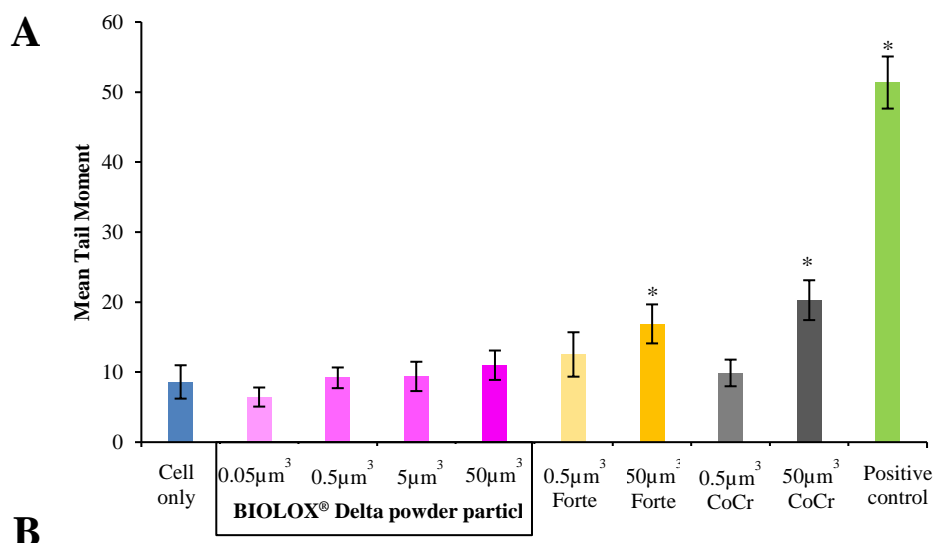
Scale bar 50µm

Figure 4.24 - The genotoxic effects of BIOLOX® Delta model ceramic particles in PBMNCs isolated from Donor 7. PBMNCs were cultured with bimodal size micrometre/sub-micron and nanoscale composite (BIOLOX® Delta) and alumina (BIOLOX® Forte) ceramic model particles, and clinically-relevant CoCr nano-particles for 24 hours. DNA damage was determined using the comet assay and presented as (A) mean tail moment and (B) images of single cells. Cells that appear circular have no DNA damage, whereas nuclei that have tails are indicative of DNA damage. A statistically significant difference ($p < 0.05$ ANOVA with post hoc Tukey test) in tail moment compared to the cells only control is indicated by an asterisk (*). A minimum of 100 cells were scored using the Comet IV software. Error bars represent $\pm 95\%$ confidence limits.



Scale bar 50µm

Figure 4.25 - The genotoxic effects of BIOLOX[®] Delta model ceramic particles in PBMNCs isolated from Donor 25. PBMNCs were cultured with bimodal size micrometre/sub-micron and nanoscale composite (BIOLOX[®] Delta) and alumina (BIOLOX[®] Forte) ceramic model particles, and clinically-relevant CoCr nano-particles for 24 hours. DNA damage was determined using the comet assay and presented as (A) mean tail moment and (B) images of single cells. Cells that appear circular have no DNA damage, whereas nuclei that have tails are indicative of DNA damage. A statistically significant difference ($p < 0.05$ ANOVA with post hoc Tukey test) in tail moment compared to the cells only control is indicated by an asterisk (*). A minimum of 100 cells were scored using the Comet IV software. Error bars represent $\pm 95\%$ confidence limits.



Scale bar 50µm

Figure 4.26 - The genotoxic effects of BIOLOX® Delta model ceramic particles in PBMNCs isolated from Donor 26. PBMNCs were cultured with bimodal size micrometre/sub-micron and nanoscale composite (BIOLOX® Delta) and alumina (BIOLOX® Forte) ceramic model particles, and clinically-relevant CoCr nano-particles for 24 hours. DNA damage was determined using the comet assay and presented as (A) mean tail moment and (B) images of single cells. Cells that appear circular have no DNA damage, whereas nuclei that have tails are indicative of DNA damage. A statistically significant difference ($p < 0.05$ ANOVA with post hoc Tukey test) in tail moment compared to the cells only control is indicated by an asterisk (*). A minimum of 100 cells were scored using the Comet IV software. Error bars represent $\pm 95\%$ confidence limits.

4.4.2.4 Oxidative stress in PBMNCs in response to model ceramic particles

The aim of this part of the study was to assess the levels of oxidative stress induced by increasing doses ($0.05\text{-}50\mu\text{m}^3$ per cell) of commercially obtained BIOLOX[®] Delta ceramic model particles in PBMNCs. This assessment was completed in PBMNCs isolated from five different healthy volunteer donors to evaluate the variability in response to the particles and controls. Oxidative stress was measured by labelling the ROS produced by PBMNCs using a DCFDA probe in the cellular reactive oxygen species detection assay kit (protocol outlined in section 4.3.2.7.4).

4.4.2.4.1 Oxidative stress in PBMNCs in response to BIOLOX[®] Delta ceramic model particles

PBMNCs isolated from five donors (donor 2, donor 5, donor 7, donor 25 and donor 26) were seeded at a density of 2×10^4 cells per well ($n=6$) in clear bottom black 96-well plates and cultured in RPMI culture media with increasing doses (0.05 , 0.5 , 5 & $50\mu\text{m}^3$ per cell) of BIOLOX[®] Delta ceramic model particles. The cell only negative control was seeded in the same way but with no particles. TBHP ($200\mu\text{M}$) was used as the positive control as it mimics ROS activity to oxidise DCFDA to fluorescent DCF and so it is commonly used to evaluate the cellular responses resulting from oxidative stress in cells and tissues (Kucera et al., 2014). The presence of ROS within the cells in response to the BIOLOX[®] Delta ceramic model particles was compared with high ($50\mu\text{m}^3$ per cell) and low ($0.5\mu\text{m}^3$ per cell) doses of BIOLOX[®] Forte ceramic model particles and high ($50\mu\text{m}^3$ per cell) and low ($0.5\mu\text{m}^3$ per cell) doses of clinically-relevant CoCr nano-particles. The plates were incubated for 24 hours at 37°C in 5% (v/v) CO_2 in air. The production of ROS in PBMNCs following incubation with the particles and controls was determined using the cellular ROS detection assay (protocol outlined in section 4.3.2.7.4). The results were expressed as average fluorescence intensity values where higher values of fluorescence intensity was directly proportional to high levels of oxidative stress. The data was analysed using one-way ANOVA and Tukey Post hoc analysis. The cells present within the wells were also imaged to correlate the fluorescence intensity values with the fluorescence emitted from within the cells.

The images captured of the PBMNCs isolated from donor 2 are shown in Figure 4.27 and are representative of all donors. The images depict the fluorescently labelled reactive oxygen species that were present in the PBMNCs isolated from Donor 2 after exposure to 485nm for 1000ms . The cell only, low dose ($0.5\mu\text{m}^3$ per cell) of CoCr nano-particles and all the doses ($0.05\text{-}50\mu\text{m}^3$ per cell) for both BIOLOX[®] Delta and BIOLOX[®] Forte demonstrated less fluorescence relative to the high dose ($50\mu\text{m}^3$ per cell) of CoCr nano-particles and positive control ($200\mu\text{M}$ TBHP). The brighter images of PBMNCs treated with $50\mu\text{m}^3$ per cell of CoCr nano-particles and TBHP were indicative of high levels of oxidative stress.

The production of ROS levels as a function of fluorescence intensity in response to the particles and controls is shown in Figure 4.28 (Donor 2), Figure 4.29 (Donor 5), Figure 4.30 (Donor 7), Figure 4.31 (Donor 25) and Figure 4.32 (Donor 26). High levels of ROS are indicated by higher fluorescence intensity relative to the cell only negative control and are visualised as brighter green fluorescence in the images (Figure 4.27). The BIOLOX[®] Delta ceramic model particles at all doses had no statistically significant effect on the level of oxidative stress (fluorescence intensity) in PBMNCs from all donors when compared to the cell only negative control. This was also evident for the BIOLOX[®] Forte ceramic model particles at low (0.5 μm^3 per cell) and high (50 μm^3 per cell) doses, where there was no significant increase in ROS production (fluorescence intensity) compared to the cell only negative control for all the donors. Similarly, the low dose (0.5 μm^3 per cell) of clinically-relevant CoCr nano-particles showed no significant increase in the level of ROS production (fluorescence intensity) when compared to the cell only negative control, except in donor 2 and donor 5, which showed significantly higher levels of oxidative stress compared with cells only negative control (ANOVA; $p < 0.05$). However, the high dose (50 μm^3 per cell) of clinically-relevant CoCr nano-particles caused a significant increase in the levels of ROS production in PBMNCs in all donors as indicated by the high levels of fluorescence intensity compared to the cells only negative control (ANOVA; $p < 0.05$). The positive control of TBHP (200 μM) caused significant levels of ROS production (fluorescence intensity) in PBMNCs from all donors compared to the cell only negative control (ANOVA; $p < 0.05$).

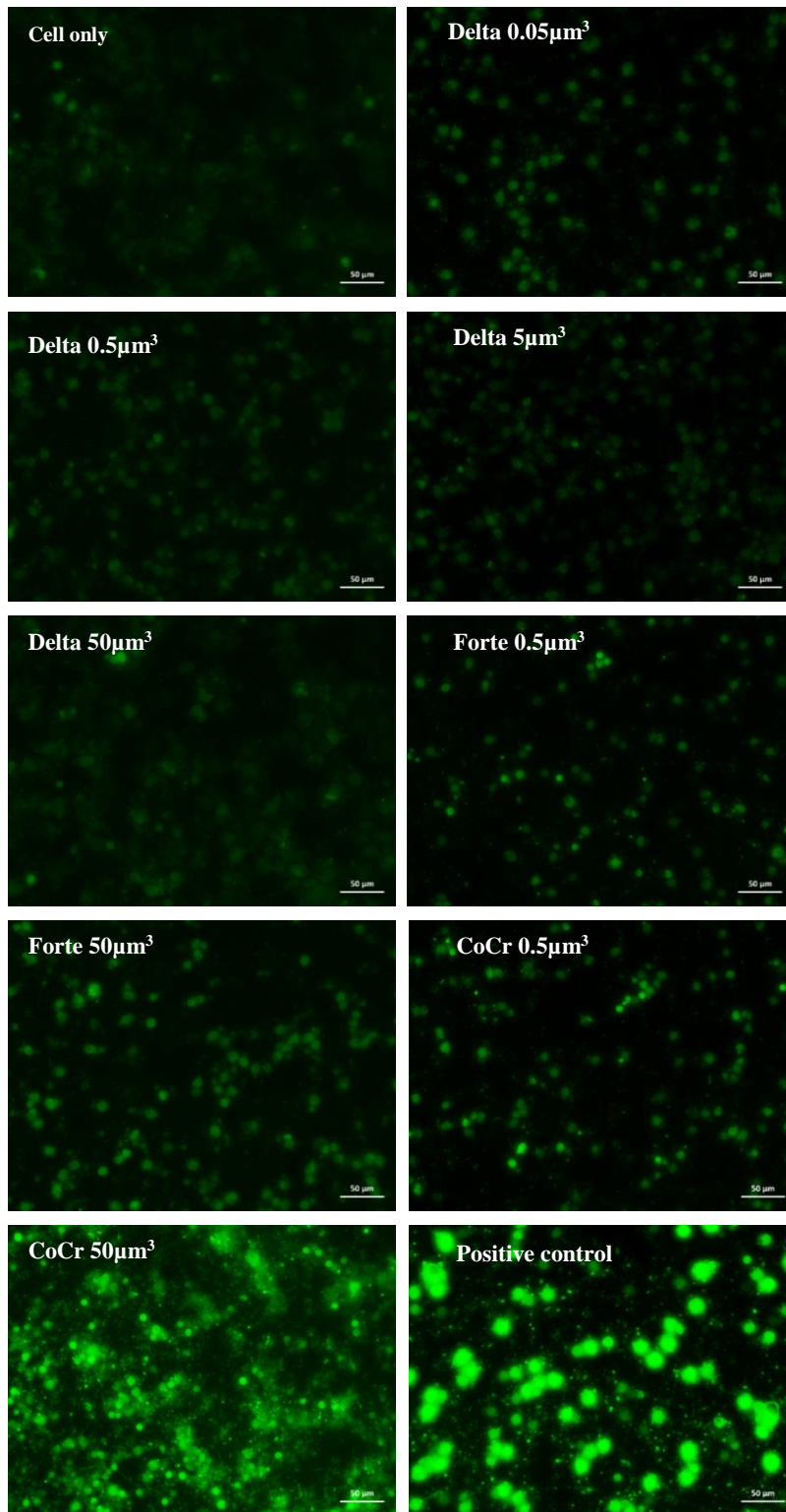


Figure 4.27 – Visualisation of the presence of ROS in PBMCs (donor 2) cultured with BIOLOX[®] Delta ceramic model particles. PBMCs were cultured with bimodal sized micrometre and nanoscale composite (BIOLOX[®] Delta) and alumina (BIOLOX[®] Forte) ceramic model particles, and clinically-relevant CoCr nano-particles for 24 hours. Oxidative stress was determined using DCFDA probe to detect the presence of ROS, which is visualised as the green fluorescence. The higher the intensity of the green fluorescence, the higher the levels of ROS produced by the PBMCs. TBHP (200µM) was used as the positive control. Size-bar 50µm in all images.

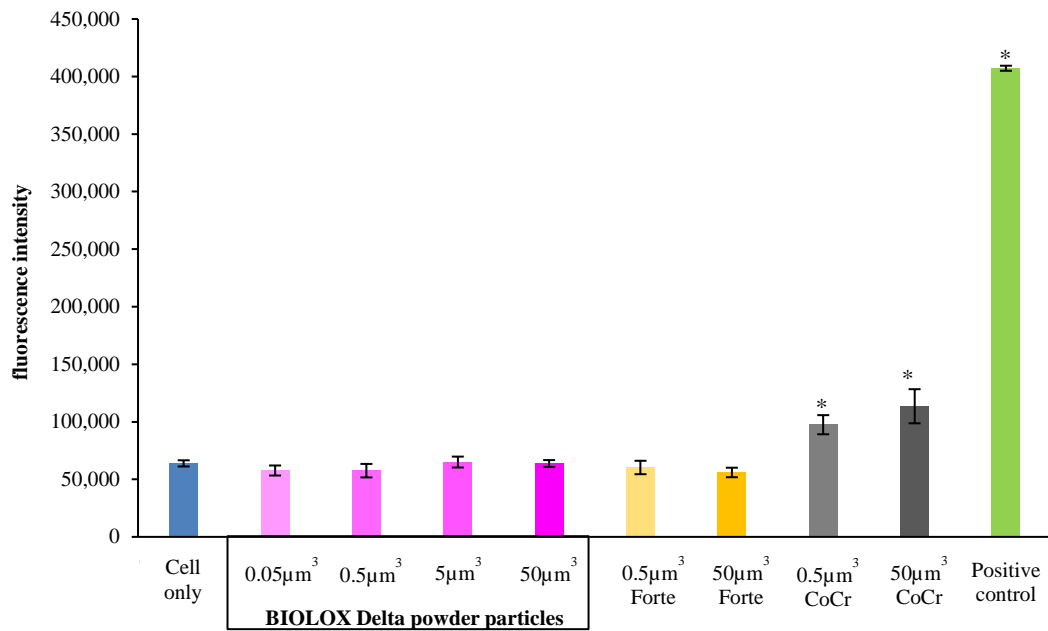


Figure 4.28 – Oxidative stress in PBMNCs isolated from Donor 2 in response to BIOLOX[®] Delta ceramic model particles. PBMNCs were cultured with bimodal sized micrometre and nanoscale composite (BIOLOX[®] Delta) and alumina (BIOLOX[®] Forte) ceramic model particles, and clinically-relevant CoCr nano-particles for 24 hours. Oxidative stress was determined using a DCFDA probe to detect the presence of ROS, which is presented as fluorescent intensity. TBHP (200µM) was used as the positive control. A statistically significant difference ($p < 0.05$ ANOVA) in fluorescence intensity compared to the cell only control is indicated by an asterisk (*). Error bars represent $\pm 95\%$ confidence limits ($n=6$).

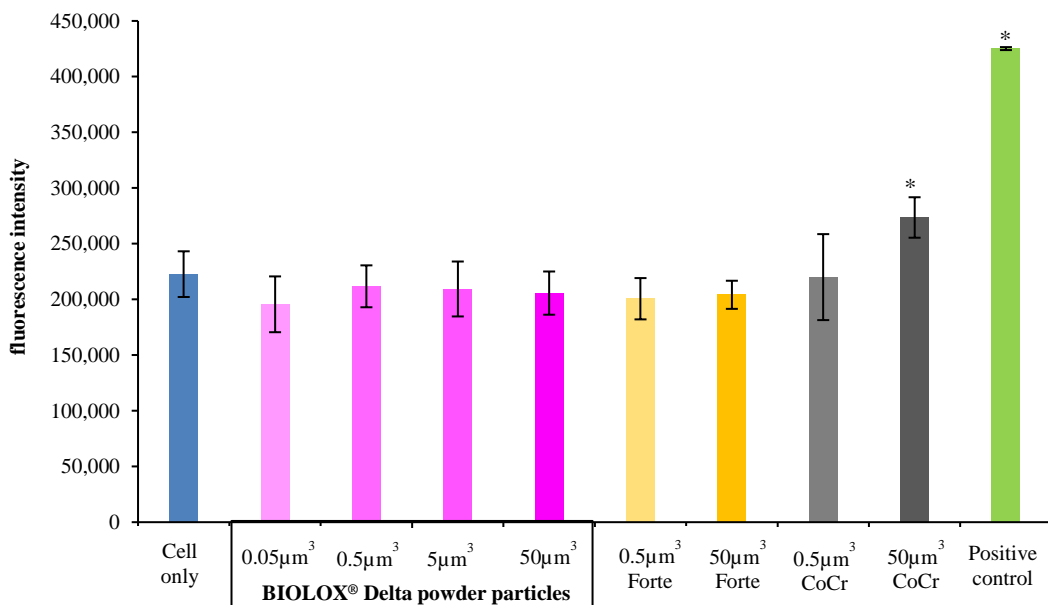


Figure 4.29 – Oxidative stress in PBMNCs isolated from Donor 5 in response to BIOLOX[®] Delta model ceramic particles. PBMNCs were cultured with bimodal sized micrometre and nanoscale composite (BIOLOX[®] Delta) and alumina (BIOLOX[®] Forte) ceramic model particles, and clinically-relevant CoCr nano-particles for 24 hours. Oxidative stress was determined using a DCFDA probe to detect the presence of ROS, which is presented as fluorescent intensity. TBHP (200µM) was used as the positive control. A statistically significant difference ($p < 0.05$ ANOVA) in fluorescence intensity compared to the cell only control is indicated by an asterisk (*). Error bars represent $\pm 95\%$ confidence limits ($n=6$).

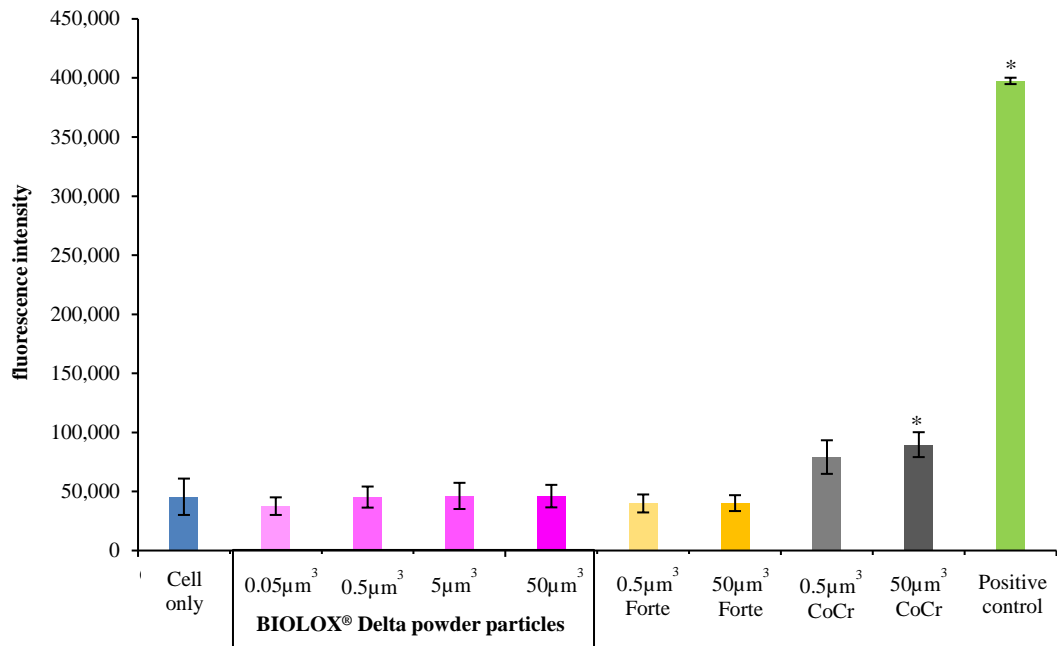


Figure 4.30 – Oxidative stress in PBMCs isolated from Donor 7 in response to BIOLOX Delta model ceramic particles. PBMCs were cultured with bimodal sized micrometre and nanoscale composite (BIOLOX[®] Delta) and alumina (BIOLOX[®] Forte) ceramic model particles, and clinically-relevant CoCr nano-particles for 24 hours. Oxidative stress was determined using a DCFDA probe to detect the presence of ROS, which is presented as fluorescent intensity. TBHP (200 μM) was used as the positive control. A statistically significant difference ($p < 0.05$ ANOVA) in fluorescence intensity compared to the cell only control is indicated by an asterisk (*). Error bars represent $\pm 95\%$ confidence limits ($n=6$).

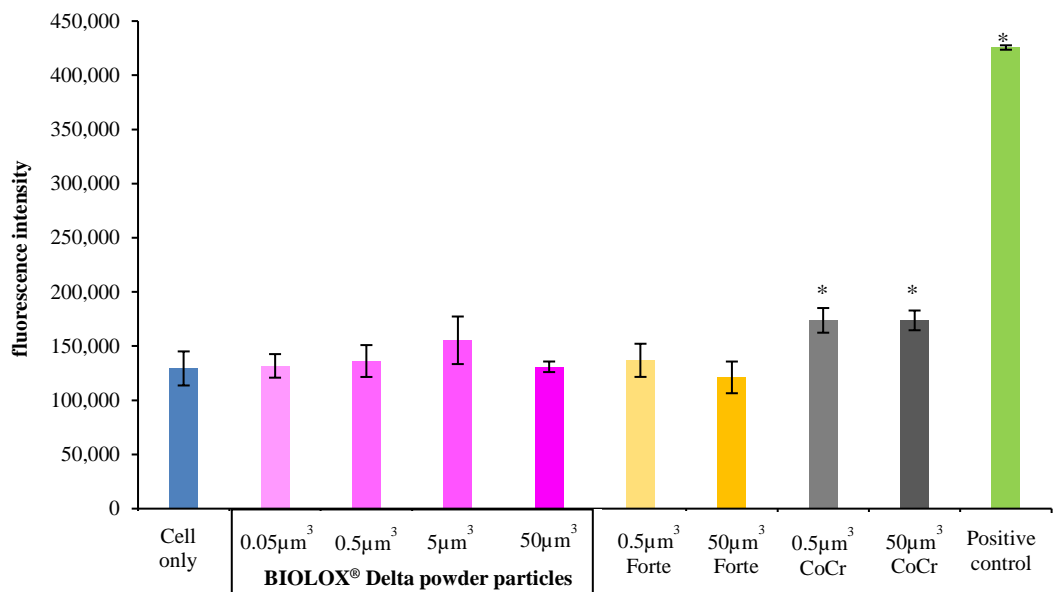


Figure 4.31 - Oxidative stress in PBMCs isolated from Donor 25 in response to BIOLOX[®] Delta model ceramic particles. PBMCs were cultured with bimodal sized micrometre and nanoscale composite (BIOLOX[®] Delta) and alumina (BIOLOX[®] Forte) ceramic model particles, and clinically-relevant CoCr nano-particles for 24 hours. Oxidative stress was determined using a DCFDA probe to detect the presence of ROS, which is presented as fluorescent intensity. TBHP (200 μM) was used as the positive control. A statistically significant difference ($p < 0.05$ ANOVA) in fluorescence intensity compared to the cell only control is indicated by an asterisk (*). Error bars represent $\pm 95\%$ confidence limits ($n=6$).

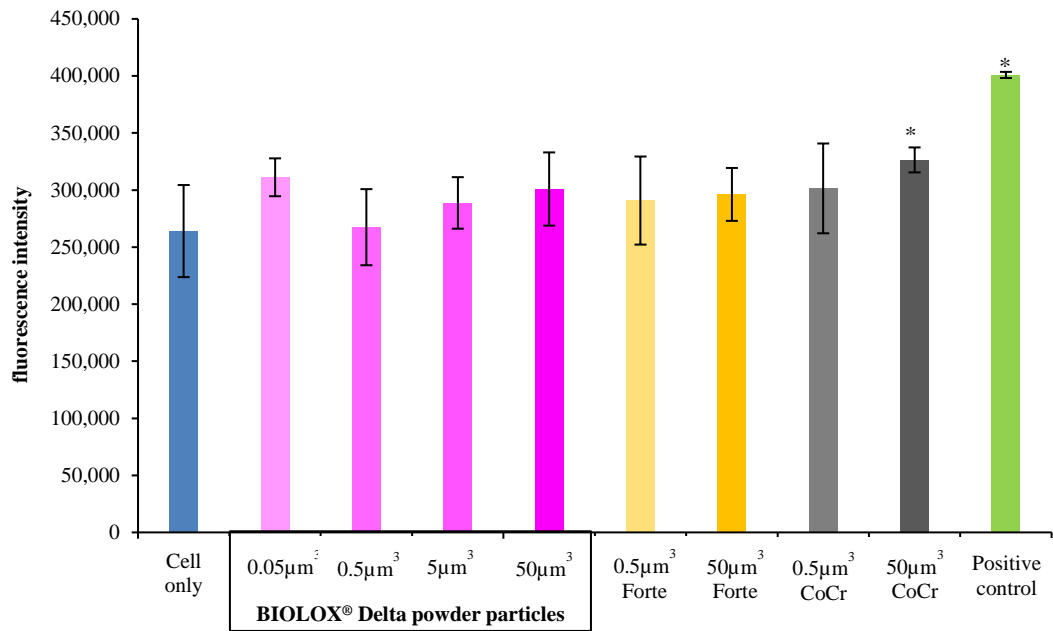


Figure 4.32 - Oxidative stress in PBMCs isolated from Donor 26 in response to BIOLOX® Delta model ceramic particles. PBMCs were cultured with bimodal sized micrometre and nanoscale composite (BIOLOX® Delta) and alumina (BIOLOX® Forte) ceramic model particles, and clinically-relevant CoCr nano-particles for 24 hours. Oxidative stress was determined using a DCFDA probe to detect the presence of ROS, which is presented as fluorescent intensity. TBHP (200µM) was used as the positive control. A statistically significant difference ($p < 0.05$ ANOVA) in fluorescence intensity compared to the cell only control is indicated by an asterisk (*). Error bars represent $\pm 95\%$ confidence limits ($n=6$).

4.4.3 Biological impact of clinically-relevant ceramic particles

The biological response to clinically-relevant BIOLOX[®] Delta ceramic wear particles (generated using the Leeds II hip simulator) was assessed using the same tool kit of assays. The biological impact of these composite BIOLOX[®] Delta ceramic wear particles was compared with clinically-relevant BIOLOX[®] Forte ceramic wear particles, which were also generated using a hip simulator and clinically-relevant CoCr nano-particles generated using a six station PoP wear rig. Stainless-steel wear particles generated using the six-station PoP wear rig were also introduced as a particle control in these experiments as the water lubricant used to generate the clinically-relevant ceramic wear particles during wear simulation was contaminated by stainless-steel wear particles (section 3.4.2.2). This was necessary as the particle suspension yielded from the hip simulator was a mixed population of ceramic wear particles and stainless-steel wear particles.

4.4.3.1 The cytotoxic effects of clinically-relevant BIOLOX[®] Delta ceramic wear particles in L929 fibroblast cells

L929 murine fibroblast cells were seeded at a density of 1×10^4 cells per well ($n=6$) in 96-well plates and cultured in DMEM culture media with increasing doses of clinically-relevant BIOLOX[®] Delta ceramic wear particles at low to high volumes ranging from $0.05\text{-}500\mu\text{m}^3$ per cell. The negative cell only control was seeded in the same way but with no particles. The cytotoxic effects of the ceramic particles were compared with clinically-relevant CoCr nano-particles at a dose of $50\mu\text{m}^3$ per cell, which was used as the positive particle control. Camptothecin, at a final concentration of $2\ \mu\text{g}\cdot\text{ml}^{-1}$ was included as the positive control to induce apoptosis. The plates were incubated for 0, 1, 3 and 6 days at 37°C in 5% (v/v) CO_2 in air. The results of the ATP-Lite assay were expressed as average absorbance values (counts per second) and as a percentage relative to the cell only negative control. The data was analysed using a one-way ANOVA and Tukey Post hoc analysis.

The cytotoxic effect of increasing doses of clinically-relevant BIOLOX[®] Delta ceramic wear particles on L929 fibroblast cells are shown in Figure 4.33. The average absorbance values, which are indicative of cellular metabolic activity and thus viability, for the cell only negative controls continued to increase over the course of the 6-day culture period as demonstrated in Figure 4.33A. The average absorbance values from day 0 to day 6 for the cells only negative control increased by approximately 8-fold, which was indicative of cell proliferation. The cell growth was adversely affected in the presence of high volumes of clinically-relevant BIOLOX[®] Delta ceramic wear particles (Figure 4.33B), where at a dose $500\mu\text{m}^3$ per cell caused a statistical significant reduction in cell viability after day 1 (ANOVA; $p<0.05$). The clinically-relevant CoCr nano-particles at a dose of $50\mu\text{m}^3$ per cell also had a statistical significant cytotoxic affect from day 1, where the cell viability was reduced to 71.3%

compared to the cell only negative control (ANOVA; $p < 0.05$). Furthermore, the clinically-relevant BIOLOX[®] Delta ceramic wear particles at a dose of $50\mu\text{m}^3$ per cell caused a statistical significant reduction in cell viability after 3 days Figure 4.33B, when compared to the cell only negative control (ANOVA; $p < 0.05$). However, after 6 days the cells cultured with $50\mu\text{m}^3$ per cell of clinically-relevant BIOLOX[®] Delta ceramic wear particles recovered after 6 days showing no statistical significant difference in cell viability compared to the cell only negative control. The highest dose ($500\mu\text{m}^3$ per cell) of clinically-relevant BIOLOX[®] Delta ceramic wear particles caused a significant reduction in cell viability after 6 days, when compared to the cell only negative control (ANOVA; $p < 0.05$). The CoCr nano-particles significantly reduced the viability of the L929 cells by approximately 54% after 6 days, when compared to the cell only negative control (ANOVA; $p < 0.05$). There was no significant reduction in the cell viability for all the other particle doses (0.05 , 0.5 , and $5\mu\text{m}^3$ per cell) tested for clinically-relevant BIOLOX[®] Delta ceramic wear particles. A significant reduction (ANOVA; $p < 0.05$) in cell viability was measured for the positive control ($2\mu\text{g}\cdot\text{ml}^{-1}$ camptothecin) after one day in culture, and after 6 days cell viability reduced by approximately 96%.

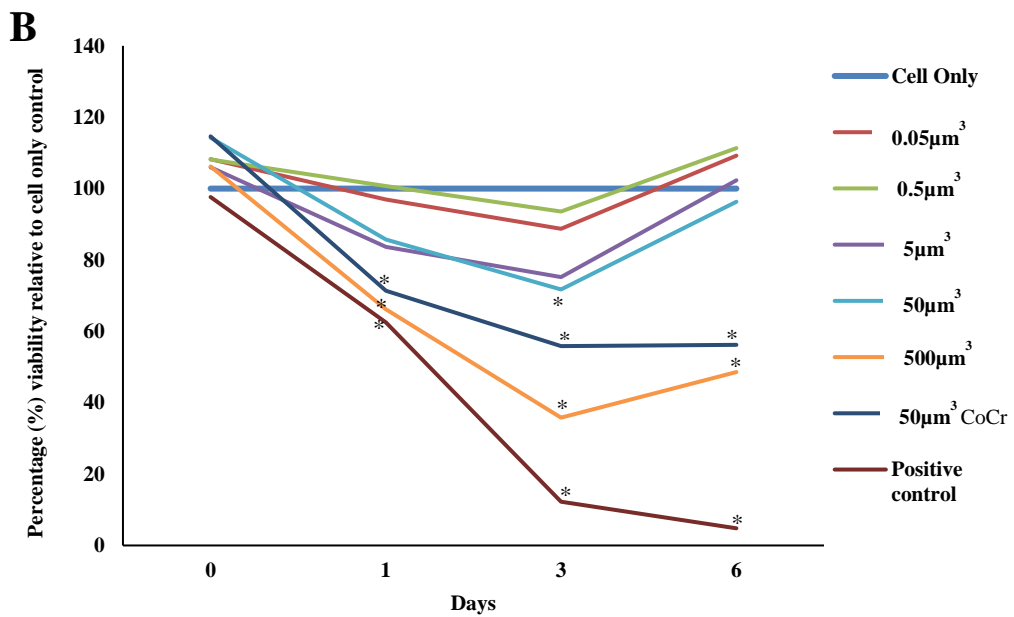
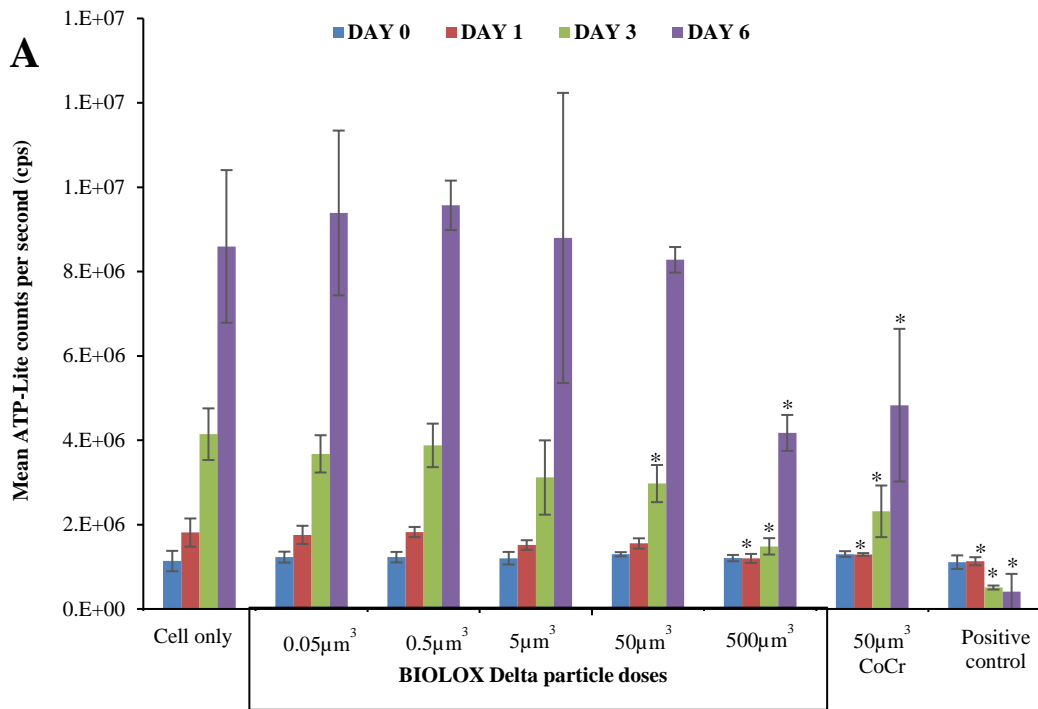


Figure 4.33 - Effects of clinically-relevant BIOLOX[®] Delta wear particles on L929 fibroblast cells using the ATP-Lite assay. L929 cells were cultured with bimodal sized micrometre and nanoscale composite ceramic wear particles generated using the Leeds II hip simulator. Cell viability was determined over a period of 6 days using the ATP-Lite assay and presented as (A) mean counts per second and (B) percentage viability relative to the cell only negative control. Positive controls were camptothecin (2 µg.ml⁻¹) and 50µm³ per cell clinically relevant CoCr nano-particles as positive particle control. A statistically significant reduction (p<0.05 ANOVA) in cell viability in comparison to the cells only control, at given time points, is indicated by an asterisk (*). Error bars represent ±95% confidence limits, n=6.

4.4.3.2 The cytotoxic and inflammatory effects of clinically-relevant ceramic wear particles on PBMNCs

The aim of this part of the study was to determine the release of TNF- α from PBMNCs in response to the increasing doses (0.05-50 μm^3 per cell) of clinically-relevant BIOLOX[®] Delta ceramic wear particles. This assessment was completed using PBMNCs isolated from the same five different healthy volunteer donors (donor 2, donor 5, donor 7, donor 25 and donor 26) to evaluate the variability in response to the particles and controls.

4.4.3.2.1 TNF- α release from PBMNCs in response to clinically-relevant BIOLOX[®] Delta ceramic wear particles

PBMNCs isolated from five donors (Donor 2, Donor 5, Donor 7, Donor 25 and Donor 26) were seeded at a density of 2×10^4 cells per well (n=6) in 96-well plates and cultured in RPMI culture media with increasing doses (0.05, 0.5, 5 & 50 μm^3 per cell) of clinically-relevant BIOLOX[®] Delta ceramic wear particles. The cell only negative control was seeded in the same way but with no particles. LPS (20ng.ml⁻¹) was used as the positive control. The cytotoxic and inflammatory effects of the clinically-relevant BIOLOX[®] Delta ceramic wear particles were compared with high (50 μm^3 per cell) and low (0.5 μm^3 per cell) doses of clinically-relevant BIOLOX[®] Forte ceramic wear particles and high (50 μm^3 per cell) and low (0.5 μm^3 per cell) doses of clinically-relevant CoCr nano-particles (positive particle control). Stainless-steel wear particles generated using the six-station PoP wear rig were also introduced at dose 50 μm^3 per cell as a particle control. The plates were incubated for 24 hours at 37°C in 5% (v/v) CO₂ in air. The cell viability of the PBMNCs following incubation with the particles and controls was determined using the ATP-Lite assay, and an ELISA was conducted on the culture supernatants to determine the concentration of TNF- α released from the cells after the 24hr culture period. The results of the ATP-Lite assay and ELISA were expressed as average absorbance values and were analysed using one-way ANOVA and Tukey Post hoc analysis.

The cell viability and TNF- α release from PBMNCs after 24hrs incubation with the particles and controls are shown in Figure 4.34 (Donor 2), Figure 4.35 (Donor 5), Figure 4.36 (Donor 7), Figure 4.37 (Donor 25) and Figure 4.38 (Donor 26). None of the conditions had a significant effect on the viability of PBMNCs from all the donors compared to the cell only negative control. The high dose (50 μm^3 per cell) of clinically-relevant CoCr nano-particles caused a significant increase in the levels of TNF- α released for all the donors when compared to the cell only negative control (ANOVA; p<0.05). Similarly, the highest dose (50 μm^3 per cell) of both clinically-relevant BIOLOX[®] Forte and BIOLOX[®] Delta ceramic wear particles caused a significant increase in the levels of TNF- α released from all the donors compared to the cell only negative control (ANOVA; p<0.05).

However, the high dose ($50\mu\text{m}^3$ per cell) of stainless steel wear particles showed no significant increase in the levels of TNF- α released for all the donors when compared to the cells only negative control. For the other particle volumes of BIOLOX[®] Delta ($0.05\text{-}5\mu\text{m}^3$ per cell) and BIOLOX[®] Forte ($0.5\mu\text{m}^3$ per cell), there was no significant increase in the levels of TNF- α released compared to the cell only negative control for all the donors. The low dose ($0.5\mu\text{m}^3$ per cell) of clinically-relevant CoCr nano-particles also showed no significant increase in TNF- α release compared to the cell only negative control for all the donors. The positive control of LPS ($200\text{ng}\cdot\text{ml}^{-1}$) caused significant levels of TNF- α released from PBMNCs from all donors compared to the cell only negative control (ANOVA; $p<0.05$).

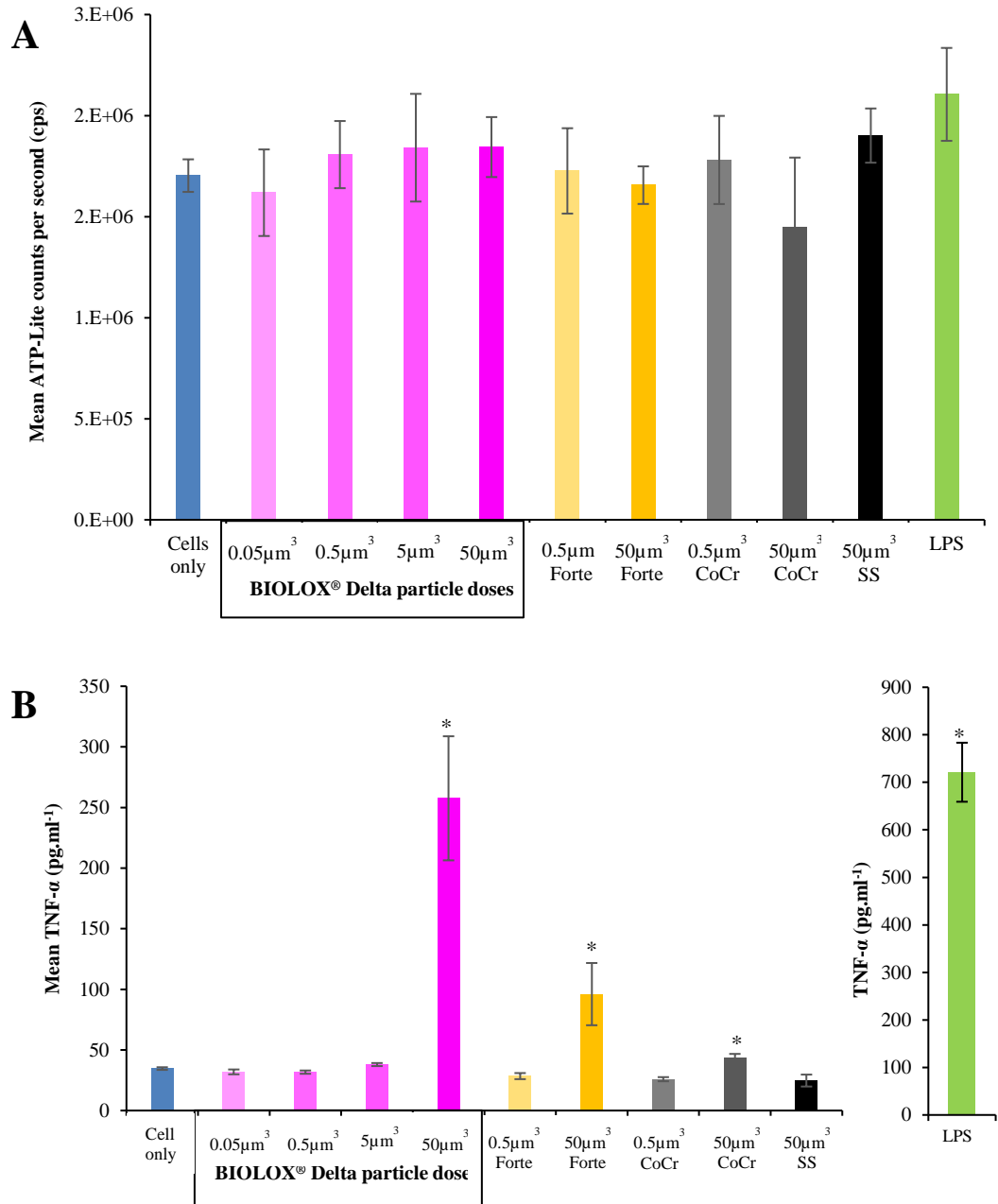


Figure 4.34 – (A) Cell viability and (B) TNF- α release from PBMCs isolated from Donor 2 in response to clinically-relevant BIOLOX[®] Delta ceramic wear particles. PBMCs were cultured with bimodal sized micrometre and nanoscale composite (BIOLOX[®] Delta) and alumina (BIOLOX[®] Forte) clinically-relevant ceramic wear particles, clinically-relevant stainless-steel wear particles and CoCr nano-particles for 24 hours. Cell viability was determined using the ATP-Lite assay and presented as (A) mean counts per second and (B) release of TNF- α was measured using ELISA. Positive control was 200ng.ml⁻¹ lipopolysaccharide. A statistically significant reduction ($p < 0.05$ ANOVA) in cell viability in comparison to the cells only control is indicated by an asterisk (*). Error bars represent $\pm 95\%$ confidence limits, $n = 6$.

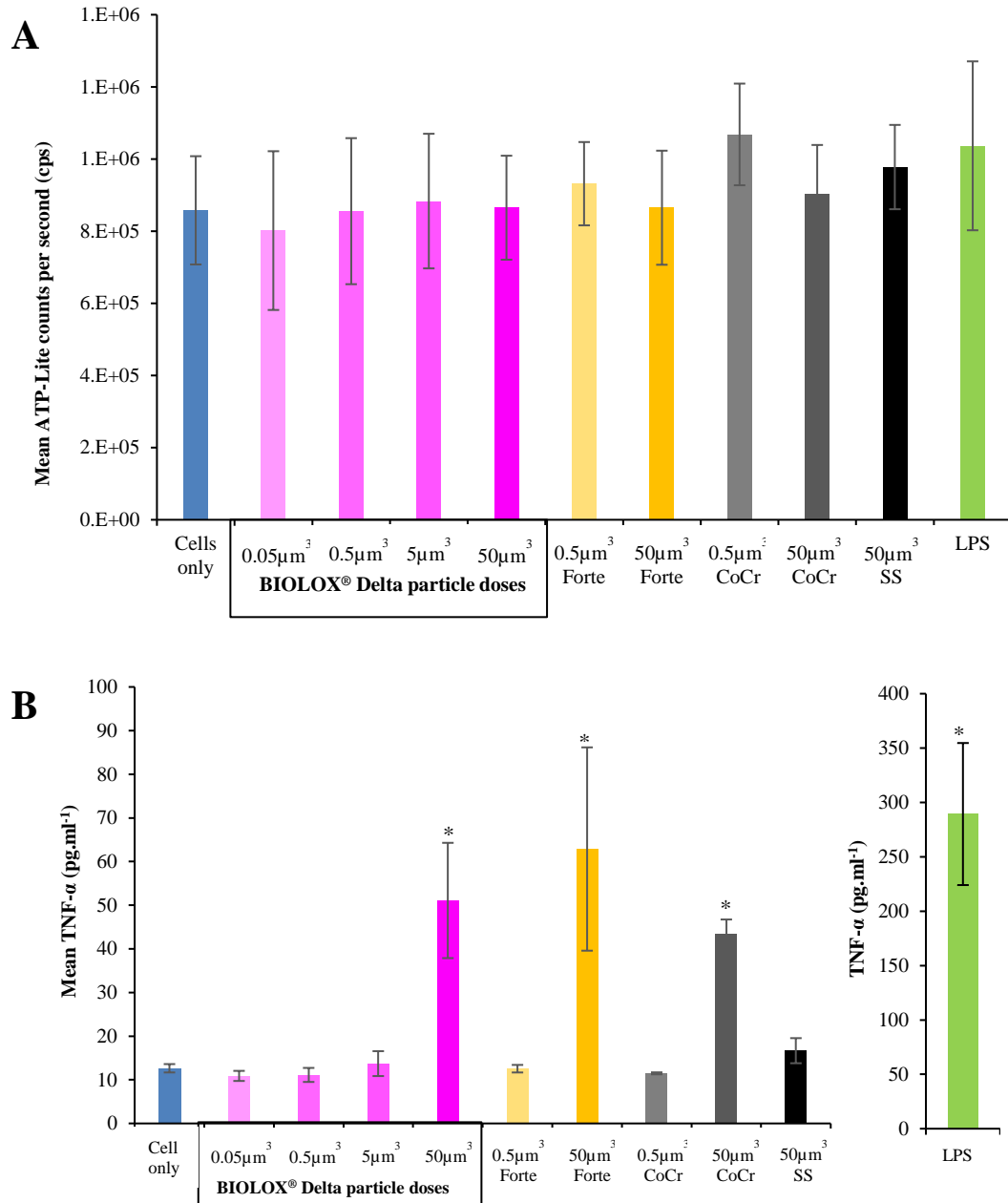


Figure 4.35 – (A) Cell viability and (B) TNF- α release from PBMCs isolated from Donor 5 in response to clinically-relevant BIOLOX[®] Delta ceramic wear particles. PBMCs were cultured with bimodal sized micrometre and nanoscale composite (BIOLOX[®] Delta) and alumina (BIOLOX[®] Forte) clinically-relevant ceramic wear particles, clinically-relevant stainless-steel wear particles and CoCr nano-particles for 24 hours. Cell viability was determined using the ATP-Lite assay and presented as (A) mean counts per second and (B) release of TNF- α was measured using ELISA. Positive control was 200ng.ml⁻¹ lipopolysaccharide. A statistically significant reduction ($p < 0.05$ ANOVA) in cell viability in comparison to the cells only control is indicated by an asterisk (*). Error bars represent $\pm 95\%$ confidence limits, $n=6$.

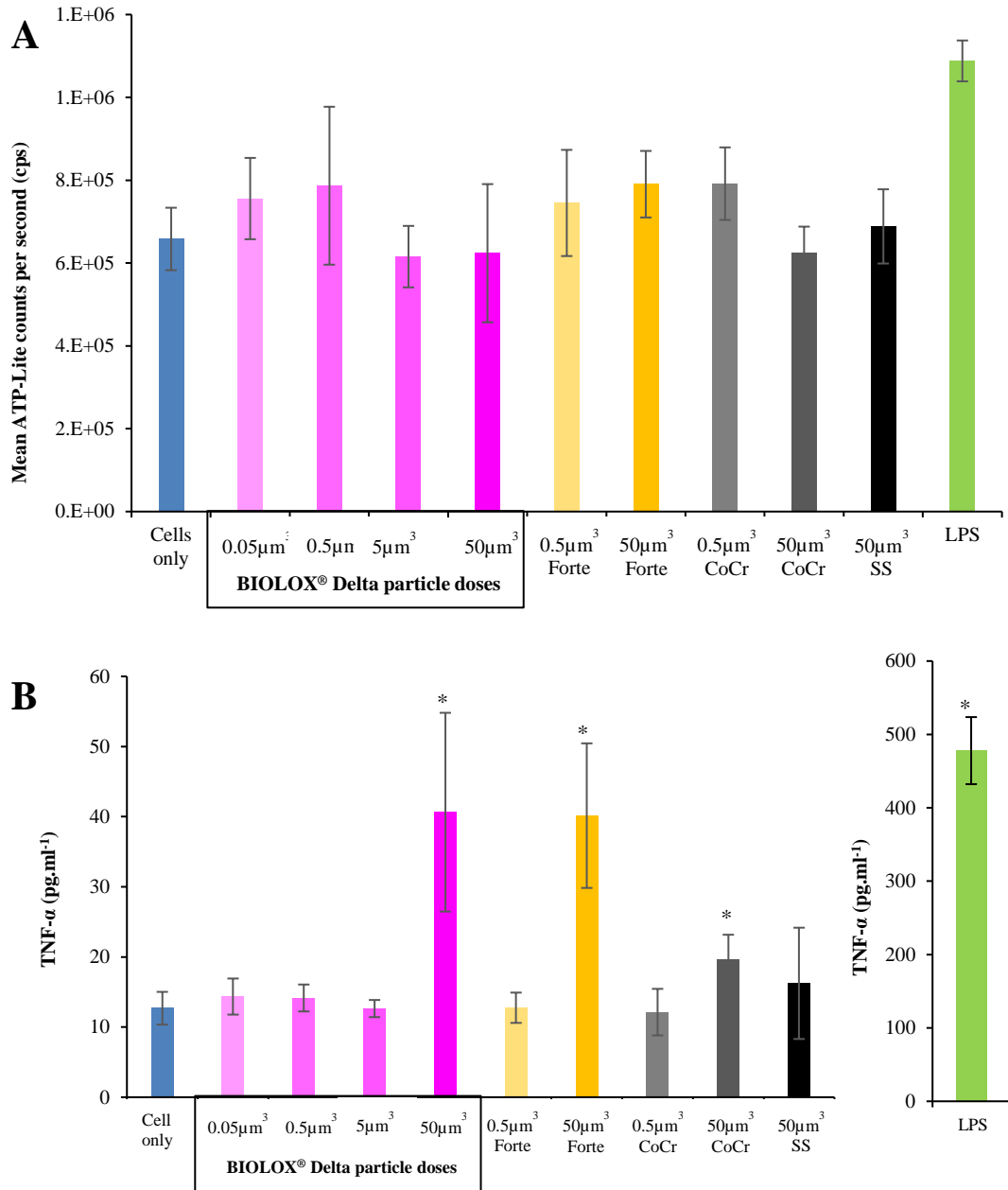


Figure 4.36 – (A) Cell viability and (B) TNF- α release from PBMCs isolated from Donor 7 in response to clinically-relevant BIOLOX[®] Delta ceramic wear particles. PBMCs were cultured with bimodal sized micrometre and nanoscale composite (BIOLOX[®] Delta) and alumina (BIOLOX[®] Forte) clinically-relevant ceramic wear particles, clinically-relevant stainless-steel wear particles and CoCr nano-particles for 24 hours. Cell viability was determined using the ATP-Lite assay and presented as (A) mean counts per second and (B) release of TNF- α was measured using ELISA. Positive control was 200ng.ml⁻¹ lipopolysaccharide. A statistically significant reduction ($p < 0.05$ ANOVA) in cell viability in comparison to the cells only control is indicated by an asterisk (*). Error bars represent $\pm 95\%$ confidence limits, $n=6$.

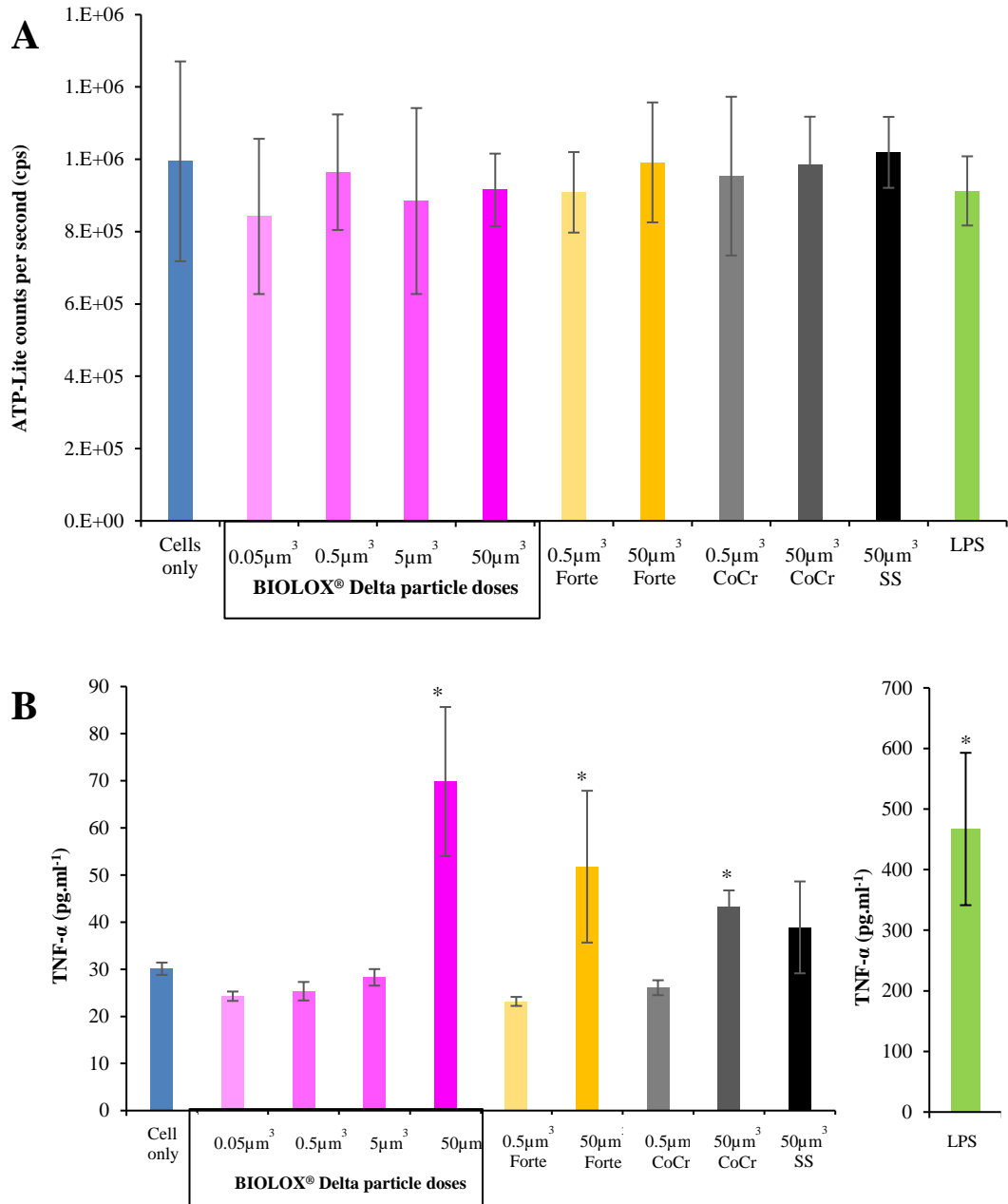


Figure 4.37 – (A) Cell viability and (B) TNF- α release from PBMNCs isolated from Donor 25 in response to clinically-relevant BIOLOX[®] Delta ceramic wear particles. PBMNCs were cultured with bimodal sized micrometre and nanoscale composite (BIOLOX[®] Delta) and alumina (BIOLOX[®] Forte) clinically-relevant ceramic wear particles, clinically-relevant stainless-steel wear particles and CoCr nano-particles for 24 hours. Cell viability was determined using the ATP-Lite assay and presented as (A) mean counts per second and (B) release of TNF- α was measured using ELISA. Positive control was 200ng.ml⁻¹ lipopolysaccharide. A statistically significant reduction ($p < 0.05$ ANOVA) in cell viability in comparison to the cells only control is indicated by an asterisk (*). Error bars represent $\pm 95\%$ confidence limits, $n=6$.

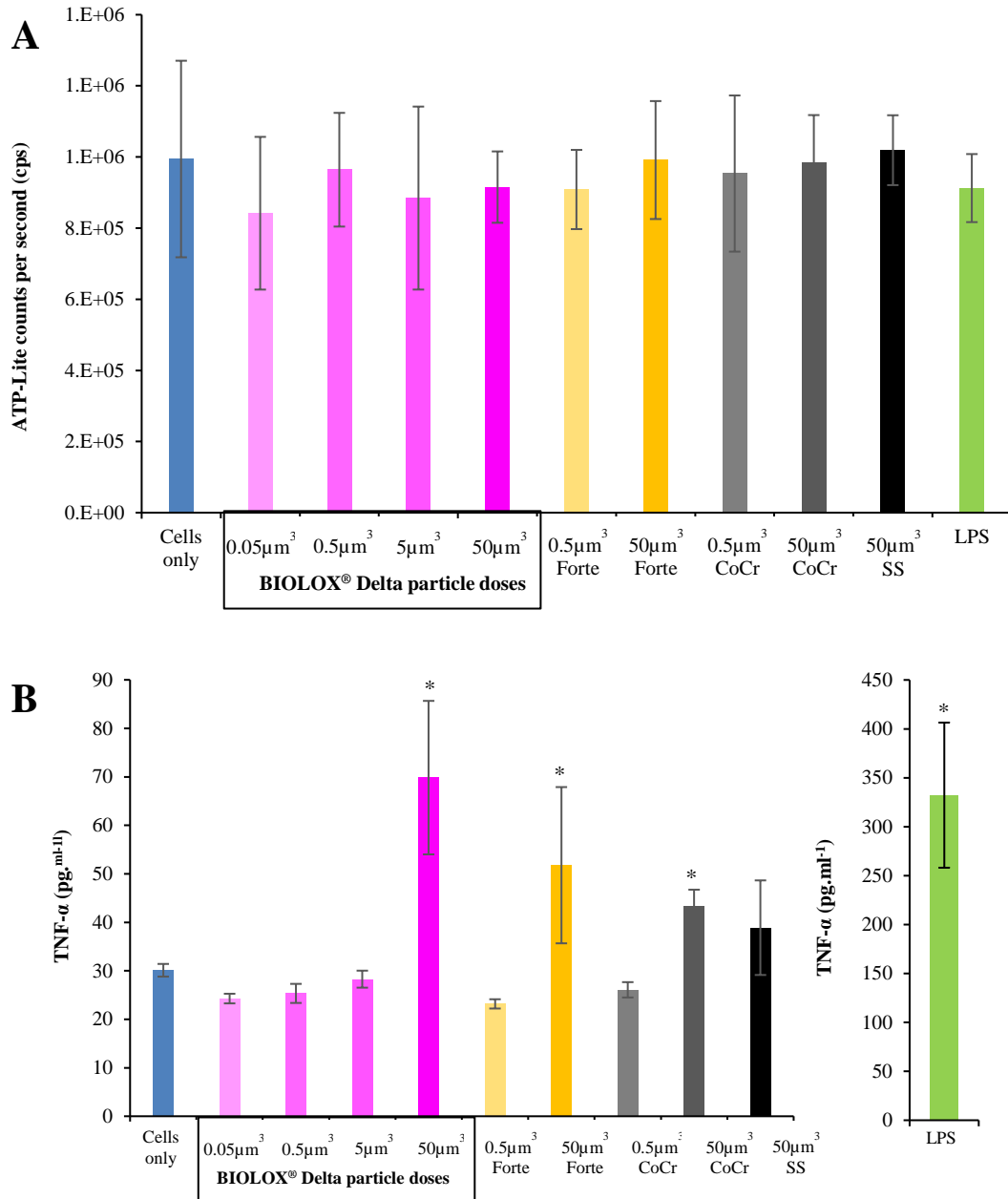


Figure 4.38 – (A) Cell viability and (B) TNF- α release from PBMNCs isolated from Donor 26 in response to clinically-relevant BIOLOX[®] Delta ceramic wear particles. PBMNCs were cultured with bimodal sized micrometre and nanoscale composite (BIOLOX[®] Delta) and alumina (BIOLOX[®] Forte) clinically-relevant ceramic wear particles, clinically-relevant stainless-steel wear particles and CoCr nano-particles for 24 hours. Cell viability was determined using the ATP-Lite assay and presented as (A) mean counts per second and (B) release of TNF- α was measured using ELISA. Positive control was 200ng.ml⁻¹ lipopolysaccharide. A statistically significant reduction ($p < 0.05$ ANOVA) in cell viability in comparison to the cells only control is indicated by an asterisk (*). Error bars represent $\pm 95\%$ confidence limits, $n=6$.

4.4.3.3 The genotoxic effects of clinically-relevant ceramic wear particles in PBMNCs

The aim of this part of the study was to assess the genotoxicity of increasing doses (0.05-50 μm^3 per cell) of clinically-relevant BIOLOX[®] Delta ceramic wear particles that were generated using the Leeds II hip simulator as described in section 3.3.3.1. This assessment was completed in PBMNCs isolated from five different healthy volunteer donors to evaluate the variability in response to the particles and controls.

4.4.3.3.1 DNA damage in PBMNCs in response to clinically-relevant BIOLOX[®] Delta ceramic wear particles

PBMNCs isolated from five donors (Donor 2, Donor 5, Donor 7, Donor 25 and Donor 26) were seeded at a density of 1×10^5 cells per well ($n=2$) in 48-well plates and cultured in RPMI culture media with increasing doses of (0.05, 0.5, 5 & $50 \mu\text{m}^3$ per cell) of clinically-relevant BIOLOX[®] Delta ceramic wear particles. The negative control was seeded in the same way but with no particles. Hydrogen peroxide ($100 \mu\text{M}$) was used as the positive control as it is known to induce single and double strand DNA damage (Driessens et al., 2009). The genotoxic effects of clinically-relevant BIOLOX[®] Delta ceramic wear particles were compared with high ($50 \mu\text{m}^3$ per cell) and low ($0.5 \mu\text{m}^3$ per cell) doses of clinically-relevant BIOLOX[®] Forte ceramic wear particles and high ($50 \mu\text{m}^3$ per cell) and low ($0.5 \mu\text{m}^3$ per cell) doses of clinically-relevant CoCr nano-particles (positive particle control). Stainless-steel wear particles generated using the six-station PoP wear rig were also introduced at dose $50 \mu\text{m}^3$ per cell as a particle control. The plates were incubated for 24 hours at 37°C in 5% (v/v) CO_2 in air and DNA damage in the PBMNCs following incubation with the particles and controls was determined using the comet assay (protocol described in section 4.3.2.7.3). During the assay protocol, the cells were embedded in agarose gel and underwent single cell electrophoresis. The output of the assay was images of single cells that were analysed using the Comet IV software. DNA damage was quantified as the comet tail moment as described in section 4.4.2.3 and the results were analysed using one-way ANOVA and Tukey Post hoc analysis.

The genotoxic effects of the particles and controls is shown in Figure 4.39 (Donor 2), Figure 4.40 (Donor 5), Figure 4.41 (Donor 7), Figure 4.42 (Donor 25) and Figure 4.43 (Donor 26). High levels of DNA damage are indicated by longer tails in the images and higher values of tail moment relative to the cells only control. Cell nuclei that appear completely circular are indicative of no DNA damage. The clinically-relevant BIOLOX[®] Delta ceramic wear particles showed genotoxic effects at high doses ($50 \mu\text{m}^3$ per cell), where statistically significant levels of DNA damage (tail moment) in PBMNCs was observed in four donors (5, 7, 25, 26) when compared to the cell only negative control (ANOVA; $p < 0.05$). The clinically-

relevant BIOLOX[®] Delta ceramic wear particles also caused DNA damage in PBMNCs at a dose of 5 μm^3 per cell for three donors (5, 7, 26). Furthermore, significant DNA damage was also observed in PBMNCs isolated from donor 25 in response to 0.5 μm^3 per cell of clinically-relevant BIOLOX[®] Delta ceramic wear particles (ANOVA; $p < 0.05$). The clinically-relevant BIOLOX[®] Forte ceramic wear particles at high doses (50 μm^3 per cell) caused significant (ANOVA; $p < 0.05$) levels of DNA damage (tail moment) in PBMNCs from all donors. This was also evident for the clinically-relevant BIOLOX[®] Forte ceramic wear particles at low doses (0.5 μm^3 per cell) whereby there was a significant (ANOVA; $p < 0.05$) increase in tail moment compared to the cells only negative control for donors 5, 7 and 25. Similarly, the high dose (50 μm^3) of clinically-relevant CoCr nano-particles caused a significant increase in the levels of DNA damage for all donors as indicated by the high levels of tail moment compared to the cell only negative control (ANOVA; $p < 0.05$). Additionally, the low dose (0.5 μm^3) of clinically-relevant CoCr nano-particles demonstrated significant levels of DNA damage (tail moment) in PBMNCs from donor 2, when compared to the cells only negative control (ANOVA; $p < 0.05$). The stainless-steel wear particles at dose 50 μm^3 per cell caused a significant increase in the levels of DNA damage for all donors as indicated by the high levels of tail moment compared to the cells only negative control (ANOVA; $p < 0.05$). The positive control of hydrogen peroxide caused significant levels of DNA damage in PBMNCs from all donors compared to the cells only negative control (ANOVA; $p < 0.05$).

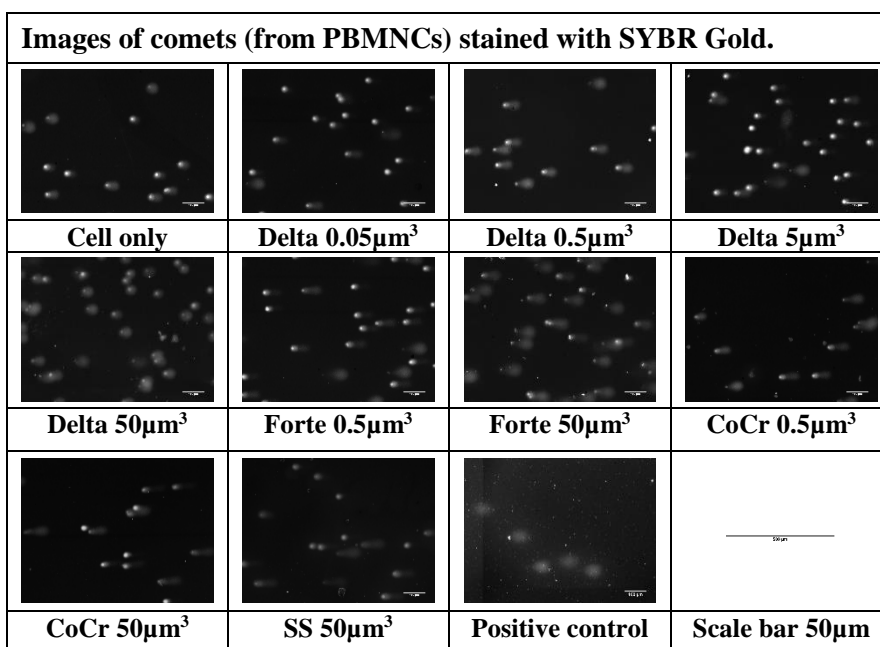
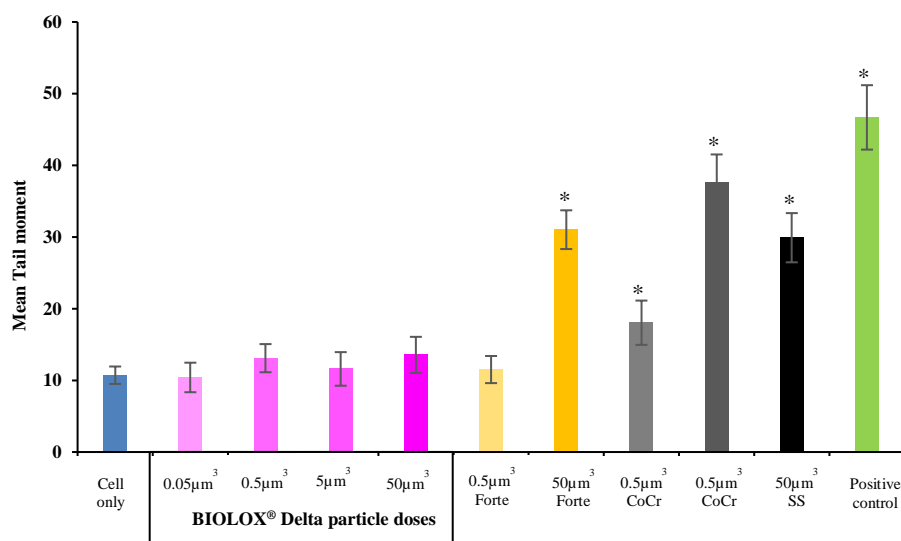


Figure 4.39 – The genotoxic effects of clinically-relevant BIOLOX[®] Delta ceramic particles wear in PBMNCs isolated from Donor 2. PBMNCs were cultured with bimodal sized micrometre/sub-micron and nanoscale composite (BIOLOX[®] Delta), alumina (BIOLOX[®] Forte) clinically-relevant ceramic wear particles, and clinically-relevant CoCr nano-particles for 24 hours. DNA damage was determined using the comet assay and presented as (A) mean tail moment and (B) images. Cells that appear circular have no detectable DNA damage, whereas nuclei that have tails is indicative of DNA damage. A statistically significant different ($p < 0.05$ ANOVA with post hoc Tukey test) in tail moment compared to the cells only control is indicated by an asterisk (*). A minimum of 100 cells were scored using the Comet IV software. Error bars represent $\pm 95\%$ confidence limits.

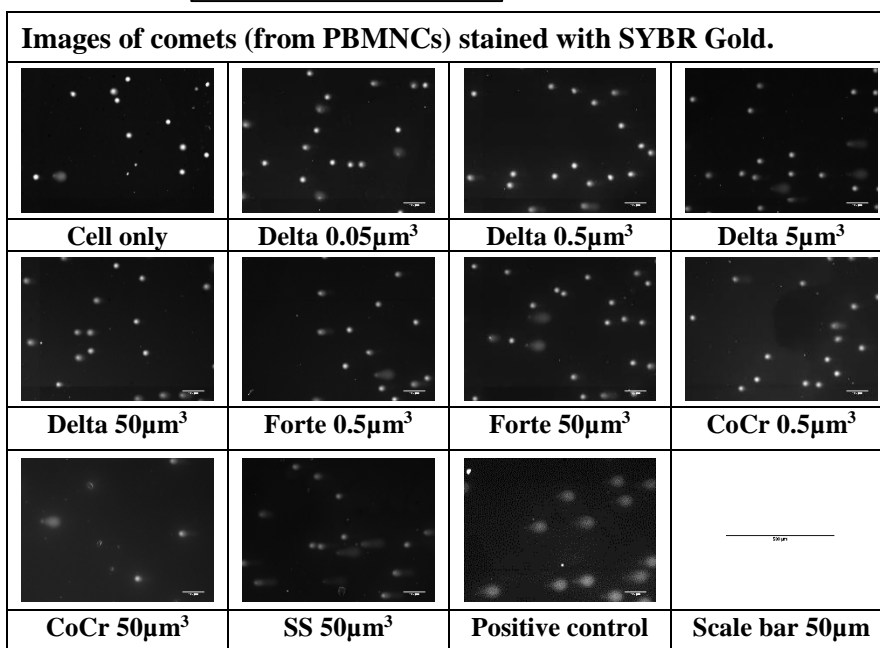
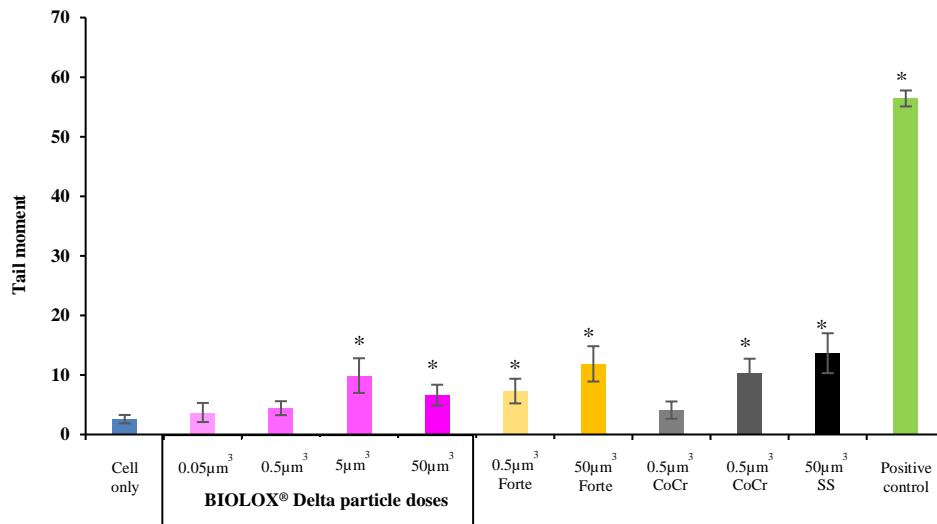
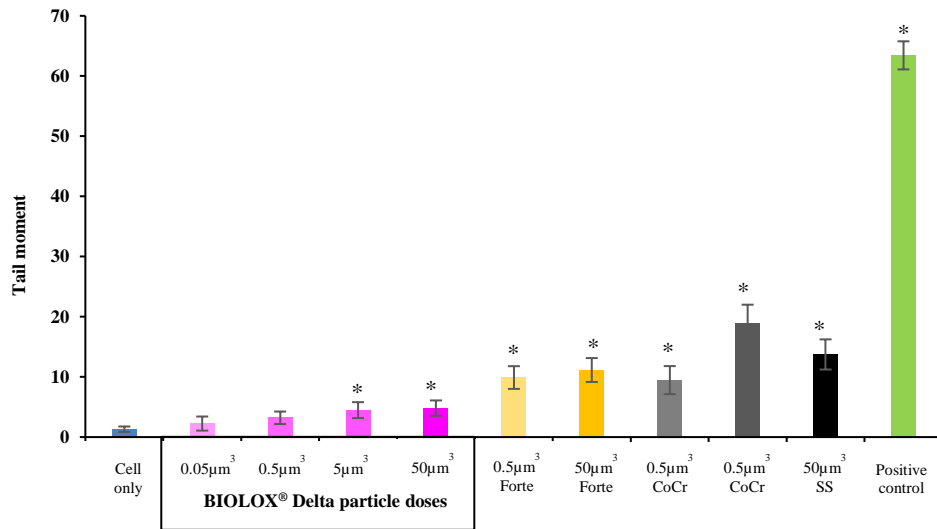


Figure 4.40 – The genotoxic effects of clinically-relevant BIOLOX® Delta ceramic particles wear in PBMNCs isolated from Donor 5. PBMNCs were co-cultured with bimodal sized; micrometre and nanoscale composite (BIOLOX® Delta) and alumina (BIOLOX® Forte) clinically-relevant ceramic wear particles, and clinically-relevant CoCr nano-particles for 24 hours. DNA damage was determined using the comet assay and presented as (A) tail moment and (B) images. Cells that appear as round have no detectable DNA damage whereas cells that have tails is indicative of DNA damage. A statistically significant different ($p < 0.05$ ANOVA) in tail moment compared to the cells only control is indicated by an asterisk (*). A minimum of 100 cells were scored using the Comet IV software. Error bars represent $\pm 95\%$ confidence limits.



Images of comets (from PBMNCs) stained with SYBR Gold.

Cell only	Delta 0.05µm³	Delta 0.5µm³	Delta 5µm³
Delta 50µm³	Forte 0.5µm³	Forte 50µm³	CoCr 0.5µm³
CoCr 50µm³	SS 50µm³	Positive control	Scale bar 50µm

Figure 4.41 – The genotoxic effects of clinically-relevant BIOLOX[®] Delta ceramic particles wear in PBMNCs isolated from Donor 7. PBMNCs were co-cultured with bimodal sized; micrometre and nanoscale composite (BIOLOX[®] Delta) and alumina (BIOLOX[®] Forte) clinically-relevant ceramic wear particles, and clinically-relevant CoCr nano-particles for 24 hours. DNA damage was determined using the comet assay and presented as (A) tail moment and (B) images. Cells that appear as round have no detectable DNA damage whereas cells that have tails is indicative of DNA damage. A statistically significant different ($p < 0.05$ ANOVA) in tail moment compared to the cells only control is indicated by an asterisk (*). A minimum of 100 cells were scored using the Comet IV software. Error bars represent $\pm 95\%$ confidence limits.

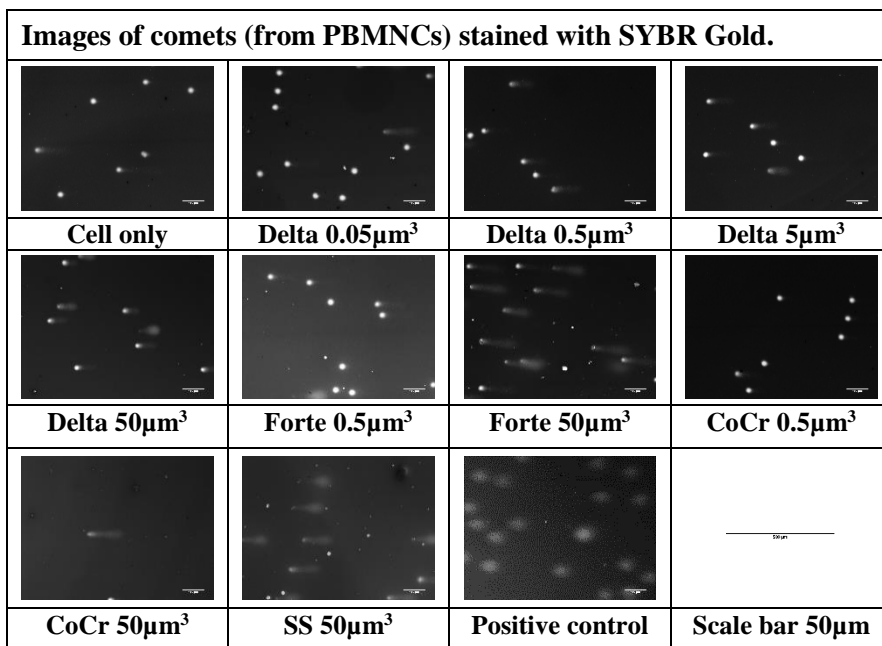
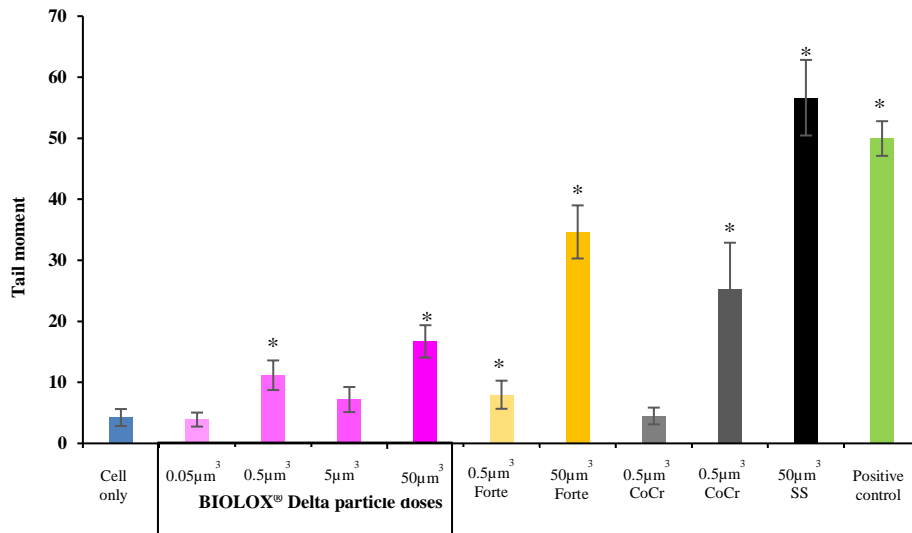
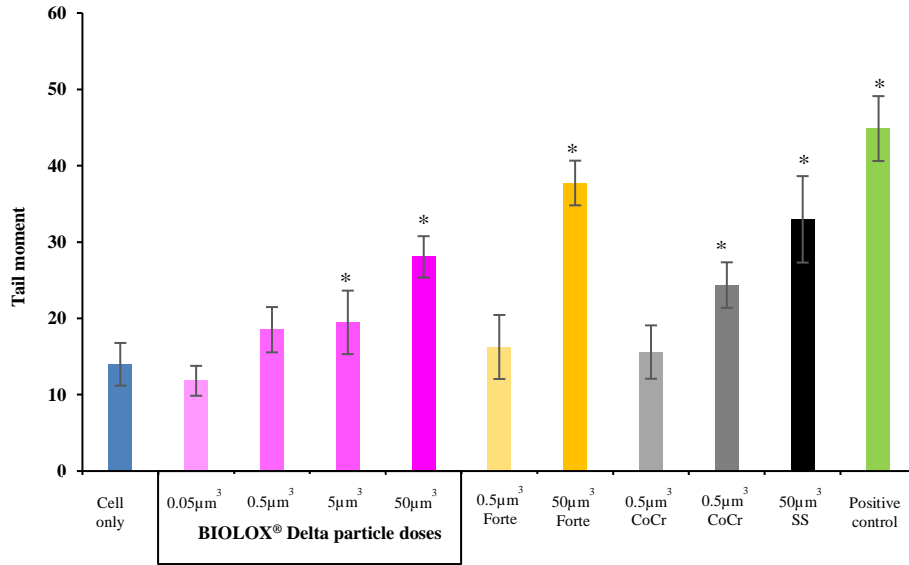


Figure 4.42 – The genotoxic effects of clinically-relevant BIOLOX® Delta ceramic particles wear in PBMNCs isolated from Donor 25. PBMNCs were co-cultured with bimodal sized; micrometre and nanoscale composite (BIOLOX® Delta) and alumina (BIOLOX® Forte) clinically-relevant ceramic wear particles, and clinically-relevant CoCr nano-particles for 24 hours. DNA damage was determined using the comet assay and presented as (A) tail moment and (B) images. Cells that appear as round have no detectable DNA damage whereas cells that have tails is indicative of DNA damage. A statistically significant different ($p < 0.05$ ANOVA) in tail moment compared to the cells only control is indicated by an asterisk (*). A minimum of 100 cells were scored using the Comet IV software. Error bars represent $\pm 95\%$ confidence limits.



Images of comets (from PBMNCs) stained with SYBR Gold.

Cell only	Delta 0.05µm³	Delta 0.5µm³	Delta 5µm³
Delta 50µm³	Forte 0.5µm³	Forte 50µm³	CoCr 0.5µm³
CoCr 50µm³	SS 50µm³	Positive control	Scale bar 50µm

Figure 4.43 – The genotoxic effects of clinically-relevant BIOLOX[®] Delta ceramic particles wear in PBMNCs isolated from Donor 26. PBMNCs were co-cultured with bimodal sized; micrometre and nanoscale composite (BIOLOX[®] Delta) and alumina (BIOLOX[®] Forte) clinically-relevant ceramic wear particles, and clinically-relevant CoCr nano-particles for 24 hours. DNA damage was determined using the comet assay and presented as (A) tail moment and (B) images. Cells that appear as round have no detectable DNA damage whereas cells that have tails is indicative of DNA damage. A statistically significant different ($p < 0.05$ ANOVA) in tail moment compared to the cells only control is indicated by an asterisk (*). A minimum of 100 cells were scored using the Comet IV software. Error bars represent $\pm 95\%$ confidence limits.

4.4.3.4 Oxidative stress in PBMNCs in response to clinically-relevant ceramic wear particles

The aim of this study was to assess the levels of oxidative stress induced by increasing doses (0.05-50 μm^3 per cell) of clinically-relevant BIOLOX[®] Delta ceramic wear particles in PBMNCs. This assessment was completed on PBMNCs isolated from five different healthy donors to evaluate the variability in response to the particles and controls. Oxidative stress was measured by labelling the ROS produced by the PBMNCs using the DCFDA probe in the cellular ROS detection assay kit (protocol outlined in section 4.3.2.7.4).

4.4.3.4.1 Oxidative stress in PBMNCs in response to clinically-relevant BIOLOX[®] Delta ceramic wear particles

PBMNCs isolated from five donors (donor 2, donor 5, donor 7, donor 25 and donor 26) were seeded at a density of 2×10^4 cells per well (n=6) in clear bottom black 96-well plates and cultured in RPMI culture media with increasing doses (0.05, 0.5, 5 & 50 μm^3 per cell) of clinically-relevant BIOLOX[®] Delta ceramic wear particles. The cell only negative control was seeded in the same way but with no particles. TBHP (200 μM) was used as the positive control as it mimics ROS activity to oxidise DCFDA to fluorescent DCF and so it is commonly used to evaluate the cellular responses resulting from oxidative stress in cells and tissues (Kucera et al., 2014). The presence of ROS within the cells in response to the clinically-relevant BIOLOX[®] Delta ceramic wear particles was compared with high (50 μm^3 per cell) and low (0.5 μm^3 per cell) doses of clinically-relevant BIOLOX[®] Forte ceramic wear particles and high (50 μm^3 per cell) and low (0.5 μm^3 per cell) doses of clinically-relevant CoCr nano-particles. Stainless-steel wear particles generated using the six-station PoP wear rig were also introduced at dose 50 μm^3 per cell as a particle control. The plates were incubated for 24 hours at 37°C in 5% (v/v) CO₂ in air. The production of ROS in PBMNCs following incubation with the particles and controls was determined using the cellular ROS detection assay (protocol outlined in section 4.3.2.7.4). The results were expressed as average fluorescence intensity values where higher values of fluorescence intensity was directly proportional to high levels of oxidative stress. The data was analysed using one-way ANOVA and Tukey Post hoc analysis. The cells present within the wells were also imaged to correlate the fluorescence intensity values with the fluorescence emitted from within the cells.

The images of fluorescently labelled ROS present in the PBMNCs from donor 2 (Figure 4.44) after exposure to 485nm for 1000ms are representative of all donors, except for the PBMNCs cultured with stainless-steel wear particles from donor 5 and donor 26, which showed brighter images of PBMNCs treated with 50 μm^3 per cell of stainless-steel wear particles. The cell only, low dose (0.5 μm^3 per cell) of CoCr nano-particles and all the doses (0.05-50 μm^3 per cell) for both BIOLOX[®] Delta and BIOLOX[®] Forte wear particles demonstrated less

fluorescence relative to the high dose ($50\mu\text{m}^3$ per cell) of CoCr nano-particles and positive control ($200\mu\text{M}$ TBHP). The brighter images of PBMNCs treated with $50\mu\text{m}^3$ per cell of CoCr nano-particles and TBHP were indicative of high levels of oxidative stress.

The production of ROS levels as a function of fluorescence intensity in response to the particles and controls is shown in Figure 4.45 (Donor 2), Figure 4.46 (Donor 5), Figure 4.47 (Donor 7), Figure 4.48 (Donor 25) and Figure 4.49 (Donor 26). High levels of ROS are indicated by higher fluorescence intensity relative to the cell only negative control and are visualised as brighter green fluorescence in the images Figure 4.44. The clinically-relevant BIOLOX[®] Delta ceramic wear particles for all the doses tested had no significant effect on the production of ROS (fluorescence intensity) in PBMNCs from all donors when compared to the cell only negative control. This was also evident for the clinically-relevant BIOLOX[®] Forte ceramic wear particles at low ($0.5\mu\text{m}^3$ per cell) and high ($50\mu\text{m}^3$ per cell) doses, where there was no significant increase in fluorescence intensity compared to the cell only negative control for all the donors. Similarly, low dose ($0.5\mu\text{m}^3$ per cell) of clinically-relevant CoCr nano-particles showed no significant increase in ROS production (fluorescence intensity) when compared to the cell only negative control. However, the high dose ($50\mu\text{m}^3$) of clinically-relevant CoCr nano-particles caused a significant increase in the levels ROS production in PBMNCs from all donors as indicated by the high levels of fluorescence intensity compared to the cell only negative control (ANOVA; $p < 0.05$). Similarly, the stainless-steel wear particles ($50\mu\text{m}^3$ per cell) caused a significant increase in the levels of ROS production in PBMNCs from donors 5 and 26 as indicated by the high levels of fluorescence intensity compared to the cells only negative control (ANOVA; $p < 0.05$). The positive control of TBHP caused significant (ANOVA; $p < 0.05$) levels of ROS production (fluorescence intensity) in the PBMNCs from all donors compared to the cell only negative control.

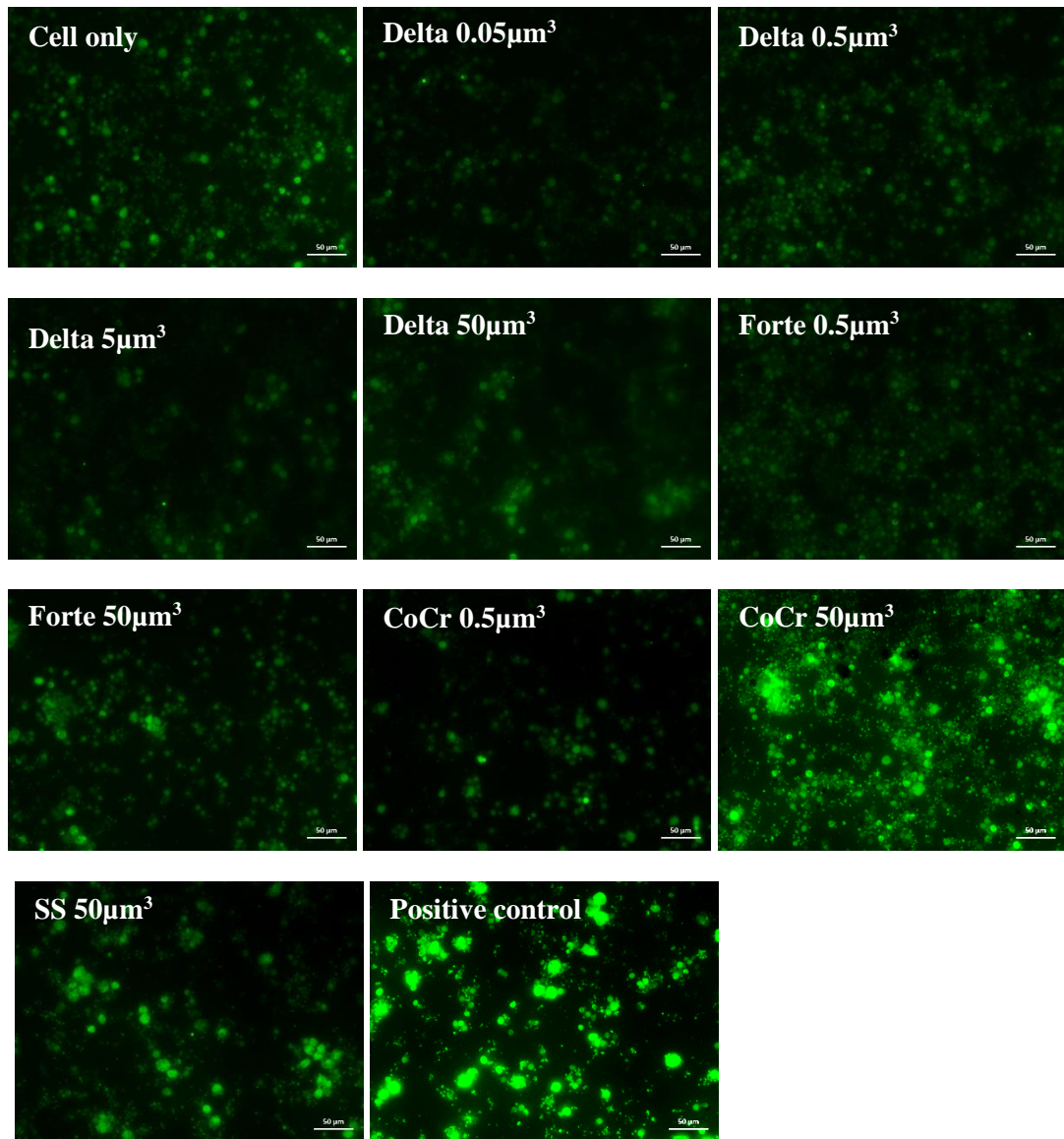


Figure 4.44 – Visualisation of the presence of ROS in PBMNCs isolated from Donor 2. PBMNCs were cultured with bimodal sized micrometre/submicron and nanoscale composite (BIOLOX[®] Delta) and alumina (BIOLOX[®] Forte) clinically-relevant ceramic particles, and clinically-relevant CoCr nanoparticles for 24 hours. Oxidative stress was determined using the DCFDA probe to detect the production of ROS, which is presented as the green fluorescence. The higher the intensity of the green fluorescence, the higher the levels of ROS produced by the PBMNCs. TBHP (200µM) was used as the positive control. Size-bar 50µm in all images.

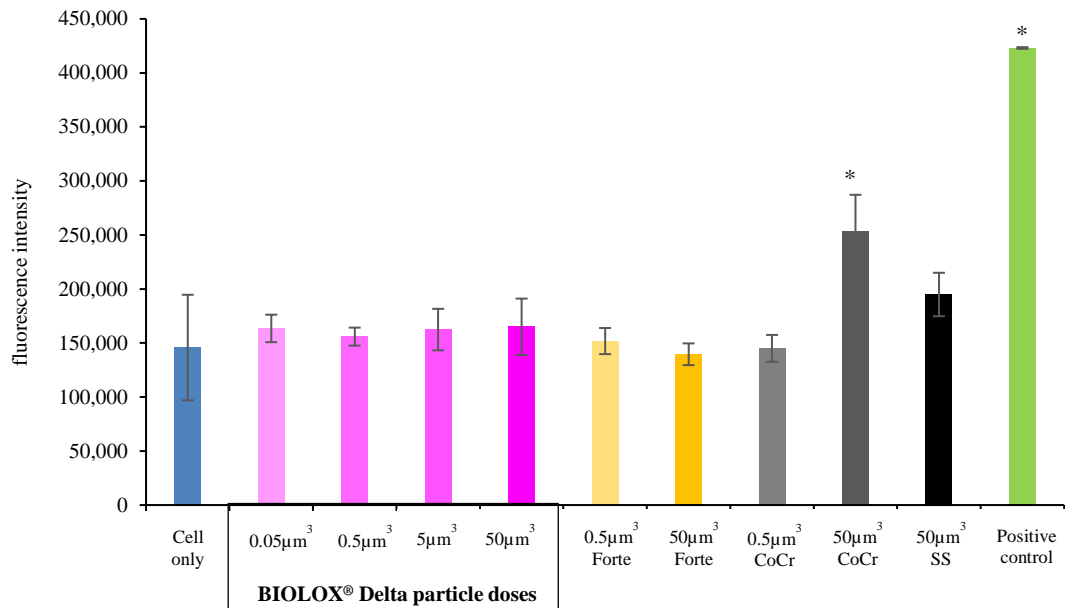


Figure 4.45 - Oxidative stress in PBMCs isolated from Donor 2 in response to BIOLOX[®] Delta model ceramic particles. PBMCs were cultured with bimodal sized micrometre/sub-micron and nanoscale composite (BIOLOX[®] Delta), alumina (BIOLOX[®] Forte) clinically-relevant ceramic wear particles, and clinically-relevant stainless steel and CoCr nano-particles for 24 hours. Oxidative stress was determined using a DCFDA probe to detect the production of reactive oxygen species, which is presented as mean fluorescent intensity. TBHP (200μM) was used as the positive control. A statistically significant different ($p < 0.05$ ANOVA) in fluorescence intensity compared to the cells only control is indicated by an asterisk (*). Error bars represent $\pm 95\%$ confidence limits ($n=6$).

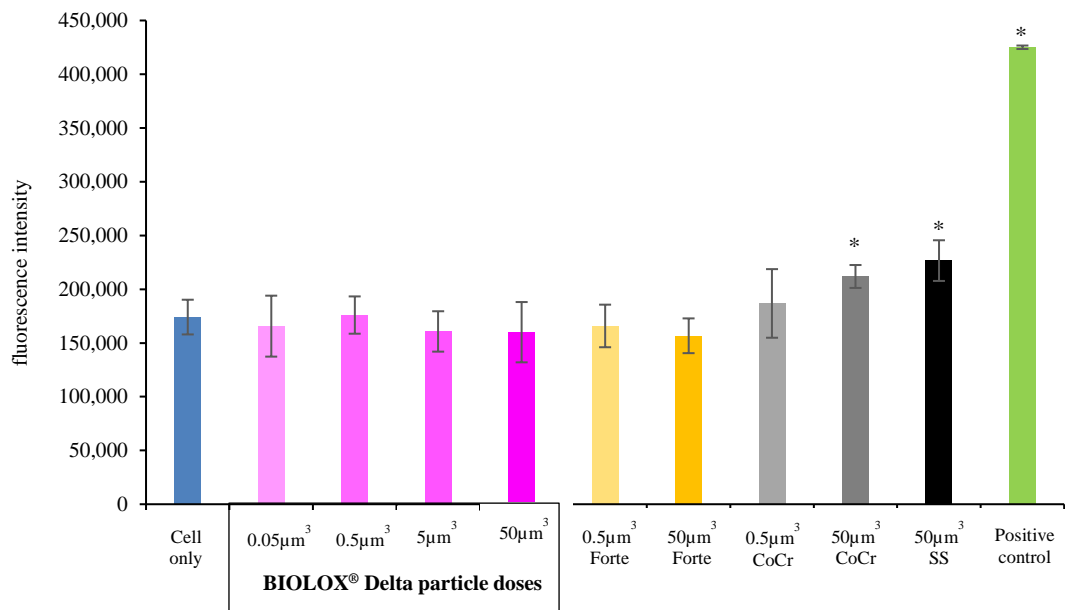


Figure 4.46 - Oxidative stress in PBMCs isolated from Donor 5 in response to BIOLOX[®] Delta model ceramic particles. PBMCs were cultured with bimodal sized micrometre/sub-micron and nanoscale composite (BIOLOX[®] Delta), alumina (BIOLOX[®] Forte) clinically-relevant ceramic wear particles, and clinically-relevant stainless steel and CoCr nano-particles for 24 hours. Oxidative stress was determined using a DCFDA probe to detect the production of reactive oxygen species, which is presented as mean fluorescent intensity. TBHP (200μM) was used as the positive control. A statistically significant different ($p < 0.05$ ANOVA) in fluorescence intensity compared to the cells only control is indicated by an asterisk (*). Error bars represent $\pm 95\%$ confidence limits ($n=6$).

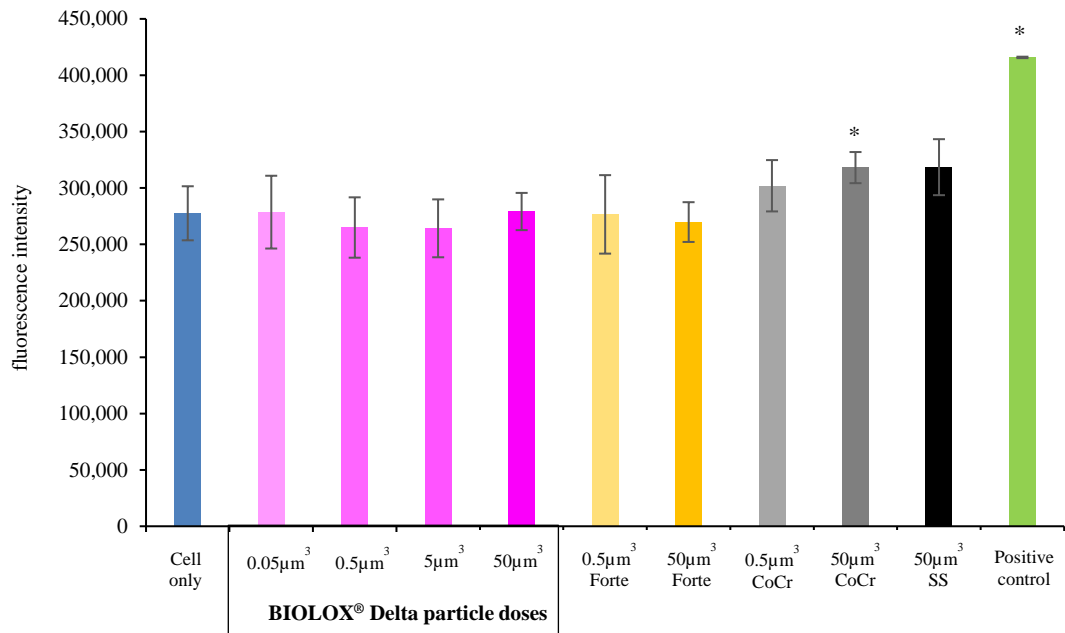


Figure 4.47 - Oxidative stress in PBMNCs isolated from Donor 7 in response to BIOLOX® Delta model ceramic particles. PBMNCs were cultured with bimodal sized micrometre/sub-micron and nanoscale composite (BIOLOX® Delta), alumina (BIOLOX® Forte) clinically-relevant ceramic wear particles, and clinically-relevant stainless steel and CoCr nano-particles for 24 hours. Oxidative stress was determined using a DCFDA probe to detect the production of reactive oxygen species, which is presented as mean fluorescent intensity. TBHP (200μM) was used as the positive control. A statistically significant different ($p < 0.05$ ANOVA) in fluorescence intensity compared to the cells only control is indicated by an asterisk (*). Error bars represent $\pm 95\%$ confidence limits ($n=6$).

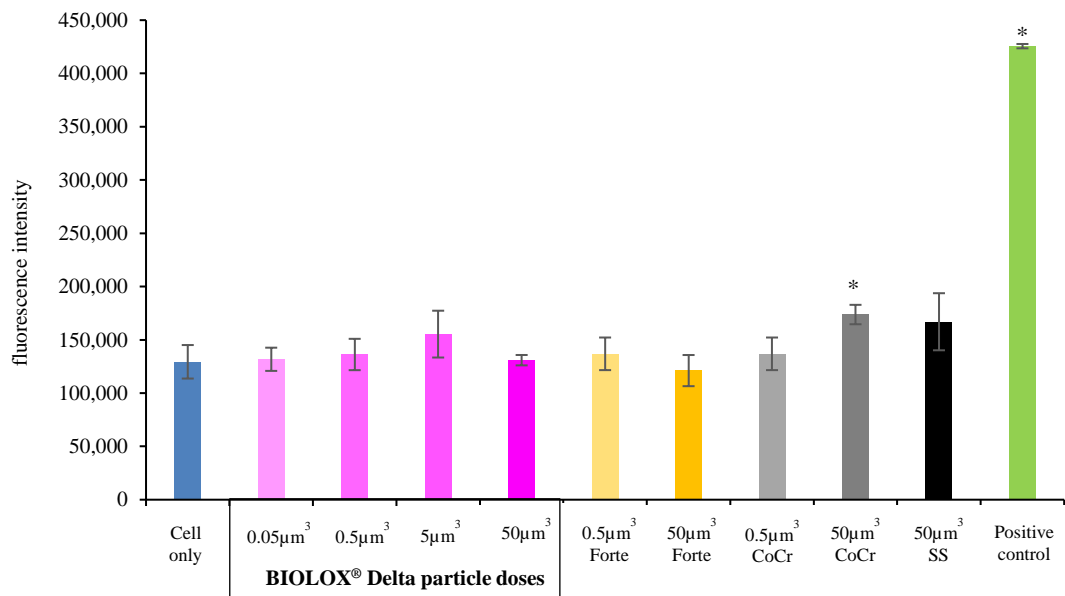


Figure 4.48 - Oxidative stress in PBMNCs isolated from Donor 25 in response to BIOLOX® Delta model ceramic particles. PBMNCs were cultured with bimodal sized micrometre/sub-micron and nanoscale composite (BIOLOX® Delta), alumina (BIOLOX® Forte) clinically-relevant ceramic wear particles, and clinically-relevant stainless steel and CoCr nano-particles for 24 hours. Oxidative stress was determined using a DCFDA probe to detect the production of reactive oxygen species, which is presented as mean fluorescent intensity. TBHP (200μM) was used as the positive control. A statistically significant different ($p < 0.05$ ANOVA) in fluorescence intensity compared to the cells only control is indicated by an asterisk (*). Error bars represent $\pm 95\%$ confidence limits ($n=6$).

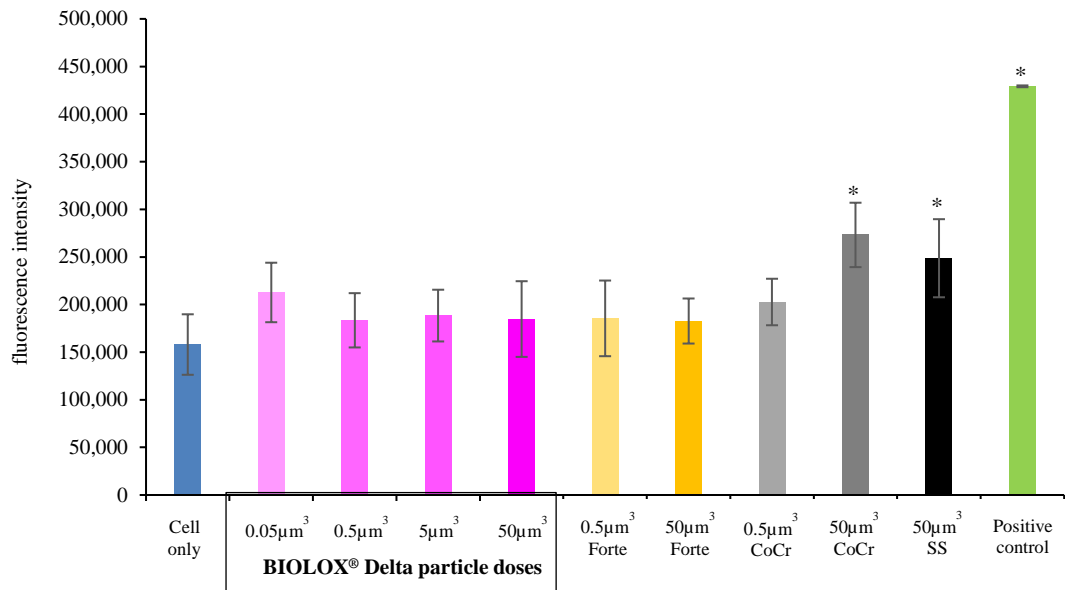


Figure 4.49 - Oxidative stress in PBMNCs isolated from Donor 26 in response to BIOLOX® Delta model ceramic particles. PBMNCs were cultured with bimodal sized micrometre/sub-micron and nanoscale composite (BIOLOX® Delta), alumina (BIOLOX® Forte) clinically-relevant ceramic wear particles, and clinically-relevant stainless steel and CoCr nano-particles for 24 hours. Oxidative stress was determined using a DCFDA probe to detect the production of reactive oxygen species, which is presented as mean fluorescent intensity. TBHP (200μM) was used as the positive control. A statistically significant difference ($p < 0.05$ ANOVA) in fluorescence intensity compared to the cells only control is indicated by an asterisk (*). Error bars represent $\pm 95\%$ confidence limits ($n=6$).

4.5 Discussion

The aim of this chapter was to assess the biological impact of model and clinically-relevant BIOLOX® Delta ceramic wear particles in terms of cytotoxicity, inflammation, genotoxicity and oxidative stress. In order to meet this aim, the cytotoxic effects of BIOLOX® Forte ceramic model particles, BIOLOX® Delta ceramic model particles and clinically-relevant BIOLOX® Delta ceramic wear particles on the viability of L929 murine fibroblast cells over a period of 6 days was initially investigated. Thereafter, a comprehensive evaluation of the biological impact of BIOLOX Delta ceramic model particles and clinically-relevant BIOLOX® Delta ceramic wear particles on PBMNCs in terms of cytotoxicity (viability), inflammation (release of TNF- α), genotoxicity (DNA damage) and oxidative stress (production of reactive oxygen species) was investigated and compared to BIOLOX® Forte ceramic model particles and clinically-relevant BIOLOX® Forte ceramic wear particles. The findings of this chapter are divided into the following sections: -

1. Characteristics of ceramic model particles compared to clinically-relevant ceramic wear particles
2. Cytotoxic effects of ceramic wear particles
3. Inflammatory response to ceramic wear particles
4. Genotoxic effects of ceramic wear particles
5. Oxidative stress in response to ceramic wear particles
6. Limitations of study

4.5.1 Characteristics of ceramic model particles compared to clinically-relevant ceramic wear particles

The work in Chapter 4 demonstrated that the wear particles generated from alumina (BIOLOX® Forte) and composite (BIOLOX® Delta) ceramic hip replacements in water lubricants were bimodal in size. The size of the wear particles generated from alumina (BIOLOX® Forte) ceramic hips had a very similar size distribution to those isolated from retrieved tissues by Hatton et al. (2001) using laser micro-dissection. Furthermore, the present study has demonstrated that there was no statistical significant difference in size distribution and morphology between the composite BIOLOX® Delta ceramic wear particles generated in serum or water under severe edge loading conditions caused by dynamic separation due to translational mismatch in the centres of rotation of the femoral head and acetabular cup. This suggested that the ceramic wear debris generated in water using the hip simulator were representative of the ceramic wear particles generated *in vivo*, and henceforth can be described as clinically-relevant.

The BIOLOX® Forte ceramic model particles described in this chapter also demonstrated a bimodal size range. What's more, there was no statistical significant difference in size

distribution and morphology between the BIOLOX[®] Forte ceramic model particles and clinically-relevant BIOLOX[®] Forte ceramic wear particles generated *in vitro* under severe edge loading conditions using the hip simulator. Both the model and clinically-relevant BIOLOX[®] Forte ceramic particles consisted of large shard-like alumina and small round alumina particles. The BIOLOX[®] Forte ceramic model particles ranged between 100-3000nm for the larger particles, with a mean size of 613nm, whereas the smaller nano-scale particles ranged between 10-80nm, with a mean size of 44nm. Similarly, the clinically relevant BIOLOX[®] Forte ceramic wear particles generated under severe edge loading conditions using the hip simulator, ranged between 100-4000nm for the larger particles, with a mean size of 736nm, whereas the smaller nano-scale particles ranged between 10-90nm, with a mean size of 50nm. However, the frequency size distributions suggested that the clinically-relevant BIOLOX[®] Forte ceramic wear particles had more particles in the nano-scale range compared to the BIOLOX[®] Forte ceramic model particles that had more particles in the submicron and micron size range. Nevertheless, both types of particles contained particles representative of the size range of particles isolated from retrieved tissues (Hatton, 2001). The similar size range between the two types of particles may be due to the fact that the BIOLOX[®] Forte ceramic model particles used in this study was comprised of the powder used to manufacture BIOLOX[®] Forte CoC hip components.

The BIOLOX[®] Delta ceramic model particles demonstrated a multimodal size distribution. The third mode of size distribution was due to the large grain-like structures of composite ZTA ceramic present in the BIOLOX[®] Delta powder. Hence, there was a significant difference in size distribution and morphology between the BIOLOX[®] Delta model ceramic particles and clinically-relevant BIOLOX[®] Delta wear particles generated *in vitro* using the hip simulator under severe edge loading conditions. The clinically-relevant BIOLOX[®] Delta ceramic wear particles generated in water in the simulator had two distinct modes (bimodal) of size distribution i.e. nano scale wear particles that ranged between 20-90nm (mean size: 48nm) and larger sized wear particles that ranged between 1000->5000nm (mean size: 3900nm). This bimodal size distribution was very similar to the BIOLOX[®] Delta wear particles isolated from hip simulator serum lubricant from BIOLOX[®] Delta CoC bearings tested under severe edge loading conditions as described in chapter 3 i.e. the larger alumina particles ranged between 100->5000nm (mean size: 2308) and the nano-scale particles range between 10-90nm (mean size: 44nm). Whereas, the BIOLOX[®] Delta model ceramic particles had a smaller size distribution, where the larger alumina particles ranged between 100-2000nm with a mean size of 508nm. The nano-scale particles however, had a similar size range (30-100; mean size: 64nm) to the clinically-relevant BIOLOX[®] Delta ceramic wear particles generated in the hip simulator under severe edge loading conditions. Even so, the frequency of the nano-scale particles for the BIOLOX[®] Delta model ceramic particles (11.7%)

was considerably lower than the frequency of nano-scale particles for clinically-relevant BIOLOX[®] Delta ceramic wear particles (26.6%). The difference in size distributions between the model and clinically-relevant BIOLOX[®] Delta ceramic particles may be due to the larger grain-like structures that were only present in the Delta model ceramic particles. These are formed during sintering where many elements in the form of raw compound materials are added to the mixture, which causes on going solid reaction and the production of these large grains and a complex ceramic microstructure. The larger alumina particles that exist in the clinically-relevant BIOLOX delta wear particle population may be as a result of grain pull-out during edge loading. These larger particles are present in the BIOLOX[®] Delta powder, however they exist within the alumina matrix, which can be observed at high magnifications as large grain-like structures using CFE-SEM. The wear particles generated from BIOLOX[®] Delta in water using the hip simulator had similar characteristics to those generated in serum, which suggested these wear particles can be considered clinically-relevant as they are more representative in terms of size and shape to those generated *in vivo* (Hatton et al., 2002). However, as previously mentioned in chapter 3, considerable stainless-steel wear particle contaminants were generated in the hip simulator, which need to be considered and mitigated for in the cell culture studies.

4.5.2 Cytotoxic effects of ceramic wear particles

Particles of composite ceramic (BIOLOX[®] Delta) have not been tested previously in terms of cytotoxic effects. Therefore, the first part of this study evaluated the cytotoxic effects of the increasing doses (0.05-500 μm^3 per cell) of composite ceramic model particles (BIOLOX[®] Delta) on L929 fibroblast cells and compared them with alumina ceramic model particles (BIOLOX[®] Forte) and clinically-relevant CoCr nano-particles that were generated using the six-station pin-on-plate wear simulator. The comparison with CoCr nano-particles was chosen as it is described in numerous studies in the literature that CoCr wear particles induce cytotoxic effects, which led to a decline in the use of MoM THR's (Germain et al., 2003a; Posada et al., 2015; Madl et al., 2015; Amanatullah et al., 2016). In addition, a comparison with wear particles from the early generation alumina BIOLOX[®] Forte CoC hips was also included, as many studies (Catelas, Petit, Marchand, et al., 1999; I Catelas, Petit, Zukor, et al., 1999; Nkamgueu et al., 2000a; Germain et al., 2003a; Faye et al., 2017) have reported the cellular response to commercially available alumina powder, which demonstrated mild cytotoxic effects that was dose dependent. Therefore, in the present study L929 fibroblast cells were exposed to increasing doses of BIOLOX[®] Forte alumina ceramic model particles ranging from 0.05-500 μm^3 per cell and the cytotoxic effects of the particles were assessed over a period of 6 days. The results showed that the highest dose (500 μm^3 per cell) of ceramic model particles for both BIOLOX[®] Forte and BIOLOX[®] Delta caused a significant reduction

in cell viability after 6 days when compared to the cell only negative control. All the other doses ($0.5\text{-}50\mu\text{m}^3$ per cell) for both BIOLOX[®] Forte and BIOLOX[®] Delta had a limited effect on the viability of the L929 cells, as no significant cytotoxic effects were observed when compared to the cell only negative control. Whereas, the CoCr nano-particles ($50\mu\text{m}^3$ per cell) had significant cytotoxic effects from day 1, which may have been due to the release of Co and Cr ions (Posada et al., 2014; Posada et al., 2015). The metal ions could have been released from the CoCr wear particles in the culture medium or within the cells once the particles were internalised. Many studies (Catelas, Petit, Marchand, et al., 1999; Catelas, Petit, Zukor, et al., 1999; Petit et al., 2002; Olivier et al., 2003; Tsaousi et al., 2010) have reported the cytotoxic effects of ceramic particles, the source, type, size and doses of these particles, in addition to the cell types used in these previous studies are shown in Table 4.14. Indeed, cytotoxicity in macrophages and fibroblasts was reported to increase in the presence of alumina wear particles, which was dependent on several factors including size and concentration. The results in the present study were in agreement with Catelas et al., (1999), who reported cytotoxic effects at high concentrations of alumina particles on J774 macrophages and that cell death increased with the size (1.3 and $2.4\mu\text{m}$) and concentration ($5\text{-}1500$ particles/cell) of the alumina particles. The authors reported that a higher concentration of smaller particles ($1.3\mu\text{m}$) compared to larger particles ($2.4\mu\text{m}$) was required to induce cytotoxic effects, thus demonstrating an overall volume effect. For example, to obtain almost the same percentage of cell death for $2.4\mu\text{m}$ at 500 particles per cell, 1500 particles per cell for $3\mu\text{m}$ alumina particles was required. Olivier et al. (2003) also demonstrated the cytotoxic effects of alumina particles ($0.43\mu\text{m}$ and $2.81\mu\text{m}$) at high concentrations ($0.025\text{-}0.5\text{mg/ml}$) in J774.2 macrophages. This study also demonstrated cytotoxic effects of alumina particles in L929 fibroblasts however alumina particle size of 0.43 did not affect the viability of L929 cells. The alumina particles were more cytotoxic for macrophages than fibroblasts (Olivier et al., 2003). This trend was also observed by Tsaousi et al. (2010), who demonstrated no significant differences in cell viability between the control and fibroblast cells treated with alumina nano-particles (0.2nm), at all doses ($0.1\text{-}10\text{mg/T75}$ flask) and time points ($24\text{-}120\text{hrs}$). Interestingly, Germain et al. (2003) in contrast demonstrated no cytotoxic affects in both U937 macrophages and L929 fibroblast cells cultured with commercial alumina ceramic particles ($0.5\mu\text{m}$) for all doses tested ($0.005\text{-}50\mu\text{m}^3/\text{cell}$). The discrepancies between the results may be partially explained by the use of particle sizes and particle doses which may not be clinically relevant. These studies used commercially-obtained alumina particles in the phagocytosable range of $0.3\text{-}10\mu\text{m}$ (Green et al., 1998), however it has been demonstrated in the present study and in previous studies that wear particles generated from ceramic hip replacements have a bimodal distribution of both micron sized and nano-scale particles (Hatton et al., 2002). Majority of these studies failed to address the nano-scale particle size

range in their cytotoxic assessment of alumina ceramic particles, which may potentially induce different cellular responses. Nonetheless, a direct comparison with these studies is valid as the model ceramic particles used in this part of the study were also commercially-obtained.

Germain et al. (2003) also used alumina wear particles generated *in vitro* under microseparation conditions using a hip simulator, as it is well established that these conditions simulate clinically-relevant wear patterns and wear mechanisms (Nevelos et al., 2000a). They reported that neither the clinically-relevant nor the ceramic powder demonstrated any cytotoxic effects on L929 cells for all the particle doses tested ($0.05\text{-}50\mu\text{m}^3$ per cell) throughout the 5-day culture period. However, the high volumetric concentrations of clinically-relevant alumina wear particles ($50\mu\text{m}^3$ per cell) caused a significant cytotoxic effect in U937 human macrophages, whereas at the same concentration the alumina powder had no cytotoxic effect. This difference in cytotoxicity seen in the U937 cells was attributed to the clinically-relevant alumina wear particles having more particles in the nanometre size range, which may be cytotoxic if taken up by cells at high volumes as nano-scale particles may release toxic ions. The model and clinically-relevant BIOLOX[®] Delta composite ceramic wear particles tested in the present study also demonstrated a similar pattern observed by Germain et al. (2003). The BIOLOX[®] Delta model ceramic particles had no effect on the viability of the L929 cells for all the particle doses tested ($0.05\text{-}50\mu\text{m}^3$ per cell), whereas the highest dose of $50\mu\text{m}^3$ per cell of clinically-relevant BIOLOX[®] Delta ceramic wear particles caused a significant reduction in cell viability after 3 days. Hence, despite the differences in composition between BIOLOX[®] Forte and BIOLOX[®] Delta, the same deduction can be made in the present study, in that the clinically-relevant BIOLOX[®] Delta composite ceramic wear particles may have had more particles in the nanometre size range, which may be cytotoxic if taken up by cells at high volumes. This suggestion is supported by the size distribution data of clinically-relevant BIOLOX[®] Delta ceramic wear particles and BIOLOX[®] Delta powder, which showed that there was a higher percentage number of nano-scale particles (mode size: 40-50nm) for the clinically-relevant BIOLOX[®] Delta ceramic wear particles (26.6%) compared to the number of nano-scale particles (mode size: 60-70nm) in the BIOLOX[®] Delta powder (11.8%). These findings were also in agreement with Catelas et al. (1998) and Catelas et al. (1999b) who showed that cell death increased with increasing concentrations of alumina particles ($0.6\text{-}4.5\mu\text{m}$), but is in disagreement with regards to particle size as the present study used both micron sized and nano-scale particles. These findings indicate that a particular threshold of wear particles in the biologically active size range may determine the severity of the biological response (Green et al., 1998; Ingham and Fisher, 2000).

The results from the present study suggest that BIOLOX[®] Delta ceramic particles exhibits similar biological activity as BIOLOX[®] Forte ceramic particles in terms of cytotoxicity,

despite the compositional differences. This was expected as zirconia, which is the second major constituent of BIOLOX[®] Delta after alumina, is reported to have a similar low cytotoxic potential as that of alumina (Catelas et al., 1998; Catelas, Petit, Marchand, et al., 1999; Faye et al., 2017). A study by Roualdes et al. (2010) reported the *in vitro* and *in vivo* effects of composite alumina-zirconia ceramic powder. They reported no deleterious effects *in vitro* on cell viability, extra-cellular matrix production (human type I collagen and fibronectin) or cell morphology in osteoblasts and fibroblasts. *In vivo*, the histology results showed no major inflammation of the synovial membrane with a very moderate and non-specific granulomatous reaction. Even so, the results from the present study demonstrated that high particle doses or volume concentrations (50-500 μm^3 per cell) of model and clinically-relevant BIOLOX[®] Delta ceramic wear particles caused significant cytotoxic effects in L929 cells. Hatton et al. (2001) reported that the mode of cytotoxicity induced by the particles at these high doses may have been due to physical damage by the high volume of debris masking the cells, which could have caused nutrient deficiency within the cells and as a result the cell viability was reduced. However, given the low wear rates of ceramic-on-ceramic bearings, it is highly unlikely that these particle doses will be achieved *in vivo*. Nevertheless, osteolysis has been associated with CoC bearings *in vivo*, but this has generally been limited to isolated cases of excessive wear (Shishido et al., 2006; Nam et al., 2007). It can be concluded from the cytotoxic evaluation of BIOLOX[®] Delta ceramic wear particles that this composite ceramic (ZTA) is relatively bioinert and concerns around its cytotoxic potential are limited (Santos et al., 2009). However, a study by Petit et al. (2002) highlighted the particle-induced apoptosis phenomenon in J774 macrophages by alumina particles. The authors hypothesised that the ability of alumina particles to induce apoptosis in macrophages may explain the lower levels of inflammatory cytokines (TNF- α) and the differences observed in osteolysis patterns between different types of THR i.e. ceramic, metal and polyethylene. Hence, in addition to cytotoxicity testing, this study set out to conduct a more comprehensive evaluation of composite ceramic wear particles in terms of inflammation, genotoxicity and oxidative stress.

Table 4.14 – Summary of previous studies that have investigated the biological response to ceramic particles

Authors	Cell type	Particle type and mean size	Particle source	Dose	Biological test	Conclusion
(Nagase et al., 1995)	human polymorphonuclear leukocytes	Alumina - 0.6, 0.8, 3.2, 7.5, 28 and 68µm	Commercially-obtained	1mg.ml ⁻¹	Production of reactive oxygen metabolites - chemiluminescence assay	Particle size of around 3µm caused the maximal production of reactive oxygen metabolites.
(Catelas et al., 1998)	J774 macrophage cell line	Alumina – 0.6, 1.3, 2.4, 4.5µm Zirconia- 0.6µm HDP – 4.5µm	Commercially-obtained	5-1250 particles per macrophage.	Cell mortality – Flow cytometry Production of TNF-α – ELISA	Macrophage response was dependent on size and concentration. Cell mortality increased with increased size (>2µm) and concentration of particles. TNF-α release increased with concentration of zirconia (0.6µm) and alumina (4.5µm) particles. TNF-α release was directly affected by particle concentration and composition.
(Catelas, Petit, Marchand, et al., 1999)	J774 macrophage cell line	Alumina – 0.6, 1.3, 2.4, 4.5µm Zirconia- 0.6µm HDP – 4.5µm	Commercially-obtained	5-2500 particles per macrophage	Cytotoxicity - Flow cytometry Inflammatory mediator tests (TNF-α, IL-1α, IL-1β)	Macrophage mortality increased with both particle size and concentration (volume effect). Higher concentration of smaller particles (1.3µm) compared to larger particles (2.4µm) was required to induce cytotoxic effects. TNF-α release increased

						with particle size and concentration. Lower concentrations of particles were required to stimulate production of TNF- α .
(I Catelas, Petit, Zukor, et al., 1999)	J774 macrophage cell line	Alumina – 0.6, 1.3, 2.4, 4.5 μ m Zirconia- 0.6 μ m HDP – 4.5 μ m	Commercially-obtained	5-500 particle per macrophage	Apoptosis – fluorescence microscopy and DNA laddering	Apoptosis increased with particle size and concentration. Induction of apoptosis reached plateau for concentrations higher than 150 particles/macrophage at 1.3 μ m.
(Nkamgueu et al., 2000b)	Human monocytes differentiate into macrophages	Alumina- 55-141 μ m (mean: 73 μ m) Zirconia- 80-175 μ m (mean: 133 μ m)	Commercially-obtained	5, 10, 30, 60mg	Changes in elemental composition – X-ray microanalysis. Cell viability – trypan blue exclusion assay Oxidative burst measurement – DCFH-DA oxidation assay	Zirconia and alumina particles affected the intracellular electrolyte concentration, where sodium concentration increased and potassium content decreased, thus resulting in increased cell mortality. The changes in cellular ionic concentration reduced phagocytic activity and oxidative metabolism, thus resulting in reduced production of hydrogen peroxide
(Petit et al., 2002)	J774 macrophage cell line	Alumina – 1.3 μ m UHMWPE – 0.5-2 μ m	Commercially-obtained	25, 125 and 250 particles/macrophage	Production of TNF- α – ELISA Apoptosis measured by protein expression of PARP and caspase-3 - Bio-Rad protein assay and western blot	UHMWPE induced higher (8-10 times) levels of TNF- α release compared to alumina particles. Induction of apoptosis was expressed higher in cells cultured with alumina particles compared to UHMWPE particles.

(Germain et al., 2003b)	U937 human histiocytic and L929 mouse lung fibroblast cell lines	Clinically-relevant CoCr – 29.5nm (range size: 5-200nm). Commercial CoCr particles– 9.87µm. Clinically-relevant alumina – Larger particles were 0.1- >10µm and smaller particles were 5-20nm. Commercial alumina powder– 0.5µm	Clinically-relevant CoCr wear particles generated using pin-on-plate tribometer and clinically-relevant ceramic particles generated using hip wear simulator. Commercially-obtained CoCr and alumina particles	50, 5, 0.5, 0.05 and 0.005µm ³ per cell	Cell viability – ATP-Lite assay	Clinically-relevant CoCr particles at dose 50 and 5µm ³ per cell reduced the viability of U937 cells by 97% and 42% and reduced the viability of L929 cells by 95% and 73%, respectively. The commercial CoCr and commercial alumina particles demonstrated no cytotoxic affects in both U937 and L929 cells.
(Hatton et al., 2003a)	Human primary peripheral blood mononuclear phagocytes	Clinically-relevant alumina – Larger particles were 0.1- >10µm and smaller particles were 5-20nm. Commercial alumina powder– 0.5µm	Commercially-obtained. Clinically-relevant particles generated using hip wear simulator.	0.1, 1, 10, 100µm ³ per cell	Cell viability – MTT assay Measurement of TNF-α release - ELISA	All six donors produced significantly elevated levels of TNF-α when stimulated with 100µm ³ , whereas PBMNCs from only three of the six donors released significantly elevated levels of TNF-α when stimulated with 100µm ³ of the clinically-relevant alumina wear particles. All donors released significant levels of TNF-α when

						stimulated with 500 μm^3 of clinically-relevant alumina wear particles.
(Warashina et al., 2003)	Murine calvarial osteolysis model (60 CL/BL6 male mice aged 12 weeks)	Alumina – 2.1 μm Zirconia-1.5 μm Titanium – 1.1 μm High density particles (HDP)- 4.1 μm	Commercially-obtained	1x10 ⁹ particles per ml	Release of IL-1 β , IL-6 and TNF- α - ELISA	The levels of IL-1 β and IL-6 were significantly elevated in response to HDP and titanium particles. Any particle type did not increase the levels of TNF- α . There were no significant differences observed in the levels of proinflammatory cytokines in response to alumina and zirconia particles.
(Olivier et al., 2003)	J774.2 macrophages and L929 fibroblasts	Alumina – 0.43 and 2.81 Polystyrene beads – 0.45 and 3.53	Commercially-obtained	Alumina - 0.01, 0.025, 0.05, 0.1, 0.5mg/ml Polystyrene beads – 0.5 and 1.0mg/ml	Cytotoxicity – trypan blue exclusion assay Apoptosis – Cell DNA analysis and Annexin V assay Release of IL-6 – ELISA	The alumina particles at both sizes and 1.0mg/ml polystyrene beads caused a significant decrease in cell number with increase in particle concentration. Particle size of 0.43 for alumina did not affect the viability of L929 cells. Particles were more cytotoxic for macrophages than fibroblasts. The death in macrophages was a combination of necrosis, caused mainly by 3.53 polystyrene beads and apoptosis caused mainly by 0.45 polystyrene beads.

						Release of IL-6 had a non-linear correlation with cytotoxicity i.e. increase in cytotoxicity caused increase in release of IL-6.
(Granchi et al., 2004)	Human osteoblasts Osteoclast precursors obtained from PBMCs from donor blood.	Alumina – 1µm UHMWPE – information on size not provided	Alumina was commercially-obtained UHMWPE was generated using CoCr vs. UHMWPE ball on a flat system.	1, 0.1, 0.01, 0.001mg/ml	Cell viability- Alamar blue Commercially available reagents were used for the immunoenzymatic determination of IL6, TNF α , GM-CSF, OPG and RANKL. Osteoclast formation	The alumina and UHMWPE particles did not affect either cell viability or TNF α and GM-CSF release. The release of IL-6 increased with particle concentration. UHMWPE increased the release of RANKL from HOB, while OPG and OPG-to-RANKL ratio were significantly inhibited. UHMWPE particles induced a large amount of multinucleated TRAP-positive giant cells, as well as significantly reduced the levels of IL6, GM-CSF and RANKL. This study showed that alumina was less inductive in terms of osteoclastogenesis.
(Rodrigo et al., 2006)	J774 cells and primary human osteoblasts	Alumina - 4µm (average diameter)	Commercially-obtained	1, 10, 50, 100, and 1mg/well	Release of IL-6 and GM-CSF – ELISA Expression of IL-6 - PCR	The levels of TNF- α were increased when J774 cells were treated with the higher doses (50 & 100mg/well) of alumina particles, but the release of TNF- α was lower when cells were cocultured with

						osteoblasts. The release of IL-6 by J744 cells was only significant when co-cultured with osteoblasts, in the presence of 50mg/well of alumina particles. Significant levels of IL-6 and GM-CSF were released from osteoblasts when stimulated with 10mg/well of alumina particles, reaching a plateau at 50mg/well. The levels of IL-6 and GM-CSF were significantly increased when osteoblasts were co-cultured with J744 cells at 50mg/well of alumina particles.
(Tsaousi et al., 2010)	Primary human fibroblasts	Alumina - Mean grain size 0.2nm CoCr – 0.56-4.74µm	Commercially-obtained	0.1–10 mg/T-75 flask	Cell viability - The trypan-blue exclusion method Genotoxicity - Micronucleus Cyt-B assay Immunostaining of gamma-H2AX foci - used as a marker of DNA double-strand breaks	There were no significant differences in cell viability between control and ceramic treated cells, at all doses and time-points studied. Cells treated with CoCr particles showed both dose- and time-dependent cytotoxicity. The induction of micronuclei was unaffected by the size or shape of the ceramic particles. There was an increase in micronucleated binucleate cells after treatment with CoCr particles. There was

						no increase in gamma-H2AX foci in cells exposed to ceramic particles, whereas there was a significant increase of these foci in cells treated with CoCr particles.
(Faye et al., 2017)	Dermal fibroblasts	Alumina or cerium-zirconia particles (50nm)	Commercially-obtained	100 and 500µg ml ⁻¹	Cell morphology, cytoplasmic ceramic incorporation - using confocal and transmission electron microscopy Cell migration -silicon insert. Sedimentation field-flow fractionation -used to evaluate the rate of incorporation of ceramic particles into the cells.	Both alumina and cerium-zirconia ceramic particles did not cause any deleterious effects on cultured cells. Confocal and electron microscopy showed that both the alumina and cerium-zirconia particles were internalized in the cells. The fluorescent membrane labelling and fluorescent alumina particles showed that a membrane formed around the particle-containing vesicles present in the cytoplasm.

4.5.3 Inflammatory response to ceramic wear particles

The inability of macrophages to degrade wear particles causes them to release pro-inflammatory cytokines for the recruitment, migration and stimulation of other cell types to the site of the foreign wear particles. As a result, the formation of a granulomatous periprosthetic tissue, which is rich in macrophages, forms around the implant to isolate the foreign matter from the surrounding tissues (Ingham and Fisher, 2005). These mediators and cytokines affect the behaviour of many cell types, particularly the interaction of osteoblasts, osteoclasts and fibroblasts which ultimately causes bone loss that can lead to osteolysis. TNF- α is a key osteolytic cytokine released by macrophages stimulated by wear particles and is reported to play an important role in osteolysis, and has been found in high levels around osteolytic implants (Ingham and Fisher, 2000). Therefore, this pro-inflammatory cytokine was used in the present study as a marker of the osteolytic response from PBMNCs in response to different doses of BIOLOX[®] Delta composite ceramic wear particles. In addition, the viability of the PBMNCs in response to the particles was measured after the 24hr culture period. The cellular response was compared with low ($0.5 \mu\text{m}^3$ per cell) and high ($50\mu\text{m}^3$ per cell) doses of the BIOLOX[®] Fore alumina ceramic wear particles. In addition, the cellular response was also compared to clinically-relevant CoCr nano-particles, which is known to induce cytotoxic and inflammatory responses (Posada et al., 2015). The cell viability and TNF- α release from PBMNCs was initially investigated in response to model ceramic particles before testing the cellular response to clinically-relevant ceramic wear particles that were generated using the hip simulator under edge loading conditions.

There was no significant effect on the viability of PBMNCs from all the five donors in response to all the conditions for both the model and clinically-relevant BIOLOX[®] Delta composite ceramic wear particles. This trend was also true for the CoCr nano-particles, which showed no significant effect on cell viability compared to the cell only negative control. This limited response in terms of cell viability may have been due to the short 24hr culture period with the wear particles and was in agreement with a study by Hatton et al. (2003), who also reported the same observation with PBMNCs cultured with alumina powder or alumina wear debris generated under microseparation conditions using the hip simulator. The levels of TNF- α produced by PBMNCs (all donors) in the present study also showed no significant difference compared to the cell only negative control in response to the BIOLOX[®] Delta model ceramic particles, for all the particle volumes tested ($50\text{-}500\mu\text{m}^3$ per cell). This was also the case for the BIOLOX[®] Forte model ceramic particles at low ($0.5 \mu\text{m}^3$ per cell) and high ($50\mu\text{m}^3$ per cell) volumetric concentrations. Several authors (Table 4.14) have suggested similar findings such as Catelas et al. (1998) who reported higher levels of TNF- α release were associated with high density polyethylene particles (size: $4.5\mu\text{m}$) compared to alumina

(size range: 0.6 – 4.5 μm) and zirconia (size: 0.6 μm) commercial particles. These authors used commercially obtained particles in the phagocytosable size range (<5 μm) and reported a direct positive correlation between TNF- α release and particle concentration. The lower levels of TNF- α release in response to alumina particles compared with UHMWPE particles (8-10 times higher) was also described by Petit et al. (2002), who reported that TNF- α release was much more intense with UHMWPE (size range: 0.5-2 μm) compared to high density polyethylene particles (size: 4.5 μm) used by Catelas et al. (1998), which is indicative of the importance of particle size in immune response. Petit et al. (2002) hypothesised that the lower levels of TNF- α associated with the alumina particles may be due to the ability of the alumina particles to induce macrophage apoptosis, which was observed through apoptotic DNA fragmentation. The suppression of inflammatory cytokine release through programmed cell death in response to ceramic particles may explain the low biological impact of ceramic hip replacements (Warashina et al., 2003). The differences between biological activity of ceramic wear particles compared to UHMWPE wear particles was also reported by Granchi et al. (2004), who described alumina particles as being less inductive of osteoclastogenesis compared to polyethylene wear particles. The authors found polyethylene wear particles increased the release of RANKL, whilst simultaneously decreasing the release of OPG, which as mentioned earlier is an inhibitor of osteoclastogenesis. Hence, these authors demonstrated that model ceramic particles were less active in promoting osteoclast formation, thus reducing the risk of bone resorption. The low biological activity of ceramic particles has been emphasised in many studies by comparing with polyethylene wear particles, which is extensively reported in the literature to cause osteolysis. However, the low-density of polyethylene wear particles presents difficulties whereby it is inherently difficult to manipulate in *in vitro* studies as it is less dense than culture medium and invariably floats on the medium surface preventing interaction with cultured monolayers of macrophages. Therefore, clinically-relevant CoCr nano-particles were used in the present study to compare the biological activity of ceramic particles. Like the low doses of model ceramic particles (0.05-5 μm^3 per cell), the low dose (0.5 μm^3 per cell) of clinically-relevant CoCr nano-particles cultured with PBMNCs also showed no significant increase in TNF- α release compared to the cells only negative control (all donors). Whereas, the high dose (50 μm^3 per cell) of clinically-relevant CoCr nano-particles caused a significant increase in the levels of TNF- α released from PBMNCs for all the donors when compared to the cell only negative control. The release of osteolytic cytokines in response to CoCr wear particles from MoM implants has been reported in numerous studies such as Brown et al. (2006) who reported high levels of TNF- α production from PBMNCs in response to 50 μm^3 per cell volumetric concentration of clinically-relevant CoCr wear particles.

The model ceramic particles (BIOLOX[®] Forte and BIOLOX[®] Delta) used in the present study did not stimulate PBMNCs (all donors) to produce significant levels of TNF- α compared to the cell only control. In contrast the highest dose (50 μm^3 per cell) of clinically-relevant BIOLOX[®] Forte and BIOLOX[®] Delta wear particles incited the PBMNCs from all donors to produce significantly higher levels of TNF- α compared to cell only negative control. All the other doses (0.05-5 μm^3 per cell) of clinically-relevant ceramic wear debris from both BIOLOX[®] Forte and BIOLOX[®] Delta failed stimulate a significant response in terms of TNF- α release from PBMNCs for all donors. The levels of TNF- α produced by the PBMNCs in response to LPS varied greatly between the five different donors evaluated in this study. This was perhaps due to the heterogeneity of human individuals as the response is determined by polymorphisms in the TNF promoter gene, which affects the susceptibility and severity of different human diseases (El-Tahan et al., 2016). Polymorphisms within genes that encode the pro-inflammatory cytokines (TNF- α , IL-1 and IL-6) associated with osteolysis may influence the risk of developing osteolysis after total hip replacement (Wilkinson et al., 2003; Gordon et al., 2008). The present study clearly demonstrated the varied response to wear particles between donors, which has been previously reported for UHMWPE wear particles (Matthews, Green, et al., 2000a). In the present study, the response of PBMNCs from donor 2 to LPS was consistently between 1.8- 2.3 times greater than that of the other donors, hence this donor was categorised as a more aggressive responder.

Nevertheless, despite the inherent variability between donors in terms of TNF- α release, the results were relatively consistent with respect to the dose of particles that stimulated a significant inflammatory response. The high levels of TNF- α released from PBMNCs (all donors) in response to clinically-relevant ceramic wear particles was initially attributed to the stainless-steel wear particle contaminants that may have been present within the culture of PBMNCs and ceramic wear particles. This was because CFE-SEM and EDX analysis of the ceramic wear particles generated *in vitro* using the Leeds II hip simulator revealed an abundance of stainless steel particle contaminants for both BIOLOX[®] Forte and BIOLOX[®] Delta particle samples, a limitation of this study that was described in chapter 3. The separation of the stainless-steel wear particles contaminants from the ceramic wear debris was extremely difficult, and so the ceramic wear particles cultured with the cells contained a mixed population of ceramic and stainless-steel wear particles. EDX mapping of the mixed population of BIOLOX[®] Delta ceramic and stainless-steel wear particles revealed that approximately $47.06 \pm 42.75\%$ ($\pm\text{CL}$) of the wear particles were ceramic (chapter 3). The percentage ratio between BIOLOX[®] Forte and stainless-steel wear particle was also similar ($44.13 \pm 31.48\%$ ($\pm\text{CL}$)). To mitigate the potential biological effects of these stainless-steel wear particle contaminants and elucidate the biological impact of the clinically-relevant ceramic wear particles, it was necessary to include a stainless-steel wear particle control. The

stainless-steel wear particle control was generated from 316L medical grade stainless-steel pins and plates using the six-station pin-on-plate wear rig (Lee, 2016). Lee et al., (2016) reported that these stainless-steel wear particles had no adverse effects on cell viability (primary astrocytes and microglia) over a 5-day culture period, for all the particle doses tested (0.5-50 μm^3 per cell). The highest dose (50 μm^3 per cell) of the stainless-steel wear particles did however produce significant levels (29.9pg.ml⁻¹) of TNF- α from primary astrocytes and microglia compared to the cell only negative control (no TNF- α released) after a 2-day culture period. However, these levels of TNF- α production were minimal when compared to the PBMNCs negative control in the present study, which produced between 12.7 - 34.6 pg/ml of TNF- α . Hence, the cytotoxic and inflammatory effects of the stainless-steel wear particles were limited, and the concerns for positive misleading results in response to the stainless-steel wear particle contaminants generated from the Leeds II hip simulator was minimal. Even so, the presence of the stainless-steel particles has some clinical-relevance, as they have been identified in retrieved tissues from hip prostheses. The source of these particles has been attributed to the fretting corrosion of the taper and so stainless-steel wear particles most definitely have the potential to invoke a biological response (Xia et al., 2017). Lee et al., (2016) reported significant DNA damage in primary astrocytes and microglia in response to all doses (5-50 μm^3 per cell) of stainless-steel particles. These genotoxic effects will therefore need be considered in this study when reporting the genotoxic effects of clinically-relevant ceramic wear particles in PBMNCs.

Considering the findings of Lee et al. (2016) regarding the cellular response to stainless-steel wear particles, it can be elucidated that the highest dose (50 μm^3 per cell) of clinically-relevant ceramic wear particles for both BIOLOX[®] Forte and BIOLOX[®] Delta, in fact caused significant levels of TNF- α produced from PBMNCs for all the donors. There is very limited literature on the biological activity of clinically-relevant ceramic wear particles generated from hip replacements as only two other studies (Germain et al., 2003a; Hatton et al., 2003a) used clinically-relevant ceramic wear particles to investigate the *in vitro* biological response to wear particles generated from ceramic hip replacements. These studies used the same BIOLOX[®] Forte alumina powder that was used in this study. But, the findings in this study were relatively dissimilar to the findings reported by Hatton et al. (2003) in that the highest dose (50 μm^3 per cell) of clinically-relevant BIOLOX[®] Forte and BIOLOX[®] Delta ceramic wear particles caused a significant increase in the levels of TNF- α released compared to the cell only negative control. The BIOLOX[®] Forte and BIOLOX[®] Delta model ceramic particles failed to stimulate a significant inflammatory response in terms of TNF- α release for all the particle volumes tested. Whereas Hatton et al. (2003) found that the BIOLOX[®] Forte alumina powder caused significantly elevated levels of TNF- α when stimulated with 100 μm^3 per cell. The lower doses (1-10 μm^3 per cell) of alumina powder showed the same response as the

present study, in that none of the donors produced significantly elevated levels of TNF- α . The differences in TNF- α release for the model ceramic particles may be because the highest dose used by Hatton et al., (2003) was double that used in this study ($50\mu\text{m}^3$ per cell). But, at dose $50\mu\text{m}^3$ per cell for the clinically-relevant or microseparation alumina ceramic wear particles, Hatton et al. (2003) reported that they failed to stimulate a significant response in terms of TNF- α release for three out of six donors. Only when the PBMNCs were stimulated with the highest dose ($500\mu\text{m}^3$ per cell) of microseparation alumina ceramic wear particles did all the donors produce significant levels of TNF- α . The authors postulated that the clinically-relevant or microseparation alumina ceramic wear particles had a greater size range and that a greater volume of clinically-relevant ceramic wear particles was required to produce similar levels of TNF- α release compared with alumina powder. The results of the present study are in contrast to this, where the model ceramic wear particles for both BIOLOX[®] Forte and BIOLOX[®] Delta were less stimulatory in terms of TNF- α release compared to the clinically-relevant ceramic wear particles for both BIOLOX[®] Forte and BIOLOX[®] Delta CoC bearings. This may have been due to the clinically-relevant BIOLOX[®] Delta ceramic wear particles having a greater size distribution and more larger particles in the phagocytosable range (up to $4.5\mu\text{m}$) compared to the BIOLOX[®] Delta model ceramic particles as demonstrated by their frequency size distributions. Thus, a lower concentration or volume of particles was required to illicit an immune response. This was supported by Catelas et al. (1998) who reported that particle size and concentration determined the macrophagic response, where TNF- α release increased with alumina particle concentration. These authors stated that macrophages respond to particle volume rather than particle number. However, the same cannot be said for the BIOLOX[®] Forte model ceramic particles and clinically-relevant BIOLOX[®] Forte ceramic wear particles as there was no significant difference in characteristics of the particles in terms of size distribution and morphology. Nevertheless, the clinically-relevant BIOLOX[®] Forte ceramic wear particles had a slightly larger size distribution compared to the BIOLOX[®] Forte ceramic model particles, and so like the clinically-relevant BIOLOX[®] Delta ceramic wear particles a lower concentration or volume of particles was required to illicit an immune response, when compared to the ceramic model particles. This possible suggestion may have been a contributing factor towards the stimulation of significantly elevated levels of TNF- α release. However, this is speculative and PBMNCs cultured with higher volumes of ceramic particles, may have given light to this observation. The only other possible explanation may be due to the presence of unknown contaminants from *in vitro* wear simulation, which may have caused a positive immune response. Nevertheless, despite the differences between this present study and the study conducted by Hatton et al. (2003), the same conclusion can be drawn in that given the low wear rates ($0.1\text{-}1\text{mm}^3$ per million cycles) of ceramic-on-ceramic bearings, these high volumes or doses of ceramic wear particles ($50\text{-}500\mu\text{m}^3$ per cell) may never be achieved

in vivo, even under malpositioning conditions. Hence, it can be concluded that CoCr hip replacements have very limited osteolytic potential as they failed to stimulate pro-inflammatory cytokine (TNF- α) production.

4.5.4 Genotoxic effects of ceramic wear particles

Genotoxicity in patients with MoM hips is of great concern regarding CoCr wear particles as previous studies have reported chromosome aberrations in patients with MoM implants (Ladon et al., 2004; Suner et al., 2012). Therefore, this study investigated the genotoxic effects of model and clinically-relevant ceramic wear particles in PBMNCs. The BIOLOX[®] Delta model ceramic particles had no significant effect on the level of DNA damage in PBMNCs from all donors when compared to the cell only negative control. Similarly, the BIOLOX[®] Forte model ceramic particles and clinically-relevant CoCr nano-particles at low dose (0.5 μm^3 per cell) caused no significant DNA damage in all the donors, when compared to the cell only negative control. However, the high dose (50 μm^3 per cell) of BIOLOX[®] Forte model ceramic particles triggered significant levels of DNA damage compared to the cell only negative control in all donors, except in donor 5. Tsaousi et al., (2010) reported that alumina ceramic particles are weakly genotoxic compared to CoCr particles. This conclusion was based upon ceramic particles (fibres, nano-particles and micro-particles) at high doses (2mg/T-75 flask or 12.5 $\mu\text{g}/\text{ml}$) causing significant increases in chromosome loss and polyploidy in primary human fibroblasts, but no DNA double-strand breaks were detected. However, the results from the present study clearly showed that high doses of model alumina particles cultured with PBMNCs can induce DNA damage, which was notably higher than the DNA damage caused by clinically-relevant CoCr nano-particles (50 μm^3 per cell) in donors 5 and 7. The difference in DNA damage observed between Forte and Delta may be due to the Forte having more submicron alumina particles compared to Delta. This is because during sintering of the Forte powder, magnesium is added to increase the growth of the grains resulting in larger particles, which may have caused significant levels of DNA damage compared to Delta that has finer particle granules. Furthermore, the compositional differences may have also been a contributing factor as Forte consists of alumina stabilised by yttria, whereas Delta consists of ZTA composite ceramic. These differences in composition can affect the agglomeration properties of the nano-particles in solution with low pH levels. The internalisation by macrophages of alumina particles within vesicles, could have exposed the alumina particles to lysosomes that create acidic conditions in order to activate the lysosomal enzymes, whose function is to break down any material present within the vesicle. These acidic conditions could have caused deagglomeration of the alumina nano-particles and potentially induced adverse effects within the cells such as DNA damage (Parry et al., 2010; Sood et al., 2011), which was clearly observed in the present study for alumina model ceramic

particles. The submicron alumina particles from Forte may suspend differently in solution compared to Delta, which may also explain the difference observed in terms of DNA damage. This statement was made as it was during preparation of the Delta and Forte model particle solutions for filtration and characterisation, it was observed that the Forte alumina powder created a cloudy solution whereas the Delta ZTA powder settled at the bottom of the universal tube. This may have been due to the two materials having different agglomeration stability/particle dispersion at the pH of water, which may also result in difference in particle generation. However, this is highly speculative and requires further investigation. Furthermore, it is evident from the literature that ceramic hip replacements do not release ions during service (Kretzer et al., 2018). The clinically-relevant CoCr nano-particles at high doses ($50\mu\text{m}^3$ per cell) consistently induced significant levels of DNA damage in PBMNCs from all donors. This was expected as it is documented in the literature that CoCr wear particles, particularly in the nano-scale size range (30 nm) induce more DNA damage than micrometre sized particles ($2.9\mu\text{m}$) (Papageorgiou et al., 2007). Furthermore, Parry et al., (2010) reported that CoCr nano-particles at a threshold of $0.0036\text{mg}/\text{cm}^2$ caused DNA double strand breaks and ten-times lower threshold of $0.00036\text{mg}/\text{cm}^2$ caused chromosome aberrations. However, these doses were much greater than the wear rates of well-functioning implants, but potentially in line with the wear rates of mal-positioned MoM THR, thus the phenomenon of such DNA damage may occur *in vivo*.

The clinically-relevant BIOLOX[®] Forte ceramic wear particles at high doses ($50\mu\text{m}^3$ per cell) also caused significant levels of DNA damage in PBMNCs from all donors. In addition, the clinically-relevant BIOLOX[®] Delta ceramic wear particles at high doses ($50\mu\text{m}^3$ per cell) caused significant levels of DNA damage in four donors (5, 7, 25 and 26) when compared to the cell only negative control. What's more, at a dose of $5\mu\text{m}^3$ per cell, significant levels of DNA damage was observed for the clinically-relevant BIOLOX[®] Delta ceramic wear particles for three donors (5, 7 and 26). This was also evident for the clinically-relevant BIOLOX[®] Forte ceramic wear particles at low doses ($0.5\mu\text{m}^3$ per cell), where there were significant levels of DNA damage for donors 5, 7 and 25. The significant genotoxic effects caused by clinically-relevant BIOLOX[®] Delta ceramic wear particles and low doses of clinically-relevant BIOLOX[®] Forte ceramic wear particles were attributed to the presence of stainless-steel wear particle contaminants in the co-culture. This was supported by results for the stainless-steel wear particle control, which demonstrated significant levels of DNA damage at doses of $50\mu\text{m}^3$ per cell. This was in agreement with the findings of Lee et al. (2016), who reported significant DNA damage in primary astrocytes and microglia in response to all doses ($5-50\mu\text{m}^3$ per cell) of stainless-steel particles. Due to the presence of stainless-steel wear particle contaminants, the results ascertained from the experiments that investigated the genotoxic effects of the clinically-relevant ceramic wear debris are considered to be

unreliable, as the stainless-steel wear particles control demonstrated significant DNA damage compared to the cells only negative control. Nevertheless, the findings from the clinically-relevant Forte wear particles support the findings from the genotoxic assessment of the model ceramic particles, as the stainless-steel wear particles were also in the submicron range and also caused DNA damage. This study showed that the biocompatibility of a material in bulk form can change when the particulate form is considered and subtle but detrimental changes such as DNA damage, that are often missed during cytotoxic evaluation of biomaterials, may be observed.

4.5.5 Oxidative stress in response to ceramic wear particles

The generation of reactive oxygen species (ROS) induced by particles also plays a vital role in genotoxicity. High levels of ROS can lead to oxidative stress within cells, which in turn can cause DNA damage and unregulated cell signalling that can eventually result in cell mortality, apoptosis and even carcinogenesis (Fu et al., 2014). Raghunathan et al. (2013) reported that genotoxicity in fibroblasts caused by exposure to CoCr wear particles is facilitated by reactive oxygen species (Raghunathan et al., 2013). It is well known that CoCr wear particles and ions released from MoM hips cause oxidative stress. Behl et al. (2013) reported that $50\mu\text{m}^3$ per cell of clinically-relevant CoCr nano-particles caused high levels of oxidative stress as observed by very strong signals of fluorescence. This was also observed in the present study with the high dose ($50\mu\text{m}^3$ per cell) of clinically-relevant CoCr nano-particles, which caused a significant increase in the levels of oxidative stress in PBMNCs from all donors as indicated by the high levels of fluorescence intensity. The quantitative method of assessing the level of reactive oxygen species production in the present study was much more reliable than the qualitative method used by Behl et al. (2013), which used post-image analysis of the fluorescence microscopy images to quantify and determine the level of oxidative stress within the cells (Behl et al., 2013). Measuring cell fluorescence from images using computer software comes with many limitations including poor image quality, which can make it difficult to accurately draw around the boundary of fluorescent cells and compute meaningful measurements. Other studies (Armstead et al., 2017; Fleury et al., 2006) also reported similar findings with high levels of oxidative stress associated with CoCr particles and highlighted that oxidative stress was mostly attributed to the combined effects of nanoparticles and ion release from the CoCr wear particles. Fleury et al. (2006) reported that oxidative stress induced by Co and Cr ions in MG-63 osteoblast cells was due to protein oxidation and protein nitration, which are biomarkers for oxidative stress. The study showed that the redox state of osteoblasts was disturbed and in turn this caused deleterious effects on protein function within the cells. The cytotoxic effects were also attributed to down-regulation of antioxidant enzymes by Co ions, which would have otherwise protected the cells from

oxidative stress induced by these ions. The *in vivo* detection of oxidative stress in tissues from patients with total hip replacements was reported by Steinbeck et al. (2014) who looked for the presence of five markers (high mobility group protein-B1; cyclooxygenase-2; inducible nitric oxide synthase; 4-hydroxynonenal; and nitrotyrosine) associated with oxidative stress. These authors found that all five markers were present in increased amounts in patient tissues revised for osteolysis when compared to normal tissues. These authors also found the markers were expressed at the high levels in localised regions with wear debris and chronic inflammation. These studies highlight the role oxidative stress can play in the inflammatory response to total hip replacements, leading to osteolysis and implant failure (Steinbeck et al., 2014). Hence, the nano-scale nature of wear particles from ceramic hip replacements poses great concern regarding oxidative stress, thus the present study investigated the production of reactive oxygen species in PBMNCs in response to model and clinically-relevant ceramic wear particles.

Interestingly, both the model and clinically-relevant BIOLOX[®] Delta ceramic wear particles for all the doses tested, had no significant effect on the level of oxidative stress (fluorescence intensity) in PBMNCs from all donors. The same observation was made for the model and clinically-relevant BIOLOX[®] Forte ceramic wear particles at low (0.5 μm^3 per cell) and high (50 μm^3 per cell) doses. What is more, despite the mixed population of clinically-relevant ceramic wear particles and stainless-steel wear particles, no significant levels of oxidative stress were detected in the PBMNCs in any donor. This was surprising as the stainless-steel wear particle control (50 μm^3 per cell) caused a significant increase in the levels of ROS in PBMNCs from donor 5 and donor 26 as indicated by the high levels of fluorescence intensity compared to the cell only negative control. However, despite these significant differences, the fluorescence intensity for the stainless-steel wear particles was only marginally higher than the cells only control, whereas the fluorescence intensity in response to the CoCr nano-particles was considerably higher. These findings for the ceramic wear particles were in agreement with the findings of Wang et al., (2002) who reported no increase in reactive oxygen and nitrogen species in response to zirconia particles (mean size: 876nm). However, the authors also reported that sub-optimal stimulation of the macrophage cells to produce TNF- α in culture with the zirconia particles caused a significant increase in reactive oxygen and nitrogen species. This study suggested that there was a synergistic effect between TNF- α and ceramic wear particles on the production of reactive oxygen and nitrogen species by human macrophage cells (Wang et al., 2002). However, this synergistic effect was not observed in the present study as the clinically-relevant BIOLOX[®] Delta and BIOLOX[®] Forte ceramic wear particles both caused significant release of TNF- α at high doses, but did not elicit oxidative stress in PBMNCs. Alumina nano-particles (30-40nm) have also been reported to induce significant oxidative stress, but the doses used were considerably higher than the

relative wear rates of ceramic-on-ceramic hip replacements, rendering these studies irrelevant (Prabhakar et al., 2012).

4.5.6 Limitations of study

The clinically-relevant ceramic wear particles generated in chapter 3 for subsequent biological testing resulted in a mixed-population of stainless-steel and ceramic wear particles. This contamination by stainless-steel wear particles in the resultant ceramic wear particle suspensions required mitigation in the cell culture studies, where it was necessary to include a stainless-steel wear particle control to determine the potential biological effects this contaminant may pose to the cells. According to the results from the stainless-steel wear particle control in each biological assay, the stainless-steel wear particles only demonstrated complications for the genotoxicity evaluation of the clinically-relevant ceramic wear particles. The significant genotoxic effects caused by clinically-relevant BIOLOX® Delta and BIOLOX® Forte ceramic wear particles at various doses was attributed to the presence of stainless-steel wear particle contaminants in the co-culture and so these results were rendered unreliable.

Another limitation of this study is that the particles used in the biological assays, were not tested for the presence of endotoxins after heat sterilisation. The presence of endotoxins on the particles could have potentially activated the cells and generated misleading results. However, the method of destroying the endotoxins (190°C for 4 hours) used in the present study has been previously validated by Germain et al. (2003) and Hatton et al. (2003) using Limulus amoebocyte lysate assay. After heat treatment of the wear debris and control standard endotoxin solution (90 endotoxin units; EU), the endotoxins levels were shown to be <0.01 endotoxin units (EU) per ml, which was below the range of the control standard endotoxin and below the accepted value of <5 EU per ml, as specified by the pharmaceutical industry for injectable pharmaceuticals (FDA, Regulatory Affairs, 1985).

4.6 Summary of findings

This part of the study aimed to investigate the biological impact of wear particles generated from CoC total hip replacements using a range of biological assays. A comprehensive evaluation of the biological impact of model and clinically-relevant ceramic wear particles (generated using a hip simulator) of BIOLOX[®] Delta ZTA ceramic wear particles in terms of cytotoxicity, inflammation, genotoxicity and oxidative stress was investigated, thus successfully addressing the aim of this chapter. The results from this comprehensive study demonstrated that both Delta composite ceramic wear particles and Forte alumina wear particles demonstrated lower biological activity compared to CoCr nano-particles. The summary of the findings from this study are presented below: -

- The present study demonstrated the potential cytotoxic effects of ceramic model particles (BIOLOX[®] Forte and BIOLOX[®] Delta) in L929 fibroblast cells at very high doses ($500\mu\text{m}^3$ per cell), despite their non-clinical relevance. All other doses ($0.05\text{-}50\mu\text{m}^3$ per cell) of ceramic model particles for both BIOLOX[®] Forte and BIOLOX[®] Delta had no cytotoxic effects in L929 cells. The clinically-relevant BIOLOX[®] Delta ceramic wear particles demonstrated cytotoxic effects in L929 cells at a lower dose of $50\mu\text{m}^3$ per cell compared to ceramic model particles. However, this dose was still not clinically-relevant and all other doses ($0.05\text{-}5\mu\text{m}^3$ per cell) had no effect on the viability of L929 cells.
- The BIOLOX[®] Delta ceramic model particles failed to stimulate an inflammatory response in terms of TNF- α release from PBMNCs for all the doses tested ($0.05\text{-}50\mu\text{m}^3$ per cell). However, the clinically-relevant BIOLOX[®] Delta ceramic wear particles caused significant levels of TNF- α release from PBMNCs at high doses ($50\mu\text{m}^3$ per cell).
- The BIOLOX[®] Forte model ceramic particles demonstrated genotoxic effects at high doses ($50\mu\text{m}^3$ per cell), whereas the BIOLOX[®] Delta ceramic model particles did not cause any DNA damage in PBMNCs from all donors. The clinically-relevant BIOLOX[®] Delta ceramic wear particles also caused DNA damage at high doses ($5\text{-}50\mu\text{m}^3$ per cell) in PBMNCs from most donors.
- The model and clinically-relevant BIOLOX[®] Delta ceramic wear particles for all the doses tested, had no significant effect on the production of ROS (oxidative stress) in PBMNCs from all donors.

CHAPTER 5

5 Final discussion

5.1 Introduction

Total hip arthroplasty (THA) is one of the most successful orthopaedic procedures of the twentieth century. The National Joint Registry reported that in 2016, there were 101,651 hip replacements performed in England, Wales, Northern Ireland and Isle of Man a rise of approximately 323% from the hip replacements carried out in 2003 (14,454) (National Joint Registry, 2017). These numbers revealed a rapid increase in the number of THA procedures, which may be due to an ageing population coupled with an increasing number of younger and more active patients in need of total hip replacement (THR) surgery (Kurtz et al., 2007). The success of THRs is determined by their longevity, their ability to alleviate pain and restore patient mobility. Many factors such as implant design and type of material affect the success rates of THRs, however, the inevitable phenomenon of wear particle generation from the bearing surfaces has a large influence on the *in vivo* longevity of the implant and the incidence of revision surgery.

The most widely used bearing couple is still the metal head on UHMWPE acetabular cup, which made up 87.1% of all cemented primary procedures and 59% of all primary THRs that were implanted between 2003 and 2016 (National Joint Registry, 2017). However, historically the high prevalence of osteolysis and aseptic loosening associated with wear particles of the conventional metal-on-UHMWPE (MoP) bearing couple led to the development of alternative hard-on-hard bearings such as metal-on-metal (MoM) and ceramic-on-ceramic (CoC). MoM bearings have reported wear rates of between 1-6 mm³ per year in comparison to <10-100 mm³ per year for MoP hip implants, which is in the order of 60 times lower compared to MoP bearings (Cuckler, 2005; Goodman et al., 2009). However, concerns over the release of metal wear particles and metal ions from MoM hips led to a dramatic decline in the use of MoM hips and an increase in the popularity of alternative CoC THRs (Haddad et al., 2011).

CoC bearings have been shown to have superior wear properties when compared with other bearing materials such as cobalt-chromium and UHMWPE. The early CoC bearings consisted of pure alumina (Al₂O₃) and had a reputation for fracture (Fritsch and Gleitz, 1996). More recent issues have centered around surgical positioning and squeaking (Nevelos et al., 2000b; Owen et al., 2014). The development of better manufacturing processing such as hot isostatic pressing (HIP) allowed major improvements of ceramics, which reduced the grain size and increased the density of the alumina, making fracture less likely to occur (Tateiwa et al.,

2008). More recently, composite ceramics such as zirconia-toughened, platelet reinforced alumina or ZTA, otherwise commercially known as BIOLOX[®] Delta have been introduced clinically. ZTA is toughened by phase transformation; dispersion of tetragonal zirconium oxide submicron/nanoparticles in the microstructure and reinforced by the formation of platelet-shaped crystals in the alumina matrix (Burger and Richter, 2000b). Composite ceramics have dramatically reduced the wear rates of CoC bearings, which can be demonstrated by their wear rates *in vitro*: BIOLOX[®] Delta composite ceramic, 0.13mm³ per million cycles compared with BIOLOX[®] Forte HIPed alumina, 1.84mm³ per million cycles (Al-Hajjar, Fisher, Tipper, et al., 2013b). In addition, retrieval studies have shown extremely low wear compared with other bearing couples (Nevelos et al., 1999; Nevelos, Ingham, et al., 2001b; Affatato et al., 2011; Esposito et al., 2012). A low wear rate is believed to be critical for extending the longevity of a prosthetic joint, and wear volumes produced by CoC bearings have been estimated to be 40-100 times lower than the current generation highly-crosslinked MoP bearings (Knahr, 2013).

Excessive wear particles have been linked with the aetiology of periprosthetic osteolysis and aseptic loosening. The relative features of wear particles in terms of their size and shape, as well as the volume of particles is reported to determine the severity of the biological response (Ingham and Fisher, 2000). Hence, there is extensive literature published on the characteristics and biological activity of UHMWPE and metal CoCr wear particles generated from MoP and MoM hips, respectively. Polyethylene wear particles in the critical size range of 0.2-1.0 μm have been reported as being the most biologically reactive in activating macrophages (Green et al., 1998). In addition to particle size, the volume of particles has also been reported as being critically important in determining the biological response. It has been well documented both *in vivo* and *in vitro* that UHMWPE wear particles stimulate macrophages to release inflammatory cytokines (TNF- α , IL-1 and IL-6), which cause osteolysis and eventually result in aseptic loosening and subsequent failure of the hip prosthesis (Matthews, Besong, et al., 2000). Furthermore, it is well established that metal wear particles and metal ions have been associated with adverse tissue reactions around the prosthetic joint in patients such as necrosis, delayed-type IV hypersensitivity reactions, and pseudotumors (Haddad et al., 2011). However, there is very limited literature on the characteristics and biological activity of ceramic wear particles generated from CoC hips. From the literature that is available, the majority of the studies have used commercially-available ceramic powder to test the biological activity, and reported cytotoxic effects at high volumes, which are not representative of the clinically-relevant wear rates of CoC bearings (Catelas et al., 1999; Catelas, Petit, Zukor, et al., 1999; Nkamgueu et al., 2000; Petit et al., 2002; Tsaousi et al., 2010). Only a few studies have reported the cytotoxic and inflammatory effects of clinically-relevant alumina ceramic wear particles, which demonstrated only mild

cytotoxic and inflammatory effects at high volumes (Germain et al., 2003b; Hatton et al., 2003b). In comparison to other bearing materials, the particles released by alumina CoC hip prostheses have been shown to induce a mild cellular response, with low cytotoxicity and inflammatory potential.

There are currently no clinically-relevant studies that report the characteristics and biological activity of wear debris generated from composite ZTA ceramic bearings, such as BIOLOX® Delta. The lack of relevant studies may be due to difficulties in generating and recovering high volumes of clinically-relevant ceramic wear debris *in vitro*. A challenge associated with ceramic wear particle isolation is that current particle isolation methods are not sensitive enough to reliably isolate the wear particles from hip simulator lubricants, due to the extremely low wear rates exhibited by CoC bearings. Hence, wear particles from composite ZTA CoC bearings have not been systematically characterised and therefore little is known about their size, morphology and biological impact. The purpose of this project was to address these gaps in the literature by developing methodology to generate and isolate clinically-relevant composite ZTA ceramic wear particles for subsequent analysis of their characteristics and investigation of their biological impact. The present study used a bank of tests to demonstrate the biological impact of Delta ZTA and Forte alumina ceramic wear particles *in vitro* e.g. cytotoxicity test, release of inflammatory cytokines, DNA damage and oxidative stress. It is important to mention that there are other forms of ZTA ceramic hip bearing materials on the market, which may have a different biological impact to Delta CoC bearings.

5.2 Development of particle isolation methodology for ultra-low wearing composite ZTA ceramic bearings

Due to the limitations of current particle isolation methods (Doorn et al., 1998b; Catelas, Bobyn, J.B. Medley, et al., 2001; Brown et al., 2007), the present study validated and optimised a newly developed particle isolation method (Lal et al., 2016) for the isolation of composite ZTA ceramic wear particles from hip simulator lubricants. Validation of the method demonstrated a recovery rate of 89% from serum spiked with the lowest volumes of ZTA particles (0.1 and 0.05 mm³), which were representative of the wear rates of CoC bearings. However, the method was ineffective at removing all of the contaminating protein from the wear particles, which was observed using CFE-SEM after application of the method to hip simulator serum lubricant. Protein contamination of the recovered wear particles is a common result for particle isolation methods, hence many studies have incorporated multiple enzymes into their digestion regimes i.e. papain and proteinase K, in order to effectively remove the proteins from the wear particles (Doorn et al., 1998a; Catelas, Bobyn, J.B. Medley, et al., 2001; Brown et al., 2007). The present study incorporated lysozyme, which breaks down bacterial cell wall proteins that may have contaminated the serum lubricant

during wear simulation testing. This modified digestion regime resulted in lower levels of protein contamination, however the isolation of ceramic wear particles remained unsuccessful as no ceramic wear particles were identified.

Another challenge encountered during optimisation of the particle isolation method was the presence of stainless-steel wear particles that were observed after batch processing of serum lubricant that was collected from one million cycles of hip simulation. This approach was implemented as the processing of aliquots of serum lubricant was not a viable approach for the low volumes of wear generated from CoC bearings, which resulted in a high ratio between the volume of serum to volume of particles (0.1:1500 - 2:1500). Previous studies processed aliquots of the serum lubricant that contained wear particles, as the higher wear rates of MoP and MoM compared to CoC bearings resulted in successful recovery of wear particles (Catelas, Bobyn, J.J. Medley, et al., 2001; Tipper et al., 2006; Brown et al., 2007). Batch processing of serum lubricants was a novel approach that had never been implemented before in any previous studies. However, the recovered stainless-steel wear particle contaminants presented a major challenge, as their large volume masked the recovery of low volumes of ceramic wear particles. A magnet was used in an attempt to separate the stainless-steel wear particles from the ceramic wear debris, which revealed the presence of large micron-sized alumina particles. However, the recovery of nano-scale particles was unsuccessful.

Further optimisation resulted in a novel two-step particle isolation method that incorporated multiple proteolytic digestion and density-gradient ultra-centrifugation steps for the purification and recovery of very low volumes of both micron-sized and nano-scale wear particles generated from composite ZTA CoC bearings (BIOLOX[®] Delta). CFE-SEM analysis revealed that the particles had a bimodal size range, with large polygonal shaped particles of alumina that had a mean size of 2308.11 ± 243.58 , and small round granular zirconia/alumina particles that were agglomerated and had a mean size of 43.73 ± 0.97 nm. The tribological properties of materials strongly determines the characteristics of wear particles produced from THRs during articulation. Equally, the characteristics of wear particles can provide vital information about the underlying wear mechanisms of bearing materials. For example, the two modes of particles sizes for wear particles generated from CoC bearings is well established in the literature, where the small nano-scale particles are believed to be as a result of relief polishing, whereas the larger micron/sub-micron sized particles were attributed to inter-granular fracture of the ceramic bearing that results in the formation of a wear stripe during edge loading (Nevelos et al., 2000a; Hatton et al., 2002; Tipper et al., 2002a).

This novel two-step particle isolation represents a major breakthrough since it has allowed for the first- time comprehensive particle characteristic analysis of clinically-relevant composite ZTA ceramic wear particles generated *in vitro*. Hatton et al. (2002) and Tipper et al. (2002)

were the last studies to report the successful isolation and characterisation of wear particles from alumina CoC bearings. The work in current study continues to increase the understanding of the characteristics of wear debris generated from ceramic hip replacements. The optimised particle isolation method will be used as a preclinical testing tool in conjunction with hip simulation testing to better understand the likely clinical performance of these materials in patients.

5.3 Generation of clinically-relevant composite ZTA ceramic wear particles *in vitro*

The development of the two-step particle isolation in chapter 2 allowed the successful recovery and characterisation of clinically-relevant ZTA ceramic wear particles from hip simulator lubricants. However, these particles could not be used for subsequent biological testing due to the risk of residual proteins and adherent endotoxins that could have caused cellular activation and produced mis-leading results, which may have not been a response to the ceramic wear particles. Therefore, it was decided in the present study to generate ceramic wear particles in water lubricants using the hip simulator under severe edge loading conditions caused by dynamic separation due to translational mismatch between the centres of rotation of the femoral head and acetabular cup. A similar approach was previously employed by Hatton et al. (2003) who used water lubricants in hip simulation to generate clinically-relevant alumina ceramic wear particles under microseparation conditions. However, there was some uncertainty whether this technique would yield sufficient volumes of ZTA ceramic wear particles, as the wear rates for composite ZTA CoC bearings (0.16mm^3 /million cycles) were considerably lower than alumina CoC bearings (1.84mm^3 /million cycles), even under microseparation conditions (Stewart et al., 2003a).

The edge loading conditions employed in wear simulation testing of CoC bearings was first introduced by Nevelos et al. (2000), who applied a 0.4-0.5mm medial-lateral displacement of the cup relative to the head using a spring during the swing phase of the gait cycle, which ultimately caused edge loading during heel strike (Nevelos et al., 2000a; Stewart et al., 2001; Stewart et al., 2003a; Stewart et al., 2003b). However, fluoroscopic studies have shown that separation and the severity of edge loading can vary considerably i.e. 1.9-5.2mm (Lombardi et al., 2000; Dennis et al., 2001). Hence, the effect of variations in translational positioning with different levels of mismatch between the centres of the cup and head on the magnitude of dynamic separation and severity of edge loading have been investigated by O'Dwyer Lancaster-Jones et al. (2017). These authors reported wear rates of up to $1.01 \pm 0.17\text{mm}^3$ per million cycles for composite ZTA CoC bearings tested under severe edge loading conditions due to translational mismatch of up to 4mm in the centres of rotation of the femoral head and acetabular cup, with inclination angle of 65° . Therefore, the present study used this technique

as an opportunity to implement these severe edge loading conditions in order to maximise the volume of ceramic wear particles that could be generated for subsequent biological impact testing.

Comparison of the size distribution and morphology (aspect ratio and circularity) between the composite ZTA ceramic wear particles generated in water or serum, revealed no significant differences. The water lubricant did not alter the characteristics (size and morphology) of the ceramic wear particles generated, thus producing ceramic wear particles that were representative of those generated *in vivo*. A study by Rainforth et al. (2012) investigated the effects of lubrication (water and 25% (v/v) new-born calf serum) on the friction and wear of BIOLOX[®] Delta. The authors found that the serum lubricant exhibited full-fluid lubrication, whilst the water exhibited both full-fluid and mixed-fluid lubrication. The water lubricant demonstrated higher wear rates and the characteristics of the worn surfaces for full-fluid lubrication regime were reported to be distinctively different compared to the water lubricated worn surfaces i.e. the presence of differential wear between grains and abrasive grooves. These features were not observed on the worn surfaces for serum lubrication tests. However, despite the higher wear rates with water lubrication, the serum lubrication tests demonstrated the most pitting. Nevertheless, all the worn surfaces exhibited pitting, which increased with load and is consistent with *in vitro* hip simulation tests that demonstrated stripe wear under edge loading conditions. The pitting was mainly attributed to intergranular fracture of the individual grains. This pitting feature was also observed in the present study for both BIOLOX[®] Delta and BIOLOX[®] Forte components. However, in the present study the formation of larger and deeper pits were observed for BIOLOX[®] Delta, which may have been due to the severe edge loading conditions employed in the wear simulation tests. Another reason for the larger pits may have been due to grain pull-out of both alumina and zirconia grains. Rainforth et al. (2012) described the formation of large pits being caused by initial grain pull-out, followed by adjacent grains being pulled out, resulting in the pit region increasing in size laterally from the source of the initial grain pull-out.

During wear simulation, the water lubricant was contaminated with stainless-steel wear particles that were generated from the fixtures or components other than the bearing surfaces, which could not be separated from the ceramic wear particles. Thus, a mixed population of stainless-steel wear particles and ceramic wear particles was presented to the cells, which required the introduction of stainless wear particle controls in all subsequent biological tests to elucidate the biological effects of the clinically-relevant ceramic wear particles. Nevertheless, the employment of severe edge loading conditions with water lubricant allowed the generation of clinically-relevant ceramic wear particles, which were successfully recovered for subsequent assessment of biological impact. The present study demonstrated that *in vitro* hip simulation can be used as a tool for the generation of clinically-relevant

ceramic wear particles, thus eliminating the need for wear particle isolation from tissues or serum lubricants that often results in particle loss and other complications such as uncertainty of complete removal of proteins and endotoxins from particles recovered from tissues or serum lubricants.

5.4 Biological impact of model and clinically-relevant composite ZTA ceramic wear particles

The generation of clinically-relevant ceramic wear particles was conducted in this study due to the limited number of studies in the literature using clinically-relevant ceramic wear particles for biocompatibility testing. This gap in the literature existed because of the difficulties in generating and isolating high volumes of clinically-relevant ceramic wear particles *in vitro*. The alternative was to use ceramic powders for biocompatibility testing. The use of ceramic powders to report the biological activity of ceramic wear particles from ceramic THR is well practised in the literature (Nagase et al., 1995; Catelas et al., 1998; I Catelas, Petit, Zukor, et al., 1999; Nkangueu et al., 2000a; Petit et al., 2002; Warashina et al., 2003; Granchi et al., 2004; Tsaousi et al., 2010; Faye et al., 2017). However, these studies are very limited in the information they provide as the characteristics of commercially-obtained ceramic particles may not clinically represent the size and shape of ceramic wear particles generated *in vivo*. In order to mitigate this concern, a few studies have used powders in the phagocytosable range ($<0.45\mu\text{m}$) to portray the clinical-relevance of their findings (Catelas et al., 1998; I Catelas, Petit, Marchand, et al., 1999; Petit et al., 2002; Warashina et al., 2003; Olivier et al., 2003; Granchi et al., 2004; Rodrigo et al., 2006; Tsaousi et al., 2010; Faye et al., 2017). However, it is important to remember when considering these findings, that other factors such as particle volume, morphology, composition and cell type also play an important role in the biological response. There is clearly a need for more studies to report the biological effects of clinically-relevant ceramic wear particles in a clinically-relevant model to better predict the likely clinical performance, hence the purpose of this thesis.

In addition to clinically-relevant ceramic wear particles, the present study also used commercially-obtained ceramic model particles to investigate the biological impact and allow a relative comparison with the published literature. Furthermore, the composite ZTA and alumina ceramic model particles used in the present study were the powders used to manufacture ceramic hip replacements BIOLOX[®] Delta and BIOLOX[®] Forte, respectively. Given this fact, the current study presents many advantages over previous studies, as it is likely that the characteristics (size and shape) of the ceramic model particles in the powder may be more representative of the ceramic wear particles produced *in vivo*. However, a comparison of the frequency (particle size) distributions and morphology (aspect ratio and circularity) between the BIOLOX[®] Delta ceramic model particles and clinically-relevant

BIOLOX[®] Delta ceramic wear particles revealed a significant difference ($p < 0.05$). Interestingly, the same comparison between BIOLOX[®] Forte ceramic model particles and clinically-relevant BIOLOX[®] Forte ceramic wear particles revealed no significant differences in particle size distribution and morphology. The similar size range between the two types of particles may be because the BIOLOX[®] Forte ceramic model particles used in this study was comprised of the powder used to manufacture BIOLOX[®] Forte CoC hip components. The contradicting significant differences in size distribution and morphology observed between the BIOLOX[®] Delta ceramic model particles and clinically-relevant ceramic wear particles was attributed to the large grain-like structure that was present in the ZTA composite ceramic model particles and not present in the clinically-relevant ZTA ceramic wear particles. During sintering of the Delta powder, many elements in the form of raw compound materials are added, which causes on going solid reaction and the production of these large grain-like structures.

A comprehensive evaluation of the biological impact of model and clinically-relevant ceramic wear particles of BIOLOX[®] Delta ZTA and BIOLOX[®] Forte alumina ceramic wear particles in terms of cytotoxicity, inflammatory cytokine release, genotoxicity and oxidative stress demonstrated that BIOLOX[®] Delta composite ceramic wear particles demonstrated lower biological impact compared to BIOLOX[®] Forte alumina wear particles. The initial assessment of cytotoxicity of ceramic model particles for both BIOLOX[®] Forte and BIOLOX[®] Delta demonstrated the potential cytotoxic effects of ceramic model particles (BIOLOX[®] Forte and BIOLOX[®] Delta) in L929 fibroblast cells at very high doses ($500\mu\text{m}^3$ per cell). This phenomenon is reported by many previous studies (Catelas et al., 1998; Catelas, Petit, Marchand, et al., 1999; Olivier et al., 2003; Granchi et al., 2004; Tsaousi et al., 2010), but it may not be clinically-relevant as it highly unlikely that these high volumes will be achieved *in vivo* due to the extremely low wear rates of CoC bearings, even under edge loading conditions. The clinically-relevant BIOLOX[®] Delta ceramic wear particles demonstrated cytotoxic effects in L929 cells at a lower dose of $50\mu\text{m}^3$ per cell compared to ceramic model particles, however again this dose was not clinically-relevant but was indicative of the differences in biological activity between ceramic model particles and clinically-relevant ceramic wear particles. These results demonstrated the importance of using clinically-relevant ceramic wear particles to test for biocompatibility, as cytotoxic effects such as those observed in the present study can be missed, which can potentially cause deleterious effects in the *in vivo* situation.

Macrophages release TNF- α in response to wear particles, which is a key cytokine involved in osteolysis and subsequent failure of hip implants (Ingham and Fisher, 2005). Hence, the present study investigated the release of TNF- α from PBMNCs in response to model and clinically-relevant ceramic wear particles. The BIOLOX[®] Delta ceramic model particles

failed to stimulate an inflammatory response in terms of TNF- α release from PBMNCs for all the doses tested (0.05-50 μm^3 per cell). However, the clinically-relevant BIOLOX[®] Delta ceramic wear particles caused significant levels of TNF- α release from PBMNCs at high doses (50 μm^3 per cell). The results of the present study were in contrast to the findings of Hatton et al. (2003), who reported that the alumina powder (model ceramic particles) were more inflammatory than the clinically-relevant alumina ceramic wear particle. Hatton et al. (2003) reported that higher doses of the clinically-relevant alumina ceramic wear particles (500 μm^3 per cell) were required to illicit the same inflammatory response as alumina powder particles (100 μm^3 per cell) (Hatton et al., 2003a). The present study demonstrated that there was no inflammatory response to the model ceramic particles in terms of TNF- α release, but significantly elevated levels of TNF- α was released from PBMNCs when stimulated with high doses (500 μm^3) of clinically-relevant BIOLOX[®] Forte and BIOLOX[®] Delta ceramic wear particles. The possible explanation provided for this observation was that the clinically-relevant BIOLOX[®] Forte and BIOLOX[®] Delta ceramic wear particles had a greater size distribution with more larger particles in the phagocytosable range (up to 4.5 μm) compared to the ceramic model particles, as demonstrated by their size distributions. Therefore, a lower concentration or volume of particles was required to illicit an immune response, a finding that was also reported by Catelas et al. 1998. Nevertheless, despite the differences between this present study and the study conducted by Hatton et al. (2003), the same conclusion was made in that given the low wear rates (0.1-1 mm^3 per million cycles) of ceramic-on-ceramic bearings, the threshold of 50 μm^3 per cell may never be achieved *in vivo*. Hence, compared to UHMWPE wear particles, the osteolytic potential of clinically-relevant ceramic wear particles is minimal as the evidence in the present study demonstrated that the clinically-relevant doses (0.05-0.5 μm^3 per cell) of ceramic wear particles failed to stimulate pro-inflammatory cytokine (TNF- α) production.

The cytotoxic and inflammatory effects of ceramic wear particles were minimal at clinically-relevant doses as reported by the literature and findings from the present study. Hence, the present study investigated other subtler changes in terms of DNA damage and oxidative stress, which may occur in exposure to exposure to ceramic wear particles over the longer term. Chromosome aberrations in patients with MoM implants have been reported by many previous studies, which is a genotoxic effect of CoCr wear particles (Ladon et al., 2004; Suner et al., 2012). Regarding ceramic wear particles, Tsaousi et al. (2010) reported alumina ceramic particles as being weakly genotoxic at high doses compared to CoCr wear particles. Weakly genotoxic means that the ceramic particles caused chromosome loss, but no DNA double-strand breaks were detected. On the contrary, the present study observed high levels of DNA damage for high doses of model and clinically-relevant alumina ceramic particles (BIOLOX[®] Forte), which was assessed using the comet assay that measures breakages in single and

double stranded DNA. Considering the literature, the results from the present study clearly showed that high doses of model alumina particles were completely genotoxic as they caused notably higher DNA damage than the clinically-relevant CoCr nano-particles ($50\mu\text{m}^3$ per cell) in some donors. The BIOLOX[®] Delta ceramic model particles did not cause any DNA damage in PBMNCs from all donors, whereas the clinically-relevant BIOLOX[®] Delta ceramic wear particles caused DNA damage at medium to high doses ($5\text{-}50\mu\text{m}^3$ per cell) in PBMNCs from four donors. The significant genotoxic effects caused by clinically-relevant BIOLOX[®] Delta ceramic wear particles were attributed to the presence of stainless-steel wear particle contaminants in the co-culture. This was supported by results for the stainless-steel wear particle control, which demonstrated significant levels of DNA damage at doses of $50\mu\text{m}^3$ per cell. Therefore, the genotoxic effects of high doses ($50\mu\text{m}^3$ per cell) of clinically-relevant ceramic wear particles for both BIOLOX[®] Forte and BIOLOX[®] Delta were considered unreliable and disregarded.

Oxidative stress has been implicated in playing an important role in the inflammatory response to total hip replacements, leading to osteolysis and implant failure (Steinbeck et al., 2014). The production of ROS and subsequent oxidative stress in cells is an important process in terms of cell signalling, and cell survival. Hence, in addition to the appropriate cytotoxicity, inflammatory and genotoxicity testing of the ceramic wear particles, the production of reactive oxygen species (ROS) in PBMNCs in response to ceramic particles was investigated as the bimodal size distribution of ceramic wear particles may have the potential to induce oxidative stress, since genotoxic effects at high doses of alumina particles were observed in previous assays. Nonetheless, this concern was negated as both the model and clinically-relevant BIOLOX[®] Delta ceramic wear particles for all the doses tested, had no significant effect on the production of ROS (oxidative stress) in PBMNCs from all donors. Previous experiments clearly showed the ingestion of ceramic wear particles by the PBMNCs, but clearly the results from the oxidative stress assay showed that the internalised ceramic wear particles had no effect in terms of ROS production. The benign response may have been due to the bioinert nature of alumina ceramics, which makes it highly suitable for clinical applications.

5.5 Future work

The present study isolated and characterised composite ZTA ceramic wear particles from hip simulator lubricants, that were generated from BIOLOX® Delta CoC bearings under severe edge loading conditions. It is well established that edge loading conditions simulated *in vitro* produce wear rates and wear mechanisms similar to those found *in vivo*. However, future work should include the isolation and characterisation of composite ZTA ceramic wear particles from retrieved tissues. This would add weight to the findings of the present study and increase the confidence of *in vitro* generated particles as being clinically-relevant.

The conditions employed in the wear simulation tests of the present study did not take in to account patient specificity in terms of geometry and anatomy. Furthermore, the tests were run consistently according to the standard walking gait cycle. The tests did not include the kinematics of running, climbing stairs or stumbling. These conditions and factors could change the characteristics of the wear particles generated from CoC bearings. Modern hip simulators now have the capability of simulating these conditions mentioned previously. Hence, using the two-step particle isolation method developed in the present study, future studies could isolate, and analyse the characteristics of the wear particles generated under different kinematic conditions. These particles could also be used for subsequent biological testing.

In the present study, it was demonstrated that high doses ($50\mu\text{m}^3$ per cell) of clinically-relevant ceramic wear particles generated from both BIOLOX® Forte and BIOLOX® Delta CoC bearings stimulated significantly elevated levels of TNF- α from PBMNCs compared to the cell only negative control. Previous studies have demonstrated the release of other inflammatory cytokines in response to UHMWPE wear particles, such as IL-1 β , IL-6 and IL-8 (Green et al., 1998; Matthews, Besong, et al., 2000; Ingham and Fisher, 2000; Ingham and Fisher, 2005). Whilst the present study showed that ceramic wear particles at clinically-relevant doses ($0.05\text{-}0.5\mu\text{m}^3$ per cell) produced low levels of TNF- α release, a more comprehensive evaluation for osteolytic cytokine release would provide valuable information for wear particles generated from composite ceramic hip replacements. Furthermore, in addition to the investigation of the release of different cytokines in response to wear particles from joint replacements, further research into the cellular pathways and mechanisms that lead to the release of these inflammatory cytokines may help to better understand the osteolysis process. Understanding this process may help to improve the longevity of bearing materials through developing therapeutic interventions, which modulates the subsequent inflammatory response after implantation.

The present study used two-dimensional (2D) cell culture to investigate the biological impact of ceramic wear particles. Whilst, this conventional technique provides vital information about cellular responses *in vitro*, the 2D cell culture environment is not always representative

of cells *in vivo*. The *in vivo* environment consists of an extracellular matrix with a complex biological environment that includes other cell types, which interact with each other through cell migration, receptors and transcriptional expressions. Hence, the 2D culture system is too simple compared to the *in vivo* environment, as it does not consider many factors that are important for accurately reproducing cell and tissue physiology (Haycock, 2011; Edmondson et al., 2014). Hence, further research investigating the biological impact of ceramic wear particles using 3D cell culture systems would support the finding in the present study. A 3D agarose gel system that better mimics the *in vivo* environment has recently been developed by Lal. et al (2017) to investigate the cellular response to prosthetic wear particles (Lal et al., 2017). The application of this method to clinically-relevant ceramic wear particles would increase the knowledge about the biological activity of prosthetic wear particles.

The present study demonstrated that high doses of alumina ceramic wear particles induced DNA damage in PBMNCs. Future studies could investigate the what impact this DNA damage has on cellular mechanisms and whether this phenomenon is responsible for the cytotoxic effects observed at similar doses. Furthermore, futures studies should investigate gene expression of general toxicology-related genes in response to ceramic wear particles. This would provide vital information about the cellular pathways leading to an inflammatory response or apoptosis/necrosis and which genes are up-regulated or down-regulated during these cellular reactions.

The work in chapter 2 of this study demonstrated that the wear particles generated from composite ZTA ceramic hip replacements consisted of both micrometre and nanoscale wear particles. Hence, future work should include the investigation of the cellular uptake mechanisms of ceramic wear particles as the cellular uptake of nano-scale particles may differ from the cellular uptake of larger micron-sized particles. In addition, the interaction of composite ceramic wear particles with the cell membrane could also be investigated as this could provide more information about the mode of toxicity these particles induce i.e. extracellularly or intracellularly.

Finally, the present study investigated the biological impact of the ceramic wear particles in PBMNCs after 24hrs of incubation. Future work should include longer incubation times to elucidate the longer term biological effects of ceramic wear particles.

5.6 Conclusions

The present study developed a two-step particle isolation method that allowed successful isolation and characterisation of composite ZTA ceramic wear particles from hip simulator lubricants for the first time. The recovered composite ZTA ceramic wear particles demonstrated a bimodal size range with large polygonal shaped particles of alumina that had a mean size of 2308nm, and small round granular zirconia/alumina particles that had a mean size of 43.7nm. In addition to methodology development that could be used as a tool for pre-clinical testing of joint replacements, this thesis has contributed to increasing the knowledge and understanding of the wear mechanisms and wear particle characteristics of composite ZTA (BIOLOX® Delta) CoC bearings. This is new benchmark information that could be used for future biomaterial development.

Wear simulation testing has provided vital information about the tribological performance and wear properties of CoC THR. The recent development of an advanced physiological *in vitro* hip simulator method that used variations in component positioning to simulate edge loading, has allowed the generation of high volumes of clinically-relevant ceramic wear particles from composite ZTA (BIOLOX® Delta) CoC bearings water lubricant to be used for subsequent biological testing. The success of the two-step particle isolation method coupled with the novel simulator method allowed the present study for the first time to generate sufficient volumes of composite ZTA ceramic wear particles for biological testing, which were validated as being clinically-relevant using the composite ZTA particle characteristics data generated from the present study.

A comprehensive evaluation of the biological impact of model and clinically-relevant ceramic wear particles (generated using a hip simulator) of composite BIOLOX® Delta ZTA ceramic wear particles was performed in terms of cytotoxicity, inflammatory cytokine release, genotoxicity and oxidative stress. The results from this study are only relevant for BIOLOX® Delta and not other manufacturers ceramics. This bank of tests demonstrated that composite BIOLOX® Delta ZTA ceramic wear particles have excellent biocompatibility with low osteolytic potential at clinically-relevant doses. The composite ZTA model particles at all doses did not illicit any biological effects in terms of cytotoxicity, inflammatory cytokine release, genotoxicity and production of ROS. However, high doses of the clinically-relevant composite BIOLOX® Delta ZTA ceramic wear particles demonstrated cytotoxic effects in L929 cells and significantly elevated levels of TNF- α release from PBMNCs. This study demonstrated that there was a threshold volume of clinically-relevant ceramic wear particles required to stimulate significant TNF- α release from PBMNCs. However, these doses were not clinically-relevant and highly unlikely to occur *in vivo* due to the extremely low wear rates of CoC bearings. Hence, it can be concluded that wear particles from composite ZTA

BIOLOX[®] Delta CoC hip replacements had a low osteolytic potential, which may enhance long-term clinical performance.

From a clinical point of view, the findings from the present study give clinicians and surgeons confidence in composite BIOLOX[®] Delta ZTA CoC bearings as they will be better able to provide a long-term prognosis to patients. Furthermore, this work continues to increase our understanding of the characteristics of ceramic wear debris and will allow industry to develop more biocompatible and longer lasting implants. Bearing materials used for total joint replacements will ultimately always produce some wear. Hence, the optimised particle isolation method and wear simulation technique developed in this study could be used as a preclinical testing technique to better understand the biocompatibility and likely clinical performance of these bearing materials in patients. In addition, the optimised bank of tests for biological impact could be used to test the biocompatibility of wear particles generated from other hard-on-hard bearing materials.

References

- Abbas, Z., Labbez, C., Nordholm, S. and Ahlberg, E. 2008. Size-Dependent Surface Charging of Nanoparticles. *The Journal of Physical Chemistry C*. [Online]. **112**(15),pp.5715–5723. Available from: <http://dx.doi.org/10.1021/jp709667u>.
- Abu-Amer, Y., Darwech, I. and Clohisy, J.C. 2007. Aseptic loosening of total joint replacements: mechanisms underlying osteolysis and potential therapies. *Arthritis Research & Therapy*. **9**.
- Affatato, S., Modena, E., Toni, A. and Taddei, P. 2012. Retrieval analysis of three generations of BioloX (R) femoral heads: Spectroscopic and SEM characterisation. *JOURNAL OF THE MECHANICAL BEHAVIOR OF BIOMEDICAL MATERIALS*. **13**,pp.118–128.
- Affatato, S., Spinelli, A., Zavalloni, M., Mazzega-Fabbro, C. and Viceconti, A. 2008. Tribology and total hip joint replacement: Current concepts in mechanical simulation. *Medical Engineering & Physics*. **30**(10),pp.1305–1317.
- Affatato, S., Traina, F. and Toni, A. 2011. Microseparation and stripe wear in alumina-on-alumina hip implants. *International Journal of Artificial Organs*. **34**(6),pp.506–512.
- Al-Hajjar, M., Fisher, J., Tipper, J.L., Williams, S. and Jennings, L.M. 2013a. Wear of 36-mm BIOLOX (R) delta ceramic-on-ceramic bearing in total hip replacements under edge loading conditions. *Proceedings of the Institution of Mechanical Engineers Part H-Journal of Engineering in Medicine*. **227**(H5),pp.535–542.
- Al-Hajjar, M., Fisher, J., Williams, S., Tipper, J. and Jennings, L. 2013. Effect of femoral head size on the wear of metal on metal bearings in total hip replacements under adverse edge-loading conditions. *JOURNAL OF BIOMEDICAL MATERIALS RESEARCH PART B-APPLIED BIOMATERIALS*. **101B**(2),pp.213–222.
- Al-Hajjar, M., Jennings, L., Begand, S., Oberbach, T., Delfosse, D. and Fisher, J. 2013a. Wear of novel ceramic-on-ceramic bearings under adverse and clinically relevant hip simulator conditions. *Journal of Biomedical Materials Research Part B-Applied Biomaterials*. **101**(8),pp.1456–1462.
- Al-Hajjar, M., Leslie, I.J., Tipper, J., Williams, S., Fisher, J. and Jennings, L.M. 2010. Effect of cup inclination angle during microseparation and rim loading on the wear of BIOLOX (R) delta ceramic-on-ceramic total hip replacement. *Journal of Biomedical Materials Research Part B-Applied Biomaterials*. **95B**(2),pp.263–268.
- Al-Hajjar, M., Williams, S., Jennings, L.M., Thompson, J., Isaac, G., E, I., Fisher, J. and Lancaster-Jones, O. 2015. Different levels of Rotational and Translational Surgical Mal-Positioning Affects the Occurrence and Severity of Edge Loading and Wear in Total Hip Replacements. *Orthopaedic Research Society*.
- Algan, S.M., Purdon, M. and Horowitz, S.M. 1996. Role of tumor necrosis factor alpha in particulate-induced bone resorption. *Journal of Orthopaedic Research*. **14**(1),pp.30–35.

- Amanatullah, D.F., Sucher, M.G., Bonadurer III, G.F., Pereira, G.C. and Taunton, M.J. 2016. Metal in Total Hip Arthroplasty: Wear Particles, Biology, and Diagnosis. *ORTHOPEDICS*. **39**(6),pp.371–379.
- Amstutz, H.C. and Grigoris, P. 1996. Metal on metal bearings in hip arthroplasty. *Clinical Orthopaedics and Related Research*. (329),pp.S11–S34.
- Arend, W.P. 2002. The mode of action of cytokine inhibitors. *The Journal of rheumatology. Supplement*. **65**,pp.16–21.
- Armstead, A.L., Simoes, T.A., Wang, X., Brydson, R., Brown, A., Jiang, B.-H., Rojanasakul, Y. and Li, B. 2017. Toxicity and oxidative stress responses induced by nano-and micro-CoCrMo particles. *JOURNAL OF MATERIALS CHEMISTRY B*. **5**(28),pp.5648–5657.
- Aspenberg, P. and Herbertsson, P. 1996. Periprosthetic bone resorption - Particles versus movement. *Journal of Bone and Joint Surgery-British Volume*. **78B**(4),pp.641–646.
- Azuma, Y., Katogi, R., Kaji, K., Takeshita, S., Naito, A., Kamimura, T., Inoue, J. and Kudo, A. 2000. Tumor necrosis factor- α induces differentiation of and bone resorption by osteoclasts. *Journal of Bone and Mineral Research*. **15**,pp.S386–S386.
- Balto, K., Sasaki, H. and Stashenko, P. 2001. Interleukin-6 deficiency increases inflammatory bone destruction. *Infection and Immunity*. **69**(2),pp.744–750.
- Barbour, P.S.M., Stone, M.H. and Fisher, J. 1999. A hip joint simulator study using simplified loading and motion cycles generating physiological wear paths and rates. *PROCEEDINGS OF THE INSTITUTION OF MECHANICAL ENGINEERS PART H-JOURNAL OF ENGINEERING IN MEDICINE*. **213**(H6),pp.455–467.
- Barrett, A.J., Rawlings, N.D., Salvesen, G. and Woessner, J.F. 2013. Handbook of Proteolytic Enzymes Introduction *In: Rawlings, ND and Salvesen, GS, ed. HANDBOOK OF PROTEOLYTIC ENZYMES, VOLS 1 AND 2, 3RD EDITION.*, pp. I–IV.
- Behl, B., Papageorgiou, I., Brown, C., Hall, R., Tipper, J.L., Fisher, J. and Ingham, E. 2013. Biological effects of cobalt-chromium nanoparticles and ions on dural fibroblasts and dural epithelial cells. *Biomaterials*. **34**(14),pp.3547–3558.
- Besong, A.A., Tipper, J.L., Ingham, E., Stone, M.H., Wroblewski, B.M. and Fisher, J. 1998. Quantitative comparison of wear debris from UHMWPE that has and has not been sterilised by gamma irradiation. *Journal of Bone and Joint Surgery-British Volume*. **80B**(2),pp.340–344.
- Billi, F., Benya, P., Ebramzadeh, E., Campbell, P., Chan, F. and McKellop, H.A. 2009. Metal wear particles: What we know, what we do not know, and why. *SAS journal*. **3**(4),pp.133–142.
- Billi, F., Benya, P., Kavanaugh, A., Adams, J., Ebramzadeh, E. and McKellop, H. 2012. The John Charnley Award: An Accurate and Sensitive Method to Separate, Display, and Characterize Wear Debris: Part 1: Polyethylene Particles. *Clinical Orthopaedics and*

Related Research. **470**(2),pp.329–338.

- Billi, F., Benya, P., Kavanaugh, A., Adams, J., McKellop, H. and Ebramzadeh, E. 2012. The John Charnley Award: An Accurate and Extremely Sensitive Method to Separate, Display, and Characterize Wear Debris Part 2: Metal and Ceramic Particles. *Clinical Orthopaedics and Related Research.* **470**(2),pp.339–350.
- Bohler, M., Mochida, Y., Bauer, T.W., Plenk, H. and Salzer, M. 2000. Wear debris from two different alumina-on-alumina total hip arthroplasties. *Journal of Bone and Joint Surgery-British Volume.* **82B**(6),pp.901–909.
- Bonner, R.F., EmmertBuck, M., Cole, K., Pohida, T., Chuaqui, R., Goldstein, S. and Liotta, L.A. 1997. Cell sampling - Laser capture microdissection: Molecular analysis of tissue. *Science.* **278**(5342),p.1481-.
- Boutin, P. 2000. Total hip arthroplasty using a ceramic prosthesis. Pierre Boutin (1924-1989). *Clinical Orthopaedics and Related Research.* (379),pp.3–11.
- Brooks, R.A., Wimhurst, J.A. and Rushton, N. 2002. Endotoxin contamination of particles produces misleading inflammatory cytokine responses from macrophages in vitro. *Journal of Bone and Joint Surgery-British Volume.* **84B**(2),pp.295–299.
- Brown, C., Fisher, J. and Ingham, E. 2006. Biological effects of clinically relevant wear particles from metal-on-metal hip prostheses. *Proceedings of the Institution of Mechanical Engineers Part H-Journal of Engineering in Medicine.* **220**(H2),pp.355–369.
- Brown, C., Williams, S., Tipper, J.L., Fisher, J. and Ingham, E. 2007. Characterisation of wear particles produced by metal on metal and ceramic on metal hip prostheses under standard and microseparation simulation. *Journal of Materials Science-Materials in Medicine.* **18**(5),pp.819–827.
- Bullough, P.G., Dicarlo, E.F., Hansraj, K.K. and Neves, M.C. 1988. PATHOLOGIC-STUDIES OF TOTAL JOINT REPLACEMENT. *Orthopedic Clinics of North America.* **19**(3),pp.611–625.
- Burger, W. and Richter, H.G. 2000a. High strength and toughness alumina matrix composites by transformation toughening and ‘in situ’ platelet reinforcement (ZPTA) - The new generation of bioceramics. *Bioceramics.* **192–1**,pp.545–548.
- Callaghan, J.J. and Liu, S.S. 2009. Ceramic on crosslinked polyethylene in total hip replacement: any better than metal on crosslinked polyethylene? *The Iowa orthopaedic journal.* **29**,pp.1–4.
- Campbell, P., Ebramzadeh, E., Nelson, S., Takamura, K., De Smet, K. and Amstutz, H.C. 2010. Histological Features of Pseudotumor-like Tissues From Metal-on-Metal Hips. *Clinical Orthopaedics and Related Research.* **468**(9),pp.2321–2327.
- Campbell, P., Ma, S., Schmalzried, T. and Amstutz, H.C. 1994. TISSUE DIGESTION FOR

- WEAR DEBRIS PARTICLE ISOLATION. *Journal of Biomedical Materials Research*. **28**(4),pp.523–526.
- Campbell, P., Ma, S., Yeom, B., McKellop, H., Schmalzried, T.P. and Amstutz, H.C. 1995. ISOLATION OF PREDOMINANTLY SUBMICRON-SIZED UHMWPE WEAR PARTICLES FROM PERIPROSTHETIC TISSUES. *Journal of Biomedical Materials Research*. **29**(1),pp.127–131.
- Campbell, P., Shen, F.W. and McKellop, H. 2004. Biologic and tribologic considerations of alternative bearing surfaces. *Clinical Orthopaedics and Related Research*. (418),pp.98–111.
- Campbell, P.A., Wang, M., Amstutz, H.C. and Goodman, S.B. 2002. Positive cytokine production in failed metal-on-metal total hip replacements. *Acta Orthopaedica Scandinavica*. **73**(5),pp.506–512.
- Case, C.P., Langkamer, V.G., James, C., Palmer, M.R., Kemp, A.J., Heap, P.F. and Solomon, L. 1994. WIDESPREAD DISSEMINATION OF METAL DEBRIS FROM IMPLANTS. *Journal of Bone and Joint Surgery-British Volume*. **76B**(5),pp.701–712.
- Catelas, I. 2011. New Insights into Wear and Biological Effects of Metal-on-Metal Bearings (vol 93, pg 76, 2011). *Journal of Bone and Joint Surgery-American Volume*. **93A**(12),p.1158.
- Catelas, I., Bobyn, J.D., Medley, J.B., Krygier, J.J., Zukor, D.J., Petit, A. and Huk, O.L. 2001. Effects of digestion protocols on the isolation and characterization of metal-metal wear particles. I. Analysis of particle size and shape. *Journal of Biomedical Materials Research*. **55**(3),pp.320–329.
- Catelas, I., Bobyn, J.D., Medley, J.J., Zukor, D.J., Petit, A. and Huk, O.L. 2001. Effects of digestion protocols on the isolation and characterization of metal-metal wear particles. II. Analysis of ion release and particle composition. *Journal of Biomedical Materials Research*. **55**,pp.330–337.
- Catelas, I., Huk, O.L., Petit, A., Zukor, D.J., Marchand, R. and Yahia, L.H. 1998. Flow cytometric analysis of macrophage response to ceramic and polyethylene particles: Effects of size, concentration, and composition. *JOURNAL OF BIOMEDICAL MATERIALS RESEARCH*. **41**(4),pp.600–607.
- Catelas, I., Medley, J.B., Campbell, P.A., Huk, O.L. and Bobyn, J.D. 2004. Comparison of in vitro with in vivo characteristics of wear particles from metal-metal hip implants. *Journal of Biomedical Materials Research Part B-Applied Biomaterials*. **70B**(2),pp.167–178.
- Catelas, I., Petit, A., Marchand, R., Zukor, D.J., Yahia, L.H. and Huk, O.L. 1999. Cytotoxicity and macrophage cytokine release induced by ceramic and polyethylene particles in vitro. *JOURNAL OF BONE AND JOINT SURGERY-BRITISH VOLUME*. **81B**(3),pp.516–

- Catelas, I., Petit, A., Zukor, D., Marchand, R., Yahia, L. and Huk, O.. 1999. Induction of macrophage apoptosis by ceramic and poly-ethylene particles in vitro. *Biomaterials*. **20**,pp.625–630.
- Chang, J.D., Lee, S.S., Hur, M., Seo, E.M., Chung, Y.K. and Lee, C.J. 2005. Revision total hip arthroplasty in hip joints with metallosis - A single-center experience with 31 cases. *Journal of Arthroplasty*. **20**(5),pp.568–573.
- Chauhan, B.S. 2008. Biochemical separation and assays *In: Principles of Biochemistry and Biophysics*. New Dehli: University Science Press, pp. 380–381.
- Chevalier, J., Gremillard, L., Virkar, A. V and Clarke, D.R. 2009. The Tetragonal-Monoclinic Transformation in Zirconia: Lessons Learned and Future Trends. *Journal of the American Ceramic Society*. **92**(9),pp.1901–1920.
- Christel, P. 1993. Ceramic for Joint Replacements *In: B. F. Morrey, ed. Biological, Material, and Mechanical Considerations of Joint Replacment*. New York: Raven Press, pp. 303–304.
- Christel, P.S. 1992. BIOCOMPATIBILITY OF SURGICAL-GRADE DENSE POLYCRYSTALLINE ALUMINA. *CLINICAL ORTHOPAEDICS AND RELATED RESEARCH*. (282),pp.10–18.
- Clarke, I.C., Green, D., Williams, P., Pezzotti, G. and Donaldson, T. 2007. *Wear performance of 36mm Biolox (R) forte/delta hip combinations compared in simulated 'severe' micro-separation test mode* (J. D. Chang & K. Billau, eds.).
- Clarke, I.C., Green, D.D., Pezzotti, G. and Donaldson, D. 2005. 20 Years Experience of Zirconia Total Hip Replacements. *Bioceramics and Alternative Bearings in Joint Arthroplasty*.,pp.67–78.
- Clohisy, J.C., Teitelbaum, S., Chen, S.P., Erdmann, J.M. and Abu-Amer, Y. 2002. Tumor necrosis factor-alpha mediates polymethylmethacrylate particle-induced NF-kappa B activation in osteoclast precursor cells. *Journal of Orthopaedic Research*. **20**(2),pp.174–181.
- Collins, A.R. 2004. The comet assay for DNA damage and repair - Principles, applications, and limitations. *Molecular Biotechnology*. **26**(3),pp.249–261.
- Correia, A., Balseiro, A., Almeida, A., Sampaio, A. and Santos, P. 2007. IL1A, IL1B, IL1R and IL1RA polymorphisms in rheumatoid arthritis. *Tissue Antigens*. **69**(5),pp.475–476.
- Crouch, S.P.M., Kozlowski, R., Slater, K.J. and Fletcher, J. 1993. THE USE OF ATP BIOLUMINESCENCE AS A MEASURE OF CELL-PROLIFERATION AND CYTOTOXICITY. *JOURNAL OF IMMUNOLOGICAL METHODS*. **160**(1),pp.81–88.
- Cuckler, J.M. 2005. The rationale for metal-on-metal total hip arthroplasty. *Clinical Orthopaedics and Related Research*. **441**,pp.132–136.

- Darowish, M., Rahman, R., Li, P., Bukata, S. V, Gelinas, J., Huang, W., Flick, L.M., Schwarz, E.M. and O'Keefe, R.J. 2009. Reduction of particle-induced osteolysis by interleukin-6 involves anti-inflammatory effect and inhibition of early osteoclast precursor differentiation. *Bone*. **45**(4),pp.661–668.
- Dayer, J.-M. 2002. Interleukin 1 or tumor necrosis factor-alpha: which is the real target in rheumatoid arthritis? *The Journal of rheumatology. Supplement*. **65**,pp.10–15.
- Dennis, D.A., Komistek, R.D., Northcut, E.J., Ochoa, J.A. and Ritchie, A. 2001. ``In vivo`` determination of hip joint separation and the forces generated due to impact loading conditions. *JOURNAL OF BIOMECHANICS*. **34**(5),pp.623–629.
- Derbyshire, B., Fisher, J., Dowson, D., Hardaker, C. and Brummitt, K. 1994. COMPARATIVE-STUDY OF THE WEAR OF UHMWPE WITH ZIRCONIA CERAMIC AND STAINLESS-STEEL FEMORAL HEADS IN ARTIFICIAL HIP JOINTS. *Medical Engineering & Physics*. **16**(3),pp.229–236.
- Doherty, A.T., Howell, R.T., Ellis, L.A., Bisbinas, I., Learmonth, I.D., Newson, R. and Case, C.P. 2001. Increased chromosome translocations and aneuploidy in peripheral blood lymphocytes of patients having revision arthroplasty of the hip. *Journal of Bone and Joint Surgery-British Volume*. **83B**(7),pp.1075–1081.
- Doorn, P.F., Campbell, P.A., Worrall, J., Benya, P.D., McKellop, H.A. and Amstutz, H.C. 1998a. Metal wear particle characterization from metal on metal total hip replacements: Transmission electron microscopy study of periprosthetic tissues and isolated particles. *Journal of Biomedical Materials Research*. **42**(1),pp.103–111.
- Driessens, N., Versteyhe, S., Ghaddhab, C., Burniat, A., De Deken, X., Van Sande, J., Dumont, J.-E., Miot, F. and Corvilain, B. 2009. Hydrogen peroxide induces DNA single- and double-strand breaks in thyroid cells and is therefore a potential mutagen for this organ. *ENDOCRINE-RELATED CANCER*. **16**(3),pp.845–856.
- Edmondson, R., Broglie, J.J., Adcock, A.F. and Yang, L. 2014. Three-Dimensional Cell Culture Systems and Their Applications in Drug Discovery and Cell-Based Biosensors. *ASSAY AND DRUG DEVELOPMENT TECHNOLOGIES*. **12**(4),pp.207–218.
- El-Tahan, R.R., Ghoneim, A.M. and El-Mashad, N. 2016. TNF-alpha gene polymorphisms and expression. *SPRINGERPLUS*. **5**.
- Eruslanov, E. and Kusmartsev, S. 2010. Identification of ROS Using Oxidized DCFDA and Flow-Cytometry *In: Armstrong, D, ed. ADVANCED PROTOCOLS IN OXIDATIVE STRESS II*. Methods in Molecular Biology., pp. 57–72.
- Esposito, C., Maclean, F., Campbell, P., Walter, W.L., Walter, W.K. and Bonar, S.F. 2013. Periprosthetic Tissues From Third Generation Alumina-on-Alumina Total Hip Arthroplasties. *Journal of Arthroplasty*. **28**(5),pp.860–866.
- Esposito, C.I., Walter, W.L., Roques, A., Tuke, M.A., Zicat, B.A., Walsh, W.R. and Walter,

- K. 2012. Wear in alumina-on-alumina ceramic total hip replacements A RETRIEVAL ANALYSIS OF EDGE LOADING. *Journal of Bone and Joint Surgery-British Volume*. **94B**(7),pp.901–907.
- Fang, H.W., Yang, C.B., Chang, C.H., Huang, C.H., Liu, H.L. and Fang, S.B. 2006. The potential role of phagocytic capacity in the osteolytic process induced by polyethylene wear particles. *Journal of International Medical Research*. **34**(6),pp.655–664.
- Faye, P.-A., Roualdes, O., Rossignol, F., Hartmann, D.J. and Desmouliere, A. 2017. Engulfment of ceramic particles by fibroblasts does not alter cell behavior. *BIOMEDICAL MATERIALS*. **12**(1).
- Firkins, P.J., Tipper, J.L., Saadatzadeh, M.R., Ingham, E., Stone, M.H., Farrar, R. and Fisher, J. 2001a. Quantitative analysis of wear and wear debris from metal-on-metal hip prostheses tested In a physiological hip joint simulator. *Bio-Medical Materials and Engineering*. **11**,pp.143–157.
- Fisher, J. 2011. Bioengineering reasons for the failure of metal-on-metal hip prostheses AN ENGINEER'S PERSPECTIVE. *JOURNAL OF BONE AND JOINT SURGERY-BRITISH VOLUME*. **93B**(8),pp.1001–1004.
- Fisher, J., Bell, J., Barbour, P.S.M., Tipper, J.L., Matthews, J.B., Besong, A.A., Stone, M.H. and Ingham, E. 2001. A novel method for the prediction of functional biological activity of polyethylene wear debris. *PROCEEDINGS OF THE INSTITUTION OF MECHANICAL ENGINEERS PART H-JOURNAL OF ENGINEERING IN MEDICINE*. **215**(H2),pp.127–132.
- Fisher, J., Jin, Z.M., Tipper, J., Stone, M. and Ingham, E. 2006. Presidential guest lecture - Tribology of alternative bearings. *Clinical Orthopaedics and Related Research*.,pp.25–34.
- Fleury, C., Petit, A., Mwale, F., Antoniou, J., Zukor, D.J., Tabrizian, M. and Huk, O.L. 2006. Effect of cobalt and chromium ions on human MG-63 osteoblasts in vitro: Morphology, cytotoxicity, and oxidative stress. *Biomaterials*. **27**(18),pp.3351–3360.
- Food and Drug Administration 2016. Food and Drug Administration (FDA) Use of international standard ISO 10993-1, “Biological evaluation of medical devices—part 1: evaluation and testing within a risk management process”. Guidance for Industry and Food and Drug Administration Staff. [Accessed 3 November 2017]. Available from: <https://www.fda.gov/downloads/medicaldevices/deviceregulationandguidance/guidancedocuments/ucm348890.pdf>.
- Fritsch, E.W. and Gleitz, M. 1996. Ceramic femoral head fractures in total hip arthroplasty. *Clinical Orthopaedics and Related Research*. (328),pp.129–136.
- Fu, P.P., Xia, Q., Hwang, H.-M., Ray, P.C. and Yu, H. 2014. Mechanisms of nanotoxicity: Generation of reactive oxygen species. *JOURNAL OF FOOD AND DRUG ANALYSIS*.

22(1, SI),pp.64–75.

- Fuller, K., Murphy, C., Kirstein, B., Fox, S.W. and Chambers, T.J. 2002. TNF α potently activates osteoclasts, through a direct action independent of and strongly synergistic with RANKL. *Endocrinology*. **143**(3),pp.1108–1118.
- Galvin, A.L., Tipper, I.L., Jennings, L.M., Stone, M.H., Jin, Z.M., Ingham, E. and Fisher, J. 2007. Wear and biological activity of highly crosslinked polyethylene in the hip under low serum protein concentrations. *PROCEEDINGS OF THE INSTITUTION OF MECHANICAL ENGINEERS PART H-JOURNAL OF ENGINEERING IN MEDICINE*. **221**(H1),pp.1–10.
- Garino, J.P. 2011. Ceramic Hip Replacement History *In: Seminars in Arthroplasty*. Pennsylvania: Elsevier.
- Garvie, R.C., Hannink, R.H. and Pascoe, R.T. 1975. Ceramic Steel. *Nature*. **258**(5537),pp.703–704.
- Germain, M.A., Hatton, A., Williams, S., Matthews, J.B., Stone, M.H., Fisher, J. and Ingham, E. 2003a. Comparison of the cytotoxicity of clinically relevant cobalt-chromium and alumina ceramic wear particles in vitro. *Biomaterials*. **24**,pp.469–479.
- Glant, T.T. and Jacobs, J.J. 1994. RESPONSE OF 3 MURINE MACROPHAGE POPULATIONS TO PARTICULATE DEBRIS - BONE-RESORPTION IN ORGAN-CULTURES. *Journal of Orthopaedic Research*. **12**(5),pp.720–731.
- Glaser, D., Komistek, R.D., Cates, H.E. and Mahfouz, M.R. 2008. Clicking and Squeaking: In Vivo Correlation of Sound and Separation for Different Bearing Surfaces. *Journal of Bone and Joint Surgery-American Volume*. **90A**,pp.112–120.
- Goodman, S.B., Barrena, E.G., Takagi, M. and Kontinen, Y.T. 2009. Biocompatibility of total joint replacements: A review. *Journal of Biomedical Materials Research Part A*. **90A**(2),pp.603–618.
- Goodman, S.B., Chin, R.C., Chiou, S.S., Schurman, D.J., Woolson, S.T. and Masada, M.P. 1989. A CLINICAL PATHOLOGIC BIOCHEMICAL-STUDY OF THE MEMBRANE SURROUNDING LOOSENED AND NONLOOSENED TOTAL HIP ARTHROPLASTIES. *Clinical Orthopaedics and Related Research*. (244),pp.182–187.
- Goodman, S.B., Fornasier, V.L., Lee, J. and Kei, J. 1990. THE HISTOLOGICAL EFFECTS OF THE IMPLANTATION OF DIFFERENT SIZES OF POLYETHYLENE PARTICLES IN THE RABBIT TIBIA. *Journal of Biomedical Materials Research*. **24**(4),pp.517–524.
- Goodman, S.B., Gibon, E. and Yao, Z. 2013. The basic science of periprosthetic osteolysis. *Instructional course lectures*. **62**,pp.201–206.
- Goodman, S.B., Huie, P., Song, Y., Schurman, D., Maloney, W., Woolson, S. and Sibley, R. 1998. Cellular profile and cytokine production at prosthetic interfaces - Study of tissues

- retrieved from revised hip and knee replacements. *Journal of Bone and Joint Surgery-British Volume*. **80B**(3),pp.531–539.
- Goodman, S.B. and Ma, T. 2010. Cellular chemotaxis induced by wear particles from joint replacements. *Biomaterials*. **31**(19),pp.5045–5050.
- Gordon, A., Kiss-Toth, E., Stockley, I., Eastell, R. and Wilkinson, J.M. 2008. Polymorphisms in the Interleukin-1 Receptor Antagonist and Interleukin-6 Genes Affect Risk of Osteolysis in Patients With Total Hip Arthroplasty. *ARTHRITIS AND RHEUMATISM*. **58**(10),pp.3157–3165.
- Granchi, D., Ciapetti, G., Amato, I., Pagani, S., Cenni, E., Savarino, L., Avnet, S., Peris, J.L., Pellacani, A., Baldini, N. and Giunti, A. 2004. The influence of alumina and ultra-high molecular weight polyethylene particles on osteoblast-osteoclast cooperation. *Biomaterials*. **25**(18),pp.4037–4045.
- Grebentchikov, N., van der Ven-Jongekrijg, J., Pesman, G.J., Geurts-Moespot, A., van der Meer, J.W.M. and Sweep, F. 2005. Development of a sensitive ELISA for the quantification of human tumour necrosis factor-alpha using 4 polyclonal antibodies. *EUROPEAN CYTOKINE NETWORK*. **16**(3),pp.215–222.
- Green, T.R., Fisher, J., Matthews, J.B., Stone, M.H. and Ingham, E. 2000. Effect of size and dose on bone resorption activity of macrophages by in vitro clinically relevant ultra high molecular weight polyethylene particles. *Journal of Biomedical Materials Research*. **53**(5),pp.490–497.
- Green, T.R., Fisher, J., Stone, M., Wroblewski, B.M. and Ingham, E. 1998. Polyethylene particles of a ‘critical size’ are necessary for the induction of cytokines by macrophages in vitro. *Biomaterials*. **19**(24),pp.2297–2302.
- Griss, P. and Heimke, G. 1981. 5 YEARS EXPERIENCE WITH CERAMIC-METAL-COMPOSITE HIP ENDOPROSTHESES .1. CLINICAL-EVALUATION. *Archives of Orthopaedic and Trauma Surgery*. **98**(3),pp.157–164.
- Haddad, F.S., Thakrar, R.R., Hart, A.J., Skinner, J.A., Nargol, A.V.F., Nolan, J.F., Gill, H.S., Murray, D.W., Blom, A.W. and Case, P. 2011. Metal-on-metal bearings THE EVIDENCE SO FAR. *JOURNAL OF BONE AND JOINT SURGERY-BRITISH VOLUME*. **93B**(5),pp.572–579.
- Hailey, J.L., Ingham, E., Stone, M., Wroblewski, B.M. and Fisher, J. 1996. Ultra-high molecular weight polyethylene wear debris generated in vivo and in laboratory tests; the influence of counterface roughness. *Proceedings of the Institution of Mechanical Engineers. Part H, Journal of engineering in medicine*. **210**(1),pp.3–10.
- Haraguchi, K., Sugano, N., Nishii, T., Miki, H., Oka, K. and Yoshikawa, H. 2001. Phase transformation of a zirconia ceramic head after total hip arthroplasty. *Journal of Bone and Joint Surgery-British Volume*. **83B**(7),pp.996–1000.

- Hartofilakidis, G., Karachalios, T. and Karachalios, G. 2005. The 20-year outcome of the Charnley arthroplasty in younger and older patients. *Clinical Orthopaedics and Related Research*. (434),pp.177–182.
- Hatton, A. 2001. The biological response to alumina ceramic wear debris. . **PhD Thesis**.
- Hatton, A., Nevelos, J.E., Matthews, J.B., Fisher, J. and Ingham, E. 2003a. Effects of clinically relevant alumina ceramic wear particles on TNF-alpha production by human peripheral blood mononuclear phagocytes. *Biomaterials*. **24**(7),pp.1193–1204.
- Hatton, A., Nevelos, J.E., Nevelos, A.A., Banks, R.E., Fisher, J. and Ingham, E. 2002. Alumina-alumina artificial hip joints. Part I: a histological analysis and characterisation of wear debris by laser capture microdissection of tissues retrieved at revision. *Biomaterials*. **23**(16),pp.3429–3440.
- Haycock, J.W. 2011. 3D Cell Culture: A Review of Current Approaches and Techniques *In*: Haycock, JW, ed. *3D CELL CULTURE: METHODS AND PROTOCOLS*. Methods in Molecular Biology., pp. 1–15.
- Henssge, E.J., Bos, I. and Willmann, G. 1994. AL₂O₃ AGAINST AL₂O₃ COMBINATION IN HIP ENDOPROSTHESES - HISTOLOGIC INVESTIGATIONS WITH SEMIQUANTITATIVE GRADING OF REVISION AND AUTOPSY CASES AND ABRASION MEASURES. *Journal of Materials Science-Materials in Medicine*. **5**(9–10),pp.657–661.
- Hernigou, P. and Bahrami, T. 2003. Zirconia and alumina ceramics in comparison with stainless-steel heads - Polyethylene wear after a minimum ten-year follow-up. *Journal of Bone and Joint Surgery-British Volume*. **85B**(4),pp.504–509.
- Horowitz, S.M. and Gonzales, J.B. 1997. Effects of polyethylene on macrophages. *Journal of Orthopaedic Research*. **15**(1),pp.50–56.
- Howie, D.W. 1993. *PROSTHESIS WEAR PARTICLE EFFECTS ON CELLS AND TISSUES* (B. F. Morrey, ed.).
- Huiskes, R., Weinans, H. and Vanrietbergen, B. 1992. THE RELATIONSHIP BETWEEN STRESS SHIELDING AND BONE-RESORPTION AROUND TOTAL HIP STEMS AND THE EFFECTS OF FLEXIBLE MATERIALS. *Clinical Orthopaedics and Related Research*. (274),pp.124–134.
- Illgen II, R.L., Bauer, L.M., Hotujec, B.T., Kolpin, S.E., Bakhtiar, A. and Forsythe, T.M. 2009. Highly Crosslinked Vs Conventional Polyethylene Particles Relative In Vivo Inflammatory Response. *Journal of Arthroplasty*. **24**(1),pp.117–124.
- Illgen II, R.L., Forsythe, T.M., Pike, J.W., Laurent, M.P. and Blanchard, C.R. 2008. Highly crosslinked vs conventional polyethylene particles - An in vitro comparison of biologic activities. *Journal of Arthroplasty*. **23**(5),pp.721–731.
- Ingham, E. and Fisher, J. 2000. Biological reactions to wear debris in total joint replacement.

Proceedings of the Institution of Mechanical Engineers Part H-Journal of Engineering in Medicine. **214**(H1),pp.21–37.

- Ingham, E. and Fisher, J. 2005. The role of macrophages in osteolysis of total joint replacement. *Biomaterials.* **26**(11),pp.1271–1286.
- Ingram, J.H., Stone, M., Fisher, J. and Ingham, E. 2004. The influence of molecular weight, crosslinking and counterface roughness on TNF-alpha production by macrophages in response to ultra high molecular weight polyethylene particles. *Biomaterials.* **25**(17),pp.3511–3522.
- Jacobs, J.J., Campbell, P.A., Konttinen, Y.T. and Implant Wear Symposium, B. 2008. How has the biologic reaction to wear particles changed with newer bearing surfaces? *Journal of the American Academy of Orthopaedic Surgeons.* **16**,pp.S49–S55.
- Jeffers, J.R.T. and Walter, W.L. 2012. Ceramic-on-ceramic bearings in hip arthroplasty STATE OF THE ART AND THE FUTURE. *Journal of Bone and Joint Surgery-British Volume.* **94B**(6),pp.735–745.
- Jimi, E., Nakamura, I., Duong, L.T., Ikebe, T., Takahashi, N., Rodan, G.A. and Suda, T. 1999. Interleukin 1 induces multinucleation and bone-resorbing activity of osteoclasts in the absence of osteoblasts/stromal cells. *Experimental Cell Research.* **247**(1),pp.84–93.
- Jin, Z.M., Firkins, P., Farrar, R. and Fisher, J. 2000. Analysis and modelling of wear of cobalt-chrome alloys in a pin-on-plate test for a metal-on-metal total hip replacement. *PROCEEDINGS OF THE INSTITUTION OF MECHANICAL ENGINEERS PART H-JOURNAL OF ENGINEERING IN MEDICINE.* **214**(H6),pp.559–568.
- Jin, Z.M., Stone, M., Ingham, E. and Fisher, J. 2006. Biotribology. *CURRENT ORTHOPAEDICS.* **20**(1),pp.32–40.
- Jolles, B.M., Genoud, P. and Hoffmeyer, P. 2004. Computer-assisted cup placement techniques in total hip arthroplasty improve accuracy of placement. *Clinical Orthopaedics and Related Research.* (426),pp.174–179.
- Joshi, M.G., Advani, S.G., Miller, F. and Santare, M.H. 2000. Analysis of a femoral hip prosthesis designed to reduce stress shielding. *Journal of Biomechanics.* **33**(12),pp.1655–1662.
- Kamali, A. 2009. Hip Joint Tribology *In: McMinn, DJW, ed. MODERN HIP RESURFACING.*, pp. 79–89.
- Kandahari, A.M., Yang, X., Laroche, K.A., Dighe, A.S., Pan, D. and Cui, Q. 2016. A review of UHMWPE wear-induced osteolysis: the role for early detection of the immune response. *BONE RESEARCH.* **4.**
- Kim, K.J., Rubash, H.E., Wilson, S.C., Dantonio, J.A. and McClain, E.J. 1993. A HISTOLOGIC AND BIOCHEMICAL-COMPARISON OF THE INTERFACE TISSUES IN CEMENTLESS AND CEMENTED HIP PROSTHESES. *Clinical*

Orthopaedics and Related Research. (287),pp.142–152.

- Kinov, P., Leithner, A., Radl, R., Bodo, K., Khoschorur, G.A., Schauenstein, K. and Windhager, R. 2006. Role of free radicals in aseptic loosening of hip arthroplasty. *JOURNAL OF ORTHOPAEDIC RESEARCH.* **24**(1),pp.55–62.
- Kinov, P., Tzoncheva, A. and Tivchev, P. 2010. EVIDENCE LINKING ELEVATED OXIDATIVE STRESS AND ASEPTIC LOOSENING OF HIP ARTHROPLASTY. *Comptes Rendus De L Academie Bulgare Des Sciences.* **63**(8),pp.1231–1238.
- Kitaura, H., Zhou, P., Kim, H.J., Novack, D. V, Ross, F.P. and Teitelbaum, S.L. 2005. M-CSF mediates TNF-induced inflammatory osteolysis. *Journal of Clinical Investigation.* **115**(12),pp.3418–3427.
- Knahr, K. 2013. Tribology and Total Hip Arthroplasty Implants. *Orthopedics.* **36**(11),pp.854–855.
- Knight, S.R., Aujla, R. and Biswas, S.P. 2011. Total Hip Arthroplasty - over 100 years of operative history. *Orthopedic reviews.* **3**(2),pp.e16–e16.
- Kobayashi, A., Freeman, M.A.R., Bonfield, W., Kadoya, Y., Yamac, T., AlSaffar, N., Scott, G. and Revell, P.A. 1997. Number of polyethylene particles and osteolysis in total joint replacements - A quantitative study using a tissue-digestion method. *JOURNAL OF BONE AND JOINT SURGERY-BRITISH VOLUME.* **79B**(5),pp.844–848.
- Kobayashi, K., Takahashi, N., Jimi, E., Udagawa, N., Takami, M., Kotake, S., Nakagawa, N., Kinoshita, M., Yamaguchi, K., Shima, N., Yasuda, H., Morinaga, T., Higashio, K., Martin, T.J. and Suda, T. 2000. Tumor necrosis factor alpha stimulates osteoclast differentiation by a mechanism independent of the ODF/RANKL-RANK interaction. *Journal of Experimental Medicine.* **191**(2),pp.275–285.
- Kopf, M., Baumann, H., Freer, G., Freudenberg, M., Lamers, M., Kishimoto, T., Zinkernagel, R., Bluethmann, H. and Kohler, G. 1994. IMPAIRED IMMUNE AND ACUTE-PHASE RESPONSES IN INTERLEUKIN-6-DEFICIENT MICE. *Nature.* **368**(6469),pp.339–342.
- Korovessis, P., Petsinis, G., Repanti, M. and Repantis, T. 2006. Metallosis after contemporary metal-on-metal total hip arthroplasty - Five to nine-year follow-up. *Journal of Bone and Joint Surgery-American Volume.* **88A**(6),pp.1183–1191.
- Kotake, S. and Kamatani, N. 2005. Association of polymorphisms in genes of osteoclastogenesis-related cytokines with severity in patients with rheumatoid arthritis. *Nihon rinsho. Japanese journal of clinical medicine.* **63**(9),pp.1574–1578.
- Kretzer, J.P., Mueller, U., Streit, M.R., Kiefer, H., Sonntag, R., Streicher, R.M. and Reinders, J. 2018. Ion release in ceramic bearings for total hip replacement: Results from an in vitro and an in vivo study. *INTERNATIONAL ORTHOPAEDICS.* **42**(1),pp.65–70.
- Kucera, O., Endlicher, R., Rousar, T., Lotkova, H., Garnol, T., Drahotka, Z. and Cervinkova,

- Z. 2014. The Effect of tert-Butyl Hydroperoxide-Induced Oxidative Stress on Lean and Steatotic Rat Hepatocytes In Vitro. *OXIDATIVE MEDICINE AND CELLULAR LONGEVITY*.
- Kummer, F.J., Stuchin, S.A. and Frankel, V.H. 1990. Analysis of removed autophor ceramic-on-ceramic components. *The Journal of arthroplasty*. **5**(1),pp.28–33.
- Kuntz, M. and Krueger, R. 2018. The effect of microstructure and chromia content on the properties of zirconia toughened alumina. *CERAMICS INTERNATIONAL*. **44**(2),pp.2011–2020.
- Kurtz, S., Ong, K., Lau, E., Mowat, F. and Halpern, M. 2007. Projections of primary and revision hip and knee arthroplasty in the United States from 2005 to 2030. *Journal of Bone and Joint Surgery-American Volume*. **89A**(4),pp.780–785.
- Kurtz, S.M., Kocagoz, S., Arnholt, C., Huet, R., Ueno, M. and Walter, W.L. 2014. Advances in zirconia toughened alumina biomaterials for total joint replacement. *JOURNAL OF THE MECHANICAL BEHAVIOR OF BIOMEDICAL MATERIALS*. **31**,pp.107–116.
- Kwon, Y.-M., Thomas, P., Summer, B., Pandit, H., Taylor, A., Beard, D., Murray, D.W. and Gill, H.S. 2010. Lymphocyte Proliferation Responses in Patients with Pseudotumors following Metal-on-Metal Hip Resurfacing Arthroplasty. *JOURNAL OF ORTHOPAEDIC RESEARCH*. **28**(4),pp.444–450.
- Kwon, Y.-M., Xia, Z., Glyn-Jones, S., Beard, D., Gill, H.S. and Murray, D.W. 2009. Dose-dependent cytotoxicity of clinically relevant cobalt nanoparticles and ions on macrophages in vitro. *Biomedical Materials*. **4**(2).
- Ladon, D., Doherty, A., Newson, R., Turner, J., Bhamra, M. and Case, C.P. 2004. Changes in metal levels and chromosome aberrations in the peripheral blood of patients after metal-on-metal hip arthroplasty. *Journal of Arthroplasty*. **19**(8),pp.78–83.
- Lal, S., Hall, R. and Tipper, J. 2017. THREE-DIMENSIONAL PARTICLE-EMBEDDED AGAROSE GELS FOR SIMULTANEOUS BIOCOMPATIBILITY TESTING OF POLYMER, METAL AND CERAMIC WEAR DEBRIS. *Orthopaedic Proceedings*. [Online]. **99-B**(SUPP 4),p.97. Available from: http://bjjprocs.boneandjoint.org.uk/content/99-B/SUPP_4/97.
- Lal, S., Hall, R.M. and Tipper, J.L. 2016. A Novel Method for Isolation and Recovery of Ceramic Nanoparticles and Metal Wear Debris from Serum Lubricants at Ultra-low Wear Rates. *Under Review, Acta Biomaterialia*.
- Lancaster-Jones, O., Williams, S., Jennings, L.M., Thompson, J., Isaac, G., Fisher, J. and Al-Hajjar, M. 2016. The influence of surgical positioning on the severity of edge loading, and wear rate in total hip replacement. *Bone Joint Journal*. **98-B**(SUPP(92)).
- Learmonth, I.D., Young, C. and Rorabeck, C. 2007. The operation of the century: total hip replacement. *Lancet*. **370**(9597),pp.1508–1519.

- Lee, H. 2016. Spinal cord cellular response to wear debris from metal-on-metal total disc replacements.
- Lee, J.M., Salvati, E.A., Betts, F., Dicarolo, E.F., Doty, S.B. and Bullough, P.G. 1992. SIZE OF METALLIC AND POLYETHYLENE DEBRIS PARTICLES IN FAILED CEMENTED TOTAL HIP REPLACEMENTS. *Journal of Bone and Joint Surgery-British Volume*. **74**(3),pp.380–384.
- Lerouge, S., Huk, O., Yahia, L., Witvoet, J. and Sedel, L. 1997. Ceramic-ceramic and metal-polyethylene total hip replacements - Comparison of pseudomembranes after loosening. *Journal of Bone and Joint Surgery-British Volume*. **79B**(1),pp.135–139.
- Lerouge, S., Huk, O., Yahia, L.H. and Sedel, L. 1996. Characterization of in vivo wear debris from ceramic-ceramic total hip arthroplasties. *Journal of Biomedical Materials Research*. **32**(4),pp.627–633.
- Liao, Y.-S. and Hanes, M. 2006. The effects of implant temperature on lubricant protein precipitation and polyethylene wear in joint simulation studies *In: Brown, SA and Gilbertson, LN and Good, VD, ed. Wear of Articulating Surfaces: Understanding Joint Simulation*. AMERICAN SOCIETY FOR TESTING AND MATERIALS SPECIAL TECHNICAL PUBLICATION., pp. 91–96.
- Liu, A., Richards, L., Bladen, C.L., Ingham, E., Fisher, J. and Tipper, J.L. 2015. The biological response to nanometre-sized polymer particles. *ACTA BIOMATERIALIA*. **23**,pp.38–51.
- Loh, N.L. and Sia, K.Y. 1992. AN OVERVIEW OF HOT ISOSTATIC PRESSING. *Journal of Materials Processing Technology*. **30**(1),pp.45–65.
- Lombardi, A. V, Mallory, T.H., Dennis, D.A., Komistek, R.D., Fada, R.A. and Northcut, E.J. 2000. An in vivo determination of total hip arthroplasty pistoning during activity. *Journal of Arthroplasty*. **15**(6),pp.702–709.
- Long, W.T. 2005. The Clinical Performance of Metal-on-Metal as an Articulation Surface in Total Hip Replacement. *The Iowa Orthopaedic Journal*. **25**,pp.10–16.
- Lu, Z. and McKellop, H. 1997. Frictional heating of bearing materials tested in a hip joint wear simulator. *Proceedings of the Institution of Mechanical Engineers Part H-Journal of Engineering in Medicine*. **211**(1),pp.101–108.
- Ma, L. and Rainforth, W.M. 2010. A study of BioloX (R) delta subject to water lubricated reciprocating wear. *TRIBOLOGY INTERNATIONAL*. **43**(10, SI),pp.1872–1881.
- Ma, L. and Rainforth, W.M. 2012. The effect of lubrication on the friction and wear of BioloX (R) delta. *ACTA BIOMATERIALIA*. **8**(6),pp.2348–2359.
- Maccauro, G., Iommetti, P.R., Raffaelli, L. and Manicone, P.F. 2011. Alumina and Zirconia Ceramic for Orthopaedic and Dental Devices *In: Pignatello, R, ed. BIOMATERIALS APPLICATIONS FOR NANOMEDICINE.*, pp. 299–308.

- Madl, A.K., Kovochich, M., Liong, M., Finley, B.L., Paustenbach, D.J. and Oberdoerster, G. 2015. Toxicology of wear particles of cobalt-chromium alloy metal-on-metal hip implants Part II: Importance of physicochemical properties and dose in animal and in vitro studies as a basis for risk assessment. *NANOMEDICINE-NANOTECHNOLOGY BIOLOGY AND MEDICINE*. **11**(5),pp.1285–1298.
- Mahendra, G., Pandit, H., Kliskey, K., Murray, D., Gill, H.S. and Athanasou, N. 2009. Necrotic and inflammatory changes in metal-on-metal resurfacing hip arthroplasties Relation to implant failure and pseudotumor formation. *ACTA ORTHOPAEDICA*. **80**(6),pp.653–659.
- Mak, M.M., Besong, A.A., Jin, Z.M. and Fisher, J. 2002. Effect of microseparation on contact mechanics in ceramic-on-ceramic hip joint replacements. *Proceedings of the Institution of Mechanical Engineers Part H-Journal of Engineering in Medicine*. **216**(H6),pp.403–408.
- Mandelin, J., Li, T.F., Lijestrom, M., Kroon, M.E., Hanemaaijer, R., Santavirta, S. and Konttinen, Y.T. 2003. Imbalance of RANKL/RANK/OPG system in interface tissue in loosening of total hip replacement. *Journal of Bone and Joint Surgery-British Volume*. **85B**(8),pp.1196–1201.
- Margevicius, K.J., Bauer, T.W., McMahon, J.T., Brown, S.A. and Merritt, K. 1994. ISOLATION AND CHARACTERIZATION OF DEBRIS IN MEMBRANES AROUND TOTAL JOINT PROSTHESES. *Journal of Bone and Joint Surgery-American Volume*. **76A**(11),pp.1664–1675.
- Maruyama, N., Hiromoto, S., Akiyama, E. and Nakamura, M. 2013. Fretting fatigue behaviour of Ni-free high-nitrogen stainless steel in a simulated body fluid. *SCIENCE AND TECHNOLOGY OF ADVANCED MATERIALS*. **14**(2).
- Masonis, J.L., Bourne, R.B., Ries, M.D., McCalden, R.W., Salehi, A. and Kelman, D.C. 2004. Zirconia femoral head fractures - A clinical and retrieval analysis. *JOURNAL OF ARTHROPLASTY*. **19**(7),pp.898–905.
- Masson, B. 2009. Emergence of the alumina matrix composite in total hip arthroplasty. *International Orthopaedics*. **33**(2),pp.359–363.
- Matthews, J.B., Besong, A.A., Green, T.R., Stone, M.H., Wroblewski, B.M., Fisher, J. and Ingham, E. 2000. Evaluation of the response of primary human peripheral blood mononuclear phagocytes to challenge with In vitro generated clinically relevant UHMWPE particles of known size and dose. *Journal of Biomedical Materials Research*. **52**(2),pp.296–307.
- Matthews, J.B., Green, T.R., Stone, M.H., Wroblewski, B.M., Fisher, J. and Ingham, E. 2000a. Comparison of the response of primary human peripheral blood mononuclear phagocytes from different donors to challenge with model polyethylene particles of

- known size and dose. *Biomaterials*. **21**(20),pp.2033–2044.
- Medel, F.J., Kurtz, S.M. and Shah, P. 2009. Retrieval Analysis of Contemporary Alternative Femoral Head Materials: Oxinium and Biolox Delta *In: 55th Annual Meeting of the Orthopaedic Research Society*. Las Vegas, NV: Trans.
- Nagase, M., Nishiya, H. and Takeuchi, H. 1995. EFFECT OF PARTICLE-SIZE ON ALUMINA-INDUCED PRODUCTION OF REACTIVE OXYGEN METABOLITES BY HUMAN-LEUKOCYTES. *Scandinavian Journal of Rheumatology*. **24**(2),pp.102–107.
- Nakashima, Y., Sun, D.H., Trindade, M.C.D., Chun, L.E., Song, Y., Goodman, S.B., Schurman, D.J., Maloney, W.J. and Smith, R.L. 1999. Induction of macrophage C-C chemokine expression by titanium alloy and bone cement particles. *Journal of Bone and Joint Surgery-British Volume*. **81B**(1),pp.155–162.
- Nam, K.W., Yoo, J.J., Kim, Y.L., Kim, Y.-M., Lee, M.-H. and Kim, H.J. 2007. Alumina-debris-induced osteolysis in contemporary alumina-on-alumina total hip arthroplasty - A case report. *Journal of Bone and Joint Surgery-American Volume*. **89A**(11),pp.2499–2503.
- National Joint Registry 2016. *Full 13th NJR Annual Report* [Online]. Available from: http://www.njrreports.org.uk/Portals/0/PDFdownloads/NJR_13th_Annual_Report_2016.pdf.
- National Joint Registry 2017. *Full 14th NJR Annual Report* [Online]. Available from: http://www.njrreports.org.uk/Portals/0/PDFdownloads/NJR_14th_Annual_Report_2017.pdf.
- Neale, S.D. and Athanasou, N.A. 1999. Cytokine receptor profile of arthroplasty macrophages, foreign body giant cells and mature osteoclasts. *Acta Orthopaedica Scandinavica*. **70**(5),pp.452–458.
- Nevelos, J., Ingham, E., Doyle, C., Streicher, R., Nevelos, A., Walter, W. and Fisher, J. 2000a. Microseparation of the centers of alumina-alumina artificial hip joints during simulator testing produces clinically relevant wear rates and patterns. *Journal of Arthroplasty*. **15**(6),pp.793–795.
- Nevelos, J.E., Ingham, E., Doyle, C., Fisher, J. and Nevelos, A.B. 1999. Analysis of retrieved alumina ceramic components from Mittelmeier total hip prostheses. *Biomaterials*. **20**(19),pp.1833–1840.
- Nevelos, J.E., Ingham, E., Doyle, C., Nevelos, A.B. and Fisher, J. 2001a. The influence of acetabular cup angle on the wear of ‘BIOLOX Forte’ alumina ceramic bearing couples in a hip joint simulator. *Journal of Materials Science-Materials in Medicine*. **12**(2),pp.141–144.
- Nevelos, J.E., Ingham, E., Doyle, C., Nevelos, A.B. and Fisher, J. 2001b. Wear of HIPed and

- non-HIPed alumina-alumina hip joints under standard and severe simulator testing conditions. *Biomaterials*. **22**,pp.2191–2197.
- Nevelos, J.E., Prudhommeaux, F., Hamadouche, M., Doyle, C., Ingham, E., Meunier, A., Nevelos, A.B., Sedel, L. and Fisher, J. 2001. Comparative analysis of two different types of alumina-alumina hip prosthesis retrieved for aseptic loosening. *Journal of Bone and Joint Surgery-British Volume*. **83B**(4),pp.598–603.
- Niedzwiecki, S., Klapperich, C., Short, J., Jani, S., Ries, M. and Pruitt, L. 2001. Comparison of three joint simulator wear debris isolation techniques: Acid digestion, base digestion, and enzyme cleavage. *Journal of Biomedical Materials Research*. **56**(2),pp.245–249.
- Nkamgueu, E.M., Adnet, J.J., Bernard, J., Zierold, K., Kilian, L., Jallot, E., Benhayoune, H. and Bonhomme, P. 2000a. In vitro effects of zirconia and alumina particles on human blood monocyte-derived macrophages: X-ray microanalysis and flow cytometric studies. *Journal of Biomedical Materials Research*. **52**(4),pp.587–594.
- O'Dwyer Lancaster-Jones, O., Williams, S., Jennings, L.M., Thompson, J., Isaac, G.H., Fisher, J. and Al-Hajjar, M. 2017. An in vitro simulation model to assess the severity of edge loading and wear, due to variations in component positioning in hip joint replacements. *Journal of Biomedical Materials Research Part B: Applied Biomaterials*. [Online]. Available from: <http://doi.wiley.com/10.1002/jbm.b.33991>.
- Olivier, V., Duval, J.L., Hindie, M., Pouletaut, P. and Nagel, M.D. 2003. Comparative particle-induced cytotoxicity toward macrophages and fibroblasts. *CELL BIOLOGY AND TOXICOLOGY*. **19**(3),pp.145–159.
- Oonishi, H., Kawanabe, K., Yamamoto, K., Dwons, B., Sorensen, K., Good, V., Braham, A., Clark, I. and Nishida, M. 1999. In vitro wear of Al₂O₃/Al₂O₃ implant combination with over 10 million cycles duration *In: Proceedings of the 45th Orthopaedic Research Society*. Anaheim CA, p. 50.
- Osserman, F.. 2012. *Lysozyme*. Academic Press.
- Owen, D.H., Russell, N.C., Smith, P.N. and Walter, W.L. 2014. An estimation of the incidence of squeaking and revision surgery for squeaking in ceramic-on-ceramic total hip replacement A META-ANALYSIS AND REPORT FROM THE AUSTRALIAN ORTHOPAEDIC ASSOCIATION NATIONAL JOINT REGISTRY. *Bone & Joint Journal*. **96B**(2),pp.181–187.
- Palmero, P., Montanaro, L., Reveron, H. and Chevalier, J. 2014. Surface Coating of Oxide Powders: A New Synthesis Method to Process Biomedical Grade Nano-Composites. *MATERIALS*. **7**(7),pp.5012–5037.
- Papageorgiou, I., Abberton, T., Fuller, M., Tipper, J.L., Fisher, J. and Ingham, E. 2014. Biological Effects of Clinically Relevant CoCr Nanoparticles in the Dura Mater: An Organ Culture Study. *NANOMATERIALS*. **4**(2),pp.485–504.

- Papageorgiou, I., Brown, C., Schins, R., Singh, S., Newson, R., Davis, S., Fisher, J., Ingham, E. and Case, C.P. 2007. The effect of nano- and micron-sized particles of cobalt-chromium alloy on human fibroblasts in vitro. *BIOMATERIALS*. **28**(19),pp.2946–2958.
- Paradowska, A. and Lacki, J.K. 2006. Pro-inflammatory cytokines gene polymorphisms in Rheumatoid Arthritis. *Central European Journal of Immunology*. **31**(3–4),pp.117–122.
- Parry, M.C., Bhabra, G., Sood, A., Machado, F., Cartwright, L., Saunders, M., Ingham, E., Newson, R., Blom, A.W. and Case, C.P. 2010. Thresholds for indirect DNA damage across cellular barriers for orthopaedic biomaterials. *BIOMATERIALS*. **31**(16),pp.4477–4483.
- Pawlik, A., Wrzesniewska, J., Florczak, M., Gawronska-Szklarz, B. and Herczynska, M. 2005. IL-6 promoter polymorphism in patients with rheumatoid arthritis. *Scandinavian Journal of Rheumatology*. **34**(2),pp.109–113.
- Pazzaglia, U.E., Dellorbo, C. and Wilkinson, M.J. 1987. THE FOREIGN-BODY REACTION IN TOTAL HIP ARTHROPLASTIES - A CORRELATED LIGHT-MICROSCOPY, SEM, AND TEM STUDY. *Archives of Orthopaedic and Trauma Surgery*. **106**(4),pp.209–219.
- Peichl, P., Ceska, M., Effenberger, F., Haberhauer, G., Broell, H. and Lindley, I.J.D. 1991. PRESENCE OF NAP-1/IL-8 IN SYNOVIAL-FLUIDS INDICATES A POSSIBLE PATHOGENIC ROLE IN RHEUMATOID-ARTHRITIS. *Scandinavian Journal of Immunology*. **34**(3),pp.333–339.
- Petit, A., Catelas, I., Antoniou, J., Zukor, D.J. and Huk, O.L. 2002. Differential apoptotic response of J774 macrophages to alumina and ultra-high-molecular-weight polyethylene particles. *JOURNAL OF ORTHOPAEDIC RESEARCH*. **20**(1),pp.9–15.
- Pezzotti, G., Munisso, M.C., Porporati, A.A. and Lessnau, K. 2010. On the role of oxygen vacancies and lattice strain in the tetragonal to monoclinic transformation in alumina/zirconia composites and improved environmental stability. *BIOMATERIALS*. **31**(27),pp.6901–6908.
- Pezzotti, G., Yamada, K., Porporati, A.A., Kuntz, M. and Yamamoto, K. 2009. Fracture Toughness Analysis of Advanced Ceramic Composite for Hip Prosthesis. *JOURNAL OF THE AMERICAN CERAMIC SOCIETY*. **92**(8),pp.1817–1822.
- Posada, O.M., Gilmour, D., Tate, R.J. and Grant, M.H. 2014. CoCr wear particles generated from CoCr alloy metal-on-metal hip replacements, and cobalt ions stimulate apoptosis and expression of general toxicology-related genes in monocyte-like U937 cells. *TOXICOLOGY AND APPLIED PHARMACOLOGY*. **281**(1),pp.125–135.
- Posada, O.M., Tate, R.J. and Grant, M.H. 2015. Effects of CoCr metal wear debris generated from metal-on-metal hip implants and Co ions on human monocyte-like U937 cells. *TOXICOLOGY IN VITRO*. **29**(2),pp.271–280.

- Prabhakar, P. V, Reddy, U.A., Singh, S.P., Balasubramanyam, A., Rahman, M.F., Kumari, S.I., Agawane, S.B., Murty, U.S.N., Grover, P. and Mahboob, M. 2012. Oxidative stress induced by aluminum oxide nanomaterials after acute oral treatment in Wistar rats. *Journal of Applied Toxicology*. **32**(6),pp.436–445.
- Premnath, V., Harris, W.H., Jasty, M. and Merrill, E.W. 1996. Gamma sterilization of UHMWPE articular implants: An analysis of the oxidation problem. *Biomaterials*. **17**(18),pp.1741–1753.
- Purdue, P.E., Koulouvaris, P., Nestor, B.J. and Sculco, T.P. 2006. The Central Role of Wear Debris in Periprosthetic Osteolysis. *HSS Journal*. **2**(2),pp.102–113.
- Quillin, M.L. and Matthews, B.W. 2000. Accurate calculation of the density of proteins. *ACTA CRYSTALLOGRAPHICA SECTION D-BIOLOGICAL CRYSTALLOGRAPHY*. **56**(7),pp.791–794.
- Raghunathan, V.K., Devey, M., Hawkins, S., Hails, L., Davis, S.A., Mann, S., Chang, I.T., Ingham, E., Malhas, A., Vaux, D.J., Lane, J.D. and Case, C.P. 2013. Influence of particle size and reactive oxygen species on cobalt chrome nanoparticle-mediated genotoxicity. *BIOMATERIALS*. **34**(14),pp.3559–3570.
- Rahman, M., Laurent, S., Tawil, N., Yahia, L. and Mahmoudi, M. 2013. *Protein-Nanoparticle Interactions, The Bio-Nano Interface*. Springer-Verlag Berlin Heidelberg.
- Rajpura, A., Kendoff, D. and Board, T.N. 2014. The current state of bearing surfaces in total hip replacement. *Bone & Joint Journal*. **96B**(2),pp.147–156.
- Ratner, B., Hoffman, A.S., Schoen, F.J. and Lemons, J.E. 2012. Orthopaedic applications *In: Biomaterials Science: An Introduction to Materials in Medicine*. Academic Press.
- Refior, H.J., Plitz, W. and Walter, A. 1997. *Ex vivo and in vitro analysis of the alumina/alumina bearing system for hip joint prostheses* (L. Sedel & C. Rey, eds.).
- Reize, P., Geiger, E. V, Suckel, A., Rudert, M. and Wulker, N. 2008. Influence of surgical experience on accuracy of acetabular cup positioning in total hip arthroplasty. *American journal of orthopedics (Belle Mead, N.J.)*. **37**(7),pp.360–363.
- Ren, W.P., Yang, S.Y., Fang, H.W., Hsu, S. and Wooley, P.H. 2003. Distinct gene expression of receptor activator of nuclear factor-kappa B and rank ligand in the inflammatory response to variant morphologies of UHMWPE particles. *Biomaterials*. **24**(26),pp.4819–4826.
- Restrepo, C., Matar, W.Y., Parvizi, J., Rothman, R.H. and Hozack, W.J. 2010. Natural History of Squeaking after Total Hip Arthroplasty. *Clinical Orthopaedics and Related Research*. **468**(9),pp.2340–2345.
- Richards, L., Brown, C., Stone, M.H., Fisher, J., Ingham, E. and Tipper, J.L. 2008. Identification of nanometre-sized ultra-high molecular weight polyethylene wear particles in samples retrieved in vivo. *Journal of Bone and Joint Surgery-British*

Volume. **90B**(8),pp.1106–1113.

- Rodrigo, A., Valles, G., Saldana, L., Rodriguez, M., Martinez, M.E., Munuera, L. and Vilaboa, N. 2006. Alumina particles influence the interactions of cocultured osteoblasts and macrophages. *JOURNAL OF ORTHOPAEDIC RESEARCH*. **24**(1),pp.46–54.
- Sabokbar, A., Fujikawa, Y., Neale, S., Murray, D.W. and Athanasou, N.A. 1997. Human arthroplasty derived macrophages differentiate into osteoclastic bone resorbing cells. *Annals of the Rheumatic Diseases*. **56**(7),pp.414–420.
- Sabokbar, A., Kudo, O. and Athanasou, N.A. 2003. Two distinct cellular mechanisms of osteoclast formation and bone resorption in periprosthetic osteolysis. *Journal of Orthopaedic Research*. **21**(1),pp.73–80.
- Sabokbar, A. and Rushton, N. 1995. Role of inflammatory mediators and adhesion molecules in the pathogenesis of aseptic loosening in total hip arthroplasties. *Journal of Arthroplasty*. **10**(6),pp.810–816.
- Santos, C., Teixeira, L.H.P., Daguano, J.K.M.F., Rogero, S.O., Strecker, K. and Elias, C.N. 2009. Mechanical properties and cytotoxicity of 3Y-TZP bioceramics reinforced with Al₂O₃ particles. *Ceramics International*. **35**(2),pp.709–718.
- Savage, N.M. 1988. The use of sodium polytungstate for conodont separations. *J. Micropalaeontol.* **7**(1),pp.39–40.
- Savarino, L., Baldini, N., Ciapetti, G., Pellacani, A. and Giunti, A. 2009. Is wear debris responsible for failure in alumina-on-alumina implants? *Acta Orthopaedica*. **80**(2),pp.162–167.
- Schmalzried, T.P. and Callaghan, J.J. 2000. Wear in total hip and knee replacements - Reply. *JOURNAL OF BONE AND JOINT SURGERY-AMERICAN VOLUME*. **82A**(12),p.1806.
- Schmiedberg, S.K., Chang, D.H., Frondoza, C.G., Valdevit, A.D.C. and Kostuik, J.P. 1994. ISOLATION AND CHARACTERIZATION OF METALLIC WEAR DEBRIS FROM A DYNAMIC INTERVERTEBRAL DISC PROSTHESIS. *JOURNAL OF BIOMEDICAL MATERIALS RESEARCH*. **28**(11),pp.1277–1288.
- Seidl, A., Hainzl, O., Richter, M., Fischer, R., Boehm, S., Deutel, B., Hartinger, M., Windisch, J., Casadevall, N., London, G.M. and Macdougall, I. 2012. Tungsten-Induced Denaturation and Aggregation of Epoetin Alfa During Primary Packaging as a Cause of Immunogenicity. *Pharmaceutical Research*. **29**(6),pp.1454–1467.
- Shanbhag, A.S., Jacobs, J.J., Black, J., Galante, J.O. and Glant, T.T. 1995. HUMAN MONOCYTE RESPONSE TO PARTICULATE BIOMATERIALS GENERATED IN-VIVO AND IN-VITRO. *Journal of Orthopaedic Research*. **13**(5),pp.792–801.
- Shanbhag, A.S., Jacobs, J.J., Glant, T.T., Gilbert, J.L., Black, J. and Galante, J.O. 1994. COMPOSITION AND MORPHOLOGY OF WEAR DEBRIS IN FAILED UNCEMENTED TOTAL HIP-REPLACEMENT. *Journal of Bone and Joint Surgery-*

British Volume. 76B(1),pp.60–67.

- Shishido, T., Yamamoto, K., Tanaka, S., Masaoka, T., Clarke, I.C. and Williams, P. 2006. A study for a retrieved implant of ceramic-on-ceramic total hip arthroplasty. *Journal of Arthroplasty. 21*(2),pp.294–298.
- Siopack, J.S. and Jergesen, H.E. 1995. TOTAL HIP-ARTHROPLASTY. *Western Journal of Medicine. 162*(3),pp.243–249.
- Solomon, N. and Solomon, I. 2010. Deformation induced martensite in AISI 316 stainless steel. *REVISTA DE METALURGIA. 46*(2),pp.121–128.
- Sood, A., Salih, S., Roh, D., Lacharme-Lora, L., Parry, M., Hardiman, B., Keehan, R., Grummer, R., Winterhager, E., Gokhale, P.J., Andrews, P.W., Abbott, C., Forbes, K., Westwood, M., Aplin, J.D., Ingham, E., Papageorgiou, I., Berry, M., Liu, J., Dick, A.D., Garland, R.J., Williams, N., Singh, R., Simon, A.K., Lewis, M., Ham, J., Roger, L., Baird, D.M., Crompton, L.A., Caldwell, M.A., Swalwell, H., Birch-Machin, M., Lopez-Castejon, G., Randall, A., Lin, H., Suleiman, M.-S., Evans, W.H., Newson, R. and Case, C.P. 2011. Signalling of DNA damage and cytokines across cell barriers exposed to nanoparticles depends on barrier thickness. *NATURE NANOTECHNOLOGY. 6*(12),pp.824–833.
- Steinbeck, M.J., Jablonowski, L.J., Parvizi, J. and Freeman, T.A. 2014. The Role of Oxidative Stress in Aseptic Loosening of Total Hip Arthroplasties. *Journal of Arthroplasty. 29*(4),pp.843–849.
- Stewart, T., Tipper, J., Streicher, R., Ingham, E. and Fisher, J. 2001. Long-term wear of HIPed alumina on alumina bearings for THR under microseparation conditions. *Journal of Materials Science-Materials in Medicine. 12*(10–12),pp.1053–1056.
- Stewart, T.D., Tipper, J.L., Insley, G., Streicher, R.M., Ingham, E. and Fisher, J. 2003a. Long-term wear of ceramic matrix composite materials for hip prostheses under severe swing phase microseparation. *Journal of Biomedical Materials Research Part B-Applied Biomaterials. 66B*(2),pp.567–573.
- Stewart, T.D., Tipper, J.L., Insley, G., Streicher, R.M., Ingham, E. and Fisher, J. 2003b. Severe wear and fracture of zirconia heads against alumina inserts in hip simulator studies with microseparation. *Journal of Arthroplasty. 18*(6),pp.726–734.
- Sukur, E., Akman, Y.E., Ozturkmen, Y. and Kucukdurmaz, F. 2016. Particle Disease: A Current Review of the Biological Mechanisms in Periprosthetic Osteolysis After Hip Arthroplasty. *The Open Orthopaedics Journal. 10*,pp.241–251.
- Sundfeldt, M., Carlsson, L. V, Johansson, C.B., Thomsen, P. and Gretzer, C. 2006. Aseptic loosening, not only a question of wear - A review of different theories. *Acta Orthopaedica. 77*(2),pp.177–197.
- Suner, S., Tipper, J.L. and Emami, N. 2012. Biological effects of wear particles generated in

- total joint replacements: trends and future prospects. *Tribology - Materials, Surfaces & Interfaces*, **6**(2),pp.39–52.
- Tateiwa, T., Clarke, I.C., Williams, P.A., Garino, J., Manaka, M., Shishido, T., Yamamoto, K. and Imakiire, A. 2008. Ceramic total hip arthroplasty in the United States: safety and risk issues revisited. *American journal of orthopedics (Belle Mead, N.J.)*. **37**(2),pp.E26-31.
- Taylor, S., Manley, M. and Serekian, P. 1998. Wear performance of a contemporary alumina-alumina bearing couple under hip joint simulation *In: Proceedings of the 44th Orthopaedic Research Society*. New Orleans, Louisiana.
- Tipper, J.L., Firkins, P.J., Ingham, E., Fisher, J., Stone, M.H. and Farrar, R. 1999. Quantitative analysis of the wear and wear debris from low and high carbon content cobalt chrome alloys used in metal on metal total hip replacements. *JOURNAL OF MATERIALS SCIENCE-MATERIALS IN MEDICINE*. **10**(6),pp.353–362.
- Tipper, J.L., Galvin, A.L., Williams, S., McEwen, H.M.J., Stone, M.H., Ingham, E. and Fisher, J. 2006. Isolation and characterization of UHMWPE wear particles down to ten nanometers in size from in vitro hip and knee joint simulators. *Journal of Biomedical Materials Research Part A*. **78A**(3),pp.473–480.
- Tipper, J.L., Hatton, A., Nevelos, J.E., Ingham, E., Doyle, C., Streicher, R., Nevelos, A.B. and Fisher, J. 2002a. Alumina-alumina artificial hip joints. Part II: Characterisation of the wear debris from in vitro hip joint simulations. *Biomaterials*. **23**,pp.3441–3448.
- Tipper, J.L., Matthews, J.B., Ingham, E., Stewart, T.D., Fisher, J. and Stone, M.H. 2003. *Wear and functional biological activity of wear debris generated from UHMWPE-on-Zirconia ceramic, metal-on-metal, and alumina ceramic-on-ceramic hip prostheses during hip simulator testing* (I. M. Hutchings, ed.).
- Tortora, G. and Derrickson, B. 2009. Joints *In: Principles of Anatomy and Physiology*. NJ, USA: John Wiley & Sons, pp. 267–289.
- Tsai, T.-Y., Li, J.-S., Wang, S., Scarborough, D. and Kwon, Y.-M. 2014. In-vivo 6 degrees-of-freedom kinematics of metal-on-polyethylene total hip arthroplasty during gait. *JOURNAL OF BIOMECHANICS*. **47**(7),pp.1572–1576.
- Tsaousi, A., Jones, E. and Case, C.P. 2010. The in vitro genotoxicity of orthopaedic ceramic (Al₂O₃) and metal (CoCr alloy) particles. *Mutation Research-Genetic Toxicology and Environmental Mutagenesis*. **697**(1–2),pp.1–9.
- Tsuboi, H., Matsui, Y., Hayashida, K., Yamane, S., Maeda-Tanimura, M., Nampei, A., Hashimoto, J., Suzuki, R., Yoshikawa, H. and Ochi, T. 2003. Tartrate resistant acid phosphatase (TRAP) positive cells in rheumatoid synovium may induce the destruction of articular cartilage. *Annals of the Rheumatic Diseases*. **62**(3),pp.196–203.
- Urban, R.M., Jacobs, J.J., Tomlinson, M.J., Gavrilovic, J., Black, J. and Peoc'h, M. 2000.

Dissemination of wear particles to the liver, spleen, and abdominal lymph nodes of patients with hip or knee replacement. *JOURNAL OF BONE AND JOINT SURGERY-AMERICAN VOLUME*. **82A**(4),pp.457–477.

- VanOs, R., Lildhar, L.L., Lehoux, E.A., Beaulé, P.E. and Catelas, I. 2014. In vitro macrophage response to nanometer-size chromium oxide particles. *Journal of Biomedical Materials Research Part B-Applied Biomaterials*. **102**(1),pp.149–159.
- Voronov, I., Santerre, J.P., Hinek, A., Callahan, J.W., Sandhu, J. and Boynton, E.L. 1998. Macrophage phagocytosis of polyethylene particulate in vitro. *Journal of Biomedical Materials Research*. **39**(1),pp.40–51.
- Wang, M.L., Hauschka, P. V, Tuan, R.S. and Steinbeck, M.J. 2002. Exposure to particles stimulates superoxide production by human THP-1 macrophages and avian HD-11EM osteoclasts activated by tumor necrosis factor-alpha and PMA. *Journal of Arthroplasty*. **17**(3),pp.335–346.
- Warashina, H., Sakano, S., Kitamura, S., Yamauchi, K.I., Yamaguchi, J., Ishiguro, N. and Hasegawa, Y. 2003. Biological reaction to alumina, zirconia, titanium and polyethylene particles implanted onto murine calvaria. *BIOMATERIALS*. **24**(21),pp.3655–3661.
- Wei, S., Kitaura, H., Zhou, P., Ross, F.P. and Teitelbaum, S.L. 2005. IL-1 mediates TNF-induced osteoclastogenesis. *Journal of Clinical Investigation*. **115**(2),pp.282–290.
- Wei, S. and Siegal, G.P. 2008. Mechanisms modulating inflammatory osteolysis: A review with insights into therapeutic targets. *Pathology Research and Practice*. **204**(10),pp.695–706.
- Wei, X., Zhang, X., Flick, L.M., Drissi, H., Schwarz, E.M. and O’Keefe, R.J. 2009. Titanium particles stimulate COX-2 expression in synovial fibroblasts through an oxidative stress-induced, calpain-dependent, NF-kappa B pathway. *American Journal of Physiology-Cell Physiology*. **297**(2),pp.C310–C320.
- White, C.A., Carsen, S., Rasuli, K., Feibel, R.J., Kim, P.R. and Beaulé, P.E. 2012. High Incidence of Migration with Poor Initial Fixation of the Accolade (R) Stem. *Clinical Orthopaedics and Related Research*. **470**(2),pp.410–417.
- Wilkinson, J.M., Wilson, A.G., Stockley, I., Scott, I.R., MacDonald, D.A., Hamer, A.J., Duff, G.W. and Eastell, R. 2003. Variation in the TNF gene promoter and risk of osteolysis after total hip arthroplasty. *JOURNAL OF BONE AND MINERAL RESEARCH*. **18**(11),pp.1995–2001.
- Williams, D.F. 1999. *The Williams Dictionary of Biomaterials*. Liverpool University Press.
- Williams, S., Butterfield, M., Stewart, T., Ingham, E., Stone, M. and Fisher, J. 2003. Wear and deformation of ceramic-on-polyethylene total hip replacements with joint laxity and swing phase microseparation. *PROCEEDINGS OF THE INSTITUTION OF MECHANICAL ENGINEERS PART H-JOURNAL OF ENGINEERING IN MEDICINE*.

217(H2),pp.147–153.

- Willmann, G. 2000. Ceramic femoral head retrieval data. *Clinical Orthopaedics and Related Research*. (379),pp.22–28.
- Wright, T. and Goodman, S. 2001. What are the wear mechanisms and what controls them? In: S. Wright, TM and Goodman, ed. *IMPLANT WEAR IN TOTAL JOINT REPLACEMENT: CLINICAL AND BIOLOGICAL ISSUES, MATERIAL AND DESIGN CONSIDERATIONS.*, pp. 176–185.
- Wu, G.-L., Zhu, W., Zhao, Y., Ma, Q. and Weng, X.-S. 2016. Hip Squeaking after Ceramic-on-ceramic Total Hip Arthroplasty. *Chinese medical journal*. [Online]. **129**(15),pp.1861–6. [Accessed 30 September 2016]. Available from: <http://www.ncbi.nlm.nih.gov/pubmed/27453238>.
- Xia, Z., Ricciardi, B.F., Liu, Z., von Ruhland, C., Ward, M., Lord, A., Hughes, L., Goldring, S.R., Purdue, E., Murray, D. and Perino, G. 2017. Nano-analyses of wear particles from metal-on-metal and non-metal-onmetal dual modular neck hip arthroplasty. *NANOMEDICINE-NANOTECHNOLOGY BIOLOGY AND MEDICINE*. **13**(3),pp.1205–1217.
- Xu, S., Ma, X.-X., Hu, L.-W., Peng, L.-P., Pan, F.-M. and Xu, J.-H. 2014. Single nucleotide polymorphism of RANKL and OPG genes may play a role in bone and joint injury in rheumatoid arthritis. *Clinical and experimental rheumatology*. **32**(5),pp.697–704.
- Yanez, M.J. and Barbosa, S.E. 2003. Changes in particle area measurements due to SEM accelerating voltage and magnification. *Microscopy Research and Technique*. **61**(5),pp.463–468.
- Yang, S.Y., Ren, W.P., Park, Y.S., Sieving, A., Hsu, S., Nasser, S. and Wooley, P.H. 2002. Diverse cellular and apoptotic responses to variant shapes of UHMWPE particles in a murine model of inflammation. *Biomaterials*. **23**(17),pp.3535–3543.
- Yoon, T.R., Rowe, S.M., Jung, S.T., Seon, K.J. and Maloney, W.J. 1998. Osteolysis in association with a total hip arthroplasty with ceramic bearing surfaces. *Journal of Bone and Joint Surgery-American Volume*. **80A**(10),pp.1459–1468.
- Zagra, L. and Ceroni, R.G. 2007. Ceramic-ceramic coupling with big heads: clinical outcome. *European Journal of Orthopaedic Surgery and Traumatology*. **17**(3),pp.247–251.